INFORMATION TO USERS

This manuscript has been reproduced from the microfilm master. UMI films the text directly from the original or copy submitted. Thus, some thesis and dissertation copies are in typewriter face, while others may be from any type of computer printer.

The quality of this reproduction is dependent upon the quality of the copy submitted. Broken or indistinct print, colored or poor quality illustrations and photographs, print bleedthrough, substandard margins, and improper alignment can adversely affect reproduction.

In the unlikely event that the author did not send UMI a complete manuscript and there are missing pages, these will be noted. Also, if unauthorized copyright material had to be removed, a note will indicate the deletion.

Oversize materials (e.g., maps, drawings, charts) are reproduced by sectioning the original, beginning at the upper left-hand corner and continuing from left to right in equal sections with small overlaps.

Photographs included in the original manuscript have been reproduced xerographically in this copy. Higher quality 6" x 9" black and white photographic prints are available for any photographs or illustrations appearing in this copy for an additional charge. Contact UMI directly to order.

Bell & Howell Information and Learning
300 North Zeeb Road, Ann Arbor, MI 48106-1346 USA
800-521-0600

UMI®

DISSERTATION

ACTIVE ZONE DEPTH AND EDGE MOISTURE VARIATION DISTANCE IN EXPANSIVE SOILS

Submitted By:

Dean Brian Durkee

Department of Civil Engineering

In partial fulfillment of the requirements

for the Degree of Doctor of Philosophy

Colorado State University

Fort Collins, Colorado

Spring, 2000

COLORADO STATE UNIVERSITY

February 1, 2000

WE HEREBY RECOMMEND THAT THE DISSERTATION PREPARED UNDER OUR SUPERVISION BY DEAN B. DURKEE ENTITLED ACTIVE ZONE AND EDGE MOISTURE VARIATION DISTANCE IN EXPANSIVE SOILS BE ACCEPTED AS FULFILLING IN PART REQUIREMENTS FOR THE DEGREE OF DOCTOR OF PHILOSOPHY.

Committee on Graduate Work

Advisor

Department Head/Director

ABSTRACT OF DISSERTATION

ACTIVE ZONE DEPTH AND EDGE MOISTURE VARIATION DISTANCE IN EXPANSIVE SOILS

Two fundamental design parameters for foundations on expansive soils are historically referred to as active zone depth and edge moisture variation distance. The purpose of this research was to investigate these two parameters in terms of their historical definitions, characterize them in terms of the effects of climate conditions, geologic conditions, and soil properties, and estimate the long term active zone depth and edge moisture variation distance at the field test sites.

Typical foundation engineering design practice for expansive soils involves the use of active zone depth for the determination of heave and pier length. Previous attempts to define the active zone depth were based on techniques for approximating its value. Common practice along the Front Range in Colorado is to approximate the active zone depth in the range of 15 to 20 feet, or less based on seasonal fluctuations observed in the natural soils.

The edge moisture variation distance is used for the design of reinforcing for slab on grade construction. This parameter has been defined as the distance measured inward from the edge of the slab over which the water content changes in response to climate fluctuations. This definition implies that the edge moisture variation distance is a function of depth. Nelson and Miller (1992) pointed out that the edge moisture variation

distance is not clearly defined for the purposes of slab design and that it is the most difficult parameter to estimate. Several methods for determining the edge moisture variation have been developed however they have not been tested and generally give unclear results.

A new definition of active zone depth is proposed in this dissertation. The active zone depth is "the zone in the soil beneath a structure that is contributing to the actual heave that takes place at some point at the surface at a given time (t)". As such the active zone depth is a time dependent and spatially dependent parameter. The historical definition of edge moisture variation distance is assumed to be appropriate based on the results of this research.

Two simulated slabs-on-grade were constructed to study these two design parameters and to evaluate the definitions presented above. In addition, the test sites provided data for analyses of the effects of climate, geology, and soil properties. One simulated slab was constructed at the CSU Expansive Soils Test Site at Colorado State University in Fort Collins, CO and one at the Waterways Experiment Station Expansive Soils Test Site at Fort Sam Houston in San Antonio, Texas. In addition, laboratory tests were conducted on soils from both sites for use in the analyses. Finally, numerical modeling was conducted to consider the long-term effects of boundary condition changes at the CSU site.

Based on the results of the field and laboratory investigations and numerical modeling conducted for this research the follow key observations and conclusions lend credibility

to the proposed definition of active zone depth and historical definition of edge moisture variation distance presented above.

- The zone of seasonal moisture fluctuation significantly underestimates the depth of the active zone. Based on water content data from the CSU site, in the uncovered soil, the depth of seasonal moisture fluctuation is approximately 5 to 7 feet. Water content increases beneath the slab have been observed as deep as 18 feet.
- Initial increases in water content in expansive soil due to the construction of a slab typically result due to the reduction in evaporation at the surface. This boundary change causes an increase in moisture to a depth that is generally consistent with the depth of seasonal moisture fluctuation. However, additional water content increases occur in soils deeper than the depth of seasonal moisture fluctuation resulting in an edge lift condition of the slab. These additional water content increases are the result of infiltration from extreme climatic events and irrigation in the uncovered soils adjacent to the slab.
- Continual increases in the depth of active zone generally follow short periods of no increase and tend to coincide with an increase in the rate of rainfall accumulation. When the rate of rainfall accumulation increase coincides with an increase in temperature the thermal gradient causes an increase in downward flow from the warmer to the cooler regions of the soil. During these periods lateral migration of moisture beneath the slab increases the depth of the active zone. This cyclical behavior will continue indefinitely.
- Climate conditions, geologic conditions, and soil properties control the rate of increase in the depth of the active zone. In general the availability of moisture is controlled by climate conditions as described above. However, the addition of water from irrigation exacerbates the problem. In addition, preferred flow paths due to geologic conditions such as bedding planes also provide conduits for flow. Hydraulic conductivity and water retention properties primarily affect time rate of development of the active zone.
- Based on model results presented herein, the long-term active zone depth for a residential foundation at the CSU test site where irrigation is applied in accordance with Northern Colorado Water Conservancy District guidelines approaches the depth of potential heave based on stress conditions, which is equal to 35 feet.
- The edge moisture variation distance measured in this investigation is equal to half the slab width, 15 feet. Therefore to determine the maximum extent of edge moisture variation distance a larger slab would be necessary.

Dean Brian Durkee
Department of Civil Engineering
Colorado State University
Fort Collins, Colorado 80523
Spring 2000

ACKNOWLEDGEMENTS

The U.S. Army Corps of Engineers, Waterways Experiment Station and Colorado State University provided financial support for this research. I am truly grateful to them for providing me with the opportunity to conduct this research project.

My sincere appreciation goes to my graduate advisor, Professor John D. Nelson, for his confidence in me and for his never ending excitement about the project and the field of geotechnical engineering in general. His enthusiasm is inspirational to anyone wishing to pursue the field. I also want to thank the other members of my graduate committee, Professor David B. McWhorter, Professor Charles D. Shackelford, and Professor Thomas V. Edgar for their advisement, patience, and accessibility throughout this research.

There have been many friends and colleagues too numerous to name at Colorado State University and at Shepherd Miller Incorporated that have helped me along the way with both technical and moral support. In particular three graduate students in the Geotechnical Engineering Program provided support for this project through completion of their Masters Theses: Kuo-Chieh Chao, Hui-Wen Cheng, and Heumggoo Yeo. Their work and their friendships are much appreciated. Thanks also to my good friends Lou and Deb Miller for their technical guidance, their encouragement to remain focused, and for being there when I needed a break.

I am particularly indebted to my family for their support. My parents have always encouraged me to pursue my dreams and their faith inspired me to complete this project. My daughters, Stephanie, Hana, and Leah have allowed me the time away from them to complete this project and I owe them for their understanding. Most of all I want to thank my wife Lisa for her love and support. Throughout this project she has been there to keep me going with encouragement and confidence and at times having to convince me as well as herself that it was worth it. This would not have been possible without her.

TABLE OF CONTENTS

LIST OF TABLES

LIST OF FIGURES

CHAPTER 1

INTRODUCTION

The term expansive soil generally refers to soil or rock that has potential for volume change (swelling) when its water content increases. Problems with slabs-on-grade constructed on expansive soil occur as a result of swelling caused by changes in the state of stress, due to an increase in water content. The increase in water content results from the decrease of evapo-transpiration from the soil surface due to placement of the slab and the introduction of water to the soil from external sources such as irrigation, broken utility lines, or extreme climatic events.

The research presented in this dissertation was conducted to investigate two fundamental expansive soil foundation design parameters historically referred to as "active zone depth" and "edge moisture variation distance". The primary objectives of this research are listed below.

1. Examine the previously proposed definitions and develop rigorous definitions for the term's "active zone depth" and "edge moisture variation distance".
2. Monitor water content, suction, and heave beneath a simulated slab foundation under controlled conditions where the evapo-transpiration has been significantly reduced.
3. Determine the active zone depth and edge moisture variation distance in terms of the observed moisture migration and heave patterns.
4. Characterize the active zone depth and edge moisture variation distance in terms of the effects of environmental conditions, geologic conditions, and soil properties.
5. Evaluate the active zone depth and edge moisture variation distance using numerical techniques to simulate boundary conditions not considered in the field investigation.

Two simulated slabs-on-grade were constructed at field test sites located in Fort Collins, Colorado (CSU), and San Antonio, Texas (FSH). The CSU site is located at the Expansive Soils Test Site on the Foothills campus of Colorado State University. The FSH site is located at the Waterways Experiment Station (WES) Expansive Soils Test Site at Fort Sam Houston. Both sites were instrumented to monitor surface heave and water content changes in the soil beneath and adjacent to the simulated slabs. The CSU site was also instrumented to monitor total suction and temperature beneath and adjacent to the simulated slab. The use of two sites allows for comparison of the effects of different geologic conditions, soil properties, and climatic conditions on water movement.

A laboratory investigation was conducted in support of the field research. Geotechnical laboratory tests were conducted to classify the soil and determine general soil properties and constitutive parameters for use in the quantitative analyses of water movement and heave. Two finite element computer models SoilCover, Geo-Analysis 2000 Ltd., and SEEP/W, GEO-SLOPE International Ltd. were used to evaluate the effects of soil properties, geologic conditions, and climatic conditions on water movement.

This dissertation presents historical information, the results of laboratory and field investigations, and the results of numerical modeling, as it pertains to active zone depth and edge moisture variation distance. An historical overview of key developments in expansive soils foundation design and previously proposed definitions of active zone depth and edge moisture variation distance are presented in the remainder of Chapter 1. In addition a rigorous definition for active zone depth is proposed in Chapter 1.4.1.

A literature review is presented in Chapter 2. The development of the mechanics of unsaturated soil, as it relates to expansive soil, an overview of soil water models, design considerations for foundations on expansive soils, and the results of previously conducted field studies are presented.

Sampling of the field test site soils and construction of the field test sites are presented in Chapter 3. Soils from the site investigation were tested in the laboratory and the results are presented in Chapter 4. The results from the laboratory investigation were also used to classify the soils in terms of swell potential. In addition, laboratory results were used in Chapters 5 and 6 to predict heave and determine constitutive parameters for the numerical modeling.

Results from the field test sites are presented in Chapter 5. The results of numerical modeling are presented in Chapter 6. Conclusions and future research topics are presented in Chapter 7.

1.1 Historical Overview

Most advances in the state-of-the-art with regard to expansive soils have taken place in the last forty years. In the late 1950's researchers began developing empirical methods to identify and classify expansive soil. Several of the early methods for identifying expansive soil correlate Atterberg limits to heave potential. The volume and moisture change behavior of soil is directly related to the percent clay and mineralogical composition, which also influence consistency limits. Generally, soil with a high plasticity index will experience greater volume change than soil with a low plasticity index.

Seed et al. (1962b) noted that two soils with the same swell potential may exhibit different swell behavior due to different environmental conditions. They made the distinction between swell potential and actual swell, and proposed that a soil be evaluated in two stages. The first stage is to determine the swell potential based on the type and amount of clay present in the soil. The second stage is to evaluate the environmental conditions to determine the actual amount of swell that can be expected.

Environmental conditions consist of climatic conditions and other external factors such as irrigation or vegetation that can effect the water content of the soil. Evaporation and evapo-transpiration cause an upward flux of water in the soil. Alternatively, a downward flow of water is caused by water at the ground surface due to precipitation or excess irrigation. In the arid and semi-arid regions of the southwestern U.S., natural soil generally exists in an unsaturated state at high negative water pressures due to the high evaporation rate and low amount of precipitation. The presence of a relatively dry expansive soil with a high affinity for water, in an area of rapid development resulting in large changes in soil moisture, typically causes serious problems in the design of foundations for light structures.

1.2 Design Considerations

A structure such as a building foundation or highway pavement significantly reduces evaporation and evapo-transpiration at the surface of the soil. Generally, an initial increase in water content occurs with subsequent swelling of the soil. Except in ideal situations, swelling occurs in an uneven pattern, due to variability in both the soil profile and water content, resulting in differential movement of the structure. If the magnitude

of differential movement is large enough, then significant damage to structures and pavements can occur.

1.3 Foundation Design Parameters

Two fundamental design parameters for design of slabs-on-grade on expansive soil are the "active zone depth" and the "edge moisture variation distance". The primary goal of this research is to define and to develop an understanding of these two parameters.

1.3.1 Definition of Active Zone Depth

The active zone depth is used to predict heave and determine pier length. A review of the literature indicates that active zone depth is not clearly defined. Previous attempts to define the active zone depth are based on techniques for approximating its value. As such, they lack rigor and a quantitative method for estimating or measuring it does not exist. Therefore, one of the first objectives of this research is to present a definition for active zone depth.

Until recently, empirical data has indicated that the zone of soil that influences heave is generally within the upper 15 or 20 feet. O'Neill and Poormoayed (1980) indicated that the active zone depth in the Denver, Colorado area ranges from 10 to 15 feet. In this zone the overburden stress is low thus providing little resistance to swell. This upper stratum of soil is typically the zone in which water content changes are the most pronounced.

Over the past 15 to 20 years practitioners and researchers have attempted to determine active zone depth by several methods which each offer their own "definition" of active zone depth.

Goode (1982) and Hamberg (1985) define the active zone depth as the "depth of water content increase" due to placement of the slab. Their studies consisted of measurement of heave and water content changes beneath simulated slab foundations constructed on expansive soils where the surrounding area was left in its natural state.

The upper 15 to 20 ft of soil are heavily influenced by climatic conditions. Nelson and Miller (1992) define active zone depth as the "zone of seasonal fluctuation". From this definition the active zone depth is a function of natural water content fluctuations and can be identified in the field by the point where the water content or suction distribution becomes constant with time.

Fredlund and Rahardjo (1993) define the active depth of swelling (active zone depth) as the depth to which the overburden stress equals the corrected swell pressure. This zone can reach depths in excess of 100 ft when typical swell pressures (10,000 psf) are considered.

Nelson, Durkee, and Bonner (1998) refer to the depth of potential heave. The depth of potential heave is synonymous to the definition of active depth of swelling proposed by Fredlund and Rahardjo (1993), and represents the maximum depth within which heave is possible.

These references provide insight into some of the factors that must be considered to estimate active zone depth for design but in and of themselves are not "definitions". The

depth at which the overburden stress equals the corrected swell pressure provides a method for estimating maximum active zone depth and can be used as a conservative estimate when data is limited.

When a relatively dry soil surface is covered, the rate of evaporation and evapo-transpiration are reduced significantly, and the water content in the soil increases to a steady-state condition based on the vapor pressure gradient in the soil. The resulting water content increases progress downward to a depth referred to as the "depth of wetting". This depth has been shown to increase with time but long-term data is limited. Thompson (1997) presented 5 to 10 years of pre-construction and post-construction water content data from residential and commercial construction sites, some of which were irrigated. All of the sites were built on flat sedimentary soil profiles. Based on this data Thompson (1997) concluded that a design depth of wetting (active zone depth) of 20 feet is conservative.

Irrigation, infiltration through backfill areas of trenches, broken water lines, and other factors can cause the depth of wetting to go much deeper. In this case the zone contributing to swell can be much deeper than the zone of seasonal fluctuation or the depth of wetting described above.

The empirical approximations discussed above are based on time dependent data and as such provide a probabilistic estimate without quantitative rigor. Thus, there have been many definitions proposed for "active zone depth". However, these are not actually definitions but rather they are methods for estimating the parameter.

Definition

The definition of Active Zone presented herein is the zone in the soil beneath a structure that is contributing to the actual heave that takes place at some point at the surface at a given time (t). As such, the depth of the active zone is a time dependent and spatially dependent parameter that is limited by the following two conditions.

1. The active zone depth can not be deeper than the depth at which the overburden pressure is equal to the swell pressure.
2. The active zone depth can not be deeper than the depth of expansive soil. This limiting condition seems obvious, but the zone of seasonal fluctuation and depth of wetting can be deeper than the zone of expansive soil.

The time dependent nature, spatial variability, and limiting conditions are illustrated in Figure 1-1. At Point A the depth of the expansive soil is 10 feet and at Point B the depth of expansive soil is 30 feet. The soils beneath the expansive soil are non-expansive. At time t_1 the wetting front in the soil beneath point A and point B has progressed to a depth z_1 of 5 feet. At this time the active zone depth is 5 feet at both locations A and B. At time t_2 the wetting front beneath points A and B has progressed to a depth z_2 of 10 feet. At this time the active zone depth is 10 feet at both locations A and B. At time t_3 the wetting front has progressed to a depth z_3 of 20 feet. At this time the active zone depth is 10 feet at point A and 20 feet at point B. Since the soil underlying point A consist of 10 feet of expansive soil over a non-expansive soil, the maximum active zone depth is 10 feet.

Similarly the maximum active zone depth at point B is 30 feet unless the swell pressure is low enough that an overburden of less than 30 feet is sufficient load to resist swell. For

example, if the swell pressure of the soil is 3,000 psf and the density of the soil is 100 pcf then at a depth of 30 feet the swell pressure is equal to the overburden load. In this case at time t_4 the soil beneath 30 feet does not contribute to heave at the surface, hence the active zone depth is 30 feet.

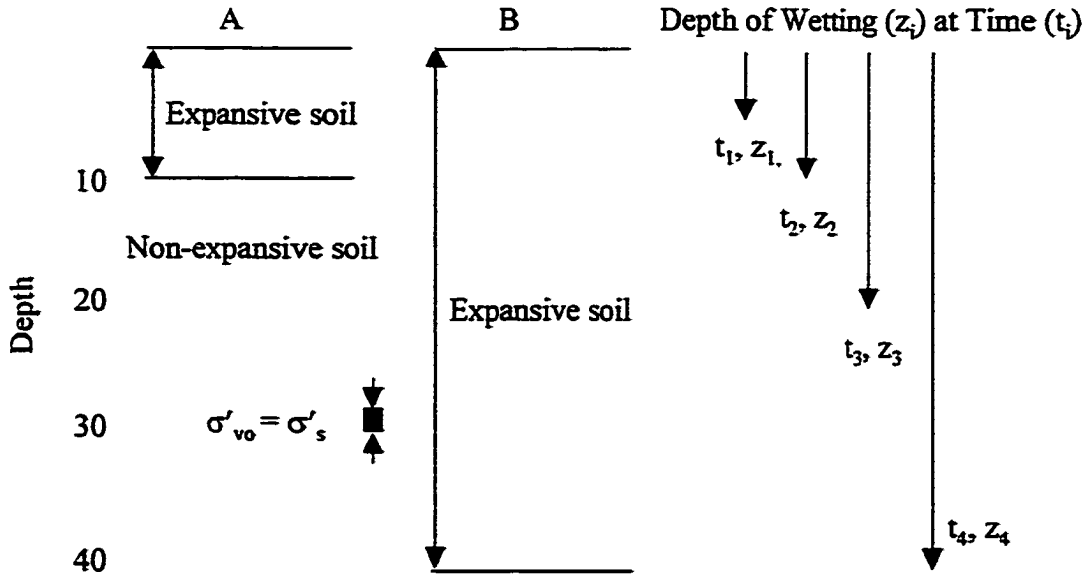

Figure 1-1 Illustration for definition of active zone depth

1.3.2 Definition of Edge Moisture Variation Distance

The edge moisture variation distance is used to design reinforcing for the slab foundations. The cyclical effects of evaporation and wetting around the edges of a foundation result in shear stresses in the concrete that contribute to cracking. For example, during hot, dry conditions water can be lost from the soil under a slab-on-grade around its edges. During wetter times of the year or during extreme precipitation events the water content will increase around the edges the slab.

The distance from the edge of the foundation inward to where these seasonal fluctuations occur is referred to as the edge moisture variation distance. PTI (1980) defines the edge moisture variation distance as the distance measured inward from the edge of the slab over which the moisture content of the soil varies. As such the magnitude of edge moisture variation distance is depth dependent. McKeen and Johnson (1990) indicate that the edge moisture variation distance can approach a distance equal to the depth of the active zone, and determine its magnitude based on suction fluctuations with depth and the depth of the slab.

Nelson and Miller (1992) point out that the edge moisture variation distance is not clearly defined and for the purposes of slab design it is the most difficult parameter to estimate. Shear stresses within a concrete slab foundation are the result of differential uplift forces beneath the slab. As such, the seasonal fluctuations in water content around the edges of the slab represent only one factor that contributes to shear stress and cracking. Geologic conditions, soil variability, and the time dependent progression of water from the edges of the slab due to irrigation also contribute to differential heave over the life of the structure. In addition, in the case of a slab type structure exposed to atmospheric conditions, such as a road or runway, temperature fluctuations above the slab can result in significant water content fluctuations beneath the surface.

CHAPTER 2

LITERATURE REVIEW

The current state of knowledge in expansive soils suggests that the methods available for predicting heave and designing slab foundations are reliable if the characteristics of the site can be defined with reasonable accuracy. As discussed in Chapter 1, two important parameters for designing foundations on expansive soil are the active zone depth and the edge moisture variation distance. The goal of this research is to characterize active zone depth and edge moisture variation distance and evaluate the effects of climatic conditions, geologic conditions, and soil properties on these parameters. The following literature review presents an overview of the fundamental theoretical background in unsaturated soils and the technical considerations for the design of slab foundations on expansive soil. The literature review is divided into four sub-chapters. The first sub-chapter discusses the current state of knowledge in the mechanics of unsaturated soil as it pertains to volume change and water movement. The second sub-chapter discusses previously developed volume change and moisture flow models. The third sub-chapter is an overview of slab-on-grade design considerations. The fourth sub-chapter presents the results of previous slab-on-grade field studies.

2.1 Mechanics of Unsaturated Soil

Fredlund and Morgenstern (1977) rigorously defined the state of stress in unsaturated soil. Prior attempts to write an effective stress equation for unsaturated soils lacked somewhat in rigor. The following sub-chapters discuss the stress state variables for unsaturated soil, particularly with respect to volume change and water movement.

2.1.1 State of Stress

Volume change behavior in soil results from changes in the state of stress within the soil. The state of stress is defined by the equations of force equilibrium and must be independent of soil properties. In geotechnical engineering the state of stress in a soil is expressed in terms of the effective stress (total stress minus pore water pressure). The original effective stress equation proposed by Terzaghi was presented in terms of a saturated soil thus allowing a single-valued effective stress. Since the late 1950's and early 1960's researchers have attempted to extend the saturated effective stress equation to unsaturated soils.

Fredlund and Rahardjo (1993) presented a review of the proposed effective stress equations for unsaturated soils. Until 1977, the most commonly used equation to define effective stress in unsaturated soils was that presented by Bishop at a lecture in Oslo, Norway in 1955 (see Bishop, 1959). Bishop's equation is given by:

$$\sigma'=(\sigma-u_a)+\chi(u_a-u_w) \qquad (2\text{-}i)$$

where:

	σ'	=	effective stress
	σ	=	total stress
	u_a	=	pore air pressure

u_w = pore water pressure
χ = dimensionless parameter related to the degree of saturation

Jennings and Burland (1962) first questioned the use of a single-valued stress state to define effective stress. Jennings and Burland (1962) conducted a series of oedometer tests and triaxial compression tests on soils ranging from silty sand to silty clay. They concluded that the equation proposed by Bishop (1959) gave different results when used for different problems. The χ-parameter, in Equation 2-1 varies with material properties including degree of saturation, and thereby introduces constitutive behavior into the stress state equation. Recognizing this, several researchers have concluded that the state of stress is not defined by a single stress state variable and must be expressed by more than one independent stress state variable (Jennings and Burland, 1962, Matyas and Radhakrishna, 1968, and Barden et al., 1969).

Fredlund and Morgenstern (1977) verified that the following three variables are valid stress state variables:

$$(\sigma-u_a),(\sigma-u_w),(u_a-u_w)$$

The third term shown above represents the matric suction of the soil. To verify and prove that the proposed stress state variables are independent; Fredlund and Morgenstern (1977) noted that:

> "A suitable set of independent stress state variables are those that produce no distortion or volume change of an element when the individual components of the stress state variables are modified but the stress state variables themselves are kept constant. Thus, the stress state variable for each phase should produce equilibrium in that phase when a stress point in space is considered."

Laboratory null tests were performed in which σ, u_a, and u_w were varied such that the stress state variables listed above remained constant. There were no measurable soil or water volume changes during the null tests indicating that the proposed stress state variables are valid. Since any two of the stress state variables can be used to determine the third one it is evident that only two of the variables are independent. Also, it has been shown experimentally that any combination of two of the stress state variables defines the state of stress in an unsaturated soil.

2.1.1.1 Soil Suction

The three stress state variables shown above represent the net normal stress with respect to the air phase, the net normal stress with respect to the water phase, and the matric suction, respectively. Fredlund and Rahardjo (1993) stated that the magnitude of the matric suction is often considerably higher than the magnitude of the net normal stress and that the variation in the soil suction profile is generally greater than variations commonly occurring in the net normal stress profile.

Variation in the matric suction profile will depend on several factors, including the environmental conditions, ground surface conditions, the location of the water table, and the permeability of the soil profile. Matric suction generally increases during dry seasons and decreases during wet seasons. During the dry season the evapo-transpiration rate at the surface is greater than the infiltration rate and the matric suction increases. During the wet season the evapo-transpiration rate at the surface decreases and hence the matric suction decreases. The surface conditions refer to whether or not the soil surface is

exposed to the atmosphere. The matric suction profile beneath an uncovered surface will vary greatly between wet and dry times of the year. The matric suction profile beneath a covered surface is less influenced by seasonal fluctuations and remains relatively constant with time. However, placement of a cover at the surface of a desiccated soil can result in an accumulation of moisture and subsequent reduction in matric suction.

The depth of the water table will generally effect the magnitude of the matric suction profile. The deeper the water table is the greater the magnitude of matric suction. The rate of migration of water due to suction changes is controlled by the permeability. This affects the ability of the soil to change matric suction when environmental conditions change.

The total suction of a soil is made up of two independent variables, matric suction (u_a-u_w) and osmotic suction, π. Changes in the total suction of a soil can result from changes in either of the independent components or a combination of both. Osmotic suction is related to the salt content of the pore-water and therefore can be associated with saturated soils as well as unsaturated soils. Changes in salt content of the pore water will result in changes in the mechanical behavior of both saturated and unsaturated soils.

Engineering problems associated with expansive soils generally result from environmental changes. The accumulation of moisture beneath a slab foundation causes a decrease in total suction (increase in pore pressure) and subsequent heaving of the structure. Fredlund and Raharjdo (1993) stated that this type of change primarily affects the matric suction component and that the osmotic suction changes are generally less significant. The results of a study on compacted Regina clay by Krahn and Fredlund

(1972) showed the relative importance of changes in osmotic suction as compared to matric suction when water content changes. When the water content changed the change in total suction was essentially equivalent to the change in matric suction.

2.1.2 Volume Change

Fredlund (1979) concluded that the stress-strain behavior of an unsaturated soil must be considered with two independent stress state variables. A three dimensional surface was used to show volume change as a function of the two independent stress state variables, thus making the relationship a constitutive surface.

Matyas and Radhakrishna (1968) tested the three dimensional surface theory using K_o compression tests on mixtures of flint powder and kaolin. The results of their tests showed that a unique surface exist in terms of $(\sigma-u_w)$ and (u_a-u_w) for samples tested on a wetting cycle. Matyas and Radhkrishna (1968) noted, however, that the surface was not unique with wetting and drying cycles due to a hysteretic effect on the soil structure.

Similar tests were conducted by Barden et al. (1969). The total, pore air, and pore water pressures were controlled during K_o loading tests. The tests were run using various stress paths on both wetting and drying cycles. Barden et al. (1969) concluded that the volume change behavior of an unsaturated soil was stress path dependent, and that it should be analyzed in terms of two independent stress state variables: $(\sigma-u_a)$ and (u_a-u_w). Although these two references recognized that the stress state variables are independent they did not show the validity of them. The work done by Fredlund and Morgenstern (1977) showed that any two of the three stress state variables can completely describe the state of stress.

Thus, the state of stress and the volume change behavior of an unsaturated soil are described by two independent stress state variables. A constitutive relationship for volume change is given by:

$$\Delta e=[C_{mi}\Delta\log(u_a-u_w)+C_{ti}\Delta\log(\sigma-u_a)]_i \qquad (2\text{-}2)$$

where:

Δe	=	the change in void ratio
(u_a-u_w)	=	matric suction stress state variable
$(\sigma-u_w)$	=	net normal stress state variable
C_m	=	matric suction index
C_t	=	effective stress index
σ	=	total stress
u_a	=	pore air pressure
u_w	=	pore water pressure.

Fredlund and Rahardjo (1993) and Nelson and Miller (1992) presented methods for finding the index parameters C_m and C_t.

2.1.3 Water Movement

Two primary approaches have been used to analyze and quantify water movement in soils, the thermodynamic approach and the mechanistic approach. Edlefsen and Anderson (1943) discussed the thermodynamic approach. They suggested that moisture movement is initiated by a gradient of the total specific free energy, which is defined as the combined effects of surface tension, hydrostatic pressure, dissolved material, and adsorptive forces. Corey and Klute (1985) listed several shortcomings to this approach. Generally, the method does not consider the effects of gravity. Corey and Klute (1985) also pointed out that the velocity term submitted by Edlefsen and Anderson (1943) is a water flux which is not necessarily the soil solution flux, therefore, it is not directly analogous to Darcy's law.

Engineers have traditionally taken a mechanistic approach to modeling water flow through soil. Fredlund and Rahardjo (1993) stated that the three concepts that engineers have used to explain the mechanical driving force that causes water flow in an unsaturated soil are the water content gradient, the matric suction gradient, and the hydraulic head gradient.

They also stated that flow is more appropriately defined in terms of a hydraulic head gradient. A water content gradient implies that water will flow from a high water content to a low water content. However, a water content gradient is not a fundamental driving potential because water can flow from low water content to high water content when soil variations are involved, (Fredlund and Rahardjo, 1993).

To show that the matric suction gradient is not the appropriate driving potential in an unsaturated soil, Fredlund and Rahardjo (1993) showed three hypothetical cases where air and water pressure are greater on the left hand side of an unsaturated element of soil, than on the right hand side. The three cases are shown in Figure. 2-1. In all three cases air and water will flow separately from left to right in response to their individual pressure gradients regardless of the matric suction gradient. If the air pressure is zero, which is the common situation in nature, the matric suction gradient is numerically equal to the pressure gradient.

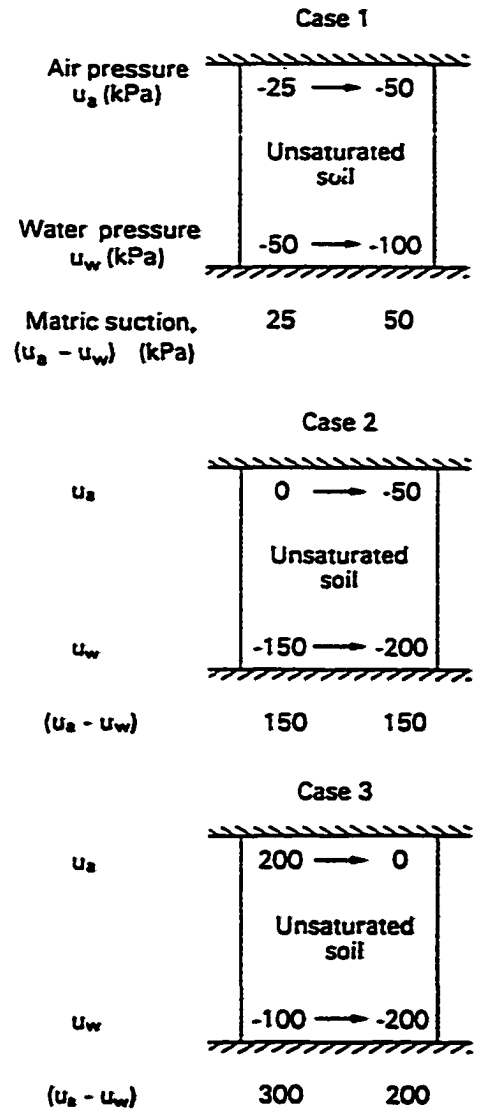

Figure 2-1 Pressure and matric suction gradients across an unsaturated soil element (Fredlund and Rahardjo, 1993)

2.2 Models for Soil Water Flow

Edgar (1983) presented a comprehensive review of the development of groundwater flow models as they have developed from modeling moisture flow through isothermal saturated rigid soil to modeling moisture flow through unsaturated deformable soil with a temperature gradient. This sub-chapter summarizes that development and presents a review of additional work since 1983.

The earliest groundwater models assumed isothermal conditions in a saturated rigid soil under steady state flow conditions. Richards (1931) developed the basic equations for isothermal flow through unsaturated rigid soil. Richards' equation uses Darcy's law to relate the rate of change of volume of water to the volumetric flux, which is proportional to the gradient of the capillary potential.

Theis (1935) developed a transient analysis for saturated isothermal flow in a rigid soil to investigate the rate of discharge from a well. Jacob (1940) showed that Theis' method also accounts for slight changes in the soil volume by considering the elastic properties of water and soil voids.

Terzaghi used the diffusion equation and the assumptions of a saturated soil, constant permeability, and a linear stress-strain relationship under small strains to develop the standard consolidation equation for isothermal flow in a deforming soil (Taylor, 1948).

Philip and De Vries (1957) developed a vapor flux equation for moisture movement in rigid porous material under temperature gradients. They coupled vapor phase and liquid phase flow by developing thermal and isothermal diffusivity coefficients for both phases.

The liquid phase flow accounts for gravity, capillary, and adsorptive forces and the vapor phase flow is controlled by diffusion.

McNabb (1960) extended Terzaghi's consolidation theory to include large strains by defining a coordinate system such that it was attached to the soil particles, thus maintaining a constant volume of solids as the soil deformed. Gibson et al. (1967) extended Terzaghi's consolidation theory to include large strains by accounting for variations in soil compressibility and permeability. Gibson et al. (1981) applied a solution to the equations developed by Gibson et al. (1967) to a thick deforming clay layer. The results of this study showed that the nonlinear finite strain theory predicts a slower dissipation of excess pore pressure than conventional theory. The authors concluded that conventional consolidation theory might therefore result in an overestimate of shear strength.

Stallman (1965) developed an equation for estimating infiltration rates due to sinusoidal fluctuations of temperature profiles at the ground surface in a saturated rigid porous media. Lapham (1987) used a finite difference method to analyze infiltration rates beneath streams with Stallman's equation. The results matched well with field measured hydraulic conductivity values.

Campanella and Mitchell (1968) showed that pore water drained from a saturated sample of illite as the sample temperature increased at a constant isotropic effective stress. As the sample was subsequently cooled, water was imbibed but not back to the initial value. The drainage of pore water upon heating was attributed to expansion of the mineral solid and pore water, and soil structure changes.

Raats and Klute (1968a, 1968b) used continuum theory of mixtures to develop equations for transport of water through saturated and unsaturated soil. They treated the soil as independent continuous phases and wrote balance of mass and balance of momentum equations for each phase. Those equations were applied to a one-dimensional deformation of the solid phase acting simultaneously with motion of the aqueous phase for saturated and unsaturated porous media (Raats and Klute, 1969).

Fredlund and Hasan (1979) developed a one-dimensional consolidation model for unsaturated soils. By considering Terzaghi's consolidation equation and the stress state variables presented by Fredlund and Morgenstern (1977) to be valid, the authors derived dual equations for pore air and pore water pressure dissipation with the application of load. Volume change of an unsaturated element of soil with a continuous air phase was defined by the total stress minus pore air pressure and capillary pressure.

Lloret and Alonso (1980) also developed a one-dimensional model for isothermal flow through a deforming unsaturated soil. The concept of relative permeability for air and water developed by Bear, and the stress state variables presented by Fredlund and Morgenstern (1977) were used in the development of a finite element model for unsaturated flow and deformation.

Chen et al. (1981) showed the effects of temperature variation in deforming soil. They developed a thermal conductive instrument for controlling a temperature gradient in a remolded expansive soil. Test results showed that for an initially constant water content distribution a linearly increasing distribution of water content could be achieved by

heating one end. The degree of redistribution of water was a function of the initial water content.

Dakshanamurthy and Fredlund (1981) developed a mathematical model for predicting moisture flow in an unsaturated deformable soil. They expanded the theory developed by Fredlund and Hasan (1979) to include nonisothermal flow conditions by applying the temperature gradient to the pore air and pore water pressure. A modified form of the pore air and pore water partial differential equations were obtained by combining the effects of the thermal and hydraulic gradients and neglecting the vapor phase flow.

The concept of total potential has been used extensively in soil physics and agronomy for analyzing soil water flow. Corey and Klute (1985) presented an historical development of the concept of total potential. They state that the most important drawback to most total potential formulations for soil water is that a distinction is not made between potential of the chemical water component and the hydraulic potential of the soil solution component.

Corey and Klute (1985) also discussed the concept of irreversible thermodynamics. The theory of irreversible thermodynamics states that any spontaneous or natural process in a system produces entropy. A balance equation can then be written for a continuous fluid mixture. The resulting balance equation relates the time rate of production of entropy per unit volume to the sum of the negative divergence of the entropy flux and an entropy source function.

Edgar et al. (1989) developed a nonisothermal, consolidation model for flow through unsaturated soil. A finite difference technique was used to analyze the effects of liquid,

gas, and heat flows on the deformable soil. A set of one dimensional equilibrium and balance equations for two and three phase soils were developed using a coordinate system defined by the soil solids. A series of example problems were used to analyze the effects of changing the environmental conditions and soil properties. A specific example, which is pertinent to this research, is the consolidation of an unsaturated soil due to placement of a cover.

The example presented in Edgar et al. (1989) considered the application of a soil cover on a soil profile consisting of three distinct layers. Prior to the placement of the cover the originally saturated soil was allowed to drain via a free draining layer at the bottom and evaporation was allowed at the surface. At some time later a cover was placed thereby eliminating evaporation at the surface. The results showed that an increase in water content occurred at the surface due to the placement of the cover. In this example a highly compressible soil was used and the model results also indicated that the soil consolidated due to the weight of the cover.

Nassar and Horton (1989) conducted experiments to observe whether the presence of a solute affects moisture migration that is controlled by a temperature gradient, in unsaturated soil. Dual tests were conducted, one with a saline soil and one without to compare the differences. A model equation for volumetric water content distribution was fitted to the data by least-squares regression. The results indicated that solute concentration does affect moisture migration due to a temperature gradient and that it can be modeled reasonably well using their empirical equation.

Bach (1992) conducted laboratory column tests to clarify the significance of nonisothermal water flow and ran a numerical simulation model for moisture and heat flow to compare the laboratory results with calculations using Philip and De Vries' formulation. Evaluation of the results indicates that temperature gradient has the most significant effect at intermediate water contents. Under nonisothermal conditions the model provided a poor fit to the measured data until the original matric potential coefficient was modified. The model results indicated that temperature gradient has less of an effect at high water contents.

2.2.1 Infiltration and Evaporation

The models discussed thus far were developed to evaluate seepage and flow in saturated and unsaturated soil. However, the analysis of seepage and flow in saturated and unsaturated soil requires the specification of a boundary condition at the surface (i.e. flow of water, pressure, and etc..). The flow of water across the surface (infiltration and evaporation) is particularly important in the investigation of expansive soils where small changes in water content near the surface can result in large volume changes and significant damage to structures.

Several models have been developed in the past for evaluating infiltration. However, in arid climates where surface soils are typically very dry or desiccated most of the time, evaporation is of particular importance. Wilson (1990) noted that the process of evaporation from the soil surface has not been fully understood and extreme difficulties frequently arise while predicting evaporation from unsaturated soil surfaces.

Wilson (1990) developed a theoretical approach for evaluating the rate of evaporation from an unsaturated soil surface. The flow of water vapor and liquid water are described by Darcy's law and Fick's law and Wilson (1990) developed a modified form of Penman's method to predict evaporation from unsaturated soil surfaces. The modified Penman formulation accounts for net solar radiation, wind speed, and relative humidity. Wilson (1990) concluded that three primary factors control the flow of moisture between the soil and the atmosphere. The first factor is the atmospheric conditions and the demand they impose on the soil, The second factor is the ability of the soil to transmit moisture; this is controlled by the hydraulic conductivity and soil water characteristic of the soil. The third factor is the influence of vegetation.

Researchers at the Unsaturated Soils Group, Department of Civil Engineering, University of Saskatchewan, Saskatoon, Canada used Wilson's model to develop a finite element computer package that models transient conditions in saturated and unsaturated soils. The model is physically based and predicts the exchange of water and energy between the atmosphere and the soil (atmospheric coupling).

2.3 Design of Stiffened Slabs-on-Grade

Design of a stiffened slab-on-grade consists of determining the bending moment, shear, and deflection for the given situation and providing reinforcing. The analysis includes the effects of structural loading and the determination of the soil conditions.

Nelson and Miller (1992) presented the design considerations for a stiffened slab-on-grade as shown in Figure 2-2. Figure 2-2a depicts the development of a mound beneath a weightless flexible slab.

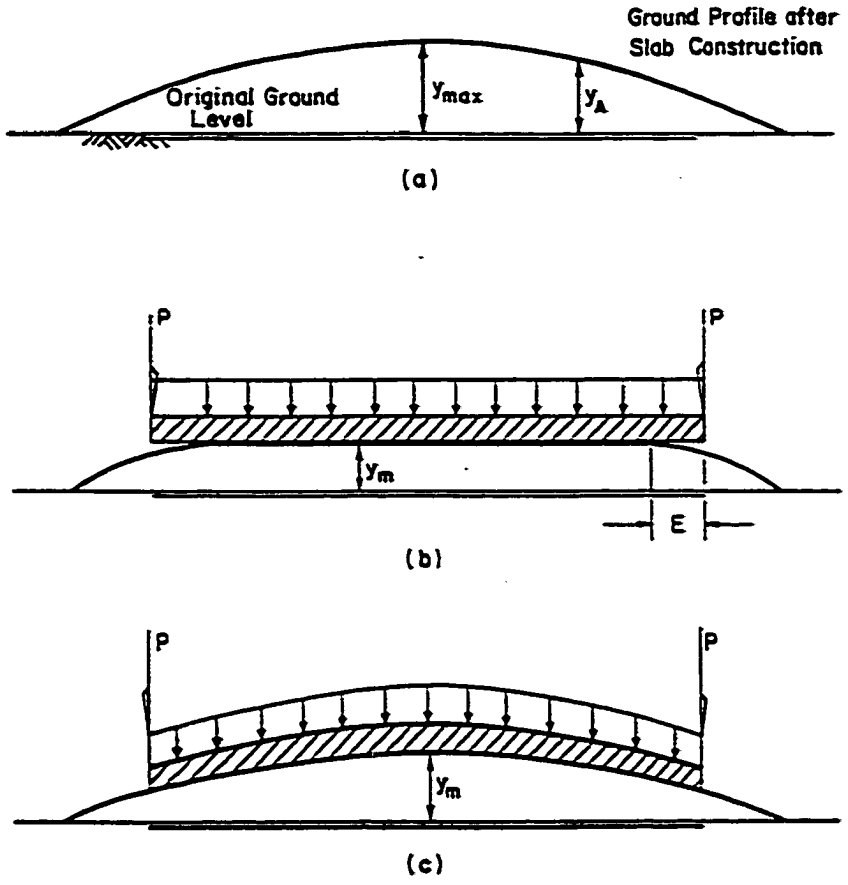

Figure 2-2 Mound profiles for various cases of slabs on grade: (a) mound profile for a weightless slab, (b) mound profile for an infinitely stiff slab with a load, (c) mound profile for a semi-rigid slab with a load (Nelson and Miller, 1992).

In Figure 2-2b the mound changes shape due to the weight and infinite rigidity of the slab. In actuality the slab will behave as shown in Figure 2-2c, which is somewhere between a and b. Theoretical design procedures for stiffened slabs-on-grade construction were presented in Nelson and Miller (1992). The present research was conducted to investigate methods for obtaining two of the parameters necessary in a typical design procedure. The reader is referred to Nelson and Miller (1992) for the specifics of the five theoretical design procedures.

The PTI (1980) design method is widely used, and is recognized by the Uniform Building Code. In this method the necessary design parameters are:

- Maximum differential heave,
- Edge moisture variation distance,
- Mound shape equation constants,
- Climatic ratings, and
- Soil properties

The maximum differential heave depends on the depth of the active zone, which is controlled by climate and soil conditions. The edge moisture variation distance, mound shape, and applied load influence the bending moment induced in the slab. Two key parameters are the active zone depth and the edge moisture variation distance, which are the subjects of this research.

2.3.1 Heave Prediction

There are several methods available for predicting heave of an expansive soil. Local engineers often use empirical methods applicable to a specific geographic location. These methods are of value within the boundaries of the local soil and environmental conditions. Theoretical and semi-empirical methods have been developed that can be further advanced and verified by current laboratory and field instrumentation methods.

The basic equation for predicting heave in expansive soil is given as (Nelson and Miller, 1992):

$$\rho = \sum_{i=1}^{n} \frac{\Delta e \cdot z_i}{(1+e_0)_i} \qquad (2\text{-}3)$$

where:

ρ = total heave

z_i = initial thickness of layer i

n = number of layers

e_0	=	initial void ratio of soil layer i
Δe	=	change in void ratio during swelling

The change in void ratio, Δe, during swelling is a function of the change in net normal stress and soil suction and the rate of change is controlled by the respective swell indices of the soil. The general equation for total heave due to changes in net normal stress and soil suction is given as:

$$\rho = \sum_{i=1}^{n} \frac{z_i}{(1+e_0)_i} \left[C_{mi} \Delta \log(u_a - u_w) + C_{ti} \Delta \log(\sigma - u_a) \right]_i \qquad (2\text{-}4)$$

where:

Δe_i	=	$C_{mi} \log (u_a\text{-}u_w)_i + C_{ti} \log (\sigma\text{-}u_a)_i$
C_{mi}	=	matric suction index for layer i
C_{ti}	=	net normal stress index for layer i
σ	=	total stress
u	=	pore pressure (a=air; w=water)

In equation 2-4 $(u_a\text{-}u_w)$ is the soil suction and $(\sigma\text{-}u_a)$ is the net normal stress. In practice there are two general approaches to predicting heave in expansive soil. Historically, the oedometer test has been used most often. More recently researchers have attempted to use soil suction as a fundamental parameter in predicting heave. The following sub-chapters discuss these two approaches.

2.3.1.1 Oedometer Tests Approach

Two general procedures for determining swell and swell pressure using an oedometer are the consolidation-swell test and the controlled strain test. In the consolidation-swell test, the soil sample is placed in an oedometer, at its natural water content, and loaded with a predetermined load, usually 500 or 1,000 psf or the in situ overburden stress. The sample is then inundated and allowed to swell under that load until equilibrium is reached. When

equilibrium has been reached the sample is loaded in the same manner as in a consolidation test with a rebound cycle. The swell pressure has traditionally been defined as the load necessary during consolidation to return the sample to its initial void ratio and the swelling index has traditionally been assumed to be the slope of the rebound curve.

The second general method is the controlled strain test. Like the consolidation-swell test, a sample is placed in an oedometer at its natural water content and loaded to some predetermined load. The sample is then inundated and pressure is applied to prohibit volume change due to swell. When the sample reaches equilibrium it is then loaded as in a consolidation test with a rebound cycle. The swell pressure is defined as the pressure developed in the constrained sample during inundation. The swell index is the slope of the rebound curve.

These two approaches represent the bounding conditions of what actually occurs in the field. The consolidation-swell test over estimates the swell pressure since it allows the soil to swell freely and then recompresses it to obtain the swell pressure. The controlled strain test on the other hand prohibits swell. Nelson, Durkee, and Bonner (1998) proposed a method for estimating the swell pressure and swell index based on results from both the swell-consolidation test and the controlled strain test. The method is based on the assumption that the percent swell obtained from the consolidation-swell test is linearly proportional to the initial surcharge pressure that is applied when the sample is saturated. Based on this assumption the swell index is a linear function between the point of maximum percent swell obtained from the consolidation-swell test with zero initial surcharge and the swell pressure from the controlled strain test.

The main shortcoming of oedometer tests is in the analysis of the data. It is of primary importance to consider the loading and wetting sequence, surcharge pressure, sample disturbance, and apparatus compressibility in the analysis. The apparatus compressibility can be accounted for by loading a steel plug and developing correction factors for each increment of loading as is normally done in a consolidation test. Nelson and Miller (1992) and Fredlund (1983) discussed the significance of sample disturbance and present methods that have been developed for establishing corrected swell parameters. Porter and Nelson (1980), Fredlund (1983), and Nelson and Miller (1992) recommended the controlled strain oedometer test as the best method for predicting heave when using an oedometer test approach. However, more recently the method presented by Nelson, Durkee, and Bonner (1998) has gained acceptance for evaluation of foundations for residential structures. Changes in soil suction are accounted for indirectly during the oedometer test method because the stress path followed during inundation represents a reduction in soil suction from the in-situ condition to zero. The resulting equation for heave is:

$$\rho = \sum_{i=1}^{n}\left[\frac{C_s z_i}{(1+e_0)_i}\log\left(\frac{\sigma'_f}{\sigma'_{sc}}\right)_i\right] \qquad (2\text{-}5)$$

where:

C_s	=	swell index (slope of the rebound curve)
σ'_f	=	final effective stress state
σ'_{sc}	=	corrected swell pressure from oedometer tests.

The term z_i is obtained by dividing the depth of the active zone into i layers and Equation 2-5 sums over the depth of the active zone.

2.3.1.2 Soil Suction Test Approach

In the oedometer tests methods, the change in suction is taken into account indirectly and the effective stress is the primary stress state variable that is used. In soil suction test methods for heave prediction, the matric suction, (u_a-u_w), is taken as the primary controlling stress state variable. A relationship between void ratio and matric suction is developed, and the matric suction index is defined as the slope of that curve. The total volume change is then a function of both the compression or swelling index obtained from oedometer tests and a void ratio-matric suction relationship.

There have been several approaches developed for determining the suction index. Of these, there are two that have been shown to predict heave reasonably well. The first method was developed at the U.S. Army Corps of Engineers Waterways Experiment Station (WES). The WES method of heave prediction is based on the relationship in Equation. 2-4. The suction index, C_m, is estimated as:

$$C_m = \frac{\alpha G_s}{100B} \tag{2-6}$$

where:
- α = the compressibility factor
- B = slope of suction versus water content
- G_s = specific gravity of solids.

The compressibility factor is the slope of the specific volume versus water content curve. Johnson (1977) noted that since the compressibility factor for highly expansive clay is close to unity, substitution of unity for α in the calculation of C_m is conservative.

The second approach to predicting heave based on soil suction tests is known as the CLOD test. It was initially developed at the New Mexico Engineering Research Institute

and developed further by Hamberg and Nelson (1984) (also see Nelson and Miller, 1992). In this test a sample of soil is coated with a saran resin that is impermeable to water but permeable to air. The volume of the coated sample can be determined by immersing it in water; and the water content at various points of drying can be determined by weighing the sample. The slope of the void ratio versus water content relationship is the CLOD index, which is analogous to the compressibility factor mentioned above. If the contribution due to change in effective stress is neglected, then Equation 2-4 can be written as:

$$\rho = \sum_{i=1}^{n} \frac{C_w \Delta w}{1 + e_0} z_i \qquad (2\text{-}7)$$

where: $C_w \Delta w$ = the change in void ratio.

Because Equation. 2-7 assumes that there is no change in effective stress, this method predicts the free-field heave (i.e., the heave at the ground surface with no load applied). The free-field heave is used in the design of lightly loaded slabs and in the prediction of pier movement (Nelson and Miller, 1992).

Hamberg (1985) and Miller, Durkee, Chao, and Nelson (1995) used data collected at the Colorado State University Expansive Soils Test Site to estimate the long-term heave for that location. Comparison with the observed behavior at the test site and in nearby structures founded on the same soil showed good agreement.

2.3.2 Active Zone Depth

The methods described above provide constitutive parameters for heave prediction and design of foundations. However a fundamental parameter for heave prediction for either

general method presented above is the active zone depth. Active zone depth, as defined in Chapter 1, is "the zone in the soil beneath a structure that is contributing to the actual heave that takes place at some point at the surface at a given time (t)." In the heave prediction equations the heave of individual soil layers is summed over the depth of the active zone. As discussed in Chapter 1 the active zone depth is a time dependent, site specific parameter and is a function of a number of variables including, soil properties, soil profile, climate, and loading conditions.

2.3.3 Edge Moisture Variation Distance

The definition of edge moisture variation distance is presented in Chapter 1. In general two modes of swelling occur beneath a slab foundation, "center lift" and "edge lift". Figure 2-3 shows both conditions with their associated design parameters. The center lift condition generally represents a long-term condition resulting from wetting beneath the center of the slab, drying around the edges of the slab, or a combination of both. The edge lift condition is considered to be a short-term condition resulting from wetting at the perimeter of the slab often as a result of irrigation or large climatic events. As water content increases at the center of the slab after sufficient time, the center will heave until a uniform field of heave or center lift conditions are developed.

The soil design parameter e_m shown in Figure 2-3 is referred to as the edge moisture variation distance (PTI, 1980). The magnitude of edge moisture variation distance depends to a large degree on climate and external conditions such as irrigation and lot grading. In arid locations with a high degree of evaporation and a center lift condition the edge moisture variation distance can be quite large. Likewise, in wetter climates with an

edge lift condition the edge moisture variation distance is large. Due to the correlation with climate, PTI (1980) presented a method for predicting edge moisture variation distance based on the Thornthwaite moisture index. This method, which was developed by Wray (1978) is shown graphically in Figure 2-4. Based on the relationship shown in Figure 2-4, the maximum edge moisture variation distance is 5 to 6 feet. A disclaimer is provided to note that for some highly active clay the edge moisture variation distance can be greater than the values given in Figure 2-4. As discussed in Chapter 1 McKeen and Johnson (1990) stated that the edge moisture variation distance is equal in magnitude to the depth of the active zone for slabs-on-grade. Also as discussed in Chapter 1, Nelson and Miller (1992) stated that the edge moisture variation distance is the most difficult parameter to determine.

2.4 Previous Field Studies

A number of field studies have been conducted which provide information that is useful for developing moisture migration and heave prediction models. Many of the field studies have been conducted on existing light structures where initial data has not always been available. Several researchers have constructed simulated slabs-on-grade where the conditions can be controlled to provide particular information for specific procedures.

Donaldson (1965) conducted a study on lightly loaded structures in South Africa. Elevation data was collected at various depths on a number of houses to establish the time necessary for equilibrium. The results showed that the soil continued to heave for approximately 5 years and that soil swelling occurred to a depth of over 40 feet. The authors also noted the time for equilibrium varied with depth and soil type.

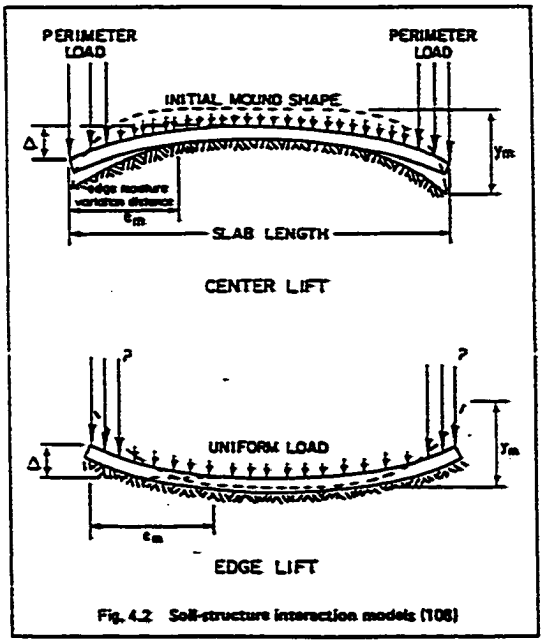

Figure 2-3 Soil structure interaction model, (PTI, 1980).

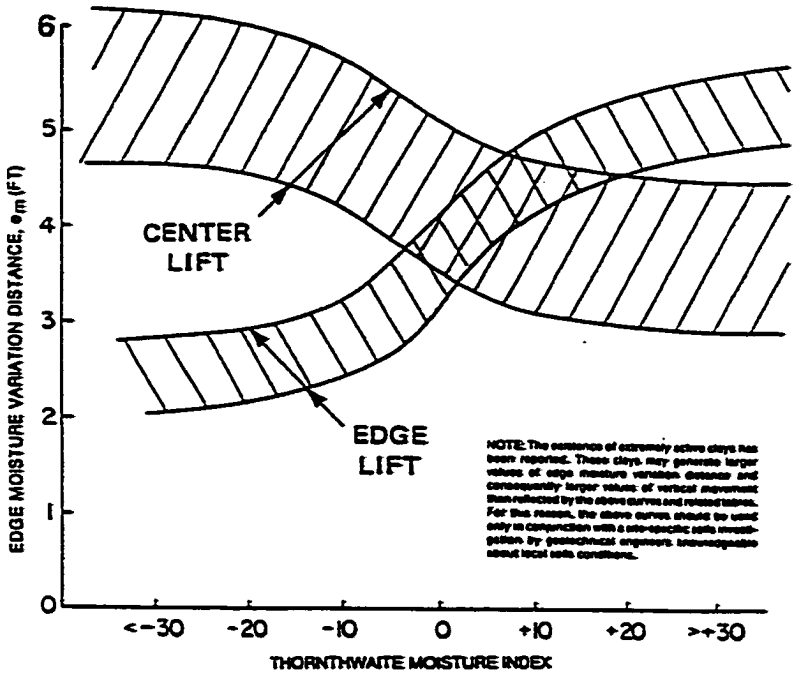

Figure 2-4 Approximate relationship between Thornthwaite Index and moisture variation distance (PTI, 1980).

Tucker and Poor (1978) conducted a comprehensive field study on residential slab foundations that had been designated for removal for the installation of a highway. The homes were founded on expansive soil and designed according to Federal Housing Authority (FHA) specifications. Among the data that was collected for their study the authors measured water content and heave from several locations beneath the slabs. The results of data collected from 69 slabs on highly expansive soils indicated the following:

- The highest water contents occurred beneath the center of the slabs and averaged about 4% higher than the perimeter measurements.
- Water content became relatively constant with depth below about 7 ft.
- Most of the slabs showed differential movement of a convex shape.
- Significant differences in differential vertical movements occurred between the winter and summer. Differential vertical movements increased almost 30% from winter to summer, even though the slabs had been in place for several years.

Uppal (1965) reported that an impermeable membrane used beneath a roadway reduced the seasonal moisture fluctuations in the soil. Water contents were taken beneath the covered section and beneath uncovered sections. The water content beneath the covered section varied only by a few percent while the water content beneath the uncovered section ranged from the shrinkage limit to the plastic limit.

Nelson and Edgar (1978) showed that an impermeable cover placed on the soil surface in an arid climate will cause moisture to move upward and accumulate near the surface. They concluded that the increase in moisture was due to the elimination of evapo-transpiration at the surface.

Goode (1982) conducted a field study on expansive Pierre shale to investigate moisture migration beneath slabs and the effectiveness of vertical barriers on controlling lateral

flow. Water content was monitored at various locations beneath the slabs. A neutron probe was used to measure water content at 1-foot intervals to a depth of 15 feet. Figure 2-5 shows two profiles from a simulated slab. The plot for location C-6 near the edge, shows an active zone depth that increased to a large depth with time. The plot for location C-1 in the center did not show a significant increase in water content. From these results Goode (1982) concluded that one-year of data is not sufficient to determine the active zone depth.

Hamberg (1985) used the field sites constructed by Goode (1982) to evaluate a laboratory method for predicting heave beneath slab foundations. Field data was collected from the same site to provide a total of three years of water content and elevation data. Water content profiles from the same two locations C-1 and C-6, from Goode's data, are shown in Figure 2-6 after three years of readings. The data from location C-1 at the center of the plot indicates that the depth of water content increase after 3 years had increased to 6 to 8 feet. Data from location C-6 indicated a depth of water content increase in excess of 15 feet. Hence, the depth of water content increase was shown to increase significantly with time. Also in comparing the data from C-1 with that from C-6 it appears that the edge moisture variation distance is as much as half the width of the slab indicating a larger slab is necessary to determine edge moisture variation distance.

Figure 2-7 shows the record of precipitation over the three-year period in which Goode (1982) and Hamberg (1985) conducted their investigations. The precipitation in 1982 and 1983 was considerably higher than in 1981 and may have contributed to the increase in wetting depth. Also the water content tended to fluctuate over a 6-month period

between times of decreasing and increasing precipitation particularly at the edge of the slab indicating the effect of climate on edge moisture variation distance.

McKeen and Johnson (1990) collected field data from airport pavements on expansive soils to use in the development of a method for estimating active zone depth and edge moisture variation distance. A simple one-dimensional diffusion equation developed by Mitchell (1979) was used to calculate suction changes in the vertical direction. The resulting movement was computed directly from the measured suction. The authors concluded that given the proper coefficients determined with reasonable accuracy in the field, the simple diffusion equation could be used to estimate soil moisture variation.

Wray (1992) constructed two field test sites for comparison of long-term shrink-swell behavior to heave prediction based on soil suction. The test sites were located in areas with different climatic conditions; one wet and the other dry. The measured total heave values at both sites approached but did not exceed the predicted values after 36 months of observation. However, the data by Goode (1982) and Hamberg (1985) indicated that 36 months is insufficient time for the maximum heave to develop as a function of climate only.

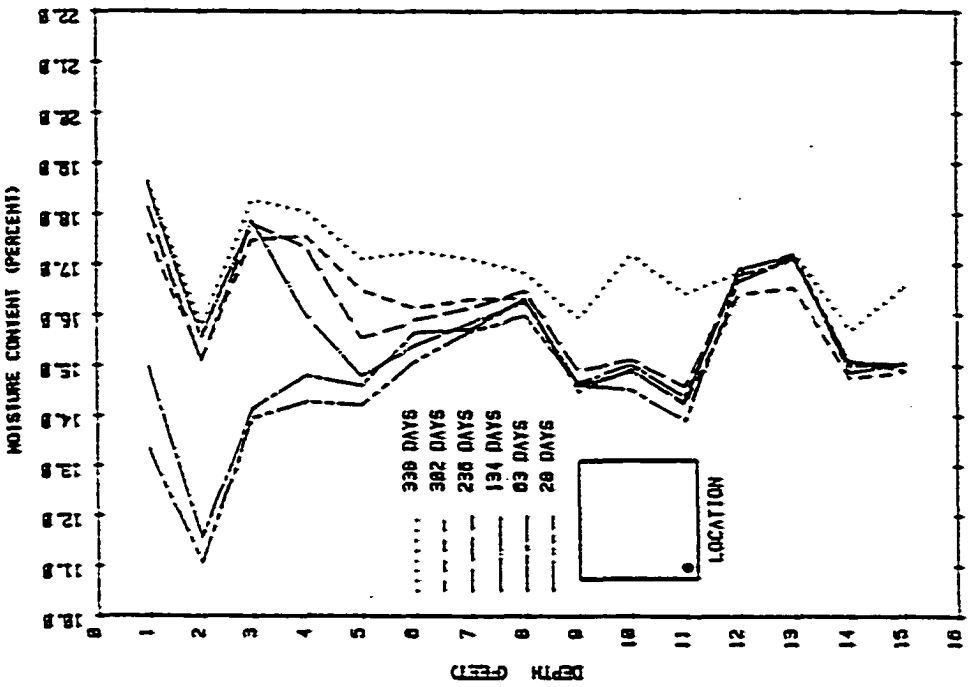

Figure 2-5b Moisture profile for hole C-6 (Goode, 1982).

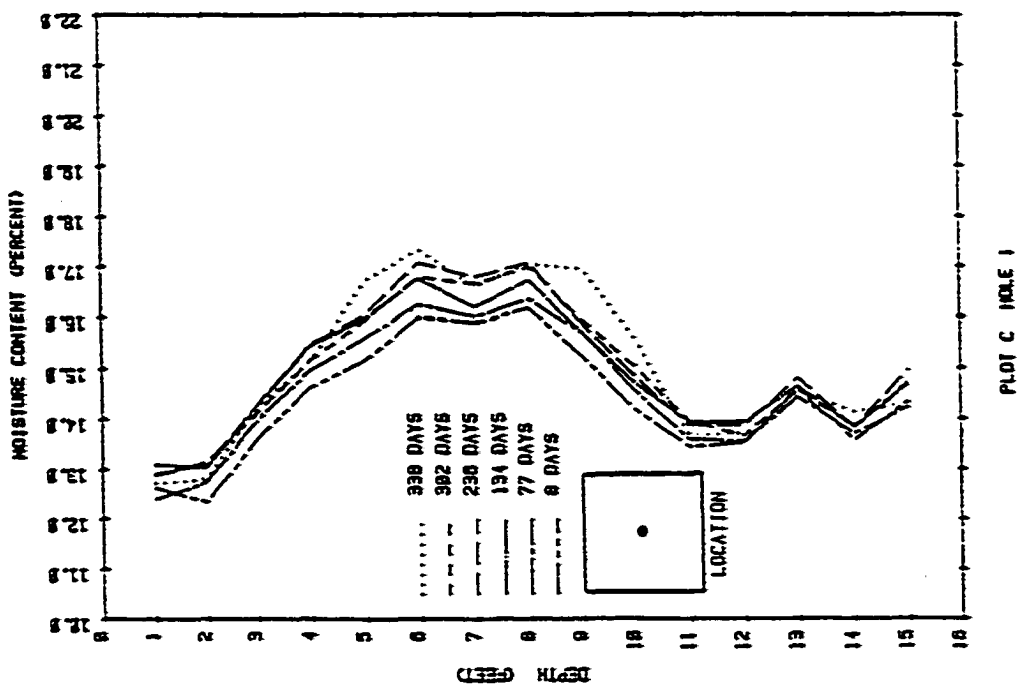

Figure 2-5a Moisture profile for hole C-1 (Goode, 1982).

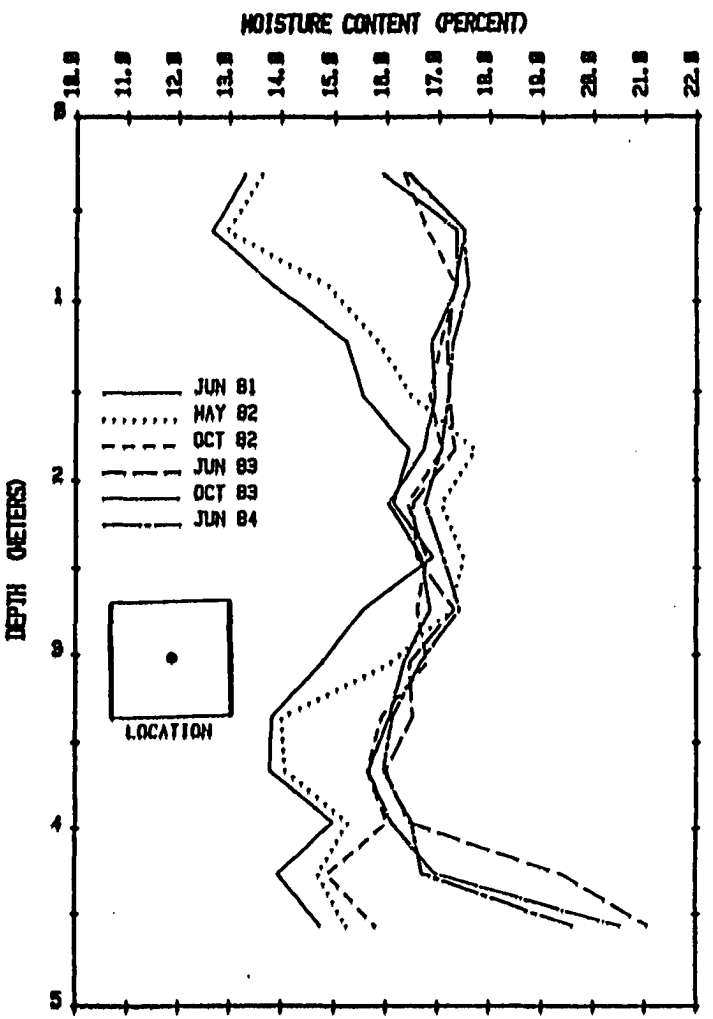

Figure 2-6a Moisture profile from hole C-1 (Hamberg, 1985).

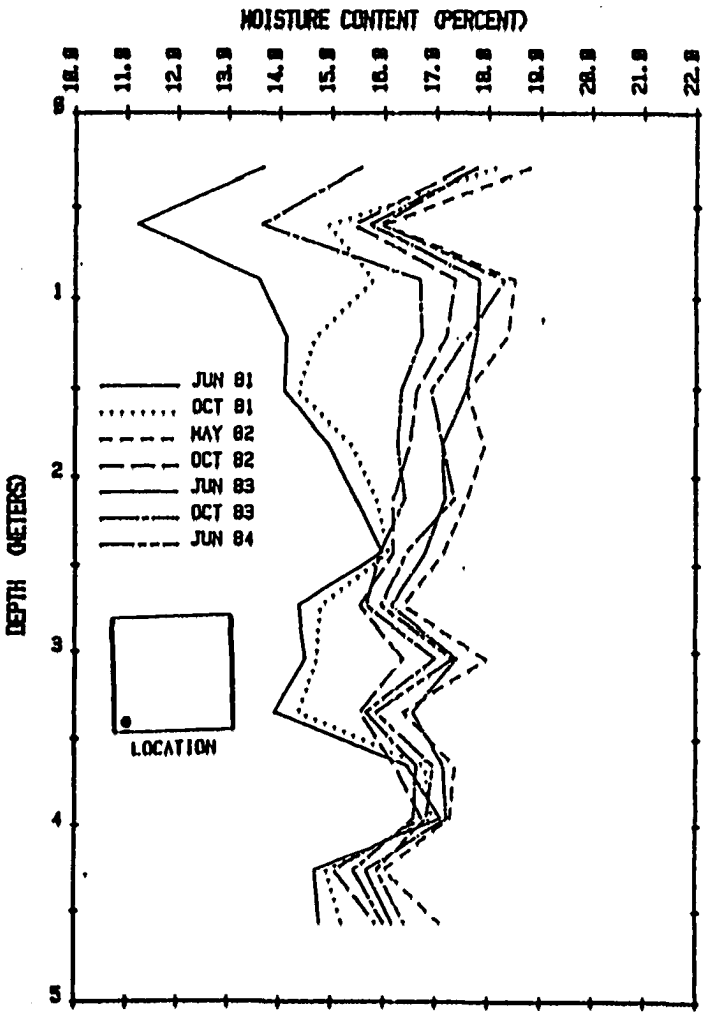

Figure 2-6b Moisture profile from hole C-6 (Hamberg, 1985).

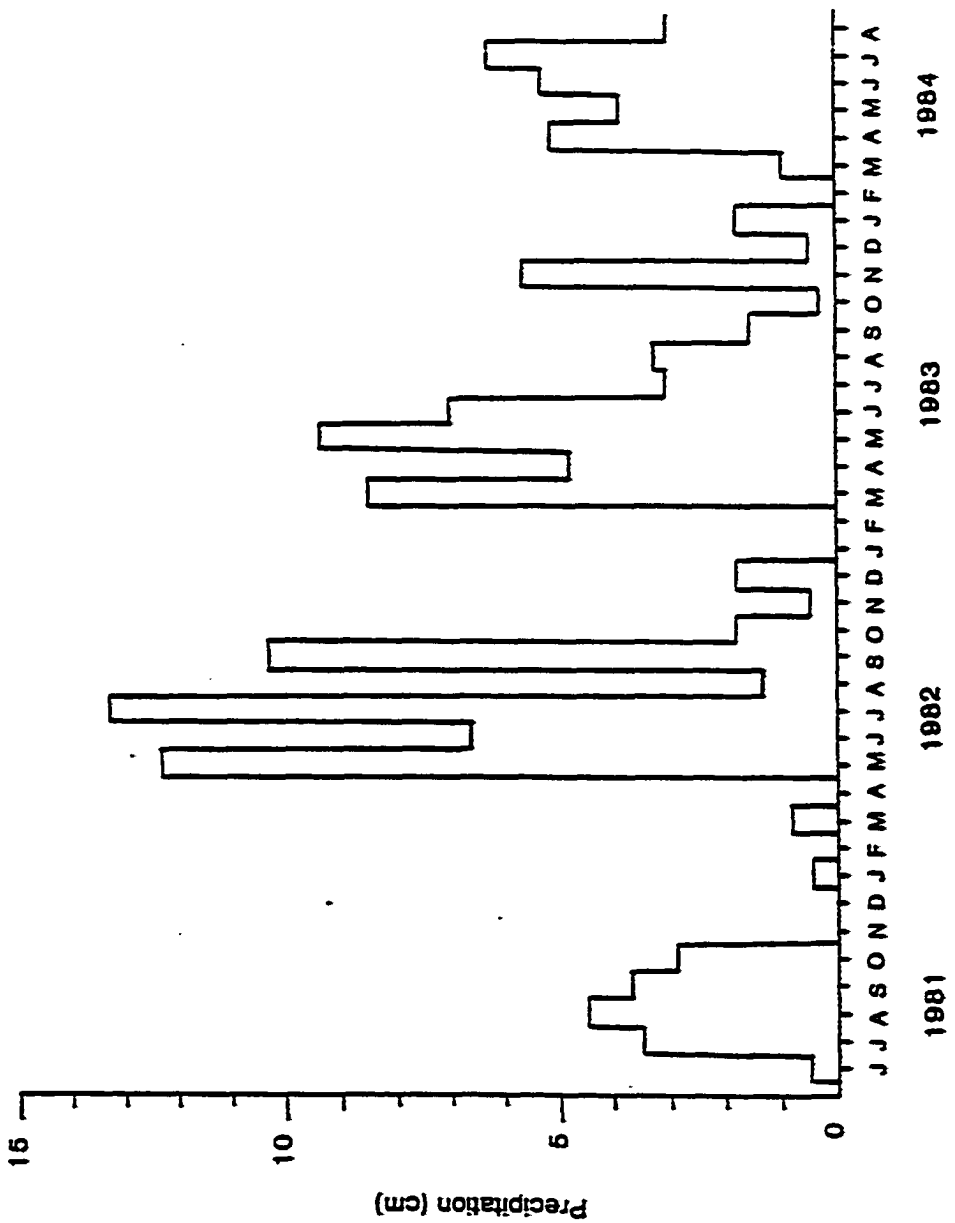

Figure 2-7 Monthly precipitation at test site area (Hamberg, 1985).

CHAPTER 3

FIELD TEST SITES

Field investigations conducted for this research utilized simulated slabs-on-grade at field test sites at Colorado State University (CSU) and Fort Sam Houston (FSH) in San Antonio, Texas. The sites were instrumented to monitor water content, soil suction, and heave.

3.1 Field Sampling

Soil samples were collected at the sites using both continuous barrel samples and California drive-samples. The samples were tested to determine soil properties and constitutive parameters for the analyses.

3.1.1 Colorado State University Soil Sampling

Three boreholes were sampled at the CSU site in September 1992 using a hollow stem auger and core barrel sampler lined with clear plexi-glass tubes shown in Figures 3-1 and 3-2. The boreholes were located along the centerline of the proposed plot in an east to west orientation with B-1 along the east edge and B-3 along the west edge. B-1 and B-3 were located approximately 1 to 2 feet inside the edge of the constructed simulated slab. B-1 was sampled to a depth of 24 feet. A California drive sampler was used for sampling to a depth of 7 feet and a split barrel sampler was used to obtain continuous samples from 7 feet to 24 feet.

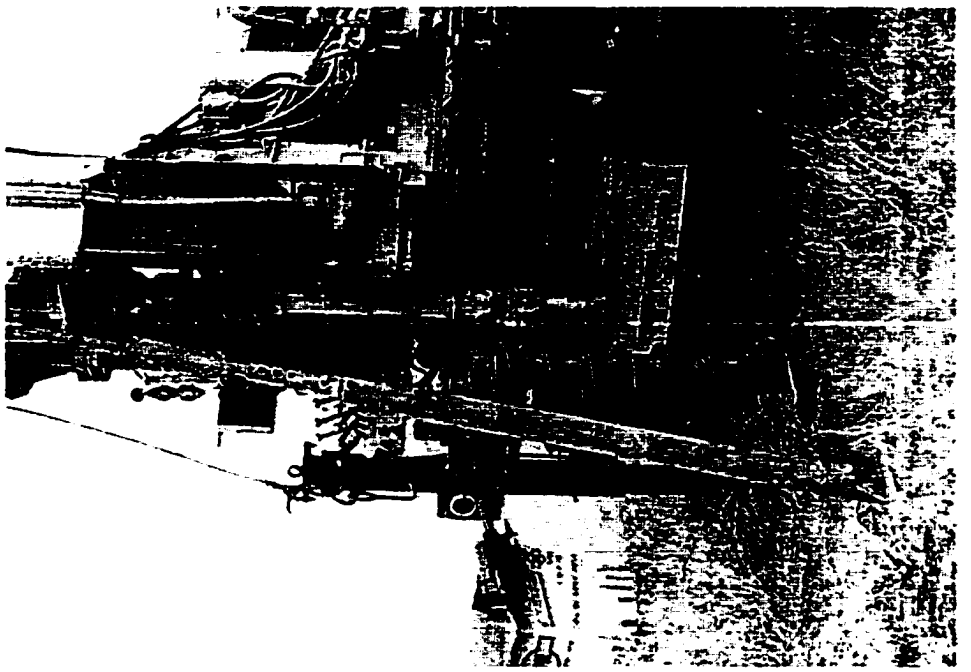

Figure 3-1 Photo of hollow stem auger used for initial sampling of CSU site.

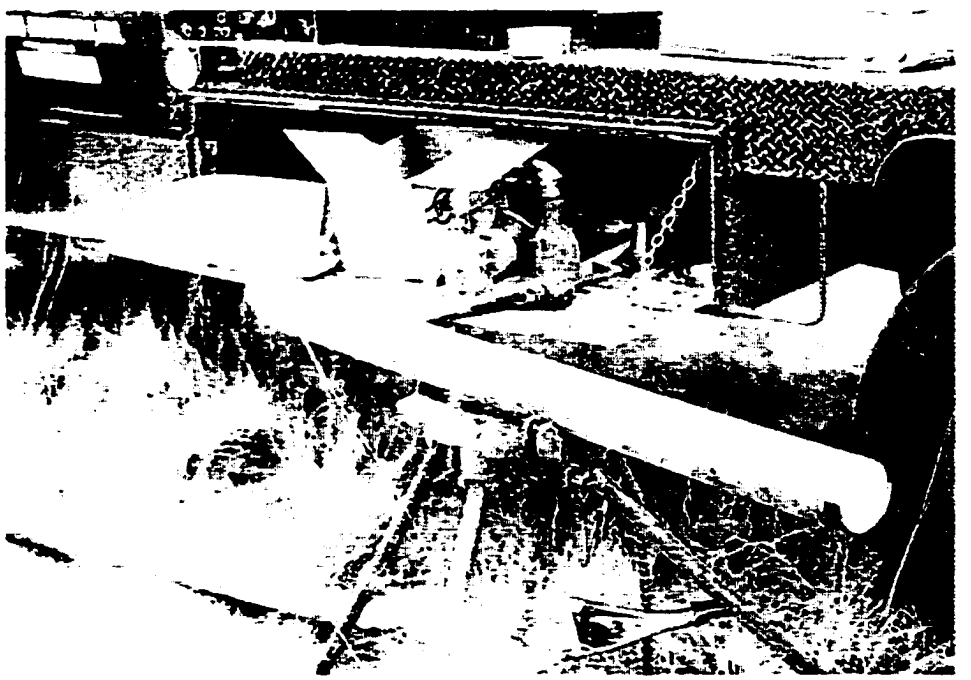

Figure 3-2 Photo of split-barrel sampler and plexi-glass tube used for sampling at the CSU site.

Boreholes B-2 and B-3 were both sampled continuously to 19.5 feet using a split barrel sampler. A total of twenty, 4-inch California samples were obtained from borehole B-1 and a total of twenty-four 2.5-foot continuous samples were obtained from the three boreholes combined.

The Pierre shale at the CSU site is characterized by varying degrees of weathering. A typical sample is shown in Figure 3-3. In each of the three boreholes, approximately 2 to 6 inches of vegetation and silt is underlain by a yellowish-tan clay to a depth of approximately 3 to 5 feet. A reddish yellow clay extending to a depth of 5 to 7 feet was found in boreholes B-1 and B-2 that was not observed in borehole B-3.

The clay is underlain by reddish brown weathered clayshale that extends to approximately 20 feet. In all three boreholes, several bentonite seams ranging from 4 to 6 inches thick were observed at various depths. In addition, a shattered weathered clayshale, approximately 1-foot thick, was observed below the deepest bentonite seam. Figure 3-4 shows the soil profile developed from the three boreholes sampled at the CSU site.

A piezometer was installed approximately 5 feet east of the foundation (see Figure 3-17). The piezometer was completed at a depth of 28 feet with a screen length of 2 feet. The hole was backfilled with sand around and up to 2 feet above the top of the screen. The remainder of the hole was backfilled to the ground surface with a bentonite grout mix. The three sampling holes also were backfilled with bentonite grout mix. To date there has not been any water present in the piezometer indicating that the water table is below 28 feet.

Figure 3-3 Photo of typical sample from the CSU site.

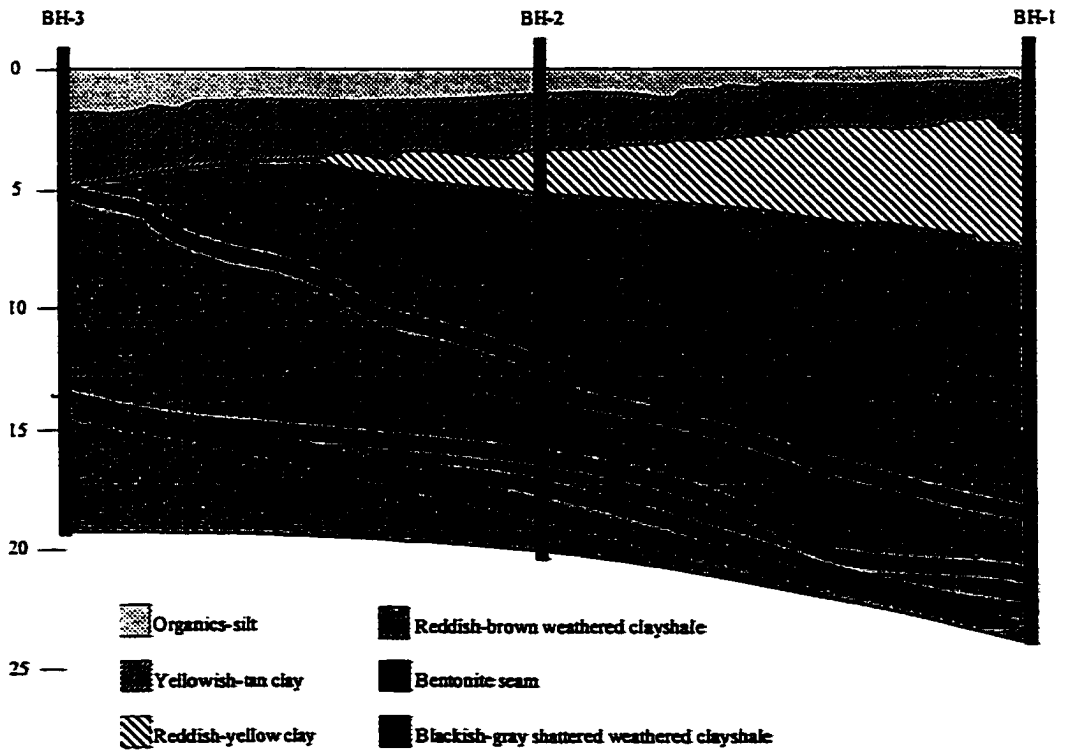

Figure 3-4 Soil profile at the CSU site

3.1.2 Fort Sam Houston Soil Sampling

Five boreholes were excavated at the FSH site using a hollow stem auger shown in Figure 3-5 and samples were collected with thin-walled tube samplers. Four of the boreholes were located 3 to 4 feet towards the center from each corner of the constructed simulated slab, and the fifth hole was located in the center. Each borehole extends to a depth of approximately 6 feet where a clayey gravel stratum was located. Three thin-walled tube samples were taken from each borehole with each tube pushed 2 feet.

The FSH site is characterized by approximately 6 inches of vegetation and white gravel underlain by black plastic clay of medium stiffness that extends to a depth of 5 to 6 feet. The black plastic clay is underlain by clayey gravel that extends to approximately 8 feet. The gravel layer is underlain by yellow gravelly medium stiff clay that extends to approximately 20 feet where stiff yellow clay shale is located. Sampling was conducted to a depth of 30 feet. Borehole logs from sampling that was done by the U.S. Army Corps of Engineers for the construction of a nearby structure shows a similar profile. Figure 3-6 shows the soil profile of the FSH test site developed from the sampling.

Two piezometers were also installed 3 feet south of the foundation plot. The first piezometer (PZ-W, see Figure 3-18) was completed at a depth of 20 feet with a screen length of 2 feet. The hole was backfilled with sand around the screen and up to 2 feet above the top of the screen. The remainder of the hole was backfilled to the ground surface with a bentonite grout mix. Before PZ-W was installed, the borehole was extended to a depth of 30 feet. California samples were obtained at 12 feet, 15 feet, 20 feet, 25 feet, and 30 feet.

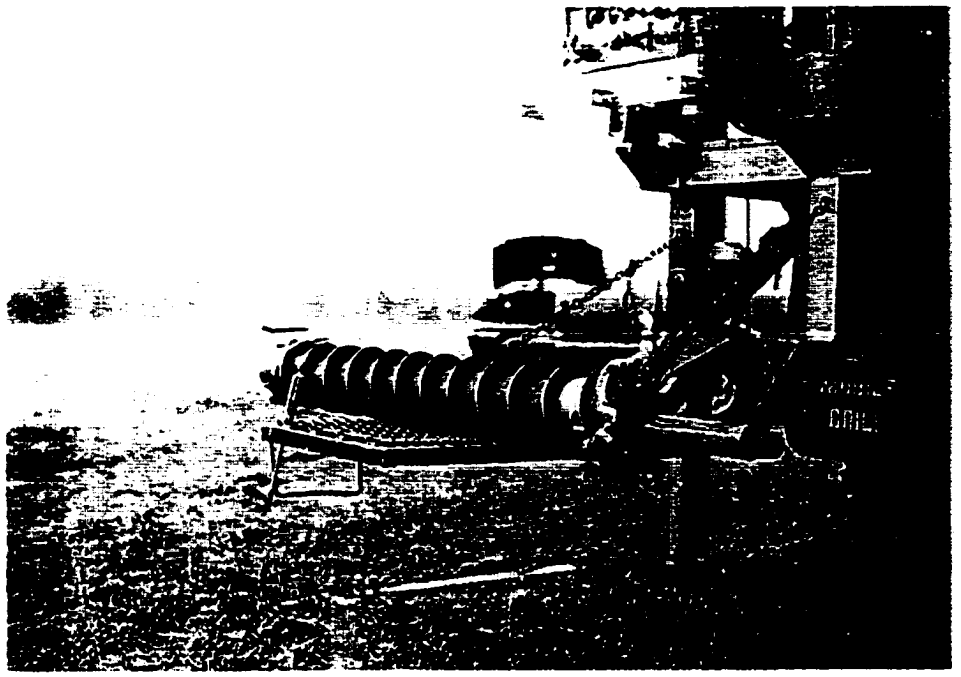

Figure 3-5 Photo of hollow stem auger used at FSH.

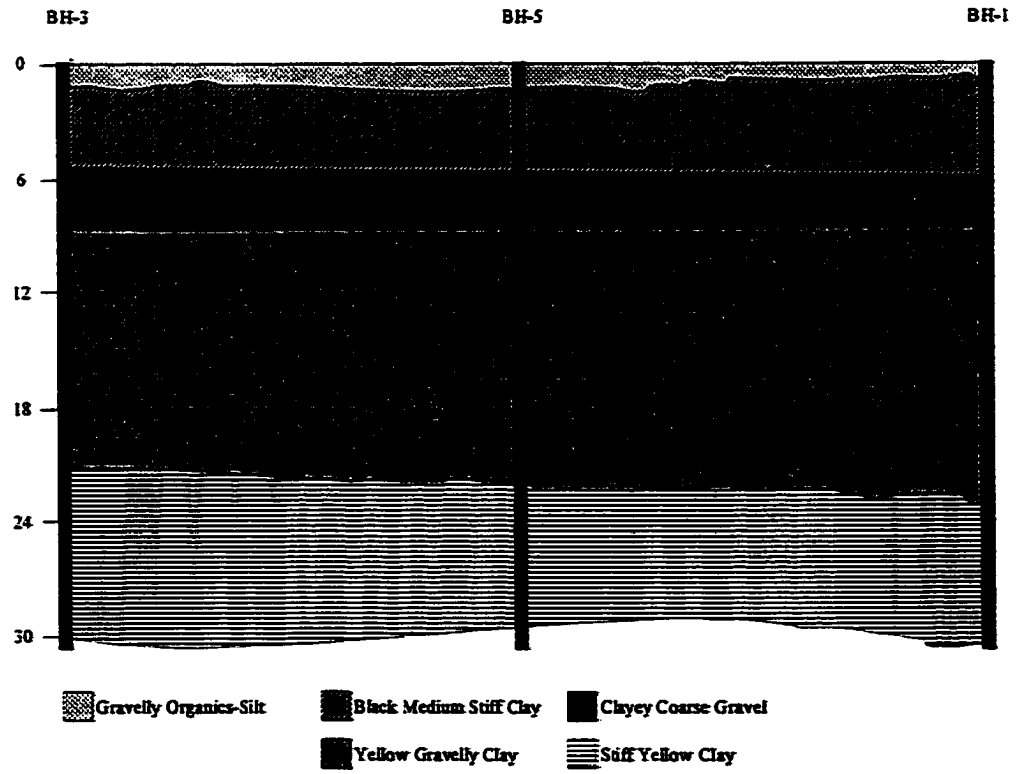

Figure 3-6 Soil profile at the FSH site

A second piezometer (PZ-E, see Figure 3-18) was installed 6 feet to the east of PZ-W. PZ-E was placed at a depth of 5 feet such that the bottom of the screen is located at the bottom of the black plastic clay. A 2-foot screen was placed using sand as a backfill to approximately 2 feet above the top of the screen. The remainder of the hole was backfilled to the ground surface with bentonite grout mix.

To date no water has been measured in either piezometer indicating that the water table is below 20 feet. However, water has been detected in a number of access tubes that were installed for measuring water content with a nuclear moisture gauge. The access tubes are sealed at the bottom with a threaded plug. The water that is present in the tubes may be due to leakage through damage incurred either during installation or as a result of lateral pressures developed during swell.

The soil at the FSH site is characterized by large desiccation cracks that form during extended dry periods. Very little precipitation had occurred at the site during the 3 months before the liner was placed. At the time of construction, large desiccation cracks were observed in the upper 2 to 3 feet of soil. When a large precipitation events follow extended dry periods at the site, the desiccation cracks provide a conduit for flow of surface water to a depth where cracking ceases. It is believed that free water is then able to migrate into the damaged water content access tubes and is not able to escape if the damage is above the bottom of the tube. The reason that water is not detected in the piezometer is that water that accumulates in the piezometers during the precipitation events is able to flow freely out, through the screened portion at the bottom.

3.2 Description of Test Sites

The FSH site is located at the Waterways Experiment Station Expansive Soils Test Site on the Fort Sam Houston Army Base. The test site is located on level ground that extends approximately 500 feet in every direction before dropping slightly to a lower elevation northeast of the site. The proximity of the test site to surrounding buildings is shown in Figure 3-7.

The CSU site is located at the Geotechnical Engineering Expansive Soils Test Site on the Foothills Research Campus of Colorado State University. The proximity of that test site to surrounding buildings and the general topography of the area are shown in Figure 3-8.

Two sites were installed to evaluate the effects of different soil properties, geologic conditions, and climatic conditions on the moisture migration patterns beneath the slab. The rate of evaporation from the soil surface has a direct effect on the active zone depth and edge moisture variation distance. Evaporation is a continuation of vapor flow from the surface and is a function of wind velocity, surface roughness, relative humidity, air temperature, vegetation, degree of saturation, and surface temperature.

Daily temperature, precipitation, and wind velocity data for the FSH site were collected by the climate center at Randolph Air Force Base in San Antonio, Texas. Daily temperature, relative humidity, solar radiation, hourly and daily precipitation, and wind velocity data for the CSU site were obtained from the Colorado Agricultural Meteorological Network (CoAgMet) Station ft01:Fort Collins, AERC, located approximately 4 miles northwest of Fort Collins at the Agricultural Engineering Research Center (AERC).

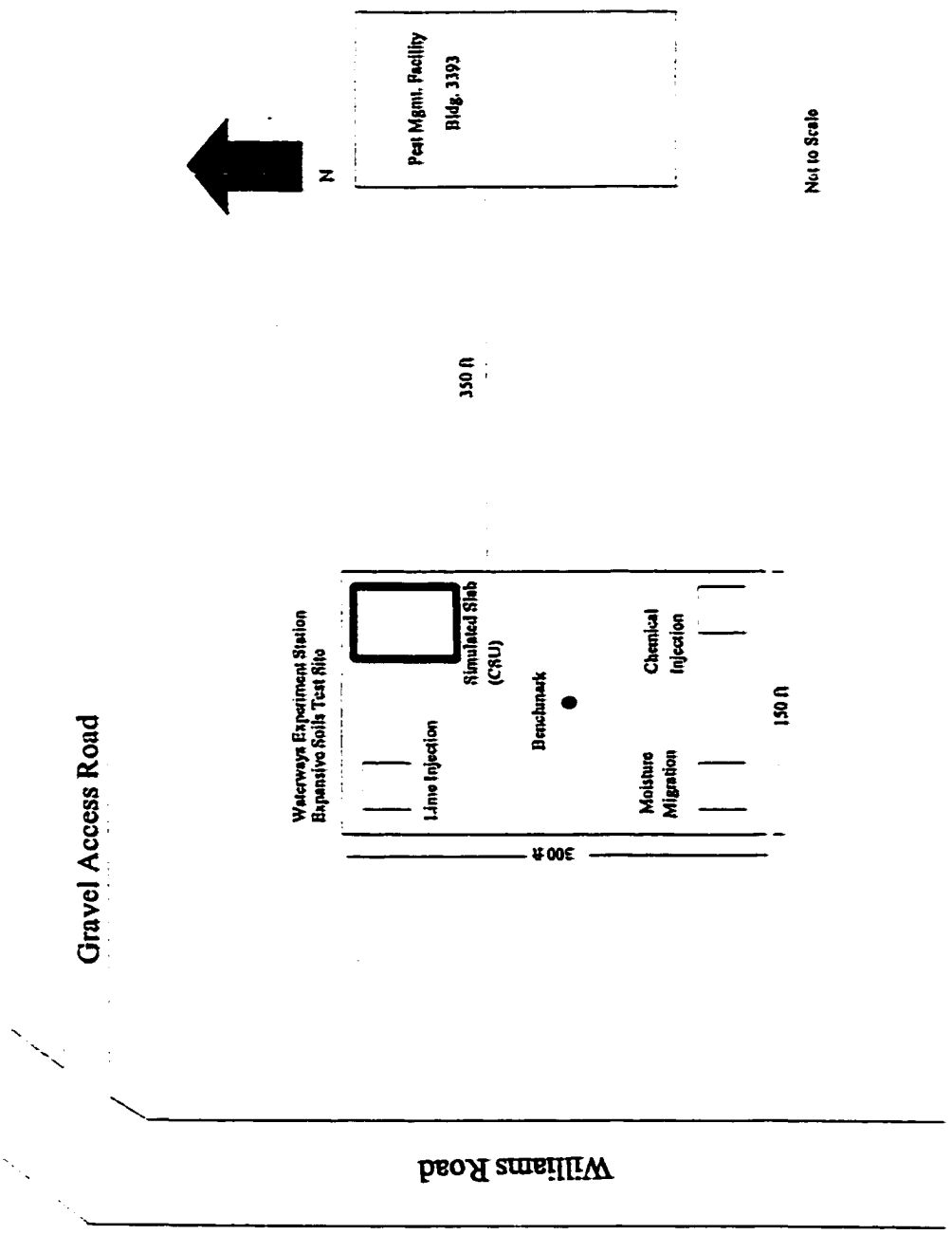

Figure 3-7 Site location at Fort Sam Houston in San Antonio, Texas.

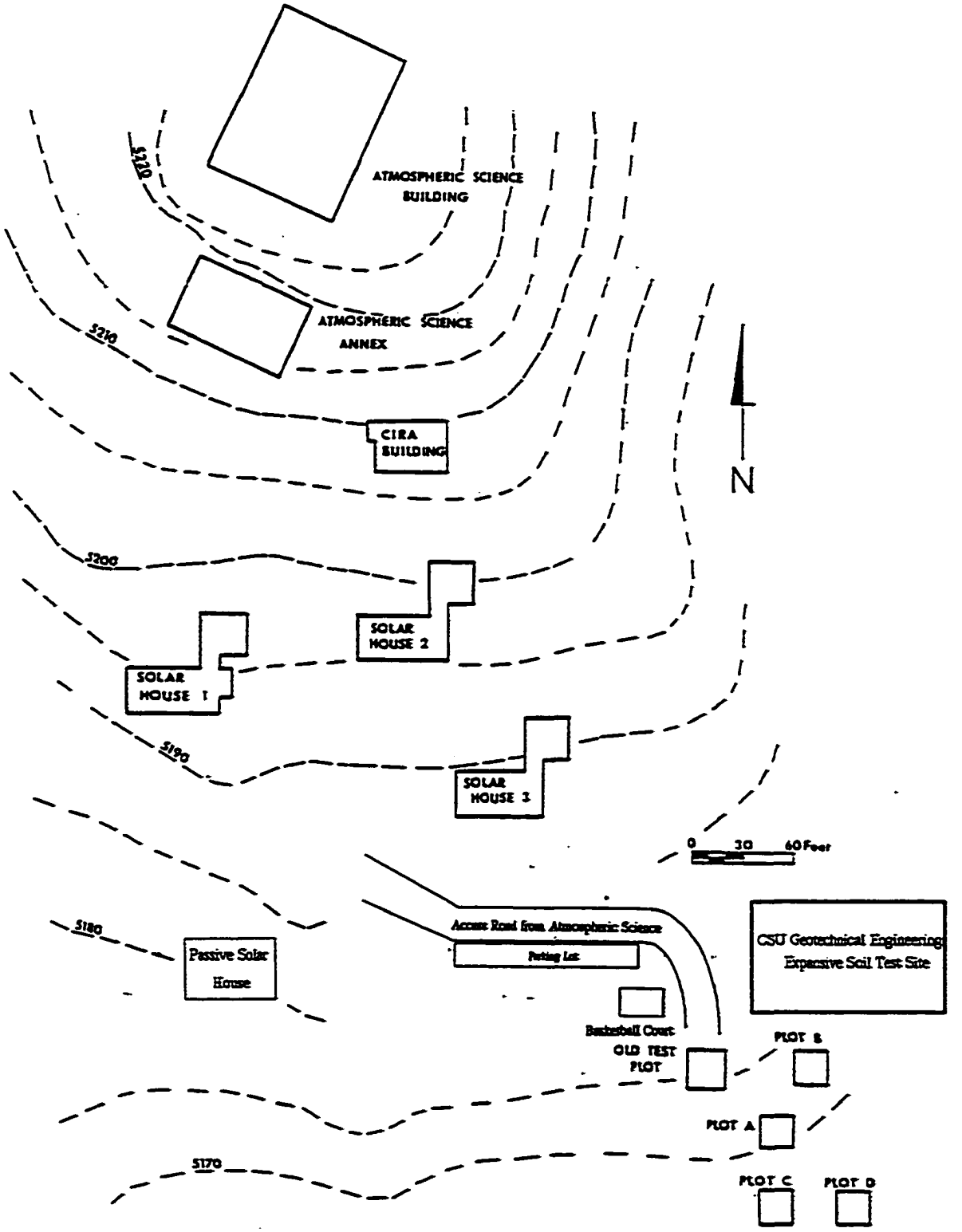

Figure 3-8 Site Location at Colorado State University in Fort Collins, Colorado.

The average temperature in San Antonio ranges from approximately 50 degrees-F in the winter to approximately 75 degrees-F in the summer. The average annual precipitation is approximately 35 inches. Fort Collins, Colorado has a semi-arid climate with approximately 15 inches of precipitation per year. The relative humidity is normally low, ranging between 10 and 50 percent. Winter temperatures can be as cold as –20 degrees-F and summer temperatures can reach 100 degrees-F. The skies are usually clear with over 300 days of sunshine each year.

3.2.1 Construction of Test Slabs

A typical cross-section of the simulated slab foundation that was installed at both sites is shown in Figure 3-9. Each site was equipped with 49 neutron probe access tubes. The access tubes were constructed with 2-inch inside diameter, schedule 40 PVC pipe. The access tubes were installed to depths of 20 feet at the CSU site and 5 feet to 6 feet at the FSH site where a gravel layer was encountered. A drag bit with compressed air was used to drill 2.25-inch diameter holes and the access tubes were then placed by hand to the required depth, see Figures 3-10 and 3-11. Plugs used at the bottom of the access tubes to keep water out are shown in Figure 3-12.

A 2-foot trench was excavated around the perimeter of each site to allow the installation of a drainage system. Gundle Lining Systems Inc. provided the Gundseal HDPE liner which was placed over the site as an impermeable cover. Figure 3-13 shows the liner and the recommended seal. The liner was placed in two 17.5-foot wide sections with a 1-foot overlap. Figure 3-14 shows the liner in place after 2.5-foot long PVC extension sections were installed on the access tubes.

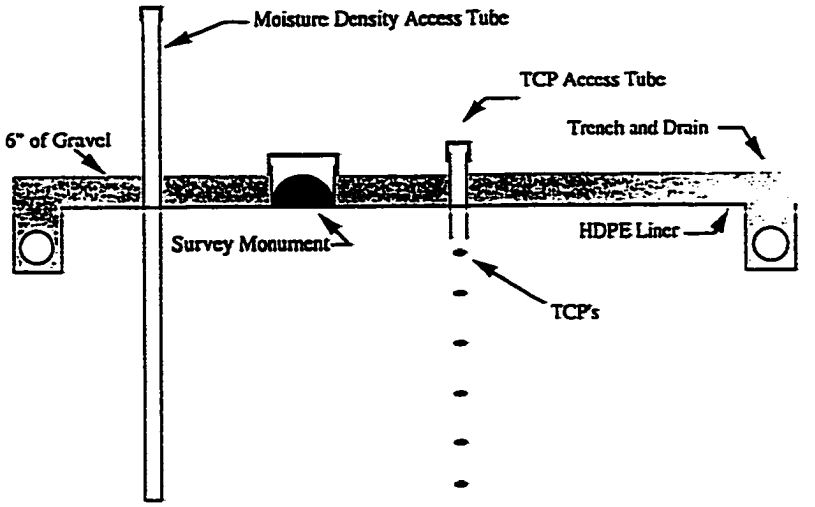

Figure 3-9 Cross-section of the simulated slab foundation.

Figure 3-10 Photo of the drag bit used for excavating access tube holes at both sites.

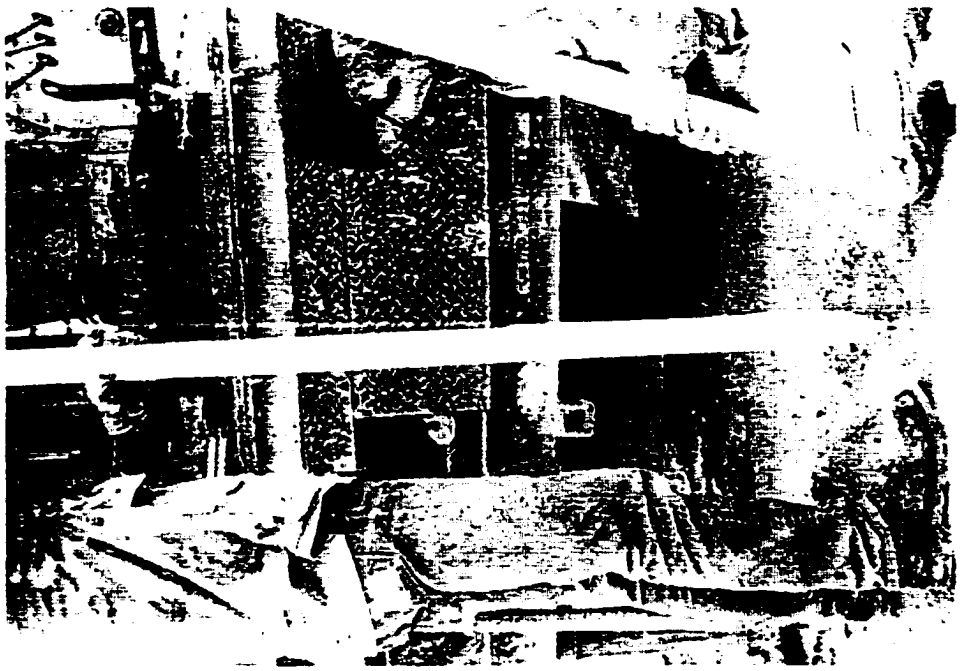

Figure 3-11 Photo of installation of PVC access tubes.

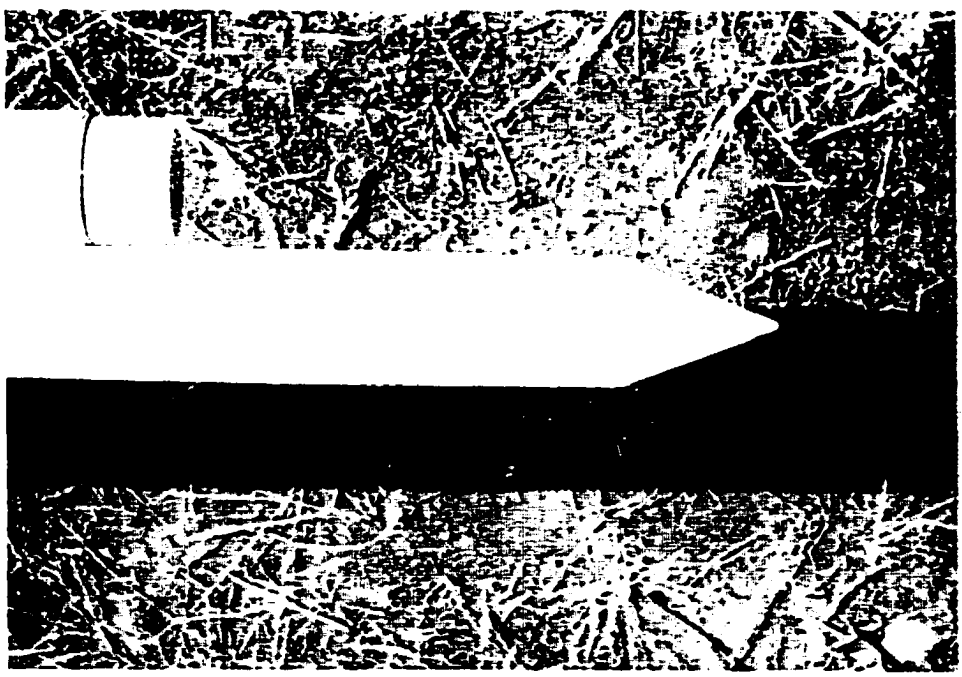

Figure 3-12 Photo of the PVC neutron probe access tube connection and bottom plug.

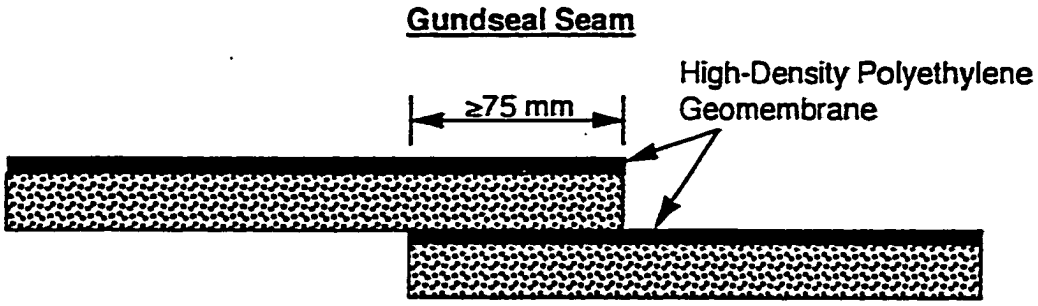

Figure 3-13 Schematic of the HDPE liner from Gundle Lining and the recommended method of seaming

Figure 3-14 Photo of liner in place with 2.5-foot PVC extensions

A small incision was made to accommodate the extensions. A rubber chimney boot was used to seal around the tube to ensure that surface water was not able to seep down along the sides of the tube.

A total of 42 survey monuments were placed on the surface of the liner. Hemispherical survey monuments were used to allow for differential movement of the monument without distorting the actual survey readings. As the hemisphere rotates, the radius from the center remains constant. The survey monuments were constructed of fiber reinforced Quickcrete in 6-inch diameter hemispherical molds. Lag screws were placed in the molded Quickcrete such that 8 inches of the screw extended from the bottom of the monument. The monuments were then placed by threading the lag screw through the liner and into the soil. A small bead of caulk was placed around the lag screw to seal the hole in the liner. The survey monuments were encased inside 6-inch diameter PVC pipes, which were caulked to the liner and equipped with covers.

A 6-inch layer of gravel was placed on the liner and the PVC pipe allowed easy access to the survey monuments, which are on the liner surface. The caulked seal between the pipe and liner keeps the area dry, reducing the possibility of water seeping through the liner at the hole made by the monument lag screw.

The HDPE liner was placed such that it extended into the 2-foot trench around the perimeter of the site. The trench was placed to ensure that the excess surface water from the area around the site did not flow onto the liner and water on the liner from precipitation was directed away from the site. Hence, any water content increase under the center of the slab is due to the liner effects on evaporation and evapo-transpiration and

lateral flow beneath the surface from wetting of the perimeter soil during precipitation events and snow melt.

A 4-inch PVC drainage pipe and ¾-inch gravel were placed in the trench to allow free flow of water away from the site. At the CSU site surface water flow is predominantly downhill to the southeast away from the plot. A pit was excavated and backfilled with gravel approximately 40 feet from the FSH site to allow drainage away from the slab. Figure 3-15 shows the site at FSH with the access tubes, survey monuments, and drains in place and the gravel being placed. Figure 3-16 shows the completed CSU site. Figures 3-17 and 3-18 show the plan views of the CSU site and the FSH site respectively.

3.3 Field Measurements

Field data was collected monthly at both sites. At the CSU site water content, density, and elevation data were collected beginning January 10, 1993. Soil suction and soil temperature data were collected monthly from September 30, 1993. At the FSH site water content and elevation data were collected monthly beginning September 10, 1993.

3.3.1 Water Content and Density Data

A Campbell Pacific Nuclear Corp. (CPN) 501 DR depth probe was used to collect water content and density data at the CSU site. Measurements were taken at 1-foot intervals to a depth of 20 feet. The model 501-DR depth density-moisture gage measures sub-surface density and moisture using a probe containing a gamma source and a Geiger mueller (GM) detector for density and a fast neutron source and thermal neutron detector for moisture (CPN, 1984).

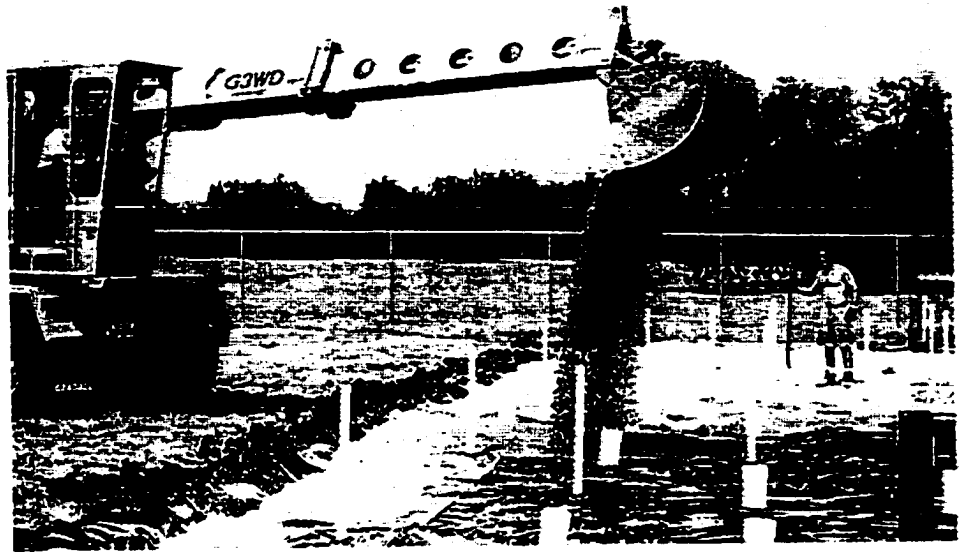

Figure 3-15 Photo of site with field instrumentation while gravel is being placed.

Figure 3-16 Photo of completed CSU site.

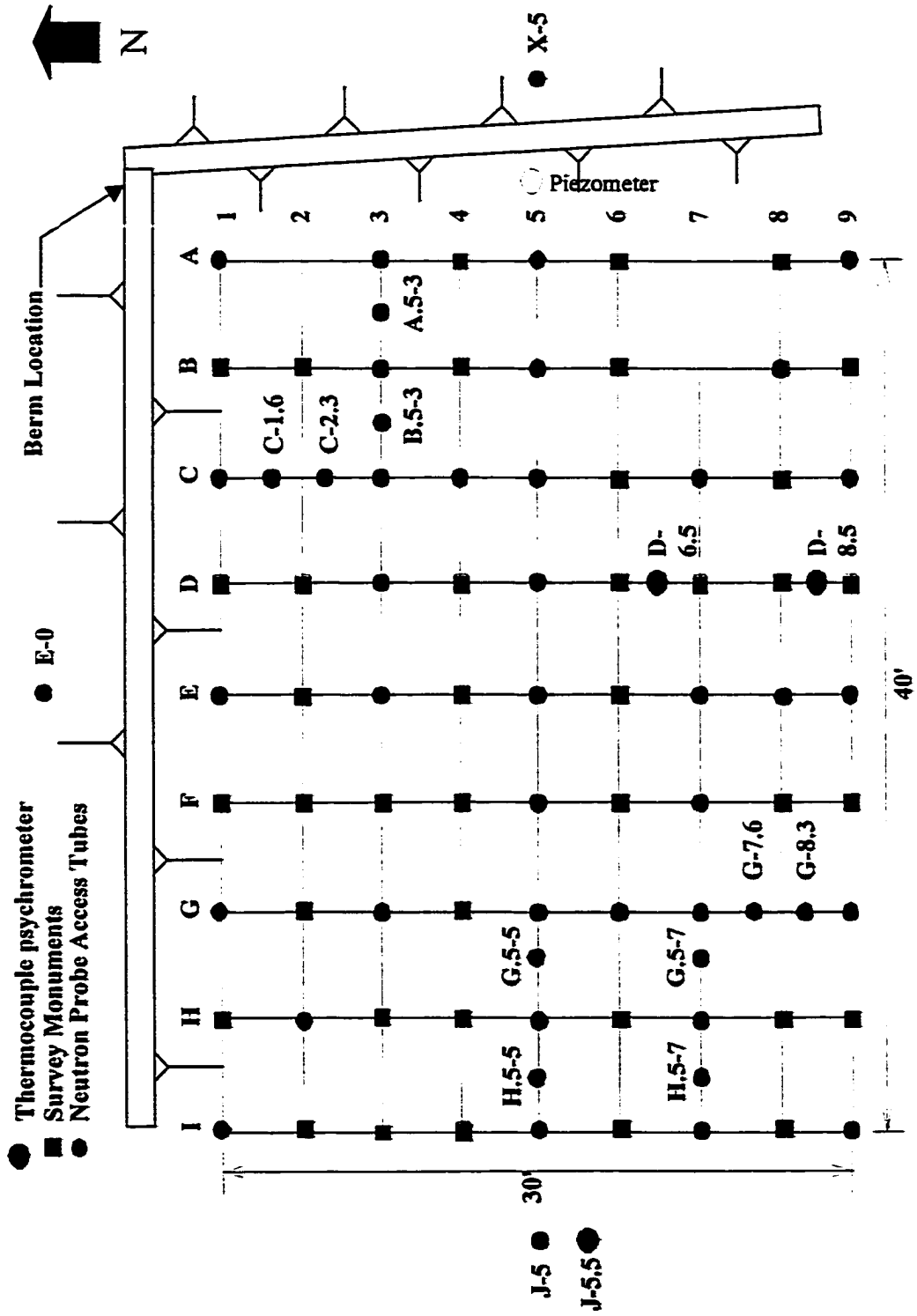

Figure 3-17 Plan view of the CSU site

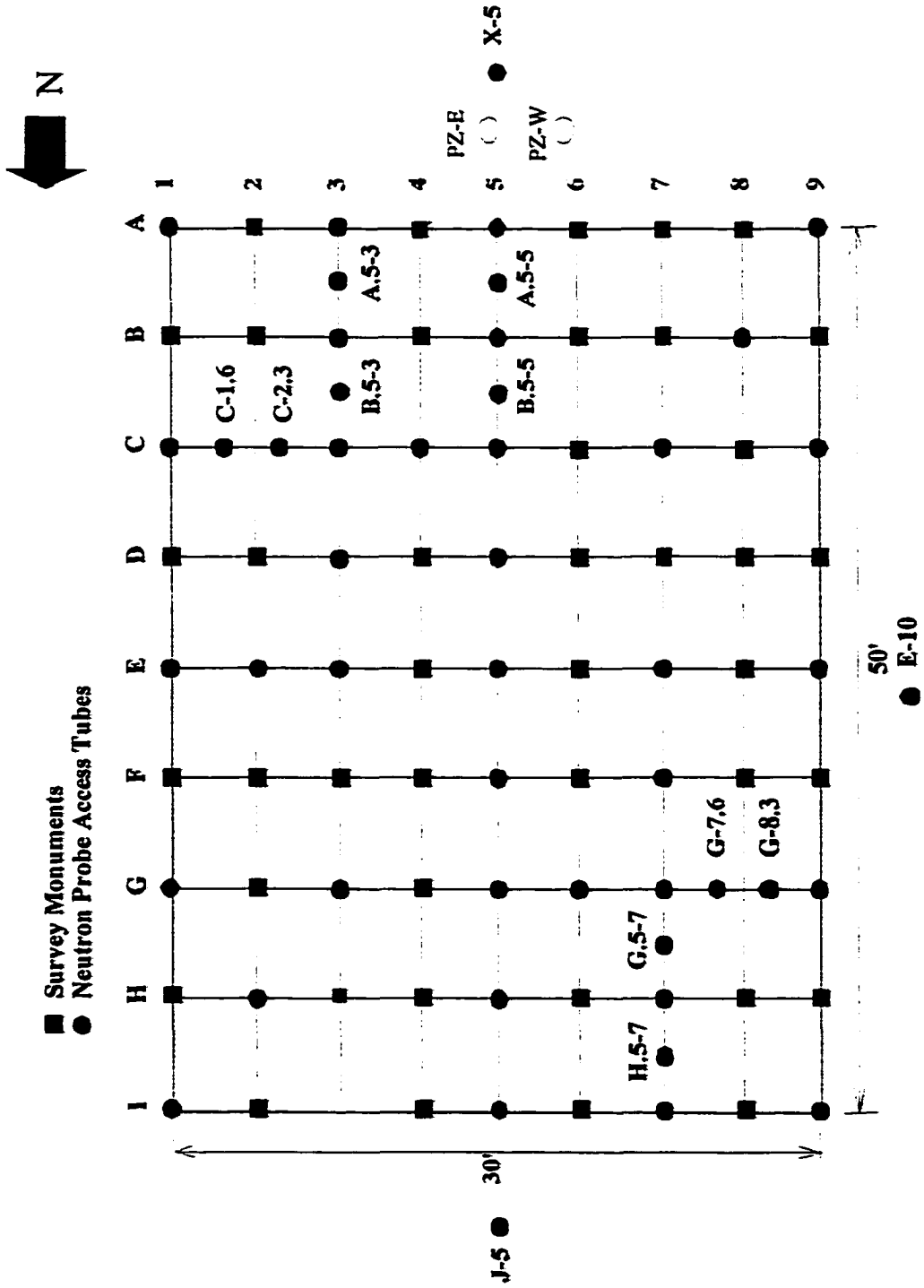

Figure 3-18 Plan view of the FSH site

The time of reading can be adjusted from 1 second to 256 seconds. The operating manual states that a count of 16 seconds is sufficient for measuring water content. The effects of count time on accuracy were also verified as part of this study. Several measurements were taken at various depths to obtain water content profiles for count times ranging from 1 second to 256 seconds. The results showed that increasing the count time to higher than 16 seconds had no effect on the water content measurements. Therefore, 16-second count times were used for this investigation. Appendix A contains the count time verification and the field calibration for the gauge.

At the FSH site a Troxler Laboratories model 105-moisture probe and a 2651 scalar rate-meter were used to collect water content data. The Troxler device does not measure density. Water content measurements were taken at 1-foot intervals to a depth of 5 feet. The field calibration for this gauge is presented in Appendix A. Count data was collected manually from the Troxler gauge and reduced using the calibration in Appendix A.

3.3.2 Elevation Data

Elevation data at the CSU site and the FSH site were collected using conventional surveying equipment. Initial elevation readings were taken immediately following the installation of the survey monuments at both sites. Benchmarks were previously installed at both sites, and were used as reference elevations. In this manner the incremental monthly elevation change and the cumulative elevation change were determined.

3.3.3 Total Suction and Temperature Data

Three sets of nested thermocouple psychrometers (TCP) were installed in drill holes at the CSU site. Two sets were placed at locations under the liner and one set was placed adjacent to the liner. The TCP's were used to monitor change in suction and temperature versus time and depth in the soil. Each hole was equipped with six TCP's at depths of 2 feet, 5 feet, 8 feet, 11 feet, 14 feet, and 17 feet.

The boreholes were excavated at each location using a 4-inch hollow stem auger and 2-inch split barrel continuous sampler. Laboratory water content and soil suction, using the filter paper method, were obtained from the core barrel samples. The cuttings from the borehole were used as backfill during installation of the TCP's.

TCP's measure relative humidity in the air phase of the soil pores. The relative humidity is related to the total suction by the relationship shown in Equation 3-1:

$$\Psi = \frac{-RT\rho_w}{\omega_v} \ln\left(\frac{u_v}{u_{v0}}\right) \qquad (3\text{-}1)$$

where:

Ψ	=	total suction
R	=	universal gas constant
T	=	absolute temperature
ρ_w	=	density of water
ω_v	=	molecular mass of water vapor
u_v	=	partial pressure of pore-water vapor
u_{vo}	=	saturation pressure of water
u_v/u_{vo}	=	relative humidity.

The TCP's used for this research were developed by J.R.D. Merrill Specialty Equipment Company in Logan, Utah. The relative humidity is measured in accordance with Peltier cooling and Seebeck thermoelectric effects. The TCP consists of two wires of different

material (in this case, constantan and chromel) which are welded together to form a junction. The other ends of the wires are connected to copper lead wires to form a reference junction where a constant temperature is maintained. The Peltier effect is used to cool the thermocouple junction to the dew point temperature of the surrounding atmosphere, condensing water vapor on the junction. When the current is stopped the water evaporates to the surrounding atmosphere, which causes a temperature drop. The decrease in temperature is a function of evaporation rate, which in turn is a function of water vapor pressure. Hence, the relative humidity can be computed, by using the Seebeck effect, to measure ambient temperature and temperature reduction due to evaporation.

The filter paper method developed at the New Mexico Engineering Research Institute (NMERI) was used for measuring soil suction for this research. Calibrated filter papers were equilibrated with field soil samples in a closed container for a period of time at a constant temperature. After equilibration, the filter papers were removed, weighed and dried for moisture content determination, and correlated with soil suction by the following relationship:

$$\text{Log}(\psi, \text{kPa}) = -0.0599w + 4.8828 \qquad (3\text{-}2)$$

where: w = gravimetric water content.

This calibration is specific to the filter paper that was used. A separate calibration should be conducted for other tests to account for moisture characteristic variability of the filter paper.

CHAPTER 4

PROPERTIES OF TEST SOILS

Geotechnical laboratory tests were conducted on samples obtained from the CSU site and the FSH site. The laboratory test results were used to classify the soil using traditional geotechnical classification methods and to determine soil properties and constitutive parameters for the analyses.

4.1 Classification

Atterberg limits tests were performed in accordance with ASTM D 4318. The liquid limit, plastic limit and plasticity index were used to classify the soil with respect to heave potential. Tables 4-1 and 4-2 show the Atterberg limits and the relative classifications by several methods for the CSU and FSH soils (Pierre shale and Texas soil), respectively. The natural water contents were obtained immediately after the samples arrived at the laboratory.

Classification of the Pierre shale indicates a "very high" potential for heave in the upper 7 feet. From 7 feet to approximately 10 feet the Pierre shale has a "high" potential for heave. Below 10 feet the Pierre shale classifies as having a "medium" potential for heave. The Texas soil appears to be homogeneous in terms of heave potential. The plasticity index increases slightly with depth, but all values indicate a "very high" or "critical" heave potential.

The data in Table 4-1 also show an important trend that has been observed in soils from arid climates. The water content, of the Pierre shale, at the time of sampling was below the plastic limit. The water content of the Texas soil, shown in Table 4-2, was approximately equal to the plastic limit. However, as mentioned above, the water content of the Texas soil at other times of the year is less than the plastic limit.

Soil profiles from a number of locations around the world are shown in Chapter 7 of Lambe and Whitman (1969). In those profiles, the natural water contents at locations having highly overconsolidated clays are about equal to the plastic limit. No sites indicated natural water contents below the plastic limit.

4.2 Consolidation Tests

Consolidation-swell tests and controlled strain tests were conducted on samples from various depths at each site to characterize the soil and determine heave prediction constitutive parameters. ASTM standards were followed for the swell tests except for minor changes due to equipment limitations.

The Pierre shale at the CSU site is highly overconsolidated and the natural water content is below the plastic limit. As a result the soil is extremely friable and it is difficult to load an undisturbed sample in a consolidometer. Therefore, remolded specimens compacted to the approximate field density were used for consolidation-swell and controlled-strain tests that were conducted on Pierre shale.

Table 4-1 Results of Atterberg limits test and heave potential classification for the Pierre shale (CSU site)

Depth (ft)	w_n(%)	LL	PL	PI	SL[1]	Heave Potential Classification: Plasticity Chart	Holtz and Gibbs (1956)[2]	Altmeye (1955)[3]	Chen (1988)[2]
2	10.4	56	22	34	12	CH	H-VH	C	H
3	12.5	64	19	45	7	CH	VH	C	VH
4	12.3	64	18	46	6	CH	VH	C	VH
5	12.9	57	22	35	12	CH-CL	M-H	M	VH
6	13.2	55	23	32	14	CH-CL	M	NC	H
7	13.4	56	21	35	11	CH-CL	H	M	VH
8	12.2	51	21	30	13	CH-CL	H	M	H
9	13.7	54	25	29	16	CL-CH	M-H	NC	H
10	12.8	46	25	21	18	CL	L-M	NC	M
11	11.9	44	24	20	18	CL	L-M	NC	M
12.5	11.5	46	20	26	13	CL	M	NC	M
14	12.3	51	20	31	12	CL-CH	H	M	H
15	11.6	43	21	22	15	CL	M	NC	M
15.5	10.7	41	23	18	17	CL	M	NC	M
16.5	11.4	41	21	20	15	CL	M	NC	M
17.5	10.4	45	23	22	16	CL	M	NC	M
19	12.6	41	23	18	17	CL	L-M	NC	M

Profiles

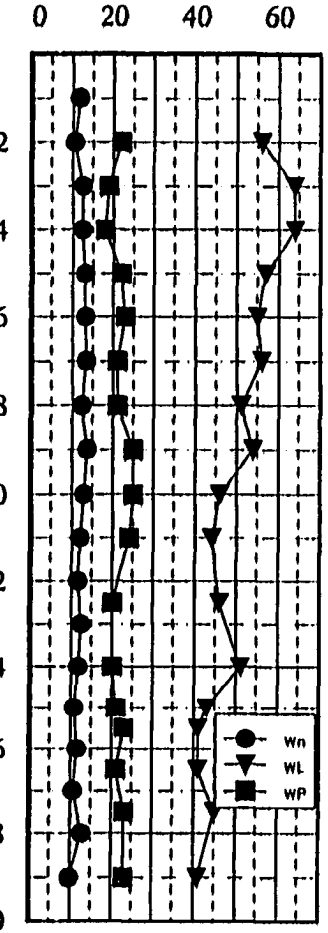

1 Computed Value (Holtz and Kovacs, 1981): $SL = 20 \pm \Delta p_I$ 2 VH=very high, H=high, M=medium, and L=low 3 C=critical, M=marginal, and NC=noncritical

Table 4-2 Results of Atterberg limits test and heave potential classification for Texas soil (FSH Site)

Depth (ft)	w_n(%)	LL	PL	PI	SL[1]	Heave Potential Classification: Plasticity Chart	Holtz and Gibbs (1956)[2]	Altmeye (1955)[3]	Chen (1988)[2]
0-0.5	32.0	66	25	41	13	CH	H-VH	N	VH
0.5	22.0	63	20	43	8	CH	VH	C	VH
1	20.5	63	20	43	9	CH	VH	C	VH
1.5	20.5	67	20	47	7	CH	VH	C	VH
2.0	24.2	73	22	51	8	CH	VH	C	VH
2.5	21.0	69	22	47	9	CH	VH	C	VH
4.5	21.7	69	21	48	8	CH	VH	C	VH
5	21.6	69	21	48	8	CH	VH	C	VH

Profiles

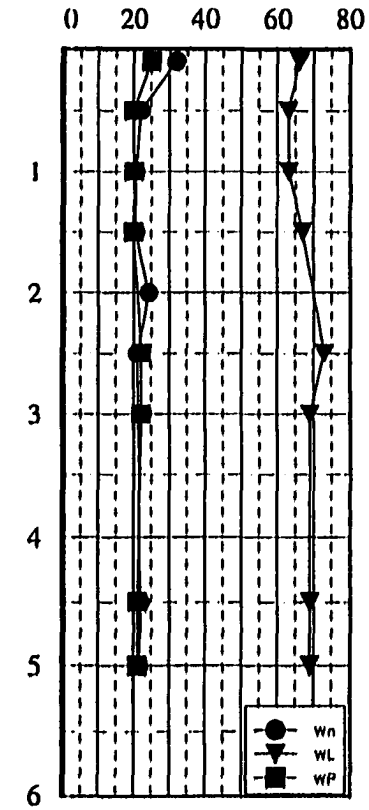

1 Computed Value (Holtz and Kovacs, 1981): SL = 20 ± Δpi 2 VH=very high, H=high, M=medium, and L=low 3 C=critical, M=marginal, and NC=noncritical

Tables 4-3 and 4-4 show the results from consolidation-swell tests and controlled strain tests conducted on remolded Pierre shale and undisturbed Texas soils, respectively. The void ratio-log σ' curves from the consolidation-swell tests and controlled strain tests are shown in Appendix B.

A standard consolidation test (ASTM D 2435) was also conducted on an undisturbed sample of Pierre shale. The soil was saturated in the sampling tube prior to extrusion thus allowing it to be loaded into the consolidometer with minimal disturbance. The results of the standard consolidation test on the undisturbed sample of Pierre shale indicates that the compression index, C_c, is equal to approximately 0.085 and the slope of the rebound curve is approximately 0.06. The swell index values presented in Tables 4-3 and 4-4 were obtained from the rebound curves of their respective tests. The value obtained from the standard consolidation test is slightly higher than the values from the consolidation-swell test and the controlled strain test.

4.3 Hydraulic Properties

The saturated hydraulic conductivity, diffusivity, and the soil water characteristic curve (SWCC) were determined for both soils as part of the laboratory investigation. The SWCC is a fundamental parameter in unsaturated flow processes and can be used with the saturated hydraulic conductivity to estimate the unsaturated hydraulic conductivity function (Fredlund and Xing (1994); Brooks and Corey (1964); Gardner (1958); Richards (1931); and others). In addition the SWCC and diffusivity function can be used to indirectly estimate the unsaturated hydraulic conductivity function (Bruce and Klute, 1956).

Table 4-3 Results of controlled strain consolidation (SC) tests and consolidation-swell (CS) tests conducted on Pierre shale.

Test Type	Sample Depth (ft)	e_o	w_i (%)	C_s[1]	%Swell	σ_{sc}' (psf)
SC	2.0	0.73	3.7	0.025	-	700
SC	5.0	0.57	10.4	0.038	-	3000
SC	10.0	0.70	9.8	0.051	-	1400
SC	17.0	0.74	11.4	0.20	-	1400
CS	5.0	0.61	10.0	0.042	5	6000
CS	8.5	0.59	10.4	0.03	3.8	9000
CS	12.5	0.57	10.1	0.022	1.9	4400
CS	17.5	0.59	11.7	0.020	3.8	6000

1. Swell index was obtained from the slope of the slope of the rebound curve.

Table 4-4 Results of strain controlled consolidation tests (SC) and consolidation-swell tests (CS) conducted on the Texas soil.

Test Type	Sample Depth (ft)	e_o	w_i (%)	C_s[1]	%Swell	σ_{sc}' (psf)
SC	1.5	0.98	28.4	0.050	-	600
SC	3.5	0.82	21.7	0.051	-	6400
SC	5.0	0.60	20.8	0.033	-	7000
CS	1.5	0.66	17.9	0.05	7.8	12400
CS	3.0	0.61	21.3	0.83	9.2	17000
CS	4.5	0.55	20.4	0.05	11.6	38000
CS	5.0	0.53	21.3	0.05	7.2	46000

1. Swell index was obtained from the slope of the slope of the rebound curve.

4.3.1 Saturated Hydraulic Conductivity

Saturated hydraulic conductivity tests were conducted on undisturbed samples of the Pierre shale and the Texas soil using a rigid-walled, falling head water-rising tail water test apparatus. Plexi-glass sampling tubes were cut into approximately 3-inch long sections and custom fitted with machined end caps and rubber o-rings for controlling water pressure through plexi-glass accumulators attached to both ends of the samples. Two tests were conducted on each soil type. The samples were loaded into the testing apparatus at their natural water content. A water pressure of 5 psi was applied to the bottom of the apparatus to initiate flow across the sample. The height of water in the accumulators was then measured daily for one-month to allow calculation of the hydraulic conductivity.

The tests were conducted until the final hydraulic conductivity values were considered to be steady-state values. Weight volume calculations after the tests were completed indicated that the degree of saturation of the samples was close to 100 percent at the completion of the tests.

The results of the tests are presented in Table 4-5. Test data are presented in Appendix B. No results were obtained for the Pierre shale in Test number 3. Attempts to induce flow in Test number 3 with a pressure gradient failed throughout the test period due to very high flow rates under low gradient. The high flow rates were attributed to either sample disturbance and fracturing or side wall leakage.

Table 4-5 Saturated hydraulic conductivity test results from falling head water rising tail water tests

Test Number	Soil Type	Void Ratio	Hydraulic Conductivity (ft/sec)
1	Pierre shale	0.75	$2.0*10^{-10}$
2	Texas soil	0.96	$2.6*10^{-10}$
3	Pierre shale	1.0	n/a
4	Texas soil	0.96	$3.2*10^{-10}$

The hydraulic conductivity values presented in Table 4-5 are low for these types of soils. It is not possible to control the stress conditions in a rigid wall test. The void ratio of the Pierre shale samples at the end of the tests was approximately 0.75 and 1.0 for Tests numbers 1 and 3 respectively. The void ratio of the Texas soil was 0.96 for both tests. Field water content and density measurements from the CSU site indicate that the void ratio of the Pierre shale ranges from approximately 0.7 to 1.2. The lower void ratio values typically occur in the deeper soils that are not as weathered and where the stress conditions are high enough to reduce swell and fracture opening. Density measurements were not obtained at the FSH site. It is believed that the samples in Tests number 1, 2, and 4 developed a significant amount of swell pressure during the test. The rigid walled apparatus prohibited swell and limited the expansion of fractures resulting in the low measured flow values.

The saturated hydraulic conductivity was also measured on the Pierre shale during the standard consolidation tests discussed in Chapter 4.1. The oedometer was instrumented with a falling head apparatus to allow measurement of the change in head across the

sample at the end of each loading increment. The measured and calculated hydraulic conductivity values and loading conditions are presented in Table 4-6. The calculated values were determined using the relationship between the coefficient of consolidation and permeability, from consolidation theory. In general the measured values are consistent with the calculated values except at the initial loading. The relatively high measured value at the initial loading is likely due to sidewall leakage at low stress.

Table 4-6 Hydraulic conductivity test results from consolidation tests

Load (psf)	Equivalent Depth (feet)	Void Ratio	Hydraulic Conductivity	
			Measured (feet/sec)	Calculated[1] (feet/sec)
647	7	0.752	$1.5*10^{-4}$	$1.3*10^{-7}$
1294	14	0.712	$2.7*10^{-7}$	$7.8*10^{-8}$
2588	28	0.666	$3.7*10^{-8}$	$1.3*10^{-8}$
5177	56	0.651	-	$9.3*10^{-9}$
10445	112	0.63	-	$5.3*10^{-9}$
20684	222	0.606	-	$3.1*10^{-9}$

1. Hydraulic conductivity calculated using $k = \frac{c_v \rho_w g a_v}{1+e_0}$ (Holtz and Kovacs, 1981)

4.3.2 Unsaturated Hydraulic Conductivity

The unsaturated hydraulic conductivity function was not measured directly as part of this research. Bruce and Klute (1956) developed an indirect method of estimating unsaturated hydraulic conductivity using the soil-water diffusivity function and the soil water characteristic curve. The soil-water diffusivity function can be developed using the Klute

cell method (Bruce and Klute, 1956). The soil water characteristic curve (SWCC) is typically obtained using the pressure plate method.

Durnford and Lorentz (1991) present the theoretical development for the Klute cell method. The Klute cell test setup is shown in Figure 4-1.

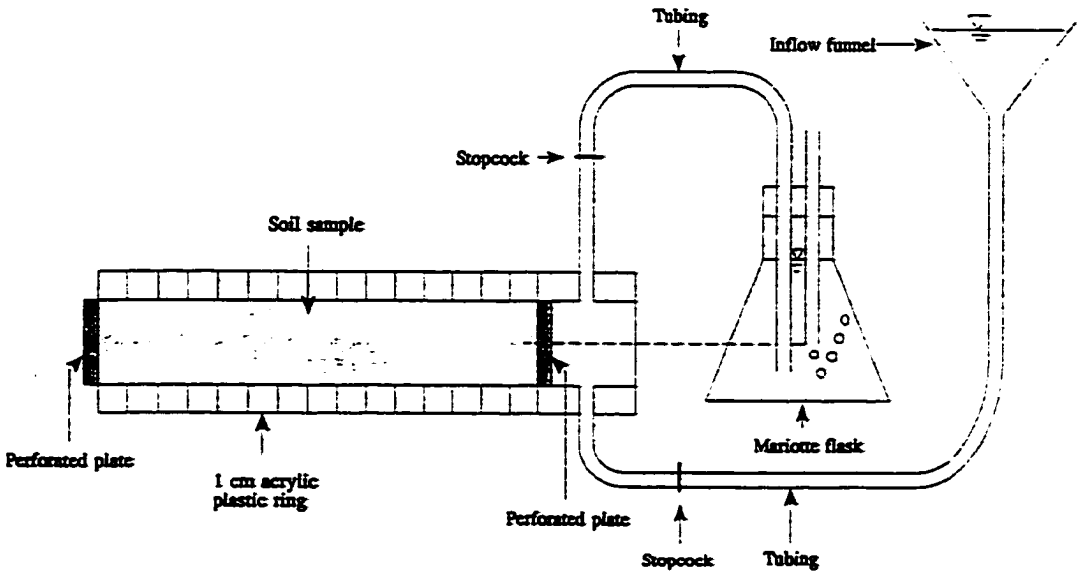

Figure 4-1 Klute Cell Apparatus.

The Bruce and Klute (1956) method was used to estimate the unsaturated hydraulic conductivity for this investigation. Cheng (1994) performed the tests as part of the requirements for his Master of Science degree. The nature of the soils tested made it difficult to load undisturbed samples in the standard apparatus, and the tests were conducted on remolded samples. The same method of compaction was used throughout both tests in an attempt to provide a consistent soil structure. The Pierre shale and Texas

soil were air-dried for 24 hours, pulverized to pass a No. 10 sieve, and compacted in the test mold.

The soil-water diffusivity tests and the pressure plate tests were then conducted using remolded soil with a dry density of 100 pcf and 87 pcf for the Pierre shale and the Texas soils respectively.

The unsaturated hydraulic conductivity results from the Bruce-Klute method are shown in Tables 4-7 and 4-8 for the Pierre shale and the Texas soil, respectively. Figures 4-2 and 4-3 show the unsaturated hydraulic conductivity as a function of volumetric water content and suction for the Pierre shale and the Texas soils, respectively. The diffusivity relationships and the soil water characteristic curves for both soils are presented in Cheng (1994).

The values presented in Tables 4-7 and 4-8 for unsaturated hydraulic conductivity are lower than expected for these types of soils. This is likely due to the fact that remolded samples were used to develop the diffusivity function. In addition the soil water characteristic curve used to develop the unsaturated hydraulic conductivity function in this case does not account for volume change.

Table 4-7 Results of Bruce-Klute tests on the Pierre shale.

Volumetric Water Content (%V)	Suction (ft-water)	Soil Water Diffusivity (ft^2/sec)	Unsaturated Hydraulic Conductivity (ft/sec)
0.3	165	$3.3*10^{-8}$	$4.7*10^{-10}$
0.313	120	$4.8*10^{-8}$	$10.4*10^{-10}$
0.325	92	$5.2*10^{-8}$	$14.8*10^{-10}$
0.338	71	$5.8*10^{-8}$	$2.6*10^{-9}$
0.350	52	$1.2*10^{-7}$	$6.5*10^{-9}$
0.363	44	$1.7*10^{-7}$	$1.1*10^{-8}$
0.375	31	$2.4*10^{-7}$	$2.3*10^{-8}$
0.388	29	$2.7*10^{-7}$	$3.3*10^{-8}$
0.4	22	$3.6*10^{-7}$	$8.2*10^{-8}$

Table 4-8 Results of Bruce-Klute tests on the Texas soil.

Volumetric Water Content (%V)	Suction (ft-water)	Soil-Water Diffusivity (ft^2/sec)	Unsaturated Hydraulic Conductivity (ft/sec)
.350	380	$5.8*10^{-9}$	$2.5*10^{-11}$
.363	228	$9.0*10^{-9}$	$5.2*10^{-11}$
.375	116	$1.2*10^{-8}$	$1.5*10^{-10}$
.388	85	$1.7*10^{-8}$	$3.4*10^{-10}$
.400	51	$2.0*10^{-8}$	$5.2*10^{-10}$
.410	36	$2.3*10^{-8}$	$8.6*10^{-10}$

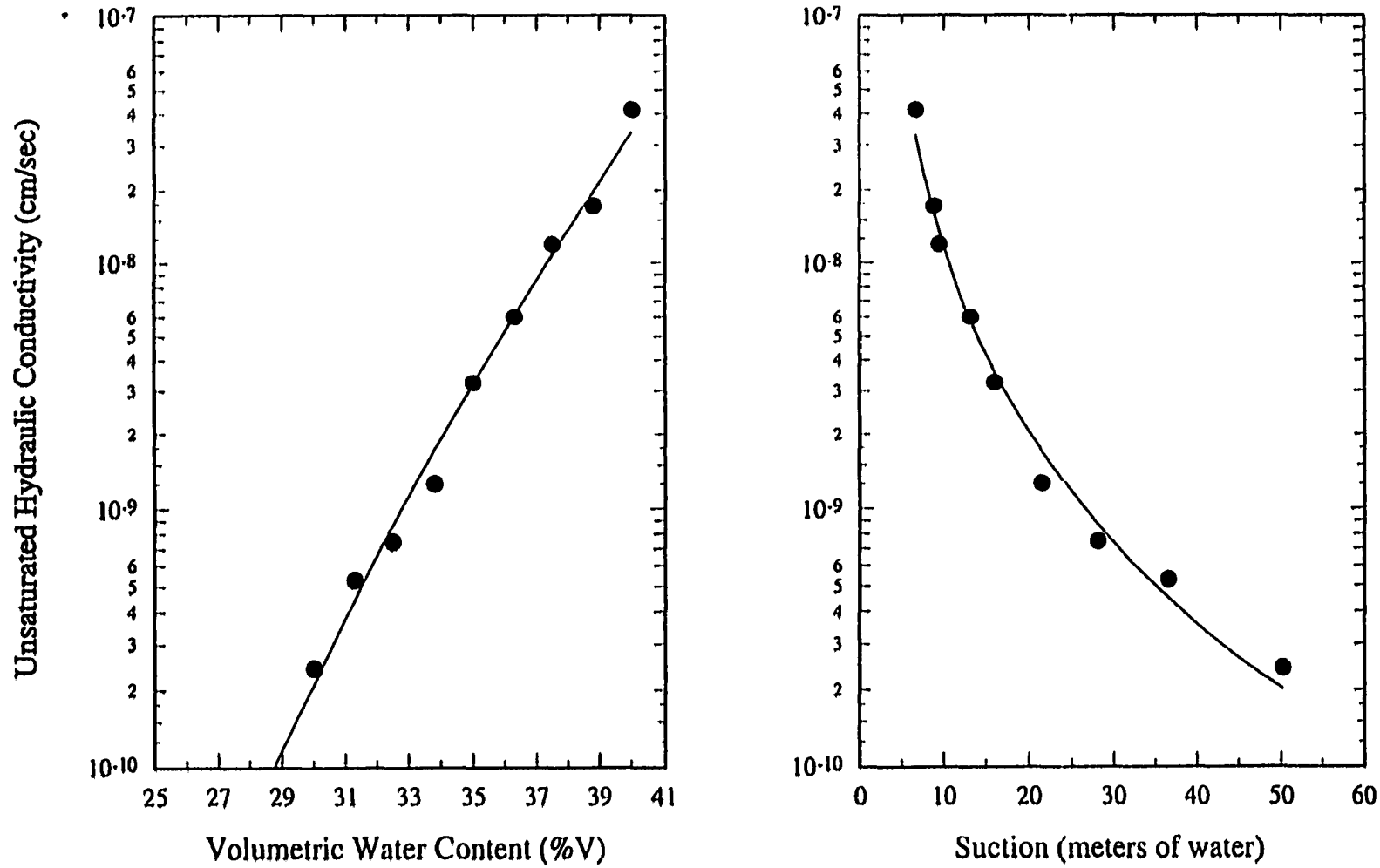

Figure 4-2 Unsaturated hydraulic conductivity as a function of volumetric water content and suction for the Pierre shale.

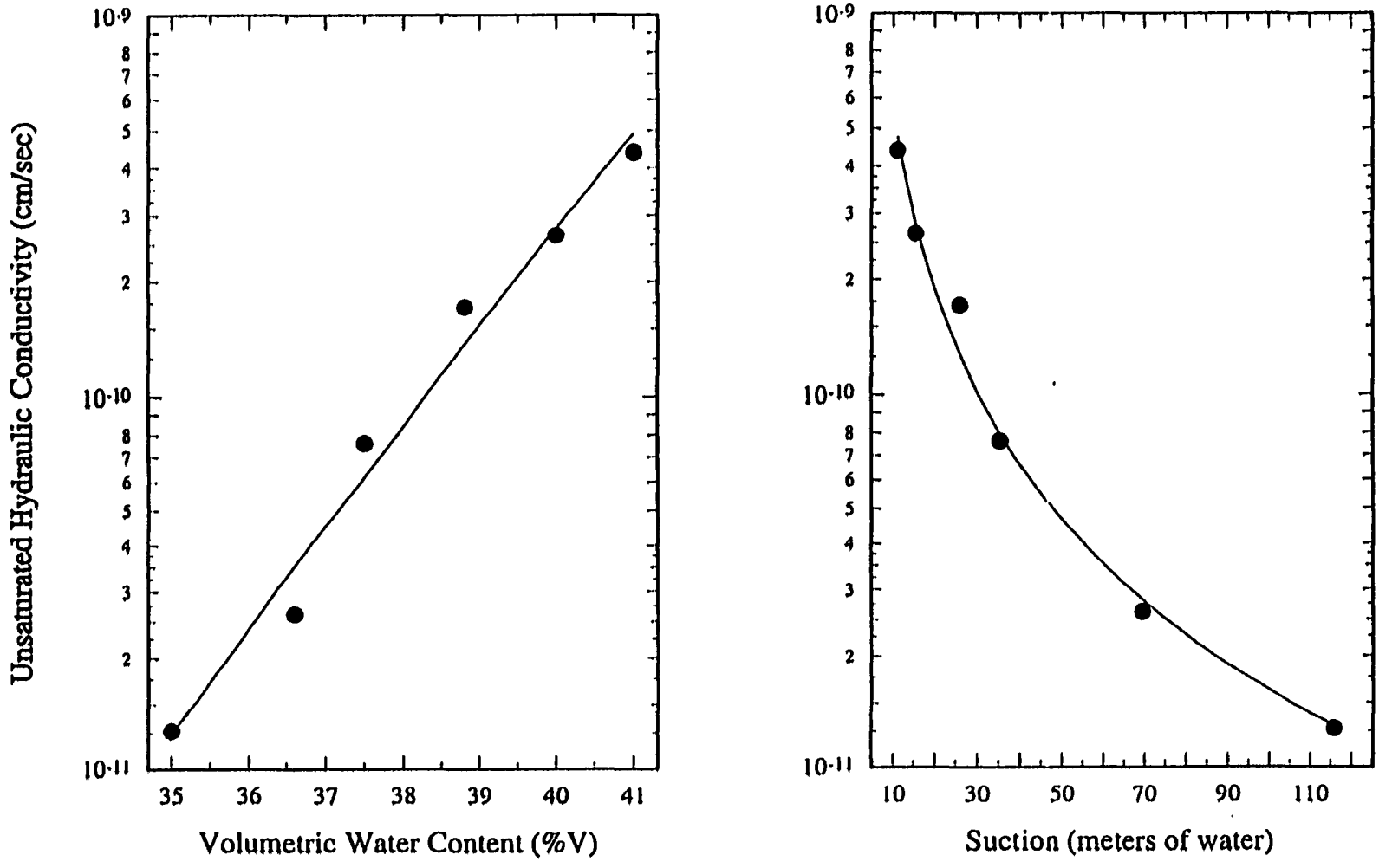

Figure 4-3 Unsaturated hydraulic conductivity as a function of volumetric water content and suction for the Texas soil.

4.3.3 Soil Water Characteristic Curve

The CLOD test described in Chapter 2 was initially developed at the New Mexico Engineering Research Center and developed further at CSU to predict free field heave (Hamberg, 1985). It provides a method for predicting heave using undisturbed samples, even for the friable soils. A soil water characteristic curve can also be obtained from the CLOD test. In the CLOD test, undisturbed samples are coated with a Saran[I] F-310 resin that is permeable to air, impermeable to water, and allows volume change of the sample. The soil water characteristic curve is then measured on a deforming undisturbed sample.

Chao (1995) conducted CLOD tests on the Pierre shale and Texas soils following the procedure outlined in Hamberg (1985). The soil water characteristic curves were obtained using a pressure plate apparatus. Clod samples coated with semi-permeable resin were placed in the apparatus and their water content was allowed to equilibrate at the applied air pressure. The water pressure in the sample was maintained at zero by placing the sample in contact with a saturated semi-permeable ceramic stone. In this manner the suction in the sample was equal to the applied air pressure. At equilibrium the samples were weighed to calculate the water content and returned to the pressure plate apparatus. The suction was then increased (decreased for the wetting curve data) to obtain the next point. The measured data are shown fitted with the Brooks-Corey and van Genuchten methods in Figures 4-4 and 4-5.

[I] Trademark of The Dow Chemical Company

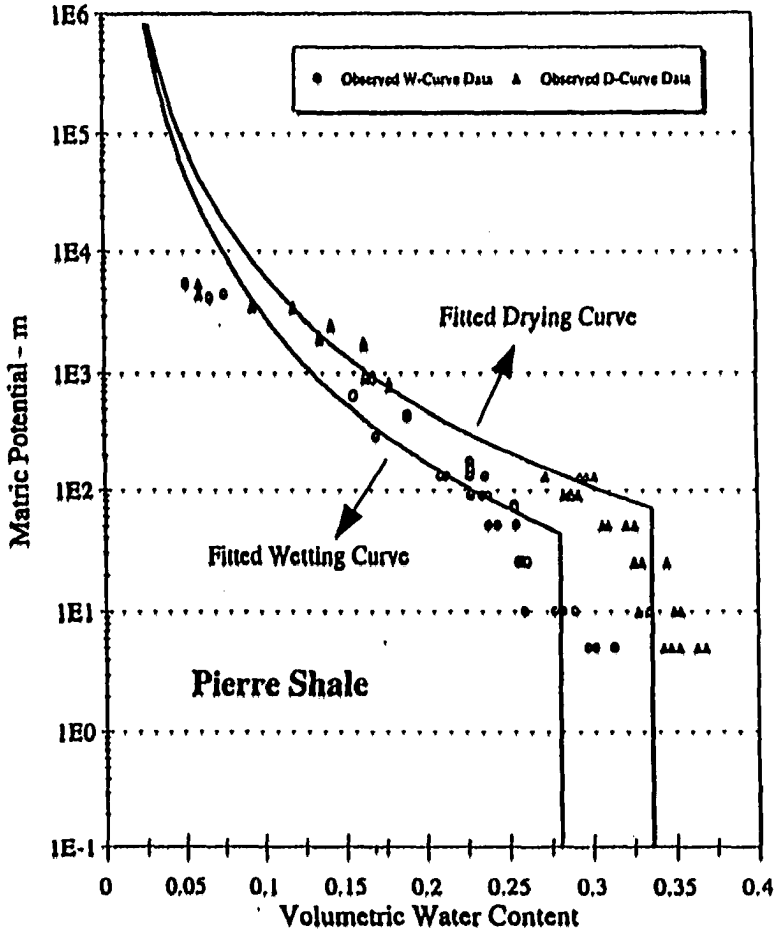

Figure 4-4a Soil water characteristic curve for Pierre shale fitted with Brooks-Corey.

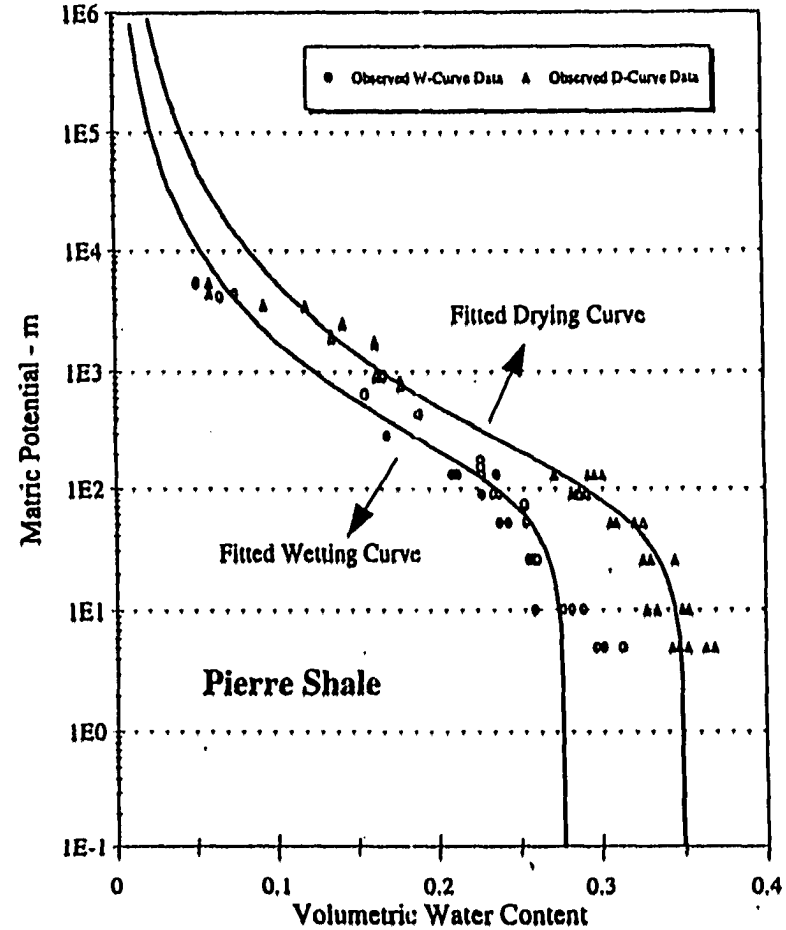

Figure 4-4b Soil water characteristic curve for Pierre shale fitted with van Genuchten.

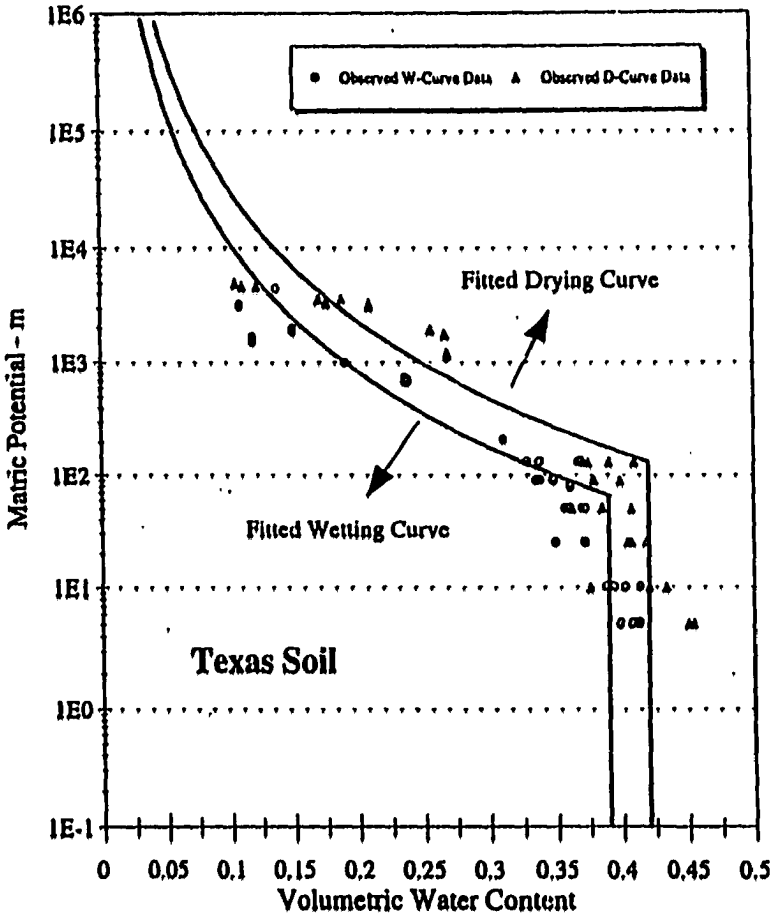

Figure 4-5a Soil water characteristic curve for Texas soil fitted with Brooks-Corey.

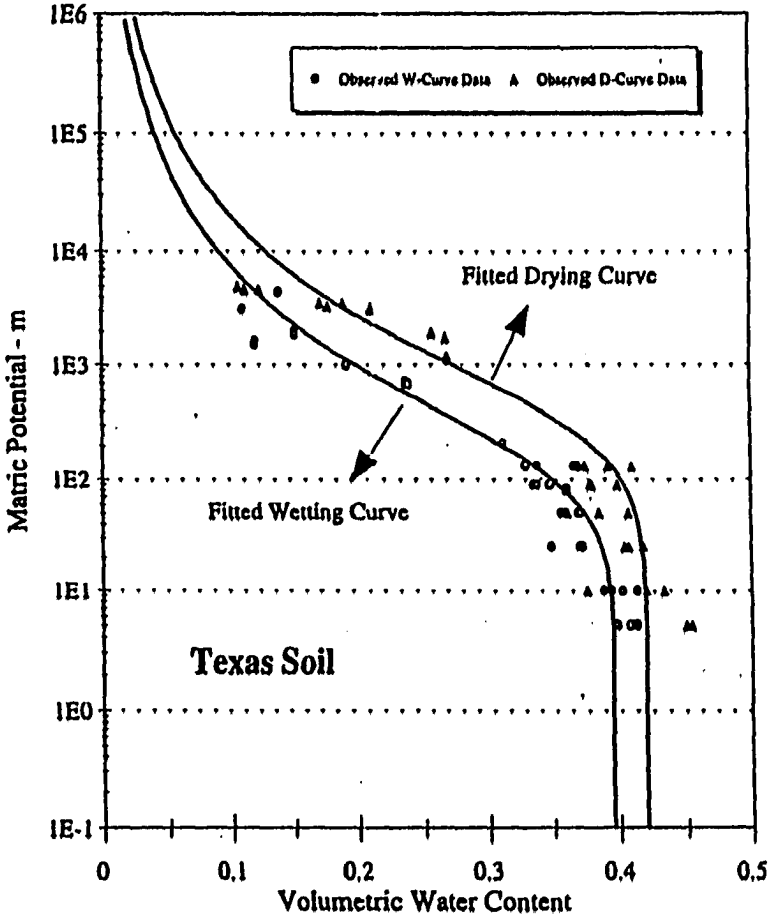

Figure 4-5b Soil water characteristic curve for Texas soil fitted with van Genuchten.

In general the Brooks-Corey and van Genuchten methods do not provide a good fit to the data. Chao, Durkee, Miller, and Nelson (1998) used the data presented in this research to investigate the effects of volume change and test traditional fitting methods. They showed that soil water retention data obtained from expansive soil while accounting for volume change is more closely represented by a bi-linear relationship than by the methods previously developed for rigid soils (Brooks-Corey and van Genuchten methods).

4.4 Summary of Soil Properties

The results of the laboratory tests that were conducted for this investigation serve to classify the soil and establish the swell potential. The hydraulic properties can be used to develop constitutive relationships and for moisture migration modeling. Further development of the hydraulic properties for use in analyses is presented in Chapter 6. A summary of index tests and the consolidation tests is shown as a function of depth in Figures 4-6 and 4-7.

Nelson and Miller (1992) discuss a method for correlating the active zone depth to natural water content and Atterberg limits. The natural water content is divided by the plasticity index, and this ratio is plotted as a function of depth. The depth at which w/PI becomes constant is assumed to be the active zone depth. There has not been much research on this technique; hence, its reliability is unknown. Plots of w/PI for the Pierre shale and Texas soils respectively are presented in Figure 4-8 and 4-9. Figure 4-8 indicates that the active zone depth in the Pierre shale can be at least 20 feet. Figure 4-9 indicates that the active zone depth in the Texas soil is less than 3 feet.

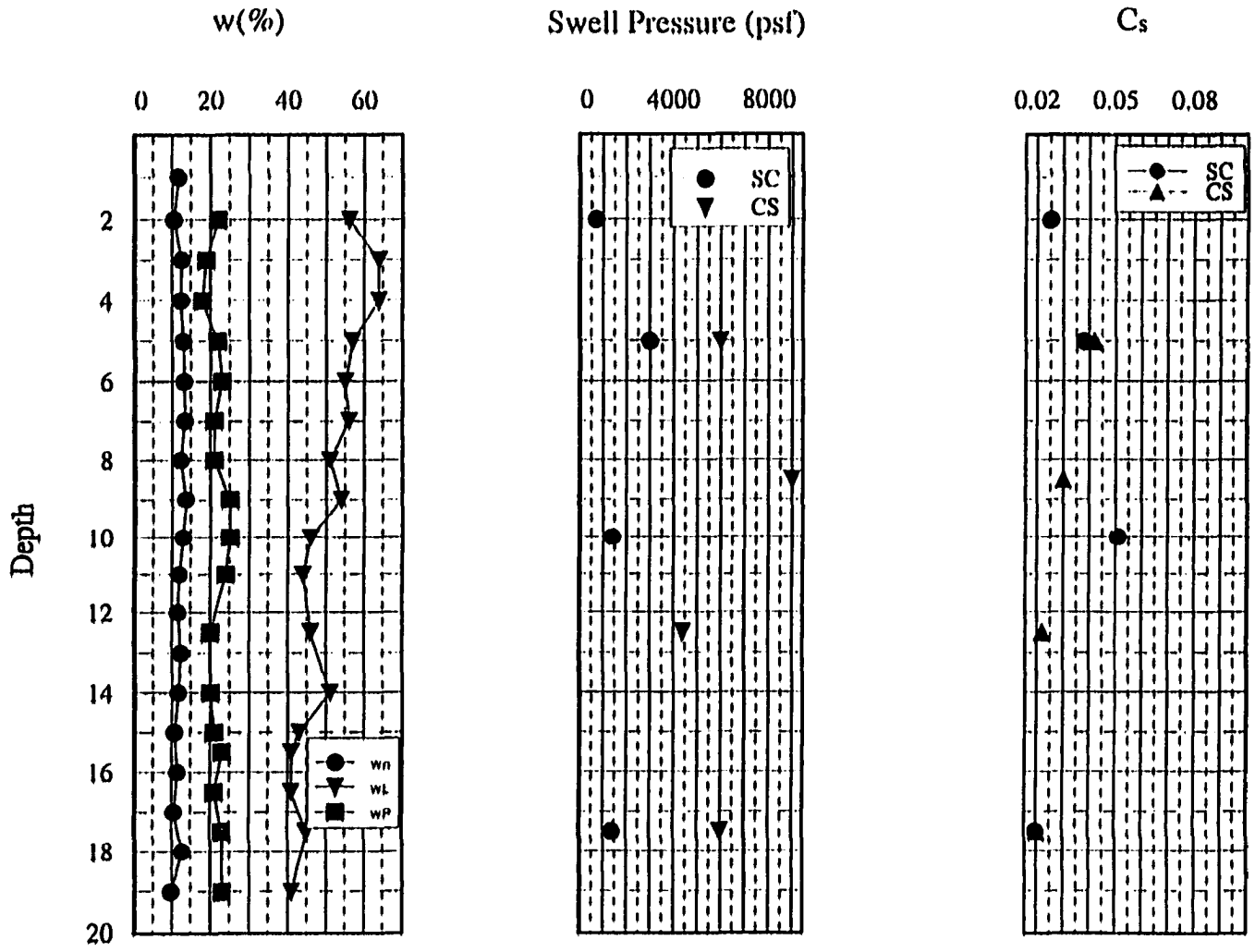

Figure 4-6 Summary of index and swell tests conducted on the Pierre shale.

Figure 4-7 Summary of index tests and swell tests conducted on the Texas soil.

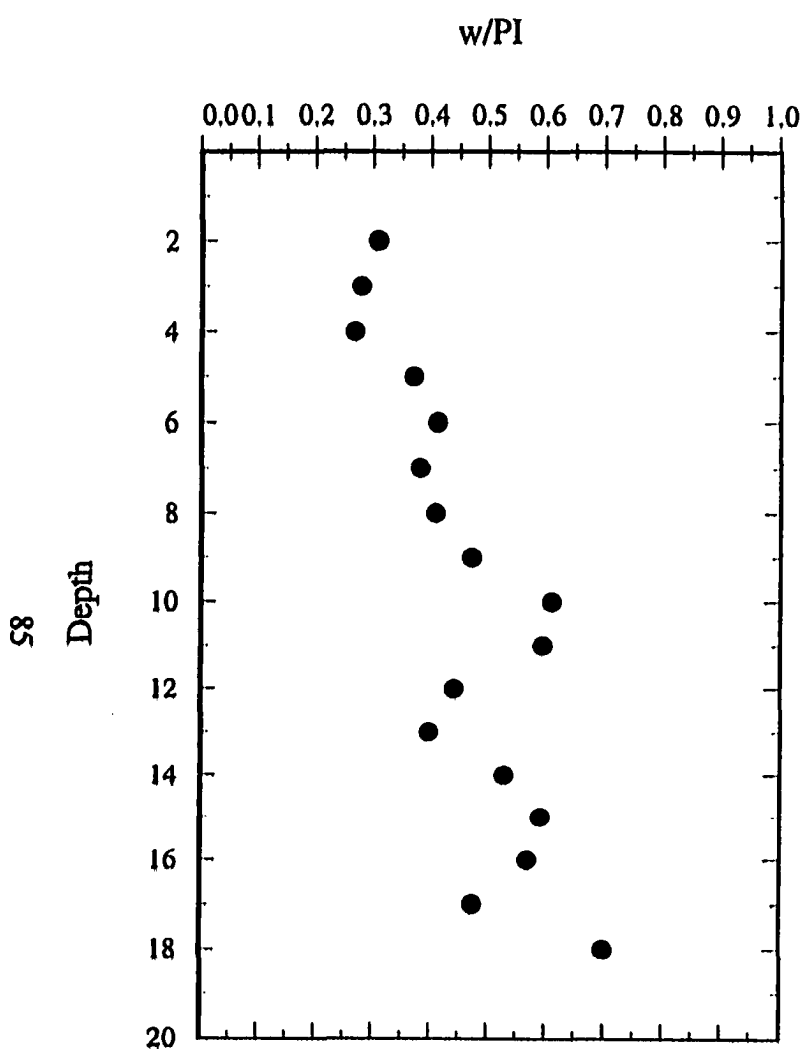

Figure 4-8 Water content normalized to the plasticity index as a function of depth for the Pierre shale.

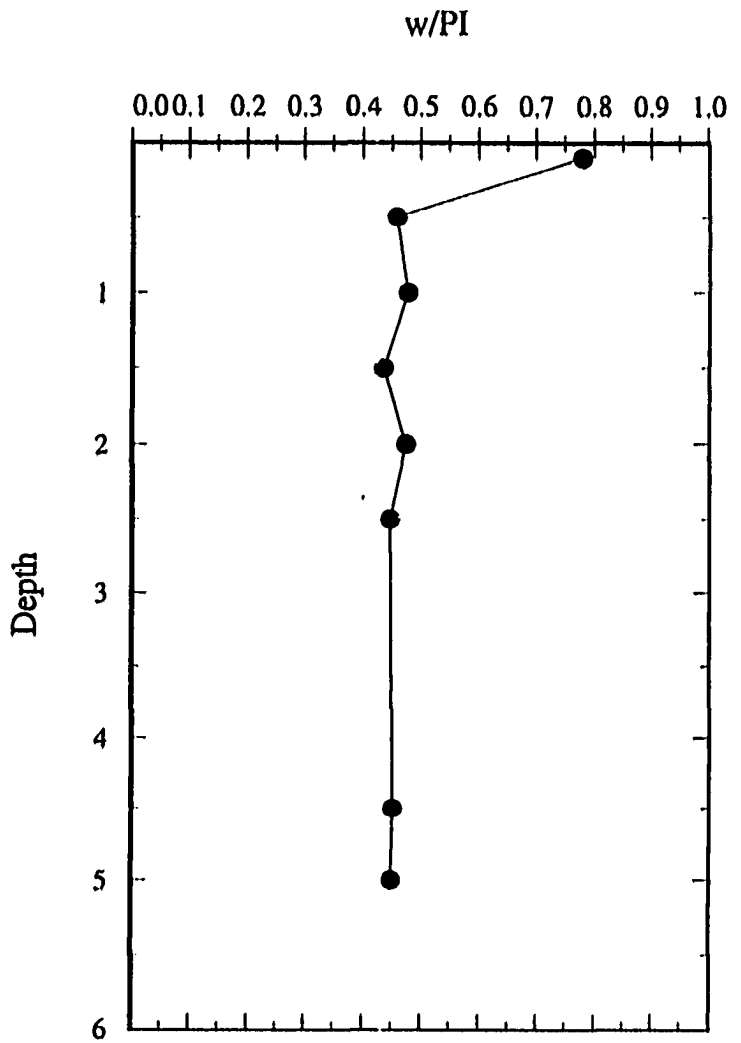

Figure 4-9 Water content normalized to the plasticity index as a function of depth for the Texas soil.

In this method the water content is divided by the plasticity index (PI) to account for varying soil types in the profile. A major limitation to the method is that it is based on the assumption that the active zone depth is equal to the depth at which the water content in the natural soil, before construction, becomes constant. As discussed in Chapters 1 and 2 this is not consistent with the definition of the active zone depth that is presented herein.

CHAPTER 5

FIELD TEST RESULTS

The goal of this research was to define and develop an understanding of the two expansive soil foundation design parameters, active zone depth and edge moisture variation distance. The purpose of the field investigation was to monitor water content, suction, and heave beneath two simulated slab foundations, located in different soils and climate environments. An HDPE geomembrane liner was used to cover a 1,000-square foot plot area at each site. The liner simulates the effects of slab foundations constructed on expansive soils by reducing evapo-transpiration. Data from the field investigation was used to determine the active zone depth and edge moisture variation distance in terms of the observed moisture migration and heave patterns. The data was also used to determine the effects of environmental conditions, geologic conditions, and soil properties on active zone depth and edge moisture variation distance.

5.1 Climate

The active zone depth and the edge moisture variation distance are strongly affected by infiltration and evaporation rates from the surrounding soil. Infiltration and evaporation rates are functions of precipitation, temperature, relative humidity, solar radiation, and wind speed. Climate data including precipitation, air temperature, relative humidity, wind speed and solar radiation data were obtained from local climate centers for both sites.

Typical monthly rainfall and daily temperature data are shown in Figures 5-1 and 5-2, for the FSH site, and Figures 5-3 and 5-4 for the CSU site, respectively. The average values presented are based on data collected for 45 years at the FSH site and 30 years at the CSU site. The majority of rainfall at FSH typically occurs between April and June, and a slight increase occurs in September and October. The majority of rainfall at the CSU site typically occurs between April and July. The average daily temperature at the FSH site varies from 50° F in the winter months to over 80° F in the summer. The average daily temperature at the CSU site varies from 25° F in winter to over 70° F in the summer.

Figures 5-5 and 5-6 show the average daily temperature trend at the FSH site and the CSU site, respectively, since the test slabs were constructed. The data in Figure 5-5 show that during the investigation the average daily temperature at the FSH site varied in a typical sinusoidal trend ranging from a low of approximately 35° F to a high of approximately 90° F. This range of fluctuation is greater than the observed average data presented in Figure 5-2. It is also important to note that at times the average daily temperature fluctuated by as much as 45° F over two to three days.

The data in Figure 5-6 shows the average daily temperature at the CSU site also varies in a typical sinusoidal trend but that the range of fluctuation is greater than at FSH. The average daily temperature at the CSU site ranges from a low of approximately 0 to 10° F to a high of approximately 80° F, which is also greater than the range observed from the average data presented in Figure 5-4. At the CSU site the average daily temperature fluctuated by as much as 50° F over two to three days.

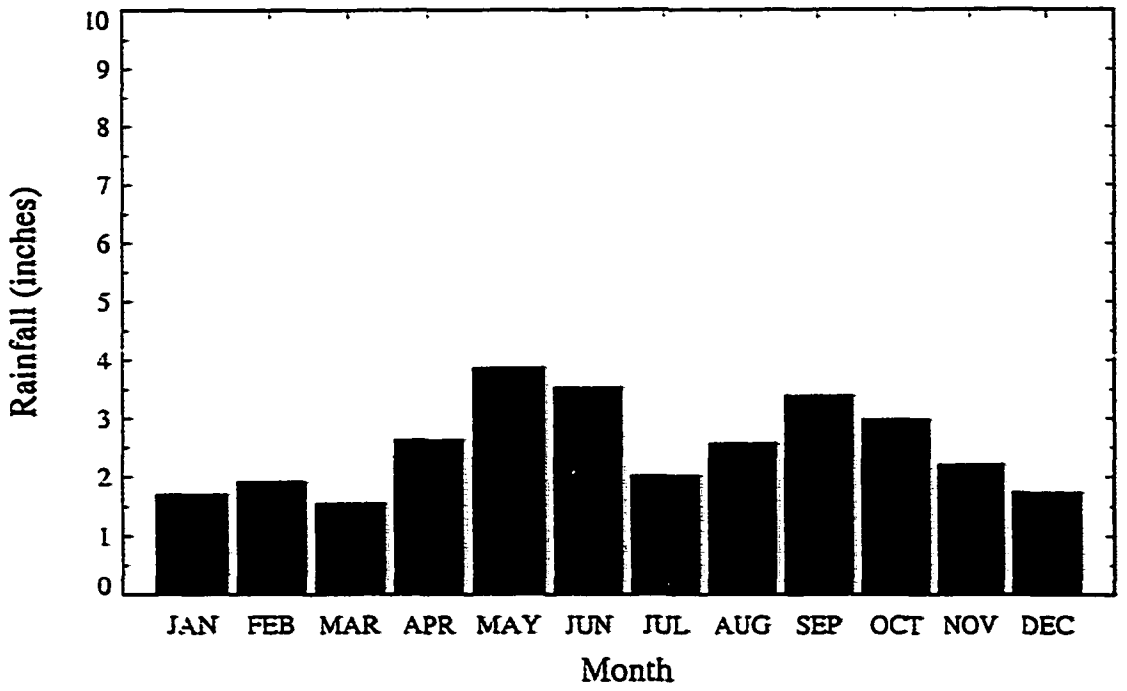

Figure 5-1 Typical monthly precipitation at the FSH site.

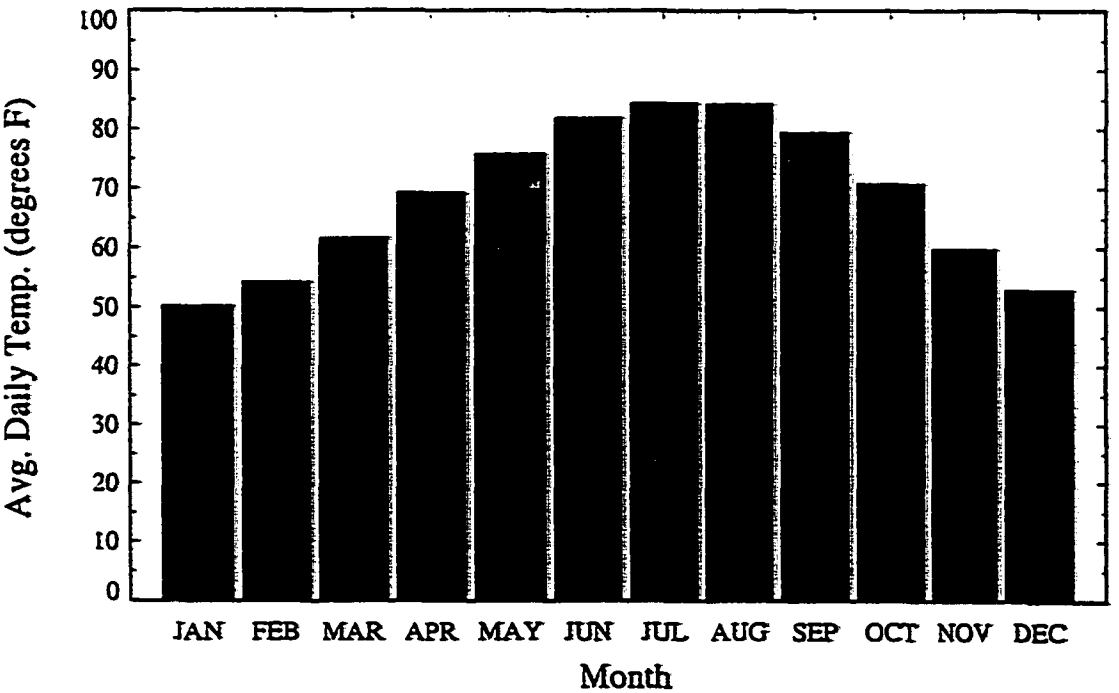

Figure 5-2 Typical average daily temperature for each month at the FSH site.

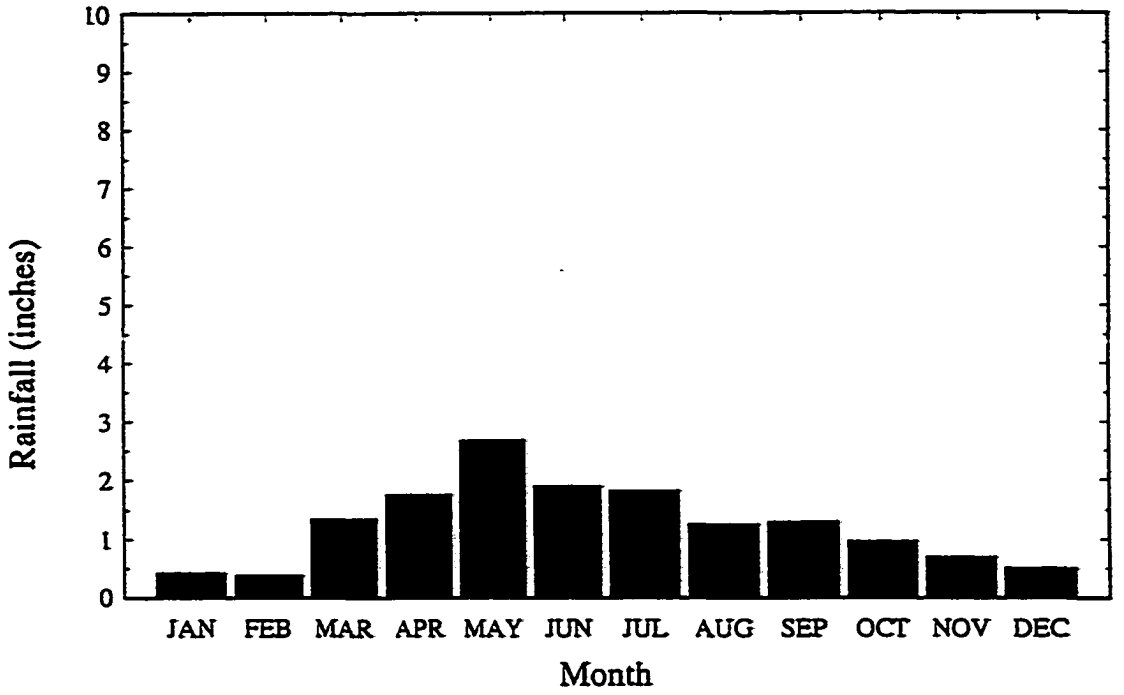

Figure 5-3 Typical monthly precipitation record for the CSU site.

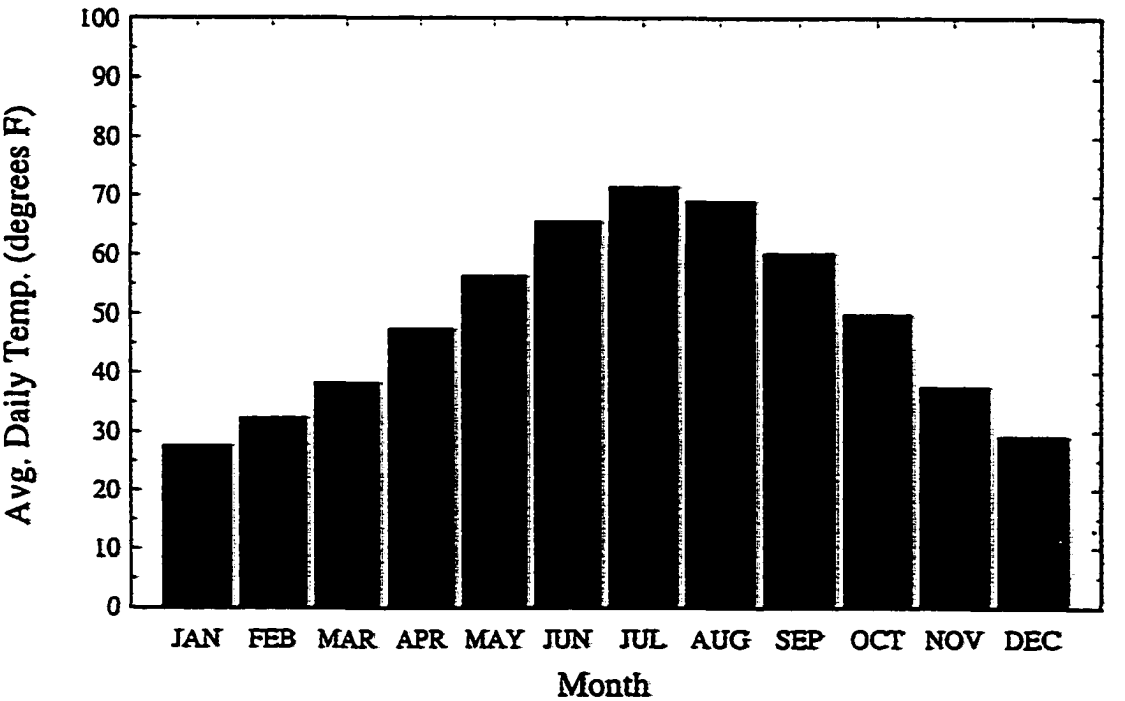

Figure 5-4 Typical average daily temperature for each month at the CSU site.

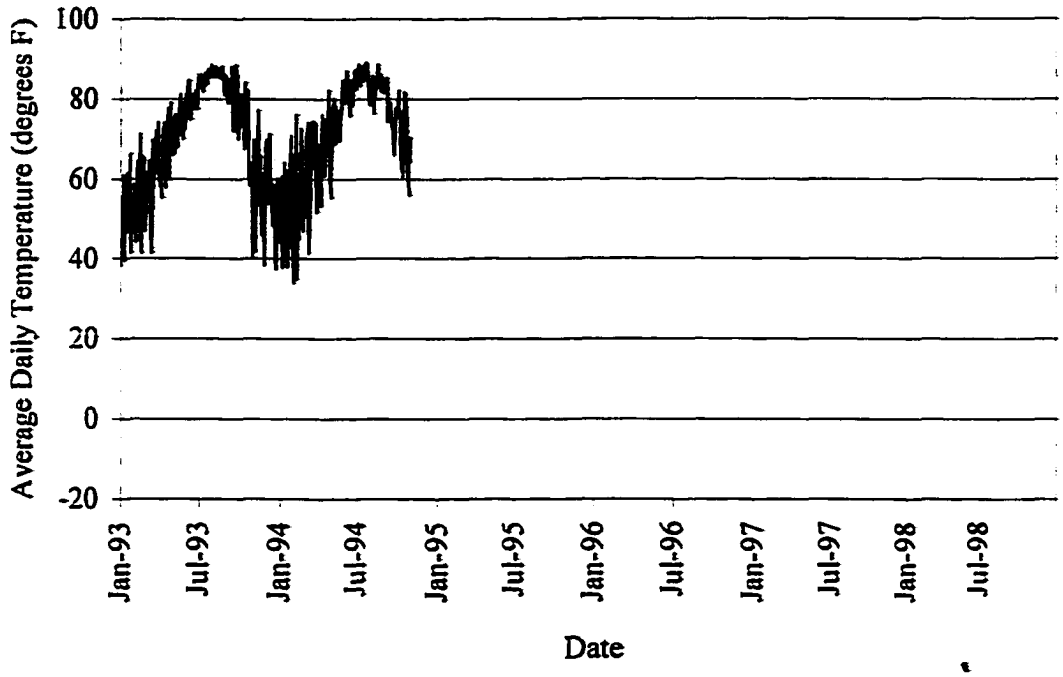

Figure 5-5 Daily average temperature data at the FSH site

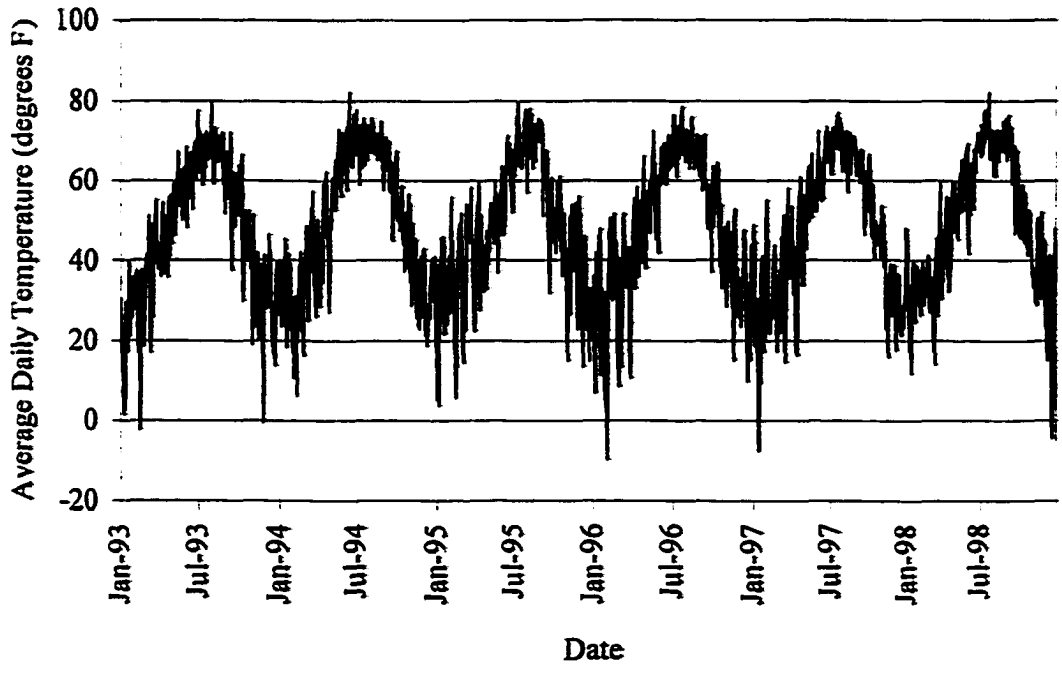

Figure 5-6 Daily average temperature data at the CSU site

Figures 5-7 and 5-8 show the cumulative precipitation at the FSH site and the CSU site, respectively. The cumulative records from both sites show how the precipitation rate increases at particular times of the year.

At the FSH site (Figure 5-7) the cumulative precipitation generally increases in the spring and early summer and again somewhat in the fall, as observed in the average data presented in Figure 5-1. Slightly more than 40 inches of precipitation occurred at the FSH site between September 1993, when the site was constructed and November 1994, when monitoring was discontinued.

At the CSU site (Figure 5-8) the cumulative precipitation generally increases in the late spring and continues into the summer. Slightly less than 120 inches of precipitation has occurred since the site was constructed in January 1993.

It should be noted at this time that the increased precipitation rate (steeper portions of the cumulative curves) generally coincide with an increase in the depth of active zone and edge moisture variation distance. This will be discussed more fully in Chapter 5.2.

Relative humidity data, wind speed data, and solar radiation data were obtained for the test sites as well. These data do not generally follow a systematic trend. However, they do influence the development of the active zone depth and edge moisture variation distance, and they are discussed more fully in Chapter 6.

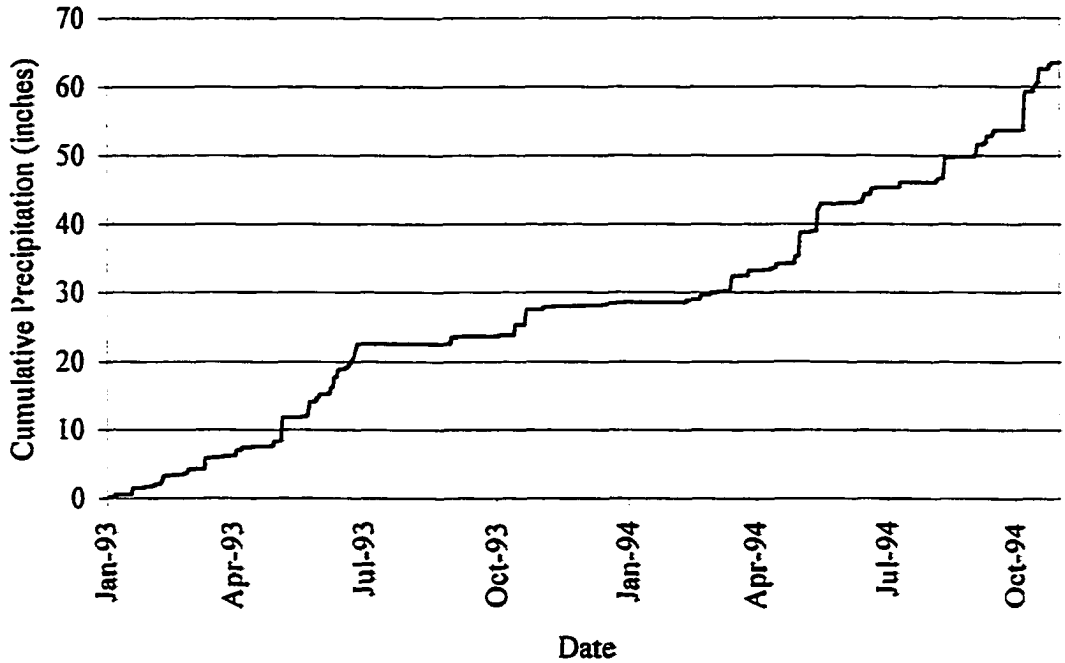

Figure 5-7 Cumulative precipitation at the FSH site

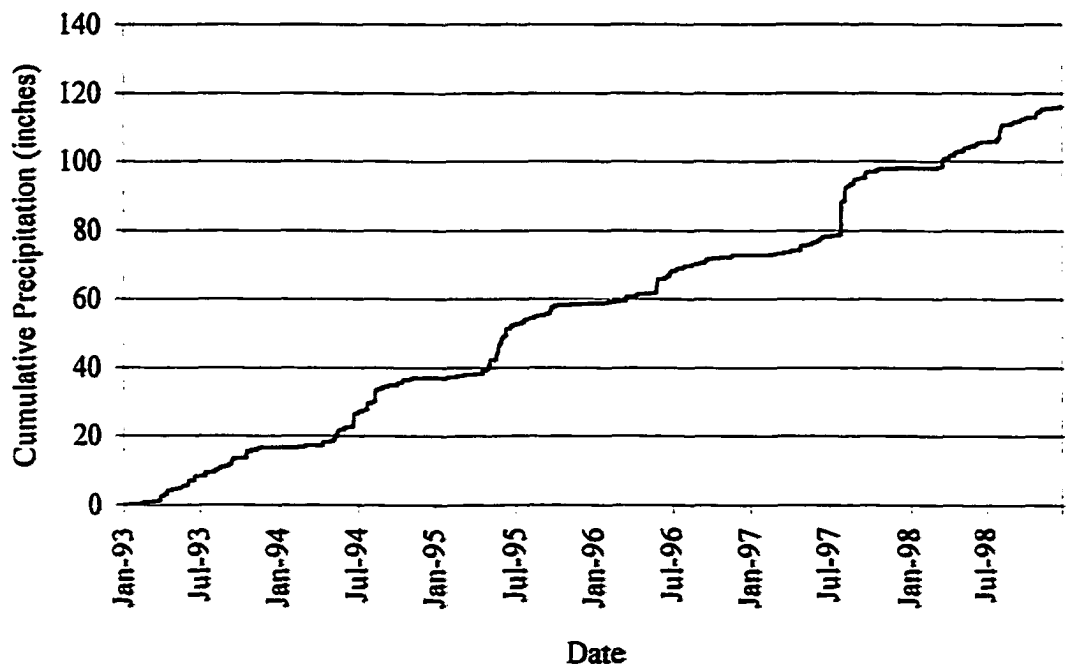

Figure 5-8 Cumulative precipitation at the CSU site

5.2 Water Content

Each test site was equipped with 49 water content access tubes. The access tubes were installed to a depth of 20 feet at the CSU site. The access tubes at the FSH site were installed to the bottom of the expansive clay where a non-expansive gravelly clay layer was encountered. The expansive clay layer at the FSH site varied between 5 and 6 feet in thickness.

The down-hole nuclear moisture gauge allows measurement at any depth within the access tubes and measurements were taken at 1-foot intervals for this investigation. The CSU site was finished on January 10, 1993 and data was collected every 4 to 6 weeks through November 2, 1997. The FSH site was finished on September 10, 1993 and data was collected monthly through November 10, 1994. The water content data for both sites are presented in Appendix C.

Figures 5-9 through 5-14 show selected water content profiles, along row 5 of the test slab, and from the uncovered soil adjacent to the test slab at the CSU site. Tube locations are shown in Figure 3-17. Access tube A-5 (Figure 5-9) is located on the eastern side of the slab, and access tube I-5 (Figure 5-13) is located on the western side. Figure 5-14 shows the average water content from access tubes J-5, E-0, and X-5 located in the uncovered soil adjacent to the slab. Data from row 5 beneath the slab are shown since it is a centerline with respect to the north-south orientation. The north south centerline is shown since a review of all the data in Appendix C indicates that water content changes along the south side of the slab generally compare well with those along the north side.

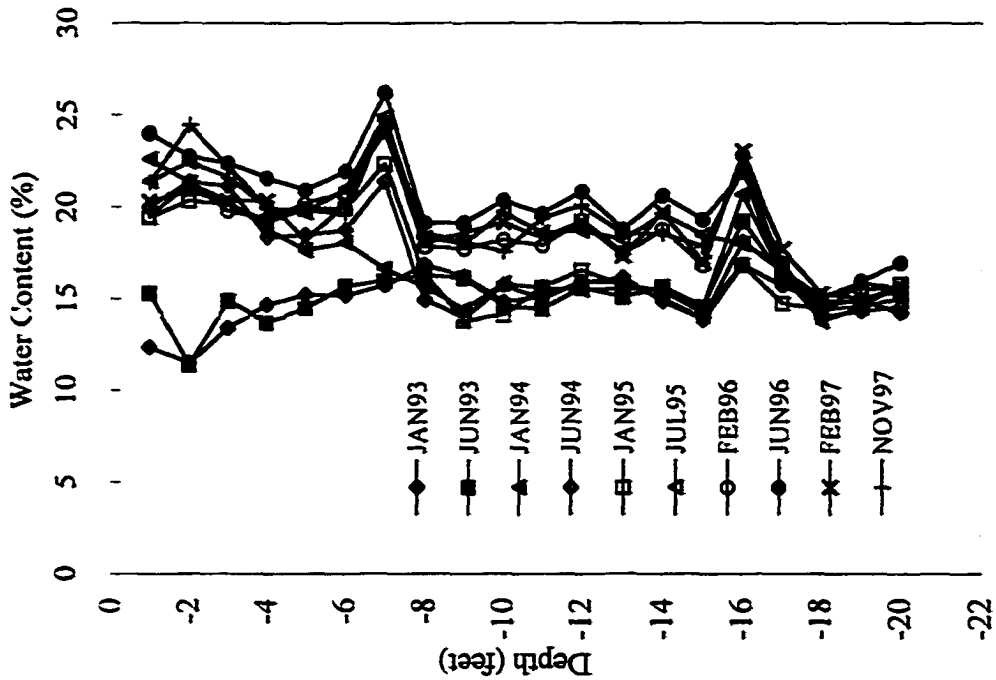

Figure 5-10 Water content profile from the CSU site (access tube B-5).

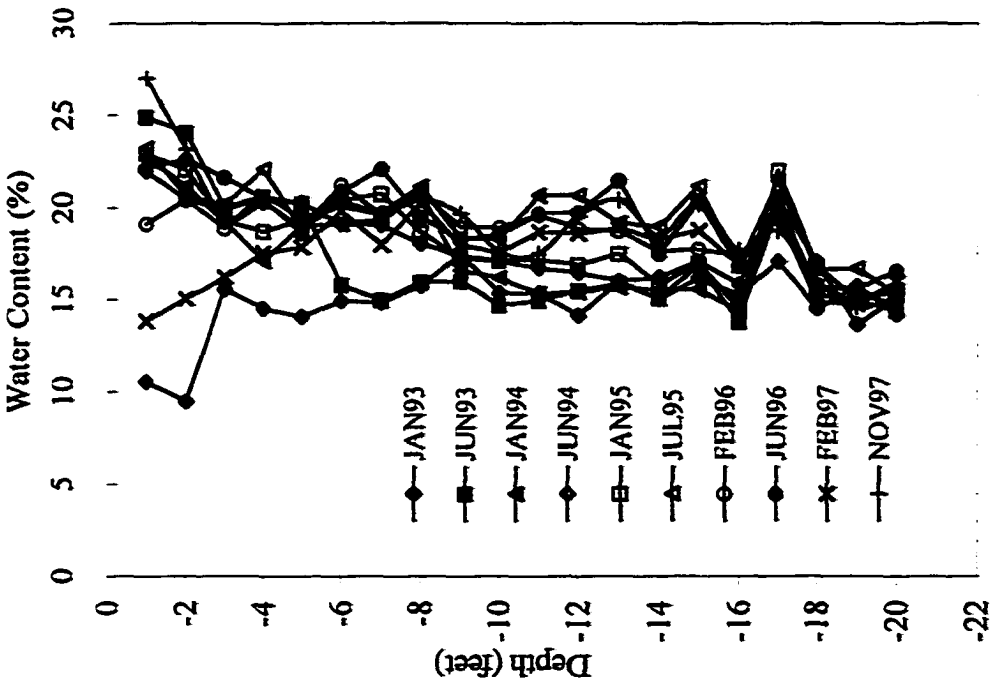

Figure 5-9 Water content profile from the CSU site (access tube A-5).

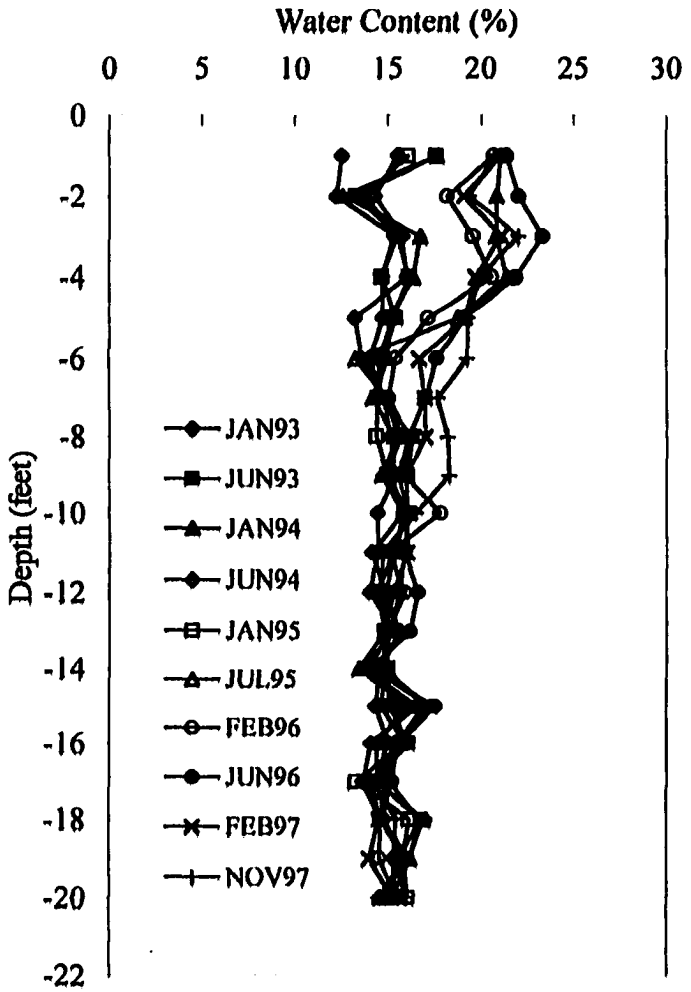

Figure 5-11 Water content profile from the CSU site (access tube C-5)

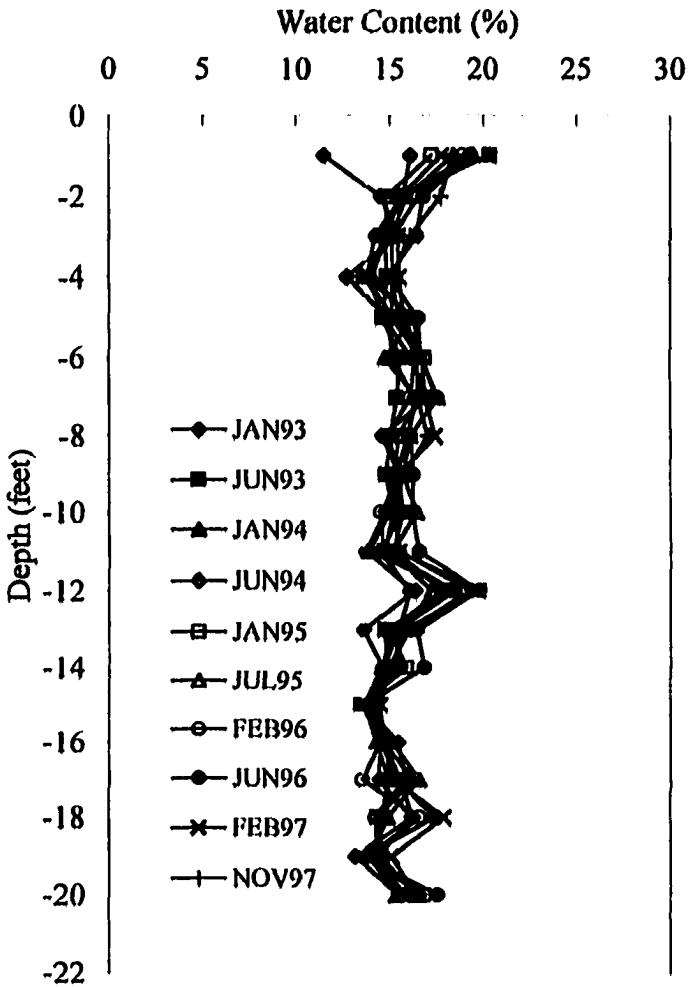

Figure 5-12 Water content profile from the CSU site (access tube E-5).

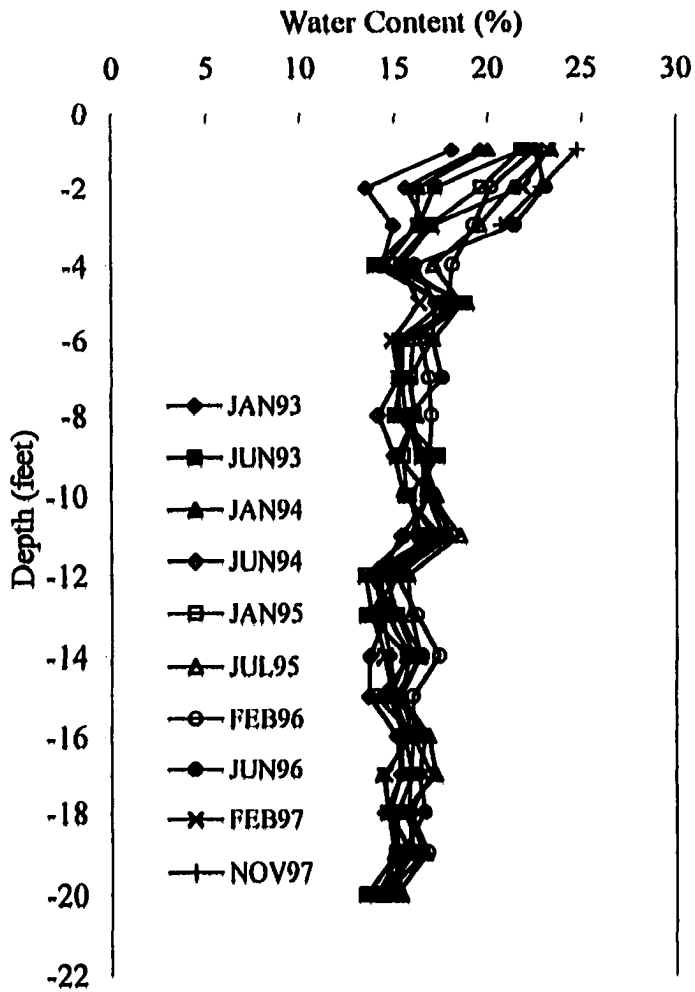

Figure 5-13 Water content profile from the CSU site (access tube I-5)

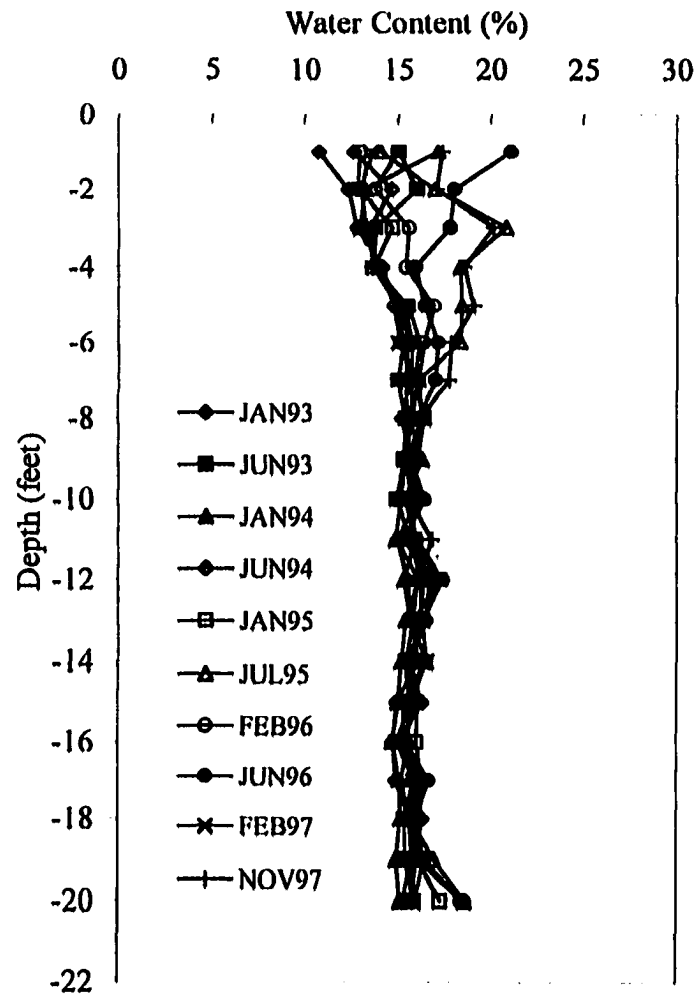

Figure 5-14 Water content profile from the uncovered soil at the CSU site (average J-5, E-0, X-5).

In general the initial water content at the site ranged from approximately 10 to 12 percent in the upper 5 to 7 feet to approximately 15 percent below 7 feet, and was relatively constant to a depth of 20 feet. Based on the profiles shown in Figures 5-9 through 5-13, the water content increase beneath the slab, west of access tube row C is limited to the upper few feet. In that area the water content near the surface has increased from the initial values of 10 percent to 12 percent to approximately 15 percent and slightly higher along the edge (see Figures 5-12 and 5-13). On the other hand the water content near the surface and at depth on the eastern side of the slab has increased to values between 25 and 30 percent (see Figures 5-9, 5-10, and 5-11). It should be noted that the plastic limit of the Pierre shale, shown in Table 4-1, ranges from 20 percent to 25 percent.

Results from previous studies conducted by Goode (1982) and Hamberg (1985) at the CSU expansive soils test site also showed a greater increase in water content generally occurred near the edge of the slab. However, in those investigations, the water content did not increase to more than 20 percent and the differential-wetting pattern from east to west was not observed.

The average water content data from access tubes J-5, E-0, and X-5 in the uncovered soil are shown in Figure 5-14. That data indicates that during dry times of the year the water content near the surface (in the upper 5 to 7 feet) of the uncovered soil decreases and during wet times of year the water content near the surface of the uncovered soil increases.

The Pierre shale is a sedimentary layer of highly overconsolidated clay shale that dips northeast at about 25°. Figure 5-15 shows a schematic of the dipping beds at the CSU site. In general, infiltration and evaporation of water from soil is a water and vapor phase flow process typically described by Darcy's law and Fick's law. In highly overconsolidated soil the particles are typically aligned parallel to the bedding plane and the transmission of water and vapor is higher along that plane.

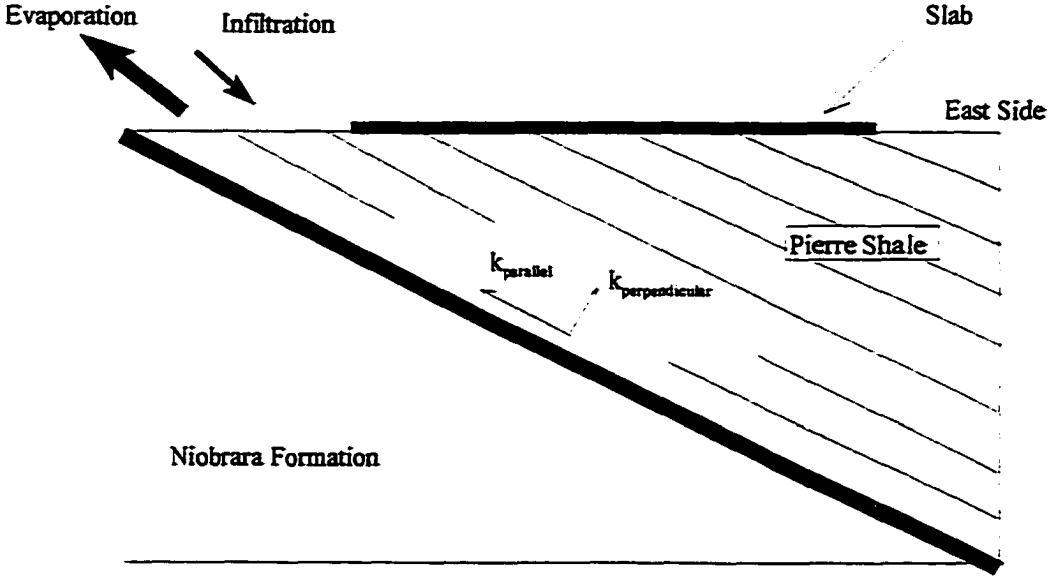

Figure 5-15 Schematic of the bedding plane at the CSU site

As a result of placing a simulated slab on the surface, infiltration and evaporation are reduced and water or vapor that flows from beneath the slab must do so laterally. Since the permeability and diffusion coefficients are functions of the tortuosity of the flow path, the rates of infiltration and evaporation will generally be higher in the direction parallel to the bedding plane. In this case the upward flow component from beneath the slab along the bedding plane is toward the western side of the slab, and flow perpendicular to the bedding plane is toward the eastern side of the slab.

It is believed that the bedding plane orientation has an effect on the wetting distribution, however, these effects can not be quantified based on the field data alone. Therefore, the effects of the bedding plane orientation were evaluated more fully with the two dimensional numerical model in Chapter 6.

The instrument accuracy must also be considered when measuring the amount of water content increase or determining the active zone depth. A series of readings were taken in two access tubes at different depths to examine the reproducibility of the CPN nuclear gauge. The results, shown in Appendix A, indicate that the gauge has a reproducibility of 2 to 3 percent. Examination of the water content data indicates that a 2 to 3 percent variation in water content occurred in all of the access tubes at all depths. This fluctuation is attributed to scatter in the gauge. Thus water content increase was based on changes greater than 2 to 3 percent.

Water content profiles from the FSH site are shown in Figures 5-16 through 5-19. Figure 5-16 is from access tube A-5 on the southern side of the slab. Figures 5-17 and 5-18 are from D-5 near the center of the slab and I-5 on the northern side of the slab, respectively. Figure 5-19 is the average from access tubes J-5, E-10, and X-5 located in the uncovered soil adjacent to the simulated slab.

The data shown in Figures 5-16 through 5-18 and in Appendix C indicate that the water content beneath the simulated slab at the FSH site increased steadily for the first 4 or 5 months, and decreases in water content during dry periods were small. In contrast the data presented in Figure 5-19 from the uncovered soil shows that the water content in the uncovered soil fluctuates seasonally. This is expected in the uncovered soil.

The FSH site was completed on September 10, 1993, following a period of 80 days without precipitation. The highest measured water content in the upper 5 to 6 feet, not including some suspected erroneous readings at the bottom of some access tubes, is approximately 19 percent. The water content beneath the center of the slab where the effects of evaporation or the introduction of water from external sources such as irrigation or flooding are minimal tends to be very close to 19 percent. However, monitoring of the FSH site was discontinued after November 1994 and the limited data does not allow comprehensive analyses. It should also be pointed out that the plastic limit of the Texas soil as shown in Table 4-2 is approximately 21 percent, still slightly higher than measured water contents beneath the slab.

5.2.1 Assessment of the Depth of the Active Zone

Active zone depth was defined in Chapter 1. The water content profiles shown in Figures 5-9 through 5-14 and in Appendix C for the CSU site show a significant amount of wetting along the eastern side and initial wetting at shallow depths over the entire site. In general the depth of water content increase at these locations identifies the depth of the active zone since the soil throughout the depth of water content increase is expansive and has a swell pressure greater than the overburden pressure within the profile.

However, an important distinction can be made at the CSU site between the depth of the active zone on the eastern side of the slab and the depth of the active zone on the western side of the slab. Figure 5-20 shows conceptual water content profiles in a soil deposit that is fairly uniform with depth.

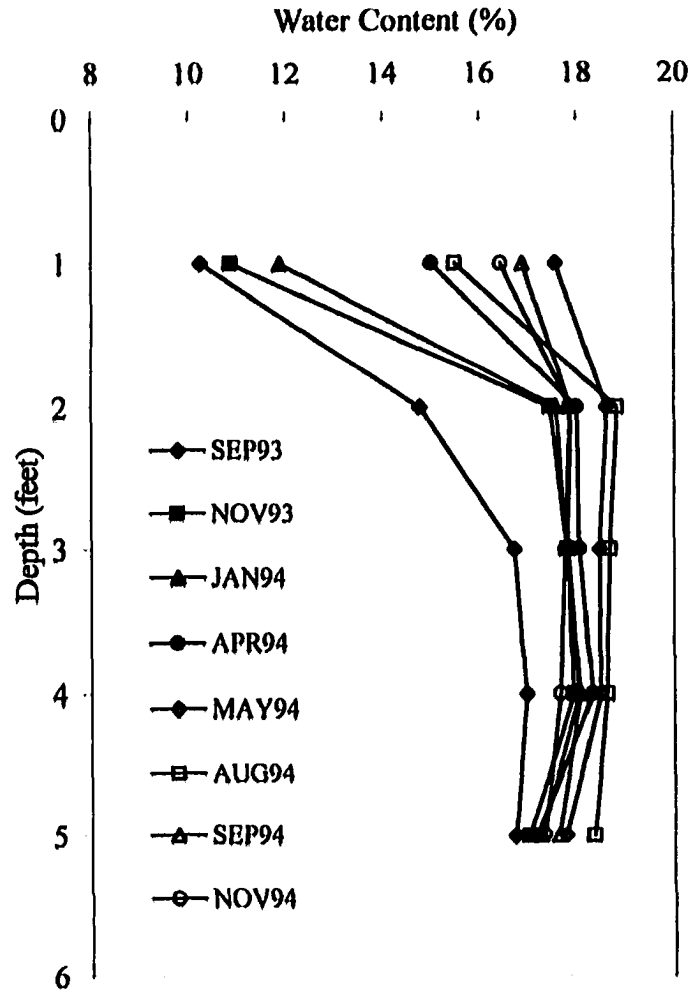

Figure 5-16 Water content profile from the FSH site (access tube A-5).

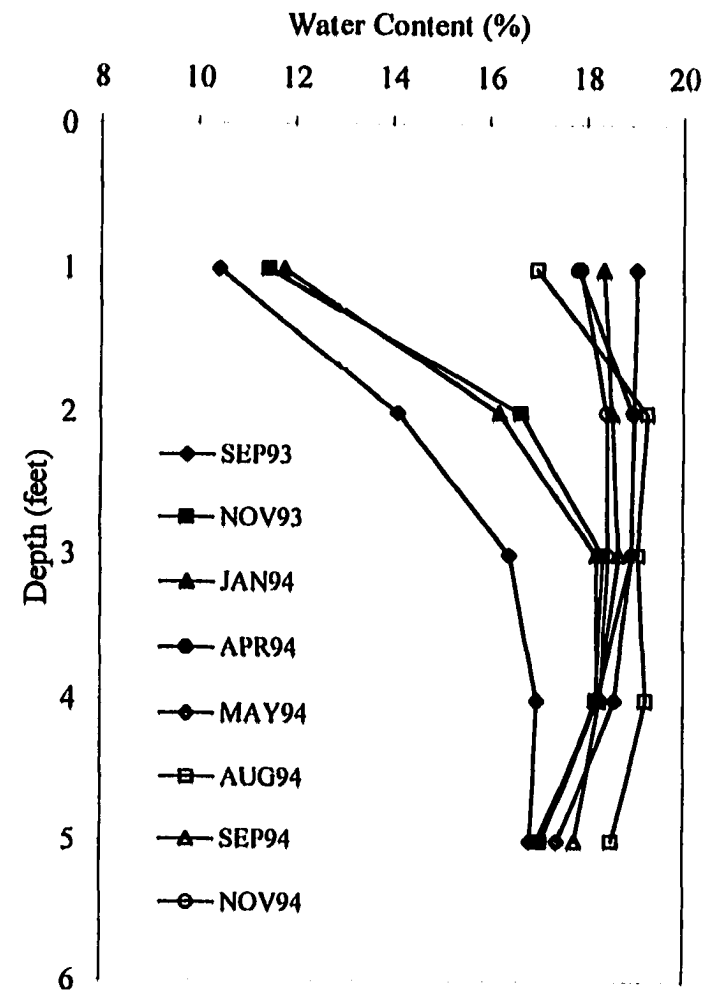

Figure 5-17 Water content profile from the FSH site (access tube D-5).

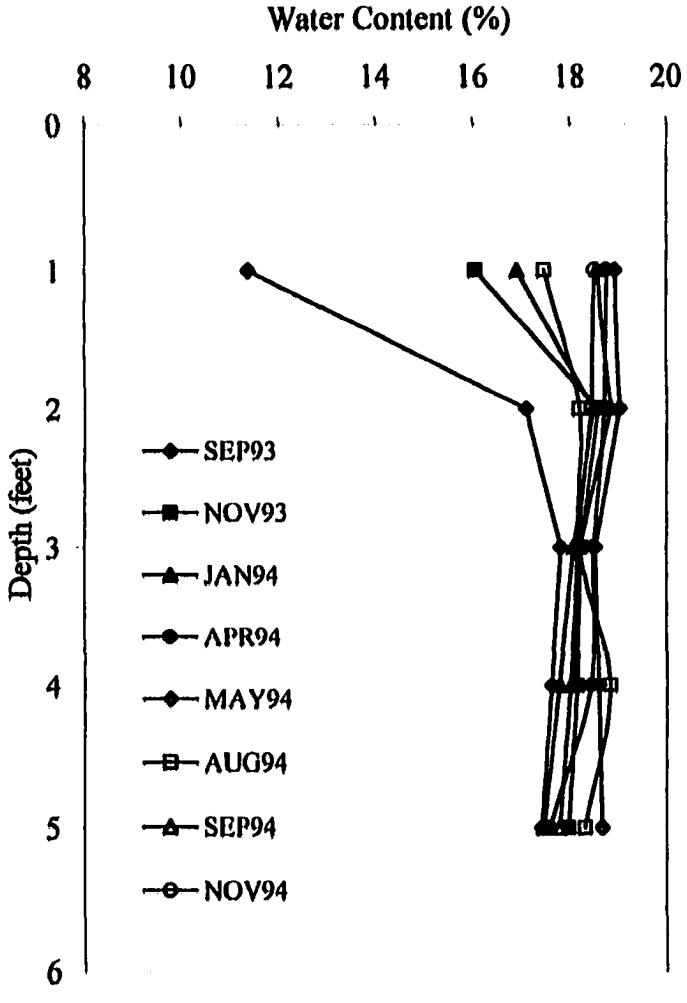

Figure 5-18 Water content profile from the FSH site (access tube I-5).

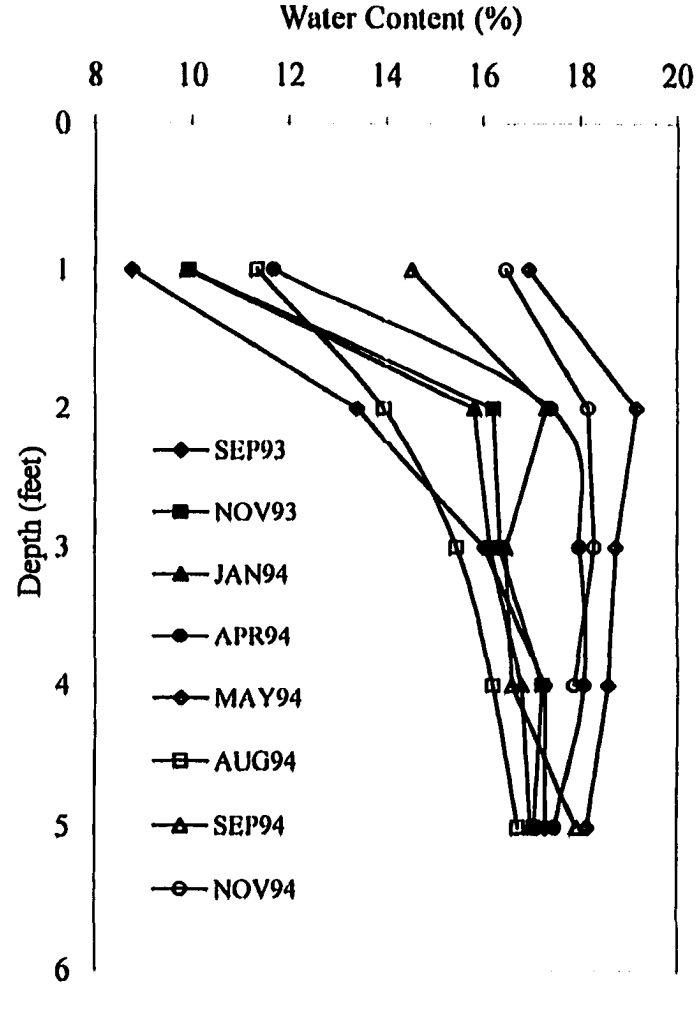

Figure 5-19 Water content profile from the uncovered soil at the FSH site (average J-5, E-10, X-5).

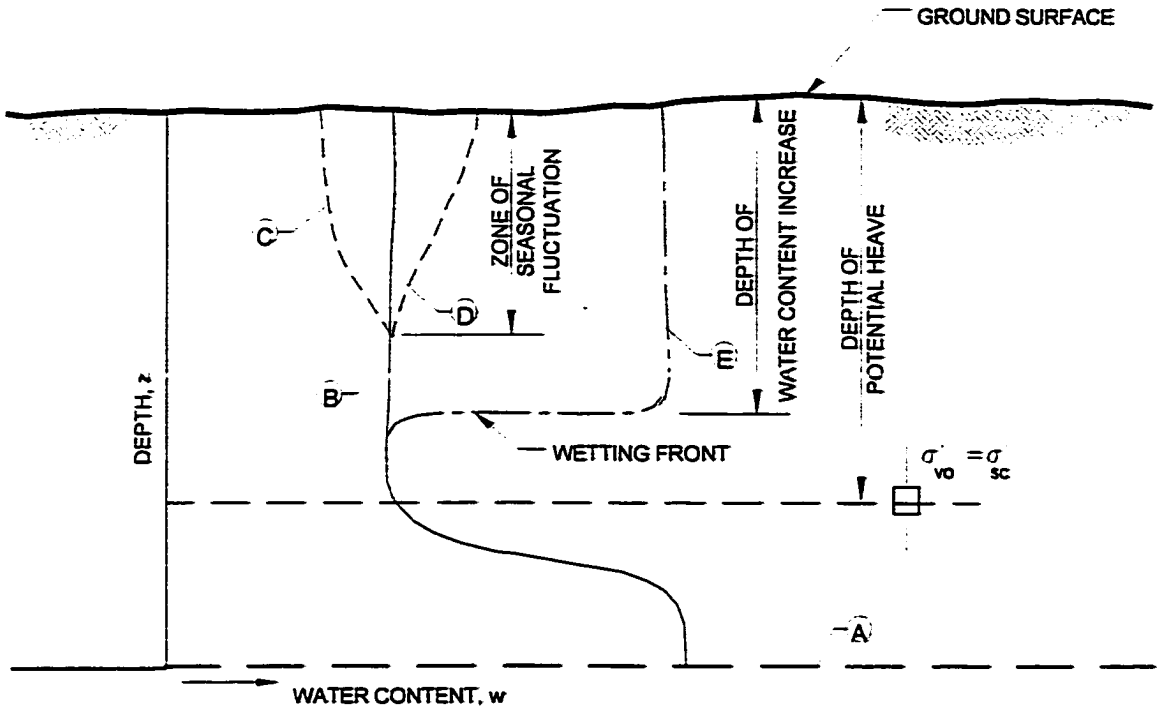

Figure 5-20 Conceptual water content profiles for a fairly uniform soil

Considering line A as a fairly deep water table, the hydrostatic equilibrium water content profile in a fairly uniform soil is represented by the soil water characteristic curve depicted by line B. During a relatively dry time of the year, the water content in the upper soil layers is depleted to below hydrostatic conditions and the distribution is represented by line C. Generally, during wetter times of the year the water content will increase in the upper soil layers and the water content distribution will look like line D in Figure 5-20. The depth to which these fluctuations between line C and line D occur is referred to as the depth of seasonal moisture fluctuation. For this investigation the water content distribution below that point is referred to as the equilibrium water content.

In general when a slab is constructed at the surface evaporation and infiltration are significantly reduced and in the ideal case of zero infiltration or evaporation the water

content approaches the soil water characteristic curve. Small fluctuations will continue with time near the surface based on the temperature fluctuations and edge effects.

When the surface of the soil at the CSU site was covered the water content in the upper few feet was approximately 10 to 12 percent and increased to approximately 15 percent at a depth of 5 to 7 feet. Below 7 feet the water content profile in January 1993 was constant with depth. Measurements in the uncovered soil shown in Figure 5-14 indicate that the water content in the upper 5 to 7 feet of soil fluctuates with climate. Therefore, the upper 5 to 7 feet at the CSU site is the depth of seasonal moisture fluctuation, and for the purposes of this investigation the water content value of 15 percent represents the equilibrium water content.

Data from the center and western side of the slab, in Figures 5-12 and 5-13 and other locations shown in Appendix C, indicate that the water content has increased to the equilibrium water content and remains relatively constant with small seasonal fluctuations. Therefore, the depth of the active zone in the center and on the western side of the CSU site is currently equal to the depth of seasonal moisture fluctuation.

Conversely, data from the eastern side of the slab, in Figures 5-9, 5-10, and 5-11 and other locations shown in Appendix C, indicate that the water content has increased to between 20 and 25 percent. Therefore, the water content on the eastern side of the site has increased to values higher than the equilibrium water content. Referring to Figure 5-20 this condition is represented by line E and results from infiltration that is introduced through irrigation, extreme climatic conditions or other external influences. This depth of water content increase is identified from the water content profiles as the depth to which

the water content has increased to greater than the equilibrium water content. Therefore, on the eastern side of the slab the depth of the active zone is equal to the depth of water content increase.

Currently the maximum depth of water content increase identified at the CSU site at access tube A-5 is approximately 18 feet, as shown in Figure 5-9. The water content increase reached 18 feet by May 1995 and based on these water content profiles has not been recorded deeper since that time.

Figure 5-21 shows the depth of water content increase for access tube A-5 at CSU and the cumulative precipitation at CSU as functions of time.

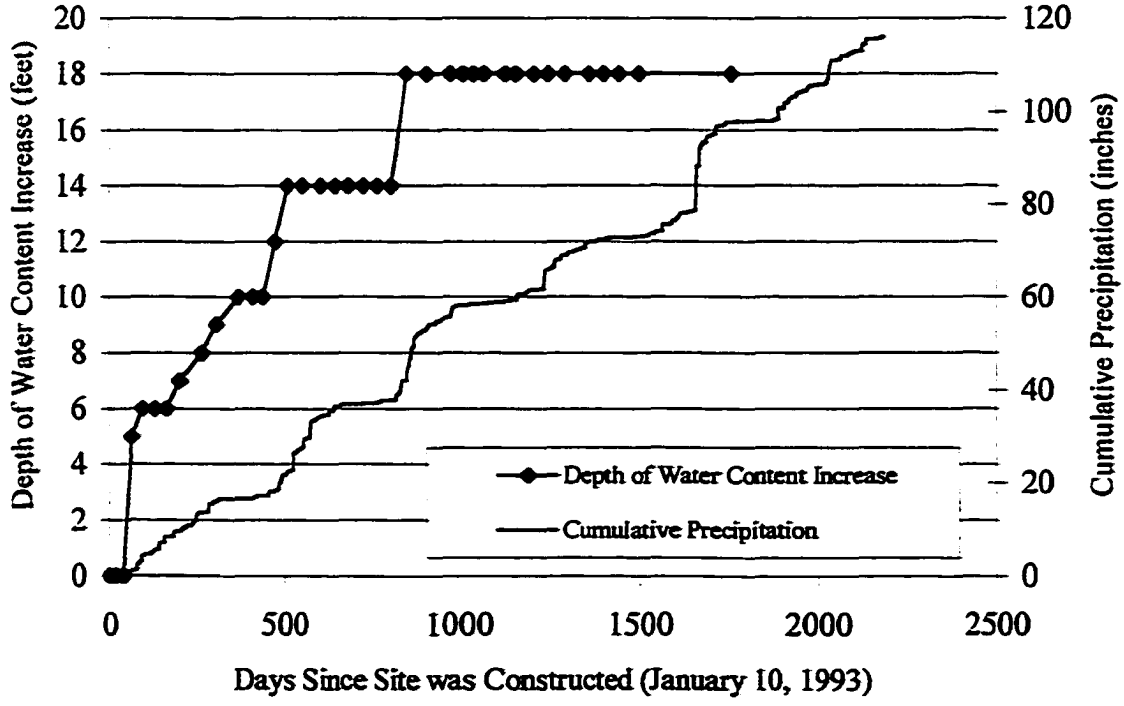

Figure 5-21 Depth of water content increase and cumulative precipitation as functions of time from access tube A-5 at the CSU site

The depth of water content increase increased steadily to approximately 18 feet, the maximum recorded for this site. However, determination of depth of water content increase from water content profiles is dependent upon interpretation of the data, and additional water content increases may have occurred that are not distinguishable within the accuracy of the gauge and frequency of measurement. There were four steep increases in the first 856 days of the study. These increases generally follow short periods of no increase and tend to coincide with an increase in the rate of rainfall accumulation. The rate of rainfall accumulation typically increases in the spring when there is also an increase in temperature. The increased surface temperature results in a thermal gradient that causes an increase in downward flow from the warmer to the cooler regions of the soil. Since May 1995 the depth of water content increase has remained constant indicating that for the current boundary conditions the soil has reached steady-state water content distribution and the depth of the active zone is 18 feet.

Figure 5-22 shows the depth of water content increase as a function of time at four locations beneath the eastern side of the slab. Access tube A-5 is located along the edge, access tube A.5-3 is located 2.5 feet inward from the edge, and access tubes B-5 and C-5 are located 5 and 10 feet inward from the edge, respectively. The depth of water content increase is deepest along the edge of the slab (A-5) and decreases with distance inward from the edge (A.5-3, B-5, and C-5). In addition the time for the water content to increase near the center of the slab (C-5) is greater than at the edge (A-5).

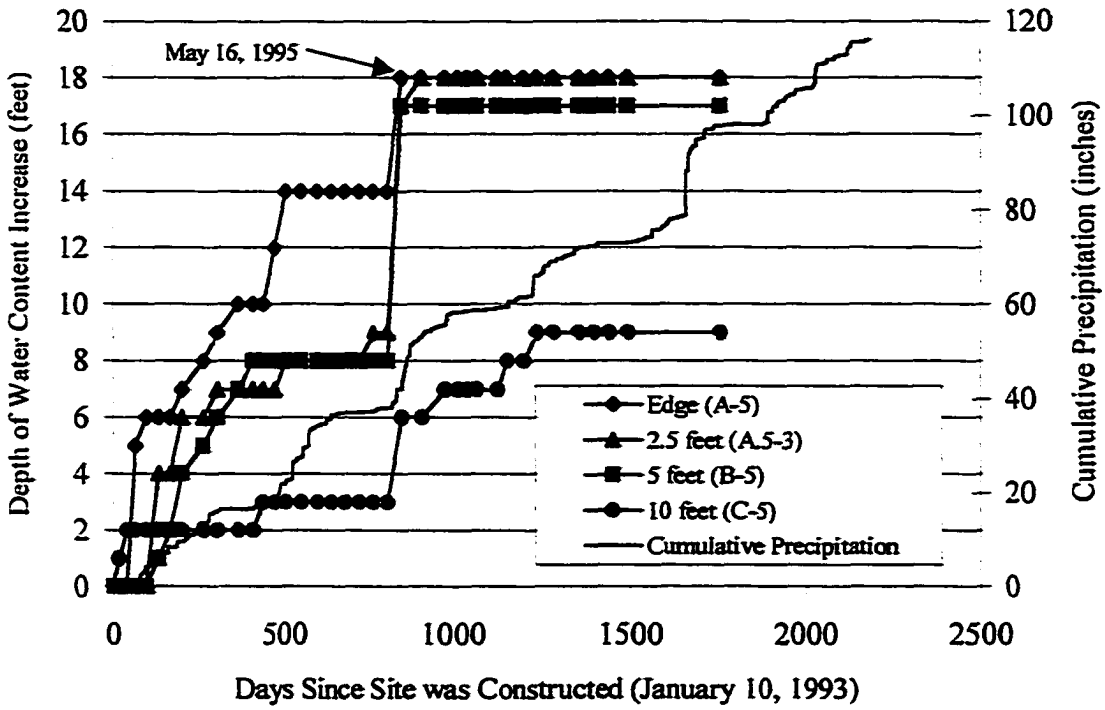

Figure 5-22 Depth of water content increase as a function of time at the edge, 2.5 feet inward, 5 feet inward, and 10 feet inward.

This behavior indicates that an edge lift condition exists at the CSU site. An edge lift condition usually exists when water is introduced at the soil surface along the edge of the slab by precipitation, sprinklers or irrigation. Sprinklers and irrigation have not been used at the site to introduce water along the east edge. However, as mentioned above, there is a berm along the eastern edge of the slab that has a tendency to pond water near the edge of the slab during precipitation events or due to snowmelt. The correlation of depth of water content increase with steep increases in cumulative precipitation and the movement of water from the edge toward the center, shown in Figure 5-22, indicate that water is infiltrating from the surface along the eastern edge of the slab and migrating laterally (westward) and downward. The effects of the berm are likely the cause of the water

content increases above 20 percent observed in this study but were not observed in previous investigations (Goode (1982) and Hamberg (1985)). Given the likelihood that water is ponding along the eastern side of the slab it is also likely that the depth of water content increase will eventually go deeper if the berm is left in place.

The depth of water content increase at the FSH site extended to a depth of 5 feet after only 53 days from the date of installing the slab. Since the expansive soil layer at the FSH site extends to approximately 5 or 6 feet and is underlain by gravelly, non-expansive clay, the maximum active zone depth, by definition, is 6 feet even if the depth of water content increase was greater than 6 feet. The depth of seasonal moisture fluctuation at the FSH site also appears to be equal to 5 or 6 feet, based on data in Figure 5-19. Water content measurements were not obtained in the non-expansive soil beneath 6 feet.

The water content data presented thus far indicate the following:

- Given the current boundary environmental conditions the depth of the active zone at the CSU site is equal to the depth of water content increase.
- The depth of the active zone at the CSU site currently is 18 feet.
- The water content at the CSU site has increased to values greater than the equilibrium water content and the plastic limit.
- The maximum active zone depth at the FSH site is 6 feet due to the limited expansive soil layer thickness.
- The water content at FSH has not reached the plastic limit

In addition the differential moisture migration patterns observed at the CSU site can be attributed to:

- Reduced evaporative flow due to the placement of the slab at the surface, and
- Ponded water along the eastern side of the slab after precipitation events.

It is also believed that the bedding plane orientation at the CSU site effects the development of the active zone and differential wetting pattern that has been observed but these effects are not definable based on field data alone.

5.2.2 Edge Moisture Variation Distance

From the water content profiles presented earlier and contained in Appendix C it can be seen that the water content in the upper few feet of soil beneath the slab continues to fluctuate with seasonal fluctuations after the soil surface has been covered. Although there is an initial increase in water content due to the slab construction the cyclical evaporative and infiltration behavior around the edge of the slab influences the water content beneath the slab and inward toward the center. The distance inward over which the water content fluctuates is referred to as the edge moisture variation distance.

The development of the edge moisture variation distance can be observed by plotting the water content distribution under the slab as a function of position and time. Because of scatter in the data and general heterogeneity of the soil, it is sometimes difficult to observe these trends. Figure 5-23 was prepared to demonstrate how idealized data would appear in such a plot. At a distance, e, sufficiently far from the edge, the water content is shown to increase initially due to the reduction of evapo-transpiration from the soil. After the increase to an equilibrium value it remains constant with time. At the edge of the slab the water content is shown to increase initially and then fluctuate cyclically with seasonal fluctuations. At intermediate distances inward from the edge of the slab the cyclic fluctuations are lower in magnitude. The distance in from the edge at which the fluctuations are no longer observed is the edge moisture variation distance.

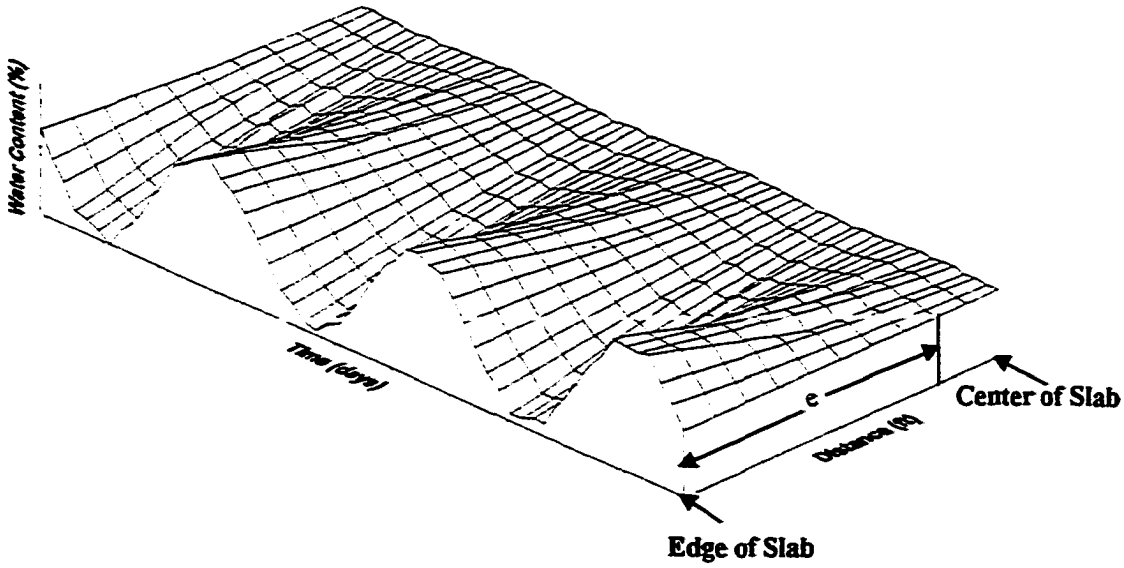

Figure 5-23 Idealized plot of water content as a function of time and distance from the edge of a slab

Figures 5-24 through 5-31 show the water content-distance-time surfaces for several locations at the CSU site. The sinusoidal shape at the edge, as shown in the idealized plot, does not appear clearly in these figures, but comparison of that data with Figure 5-23 allows the reader to observe the pattern of changes that would indicate edge moisture variation distance.

It was shown in Chapter 5.2.1 that the eastern side of the test slab has experienced a greater increase in water content than the western side of the slab. Figures 5-24 and 5-25 are for instrumentation lines in the eastern half of the slab. Although the cyclic seasonal fluctuations are not as definite as depicted in Figure 5-23 it is evident that the water content fluctuations near the edge of the slab are greater than near the center of the slab. In Figure 5-24 relatively large fluctuations occur between 0 and 10 feet from the edge of the slab and some argument could be made that the edge moisture variation distance is as

high as 17 to 20 feet, half the length of the slab. However, the maximum edge moisture variation distance is equal to half of the shorter lateral dimension, in this case 15 feet north to south.

Figures 5-26 and 5-27 show water content-distance-time surfaces for the western half of the site. An apparent edge moisture variation distance of about 15 feet can be seen. The remaining figures for the north and south edges of the slab do not indicate clear results with regard to edge moisture variation distance.

The data presented in Figures 5-24 through 5-31 represents approximately 5 years of data. When one considers that active heave can continue for 10 or more years and the edge moisture variation distance is intended to represent a steady state condition, it is evident that a longer record of data is needed to draw conclusions. However, two-dimensional numerical simulations were conducted in Chapter 6 that can be used to better estimate the long-term conditions.

Figures 5-32 through 5-39 show the water content-distance-time surfaces for various locations at the FSH site after 14 months. In all of those plots the initial water content increase is large compared to the fluctuations due to climate and no trends with regard to edge moisture variation distance are evident. In addition, monitoring of the FSH site was discontinued after 14 months and the limited data does not provide for an assessment of edge moisture variation distance.

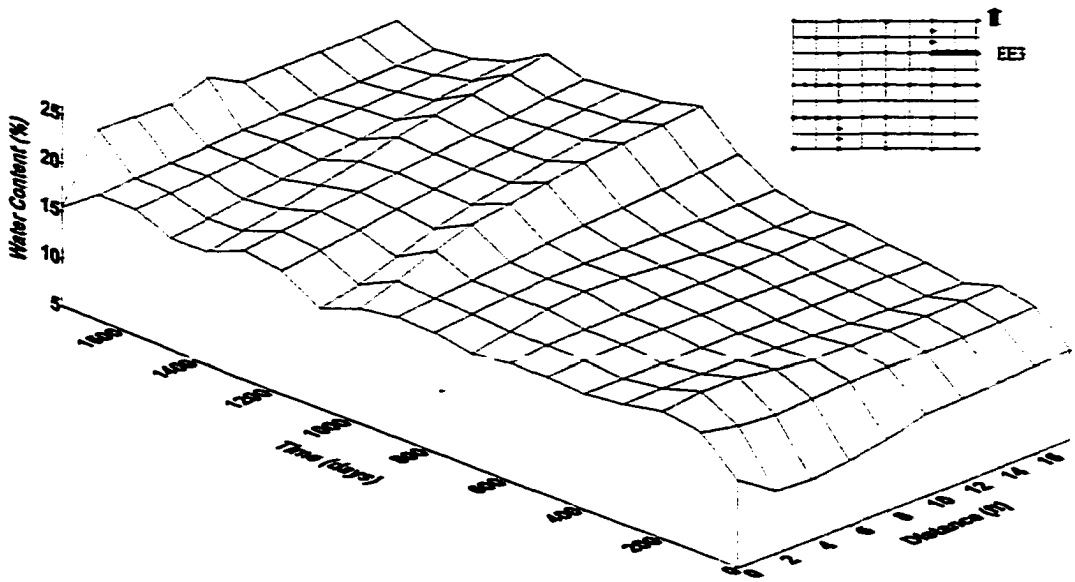

Figure 5-24 Water content as a function of time and distance from the east edge along row 3 (EE3) of the CSU site at a depth of 1 feet.

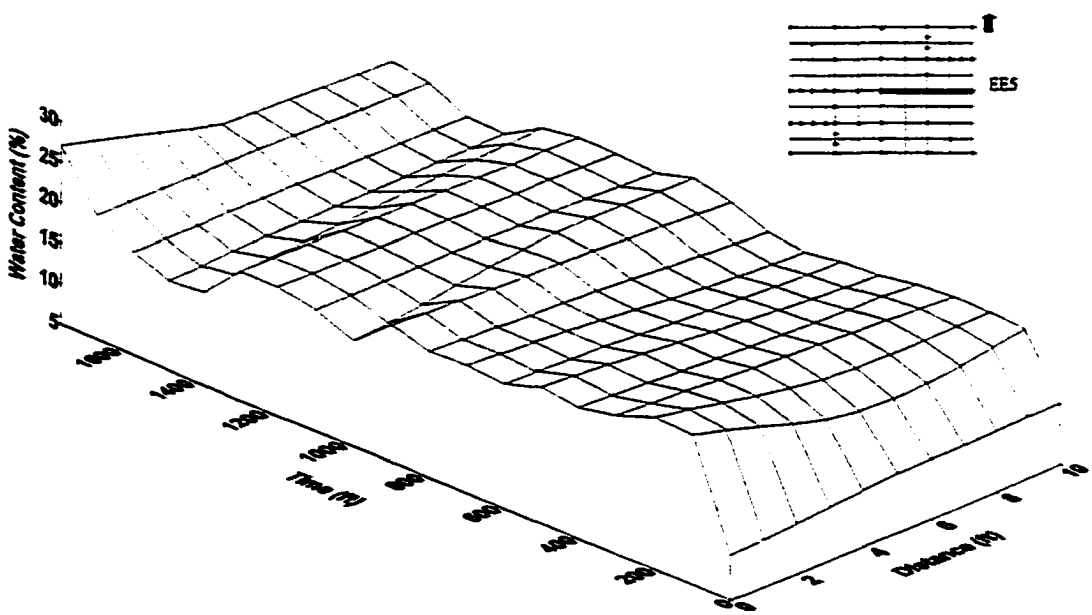

Figure 5-25 Water content as a function of time and distance from the east edge along row 5 (EE5) of the CSU site at a depth of 1 feet.

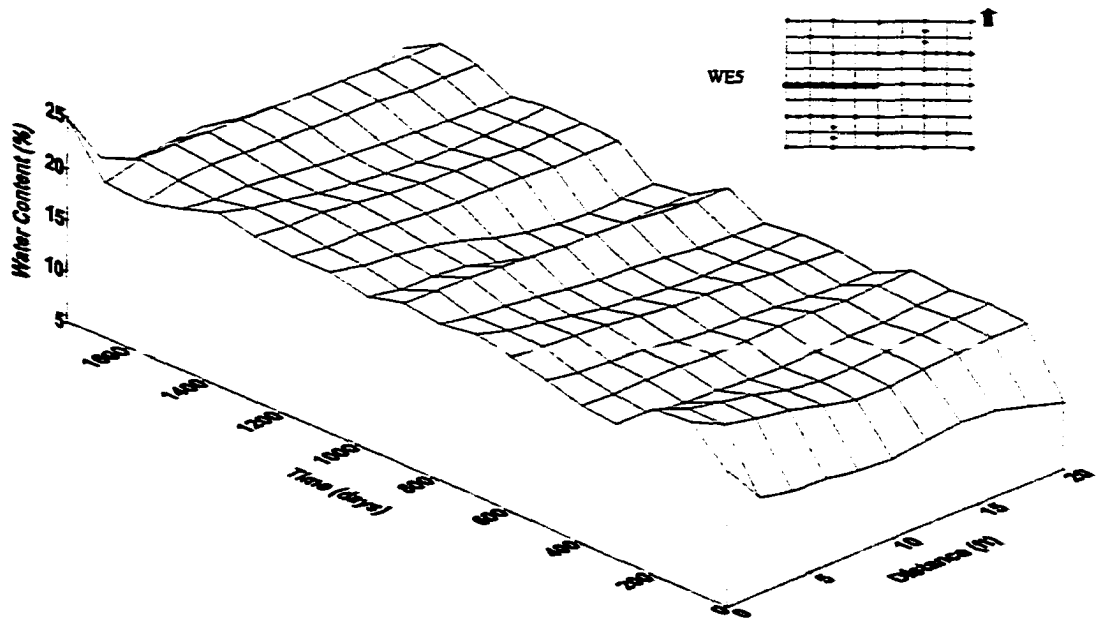

Figure 5-26 Water content as a function of time and distance from the east edge along row 5 (WE5) of the CSU site at a depth of 1 feet.

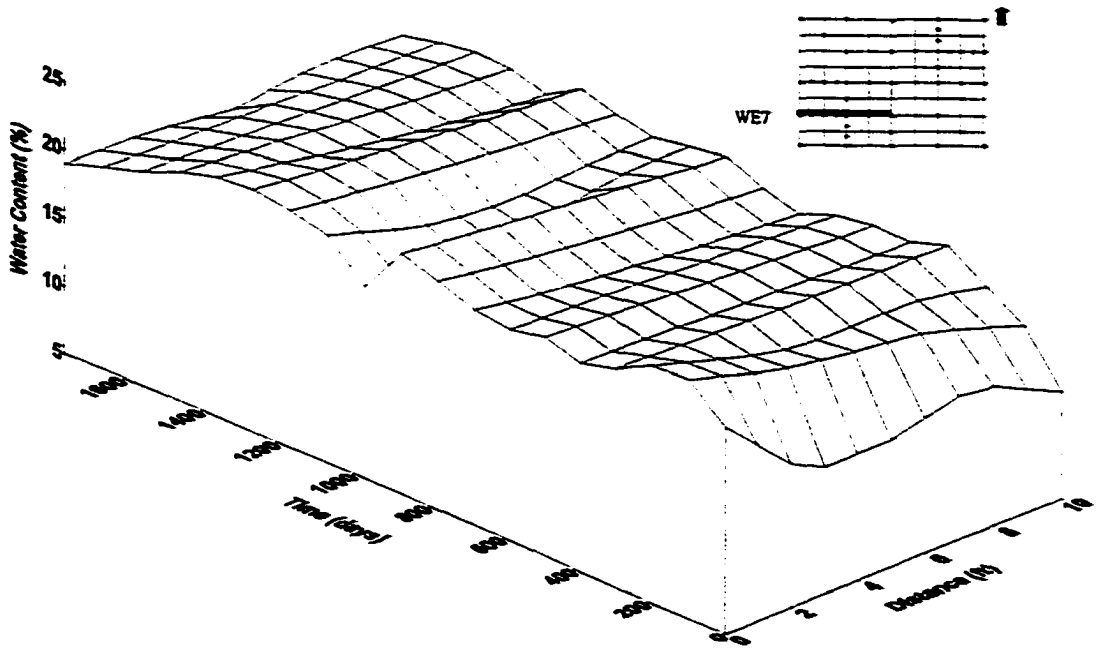

Figure 5-27 Water content as a function of time and distance from the west edge along row 7 (WE7) of the CSU site at a depth of 1 feet.

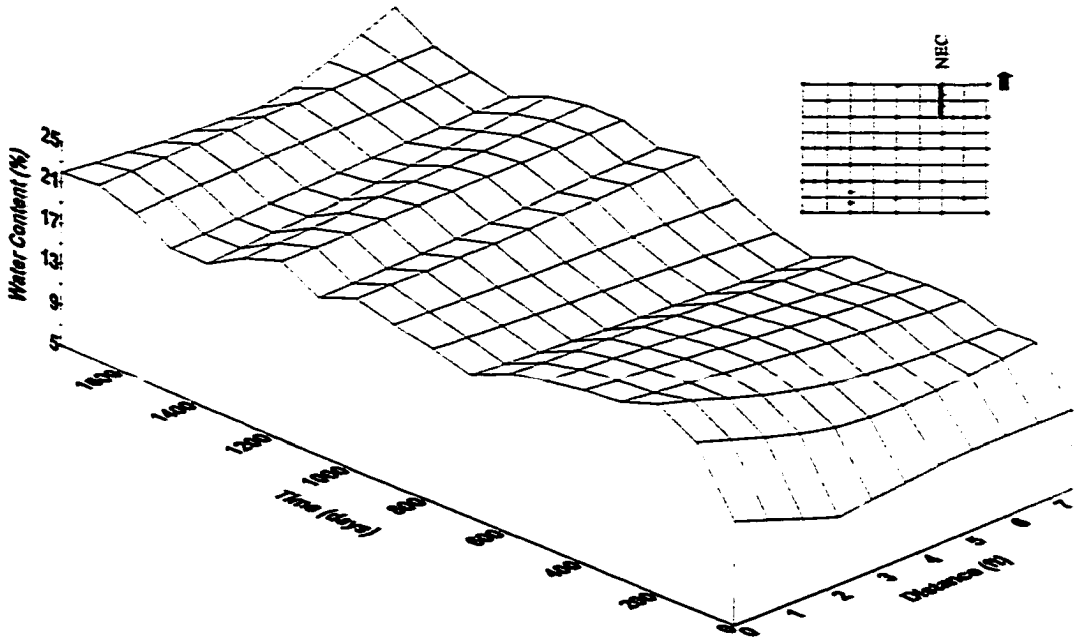

Figure 5-28 Water content as a function of time and distance from the north edge along line C (NEC) of the CSU site at a depth of 1 feet.

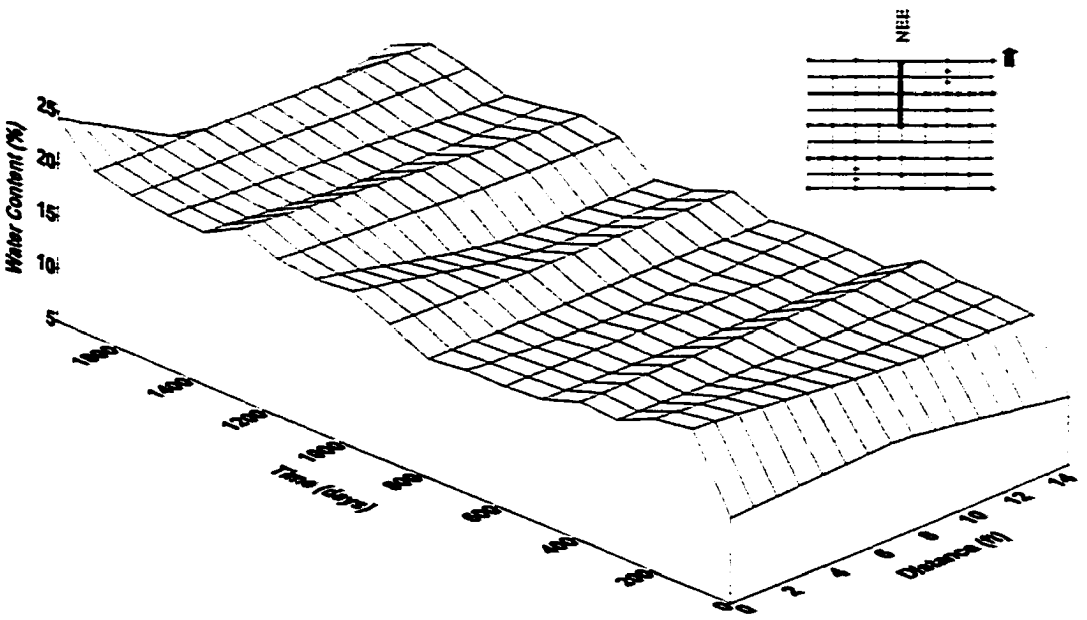

Figure 5-29 Water content as a function of time and distance from the north edge along line E (NEE) of the CSU site at a depth of 1 feet.

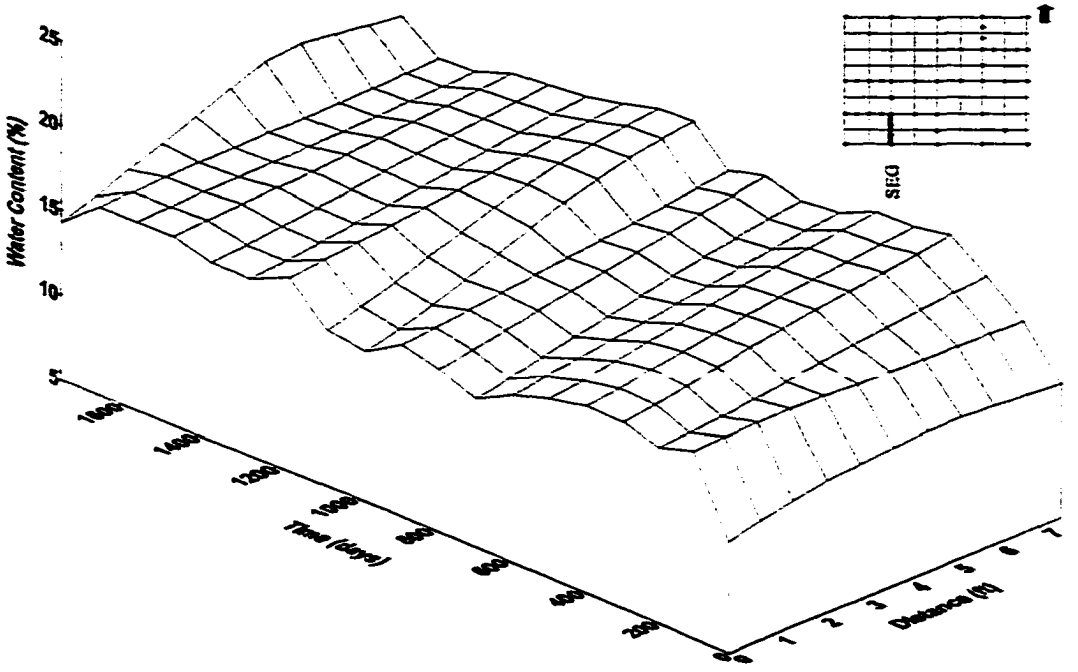

Figure 5-30 Water content as a function of time and distance from the south edge along line G (SEG) of the CSU site at a depth of 1 feet.

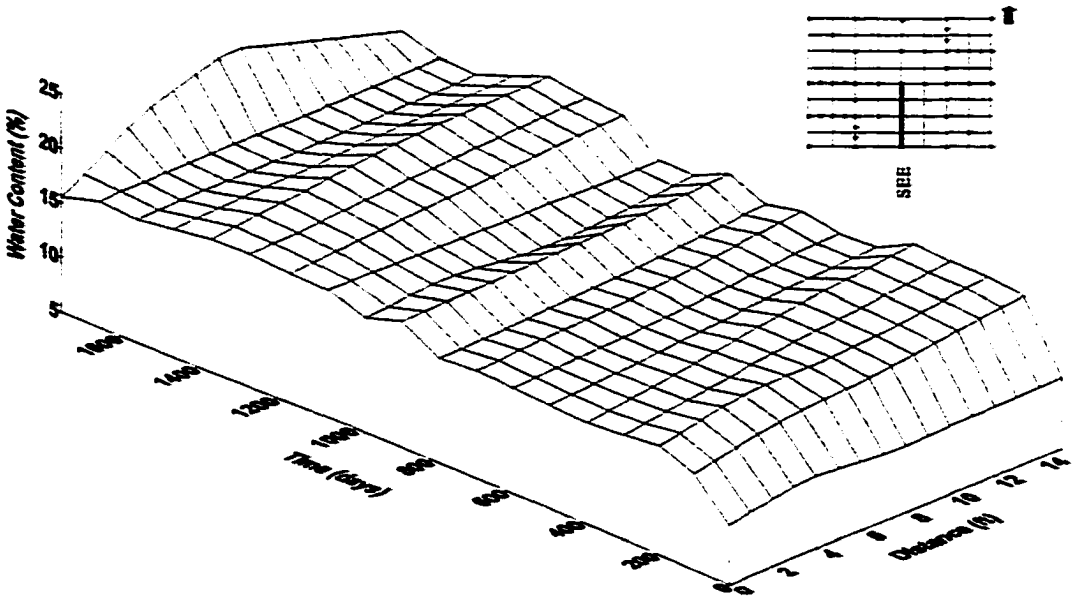

Figure 5-31 Water content as a function of time and distance from the south edge along line E (SEE) of the CSU site at a depth of 1 feet.

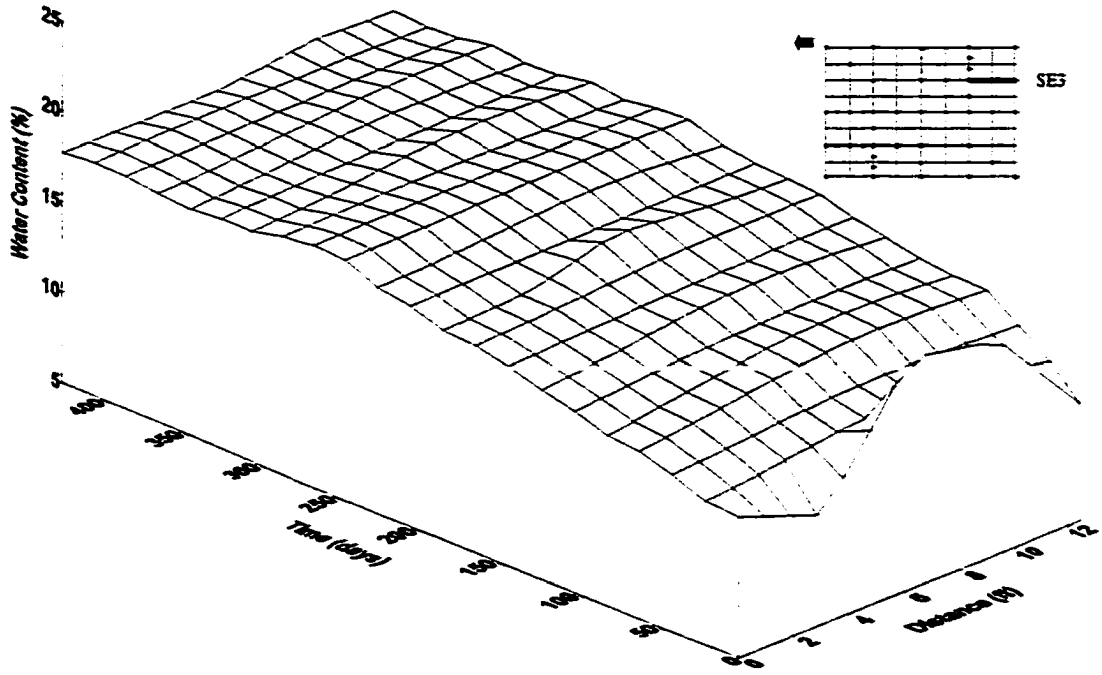

Figure 5-32 Water content as a function of time and distance from the south edge along row 3 (SE3) of the FSH site at a depth of 1 feet.

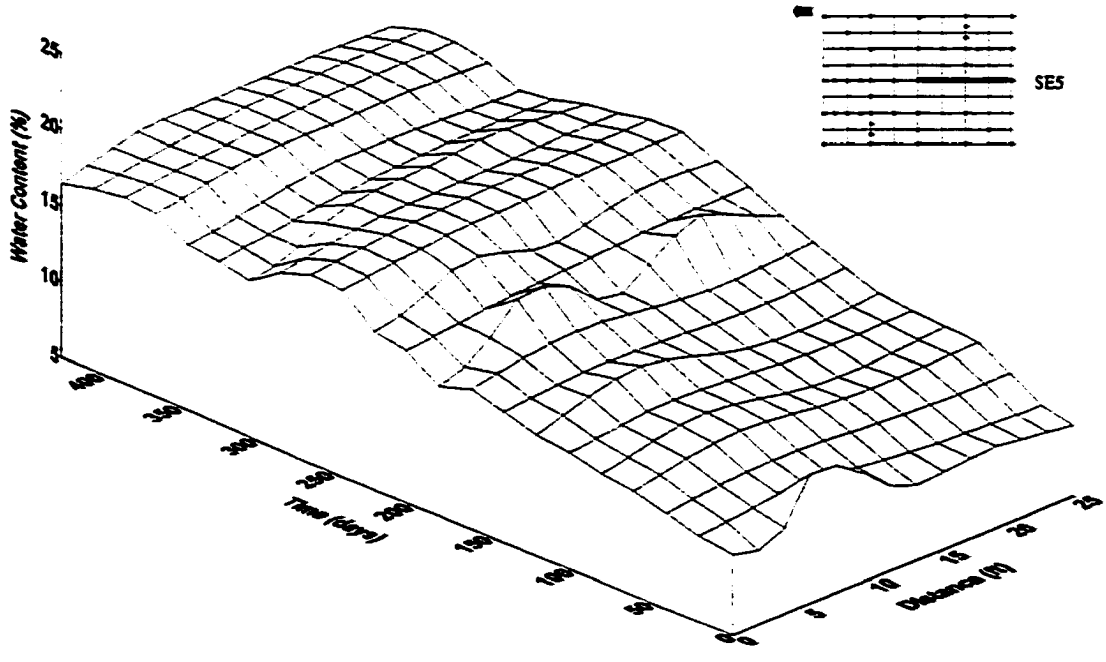

Figure 5-33 Water content as a function of time and distance from the south edge along row 5 (SE5) of the FSH site at a depth of 1 feet.

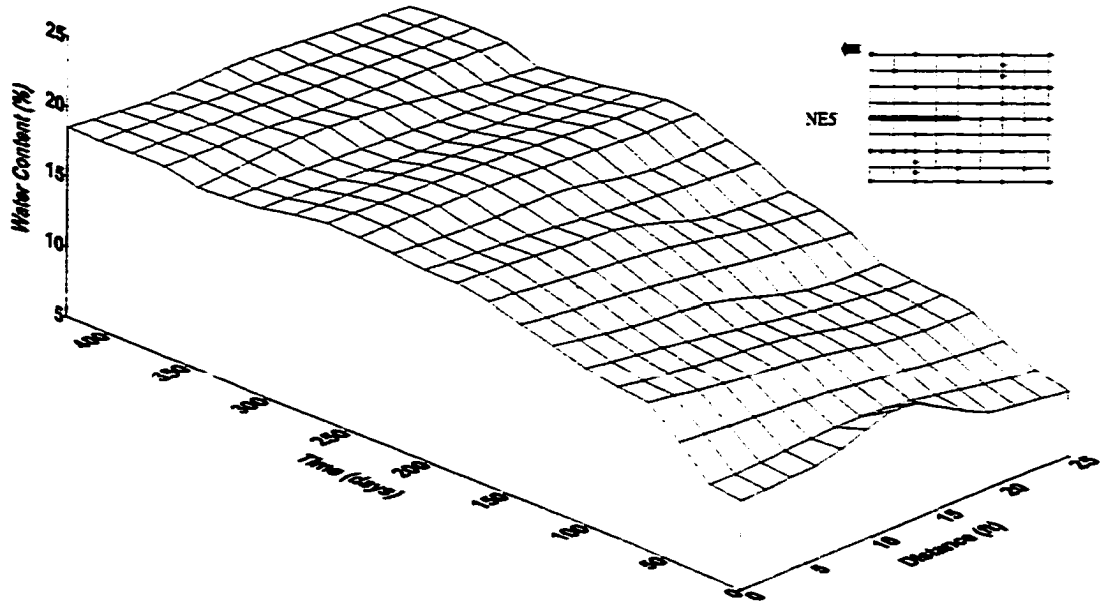

Figure 5-34 Water content as a function of time and distance from the north edge along row 5 (NE5) of the FSH site at a depth of 1 feet.

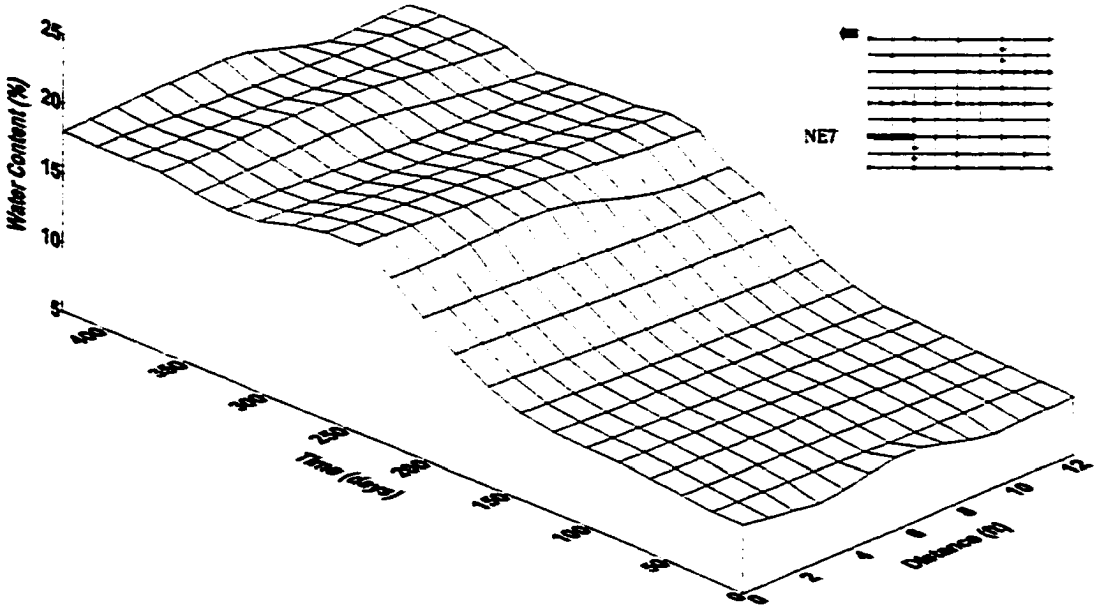

Figure 5-35 Water content as a function of time and distance from the north edge along row 7 (NE7) of the FSH site at a depth of 1 feet.

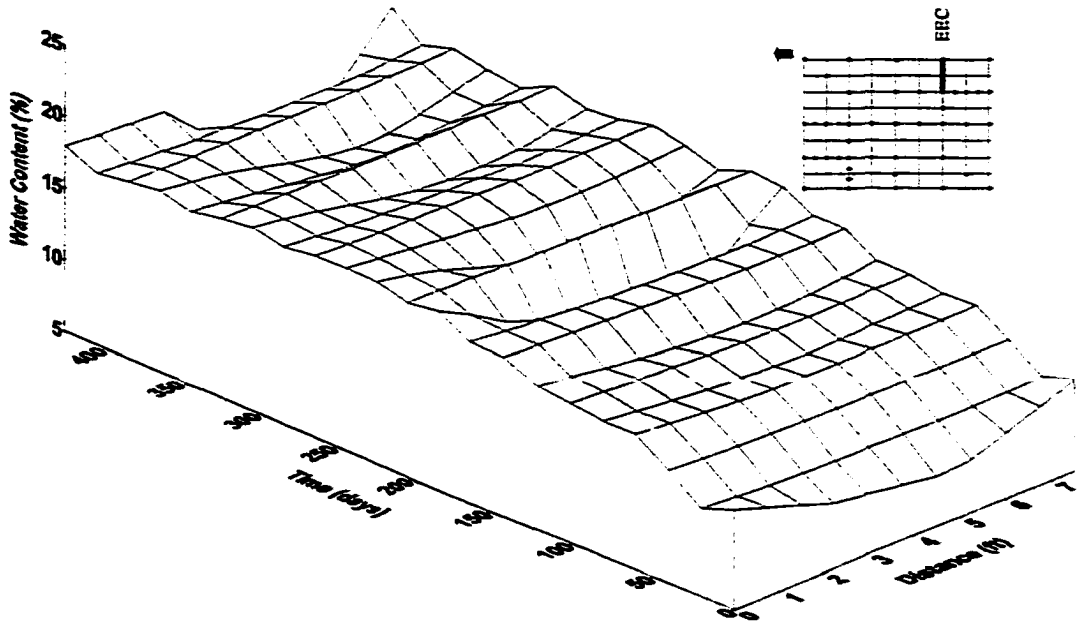

Figure 5-36 Water content as a function of time and distance from the east edge along line C (EEC) of the FSH site at a depth of 1 feet.

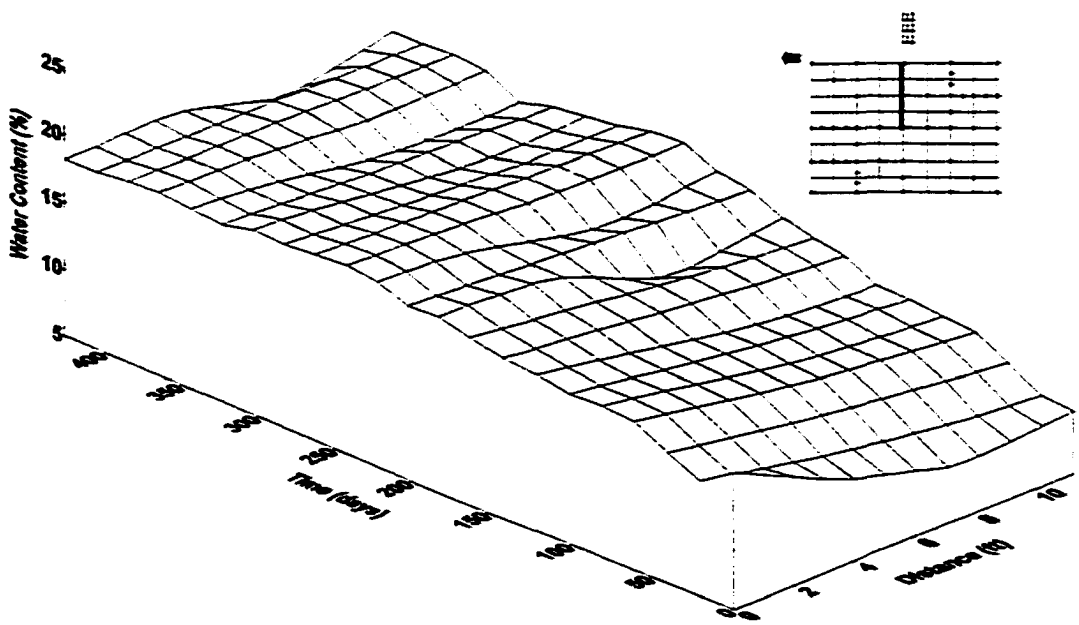

Figure 5-37 Water content as a function of time and distance from the east edge along line E (EEE) of the FSH site at a depth of 1 feet.

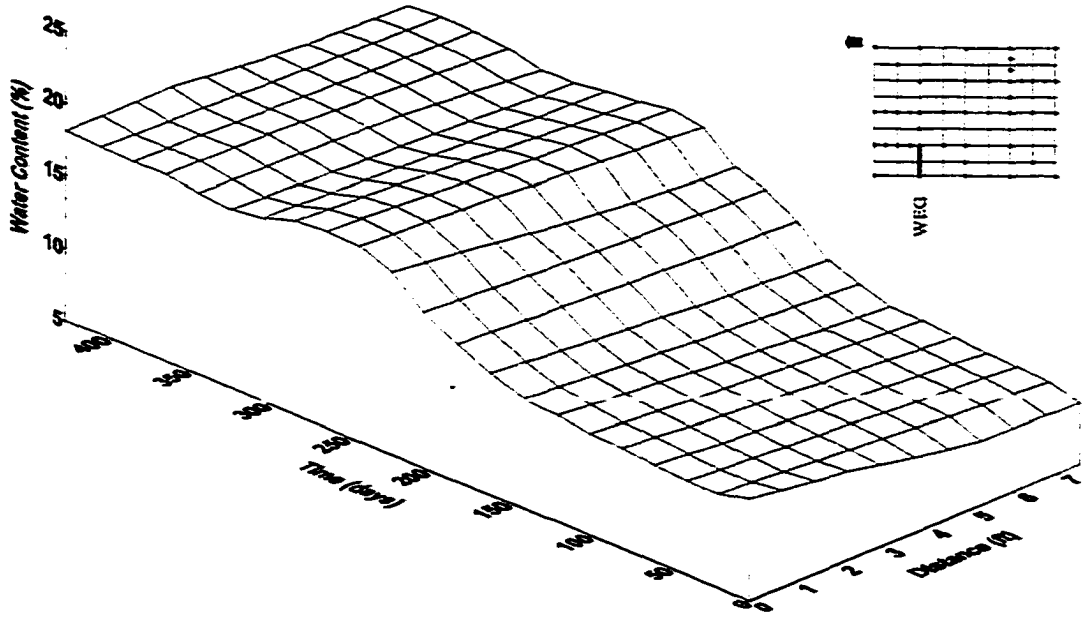

Figure 5-38 Water content as a function of time and distance from the west edge along line G (WEG) of the FSH site at a depth of 1 feet.

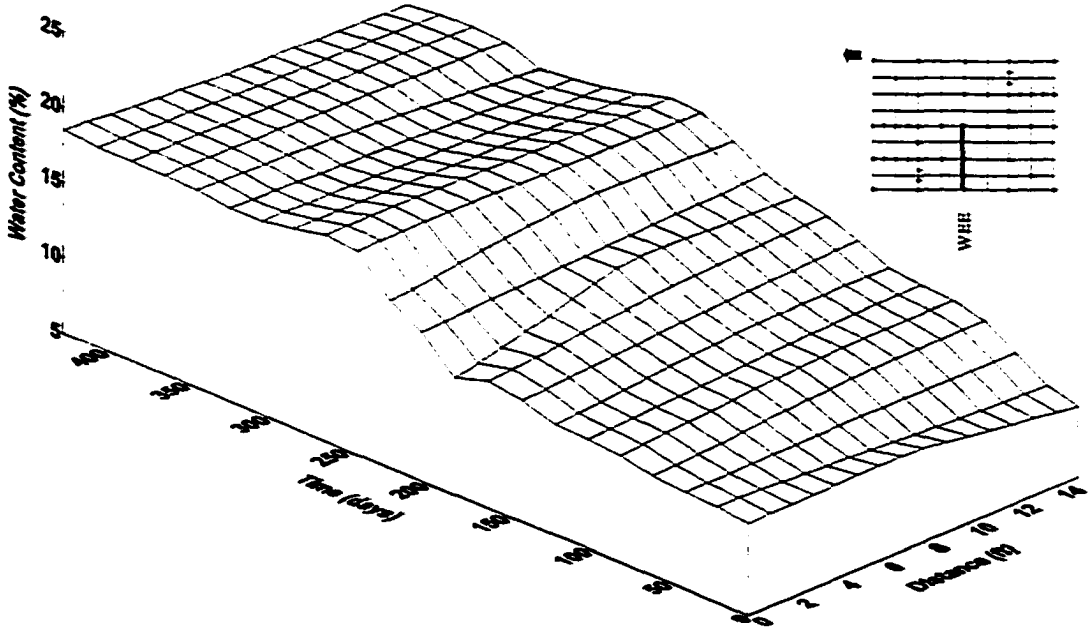

Figure 5-39 Water content as a function of time and distance from the west edge along line E (WEE) of the FSH site at a depth of 1 feet.

5.3 Elevation

Elevation data was collected monthly at the CSU and FSH sites from the 42 survey monuments shown in Figures 3-17 and 3-18, respectively. Figures 5-40 and 5-41 show the total measured change in elevation for the two sites. The data from CSU was collected on June 20, 1998 and the data from FSH was collected on November 10, 1994. The incremental monthly elevation data for both sites are presented in Appendix C.

The maximum measured heave at the CSU site is approximately 6 inches and was measured at survey monument A-8, along the east edge of the simulated slab where the water content increase was the greatest. Less than 1 inch of elevation change has been recorded along the west edge of the CSU site to date. The elevation change over the whole site tends to vary approximately in a linear mode (see Figure 5-40) from east to west, which is consistent with the water content data for the site. The elevation change at the FSH site has been relatively uniform (see Figure 5-41) ranging approximately from 1.5 to 3 inches. Monitoring was discontinued at the FSH site in the fall of 1994.

In general expansive soil will continue to heave as long as the water content of the soil and active zone depth continue to increase. Figures 5-42 and 5-43 show the heave as a function of time at several survey monuments along row 5 and the heave as a function of distance from the edge, respectively, for the CSU site. Figures 5-42 and 5-43 indicate that the CSU site is continuing to heave. However, the rate of heave along the eastern edge of the slab is decreasing and the rate of heave near the center and on the western edge of the slab is increasing.

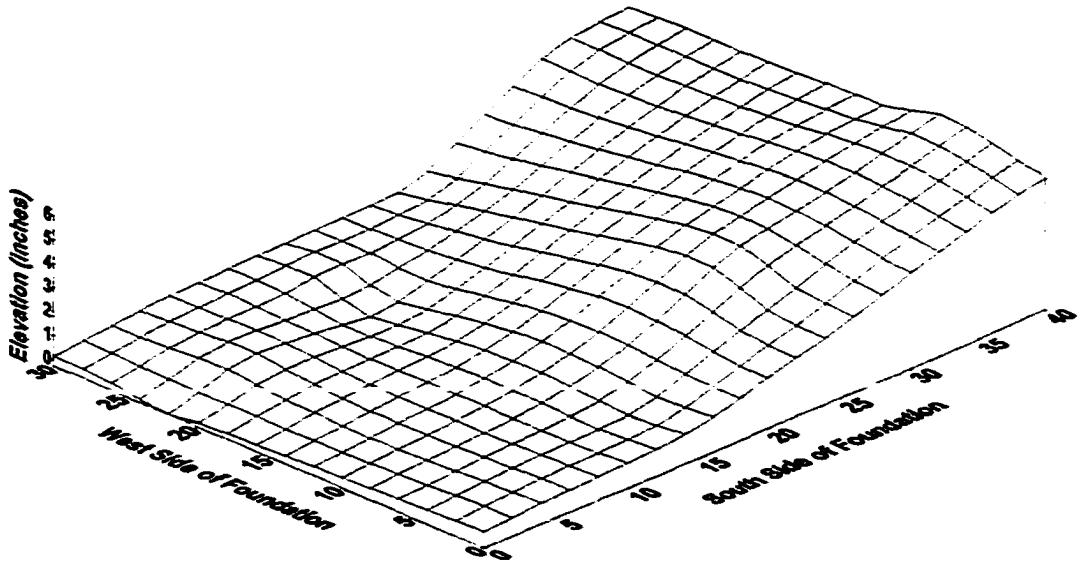

Figure 5-40 Total change in elevation of the CSU site as of June 20, 1998.

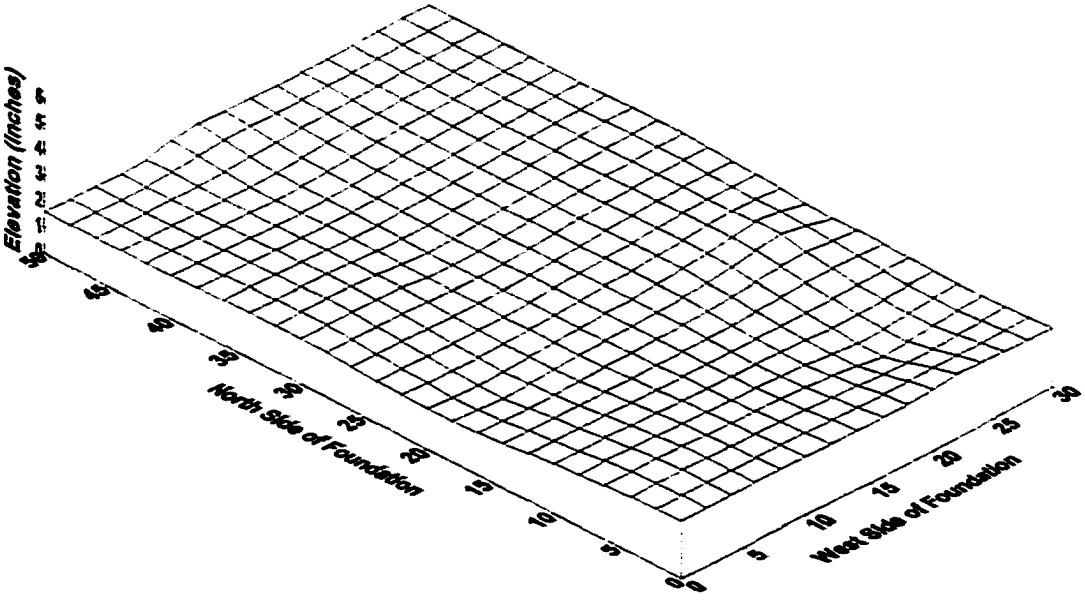

Figure 5-41 Total change in elevation of the FSH site as of November 10, 1994.

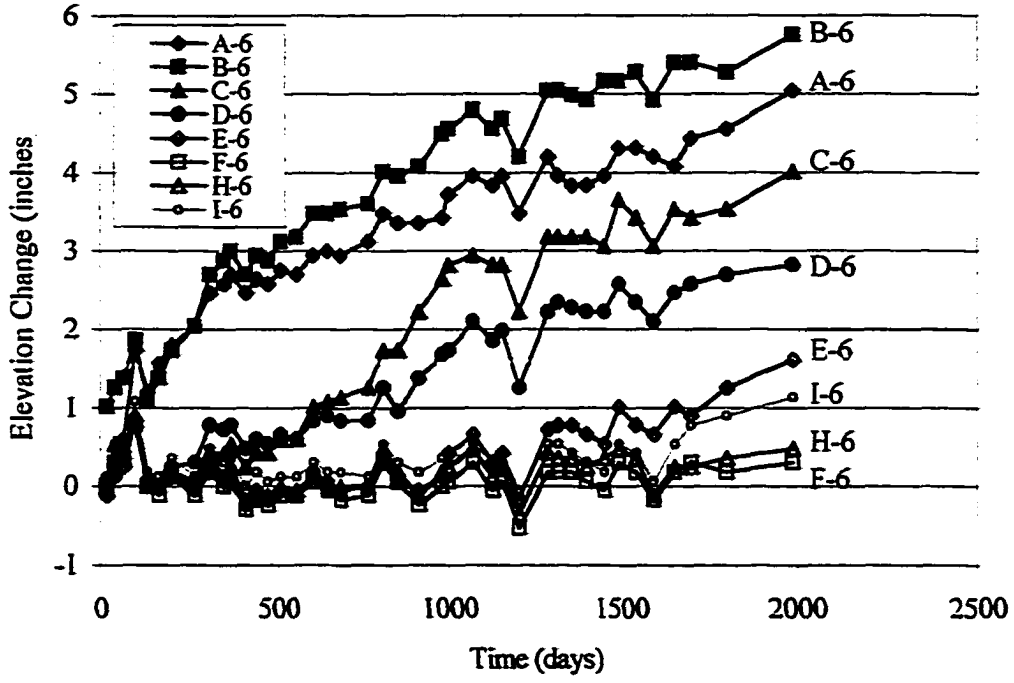

Figure 5-42 Heave as a function of time at various points along row 5 at the CSU site

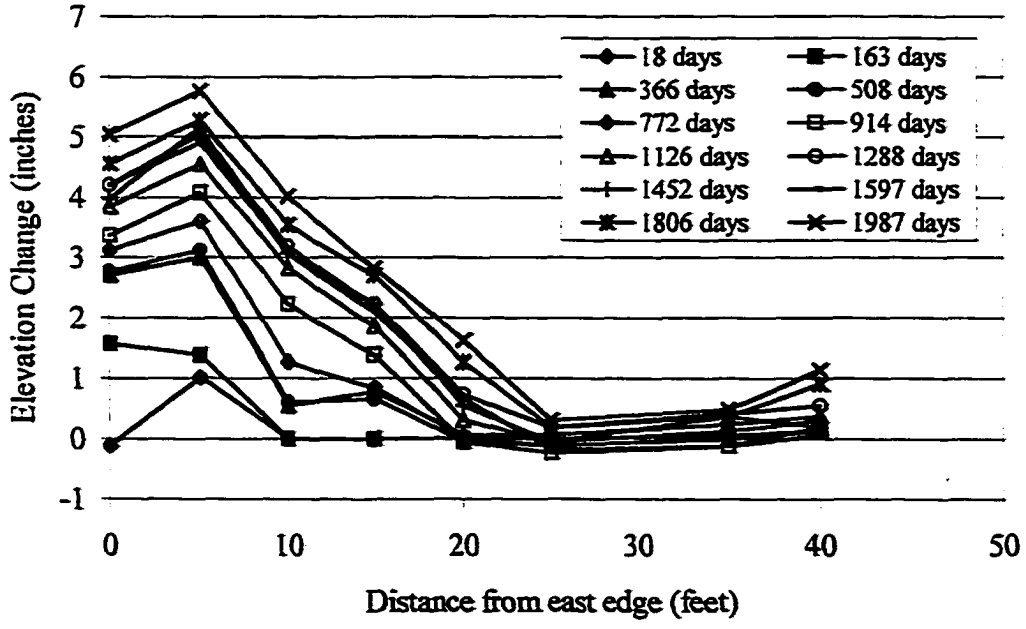

Figure 5-43 Heave as a function of distance from the east edge and time at the CSU site

The data also shows that the amount of heave that has occurred at locations toward the center is less than along the edge, as would be the case for edge lift conditions. Heave in the center and along the western side of the slab is considerably less than along the eastern edge.

Also important to note is that the heave in the center of the slab (E-6) increased from a value of 0.3 inches in February 1996 (3 years after construction) to 1.6 inches in June 1998, five and a half years after construction. This indicates that water continues to migrate from the eastern side of the slab toward the western side of the slab and that the site has not reached equilibrium.

The concept of equilibrium with regard to water content profiles and depth of the active zone has been discussed. However, with respect to heave, equilibrium can not be evaluated based on active zone depth alone. Water content profiles presented in the previous chapter indicated that the water content had not increased significantly, west of row C of the CSU slab. This would indicate that heave is not occurring there either. However, as seen in Figures 5-42 and 5-43, heave has occurred at E-6. Figure 5-44 shows the water content versus time at various depths in the center of the slab (access tube E-5). From that data it appears that the water content is increasing slightly, and it is likely that moisture is migrating from the eastern (wetter) side toward the west.

This behavior is very important from the standpoint of heave prediction. It has been shown that estimating the depth of the active zone is dependent upon interpretation of the depth of water content increase data. However, in addition to the depth of water content increase, the magnitude of water content increase also effects the amount of heave. From

the data presented thus far the depth of the active zone in the center of the slab does not appear to be increasing. However, the magnitude of water content in the upper soil layers is increasing slightly and those slight increases are large enough to result in continuation of heave with time.

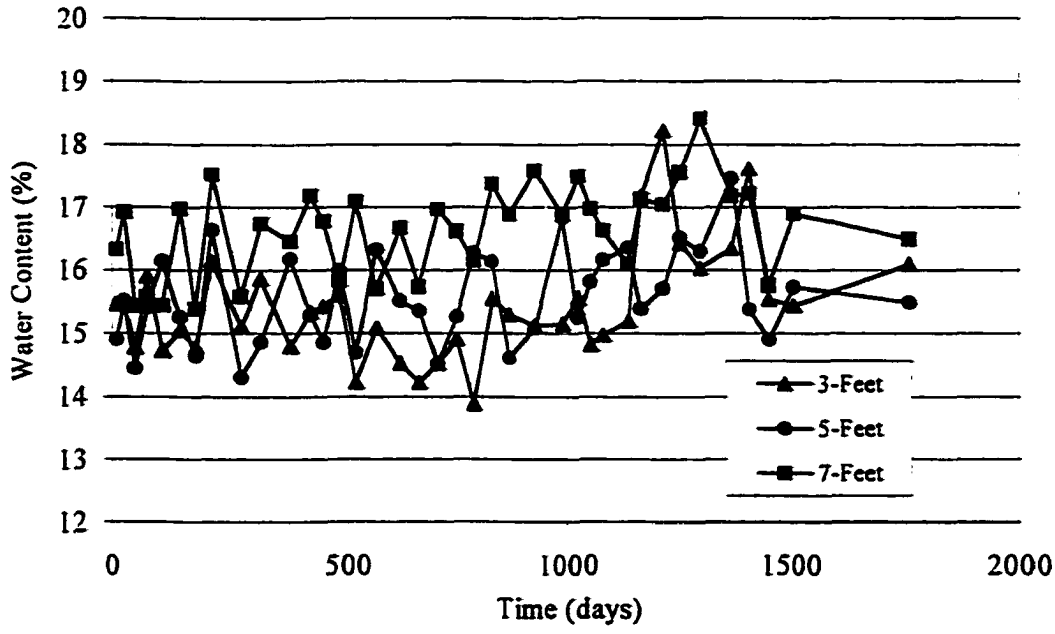

Figure 5-44 Water content as a function of time at the center of the slab (E-5) at CSU

Figures 5-45 and 5-46 show the heave as a function of time and distance from the edge at the FSH site. The data in Figures 5-45 and 5-46 generally indicate the same trend as at the CSU site. However, since there were instrumentation problems during the first six months of the study there is no data available until day 222 for most of the locations shown. The small decreases after 300 days, for locations A-6 and I-6, which are both near the edge of the slab, are attributed to shrinkage along the edge following a hot and dry summer. As was the case with the water content data the limited time of monitoring does not allow comprehensive characterization of the FSH site.

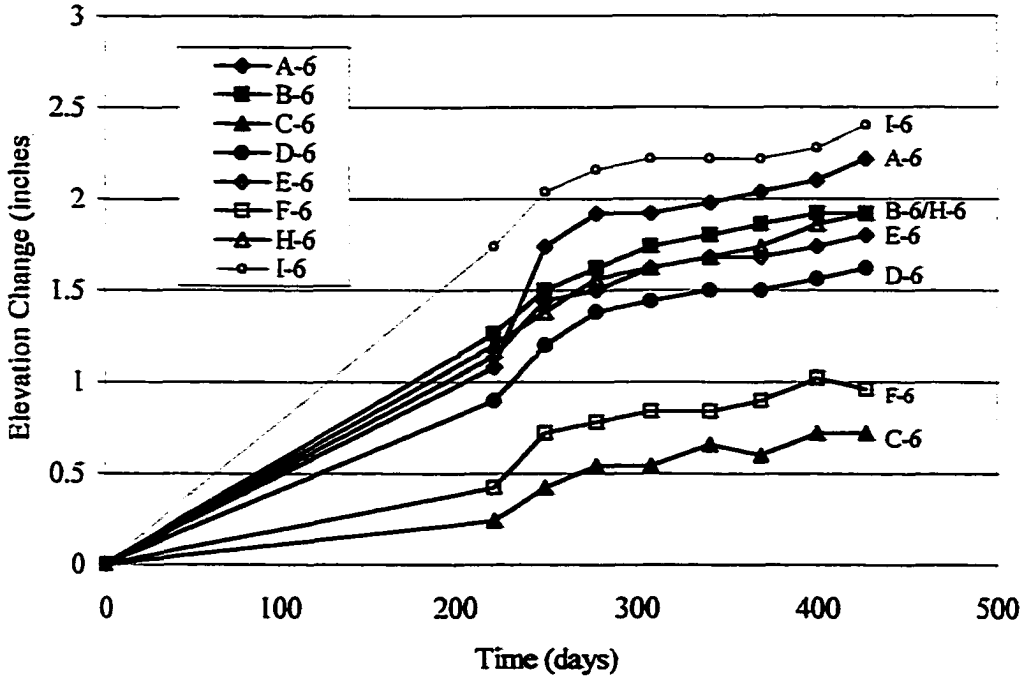

Figure 5-45 Heave as a function of time at various points along row 5 at the FSH site

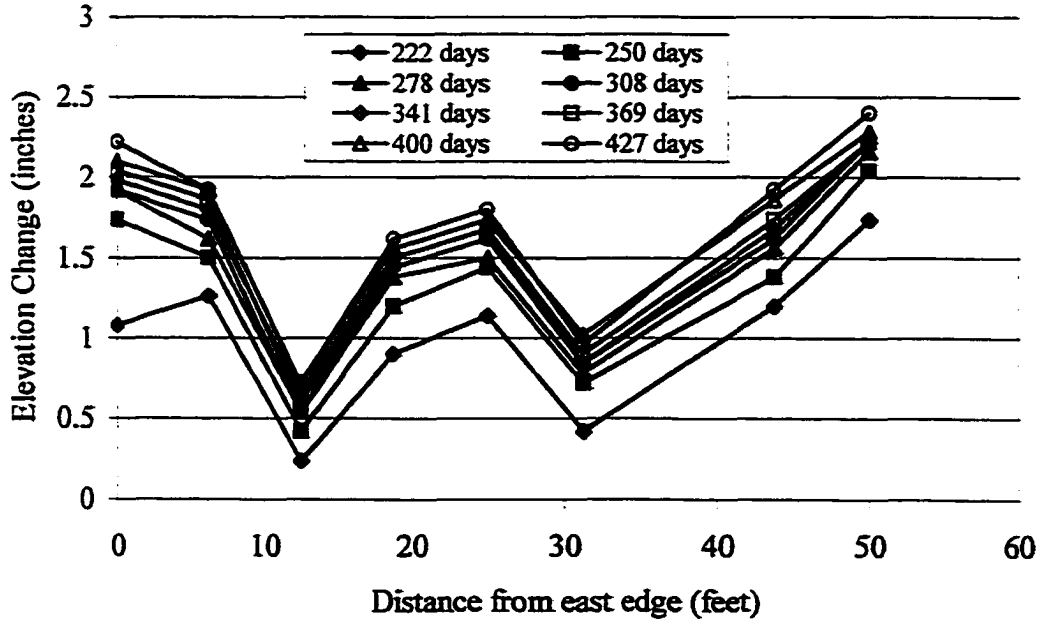

Figure 5-46 Heave as a function of distance from the edge and time at the FSH site

5.3.1 Heave Predictions

Heave predictions were performed for the CSU site and the FSH site using data from the field and laboratory investigations. The predicted heave values for both sites are consistent with total measured heave at both sites. The heave prediction methodologies are presented in Chapter 2.

Table 5-1 shows the results of heave predictions on Pierre shale and the Texas soil using the CLOD test method. The swell index parameters were obtained from CLOD tests conducted by Chao (1995). The calculation spreadsheets for the predicted heave values shown below are presented in Appendix D. Field measured heave values were obtained at survey monuments in the immediate vicinity of the water content access tubes that were used to calculate the predicted heave.

Table 5-1 Results of CLOD test heave prediction on Pierre shale and Texas soil.

Soil	z_i (ft)	Number Of Layers	Thickness of Layers (ft)	C_w	Total Corrected Heave (in)	Field Measured Heave (in)
Pierre Shale	13	13	1	0.016-0.019	4.1	4.9
	14	14	1	0.016-0.019	5.6	5.3
	15	15	1	0.016-0.019	5.2	4.3
	15	15	1	0.016-0.019	4.1	3.7
	15	15	1	0.016-0.019	4.6	4.9
	18	18	1	0.016-0.019	5.5	5.5
Texas Soil	5	5	1	0.023	1.6	1.7
	5	5	1	0.023	2.3	1.8
	5	5	1	0.023	1.8	1.8

The total corrected heave presented in Table 5-1 was adjusted for lateral restraint and anisotropy using the correction factor, f, presented in Hamberg (1985). The CLOD test prediction method assumes that total volume change in the CLOD sample represents

vertical heave in the field. Hamburg (1985) presented the development of the correction factor, f, to account for anisotropic soil conditions and the effects of lateral constraint. Hamberg (1985) concluded that the correction factor, f, varies between 0.33 and 1 for most soil types. The correction factors for Pierre shale and the Texas soil are 0.56 and 1.0, respectively (Chao, 1995).

The total heave at the FSH site closely agrees with that predicted by the CLOD tests. However, the correction factor, f=1, at the FSH site is based on the assumption of total lateral restraint. At the time of construction, however, it had not rained in the San Antonio area for over 80 days and large desiccation cracks were observed at the site. This indicates that total lateral restraint conditions did not exist at the site during the time of monitoring.

Heave is still occurring at the CSU site. The CLOD test prediction method accounts for this by utilizing the measured depth and magnitude of water content changes at a given time to calculate heave. If the water content at the time of maximum heave (swelling limit) and the maximum long term active zone depth were known then the total maximum heave at the site could be predicted by the CLOD test. However, very little research has been conducted on the swelling limit (analogous to the shrinkage limit) and it is not rigorously defined.

Total maximum heave was also predicted using swell parameters obtained from consolidation-swell tests results that were presented in Chapter 4. The swelling index was determined from consolidation-swell test results using the method proposed by Nelson, Durkee, and Bonner (1998). Results from maximum total heave predictions on the Pierre

shale and the Texas soils are shown in Table 5-2. The calculation sheets are shown in Appendix D.

Table 5-2 Results of total maximum heave predictions on Pierre shale and Texas soil using Nelson, Durkee, and Bonner (1998) method.

Soil Type	Layer #	$C_\rho/(1+e_0)$	σ_s' (psf)	$\sigma_{s(adj.)}'^{(1)}$ (psf)	Seating Load (psf)	Total Heave (inches)
Pierre Shale	1	0.057	6000	3,800	500	
	2	0.036	9000	5,600	500	
	3	0.025	4400	2,840	500	
	4	0.043	6000	3,800	500	**8.23**
Texas Soil	1	0.066	12,400	7,640	500	
	2	0.070	17,000	10,400	500	
	3	0.070	38,000	23,000	500	
	4	0.041	46,000	27,800	500	**5.62**

(1) Adjusted swell pressure based on Nelson, Durkee, and Bonner (1998).

Heave calculations using the consolidation-swell test predicts a total maximum heave of 8.23 inches at the CSU site. The maximum active zone depth, based on the depth at which the overburden pressure is equal to the swell pressure, at the CSU site is 35.1 feet. Initial sampling at the CSU site included one boring for a piezometer to a depth of approximately 30 feet. Clayshale was identified to the depth of 30 feet and it is likely that it continues to a depth of 35.1. Therefore, based on the laboratory consolidation-swell test results and the definition presented in Chapter 1, the maximum active zone depth at the CSU site is approximately 35 feet. The maximum heave at the CSU site assuming the clayshale does not extend beyond 30 feet is approximately 8.15 inches.

The maximum measured heave thus far at the CSU site is 6 inches. The predicted heave from the consolidation-swell test method inherently assumes total saturation of the soil since the soil is saturated to obtain the swell prediction parameters. Therefore, the predicted heave value from this method represents the maximum heave, assuming the water content in the active zone has reached the swelling limit.

The water content distribution from actual field profiles where heave was measured is continuing to increase. In addition, Chao (1995) showed that the void ratio of samples from the CSU site continues to increase as the water content increases to above 20 percent. The water content measured in the access tubes in the immediate vicinity of the measured heave locations is less than 20 percent indicating that heave will continue as the water content at depth increases. In addition, due the extremely friable nature of the Pierre shale it was difficult to load undisturbed samples in a consolidometer. Therefore, remolded soil compacted to the approximate field density was used for all of the consolidation tests and the loss of soil structure during compaction results in error in the predicted values that can not be quantified.

The maximum predicted heave at the FSH site is 5.62 inches. The maximum heave measured in the field at the FSH site is approximately 3 inches. As was the case with the CSU site, it is likely that the water content of the soil at the FSH site has not reached the swelling limit. The maximum water content measured at the site is approximately 19 to 20 percent. Chao (1995) showed that the void ratio of samples from the FSH site continues to increase as the water content of the CLOD samples approaches 30 percent. The

maximum predicted heave at the FSH site was determined assuming a 6-foot thick layer of expansive soil (i.e. 6-foot active zone depth).

5.4 Total Suction and Temperature

The CSU site was instrumented with thermocouple psychrometers (TCP) nine months after construction (September 1993). The TCP's were placed in locations D-6.5, D-8.5, and J-5.5 (Figure 3-17). This provided for one set near the center of the slab, one near the edge and one in the uncovered soil. Each set consisted of six TCP's, at depths of 2, 5, 8, 11, 14, and 17 feet. Figures 5-47, 5-48, and 5-49 show the monthly total suction and temperature profiles at locations D-6.5, D-8.5, and J-5.5, respectively.

A limited number of practitioners have used total suction data to predict active zone depth. They generally install TCP's in the soil in an area of proposed construction to monitor suction changes as a function of depth. McKeen and Johnson (1990) developed a method for predicting active zone depth and edge moisture variation distance based on the depth of equilibrium suction and the sinusoidal patterns of climate data. They define the term equilibrium suction value as the soil moisture suction value below the depth of seasonal moisture variation. The equilibrium suction value is determined based on a minimum range of suction change considered significant. The determination of equilibrium suction is dependent upon interpretation and relies on the assumption that the active zone depth is obtained from the depth of seasonal moisture variation.

Figure 5-50 shows the average suction, and minimum and maximum suction values measured in the uncovered soil at J-5.5 over a time period of approximately six years.

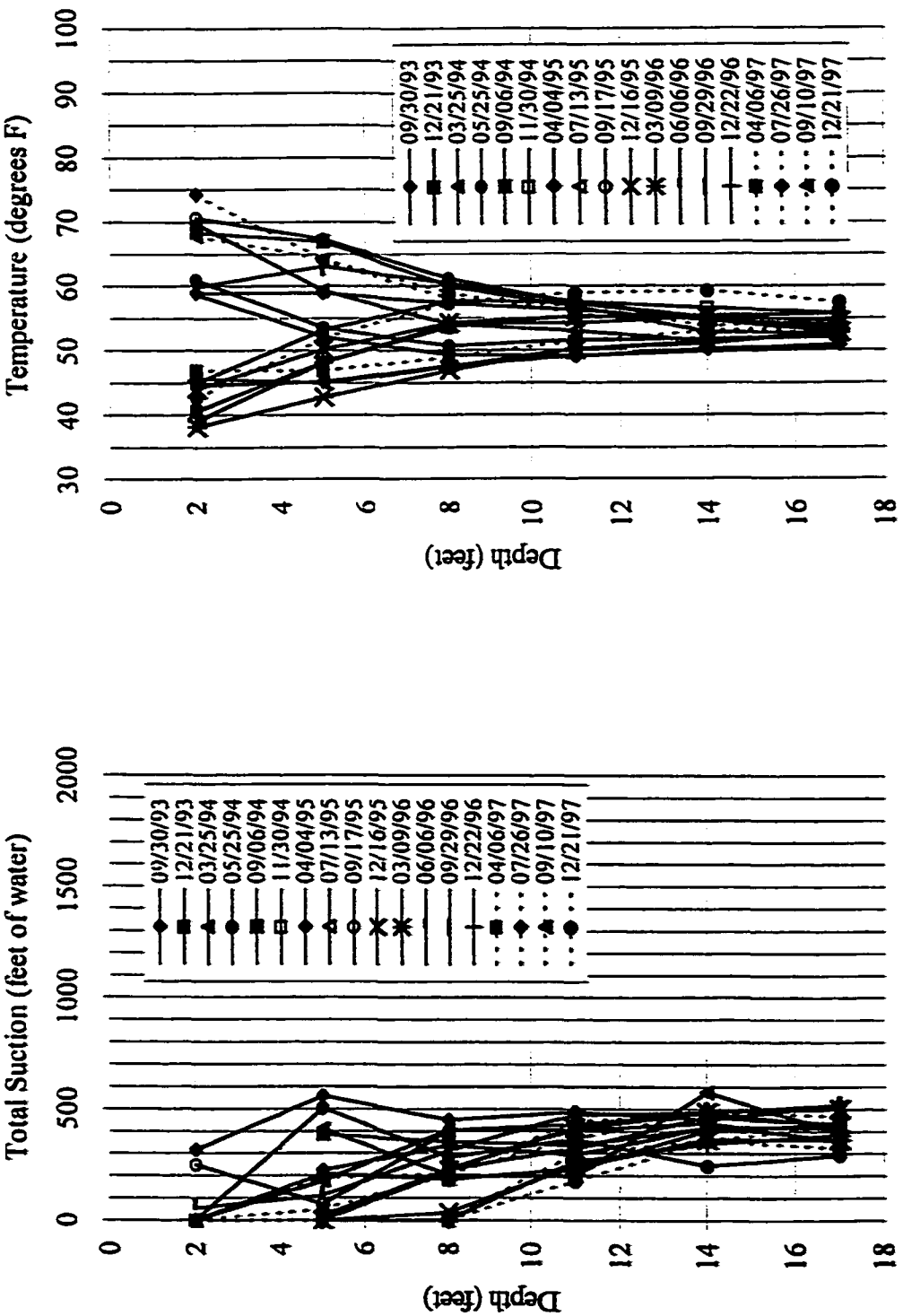

Figure 5-47 Total suction and temperature as a function of depth and time at location D-6.5 at the CSU site.

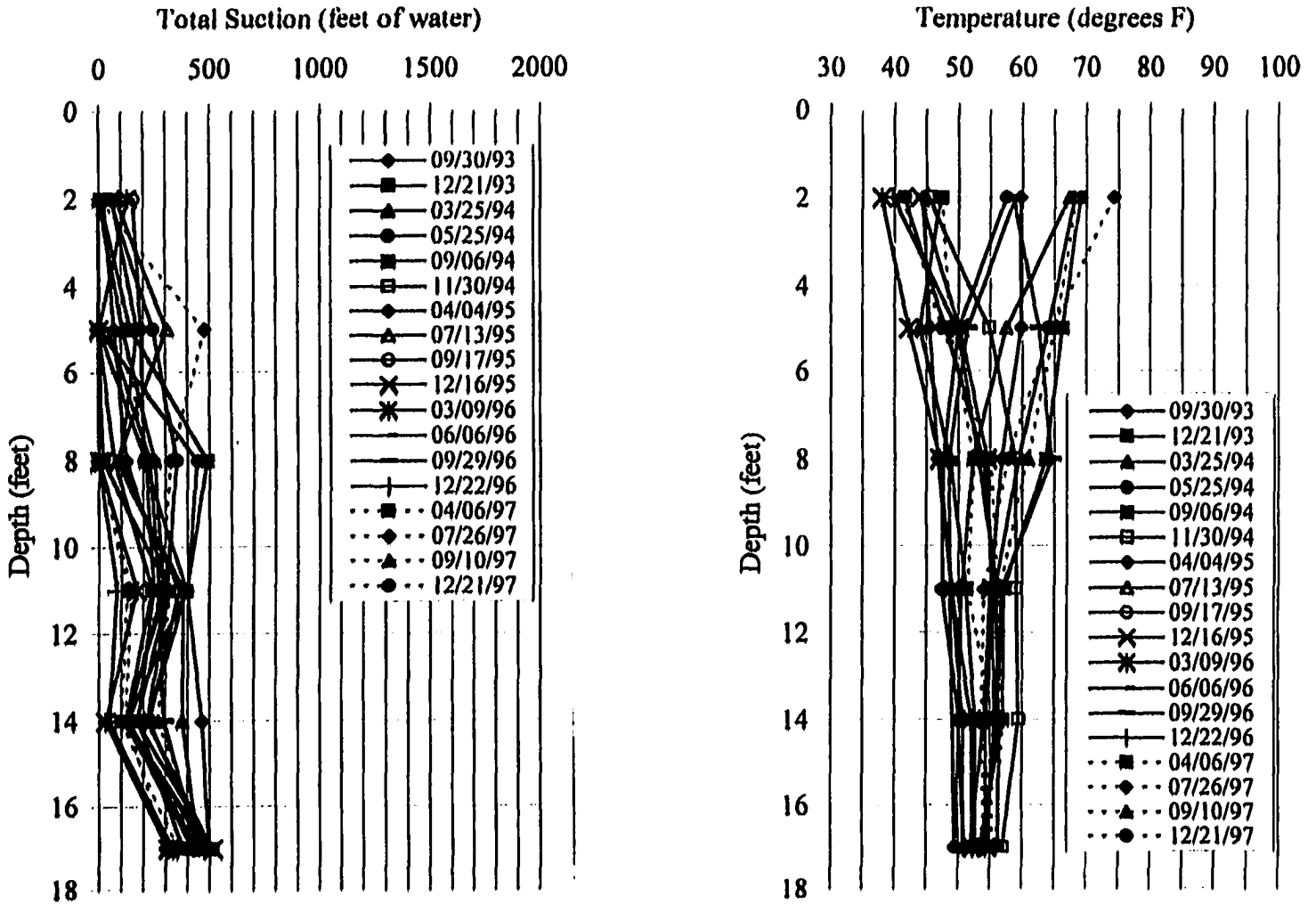

Figure 5-48 Total suction and temperature as a function of depth and time at location D-8.5 at the CSU site.

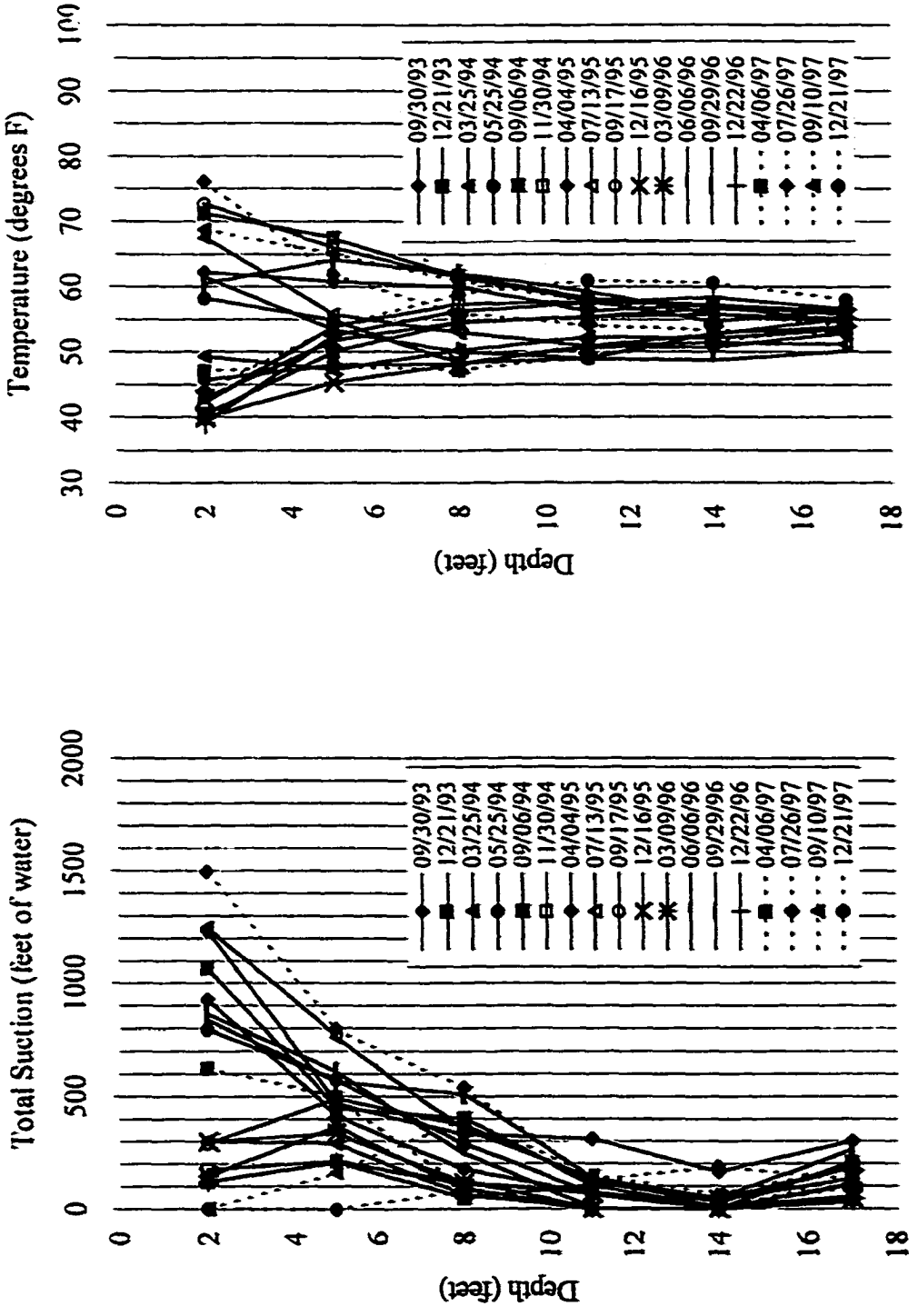

Figure 5-49 Total suction and temperature as a function of depth and time at location J-5.5 at the CSU site.

At that location the soil suction at a depth of 17 feet ranges between zero and 300 feet and the average suction value is approximately 128 feet. This indicates that the depth of equilibrium suction is greater than 17 feet. This also agrees with the depth of water content increase of 18 feet measured beneath the slab at access tube A-9 in Figure 5-9. However, since soil suction measurements were not obtained below 17 feet the equilibrium suction from McKeen and Johnson's method can not be evaluated below that depth.

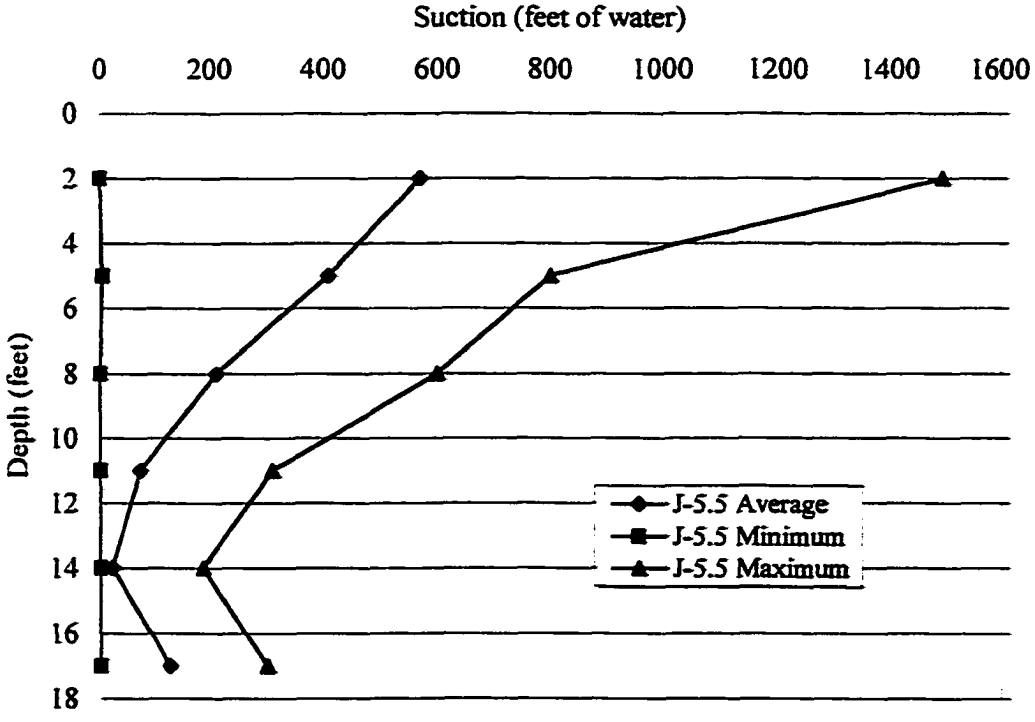

Figure 5-50 Average, minimum and maximum suction profiles from J-5.5

The zone of seasonal moisture fluctuation determined from water content access tube J-5, which is in the uncovered soil approximately 5 feet north of TCP location J-5.5, is approximately 6 feet. This suggests that the suction fluctuates with climate at that

location to a depth of at least 17 feet but that the water content within that same 17 feet does not respond to the suction changes. If this is the case then the active zone depth could only be evaluated in a soil profile using suction measurements, and the water content increase would not manifest itself to the depth of equilibrium suction until after the surface was covered. However, it should be pointed out that in this range of suction, the water content change is close to the accuracy of the nuclear moisture density gauge (2 to 4 percent for the CPN 501DR). From the soil water characteristic curve presented in Chapter 4 a suction change of 300 feet is associated with water content changes of 2 to 4 percent. Therefore, based on the accuracy of the nuclear moisture density gauge a change in suction of less than 300 feet can result in zero change in water content. Yeo (1995) compared suction measurements in Pierre shale under controlled conditions in a laboratory using thermocouple psychrometers (TCP) and the filter paper method. The results indicated that in a range of suction between 1,200 and 2,700 feet the water content ranged from 15 to 19.5 percent. This indicates that for a change in suction of 300 feet a water content change of less than 1 percent can be expected.

However, the main limitation to McKeen and Johnson's method is that it assumes the depth of the active zone will not be deeper than the depth of seasonal moisture variation. Thus far, the water content has not increased in the soil below 18 feet due to placement of the slab. However, future data is likely to indicate otherwise. In addition, if water were introduced at the surface near the edge of the foundation, as is expected for lawn watering in residential areas, the depth of water content increase would go deeper, thereby increasing the depth of the active zone. Also the water content measured below the

current active zone depth is less than the swelling limit indicating that if water is made available at that depth additional swelling will occur.

McKeen and Johnson (1990) also proposed that the edge moisture variation distance is equal to the difference between the active zone depth and the depth of the foundation. Hence, for the simulated slab constructed at the surface for this investigation the edge moisture variation distance is equal to the active zone depth. The relationship between water content at 1-foot depth, time, and distance from the edge of the slab at the CSU site was presented in Figures 5-24 through 5-31. Although there is considerable scatter in the data the edge moisture variation distance at the CSU site appears to be as high as 20 feet.

Figures 5-51, 5-52, and 5-53 show the total suction as a function of time measured by each TCP at locations J-5.5, D-8.5, and D-6.5, respectively. The data in Figure 5-51 demonstrates the cyclical behavior of soil suction and the effects of seasonal fluctuations in the soil, as was seen in Figures 5-24 through 5-31. The highest total suction values were measured at 2 feet, the shallowest location monitored. At a depth of 2 feet the total suction ranges from 0 feet to 1,500 feet. As expected, the range of total suction measured in the profile decreases with depth. However as mentioned above, the data in Figure 5-51 shows that the total suction at 17 feet fluctuates by as much as 300 feet.

The data in Figures 5-52 and 5-53 demonstrate the effects of covering the surface. The seasonal fluctuations in total suction are apparent, but the magnitude of the variations is much less than in the uncovered soil. In addition, the lowest suction values are in the upper 5 feet where moisture has accumulated do to placement of the slab. The highest suction values at D-8.5 (Figure 5-52) are measured at 17 feet.

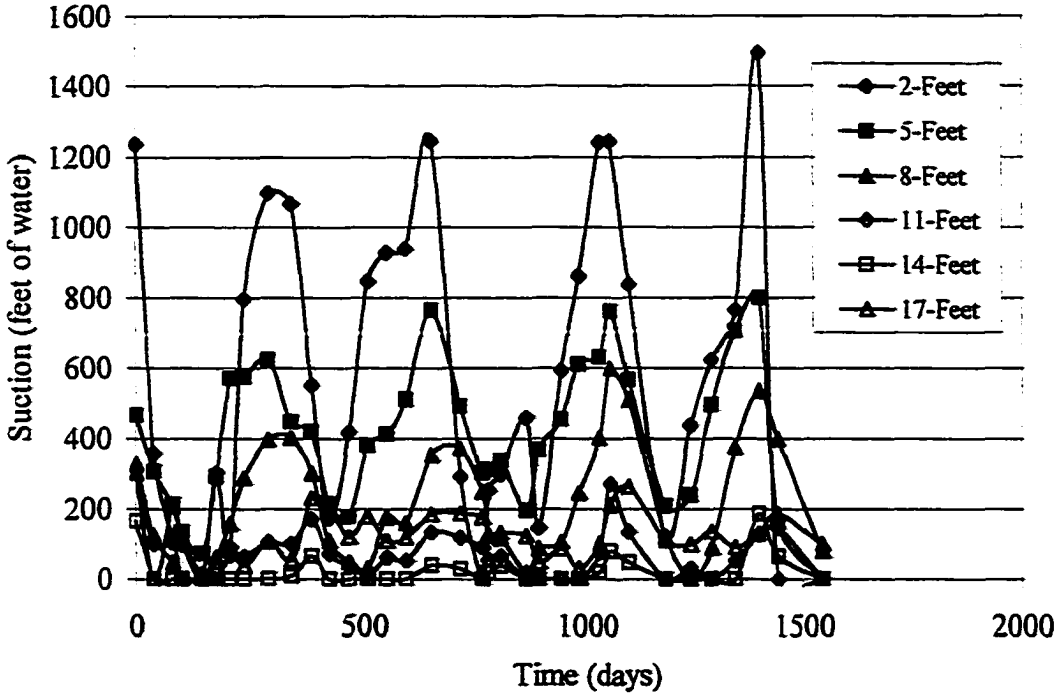

Figure 5-51 Total suction as a function of time and depth in the natural soil, J-5.5

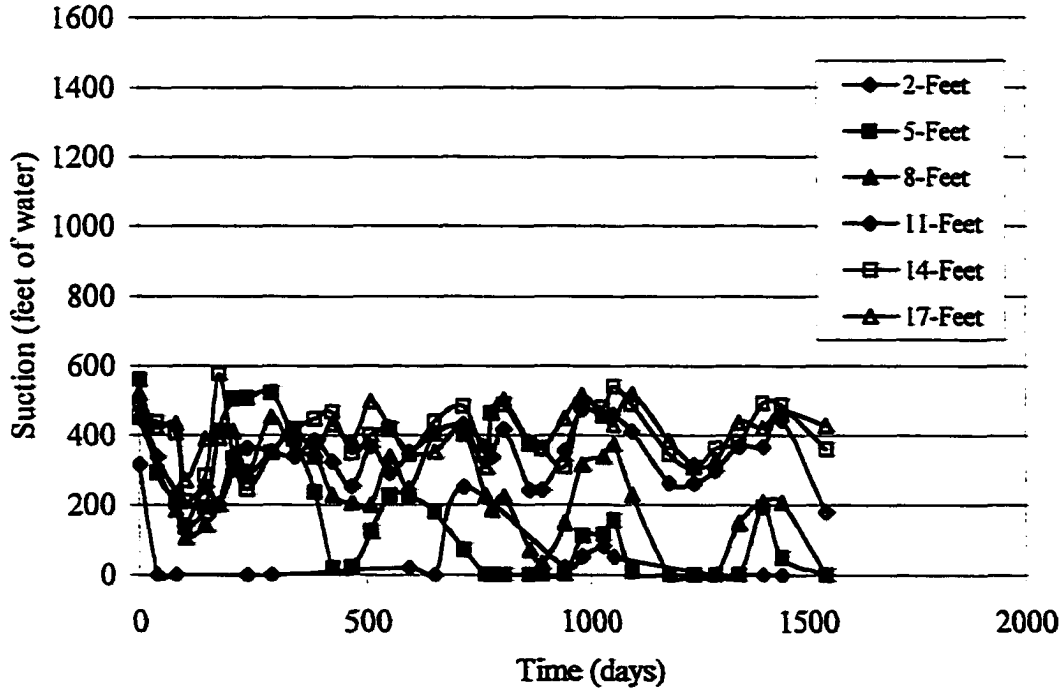

Figure 5-52 Total suction as a function of time and depth beneath the slab, D-6.5.

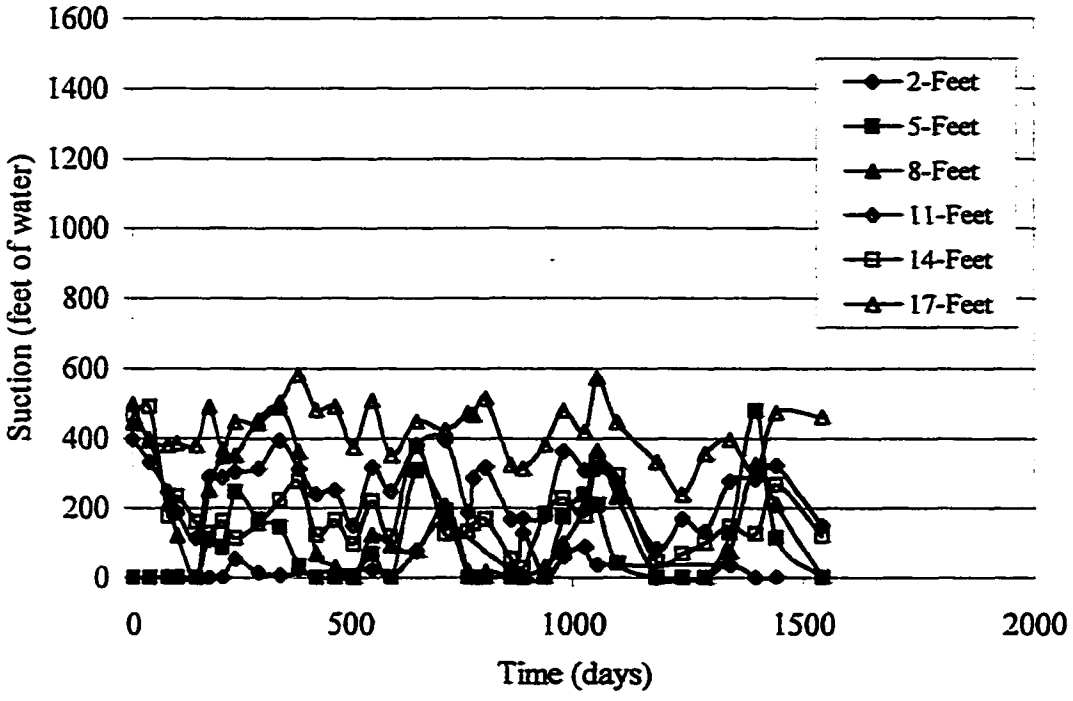

Figure 5-53 Total suction as a function of time and depth beneath the slab, D-8.5.

The lower magnitude of suction change with time at D-8.5 and D-6.5 suggest that temperature changes at the surface are controlling behavior at those two locations, and that the difference in magnitude of fluctuation between those two locations and J-5.5 is due to the reduction of evapo-transpiration at the surface. In addition, it should be noted that there is very little difference between the data measured at D-8.5, near the edged of the slab and D-6.5, near the center of the slab.

Figures 5-47, 5-48, and 5-49 do not indicate that covering the surface has an effect on soil temperature. Generally, the temperature at 2 feet ranges from 37° F to 75° F. The range varies linearly to a depth of 17 feet where it ranges from 50° F to 58° F.

CHAPTER 6

NUMERICAL MODELING

Historical definitions of active zone depth and edge moisture variation distance were discussed in Chapters 1 and 2. A new definition of active zone depth was proposed and this research was conducted in part to validate that definition. The historical definition of edge moisture variation distance is consistent with trends observed in the field. The field and laboratory investigations presented in Chapters 3, 4, and 5 provide a characterization of the active zone depth and edge moisture variation distance in terms of environmental conditions, geologic conditions, and soil properties.

The active zone depth at the CSU site, based on approximately 6 years of water content, suction, and heave data, is currently 18 feet. The depth of the active zone varies across the slab from east to west. In general the water content profiles indicate that the active zone depth is in equilibrium with the boundary conditions at the site. However, heave data indicates that the site is still moving and that the wetting front is continuing to move westward. The water content changes associated with the continued movement may be smaller than accurately measurable with the instrumentation that was used. The water content data also indicates that the edge moisture variation distance may be as high as 20 feet.

Suction data from beneath the slab at the CSU site does not provide an estimate of active zone depth because the TCP's were installed 9 months after the site was constructed.

Suction data from the uncovered soil adjacent to the slab at the CSU site indicate that the zone of seasonal moisture fluctuation is approximately 17 feet compared with 5 to 7 feet from the water content data. This inconsistency may be due to the relatively small changes in water content in response to suction changes and accuracy limitations of the instrumentation. Water content data from beneath the slab indicate that the maximum depth of wetting thus far, of 18 feet, is consistent with the depth of equilibrium suction. However, as discussed in Chapters 1 through 5, the active zone depth is not defined as the depth of seasonal moisture fluctuation.

Water content and heave data were collected at the FSH site for a period of 14 months and provide only a limited view of behavior in terms of expansive soil foundation design parameters. In addition, the FSH site is limited to a 6-foot thick expansive soil layer. Since the depth of water content increase and the zone of seasonal moisture fluctuation beneath a slab typically go much deeper than 6 feet, the data from the FSH site does not allow for a comprehensive analysis.

Based on the field and laboratory results from this investigation the active zone depth and edge moisture variation distance at the CSU site were characterized in terms of the effects of environmental conditions, geologic conditions, and soil properties. The results demonstrate the significance of the environmental conditions, geologic conditions, and soil properties, within the context of time over which the study has been conducted. However, environmental conditions include climate conditions as well as manmade surface boundary conditions such as irrigation and broken utilities that have not been investigated in the field study. In addition, geologic conditions include anisotropy,

bedding plane orientation, and fracturing within the soil, the effects of which have been discussed on a qualitative basis.

Hence, there are several questions that have not been addressed by the field and laboratory investigations because of the limits of time and budget. To provide a more comprehensive characterization of the active zone depth and edge moisture variation distance, the scope of the investigation included numerical modeling analyses. The numerical analyses were conducted based on the CSU site only. As mentioned previously, the limited depth of expansive soil and the fact that the FSH site was monitored for only 14 months does not allow a comprehensive analysis of that site.

The goal of the modeling phase of this research was to address several questions that were not fully evaluated in the field and laboratory investigation. Generally:

- How do soil properties affect the active zone depth and edge moisture variation distance?
- What affect does bedding plane orientation have on wetting and heave pattern development?
- What are the effects of ponding and watering near the foundation?
- How deep can the active zone go and how long will it take?

6.1 Model Descriptions

Two commercially available computer models were used to model moisture flow, in the soil, and evaluate the effects of placing a simulated slab on the surface, SoilCover (Geo2000, Ltd.) and SEEP/W (GEO-SLOPE, International). The SoilCover model is a one-dimensional finite element, boundary flux model that couples flow in the soil with atmospheric conditions on a time-dependent basis. Evapo-transpiration and infiltration in saturated and unsaturated soil are modeled for up to one year, at which time the initial

conditions can be updated and the model restarted for the next year of modeling. Climate parameters including minimum and maximum temperature and relative humidity, solar radiation, precipitation, and wind speed can be updated daily.

The SEEP/W model is a two-dimensional finite element computer model developed for simulating saturated and unsaturated flow through soils. The boundary conditions at the surface are controlled by the user and can be updated at regular intervals to account for changing environmental conditions.

In this investigation the SoilCover model was used to determine daily infiltration and evaporation rates at the uncovered soil surface around the slab, based on the climate conditions and the stress-state in the soil. The simulations were also conducted assuming the surface was covered to simulate the effects of the slab. To simulate the covered surface, the relative humidity of the air was set equal to 100 percent and the solar radiation value was set to zero throughout the simulations. The daily infiltration and evaporation rates were then used as boundary conditions in the SEEP/W model. The theoretical framework for modeling flow with these two models is presented in the following two sub-chapters.

6.1.1 SoilCover Model

The SoilCover model utilizes the heat and mass transfer equations derived by Wilson (1990) to model coupled one-dimensional transient heat and mass flow in soil. The liquid water and water vapor flow equations derived in Wilson (1990) are presented below.

The flow of water vapor and liquid water are described on the basis of Fick's law and Darcy's law as follows:

$$\frac{\delta h_w}{\delta t} = C_w^1 \frac{\delta}{\delta y}\left(k_w \frac{\delta h_w}{\delta y}\right) + C_w^2 \frac{\delta}{\delta y}\left(D_v \frac{\delta P_v}{\delta y}\right) \qquad (6\text{-}1)$$

where:

h_w	=	Total head (m)
t	=	time (s)
C_w^1	=	Coefficient of consolidation with respect to the liquid phase
	=	$1/m_2^w \rho_w g$
ρ_w	=	mass density of water (kg/m^3)
g	=	acceleration due to gravity (m/s^2)
y	=	position (m)
k_w	=	hydraulic conductivity (m/s)
C_w^2	=	Coefficient of consolidation with respect to the vapor phase
	=	$\frac{(P+P_v)}{P\rho_w^2 g m_2^w}$
m_2^w	=	slope of the moisture retention curve (1/kPa)
P	=	total gas pressure in the air phase (kPa)
P_v	=	partial pressure due to water vapor (kPa)
D_v	=	diffusion coefficient of water vapor through the soil (kg·m/kn·s)
	=	$\alpha\beta(D_{vap}\frac{W_v}{RT})$
α	=	tortuosity factor of soil ($\beta^{2/3}$)
β	=	cross sectional area of soil available for vapor flow
D_{vap}	=	molecular diffusivity of water vapor in air (m^2/s)
	=	$0.229\times10^{-4}(1+\frac{T}{273.15})^{1.75}$
T	=	temperature (°K)
W_v	=	molecular weight of water (0.18 kg/kmole)
R	=	universal gas constant (8.314 J/mole/°K)

Temperature is evaluated on the basis of conductive and latent heat transfer as follows:

$$C_h \frac{\delta T}{\delta t} = \frac{\delta}{\delta y}\left(\lambda \frac{\delta T}{\delta y}\right) - L_v\left(\frac{(P+P_v)}{P}\right)\frac{\delta}{\delta y}\left(D_v \frac{\delta P_v}{\delta y}\right) \qquad (6\text{-}2)$$

where: T = Temperature(°C)

C_h	=	Volumetric specific heat of the soil as a function of water content ($J/m^3/°C$)
	=	$C_v\rho_s$
C_v	=	Specific heat of the soil (J/kg/°C)
ρ_s	=	Mass density of the soil (kg/m^3)
λ	=	Thermal conductivity of the soil (W/m/°C)
L_v	=	Latent heat of vaporization of water (J/kg)

The vapor pressure is calculated on the basis of the total suction of the liquid phase after Edlefsen and Anderson (1943).

$$P_v = P_{sv} h_r \tag{6-3}$$

where:			
	P_v	=	actual vapor pressure in the soil
	P_{sv}	=	saturation vapor pressure of the soil at it's temperature, T
	h_r	=	relative humidity of the soil surface as a function of total suction and temperature
		=	$e^{(\frac{\Psi g W_v}{RT})}$
	Ψ	=	total suction in the soil (m)

In Equation 6-1 the hydraulic conductivity is a key input variable for modeling water flow with the SoilCover model. In unsaturated soils the vapor phase flow component becomes particularly important. In the SoilCover model the diffusion coefficient, which is the fundamental parameter for the vapor phase flow component, is calculated based on the temperature in the soil. For this investigation, the evaluation of the effects of soil properties on active zone depth and edge moisture variation distance is limited to the hydraulic conductivity.

The unique aspect of the SoilCover model that lends itself well to modeling the development of the active zone depth and the edge moisture variation distance is the

capability of atmospheric coupling. This is achieved by calculating the soil evaporative flux. Using the modified Penman formulation developed by Wilson (1990) the soil evaporative flux is calculated based on the vapor pressure gradient between the soil surface and the atmosphere. Wilson (1990) presents the vertical evaporative flux equation as:

$$E = \frac{\Gamma Q + v E_a}{\Gamma + Av} \tag{6-4}$$

where:

E	=	vertical evaporative flux (mm/day)
Γ	=	slope of the saturation vapor pressure versus temperature curve at the mean temperature of the air
Q	=	net radiant energy available at the surface (mm/day)
v	=	psychometric constant
E_a	=	$f(u)P_a(B-A)$
f(u)	=	function dependent on wind speed, surface roughness, and eddy diffusion
	=	$0.35(1+0.15U_a)$
U_a	=	wind speed (km/hr)
P_a	=	vapor pressure in the air above the evaporating surface
B	=	inverse of the relative humidity of the air = $1/h_a$
A	=	inverse of the relative humidity at the soil surface = $1/h_r$

The modified Penman formulation accounts for net radiation, wind speed, and the relative humidity of both the air and soil surface while calculating evaporation from an unsaturated soil surface. The relative humidity of the soil surface is evaluated by simultaneously solving the moisture flow equation and the modified Penman formulation.

6.1.2 SEEP/W Model

The governing differential equation used in the formulation of SEEP/W is:

$$\frac{\delta}{\delta x}\left(k_x \frac{\delta H}{\delta x}\right) + \frac{\delta}{\delta y}\left(k_y \frac{\delta H}{\delta y}\right) + Q = \frac{\delta \theta}{\delta t} \tag{6-5}$$

H	=	total head
k_x	=	hydraulic conductivity in the x-direction
k_y	=	hydraulic conductivity in the y-direction
Q	=	applied boundary flux
θ	=	volumetric water content
t	=	time

This equation is essentially the same fundamental equation as is used by SoilCover except that the SEEP/W equation is written for two-dimensional flow and includes an applied boundary flux. The SoilCover version however, is written for one-dimensional flow, includes a vapor phase component, and uses the modified Penman formulation to calculate the boundary flux. In addition the SoilCover model considers soil temperature and the SEEP/W model does not.

The majority of moisture flow in this investigation occurs near the surface of the soil. The SoilCover model uses the atmospheric coupling approach to calculate the net infiltration across the surface while considering soil temperature and vapor phase flow. Therefore, the coupling of these two models provides a two-dimensional moisture flow model that considers soil temperature, vapor phase flow, and is physically based in terms of evaporation.

6.2 SoilCover Modeling

The SoilCover model was used to determine evaporation and infiltration rates from a one-dimensional profile at the CSU site. Soil, climate, and model parameters were obtained from the results of the laboratory and field investigations and from default methods available within the model.

6.2.1 Model Parameters

Model parameters were determined from the results of the laboratory and field investigations presented in Chapters 4 and 5. The SoilCover model requires two general types of input data, soil data and climate data. There are also options for modeling vegetation and soil freeze-thaw that require additional input data. The user develops the mesh geometry, initial water content or suction distribution, initial temperature conditions, and boundary conditions.

6.2.1.1 Soil Input Data

Soil input data include specific gravity, hydraulic conductivity, coefficient of volume change, and the soil water characteristic curve (SWCC). The model develops functions for unsaturated hydraulic conductivity, thermal conductivity, and volumetric specific heat. The specific gravity, the saturated hydraulic conductivity, and coefficient of volume change used for modeling the CSU site, were determined from laboratory testing presented in Chapter 4, and are presented in Table 6-1.

Table 6-1 Soil parameters for CSU site used in SoilCover modeling

Parameter	Value
Specific Gravity	2.72
Saturated Hydraulic Conductivity, k (ft/s)	1.3E-07
Coefficient of Volume Change, m_v (1/psf)	7.0E-03

The specific gravity was determined by Cheng (1994), as part of his investigation of soil-water diffusivity. The saturated hydraulic conductivity, k, and the coefficient of volume change, m_v, were determined from the consolidation test conducted on an undisturbed sample of Pierre shale.

The hydraulic conductivity values determined in Chapter 4 are summarized in Figure 6-1. As discussed in Chapter 4 the measured value from falling headwater rising tailwater tests is quite low. A rigid-walled test cell was used for those tests. The rigid-walled apparatus does not allow control or measurement of the stress-state in the sample and it is not possible to insure the specimen is saturated during the tests.

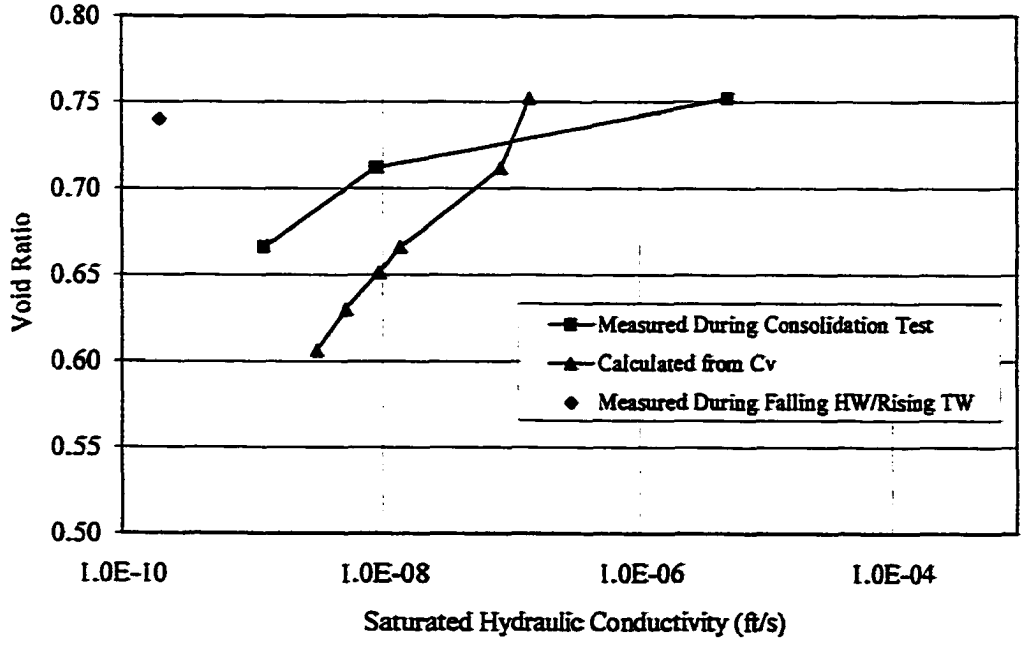

Figure 6-1 Results from laboratory hydraulic conductivity measurements on Pierre shale

The saturated hydraulic conductivity values from direct measurement during consolidation tests ranged from approximately 10^{-5} feet per second to 10^{-9} feet per second within a void ratio range of less than 0.1. The consolidation test is also conducted in a rigid-walled apparatus, and hence, involves the same difficulties as the falling headwater rising tailwater test. It is also possible that the initially high measured value is a result of sidewall leakage. The values determined from indirect calculations using the coefficient of consolidation ranged from approximately 10^{-7} to 10^{-9} feet per second.

Evaporation and infiltration are primarily a function of the soil conditions in the upper layers, in this case the weathered clay in the upper 5 to 7 feet. Laboratory tests were not conducted on soil samples from enough locations in the profile to accurately model subtle differences associated primarily with weathering. Therefore, for the purposes of this investigation the soil was modeled as a 20-foot thick homogeneous layer of soil. The saturated hydraulic conductivity values from the indirect method are shown plotted as a function of equivalent depth in Figure 6-2. The hydraulic conductivity used for this investigation was obtained from the relationship shown in Figure 6-2 at a depth of 7 feet, 1.3E-07 feet per second. This hydraulic conductivity value is within a reasonable range for this soil type and provided good results with respect to infiltration and evaporation during preliminary modeling.

Similarly Figure 6-3 presents the coefficient of volume change as a function of depth. The coefficient of volume change was also calculated from the consolidation tests results. The value of the coefficient of volume change from a depth of 7 feet in Figure 6-3 was used for the SoilCover modeling.

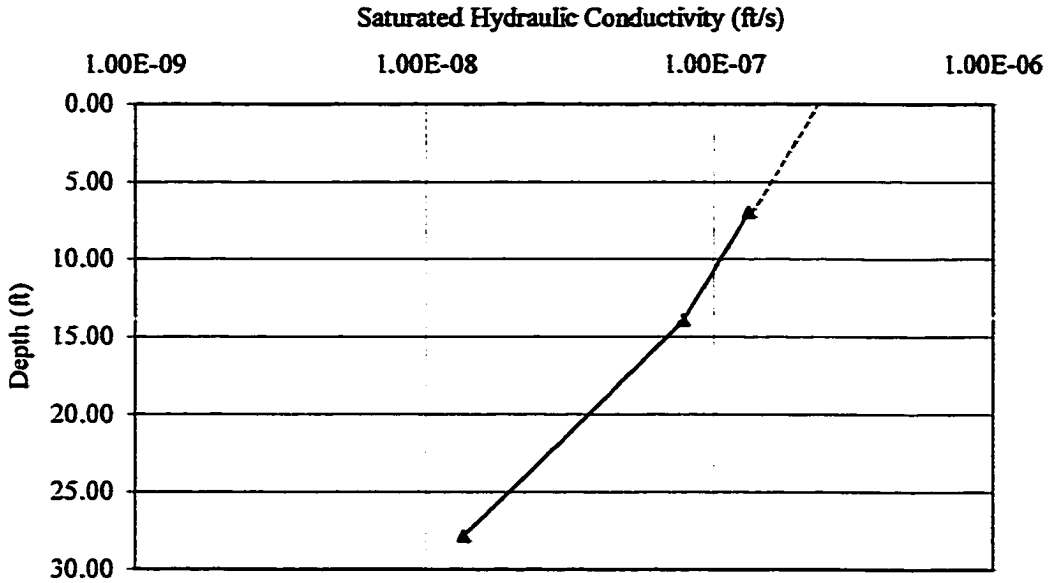

Figure 6-2 Saturated hydraulic conductivity as a function of depth in Pierre shale

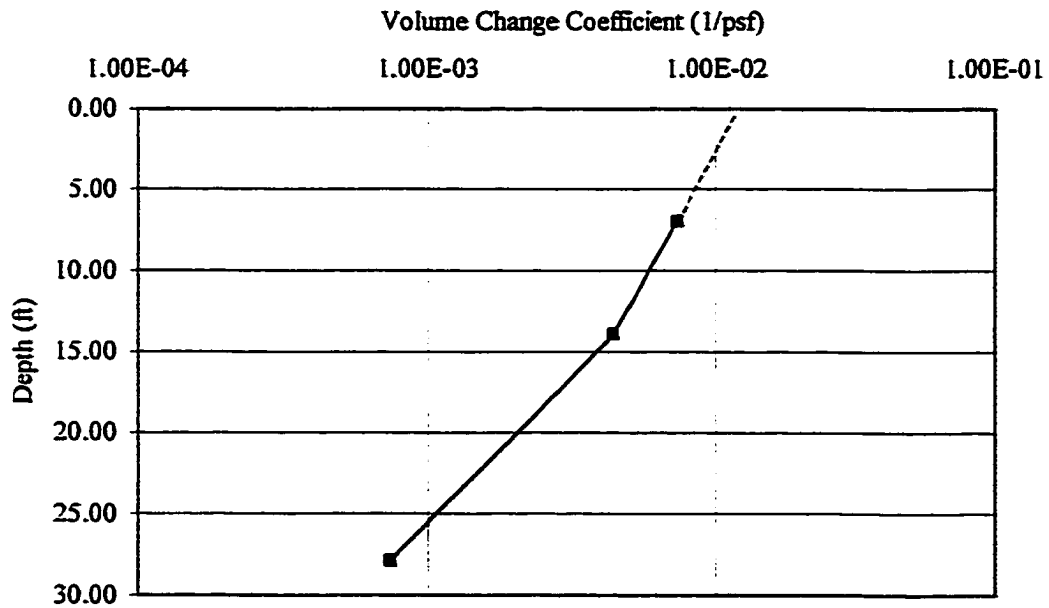

Figure 6-3 Coefficient of volume change as a function of depth in Pierre shale

Water retention data obtained by Chao (1995) and presented in Chapter 4 was used to develop the SWCC for the numerical analyses. Drying curve and wetting curve data were input directly to the model and the curve fitting routine developed by Fredlund and Xing (1994) was used to develop the SWCC. Preliminary modeling was conducted using both the drying curve and wetting curve data. The results from the drying and wetting curves are presented in Chapter 6.3 Model Validation.

The model uses the method developed by Fredlund et.al. (1994) to determine the unsaturated hydraulic conductivity function based on an integration form of the suction versus water content relationship (SWCC), equation proposed by Fredlund and Xing (1994). However, as stated in their paper and in the case of typical SWCC fitting routines, the function is unique as long as the volume change of the soil structure is negligible. In an expansive soil the majority of volume change takes place at the surface and in the upper few feet. The upper few feet of soil is also the most critical with respect to infiltration and evaporation. Preliminary modeling conducted with the unsaturated hydraulic conductivity function developed using the method proposed by Fredlund et.al. (1994) resulted in poor results when compared to the field measured results. A much better result was obtained using the method developed by Brooks and Corey (1964) combined with an adjustment for volume change based on the Kozeny-Carmen equation.

Brooks and Corey (1964) present the function for unsaturated hydraulic conductivity as follows:

$$k_w = k_s \qquad \text{For } h \le h_d \qquad (6\text{-}1a.)$$

$$k_w = k_s\left(\frac{h_d}{h}\right)^{\eta} \qquad \text{For } h > h_d \qquad (6\text{-}1b)$$

where:

k_w	=	unsaturated permeability
k_s	=	saturated permeability
h_d	=	displacement pressure
h	=	matric suction
η	=	empirical constant

The empirical constant, η, is related to the pore size distribution index, λ, by:

$$\eta = 2 + 3\lambda \qquad (6\text{-}2)$$

The pore size distribution index is equal to the slope of the matric suction versus effective degree of saturation curve. From the water retention data that was presented in Chapter 4, the pore size distribution index for the Pierre shale was determined to be approximately 0.53 for the drying curve and 0.4 for the wetting curve. These values are consistent with well-aggregated soils in an undisturbed state (Corey, 1986).

The difficulties involved in determining the displacement pressure in expansive soil have been documented by others and are discussed in Chapter 4. For the purposes of this investigation it was assumed that at a degree of saturation of 85 percent or greater the air phase is not continuous and changes in hydraulic conductivity are not significant. Therefore, the displacement head was assumed to be the suction value from the water retention data at which the degree of saturation is equal to 85 percent. From the drying curve data presented by Chao (1995), the value of suction at a degree of saturation of 85 percent is approximately 160 feet. However, data presented by Chao (1995) also indicates that volume change does occur as the degree of saturation goes above 85 percent and

approaches 100 percent. Therefore the hydraulic conductivity was adjusted in that range of suction using the Kozeny-Carmen equation only.

The unsaturated hydraulic conductivity functions based on the Brooks and Corey (1964) method and the Fredlund et al. (1994) method, are shown in Figure 6-4. As discussed in Chapter 5, the suction in the uncovered soil near the surface ranges from zero to 1,600 feet of water. In that range the difference between the two curves is very large when considering its effects on infiltration and evaporation.

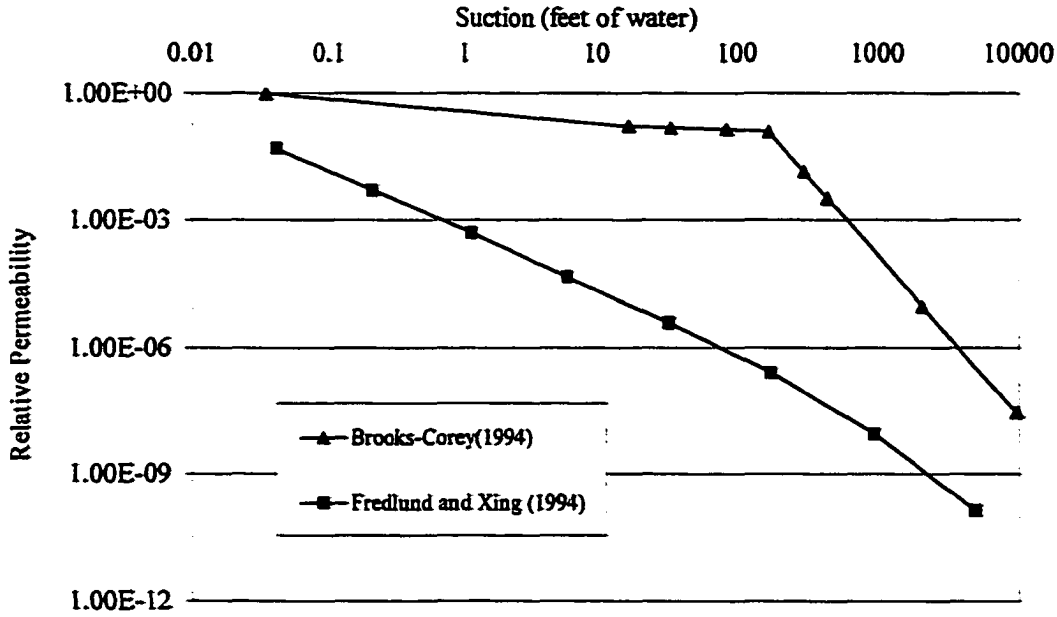

Figure 6-4 Unsaturated hydraulic conductivity functions for Pierre shale

Since the unsaturated hydraulic conductivity was not measured for this investigation, comparison can not be made to actual data. In addition, rigorous evaluation of curve fitting methods for the SWCC and methods for developing the unsaturated hydraulic conductivity function are beyond the scope of this investigation. However, model results

from simulations that utilized the Brooks Corey relationship more closely matched the water content distributions measured in the field over time. It is evident that rigorously evaluated analyses of these important hydraulic functions are necessary for the development of moisture flow modeling in expansive soil.

Thermal conductivity affects the ability of soil to transmit heat just as the hydraulic conductivity affects the ability of soils to transmit water. The rate of heat transfer in soil is a function of the temperature gradient and the thermal conductivity. The thermal conductivity is in turn a function of water content. The SoilCover model uses a method developed by Johansen (1975) to determine the thermal conductivity function. The user specifies a composite percentage of quartz in the soil. The quartz percentage for various soil types ranges from 1.0 for pure sand to 0.7 for pure clay. For this investigation the percent quartz was assumed to be 0.75.

Volumetric specific heat of a soil is defined as the amount of stored heat required to change the temperature of a unit volume of soil by one degree Celsius, and is also a function of water content of the soil. The SoilCover model calculates the volumetric specific heat function based on the mass density of the soil.

6.2.1.2 Climate Data

Climate data include the minimum and maximum temperature, net solar radiation, minimum and maximum relative humidity, and wind speed. The top boundary condition can be updated daily as pressure, water content, or precipitation. The top boundary condition can also be partitioned to occur during specific hours of the day.

Climate data was obtained from the Colorado Agricultural Meteorological (CoAgMet) Station ftc01 located approximately 4 miles northwest of Fort Collins at the Agricultural Engineering Research Center (AERC). Complete data was available from February 1, 1992 to present.

In addition to the daily climate data input, the model allows the user to specify periods of vegetation growth and freeze-thaw. The vegetation model is based on the vegetation uptake source term method combined with a shade, or cover factor term. Input data for the vegetation model includes root depth, the moisture limiting point, the moisture wilting point, and the leaf area index. In addition the user specifies the time of year over which the vegetation is active.

Vegetation at the CSU site consists primarily of native perennial grasses and sparsely scattered forbs and shrubs. The dominant species of grasses include blue grama, Japanese brome, cheatgrass, Buffalo grass, and green needle grass. Root depths for these species range from 0.5 feet to 5 feet.

Lack of available plant water causes most plants to biologically react by closing stoma and reducing transpiration. At a suction value of approximately 33 feet (100 kPa) the plant limiting factor is reduced linearly as a function of the log of matric suction, and plant transpiration is reduced to zero at a suction of 500 feet (1,500 kPa). This plant-limiting model is one of several from the plant science and soil physics literature. As a simple method for estimating transpiration this default function was used for vegetation modeling at the CSU site.

The leaf area index function is automatically generated within the SoilCover model based on the grass quality and growing season specified by the user. The average growing season for the Denver/Fort Collins area is from May 1st to October 13th and this was the assumed growing season for all of the simulations that were conducted.

SoilCover also allows the user to specify a time of year over which the soil is frozen. The model develops a soil-freezing curve using the Clapeyron equation (see SoilCover (1997)). They state however that the Clapeyron equation is severely limited, as it is not ideal for use in soils that contain a mixture of capillary and adsorptive water forces. During the time over which the soil is frozen, evaporation and infiltration does not occur. Since this time period can be significant at the CSU site the soil-freezing model was used.

The time over which the soil is frozen was determined by plotting daily soil temperature data versus time. The data was obtained at the CoAgMet site from a depth of 2 inches and is shown in Figure 6-5. It was assumed for this investigation that if the temperature at a depth of 2 inches was less than one degree Celsius then the surface of the soil was frozen. This allows for a gradient in temperature of one degree Celsius between the surface of the soil and the soil at a depth of 2 inches.

The soil freeze-thaw model also allows the user to specify a depth of surface water to simulate snow melting on the surface as warming occurs at the end of the freeze-thaw period. Snow accumulation at the CSU site is sporadic and sufficient data was not available to accurately simulate it. However, precipitation that was measured during that time period was introduced as water on the surface.

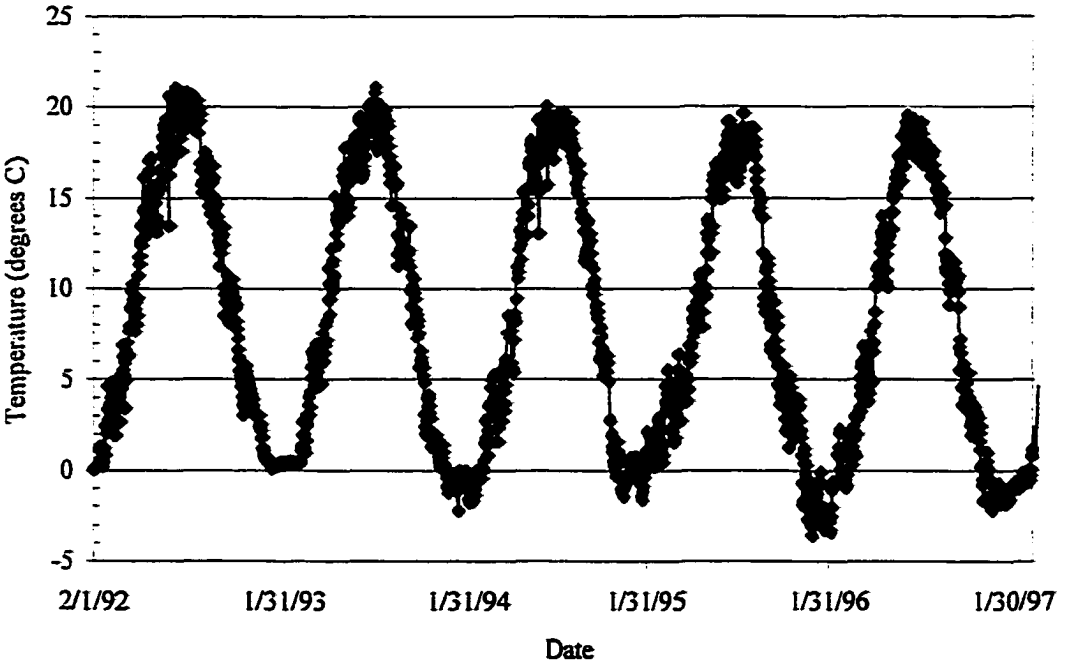

Figure 6-5 Ground temperature measured at 2 inches depth at CSU site

6.3 Model Validation

The accuracy of the SoilCover model was evaluated in the uncovered soil and in the covered soil using the field measured water content data. Field data for comparison in the uncovered soil was obtained from access tubes E-0, X-5, and J-5, adjacent to the slab. Field data for comparison in the covered soil was obtained from access tubes D-5, E-3, E-5, E-7, and F-5 from the center of the slab. In addition TCP data collected at J-5.5, D-8.5, and D-6.5 were compared to model output for suction and temperature.

In the uncovered soil the surface flux will vary between evaporation and infiltration conditions dependent upon the daily climate conditions. In ideal conditions beneath the center of the simulated slab, an initial relatively dry soil profile will increase in water content due to the reduction of evaporation at the soil surface. When the total head

becomes constant with depth, moisture migration in the vertical direction is controlled by temperature fluctuations at the surface. Under these conditions the water content profile, assuming a homogeneous soil profile, is roughly constant with depth except for fluctuations near the surface due to temperature. A one-dimensional column of homogeneous soil 20 feet in depth was used to model the CSU site. Model soil and climate input data were discussed above and typical model input pages from 1993 model simulations that used drying curve SWCC are shown in Appendix E.

6.3.1 Uncovered Soil

6.3.1.1 Water Content Data

Water content data was collected from January 1993 to November 1997. The initial water content conditions in the soil were determined from the average of the measured water content values from access tubes E-0, X-5, and J-5, the three locations in the uncovered soil and access tubes D-5, E-3, E-5, E-7, and F-5 from the center of the slab. Comparisons of the water content trends at the three locations on the north, east, and west sides of the slab respectively, and the five locations in the center of the slab indicate that the soil profiles are similar and the variations in water content with depth and time are consistent. These eight locations provide an average representation spatially for the site. The initial water content distribution based on the average data is shown in Figure 6-6.

The initial water content profile varies from approximately 12 percent at 1 foot to 15 percent at 7 feet. Below 7 feet the water content is a relatively constant 15 percent with depth. For the purposes of modeling, this was the assumed initial water content distribution at the CSU site on February 1, 1992.

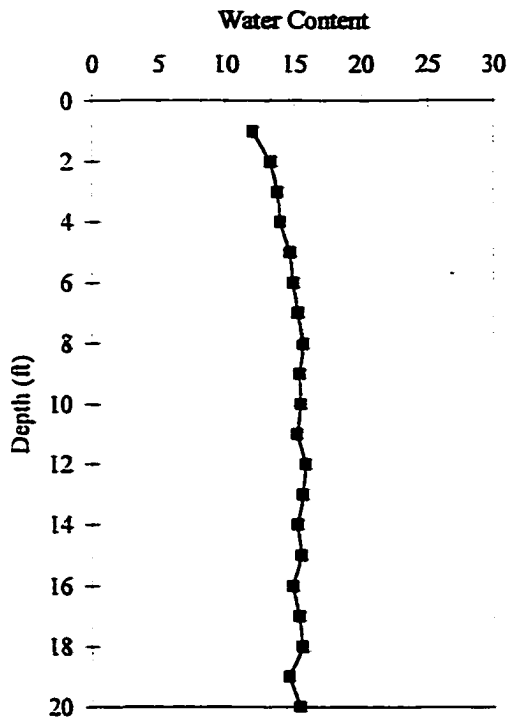

Figure 6-6 Initial water content distribution for SoilCover modeling

A preliminary simulation was conducted from February 1, 1992 to October 31, 1992 to allow the model to equilibrate to the initial conditions. The SoilCover model allows maximum simulation periods of one-year. Therefore at the end of each simulation the final suction profile was used as the initial conditions for the subsequent simulation. On November 1, 1992 the suction profile from October 31, 1992 was used to start the second year of modeling, and subsequent simulations were conducted from November 1st to October 31st of the respective years.

To evaluate the accuracy of the model measured water content profiles from the field were compared to the water content profiles from the model for the same days. Figures 6-7 through 6-16 show the measured water content profiles and the profiles for the same days from the model simulations for years 1993 through 1997, respectively.

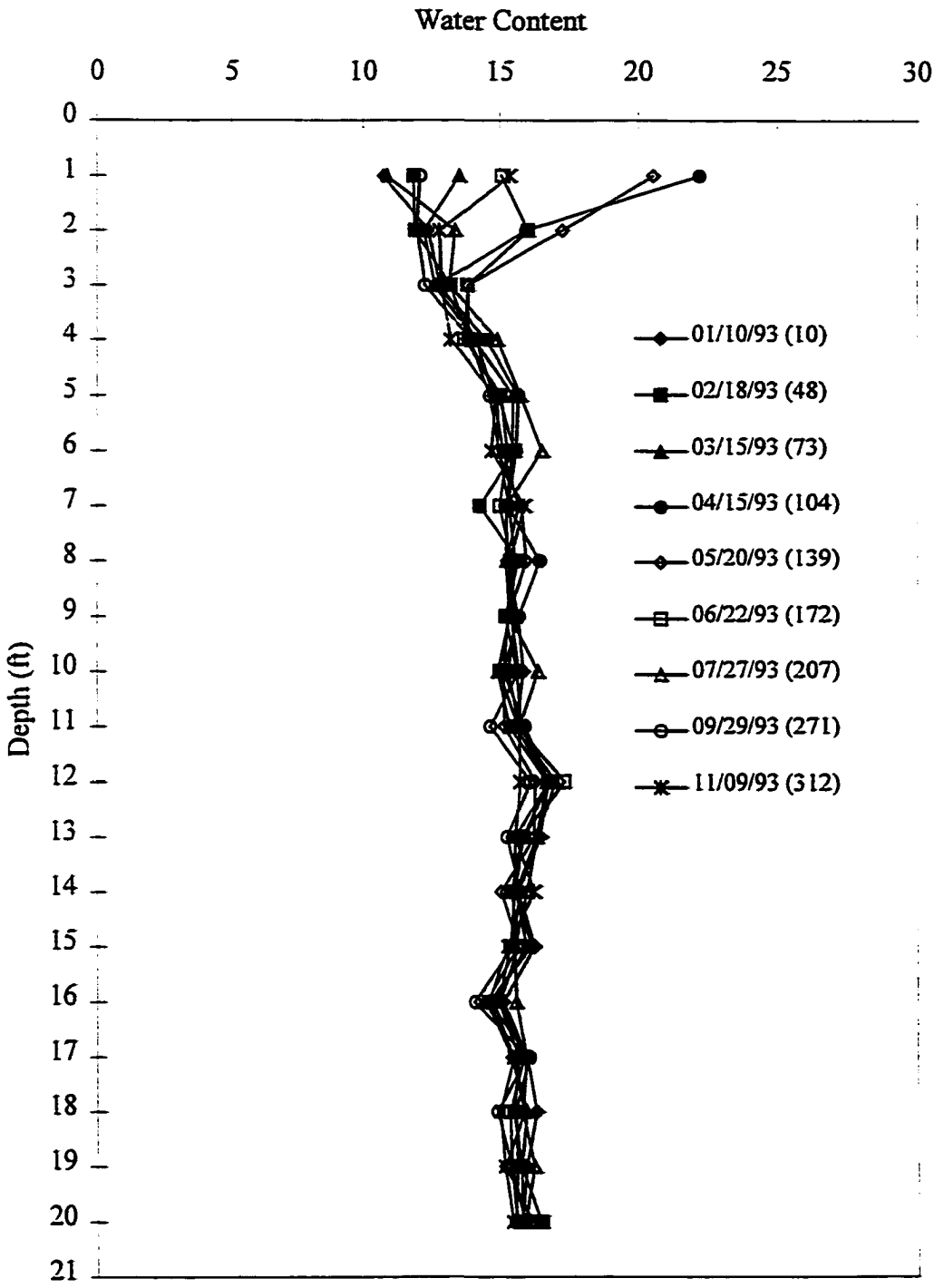

Figure 6-7 Measured water content profiles from 1993 in uncovered soil at CSU (based on average from X-5, J-5, and E-5)

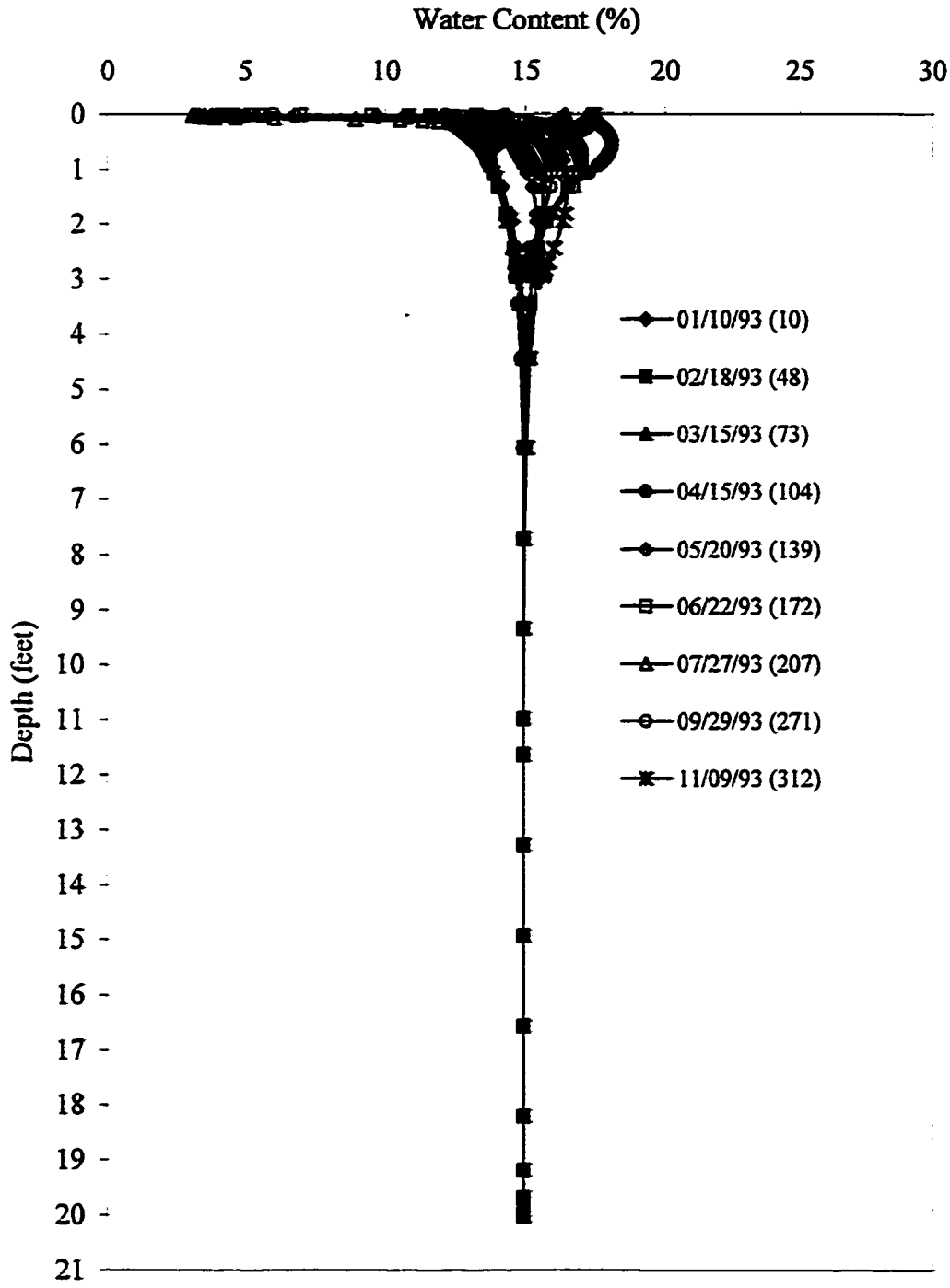

Figure 6-8 Model predicted water content profiles from 1993 in uncovered soil at CSU

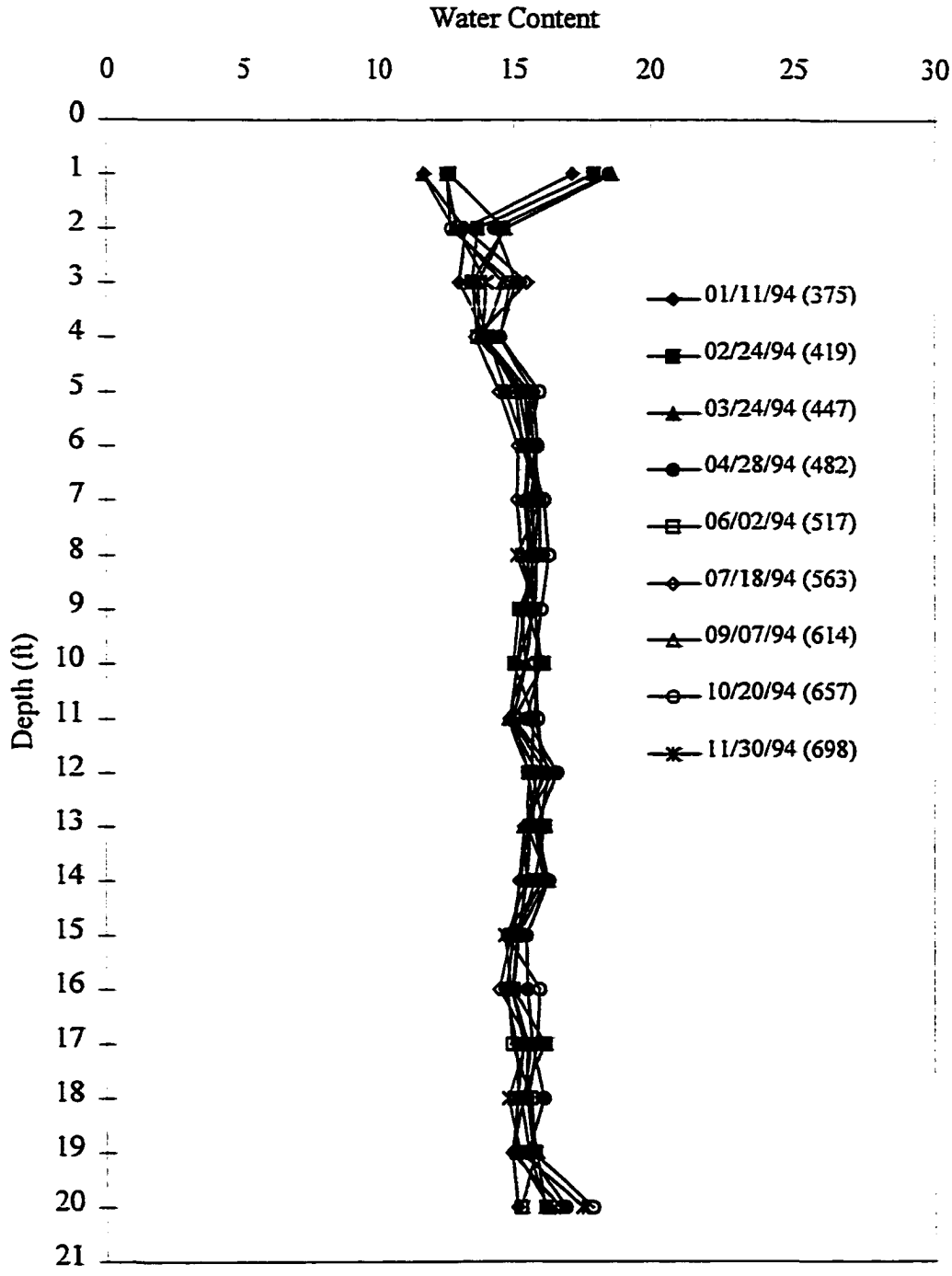

Figure 6-9 Measured water content profiles from 1994 in uncovered soil at CSU (based on average from X-5, J-5, and E-5)

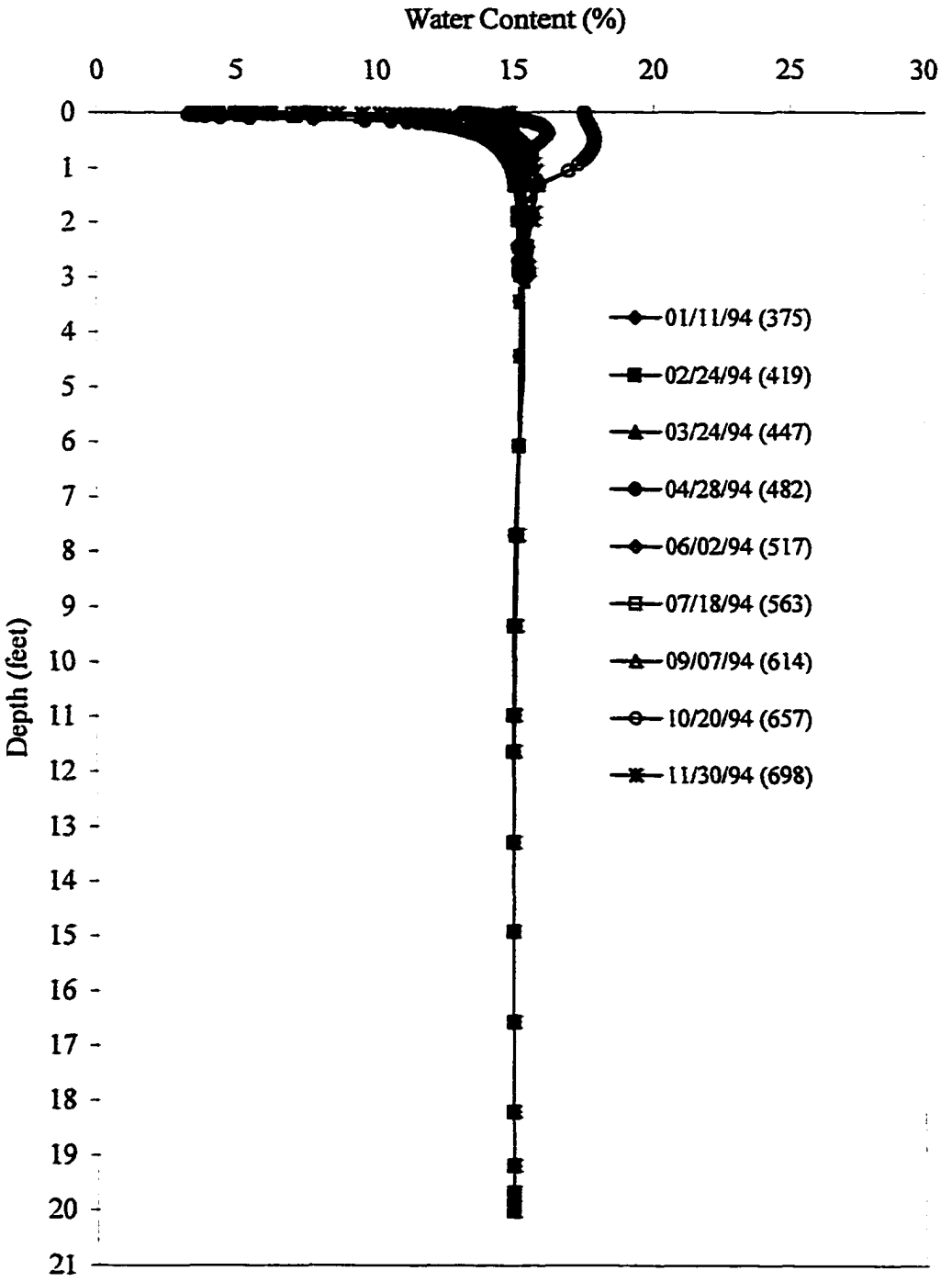

Figure 6-10 Model predicted water content profiles from 1994 in uncovered soil at CSU

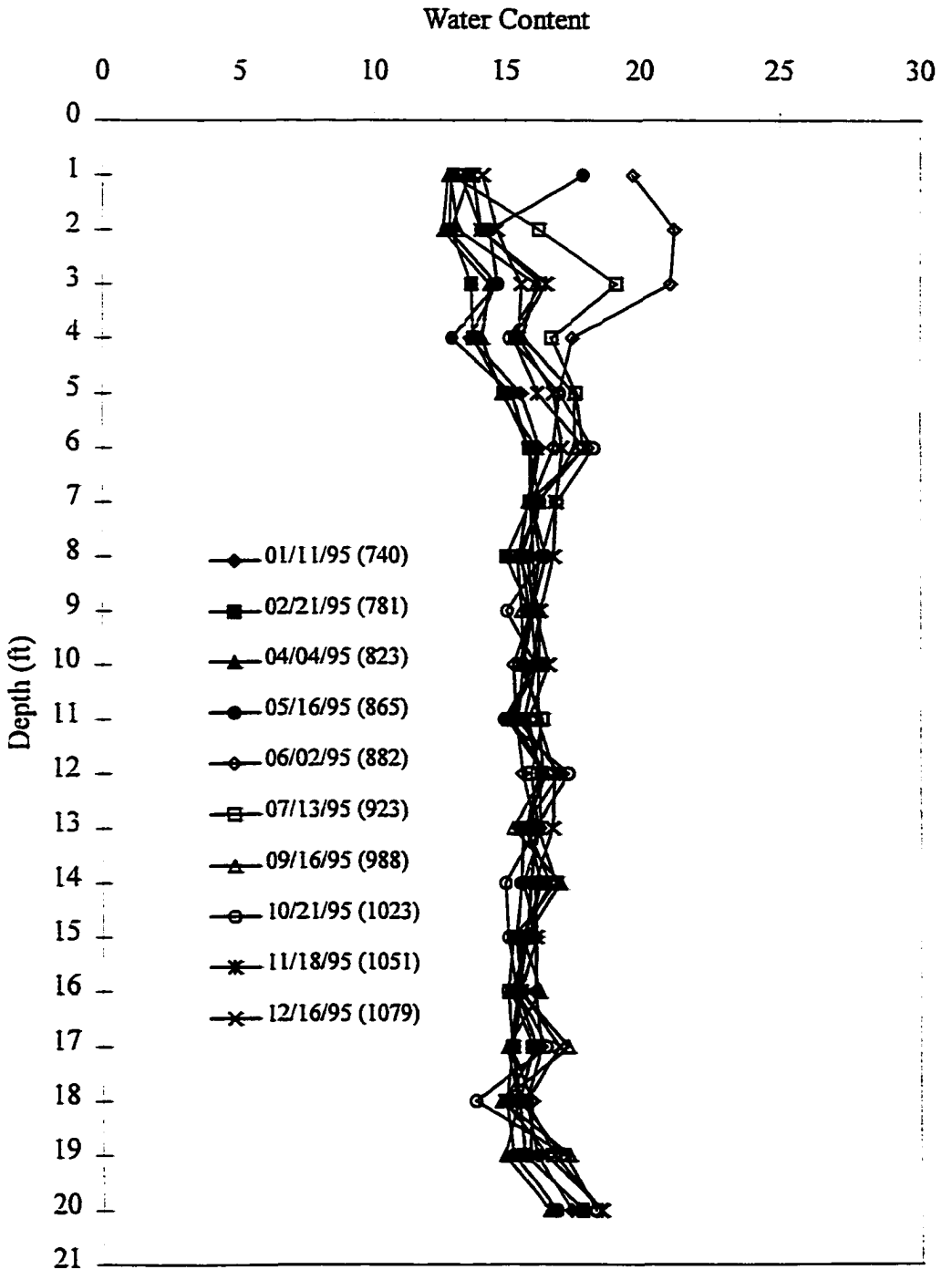

Figure 6-11 Measured water content profiles from 1995 in uncovered soil at CSU (based on average from X-5, J-5, and E-5)

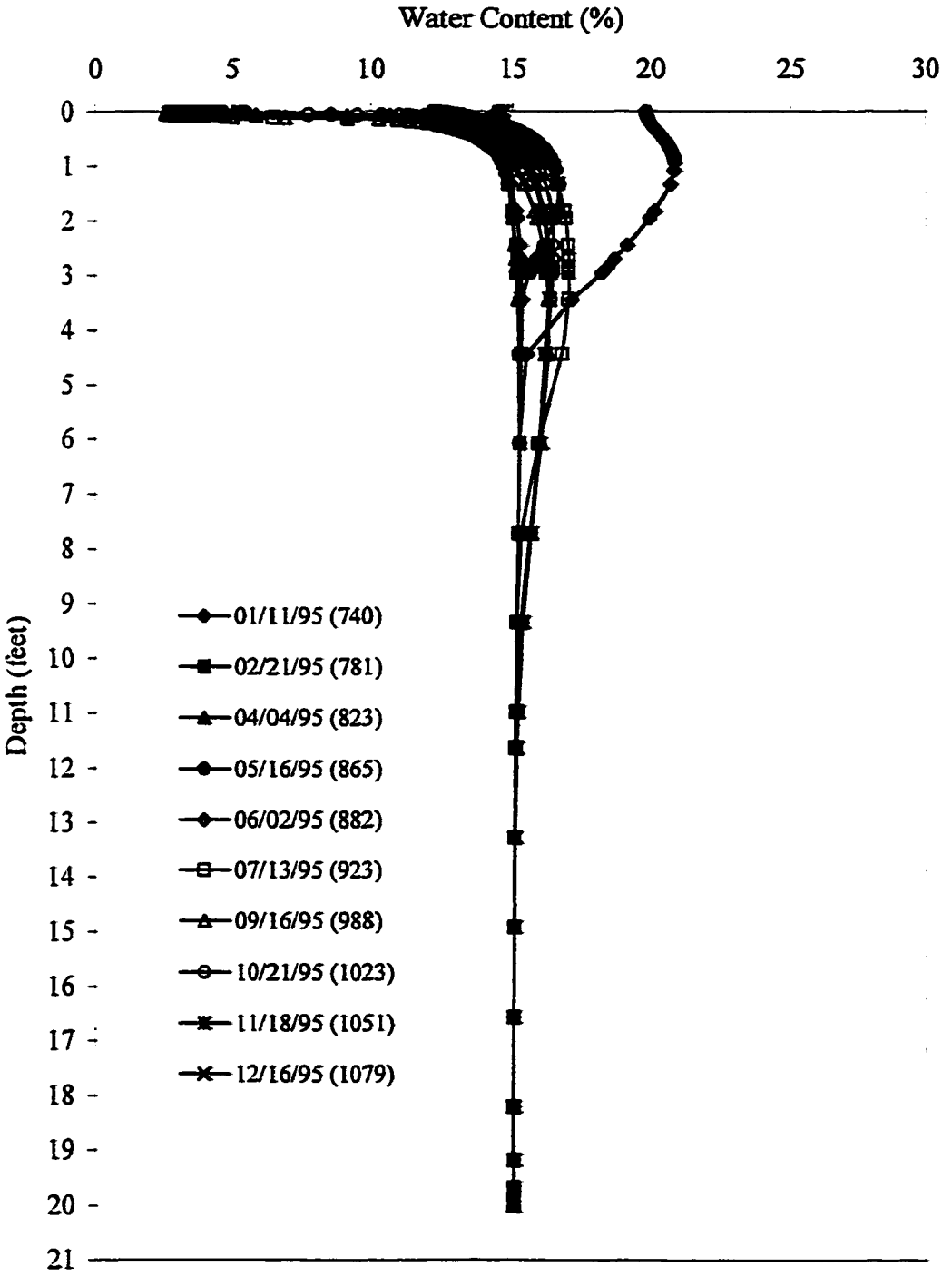

Figure 6-12 Model predicted water content profiles from 1995 in uncovered soil at CSU

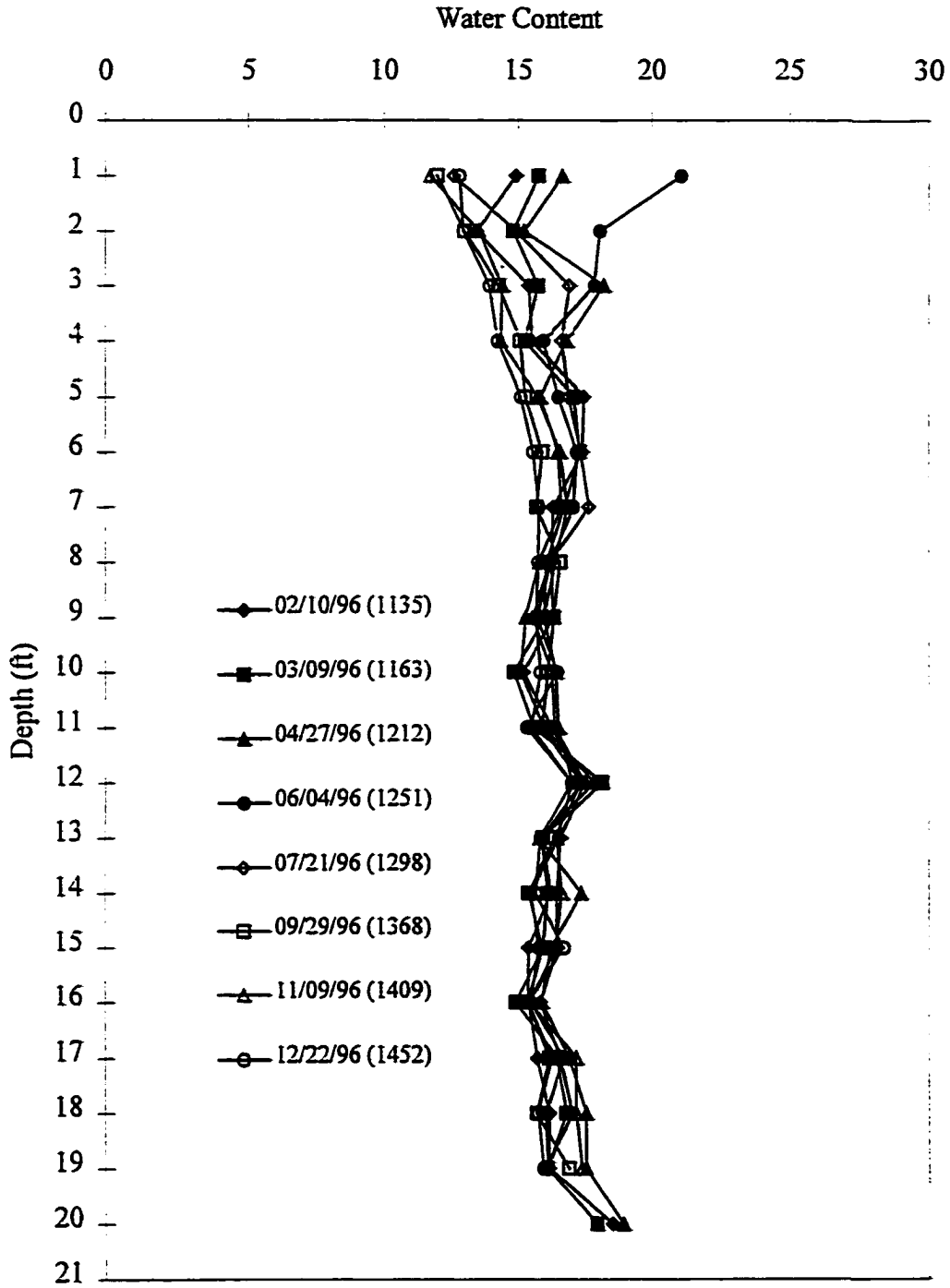

Figure 6-13 Measured water content profiles from 1996 in uncovered soil at CSU (based on average from X-5, J-5, and E-5)

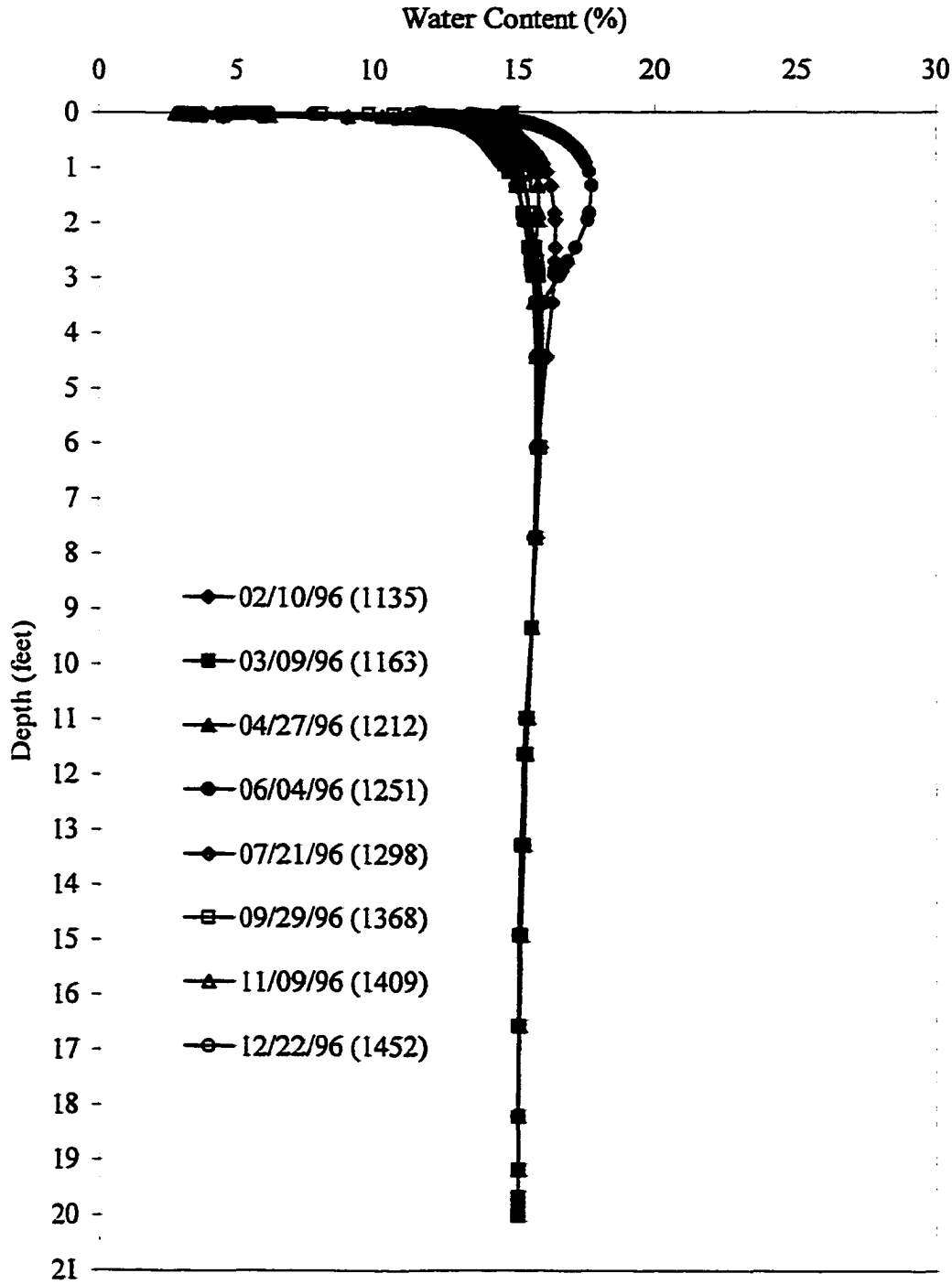

Figure 6-14 Model predicted water content profiles from 1996 in uncovered soil at CSU

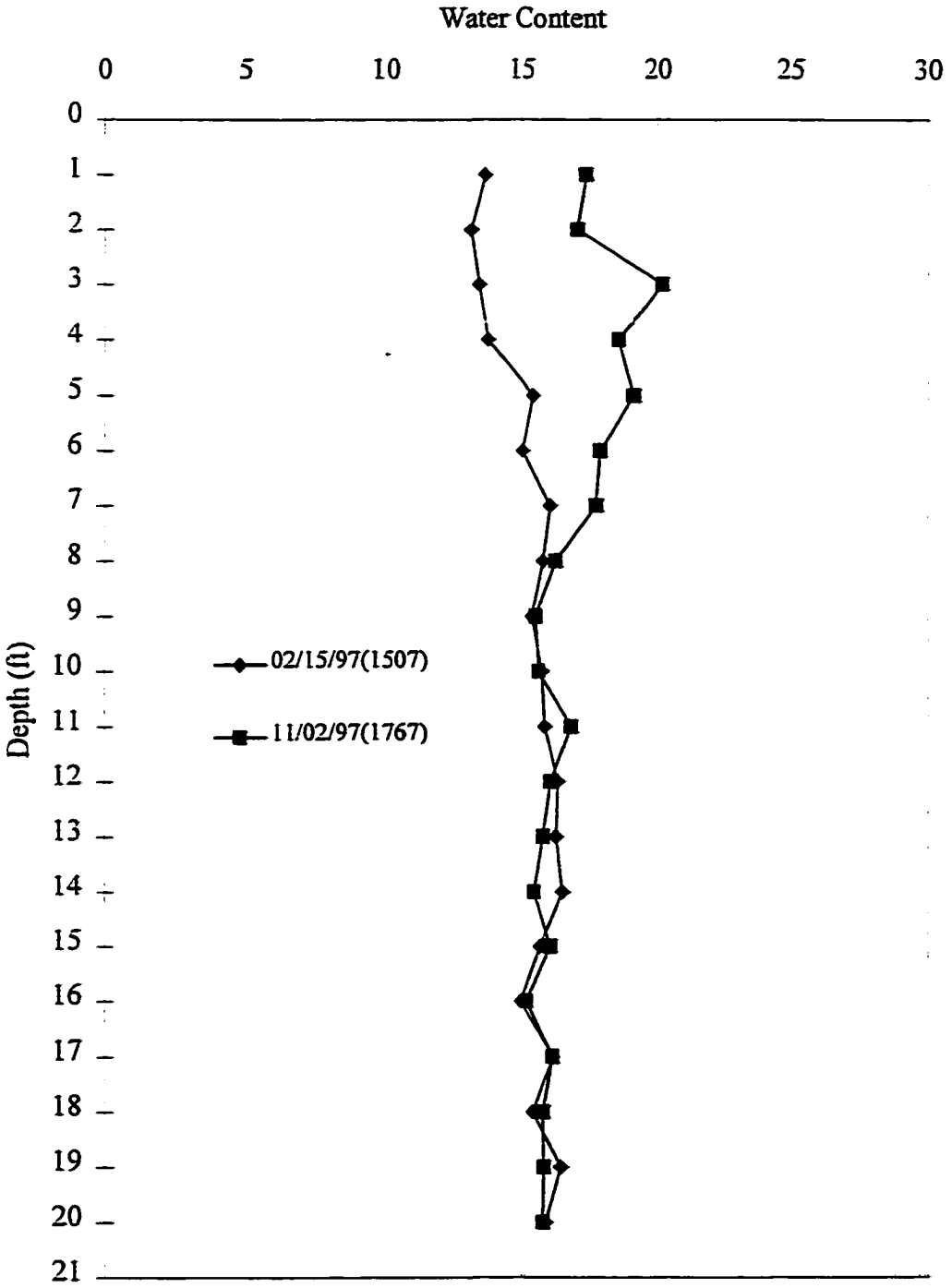

Figure 6-15 Measured water content profiles from 1997 in uncovered soil at CSU (based on average from X-5, J-5, and E-5)

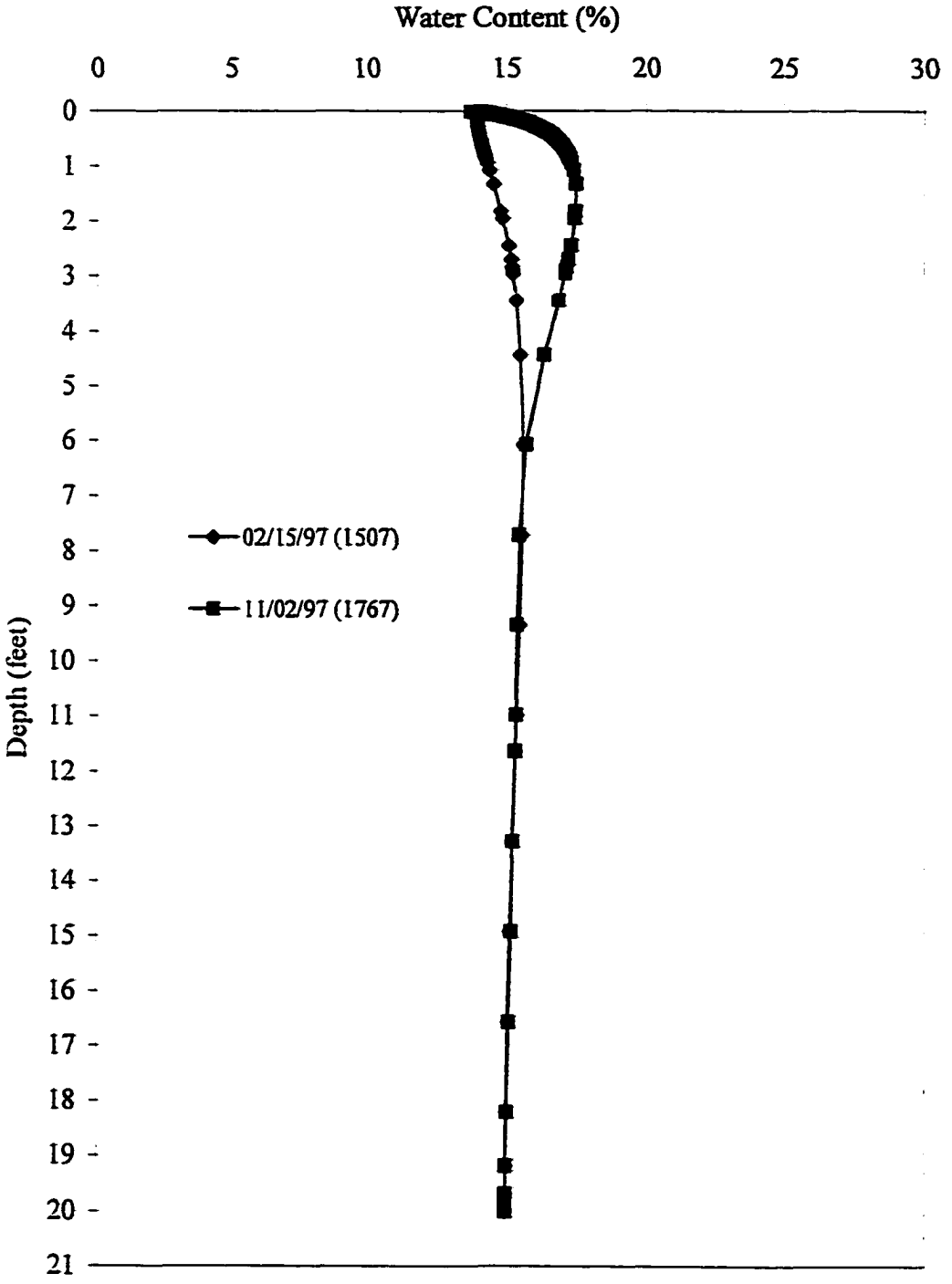

Figure 6-16 Model predicted water content profiles from 1997 in uncovered soil at CSU

The last water content measurement at the site was on November 2, 1997. The water content profiles from model results are from the drying curve model simulations. The wetting curve model simulations are discussed later.

In general the water content profiles from the model simulations follow the same trends with time as the measured water content profiles. The water content values from the model, at depth, are constant at 15 percent. The measured water content at depth also remains relatively constant at approximately 15 percent. The depth of seasonal moisture fluctuation varies from year to year between approximately 2 feet and 7 feet in both the measured and modeled profiles. The water content fluctuations measured within the upper few feet of soil vary between approximately 10 and 25 percent. In the same zone the water content from the model fluctuates between approximately 12 and 20 percent.

This difference between the model results and the field-measured values can be seen in Figures 6-17 through 6-22. The water content values measured at various depths in the soil and obtained from the model are plotted as a function of time. The results from the model using the wetting and drying curves are presented for comparison.

The results shown in Figures 6-17 through 6-22 show generally good agreement between the model and the field. In general, the field measured water content data fluctuates between the water content from models that used the drying curve SWCC and the water content from models that used the wetting curve SWCC. This is expected since near the surface of the soil the flux varies between infiltration and evaporation depending on the climate conditions. Since SoilCover is not capable of modeling the hysteretic nature of the soil at the surface there is some error during the transition between flux states.

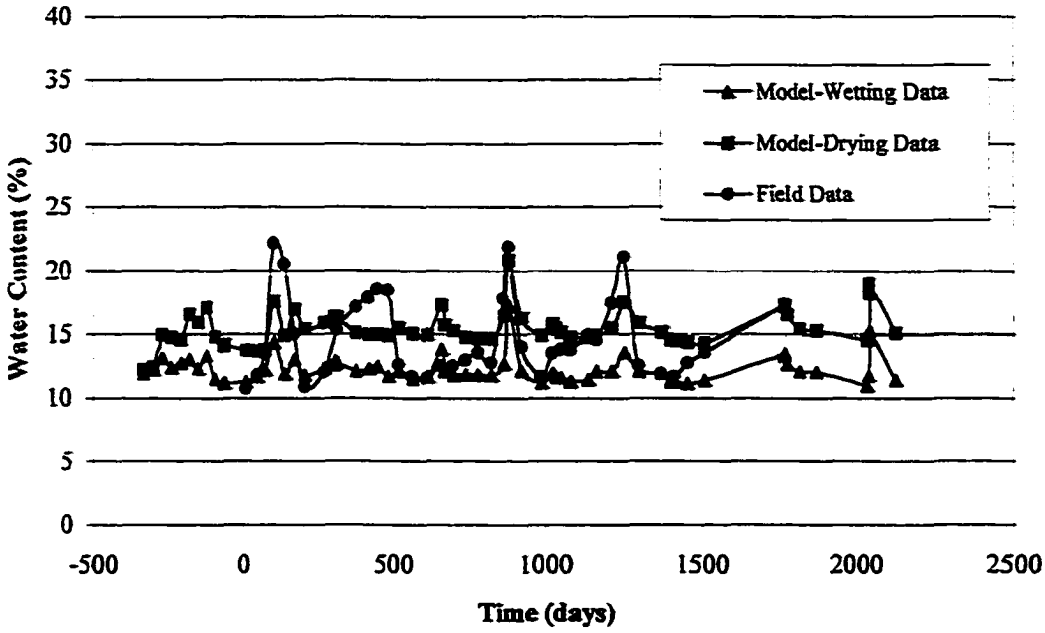

Figure 6-17 Water content at 1 foot in the uncovered soil from the CSU site

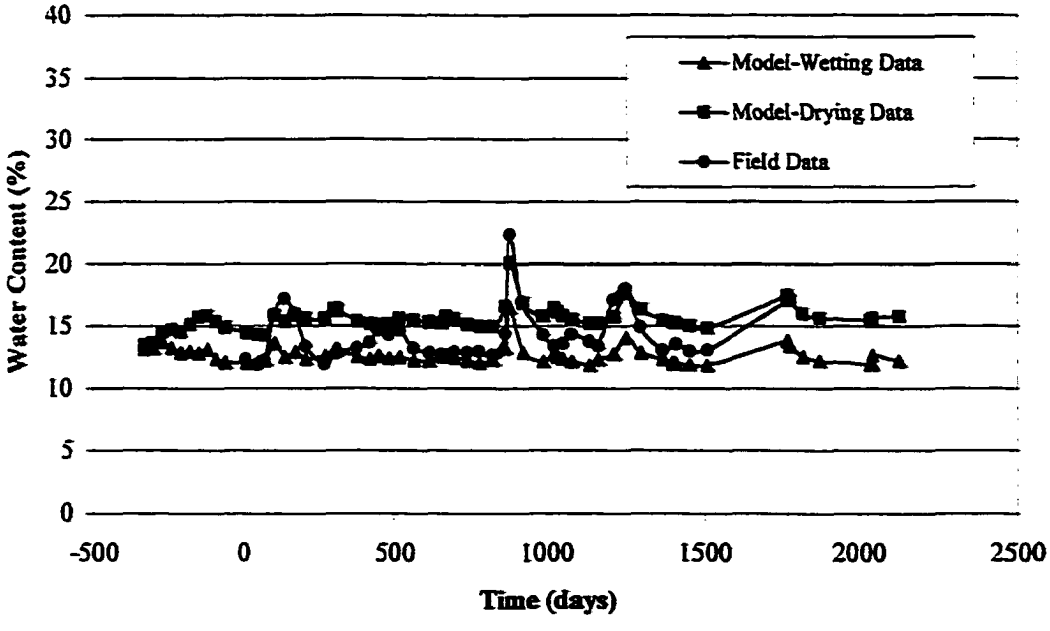

Figure 6-18 Water content at 2 feet in the uncovered soil from the CSU site

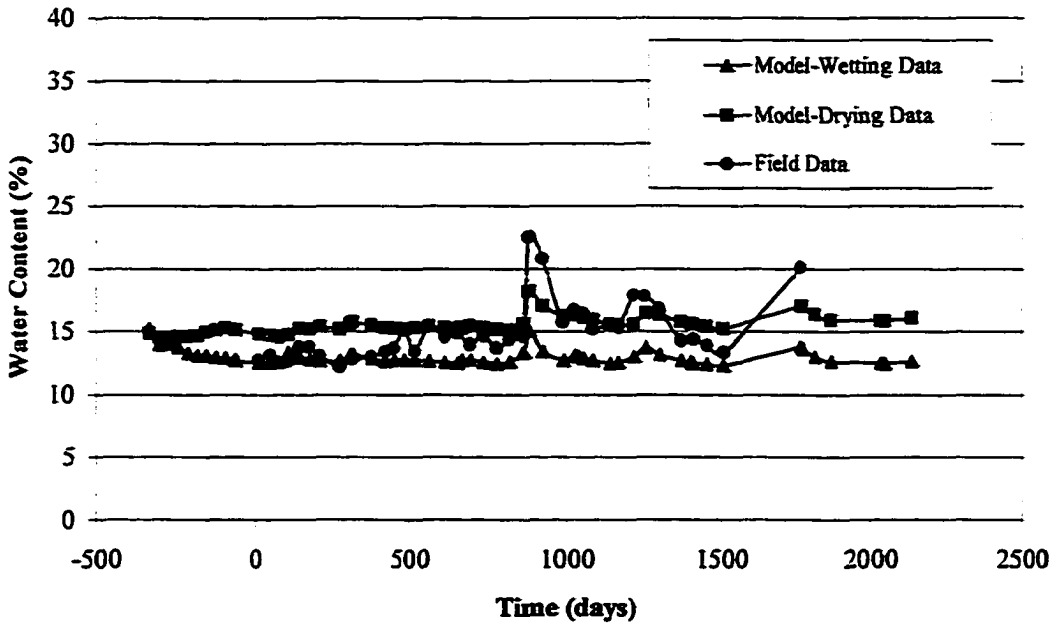

Figure 6-19 Water content at 3 feet in the uncovered soil from the CSU site

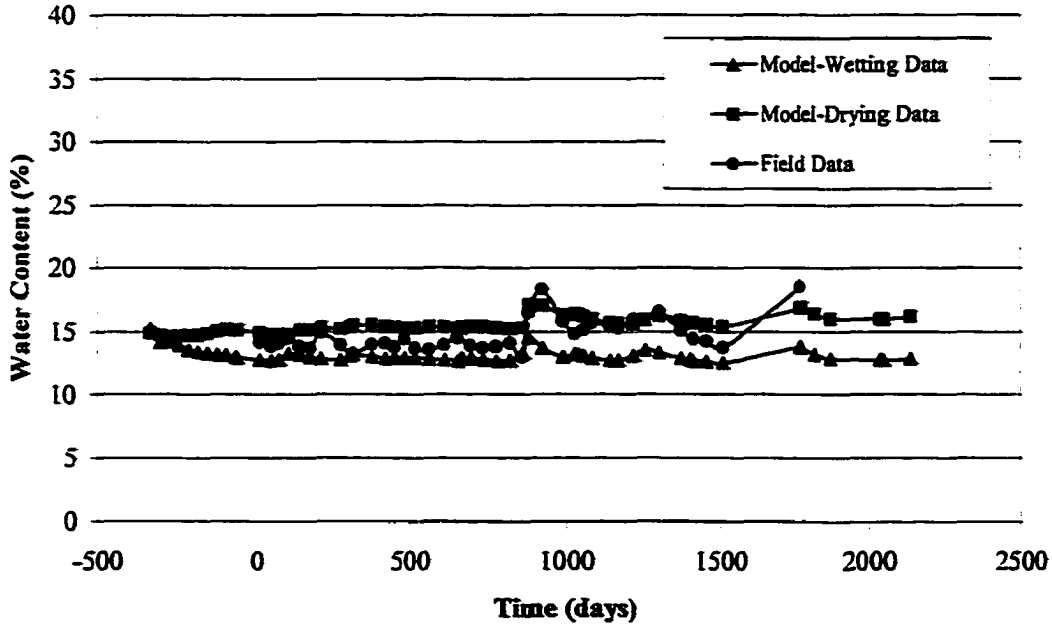

Figure 6-20 Water content at 4 feet in the uncovered soil from the CSU site

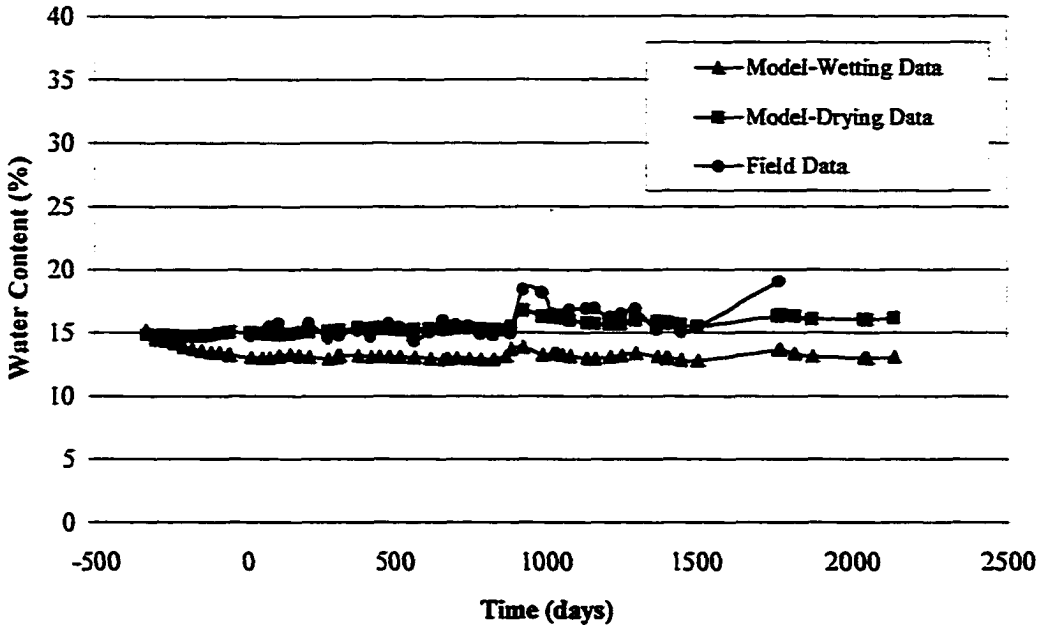

Figure 6-21 Water content at 5 feet in the uncovered soil from the CSU site

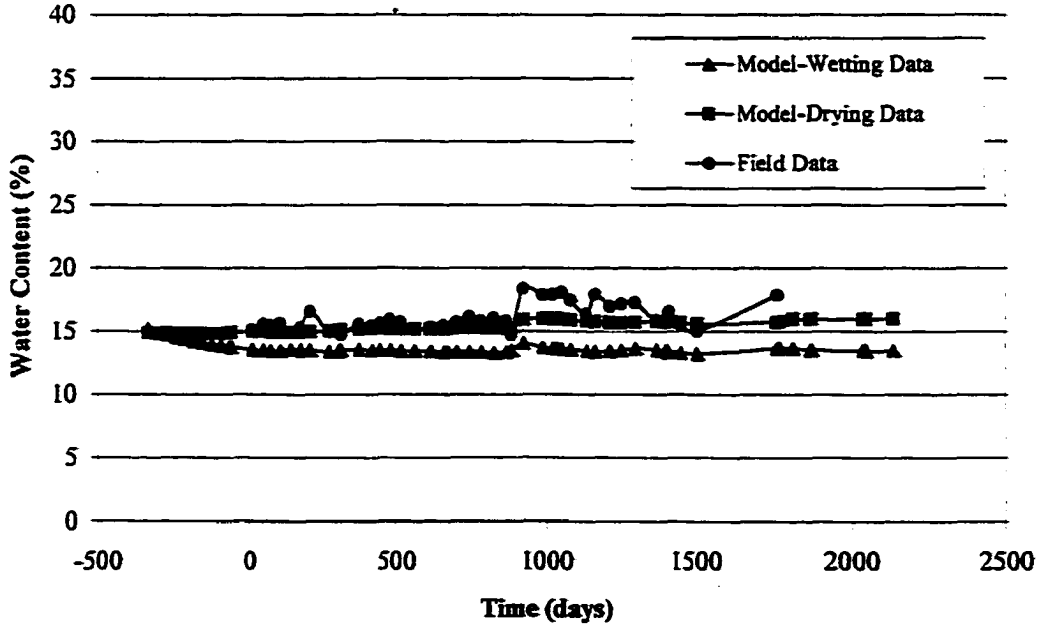

Figure 6-22 Water content at 6 feet in the uncovered soil from the CSU site

This pattern is more noticeable near the surface than at depth. At depths of 5 and 6 feet the measured water contents correlate more closely with the water contents obtained from the model simulations that used the drying data.

6.3.1.2 Suction Data

Suction data was collected at J-5.5 in the uncovered soil between September 1993 and November 1998. TCP's were installed at depths of 2, 5, 8, 11, 14, and 17 feet. Suction data from each location as a function of time, from the model and from the field, are shown in Figures 6-23 through 6-28, respectively. The field measured suction data tend to fluctuate significantly at each depth compared to the model output, and by a higher magnitude closer to the surface. Suction values below 5 feet tend to correlate better with the modeled suction values that were obtained using the wetting curve SWCC.

Figure 6-29 shows the measured water content at access tube J-5 and suction at TCP location J-5.5 from 2 feet, as a function of time on the same graph. In general the water content-suction relationship from the field is consistent with expected trends. However, there is a slight lag time in the response of water content change to change in suction. This is expected since the seepage velocity is a function of hydraulic conductivity and the total head gradient.

Figure 6-30 shows the model simulated water content and suction, from 2 feet, as a function of time on the same graph. The water content-suction relationship from the model is consistent with expected trends. The lack of the lag time effect in the model output results from the inability of the model to simulate the hysteresis effect.

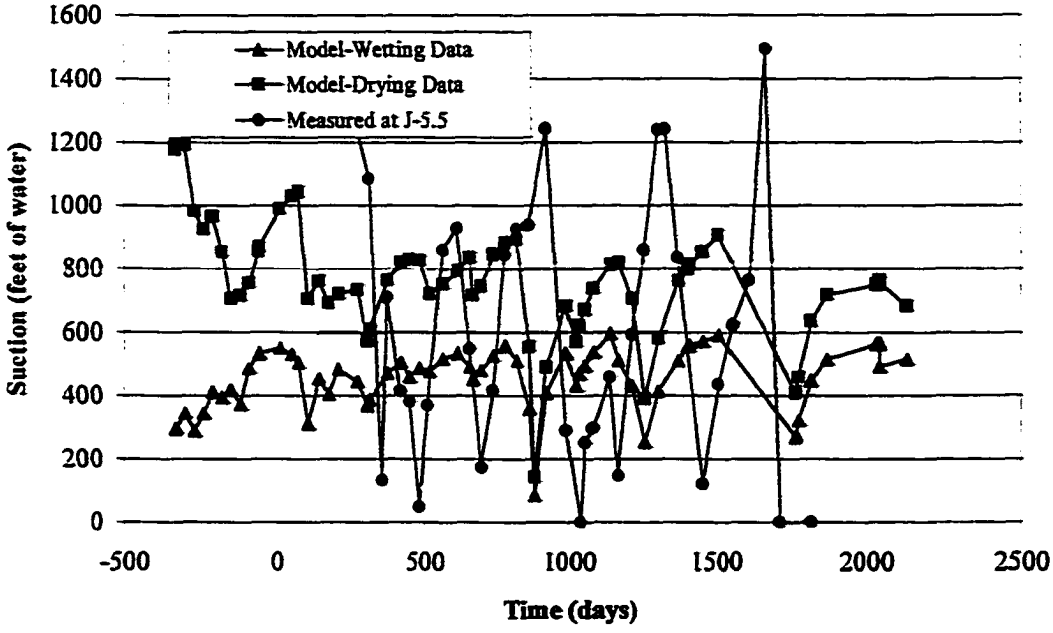

Figure 6-23 Suction at a depth of 2 feet in the uncovered soil at the CSU site

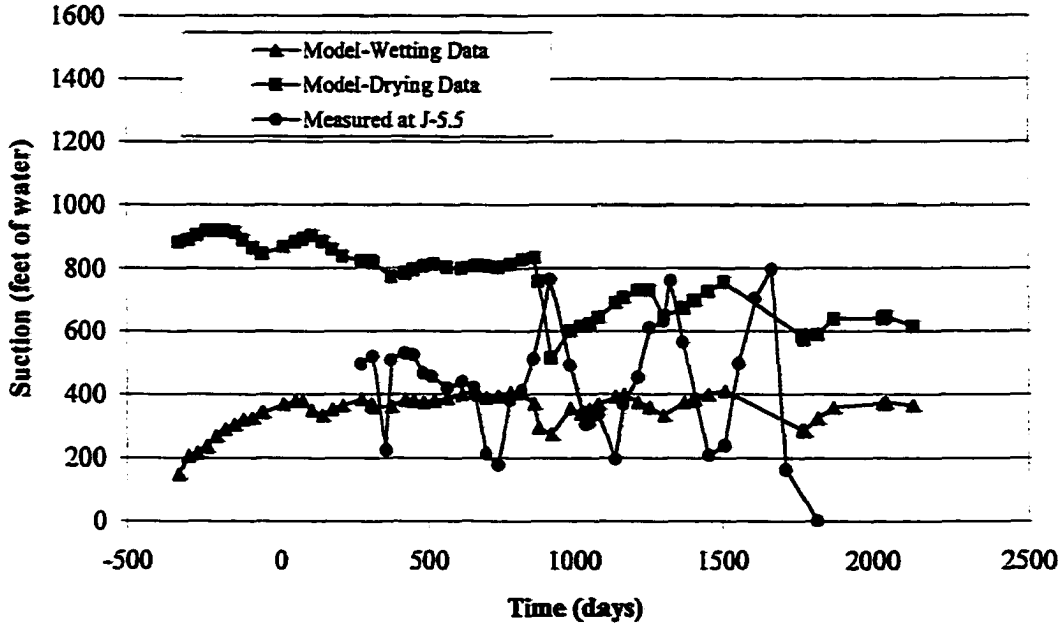

Figure 6-24 Suction at a depth of 5 feet in the uncovered soil at the CSU site

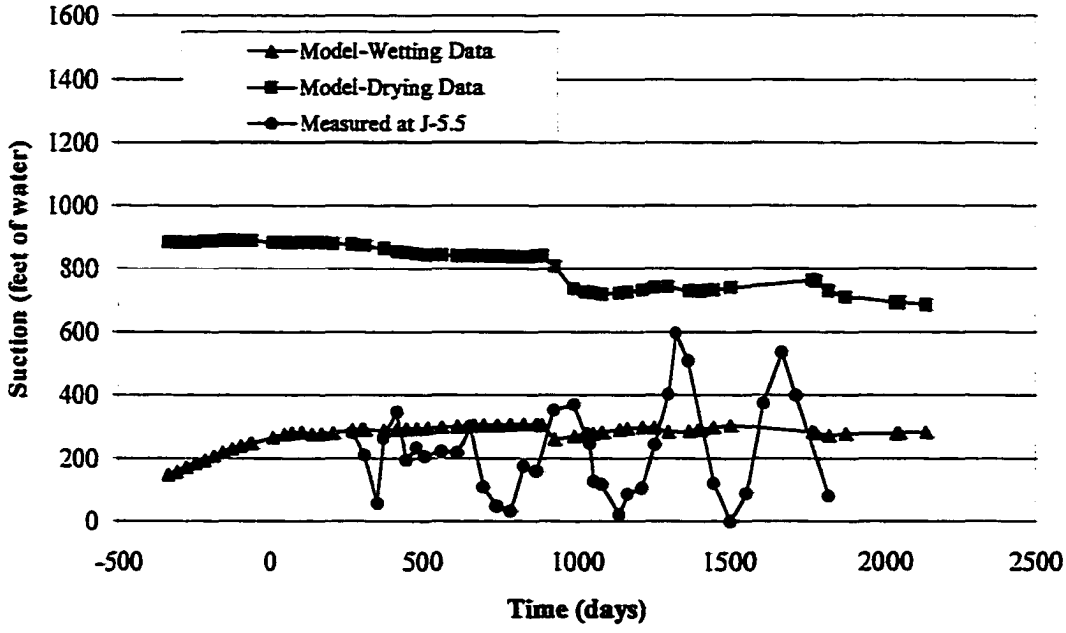

Figure 6-25 Suction at a depth of 8 feet in the uncovered soil at the CSU site

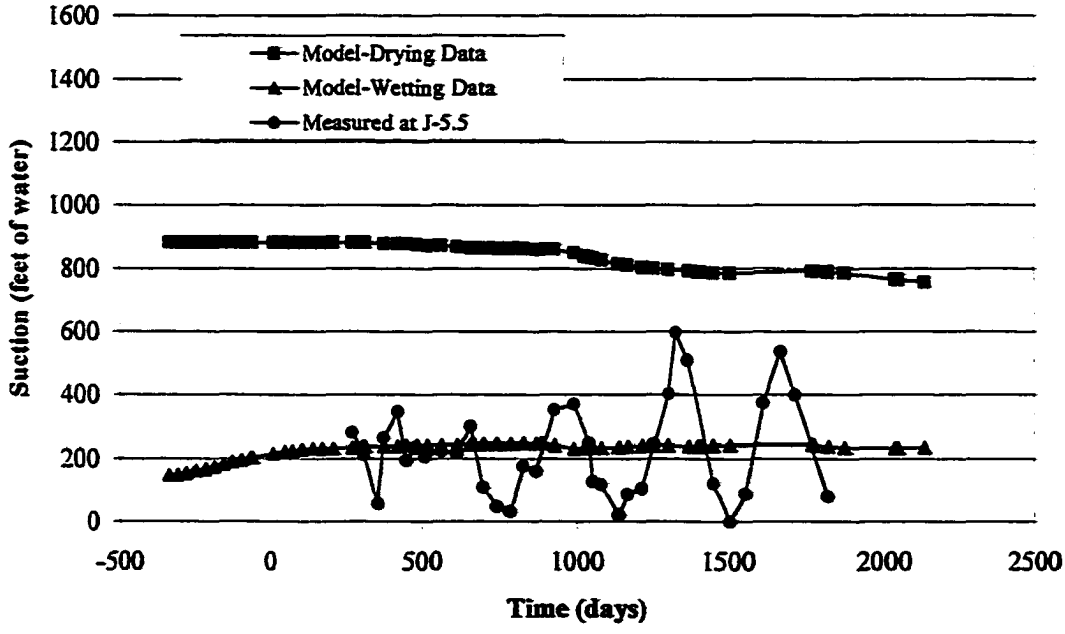

Figure 6-26 Suction at a depth of 11 feet in the uncovered soil at the CSU site

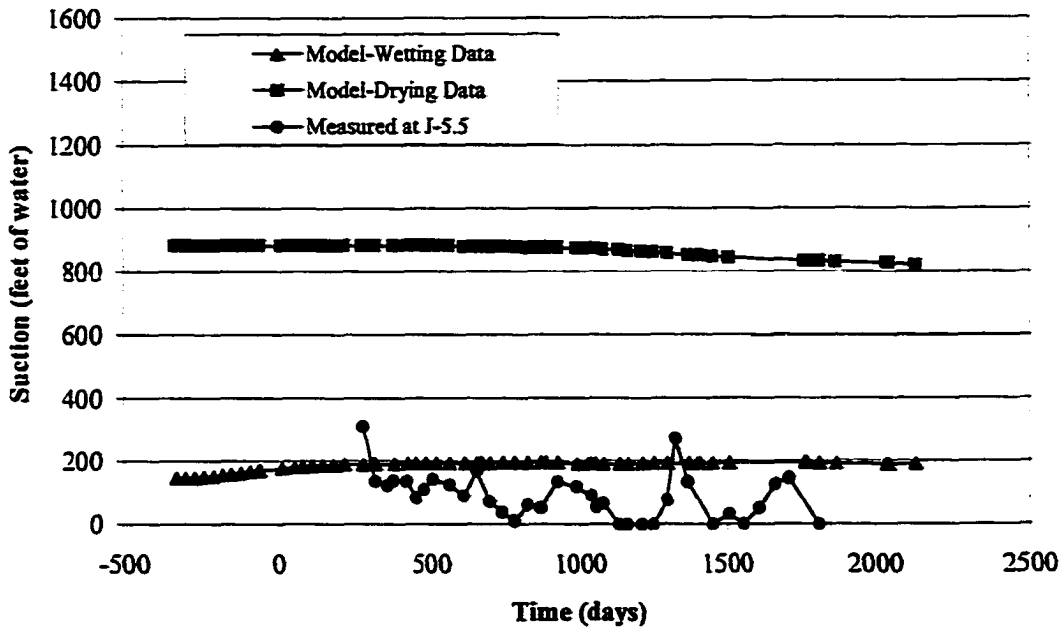

Figure 6-27 Suction at a depth of 14 feet in the uncovered soil at the CSU site

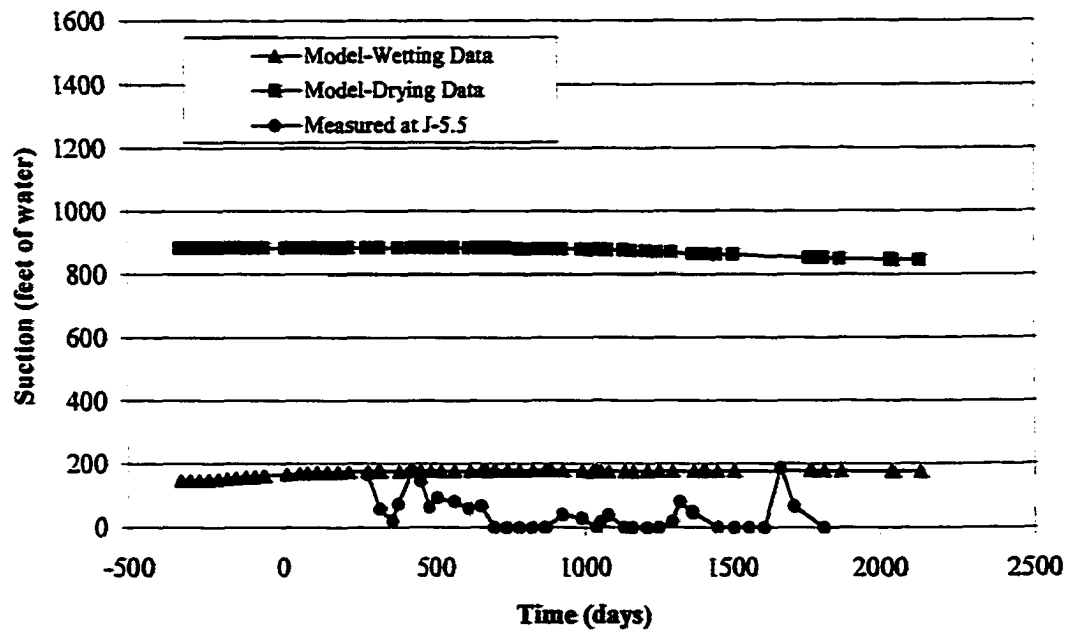

Figure 6-28 Suction at a depth of 17 feet in the uncovered soil at the CSU site

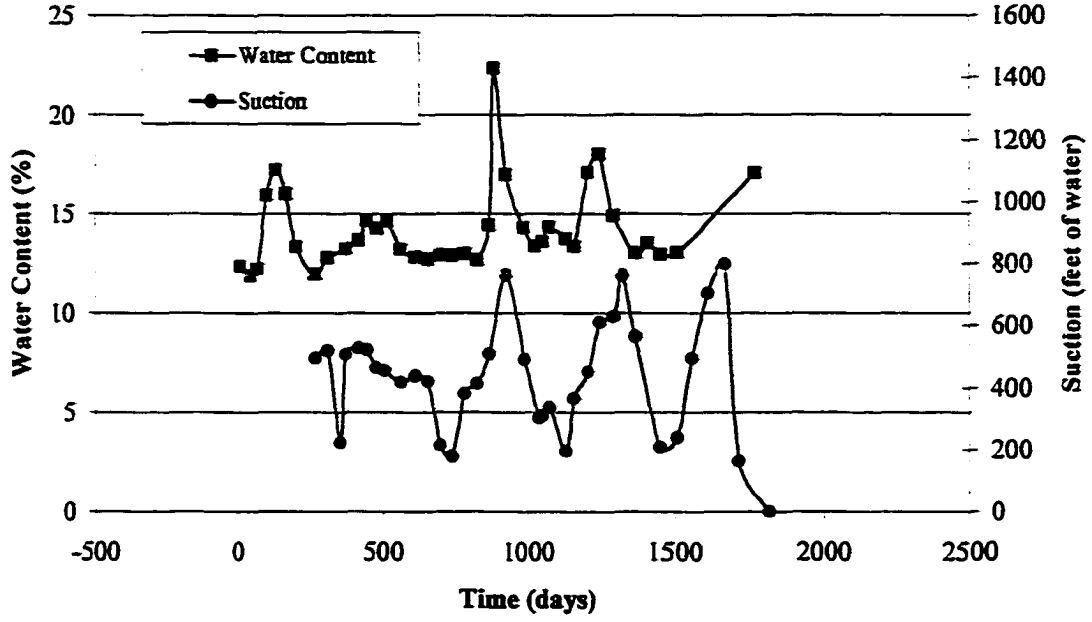

Figure 6-29 Measured water content and suction at a depth of 2 feet in the uncovered soil at the CSU site

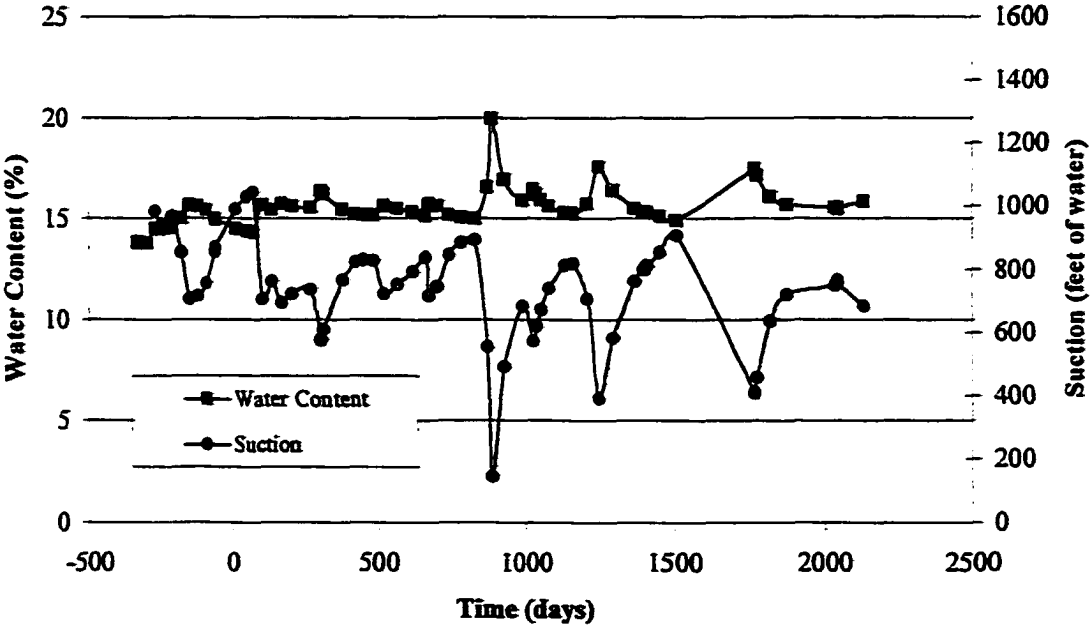

Figure 6-30 Modeled water content and suction at a depth of 2 feet in the uncovered soil at the CSU site

Figure 6-31 illustrates the effect of hysteresis and shows the actual field data compared with the model SWCC data. The water content data is from access tube J-5 and the suction data is from TCP location J-5.5. In general the field measured suction and water content data plot between the wetting and drying curves. However, the water content-suction relationship based on data from below 8 feet tends to be steeper than the laboratory curves.

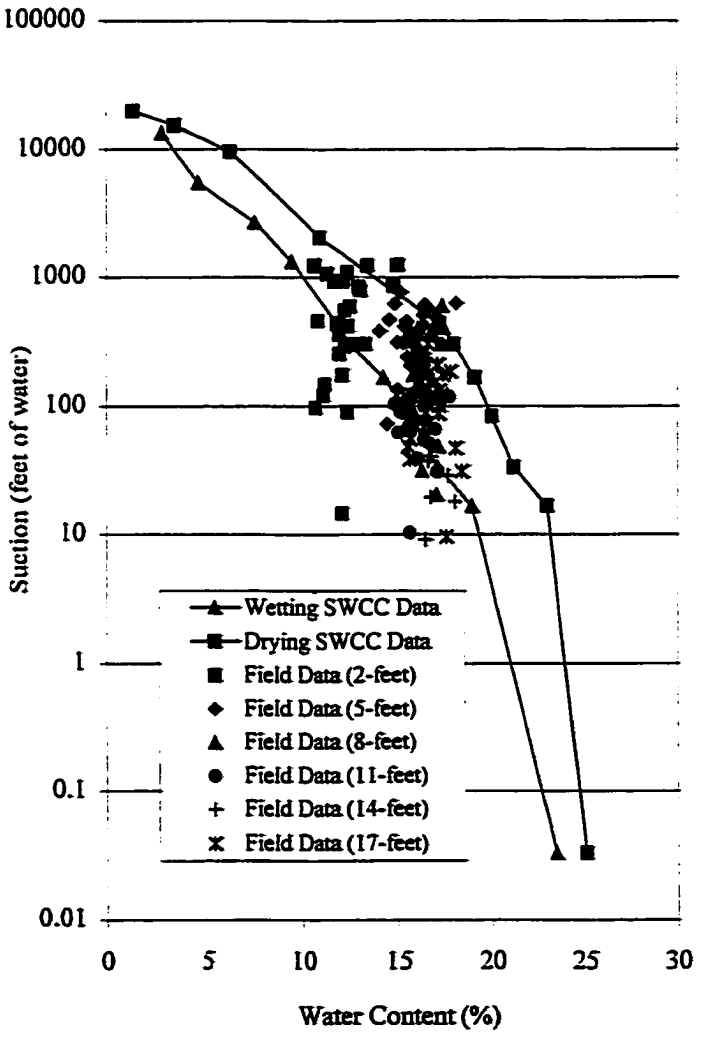

Figure 6-31 Field measured suction-water content data and laboratory SWCC data

The model is very sensitive to the SWCC and hydraulic conductivity functions. As such, the exact combination of parameters that results in output that matches precisely the field measured water content and suction values is difficult to obtain. The input parameters were obtained from laboratory testing, and the model shows generally close agreement with measured water content data. The one-dimensional modeling in the uncovered soil was conducted in part to obtain infiltration data. It is believed that the water content results from the SoilCover simulations indicate that the model gives reasonable results with respect to storage changes in the upper 5 to 10 feet of soil. Therefore it is assumed that the model can be relied upon with confidence to predict future trends with respect too active zone depth and edge moisture variation distance.

6.3.1.3 Temperature Data

The variations in temperature with time from each TCP and from the model are presented in Figures 6-32 through 6-37. The results from simulations with the drying curve SWCC and wetting curve SWCC are the same. The measured temperature values closely match the model results at all locations.

Based on the model results from the uncovered soil and data measured in the field, the drying curve model generally correlates better with the field measured water content data than the wetting curve model. As stated above, the one-dimensional modeling in the uncovered soil was conducted in part to obtain infiltration values. Since infiltration is essentially a storage change in the near surface soils, the model that results in water content changes in the near surface soils that closely match the field measured water content values is the most appropriate model to use.

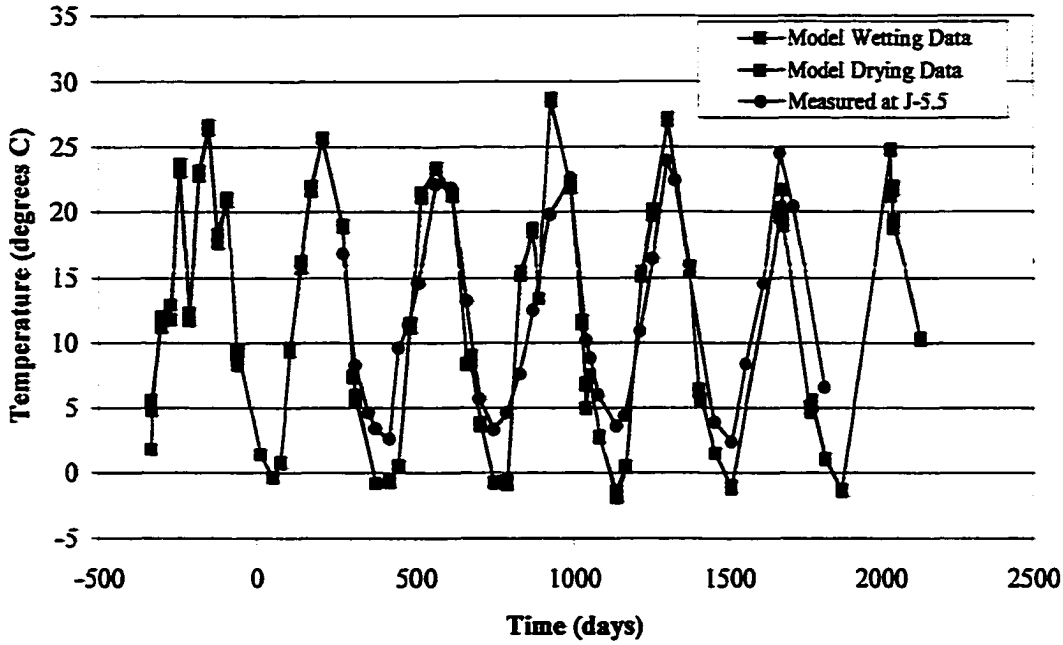

Figure 6-32 Temperature at a depth of 2 feet in the uncovered soil at the CSU site

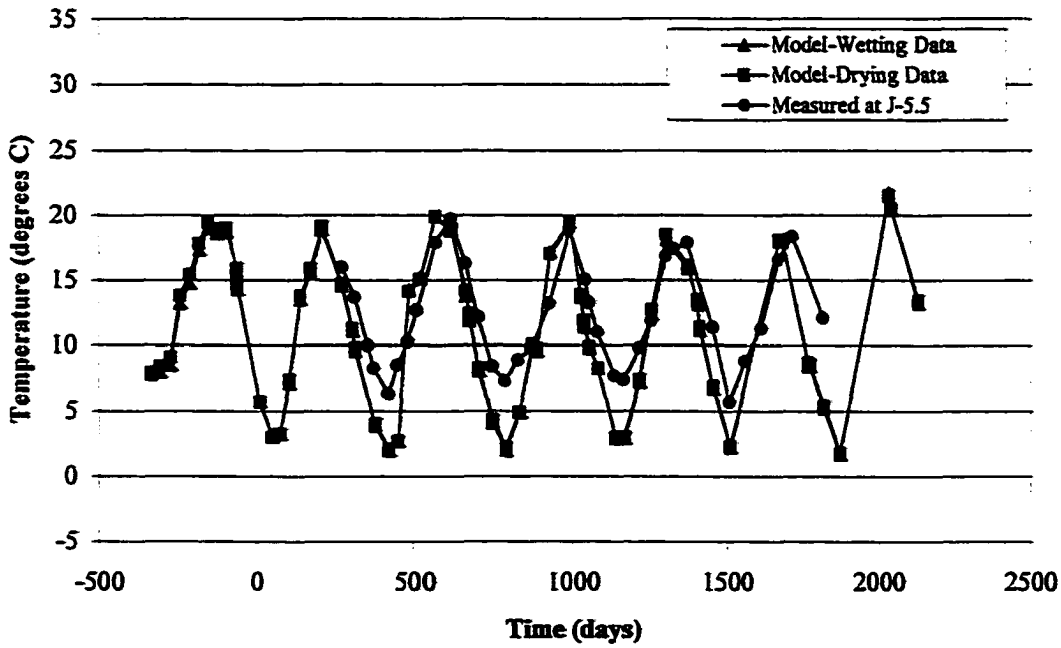

Figure 6-33 Temperature at a depth of 5 feet in the uncovered soil at the CSU site

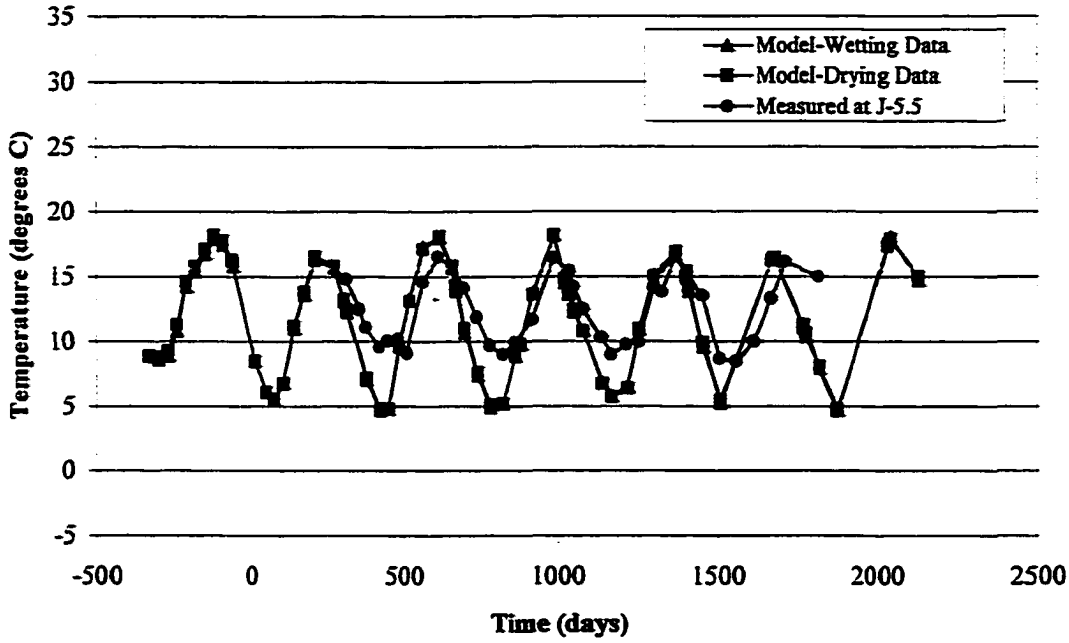

Figure 6-34 Temperature at a depth of 8 feet in the uncovered soil at the CSU site

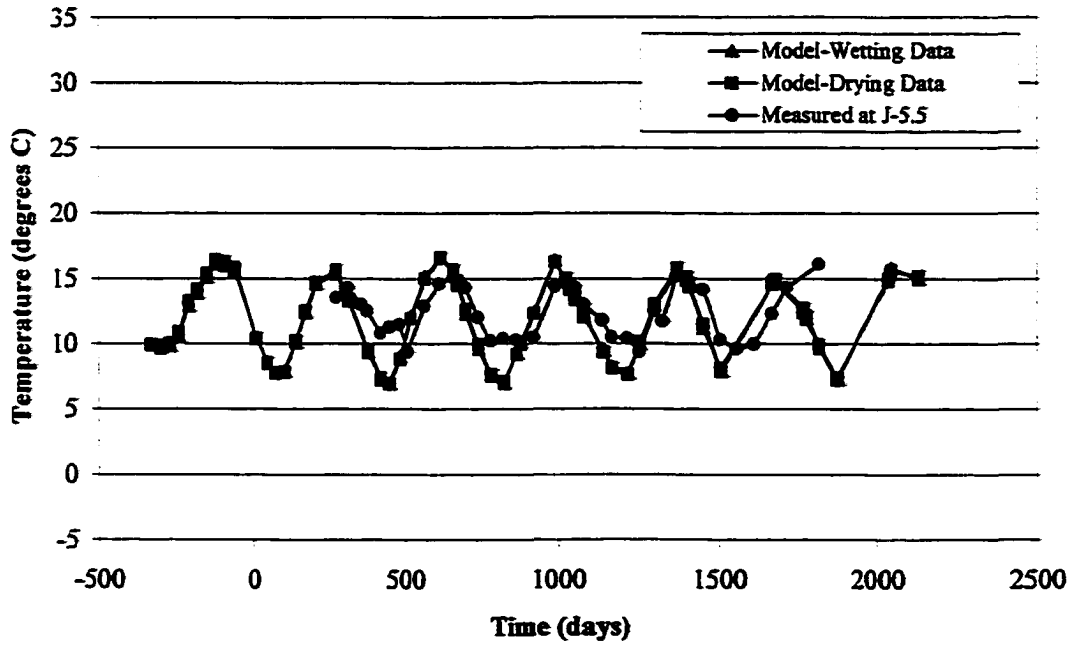

Figure 6-35 Temperature at a depth of 11 feet in the uncovered soil at the CSU site

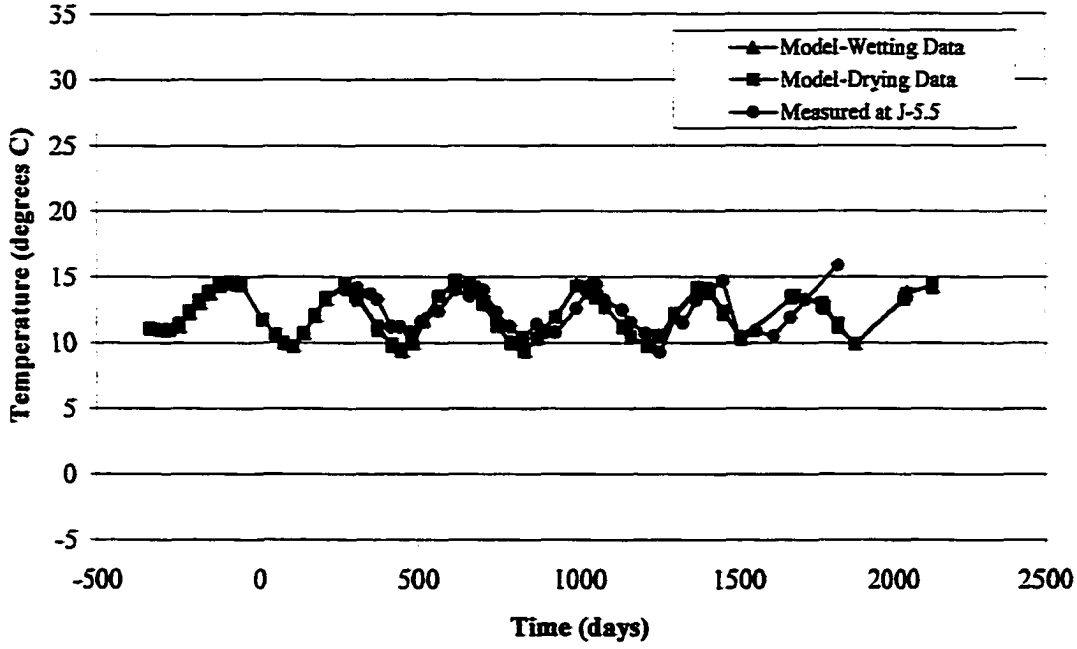

Figure 6-36 Temperature at a depth of 14 feet in the uncovered soil at the CSU site

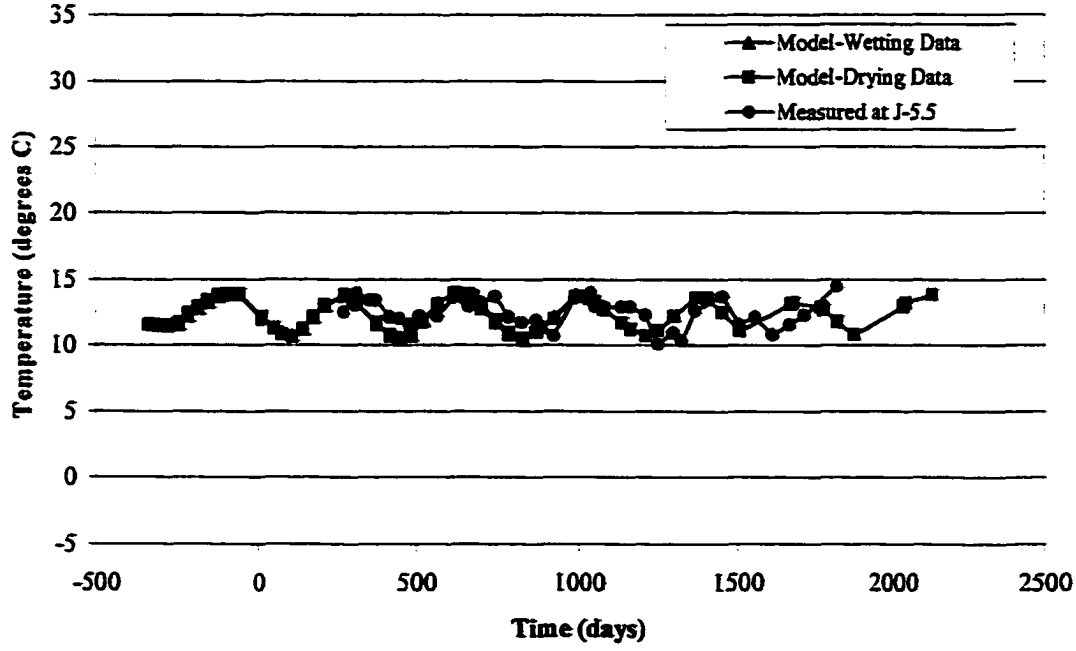

Figure 6-37 Temperature at a depth of 17 feet in the uncovered soil at the CSU site

6.3.2 Covered Soil

The initial soil profile, shown in Figure 6-6, and soil properties and climate data presented in Chapter 6.2 were used to model the covered soil. To model the geosynthetic cover and 6 inches of rock used for the simulated slab, the solar radiation was set equal to zero and the relative humidity was set equal to 100 percent beginning on January 10, 1993, the day the liner was placed. Setting solar radiation to zero and relative humidity to 100 percent eliminates evaporation from the model. This results in accumulation of moisture due to vapor flow from the wetter soils at depth toward the drier soils near the surface.

The SoilCover model was not developed to model the placement of a geosynthetic liner and condensation of moisture beneath it. The boundary conditions mentioned above are a simple way of eliminating evaporation and accumulating moisture near the surface of a desiccated soil in the ideal one-dimensional case of a covered soil. Koerner (1990) presents a test method for measuring water vapor flow through a geomembrane. The water vapor transmission (WVT) test is used to measure the rate of water vapor transmission through a geomembrane based on a relative humidity gradient across the liner. The equivalent hydraulic conductivity of the geomembrane is then calculated based on the pressure gradient required to achieve the WVT rate and the density of water. Koerner (1990) demonstrates that the equivalent hydraulic conductivity of a 30-mil geomembrane is on the order of 2.6E 10^{-13} feet per second. In this investigation the field test site included 6 inches to 1 foot of gravel placed on top of the geomembrane, which reduces the relative humidity gradient across the liner thereby reducing WVT rate. In

addition, the hydraulic conductivity of the liner is 5 to 6 orders of magnitude lower than the soil hydraulic conductivity. Therefore for the purposes of modeling covered soil in this investigation it is assumed that the surface of the liner creates a no flow boundary.

Model simulations were then performed over the same time periods as in the case of the uncovered soil. At the end of each year the suction profile was updated and the following year was simulated using the respective climate data.

6.3.2.1 Water Content Data

The water content profiles from the model and the average measured profile from the center of the covered surface are shown in Figures 6-38 through 6-47. The measured results are based on the average of water content data collected at access tubes D-5, E-3, E-5, E-7, and F-5. The model results are based on the results from the drying curve simulations. The results from simulations that used the wetting curve are discussed later.

In general the model results compare well with the field-measured water content profiles. The drier soil near the surface begins to increase in water content immediately after placement of the liner. The rate of increase in water content decreases after approximately 4 months and the water content remains relatively constant from that point on. This is expected since the gradient for upward flow is now very low or zero after the initial wetting.

The field profiles tend to be slightly wetter near the surface than the model results indicate. The reason for this is that in the field the near surface soils are highly weathered and their hydraulic properties are likely to be slightly different than those used for the

modeling. Given the close agreement in the results and the lack of laboratory data on the weathered soil, the subtle differences due to weathering were not considered.

The measured and modeled water content from beneath the center of the slab at 1-foot intervals to a depth of 6 feet, as a function of time, are shown in Figures 6-48 through 6-53, respectively. Model results based on the drying SWCC and the wetting SWCC are shown for comparison. In general, the data in Figures 6-48 through 6-53 indicate that the model results compare well with the water content changes measured in the field. As with the uncovered soil results the water content values obtained using the wetting curve SWCC are slightly less than the water content values obtained using the drying curve SWCC.

As discussed above and in Chapter 5.2.2 there was an initial rapid increase in water content measured at a depth of 1 foot. The rapid increase in water content occurred near the surface at most monitoring locations on the simulated slab at CSU (see field data plots in Appendix C). The model does not show the same result. However, after the initial increase at access tubes near the center of the slab, the water content from the model and the measured water content remained relatively constant over time showing some cyclical behavior associated with climatic trends.

The initial increase in water content noted in the measured data may be associated with climatic trends. Another significant increase in measured water content occurred between approximately 1,100 and 1,200 days (fall/winter 1995). A similar increase was documented to a depth of 5 feet in the uncovered soil, between approximately 850 and 1,000 days during the summer of 1995.

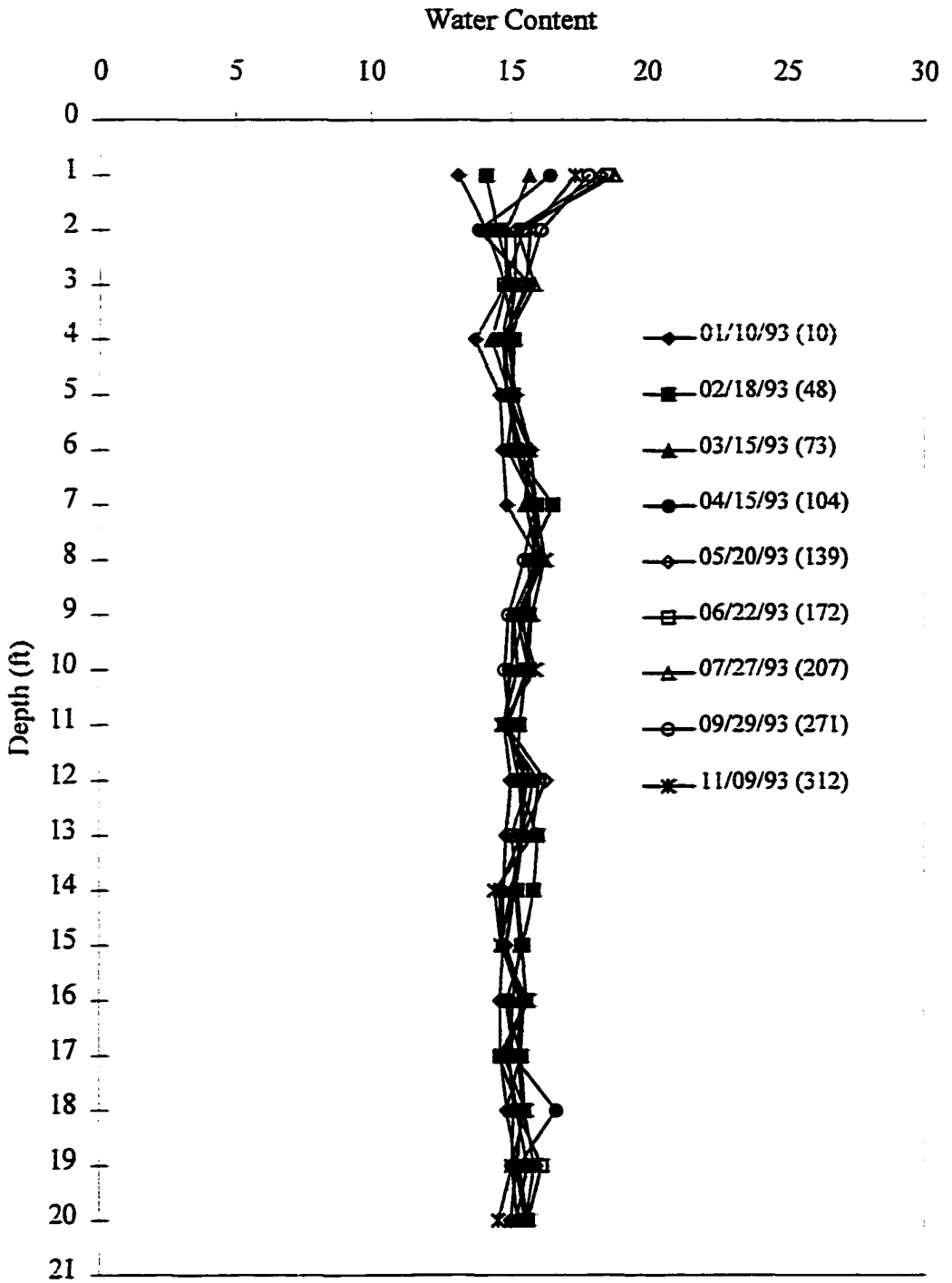

Figure 6-38 Measured water content profiles from 1993 in covered soil at CSU (based on the average from D-5, E-3, E-5, E-7, and F-5)

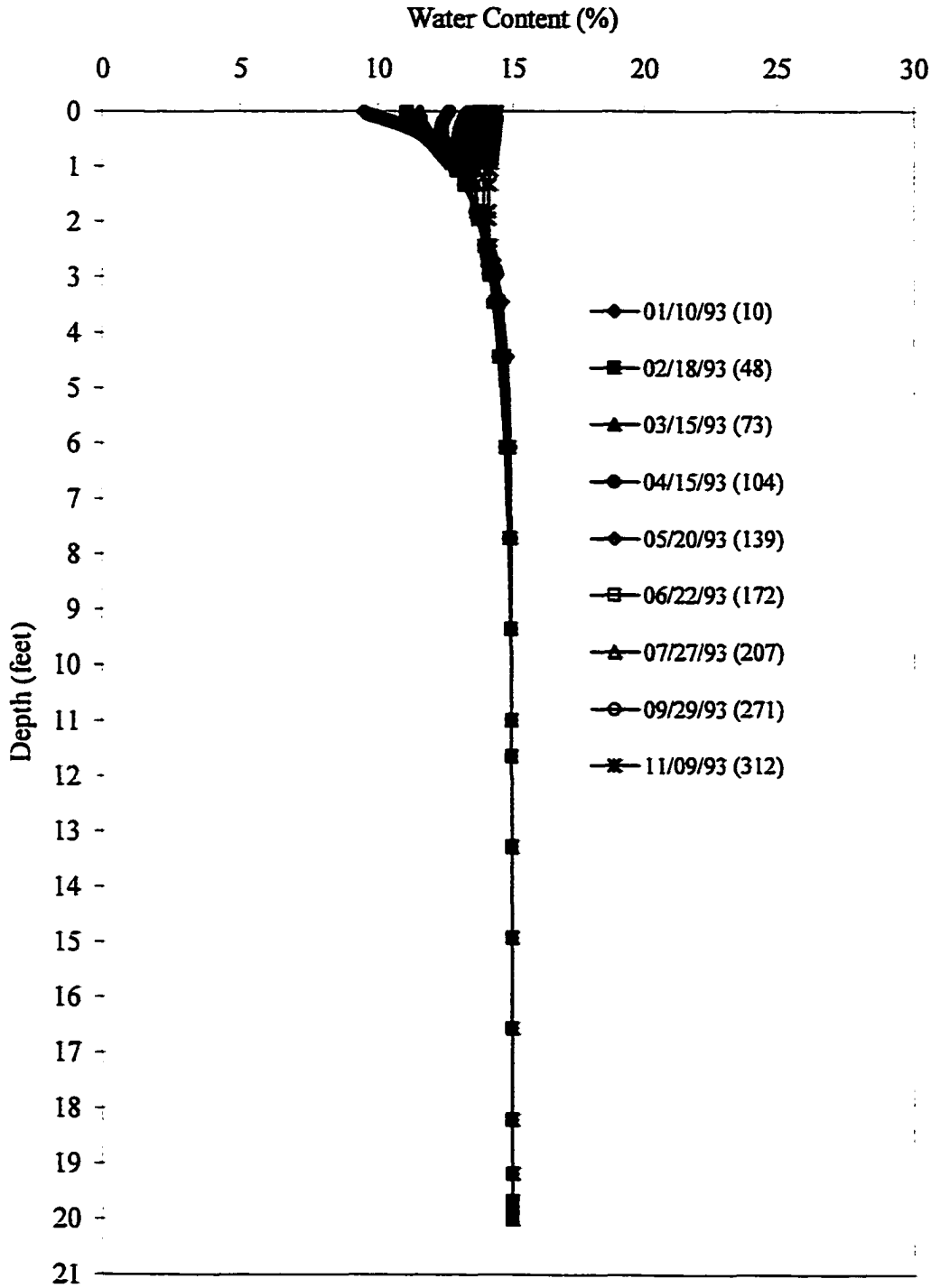

Figure 6-39 Model predicted water content profiles from 1993 in covered soil at CSU

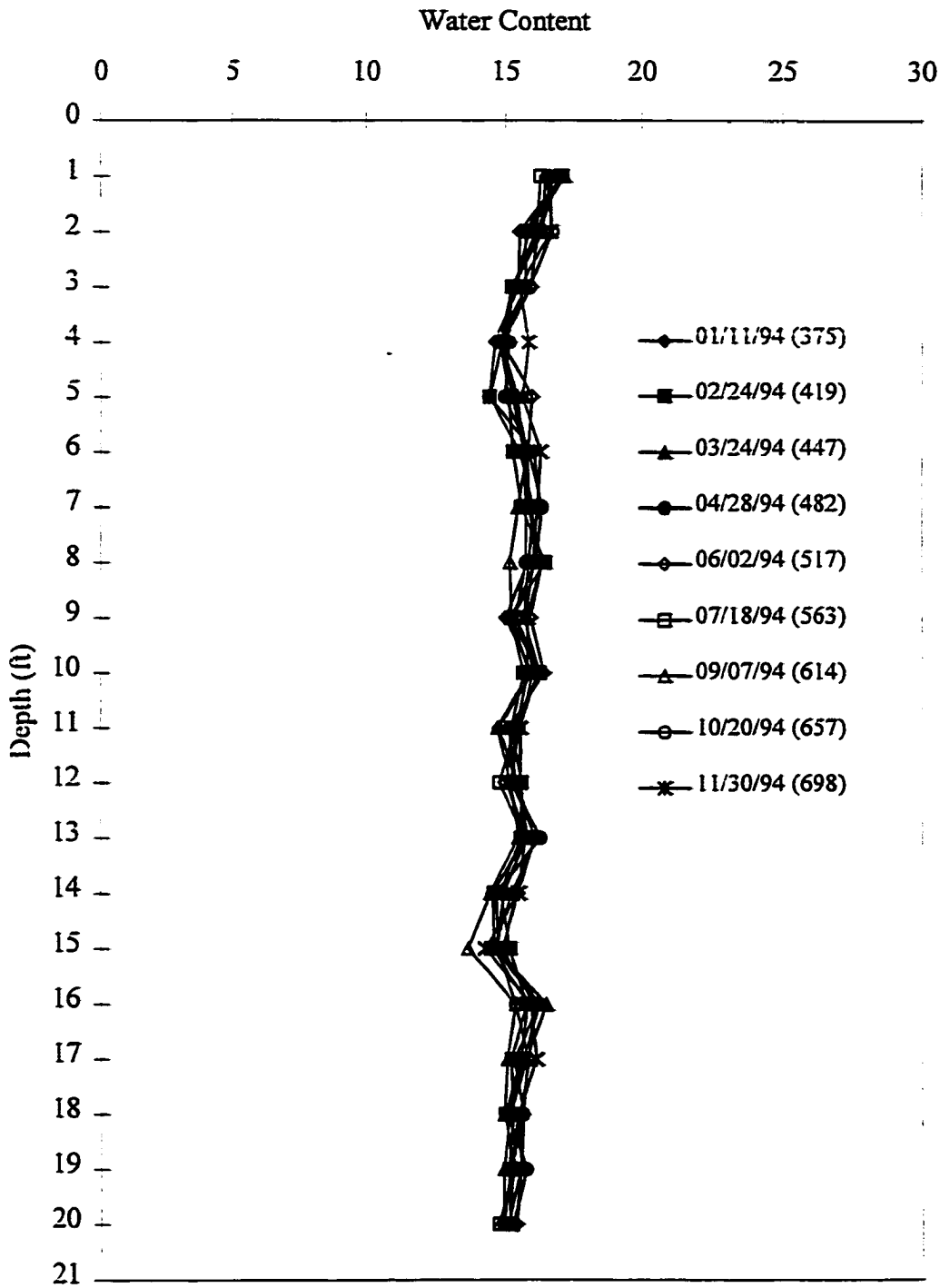

Figure 6-40 Measured water content profiles from 1994 in covered soil at CSU (based on the average from D-5, E-3, E-5, E-7, and F-5)

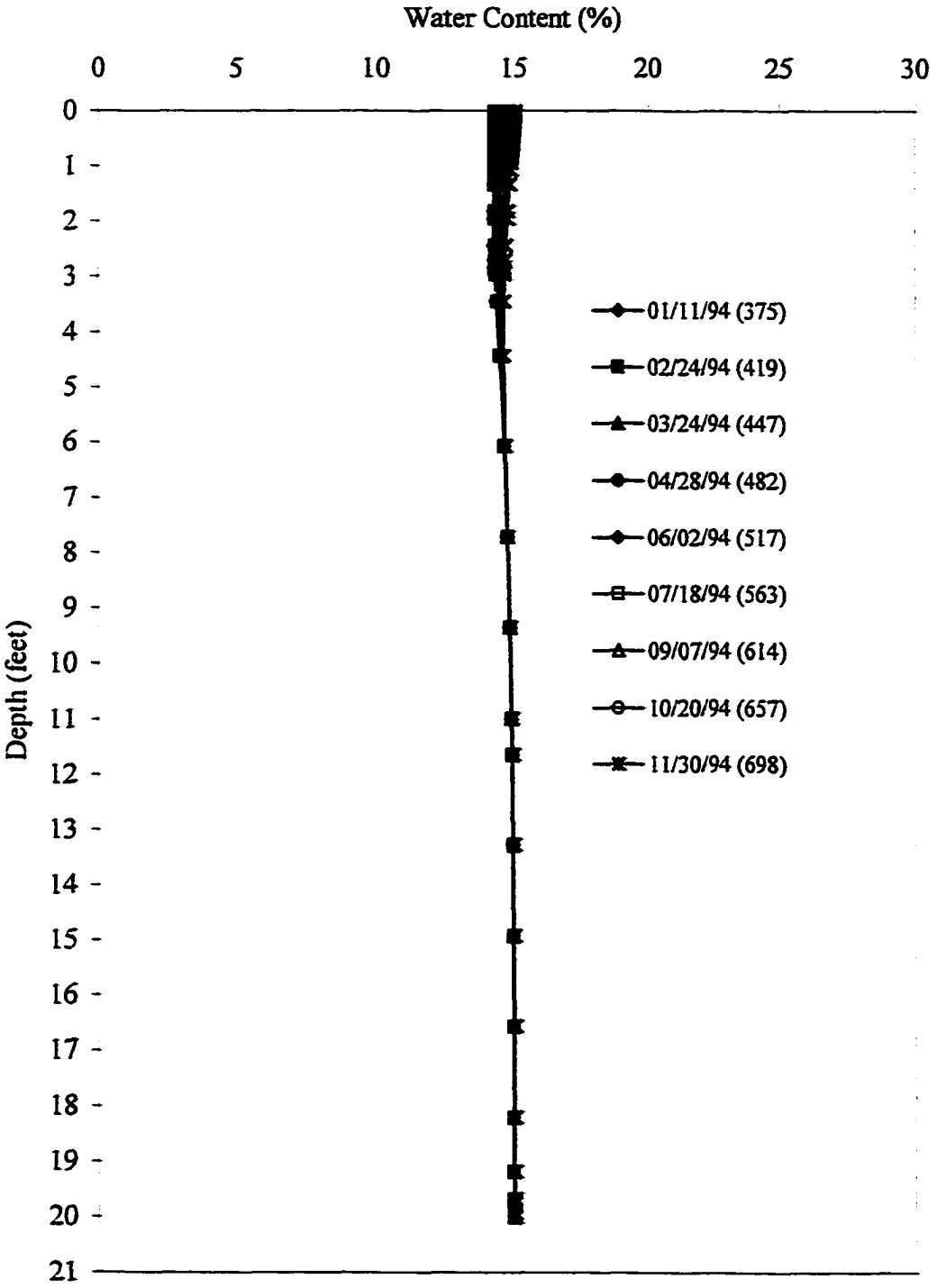

Figure 6-41 Model predicted water content profiles from 1994 in covered soil at CSU

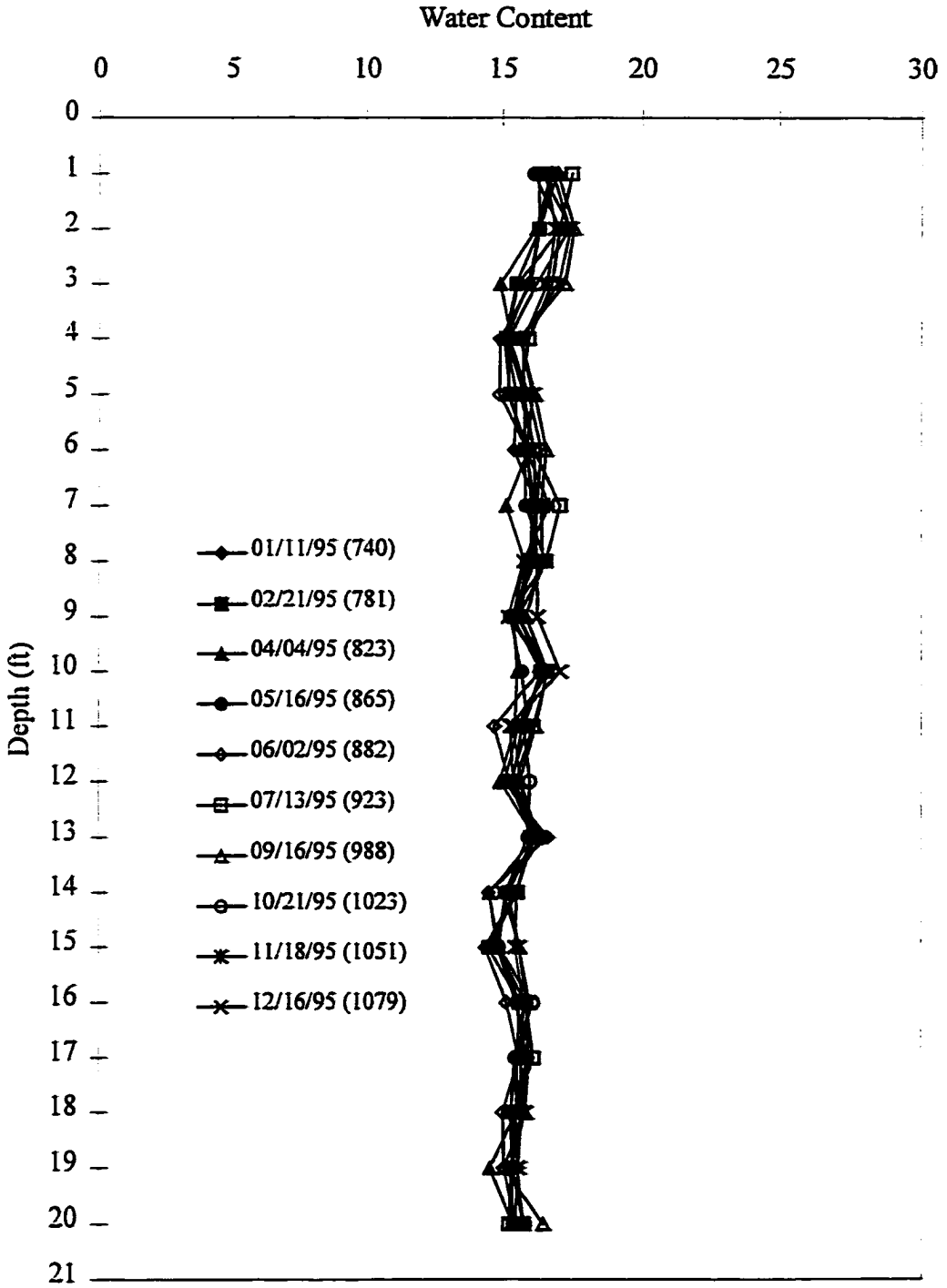

Figure 6-42 Measured water content profiles from 1995 in covered soil at CSU (based on the average from D-5, E-3, E-5, E-7, and F-5)

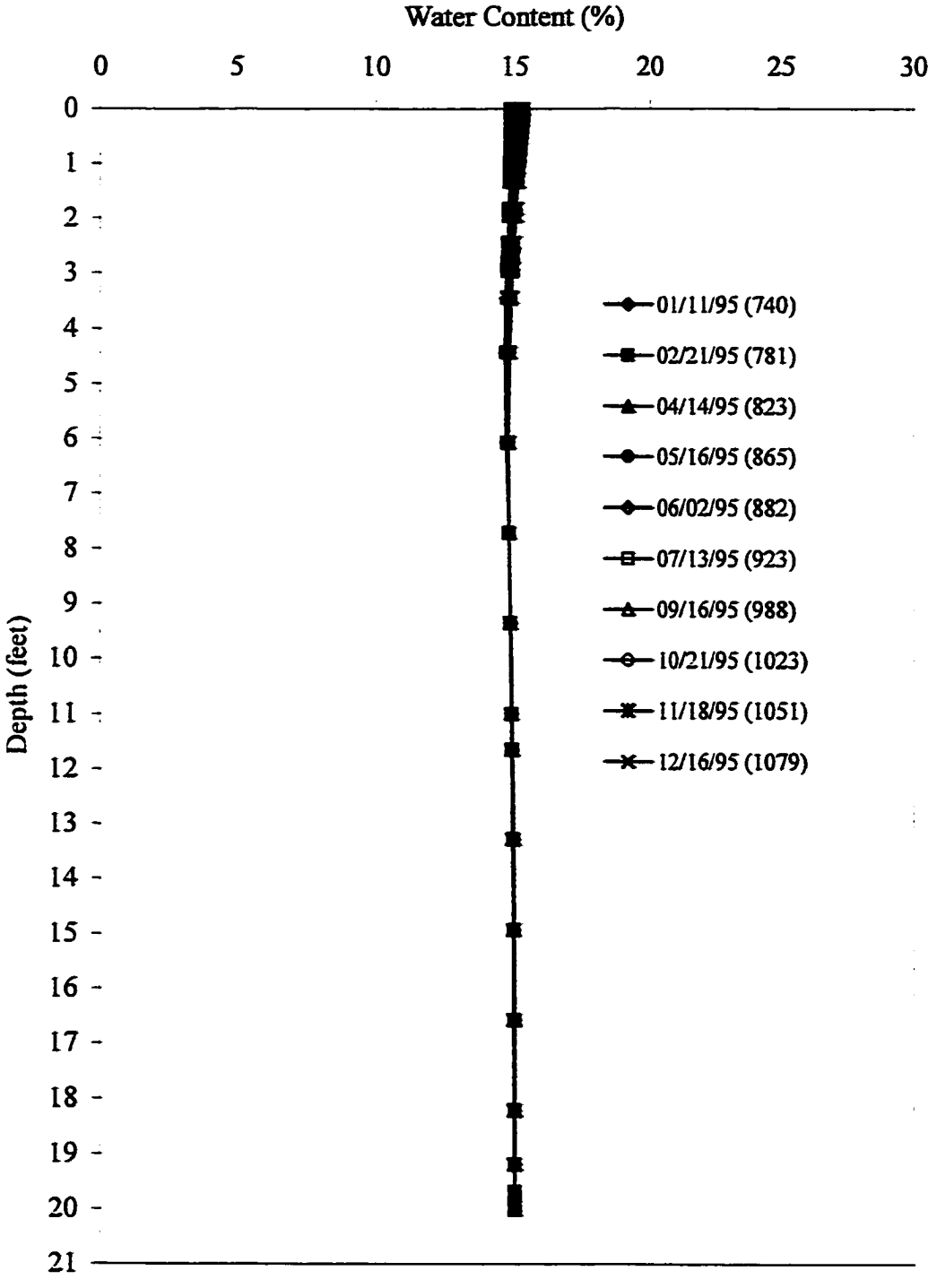

Figure 6-43 Model predicted water content profiles from 1995 in covered soil at CSU

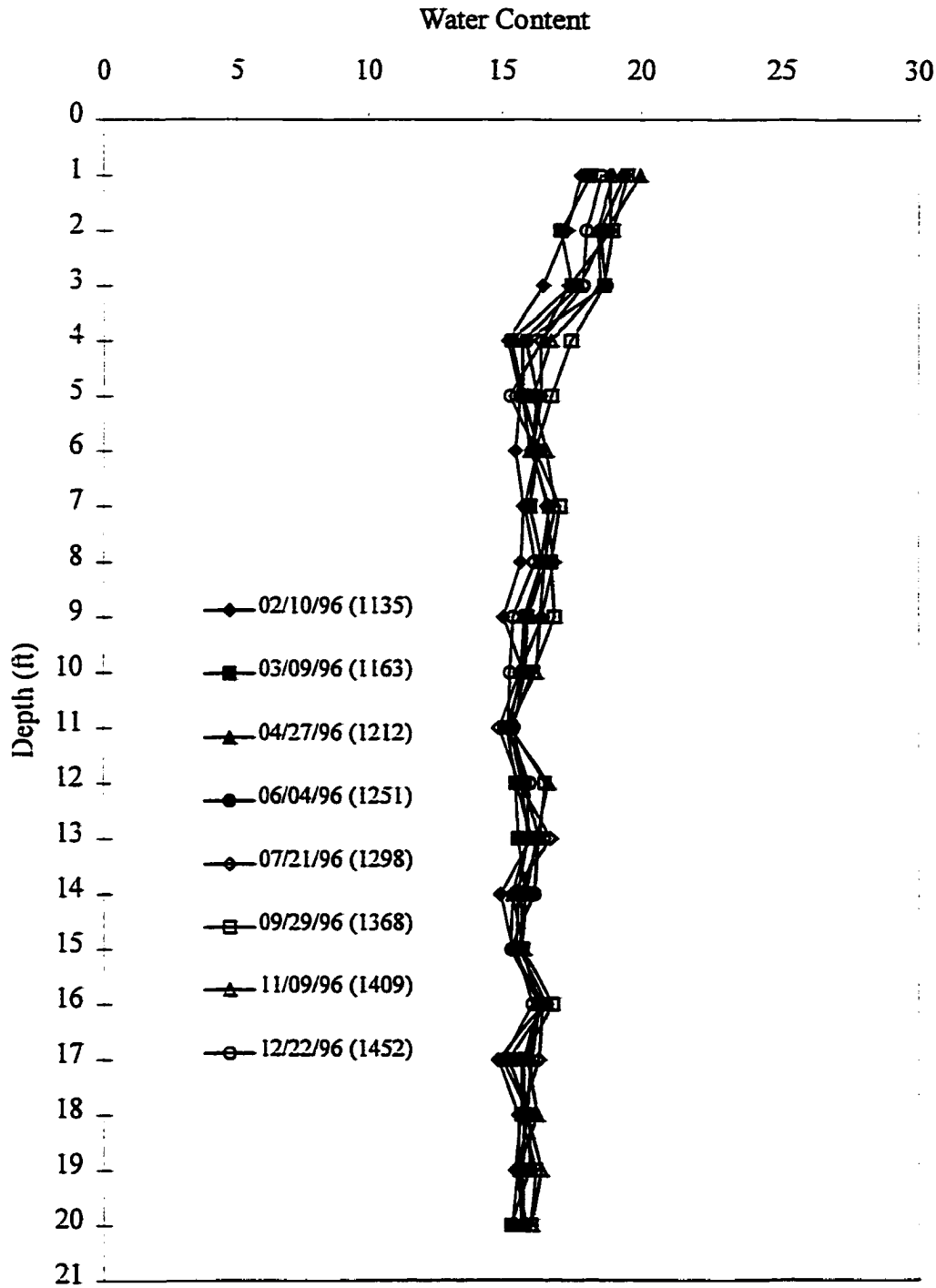

Figure 6-44 Measured water content profiles from 1996 in covered soil at CSU (based on the average from D-5, E-3, E-5, E-7, and F-5)

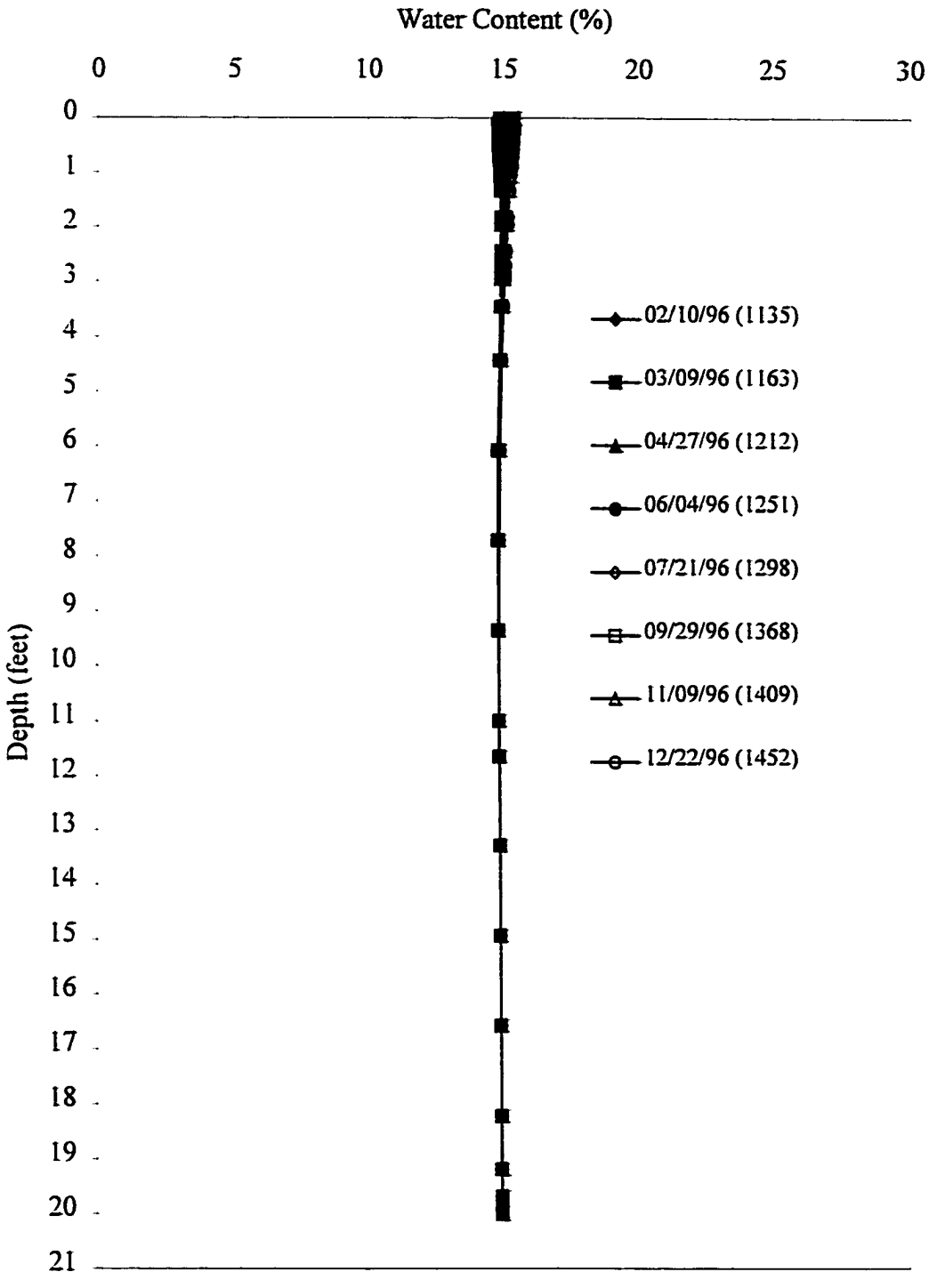

Figure 6-45 Model predicted water content profiles from 1996 in covered soil at CSU

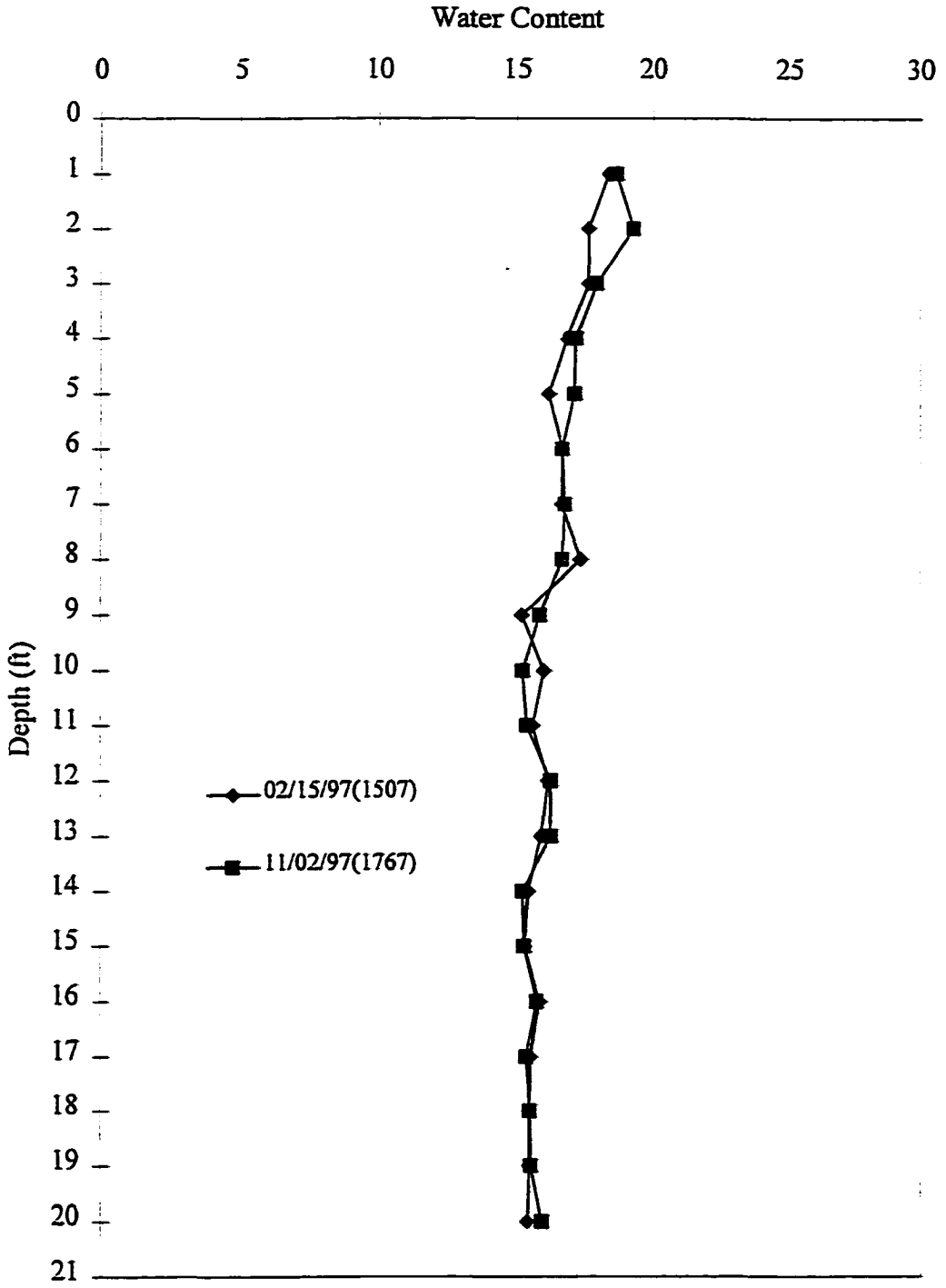

Figure 6-46 Measured water content profiles from 1997 in covered soil at CSU (based on the average from D-5, E-3, E-5, E-7, and F-5)

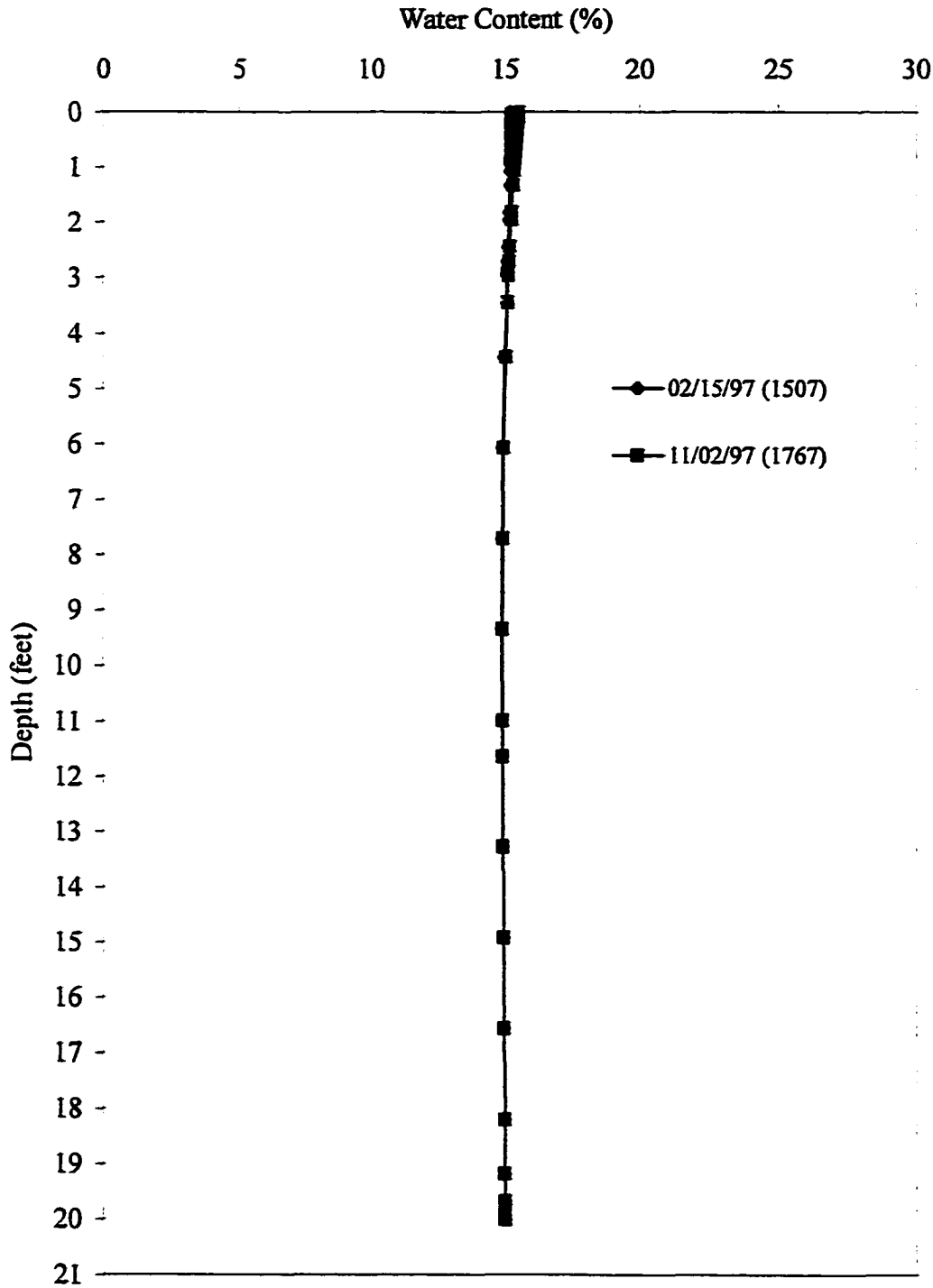

Figure 6-47 Model predicted water content profiles from 1997 in covered soil at CSU

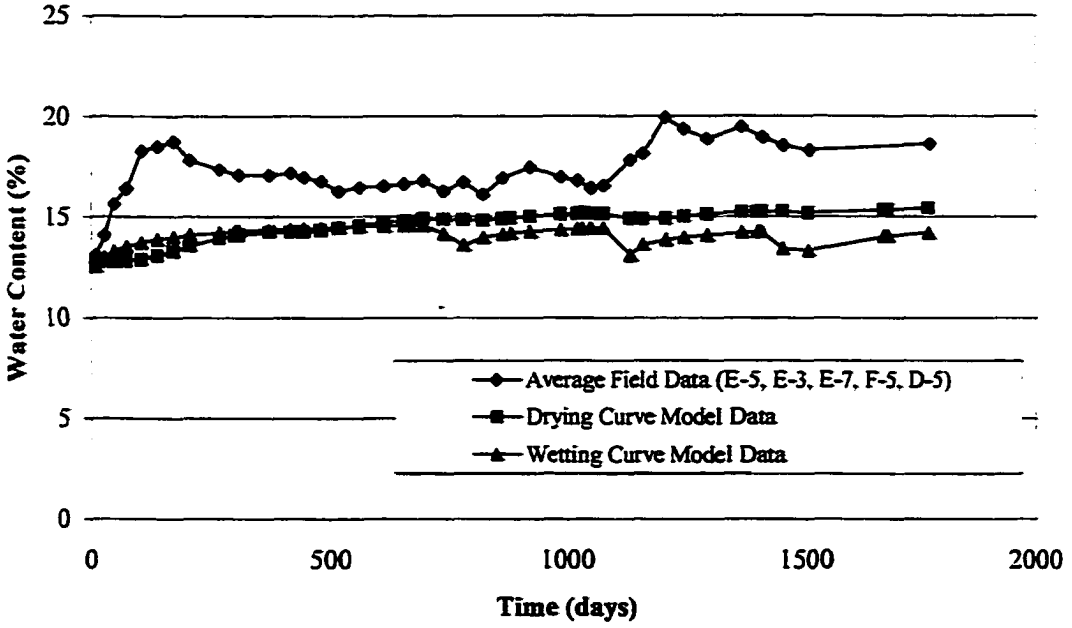

Figure 6-48 Water content at 1 foot in the covered soil from the CSU site

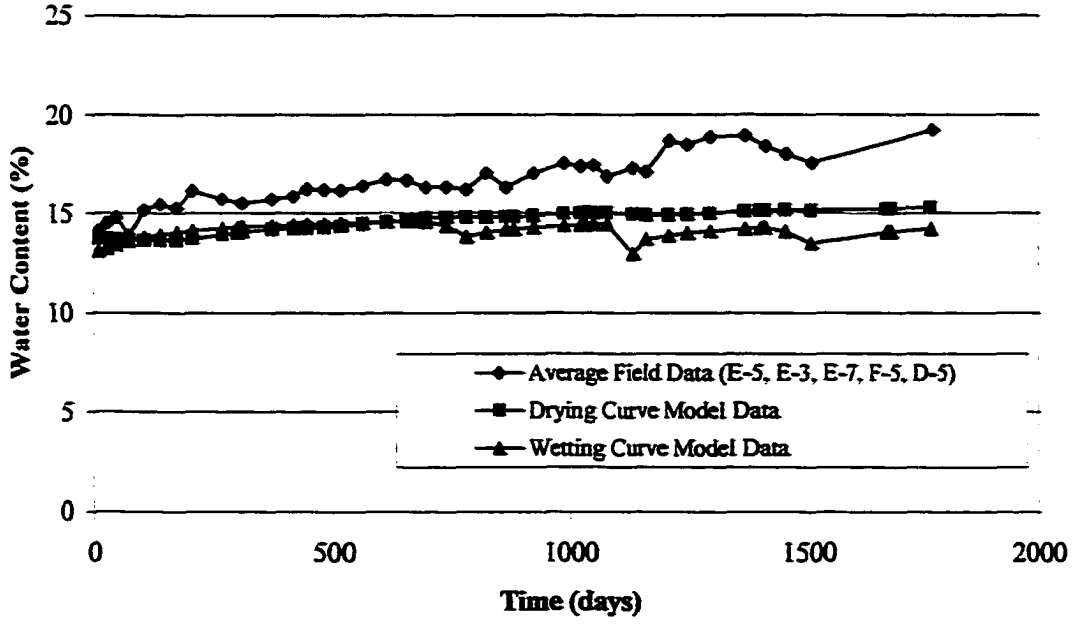

Figure 6-49 Water content at 2 feet in the covered soil from the CSU site

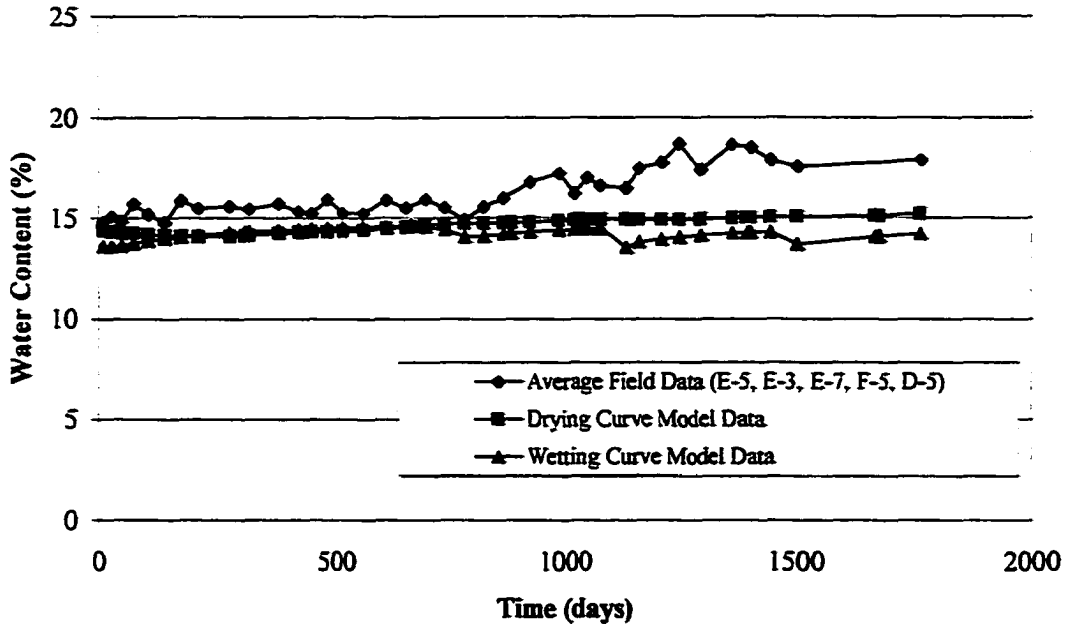

Figure 6-50 Water content at 3 feet in the covered soil from the CSU site

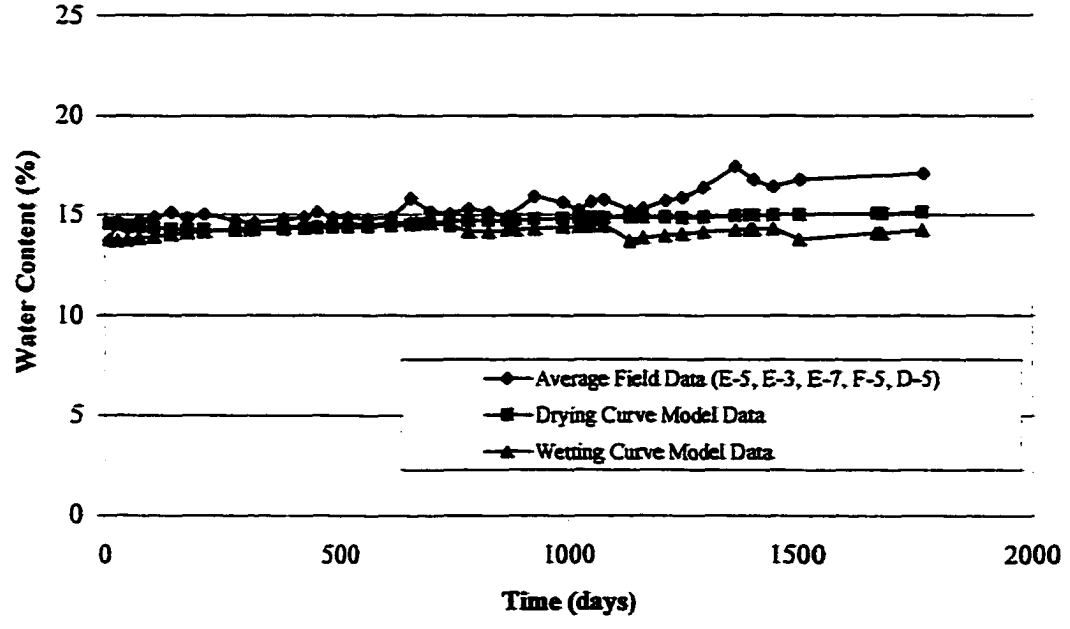

Figure 6-51 Water content at 4 feet in the covered soil from the CSU site

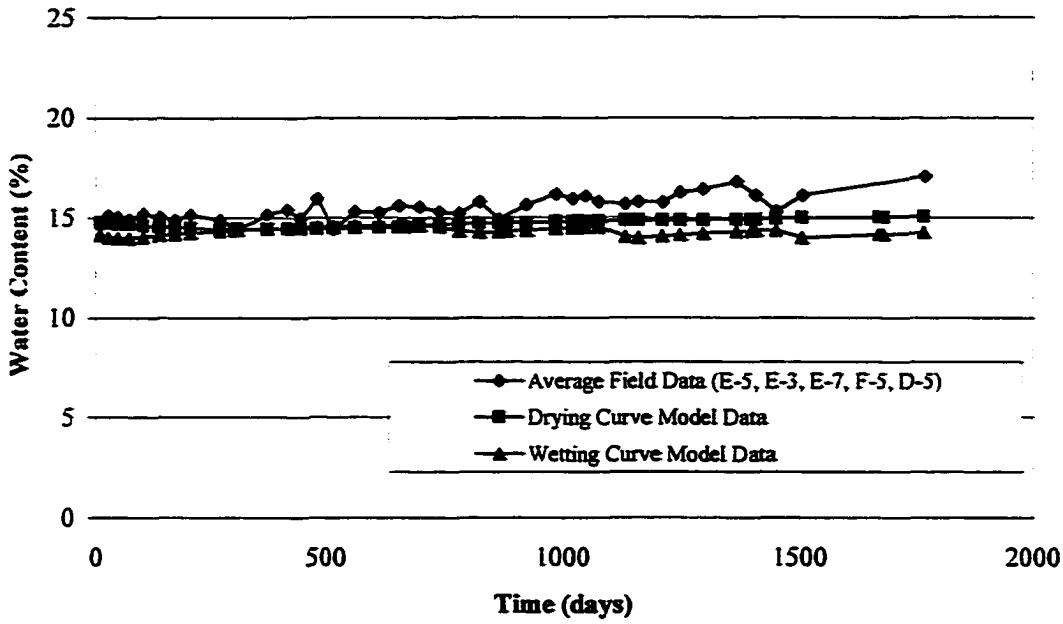

Figure 6-52 Water content at 5 feet in the covered soil from the CSU site

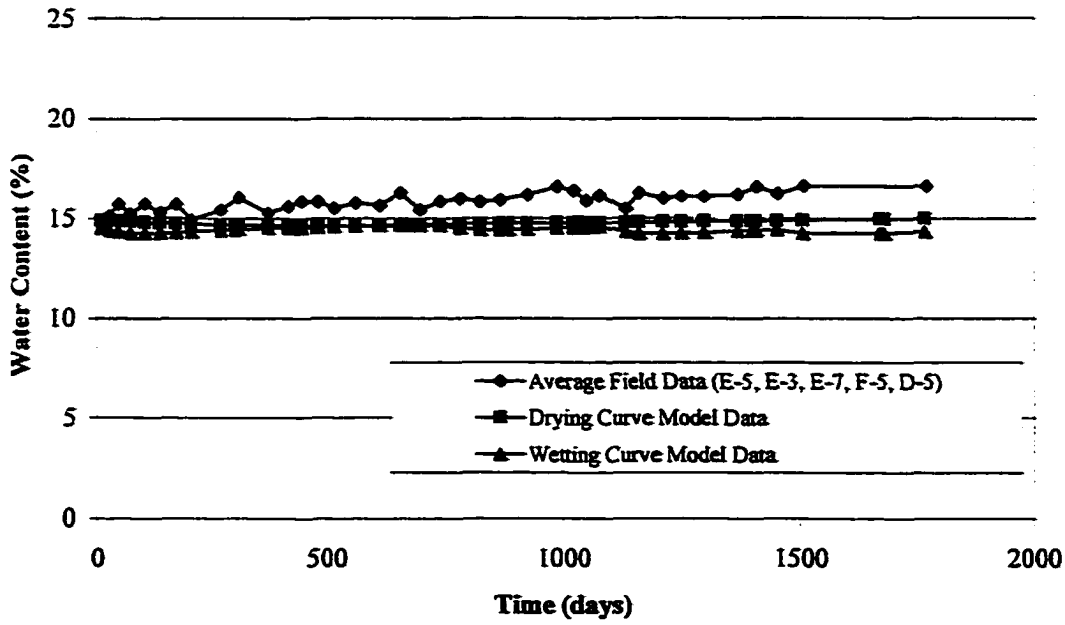

Figure 6-53 Water content at 6 feet in the covered soil from the CSU site

Since the increase in the center of the slab occurs after more than 3 years of monitoring and was preceded by an increase in the uncovered soil, it is likely due to moisture migration from the edge of the slab after large precipitation events.

Review of the climate data indicates that the summer of 1995 was the wettest period during the investigation and the results presented in Figures 6-17 through 6-22 indicate that a significant increase in water content occurred in the uncovered soil in the summer of 1995. Since the SoilCover model is a one-dimensional model it is not possible to account for moisture that migrates laterally beneath the slab. However, the predicted water content data in Figures 6-48 through 6-53 is reasonable for an ideal one-dimensional situation. In addition, the large increase in water content in the center of the slab after over 3 years of monitoring indicates that the edge moisture variation distance is as high as 15 feet, half the width of the simulated slab.

6.3.2.2 Suction Data

Figures 6-54 through 6-59 show the measured and modeled suction beneath the slab as a function of time from depths of 2, 5, 8, 11, 14, and 17 feet. Measured suction values represent the average of data obtained from TCP locations, D-8.5 and D-6.5. As was the case in the uncovered soil, the field measured suction data tends to agree more closely with the model results from simulations conducted using the wetting SWCC. In addition the measured suction data fluctuates significantly at each depth compared to the model output. However, in contrast to the uncovered soil, the suction values in the upper 2 to 5 feet are lower than at depth. This is expected since the water content near the surface has increased due to the reduced evaporative flux.

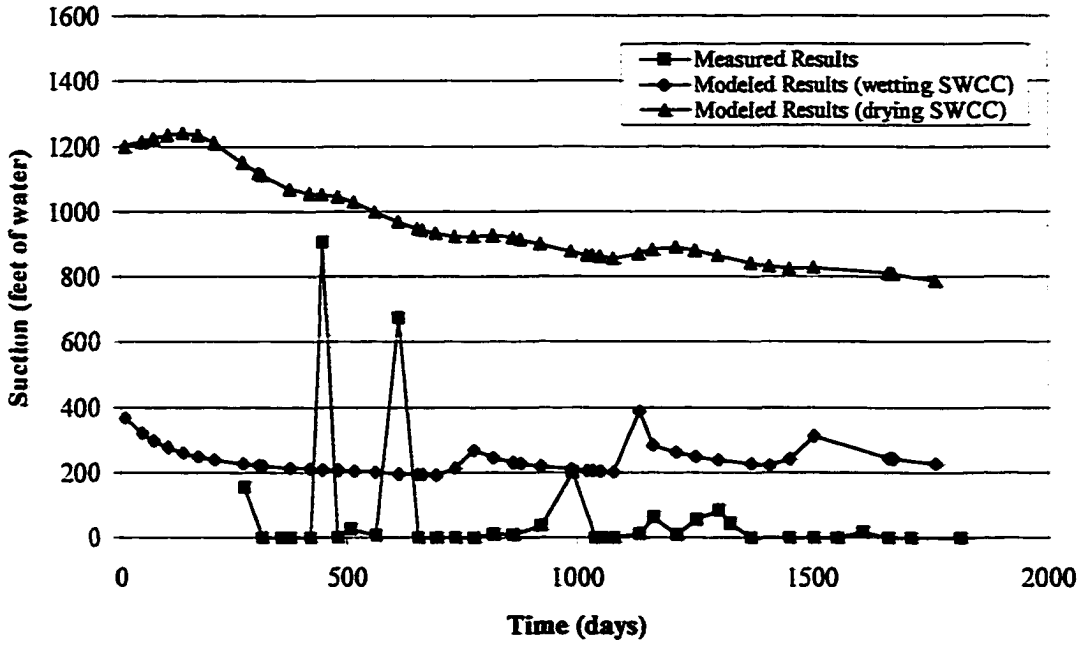

Figure 6-54 Suction at a depth of 2 feet in the covered soil at the CSU site

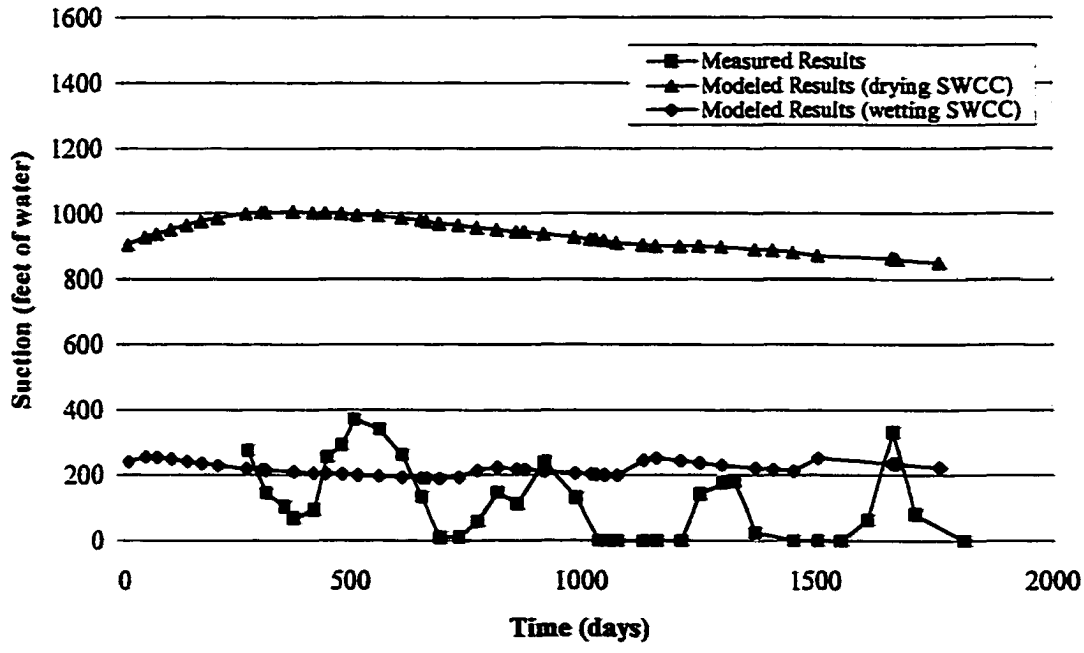

Figure 6-55 Suction at a depth of 5 feet in the covered soil at the CSU site

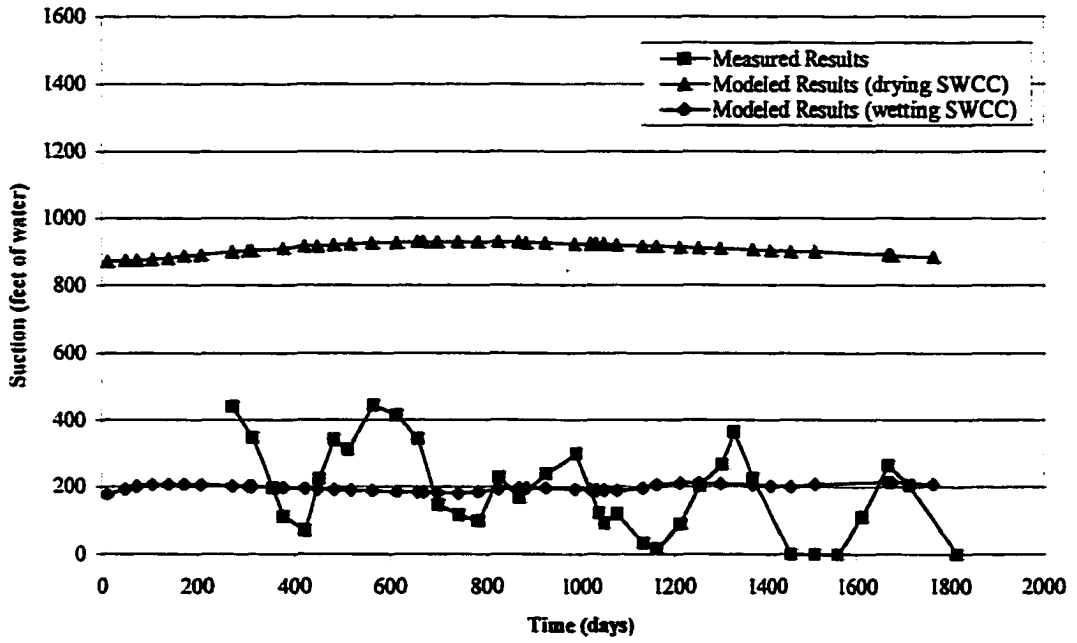

Figure 6-56 Suction at a depth of 8 feet in the covered soil at the CSU site

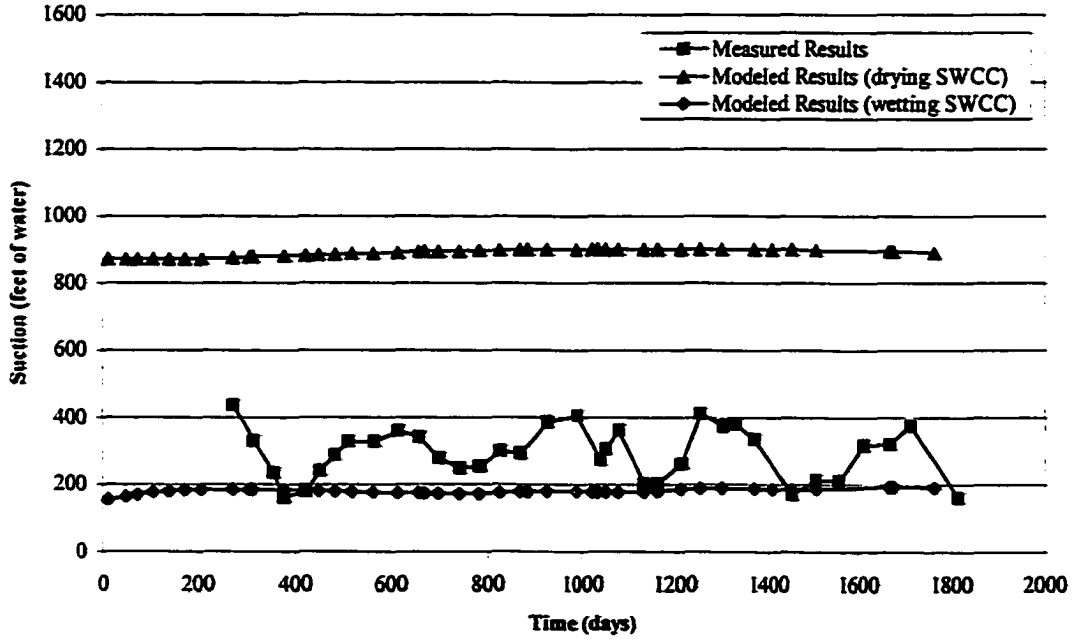

Figure 6-57 Suction at a depth of 11 feet in the covered soil at the CSU site

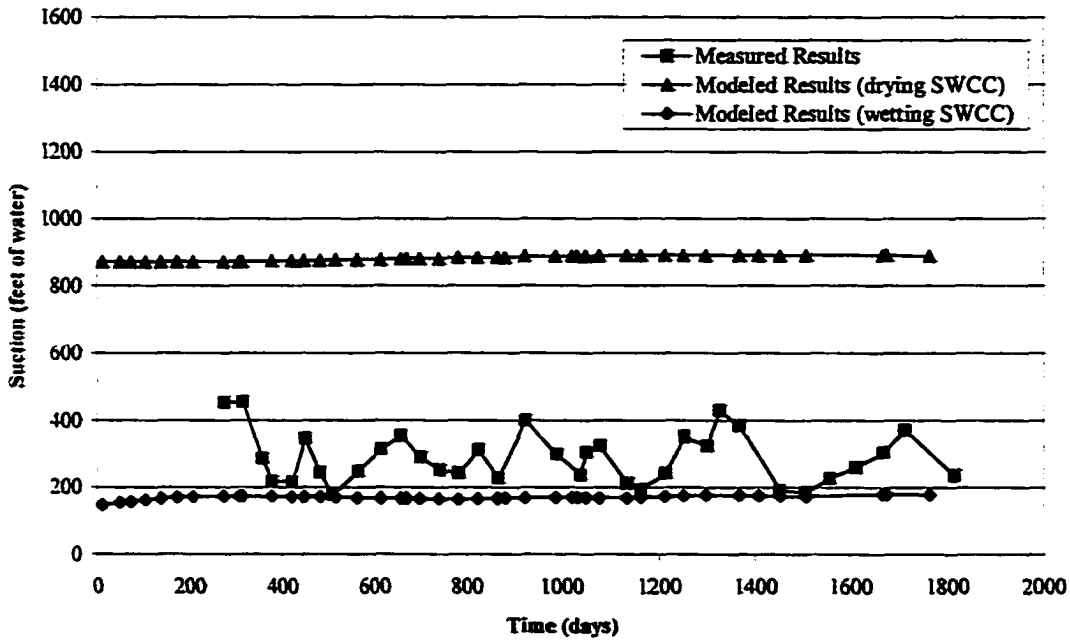

Figure 6-58 Suction at a depth of 14 feet in the covered soil at the CSU site

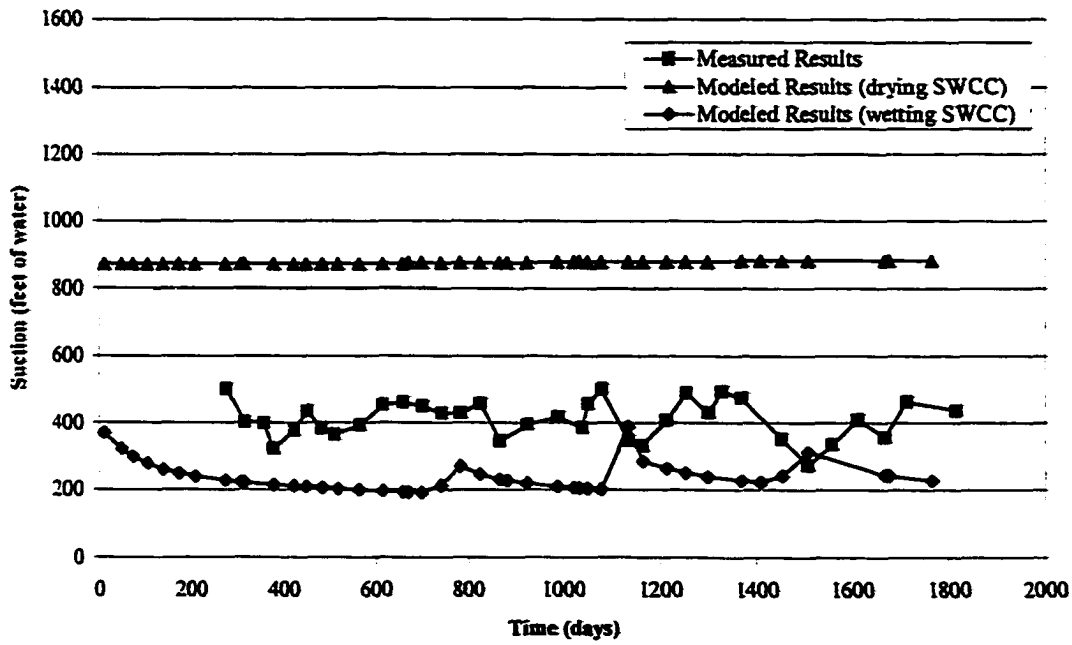

Figure 6-59 Suction at a depth of 17 feet in the covered soil at the CSU site

At a depth of 2 feet (Figure 6-54) there were two relatively high suction readings in the first year or two. For most of the remaining monitoring period the suction has been close to zero, indicating that the upper 2 feet of soil is saturated, or that the TCP has been damaged from wetting. The degree of saturation profiles from the center of the slab (access tube E-5) from the first and most recent monitoring are shown in Figure 6-60. The degree of saturation in the upper few feet originally ranged from approximately 40 percent at the surface to approximately 85 to 90 percent at a depth of 20 feet. Currently the degree of saturation in the center of the slab ranges from approximately 65 percent near the surface to approximately 85 to 90 percent at a depth of 20 feet. Fredlund and Rahardjo (1993) state that the limits of suction measurement, with TCP's, range from a lower limit of approximately 33 feet (100 kPa) to an upper limit of approximately 2,640 feet (8,000 kPa). The relative humidity in that range of suction ranges from approximately 100 percent down to approximately 94 percent, respectively.

The zero suction readings in the upper soils beneath the cover indicate the suction is less than 33 feet. These low suction values (high relative humidity), associated with a relatively high degree of saturation in the upper soils, indicate that the limits of suction measurement may have been reached in the TCP's at shallow depth beneath the slab. The measured degree of saturation data in Figure 6-60 indicates that significant increases in the degree of saturation (and heave) are still possible even though the suction measurements near the surface are close to zero.

The suction data from below 2 feet, shown in Figures 6-55 through 6-59, fluctuate by approximately 300 feet on an annual basis at all monitoring locations deeper than 2 feet.

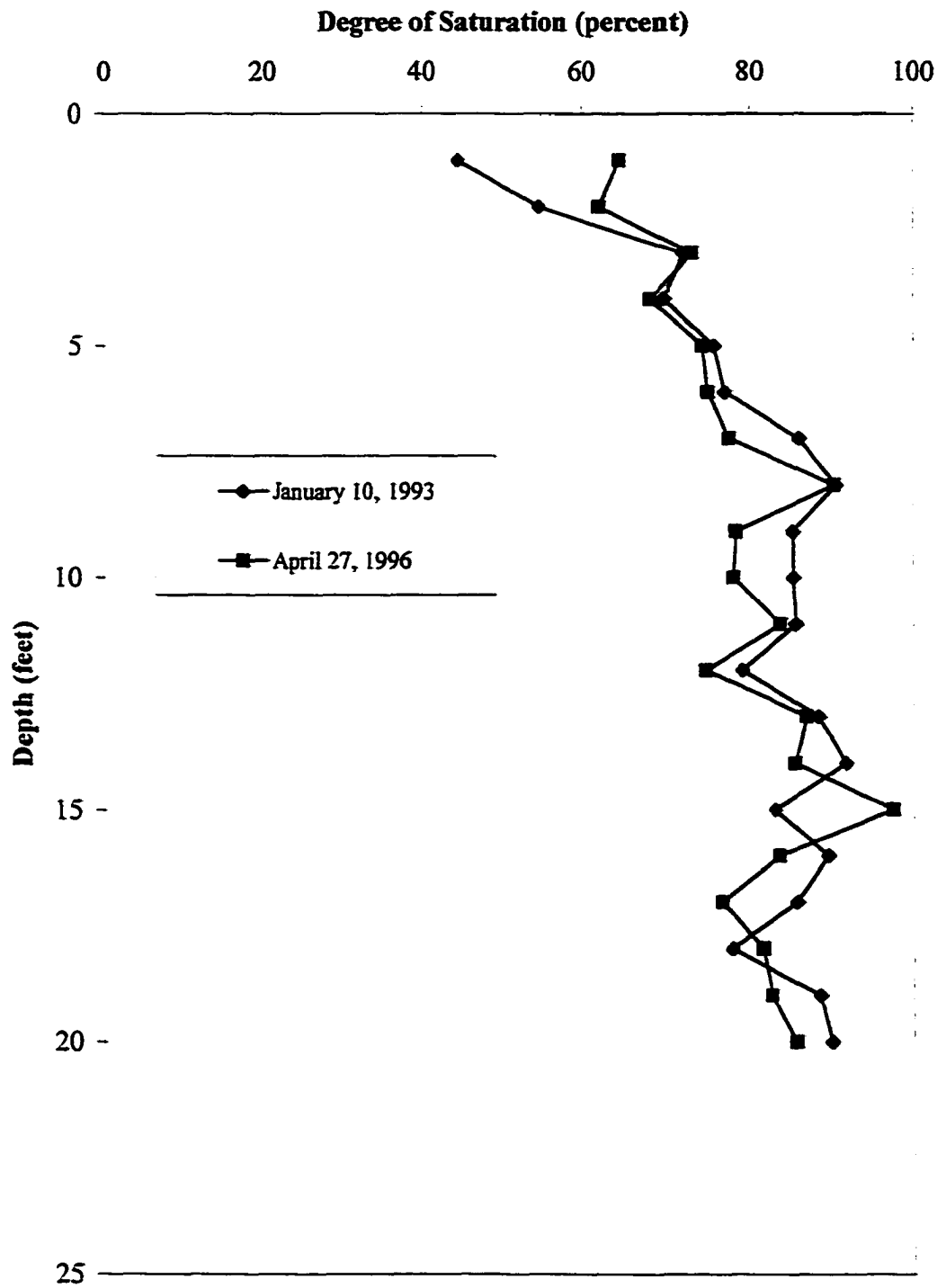

Figure 6-60 Initial and final degree of saturation beneath the center of the slab

However, the average suction value increases from approximately 100 feet at a depth of 5 feet to approximately 400 feet at a depth of 17 feet.

In general the suction data from the model simulations beneath the slab are consistent with the expected trends. The suction decreases with time as the water content of the soil increases. As was the case in the model simulations in the uncovered soil, the measured suction values fluctuate more than the model values and agree more closely with the suction data from the wetting SWCC model. Also as discussed in Chapter 6.3.1.2 this is a result of hysteresis effects not accounted for in the model and a slightly different SWCC used for the model than what actually exist in the field.

6.3.2.3 Temperature Data

The temperature results from model simulation beneath the slab were the same as in the uncovered soil. The results from the uncovered soil are shown in Figures 6-32 through 6-37.

6.3.3 Summary

In summary, the results presented above indicate that the SoilCover model can be relied upon with confidence to predict water content changes associated with changing boundary conditions. The model output shows generally close agreement with field measured water content and temperature data collected at the CSU Expansive Soils Test Site. The suction values from the model are reasonable for the field conditions. However, the field measured suction values vary significantly with time compared with the model generated suction values.

The time rate of variation is consistent with climatic trends. However, field measured water content values from locations where the suction measurements were obtained do not show significant variation in response to the large suction changes. This indicates, as mentioned previously, that in the field small changes in water content are associated with large changes in suction.

The results presented thus far indicate the limits of currently available hydraulic functions that were developed for rigid soils, for modeling flow in expansive soil. The trends observed in the field are reflective of volume changes that occur in the soil throughout the wetting and drying process. Since the models assume a rigid soil matrix and the constitutive parameters used for modeling flow are based on a rigid soil matrix there is an inherent error in the theoretical framework. However, the general trends that are observed in the field are represented in the model results. As such, the model can be used to evaluate the relative effects of soil properties, geologic conditions, and climate conditions on the development of the active zone and edge moisture variation distance.

It should be noted that there are one-dimensional flow models available such as DEFORM (Edgar, 1983), that account for volume change. However, the DEFORM model and others like it are not physically based models in terms of infiltration. Since the results from the field investigation indicate the active zone depth and edge moisture variation distance are more strongly influenced by infiltration processes and climatic effects than by soil volume changes, the SoilCover model is considered to be a more appropriate model for this investigation.

For this investigation water content has been used as the primary variable for evaluating active zone depth and edge moisture variation distance. Given that the model is particularly sensitive to soil water characteristic and unsaturated hydraulic conductivity input parameters, and that the state of knowledge in the area of interpretation of these parameters for expansive soil is limited, the modeling results presented above are considered to be quite good. The continued use of the SoilCover model for this research to obtain infiltration values for use in a two-dimensional flow model and to evaluate water content profile response to changing boundary conditions is appropriate.

The SEEP/W model (GEOSLOPE, International) was used for two-dimensional flow modeling. The primary input parameters for both the SoilCover and SEEP/W models are the SWCC, the saturated hydraulic conductivity, and an unsaturated hydraulic conductivity function. Therefore it is assumed after evaluation of these parameters with the SoilCover model that the same ones are appropriate for the SEEP/W model.

6.4 Modeling Results

The results from the field investigation and from the model simulations presented above indicate that the water content beneath the center of a slab-on-grade foundation increases to a steady state value to a depth that is approximately equal to the depth of seasonal moisture fluctuation. The magnitude of the steady state water content is a function of the SWCC of the soil and the equilibrium suction of the soil. The edge effects, and the reduction in the upward gradient for flow upon wetting of the upper soil layers, limit the magnitude and depth of initial increase.

After the initial increase in water content, boundary changes at the surface adjacent to the structure control the long-term development of active zone depth and edge moisture variation distance. Hence, continued wetting of the soil beneath a slab foundation appears to be the result of lateral migration of water from extreme climatic conditions and from manmade sources such as irrigation. In addition, the flow patterns that contribute to differential heave are a function of the geologic conditions of the soil and variation in boundary conditions around the foundation. Finally, the time rate of development and the magnitude of water content increase are functions of the soil properties, primarily hydraulic conductivity and the soil water characteristic curve.

In general, irrigation water and water from extreme climatic events migrates beneath the slab, and the ability of the soil to transmit water back upward, to the surface in the form of water or vapor phase flow is limited by the obstruction of the slab. Additionally, water that migrates during specific environmental events, to depths in excess of the depth of seasonal moisture variation (evaporative depth), remains in the soil when the surface boundary conditions change. That water is available for lateral flow to the drier soils beneath the slab. As a result, the long-term condition is one of continued temporary steady-state behavior followed by an increase in the depth of wetting beneath the slab, associated with a boundary condition change at the surface adjacent to the slab.

The above description indicates that the development of the active zone is a three-dimensional problem and can not be fully evaluated with one-dimensional models, and that it is a time-dependent problem that can not be evaluated with steady state models. The one-dimensional modeling presented thus far does not address the issues of

differential wetting or edge boundary effects. In addition, the use of the depth of seasonal moisture variation to predict the active zone depth, is an example of the limits of using a one-dimensional conceptual model to predict three-dimensional behavior.

The field data presented thus far indicates that the active zone depth will continue to increase to its maximum depth based on stress conditions and the soil profile, at a rate that is controlled by the hydraulic conditions of the soil and the frequency and magnitude of boundary changes. Furthermore, development of the active zone appears to be strongly affected by anisotropy in the soil and environmental conditions at the site. This indicates that the use of an active zone depth value that is less than the maximum value based on stress conditions, for the design of foundations, is not conservative.

The characterization of active zone depth and edge moisture variation distance presented in the following chapters is based on the results from the SoilCover and SEEP/W models. It was demonstrated in Chapter 6.3 that the models are not capable of simulating exact behavior in terms of water content, suction, and temperature but that the trends noted in the field are generally well represented in the model results. If the exact hydraulic parameters for the soil were known the modeling results would more closely match the field results, however, the models are also limited in that they do not account for volume change and stress distribution in the soil. To evaluate the effects of soil properties, geologic conditions and climatic conditions, the independent effects of each condition are considered in terms of general trends.

6.4.1 Soil Properties

The most important soil property with respect to flow through soil is the hydraulic conductivity (saturated and unsaturated). Generally, the hydraulic conductivity controls the rate of flow and is a function of the soil density, percent clay, and soil structure. These properties are typically considered constants thereby making the hydraulic conductivity a constant with respect to soil volume. The soil water characteristic curve (SWCC) describes the water holding capacity of the soil at a given suction and is also a function of soil density, percent clay, and soil structure as well as the wetting and drying process. The SWCC data presented in Chapter 4 and the modeling results presented earlier in this chapter illustrate the effects of wetting and drying on the SWCC.

Volume changes in an expansive soil are of significant magnitude to have an effect on density and soil structure resulting in large changes in hydraulic conductivity and the SWCC. The volume changes are particularly important near the surface of the soil where stresses are low and water content changes dramatically with climate. As such, the hydraulic conductivity and SWCC are technically not fundamental soil properties in an expansive soil, but rather their relationship to volume change is a fundamental function that controls the rate of flow and water holding capacity.

For the purposes of modeling presented in Chapter 6.3 the hydraulic conductivity was assumed to be equal to 1.3E-07 feet per second, based on laboratory consolidation test results. The SWCC determined by Chao (1995), presented in Chapter 4, was used for the modeling presented in Chapter 6.3. The results from those model simulations compared fairly well with field measured results in terms of water content changes in the soil.

However, the consolidation test results indicate that there is a large variation in hydraulic conductivity with stress. In addition the effects of volume change on the SWCC were discussed previously. Since the effects of these two parameters combine to control the infiltration rate and because their behavior in terms of expansive soil is not fully understood, it is difficult to determine the appropriate values for each parameter independently.

Because the results from the modeling presented in Chapter 6.3 compare well with the field results, and because of the hysteresis effects shown in Figure 6-31, it was assumed for this investigation that the laboratory measured SWCC data presented in Chapter 4 is appropriate. As discussed earlier, the proper representation of water retention data in an expansive soil for the purposes of modeling moisture flow and evaporation is a topic of current research. The CLOD test method has been proposed for this purpose and was used by Chao (1995) to obtain the SWCC used here.

Given the current state of technology for modeling evaporation and infiltration in an expansive soil the hydraulic conductivity was selected for this research as the primary variable in terms of evaluating the effects of soil properties on active zone depth and edge moisture variation. To evaluate the effects of hydraulic conductivity, the initial value of 1.3E-07 feet per second, used for preliminary modeling presented in Chapter 6.3, was varied by an order of magnitude in each direction (1.3E-06 to 1.3E-08 feet per second) in the SoilCover model. The model simulations were conducted on the CSU site from February 1, 1992 to October 31, 1998. The input climate parameters used in Chapter 6.3 were also used here.

Figure 6-61 shows the results of three SoilCover model simulations utilizing hydraulic conductivity values of 1.3E-06, 1.3E-07, and 1.3E-08 feet per second.

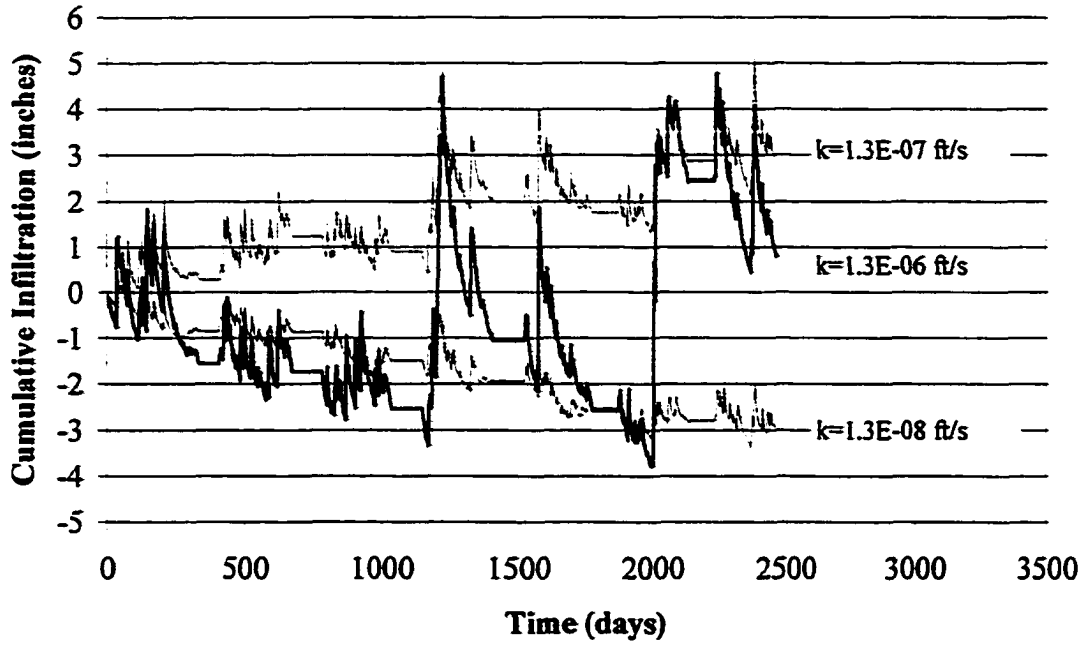

Figure 6-61 Cumulative net infiltration as a function of hydraulic conductivity

The effects of hydraulic conductivity are most clearly visible with respect to the net infiltration at the surface, the key component of flow effecting active zone depth and edge moisture variation distance. The net infiltration at the surface given by the SoilCover model is the difference between inflow and outflow across the soil surface over a given time step.

As expected the cumulative infiltration results presented in Figure 6-61 indicate that the hydraulic conductivity controls the flux rate at the surface. However, there appears to be an optimum hydraulic conductivity in terms of flux rate. For example when the hydraulic conductivity is equal to 1.3E-06 feet per second the cumulative infiltration fluctuates

between –4.0 inches and +4.0 inches. When the hydraulic conductivity is decreased to 1.3E-07 feet per second the cumulative infiltration continues in the positive range fluctuating between the initial value of zero and a maximum value of approximately 5 inches. However, when the hydraulic conductivity is decreased further to 1.3E-08 feet per second, the cumulative infiltration is negative (net evaporation) due to the inability of the soil to transmit moisture before it evaporates at the surface or runs off.

The cumulative infiltration and the cumulative precipitation are shown in Figure 6-62.

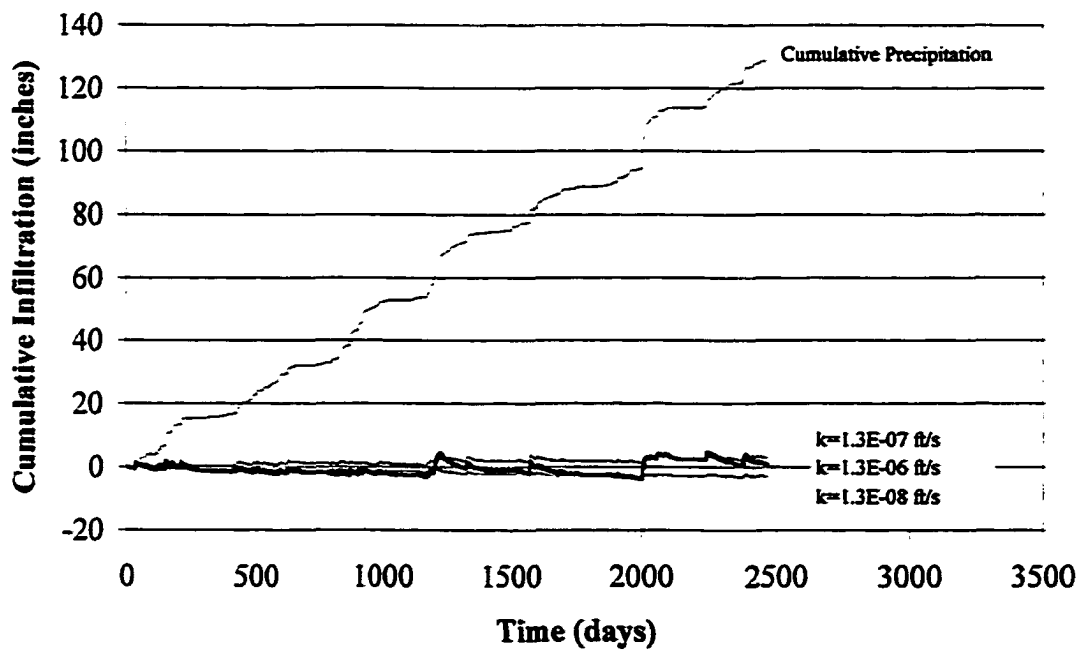

Figure 6-62 Cumulative net infiltration and precipitation as a function of time

The cumulative infiltration is very low for all three cases presented when compared to the cumulative precipitation over the same time. The cumulative precipitation is approximately 140 inches compared with cumulative infiltration that ranges from –4 to +4 inches. This indicates that the majority of precipitation is lost to evaporation or

runoff, and that the relative effect of hydraulic conductivity, in this range of values and in this soil type, is minimal.

These results are for an ideal case of infiltration into a one-dimensional column of homogeneous soil on a flat surface. The soil adjacent to the slab is not a flat surface. Generally the area around the slab slopes to the southeast. In addition, when the simulated slab was installed a berm was constructed adjacent to the slab on the north and east sides to divert runoff from accumulating on the slab. On the north side the toe of the berm intersects the surface of the simulated slab. However, on the east side of the slab the toe of the berm is approximately 5 to 10 feet east of the slab edge and the soil surface between the toe of the berm and the slab is irregular with moderately dense low vegetation. It is believed that during snow melt and significant precipitation events water accumulates in some of the undulations scattered within the area between the berm and the slab, and this has contributed to the excess increase in water content along the east side of the slab.

To demonstrate the effects of ponding on the eastern side and the effects of the geologic dip and anisotropic structure of the Pierre shale on the development of the active zone depth it was necessary to incorporate the two-dimensional flow model SEEP/W. The results of two-dimensional modeling are presented in the following sub-chapter.

6.4.2 Geologic Conditions

The prominent geologic feature of the Pierre shale at the CSU test site is the bed dip. It was proposed in Chapter 5 that the bed dip and anisotropic nature of the Pierre shale contributes to the differential water content and heave patterns that have been observed.

This description is purely qualitative, based on field observations, and has not been validated from a numerical or quantitative stand point. To more fully investigate the effects of bed dip on the observed behavior, a two-dimensional numerical model, SEEP/W, was employed.

As discussed in Chapter 6.3.3 the primary input parameters for the SEEP/W model are the SWCC, saturated hydraulic conductivity, and the unsaturated hydraulic conductivity function. The same soil conditions were used for the two-dimensional modeling as were used in the one-dimensional modeling with SoilCover. The finite element mesh geometry used for the two-dimensional modeling is presented in Appendix E.

The SEEP/W model allows the user to specify a hydraulic conductivity direction. The hydraulic conductivity direction simulates the angle of dip by orienting a set of x'-y' axes by the specified angle relative to the x-y plane. The new axis orientation, x'-y', represents the bed dip where, x' is parallel to the bedding plane, and y' is perpendicular to the bedding plane. Assuming that the x-plane in this case represents the east-west direction at the site, rotating the x-y plane 25 degrees from the horizontal to obtain x'-y', simulates the general bed dip at the CSU site. In addition, the ratio between the horizontal and vertical hydraulic conductivity (K_h/K_v) can range between 2 and 10 for normally consolidated sedimentary clay (Lambe and Whitman, 1969). Horizontal permeability tests were not performed on samples from the CSU site. Therefore, as an approximation the K_h/K_v ratio was assumed to be 10.

To evaluate the effects of bed dip and anisotropy, two model simulations were conducted, one with a horizontal (zero bed dip) orientation and isotropic conditions, and a second

with a 25-degree bed dip orientation and anisotropic conditions. The results from the two model simulations are presented in Figures 6-63 through 6-72.

Figures 6-63 through 6-72 show the water content, at a depth of 1 foot below the slab, as a function of distance from the west edge of the slab. Figures 6-63 and 6-64 show the results from 1993 with and without considering bed dip and anisotropy, respectively. In general the bed dip and anisotropy result in a slight increase in infiltration beneath the west side of the slab, in the direction of dip and higher permeability. The same result is evident in Figures 6-65 through 6-72. The model results indicate that the water content beneath the slab increases during large precipitation events and that the increase is larger due to the bed dip and anisotropy along the western side of the slab.

Field measured water content data from the CSU site taken at a depth of 1 foot is shown in Figures 6-73 through 6-77. In general there is more variability in the field-measured water content laterally beneath the slab. This is due to the natural variability in soil structure at the site. Also, the data from 1993 shows a large increase in water content that does not appear in the first year of modeling. This does not appear in the model results because of the initial conditions that were used for the modeling. It was assumed for the SEEP/W modeling that the initial wetting due to slab placement and subsequent decrease in evapo-transpiration had already occurred, and that the water content profile was a constant 15 percent with depth. As was the case in the preliminary SoilCover simulations the magnitude of the water content from the model is less than the measured values. This is due to the SWCC that was used for modeling compared with actual conditions.

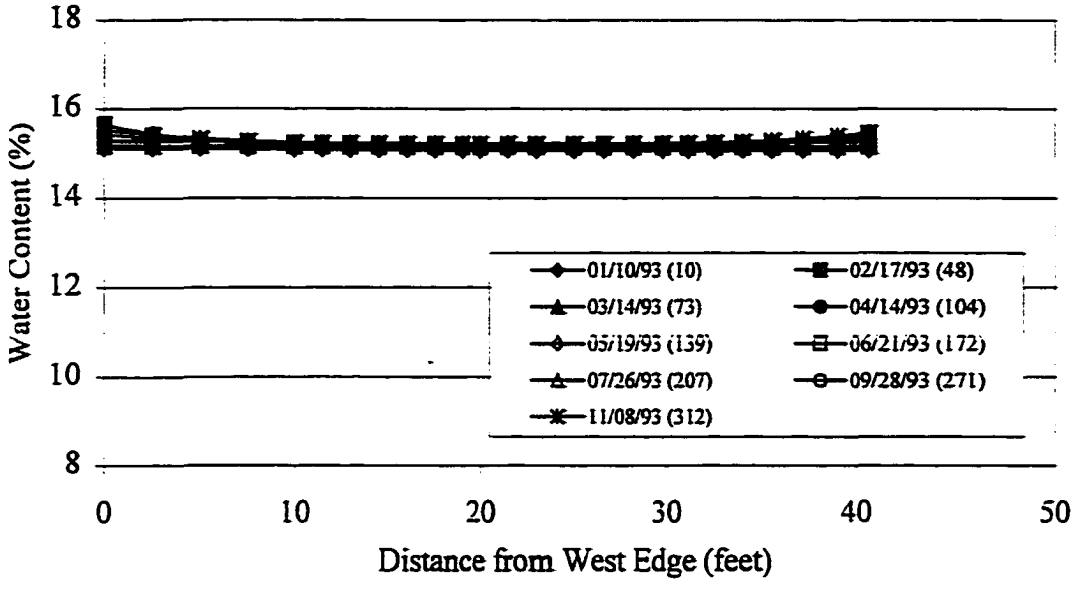

Figure 6-63 Predicted water content in 1993 as a function of lateral position at a depth of 1-foot beneath the slab – bed dip = 0, K_h/K_v=1

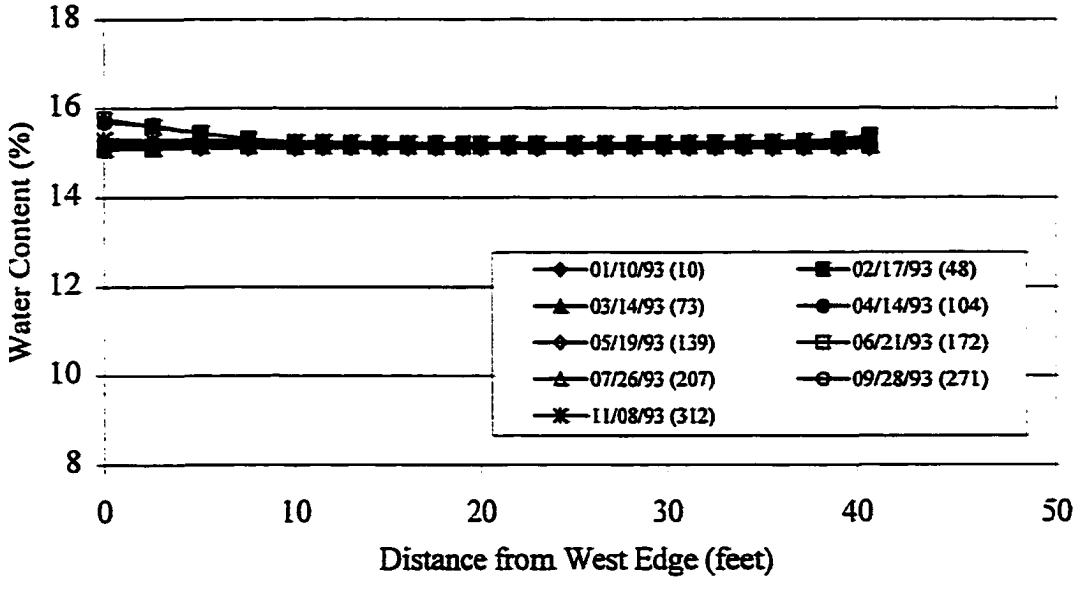

Figure 6-64 Predicted water content in 1993 as a function of lateral position at a depth of 1-foot beneath the slab – bed dip = 25°, K_h/K_v=10

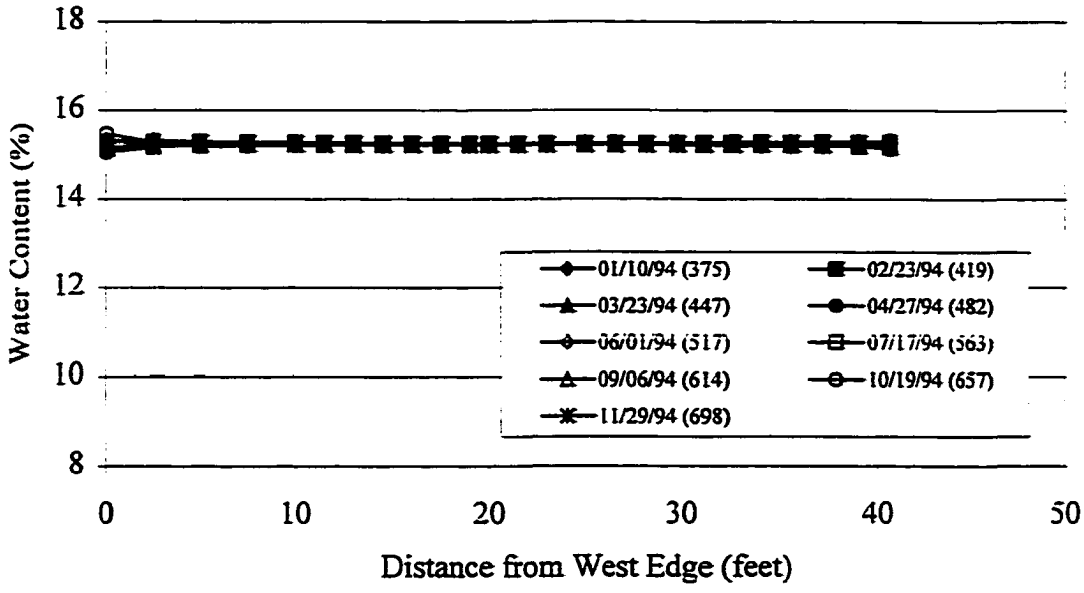

Figure 6-65 Predicted water content in 1994 as a function of lateral position at a depth of 1-foot beneath the slab – bed dip = 0, K_h/K_v=1

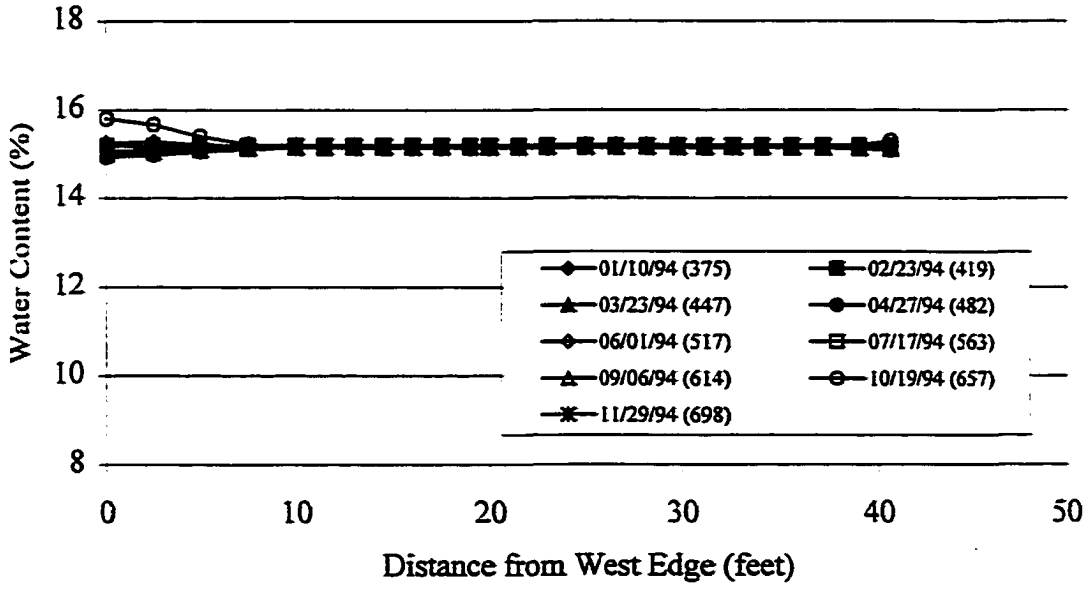

Figure 6-66 Predicted water content in 1994 as a function of lateral position at a depth of 1-foot beneath the slab – bed dip = 25°, K_h/K_v=10

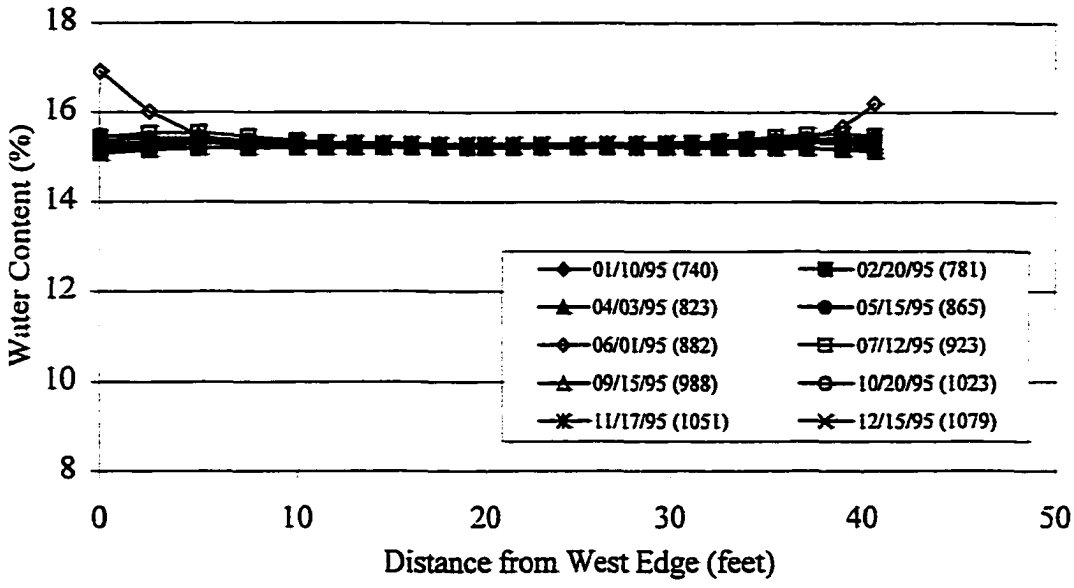

Figure 6-67 Predicted water content in 1995 as a function of lateral position at a depth of 1-foot beneath the slab – bed dip = 0, K_h/K_v=1

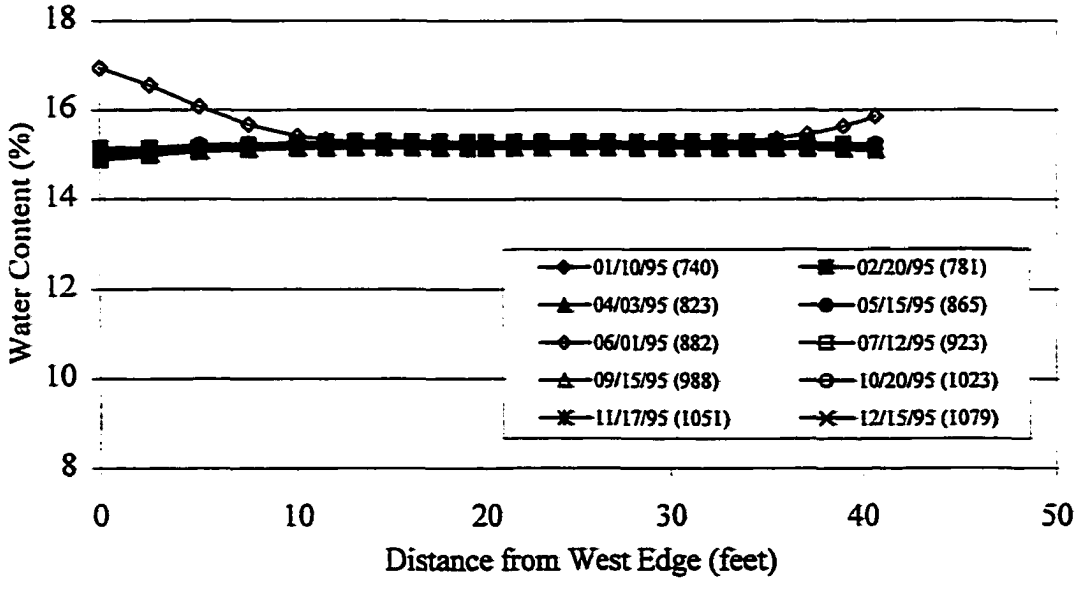

Figure 6-68 Predicted water content in 1995 as a function of lateral position at a depth of 1-foot beneath the slab – bed dip = 25°, K_h/K_v=10

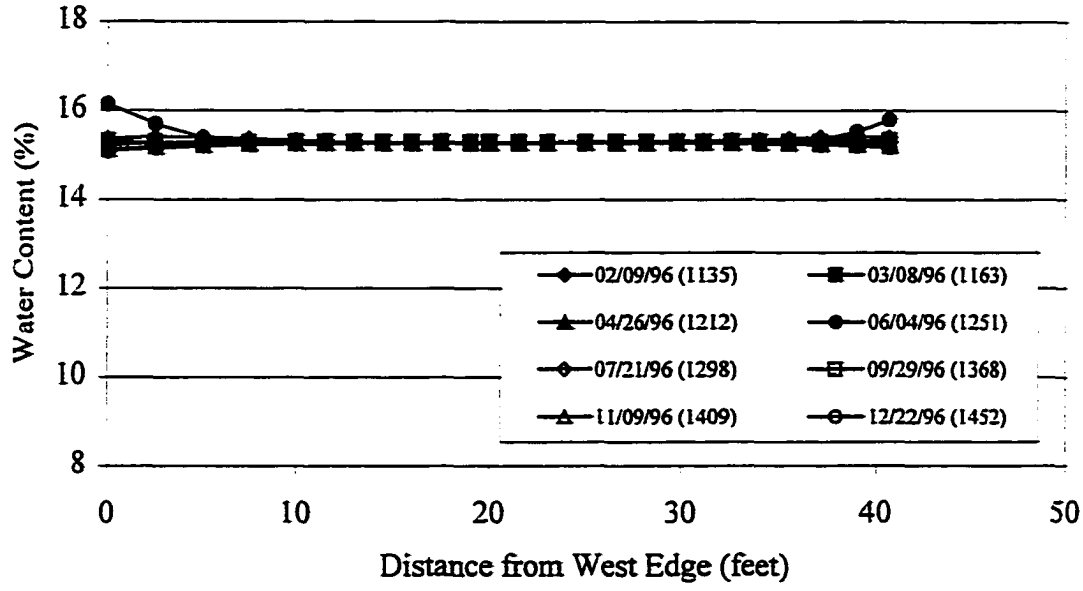

Figure 6-69 Predicted water content in 1996 as a function of lateral position at a depth of 1-foot beneath the slab – bed dip = 0, K_h/K_v=1

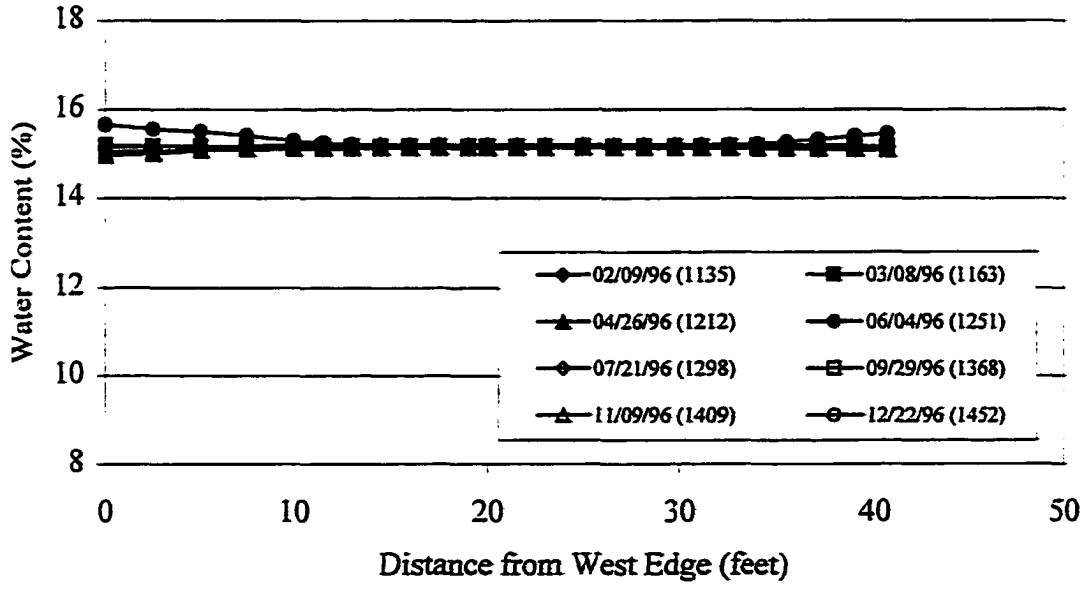

Figure 6-70 Predicted water content in 1996 as a function of lateral position at a depth of 1-foot beneath the slab – bed dip = 25°, K_h/K_v=10

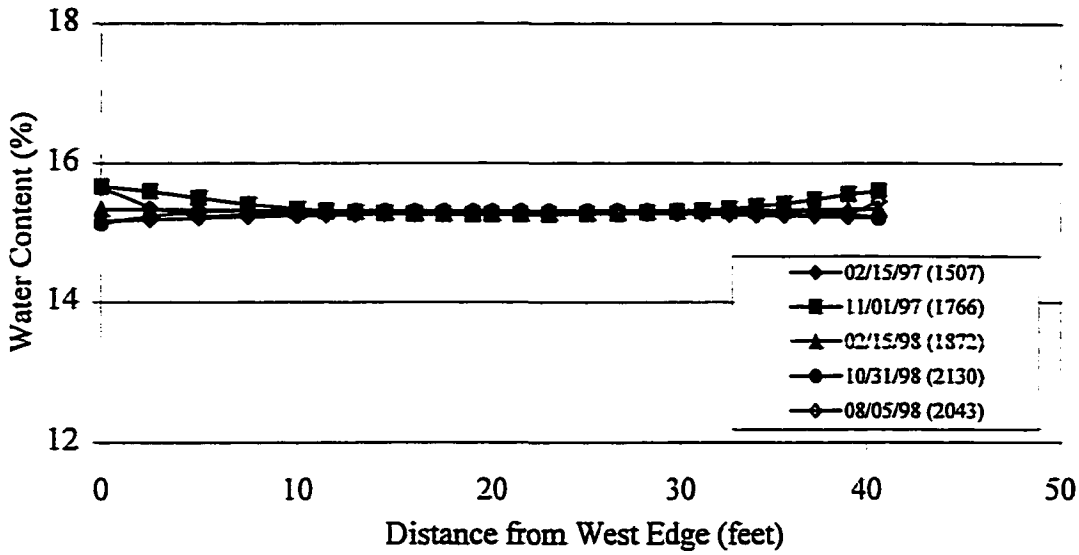

Figure 6-71 Predicted water content in 1997 as a function of lateral position at a depth of 1-foot beneath the slab – bed dip = 0, K_h/K_v=1

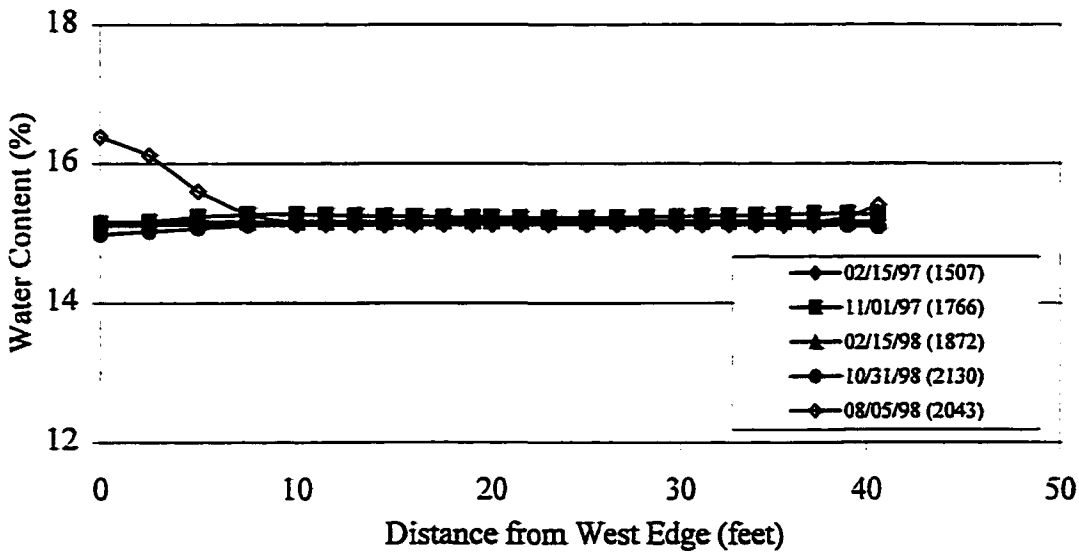

Figure 6-72 Predicted water content in 1997 as a function of lateral position at a depth of 1-foot beneath the slab – bed dip = 25°, K_h/K_v=10

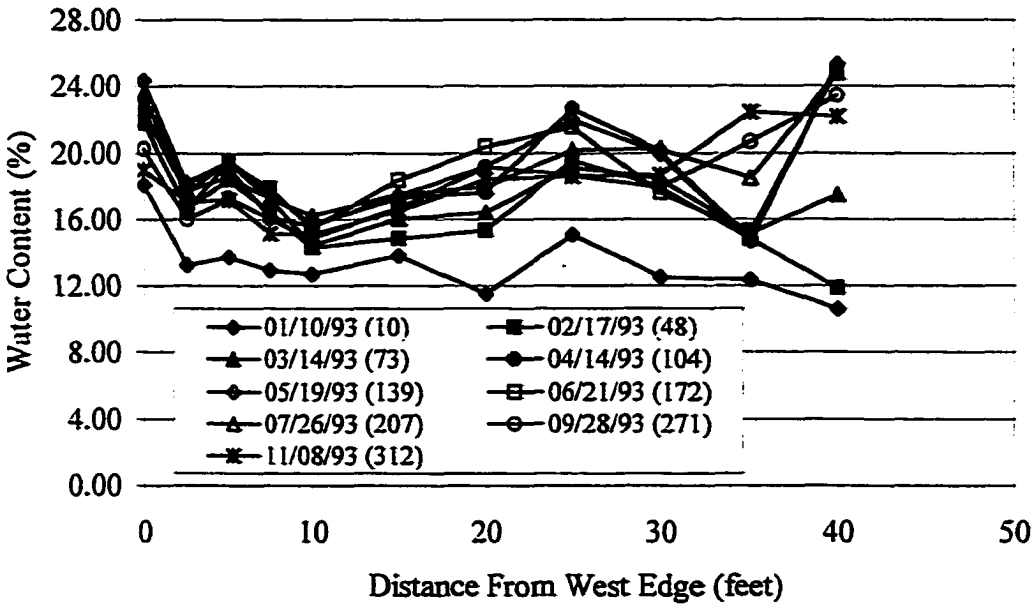

Figure 6-73 Field measured water content in 1993 as a function of lateral distance from the west edge of the slab, at a depth of 1-foot

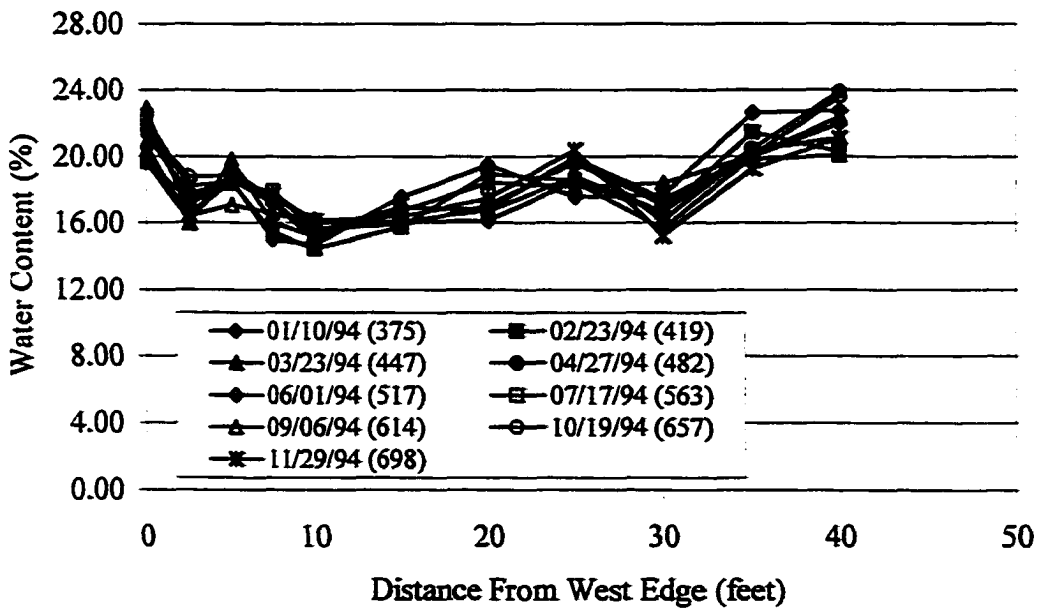

Figure 6-74 Field measured water content in 1994 as a function of lateral distance from the west edge of the slab, at a depth of 1-foot

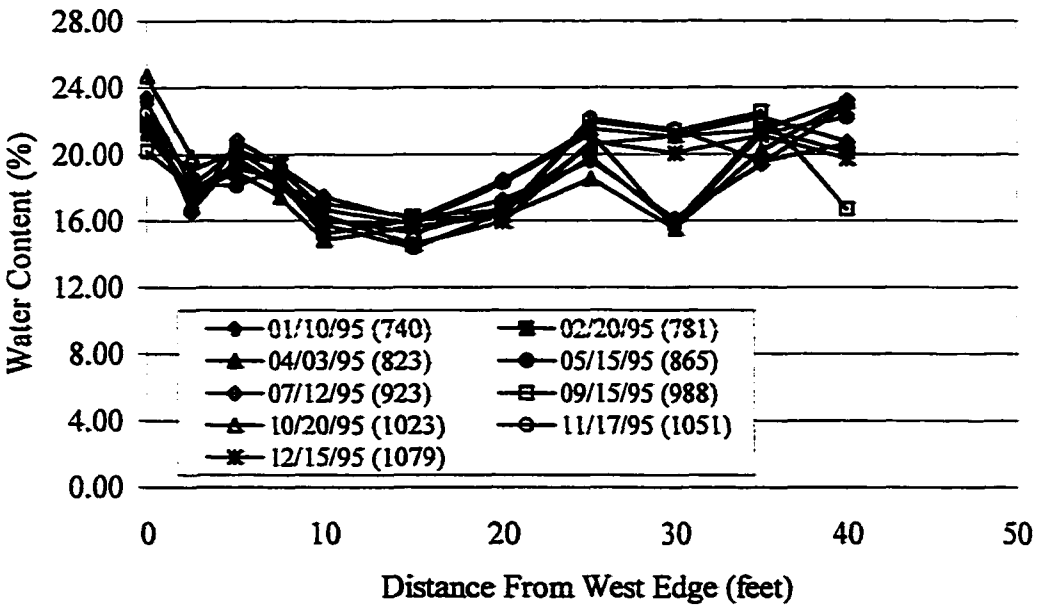

Figure 6-75 Field measured water content in 1995 as a function of lateral distance from the west edge of the slab, at a depth of 1-foot

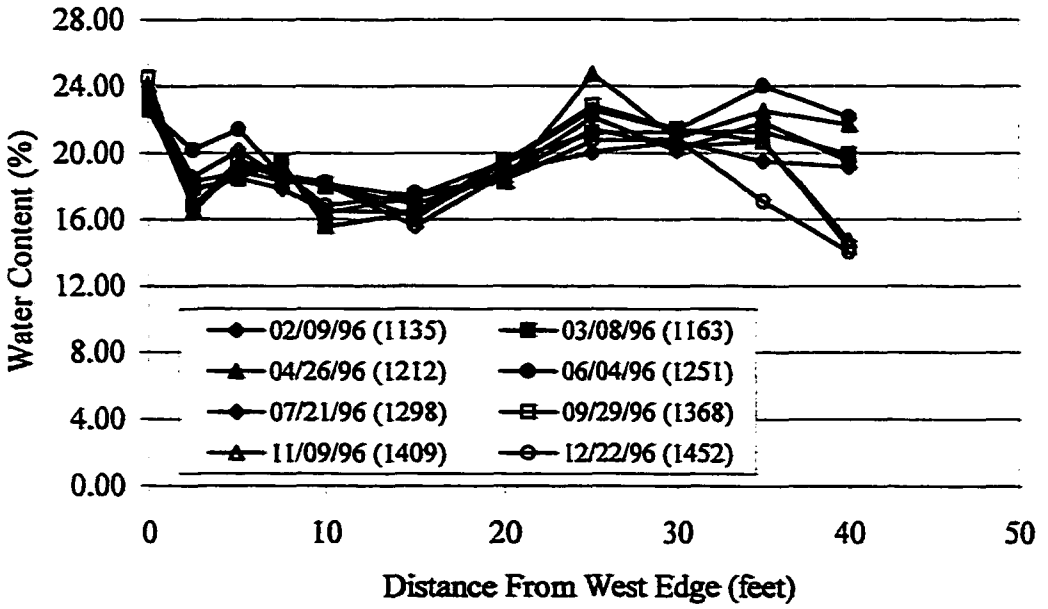

Figure 6-76 Field measured water content in 1996 as a function of lateral distance from the west edge of the slab, at a depth of 1-foot

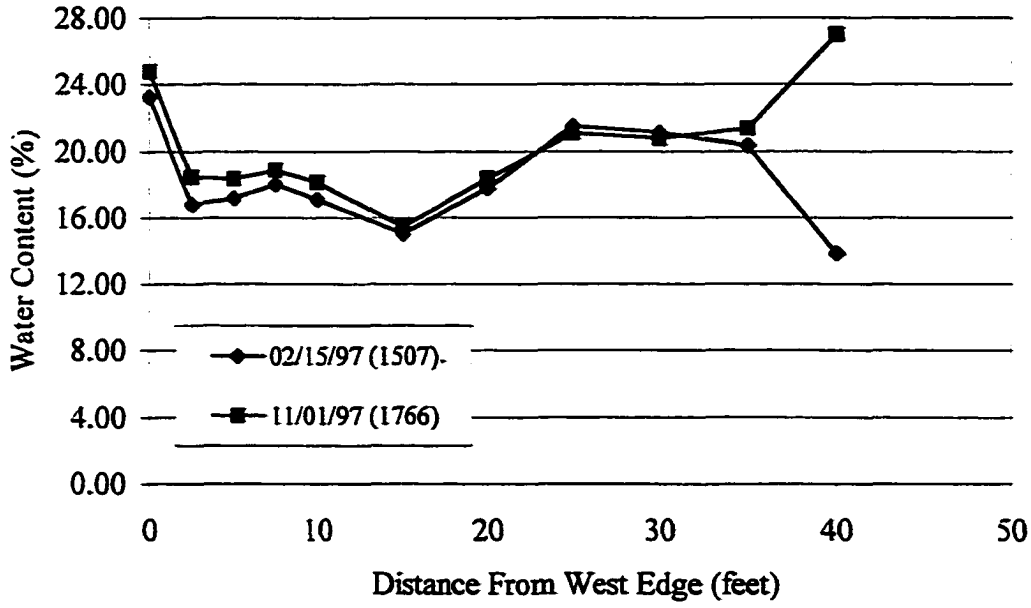

Figure 6-77 Field measured water content in 1997 as a function of lateral distance from the west edge of the slab, at a depth of 1-foot

Given these differences the model results are considered reasonable. They demonstrate the effects of extreme climatic events on infiltration from the adjacent soils. The seasonal fluctuations near the edges of the slab due to cyclical climatic events are consistent with the observed behavior.

The field measured water content data from the eastern side of the slab however, shows the progression of water downward along the edge of the slab and to a lesser degree at 5 feet and 10 feet inward from the edge of the slab. This was presented in Chapter 5 and can be seen in water content profiles for monitoring locations A-5, B-5, and C-5 in Appendix C and in Chapter 5. The progression of water downward has not yet been demonstrated numerically by the modeling. The model results presented here that include the bed dip and anisotropy do not account for this observed behavior.

As discussed above the stress distribution in the soil is not accounted for in the models used in this investigation. As an indirect approach to accounting for the stress distribution, the soil profile can be distributed in layers consistent with the geologic layering at the site. In the case of the CSU site, four general layers were identified and discussed in Chapter 3. For flow modeling, the stress distribution of the soil can be accounted for by decreasing the hydraulic conductivity in each soil layer with depth. The model results presented thus far indicate that infiltration is relatively low given the current boundary conditions and the effects of decreasing hydraulic conductivity at depth are not significant. Therefore, this aspect of the geologic conditions is addressed in Chapter 6.4.3 after the environmental boundary conditions of the model are evaluated.

6.4.3 Environmental Conditions

It was suggested in Chapter 5 that water impounded along the eastern side of the slab has affected the moisture migration patterns that have been observed beneath the slab. A review of the data from Goode (1982) and Hamberg (1985), presented in Chapter 2, shows that the maximum water content values observed along the edge of their simulated slabs were approximately 17 to 19 percent. The maximum water content values observed in this investigation are approximately 25 to 30 percent, see for example water content profiles A-1, A-3, A-5, A-9, B-5, and C-5. The climate conditions and soil types in these two investigations are the same. However, as mentioned above there is a berm on the eastern side of the slab in this investigation and impounded water at that location may be contributing to the higher water content values measured on the eastern side of the slab.

A ponding scenario was introduced in the SEEP/W model to more fully investigate the effects of the boundary conditions at the site. SEEP/W simulations were conducted assuming that during precipitation events a constant inflow boundary condition, equal to the permeability of the soil, occurs along the eastern edge of the slab. The results from those model simulations are presented in Figures 6-78 through 6-82. The water content beneath the slab as a function of lateral distance from the western edge is shown for years 1993 through 1998 in Figures 6-78 through 6-82, respectively.

The results shown in Figures 6-78 through 6-82 indicate that water impounded along the eastern side of the slab during precipitation events, will migrate inward toward the drier soils beneath the center of the slab. This is consistent with the measured field data shown in Figures 6-73 through 6-77. However, the magnitude of water content from the model (Figures 6-78 through 6-82) is less than that observed in the field, (Figures 6-73 through 6-77) for reasons discussed in Chapter 6-2. The general trend however, of water content increase along the edge and migration laterally resulting in water content increases at locations inward from the edge over time is apparent in both the model and field results.

Figure 6-83 shows the time rate of water content increase from the model at a point located 5 feet inward from the eastern edge of the slab, at three depths in the soil near the surface. Similar model results from the center of the slab and from a point located 4 feet inward from the western edge of the slab are shown in Figures 6-84 and 6-85. In general, the model results show that the water content beneath the slab is gradually increasing and the magnitude of increase is significantly higher along the eastern side, as expected.

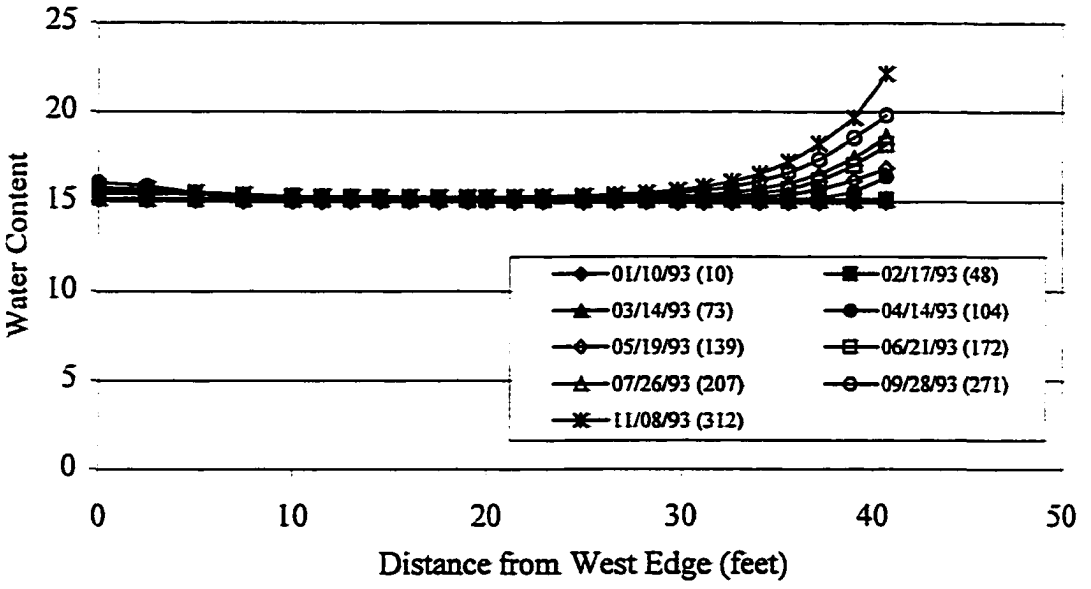

Figure 6-78 Predicted water content in 1993 as a function of lateral position at a depth of 1-foot beneath the slab – bed dip = 25°, K_h/K_v=10, with ponding

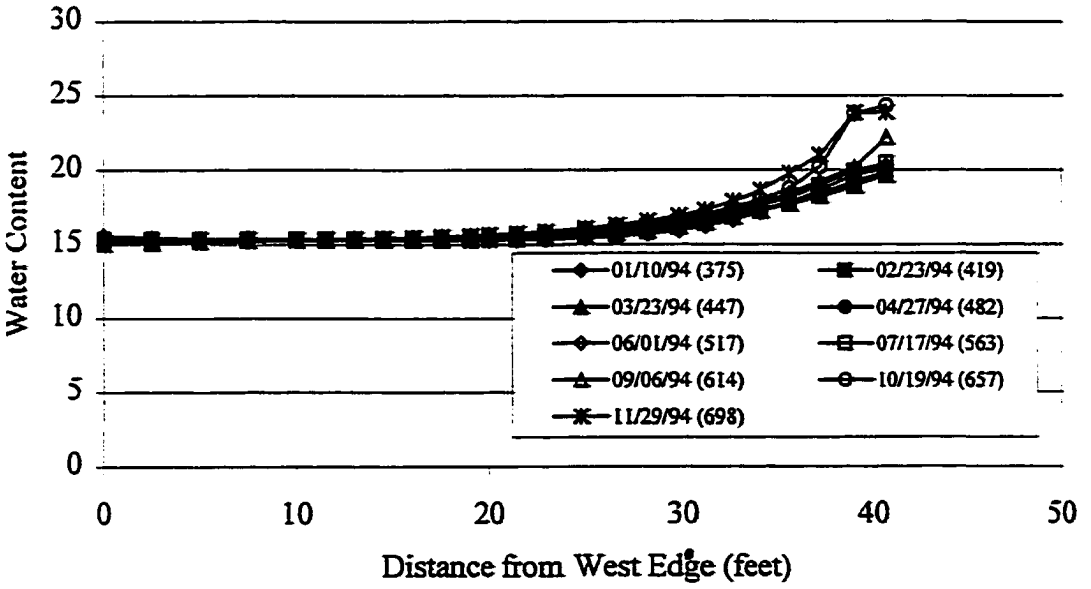

Figure 6-79 Predicted water content in 1994 as a function of lateral position at a depth of 1-foot beneath the slab – bed dip = 25°, K_h/K_v=10, with ponding

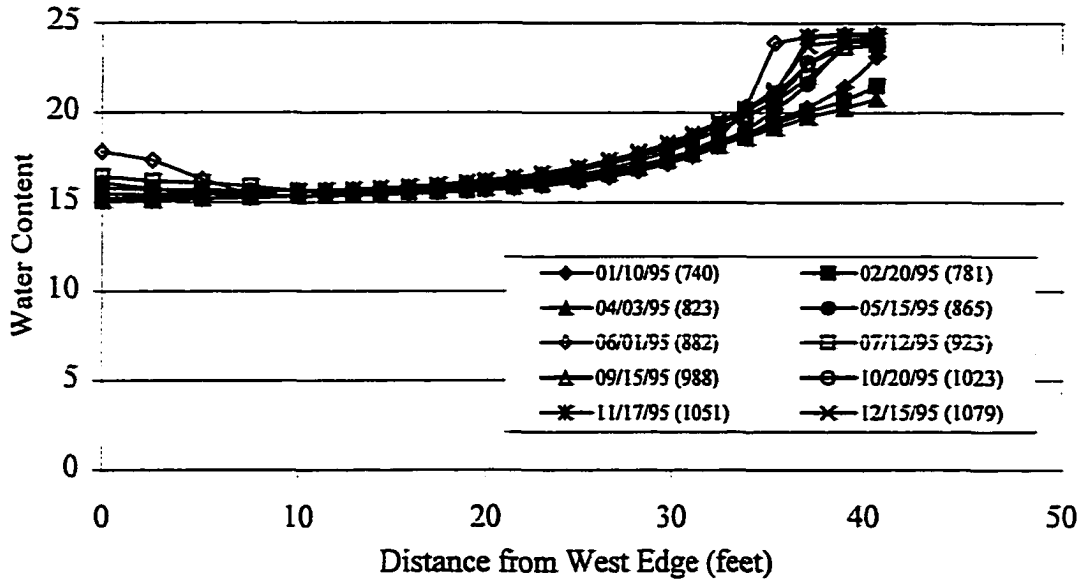

Figure 6-80 Predicted water content in 1995 as a function of lateral position at a depth of 1-foot beneath the slab – bed dip = 25°, K_h/K_v=10, with ponding

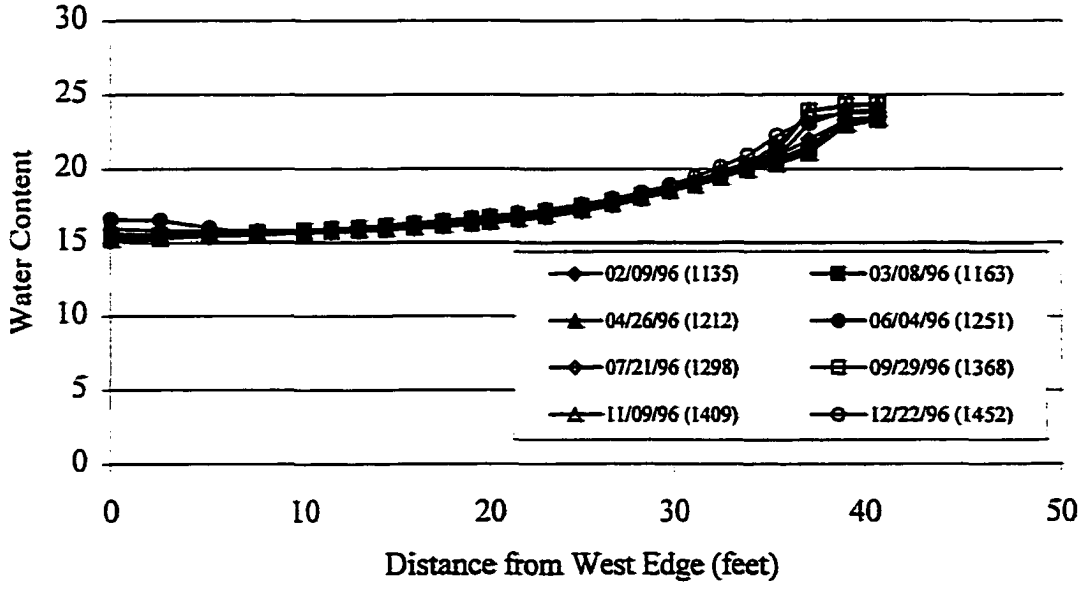

Figure 6-81 Predicted water content in 1996 as a function of lateral position at a depth of 1-foot beneath the slab – bed dip = 25°, K_h/K_v=10, with ponding

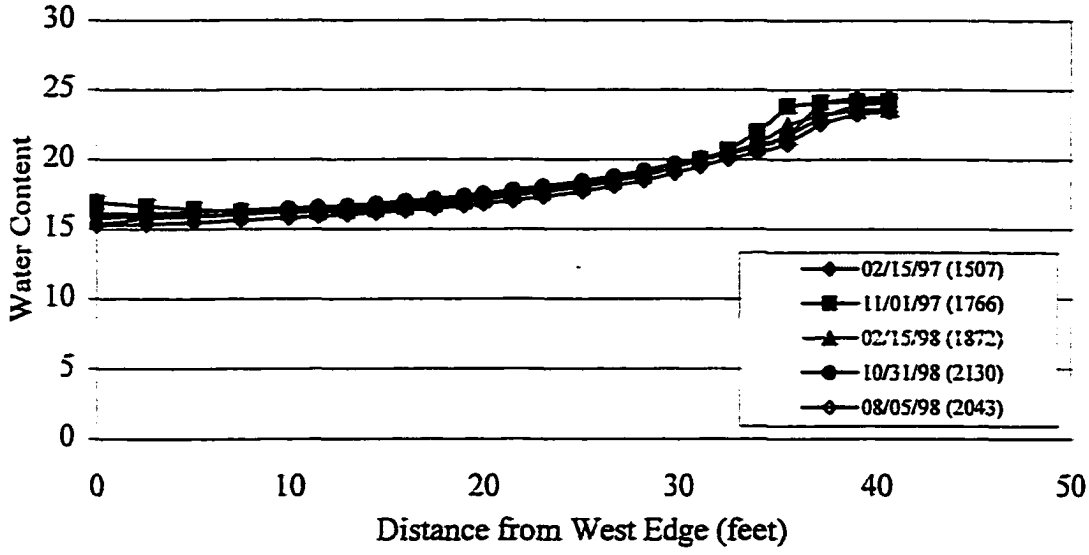

Figure 6-82 Predicted water content in 1997 as a function of lateral position at a depth of 1-foot beneath the slab – bed dip = 25°, K_h/K_v=10, with ponding

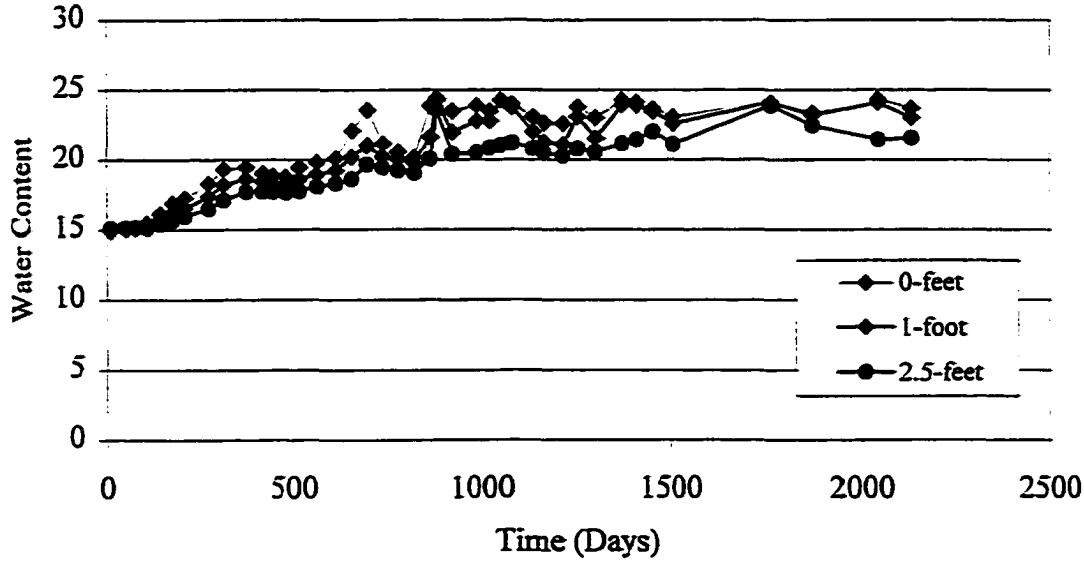

Figure 6-83 Predicted water content at a point located 5 feet inward from the east edge as a function of time – bed dip = 25°, K_h/K_v=10, with ponding

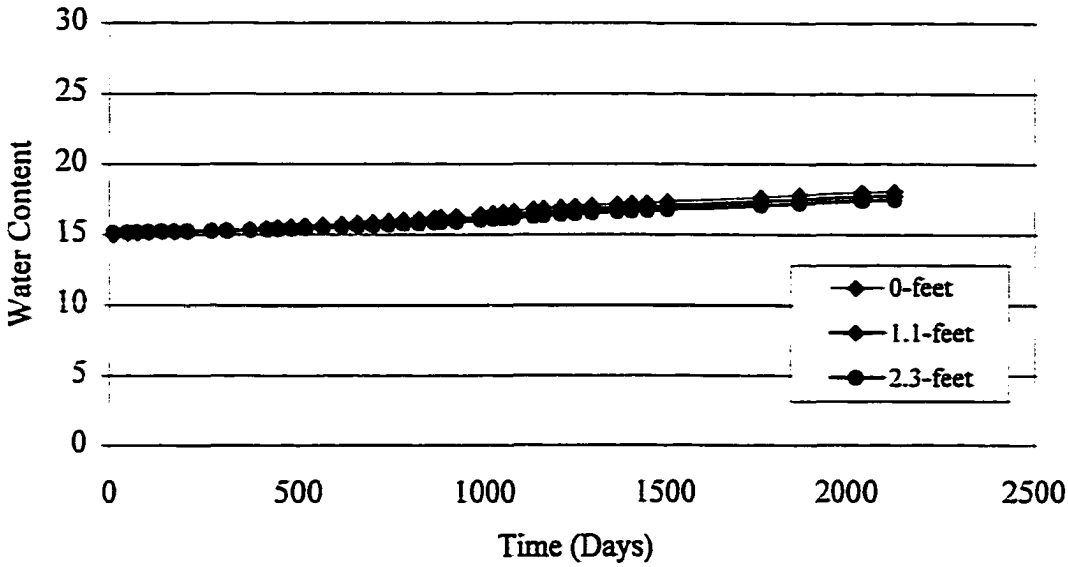

Figure 6-84 Predicted water content at a point located in the center of the slab as a function of time – bed dip = 25°, K_h/K_v=10, with ponding

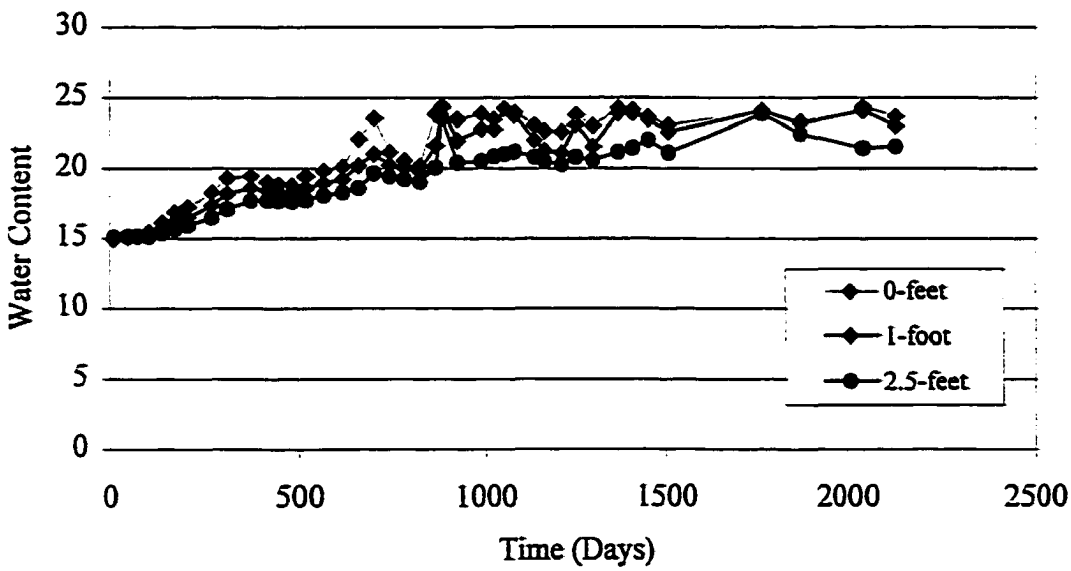

Figure 6-85 Predicted water content at a point located 4 feet inward from the west edge as a function of time – bed dip = 25°, K_h/K_v=10, with ponding

The modeled water content from the eastern edge of the slab to approximately 5 feet inward from the edge is approaching 25 percent. Based on the weight-volume relationship of the soil, 25 percent gravimetric water content represents a saturated soil in the model. The measured degree of saturation was presented in Figure 6-60. The difference between the measured degree of saturation and the degree of saturation obtained from the model is due to the inability of the model to account for volume change.

Field data from depths of 1, 2, and 3 feet at access tubes located along the centerline of the slab at the field test site is shown in Figures 6-86 through 6-94. The field data show the same trend as seen in Figures 6-83 through 6-85. Figure 6-86 shows that at the edge of the slab (A-5) the water content increased rapidly and has since continually fluctuated with climatic trends.

At locations B-5 (Figure 6-87) and C-5 (Figure 6-88) the water content increases later than at A-5, indicating that water is migrating from the eastern edge (near A-5). In addition, the field results in Figures 6-86 through 6-94 indicate that the water content beneath the center and edge of the slab fluctuates with climatic trends.

As discussed in Chapter 6-2, the model results differ somewhat in magnitude from the field results due to the infiltration-evaporation boundary conditions that were predicted by the SoilCover model. The reasons for the difference between the model and the field results can be divided into two groups; those related to the assumptions that are made during the formulation of the model and those related to the difficulties in determining and applying the appropriate constitutive parameters for the models.

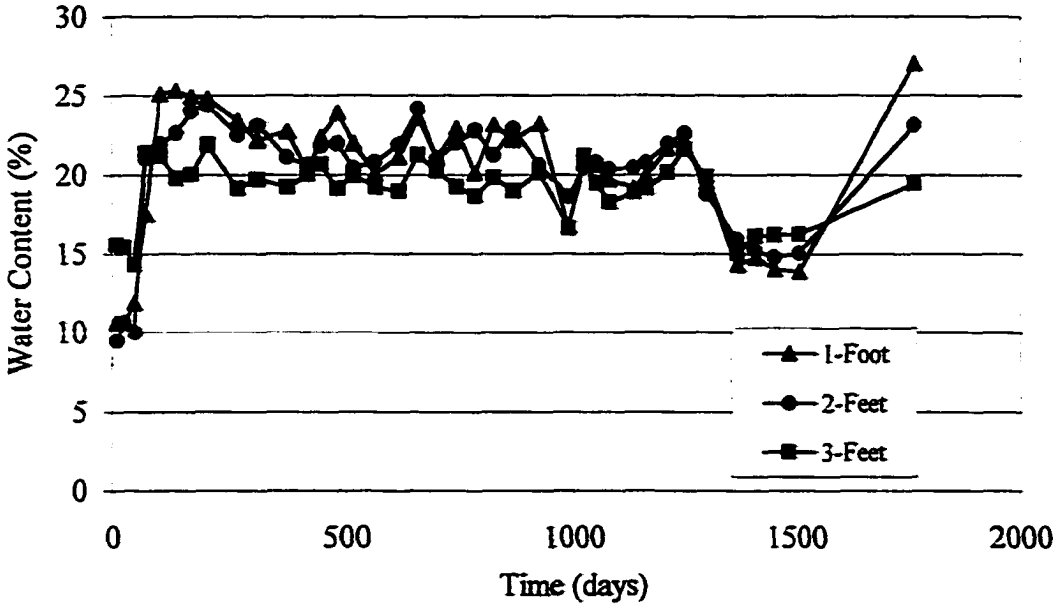

Figure 6-86 Measured water content as a function of time from Access Tube A-5 located along the eastern edge of the slab

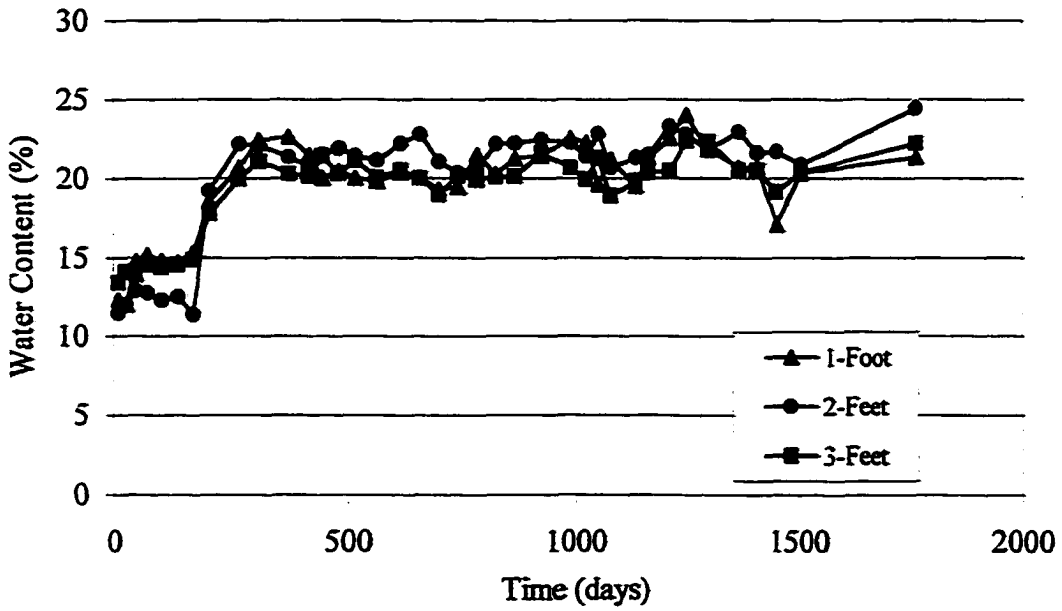

Figure 6-87 Measured water content as a function of time from Access Tube B-5 located 5 feet inward from the eastern edge of the slab

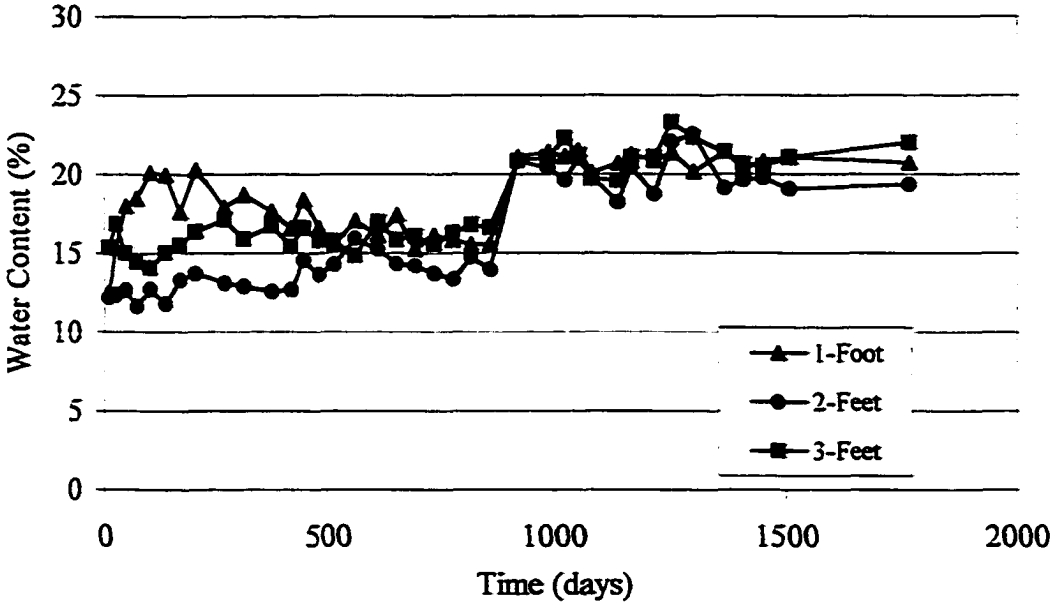

Figure 6-88 Measured water content as a function of time from Access Tube C-5 located 10 feet inward from the eastern edge of the slab

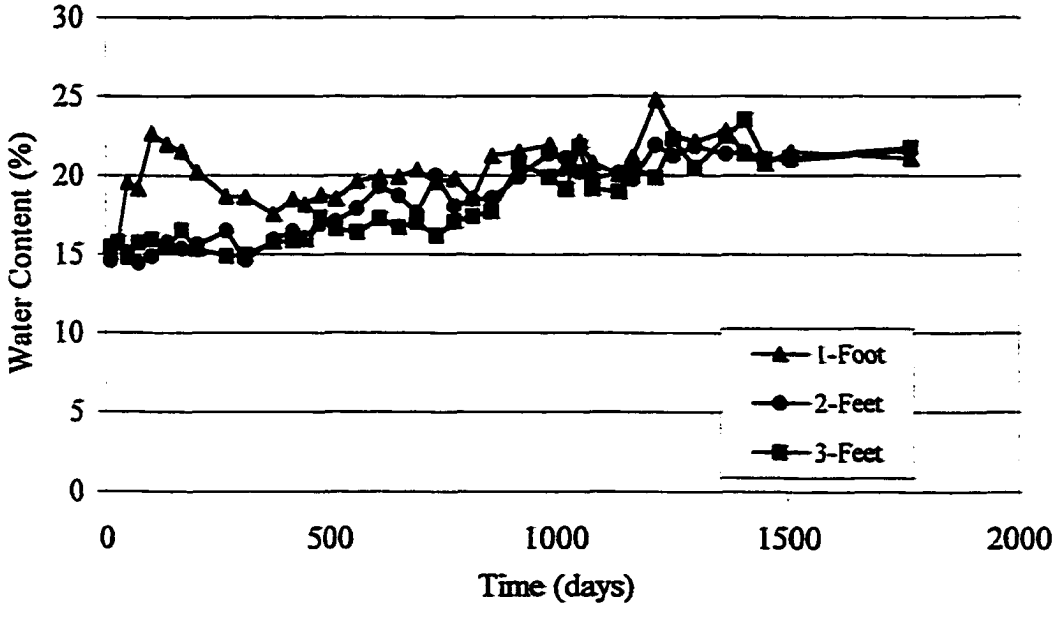

Figure 6-89 Measured water content as a function of time from Access Tube D-5 located 15 feet inward from the eastern edge of the slab

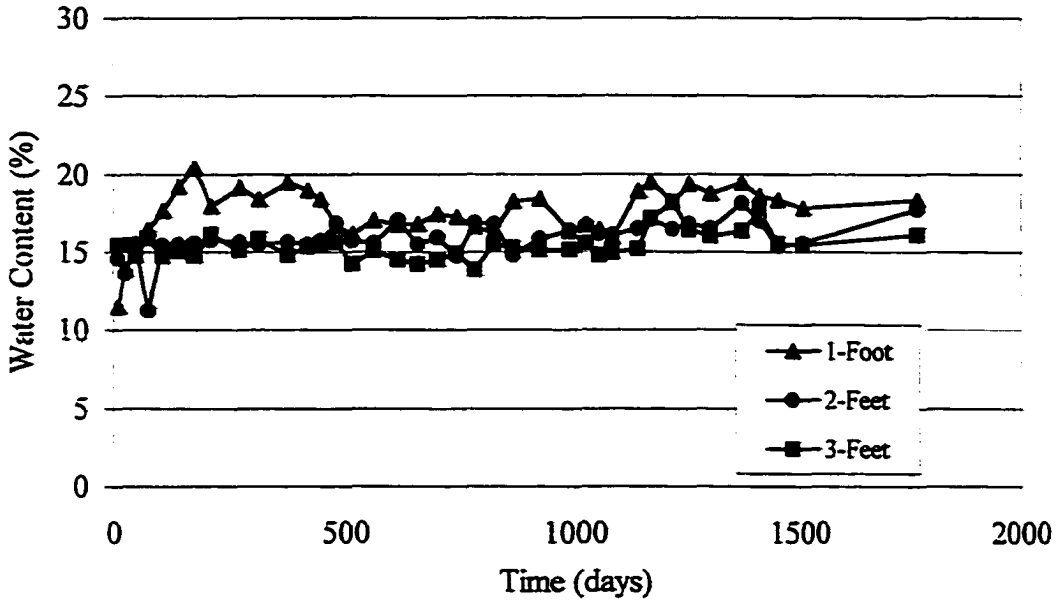

Figure 6-90 Measured water content as a function of time from Access Tube E-5 located in the center of the slab

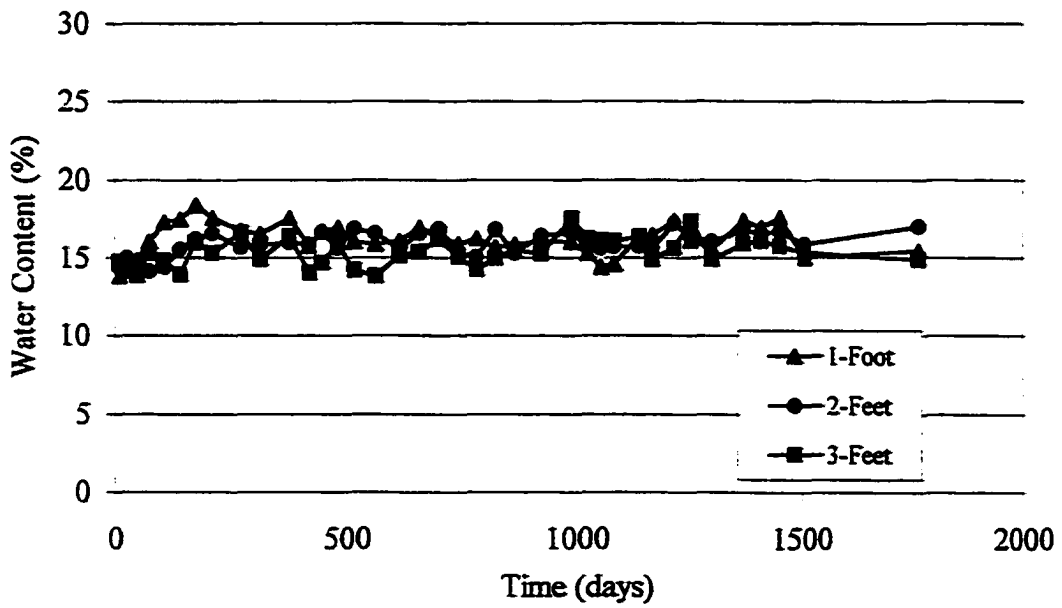

Figure 6-91 Measured water content as a function of time from Access Tube F-5 located 15 feet from the western edge of the slab

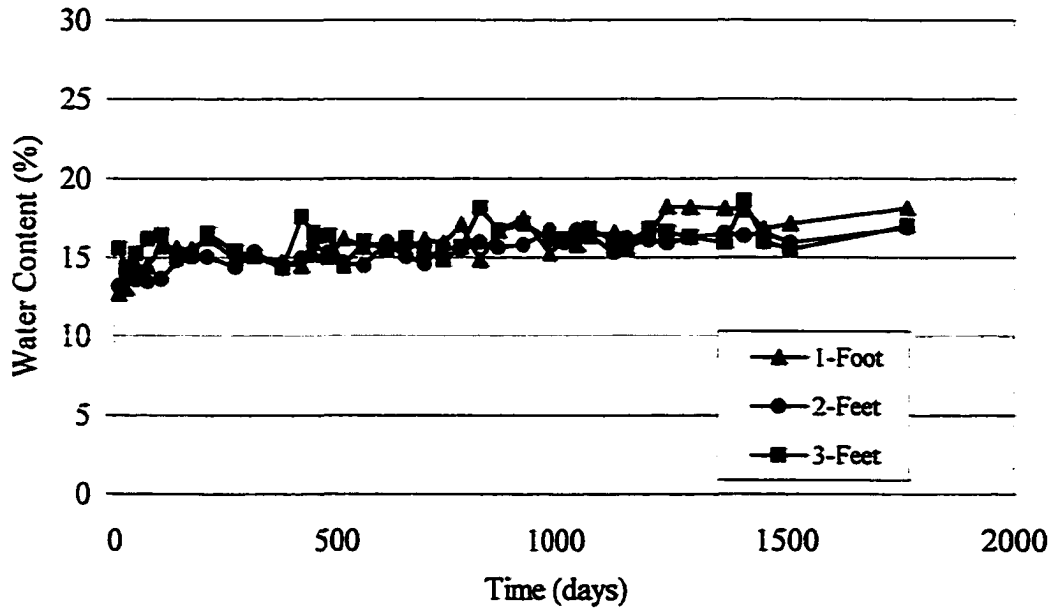

Figure 6-92 Measured water content as a function of time from Access Tube G-5 located 10 feet from the western edge of the slab

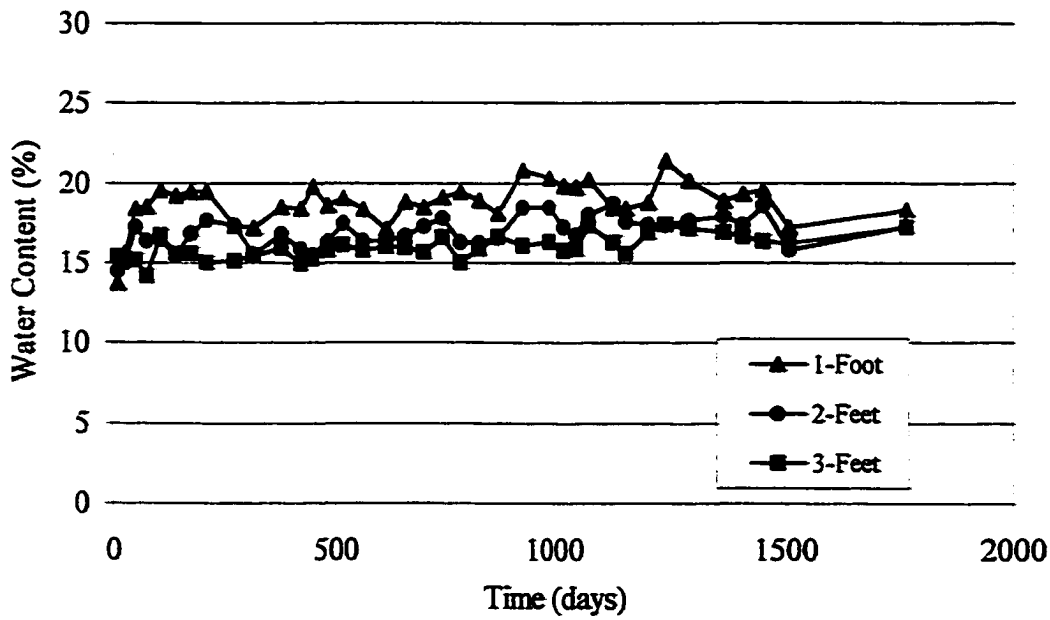

Figure 6-93 Measured water content as a function of time from Access Tube H-5 located 5 feet from the western edge of the slab

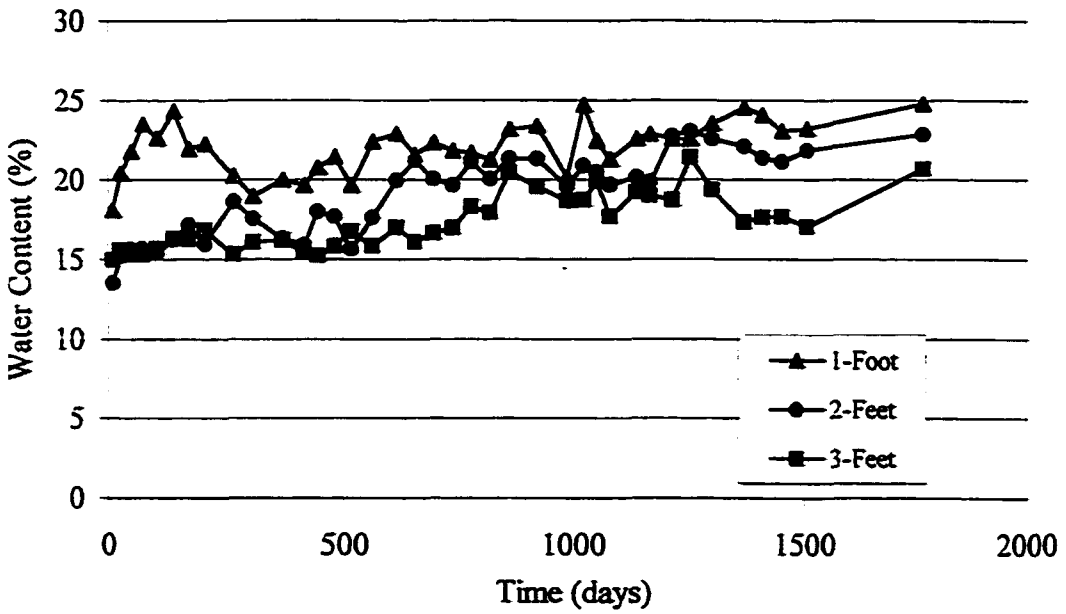

Figure 6-94 Measured water content as a function of time from Access Tube I-5 located along the western edge of the slab

The constitutive parameters used in this investigation were discussed in Chapter 4 and Chapter 6.2. Wilson (1990) lists several limitations to the theoretical development for the evaporation and infiltration formulations that he derived and which are used for the SoilCover model. Generally, the theoretical development used in the SoilCover model is based on a constant volume soil structure, and as mentioned earlier, the SWCC is significantly affected by volume change. The development of the SWCC used for this investigation and the effects of volume change were discussed in Chapter 4 and Chapter 6.3. Also important to the application of the SoilCover model to expansive soils is the occurrence of desiccation. The SoilCover model does not account for this phenomenon and Wilson (1990) did not investigate the effects of shrinkage and cracking on evaporation and infiltration. Shrinkage and cracking near the surface of the soil may

account for the larger fluctuations in water content at shallow depths observed in the field than were obtained from the model.

In addition, Wilson points out that the SWCC must be defined at the same temperature as the soil during the evaporative process. Laboratory tests conducted by Wilson (1990) show that the SWCC for sand, silt, and clay are particularly sensitive to temperature at high values of total suction. The TCP data presented in Chapter 4 shows that the maximum suction measured in the upper two feet of the surrounding soil at the CSU test site is 1,500 feet of water. Wilson (1990) suggests the sensitivity may be related to changes in osmotic suction with temperature, a condition also proposed by Miller (1996). Figure 6-95 shows the suction-water content data measured at the CSU site in the uncovered soil plotted as a function of temperature. Although there is considerable scatter in the data, linear trend lines indicate that field measured suction can vary by as much as 500 feet when temperature conditions are considered.

The effects of layering were briefly discussed in Chapter 6.4.2, and are more fully evaluated here. The soil profile at the CSU site is presented in Figure 3-4. A two-layered soil was considered by assuming that soils in the upper approximately 5 feet (organic-silt, yellow-tan clay, and reddish-yellow clay) are layer one, and the deeper soil (reddish-brown weathered clayshale) are layer two. The soil properties of the two layers were the same as in previous modeling except that the hydraulic conductivity of the deeper soil was decreased to 7.8E-8 feet per second, based on data presented in Figure 6-2. The bentonite seams and the shattered clayshale were not considered in these model simulations, and are discussed later.

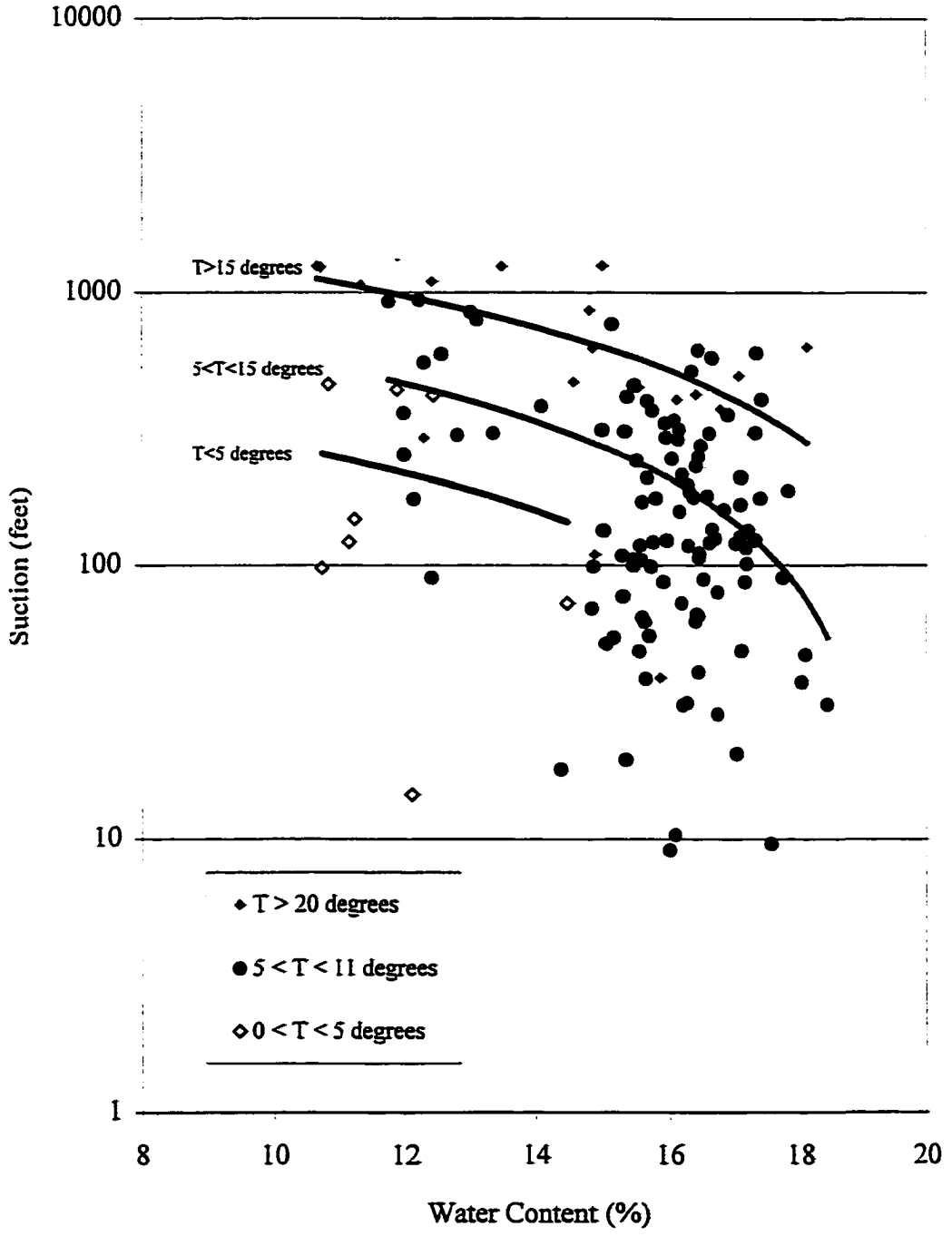

Figure 6-95 Measured suction-water content from J-5.5 in the uncovered soil adjacent to the slab

The model conditions used for the ponding scenario presented above were used for the two layered soil simulations. The effects of layering can be seen in Figures 6-96 through 6-99. Figure 6-96 shows the modeled water content as a function of lateral distance from the western edge of the slab for 1997, from the two-layered soil simulations. To see the effects of layering the results in Figure 6-96 can be compared with results presented in Figure 6-82 for the homogeneous soil. In general, the lower hydraulic conductivity soil below 5 feet results in a slower progression of water downward and an increase in the rate of lateral migration toward the center of the slab. Figure 6-97 shows the time rate of increase in water content at a point located 5 feet inward from the eastern edge of the slab. Those results, compared with results in Figure 6-83 for a homogeneous soil, indicate that the water content increases more rapidly beneath the slab when the lower hydraulic conductivity of the deeper soils is considered. Figures 6-98 and 6-99 show the modeled water content profiles at a point located 5 feet inward from the eastern edge of the slab, from the first and last days of monitoring at the site, based on a homogeneous soil and the two-layered soil, respectively. Those results show the lateral migration of water from the edge of the slab inward and how it is affected by the lower hydraulic conductivity in the deeper soils.

Generally, the results presented thus far indicate that the models agree with the trends observed in the field and can be used to further predict the long-term behavior. The exact inflow value or function to account for ponding along the eastern side of the slab is not known. However, the preliminary estimates based on reasonable assumptions give reasonable results. The final phase of this research was to evaluate the development of the maximum active zone depth at the CSU site.

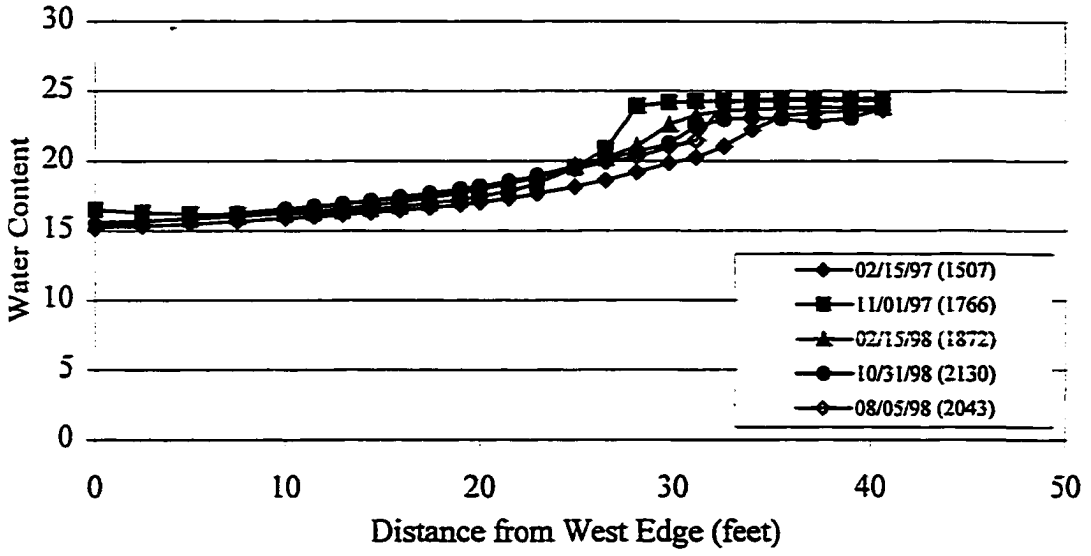

Figure 6-96 Predicted water content in 1997 as a function of lateral position at a depth of 1-foot beneath the slab – bed dip = 25°, K_h/K_v=10, with ponding in a 2-layered soil

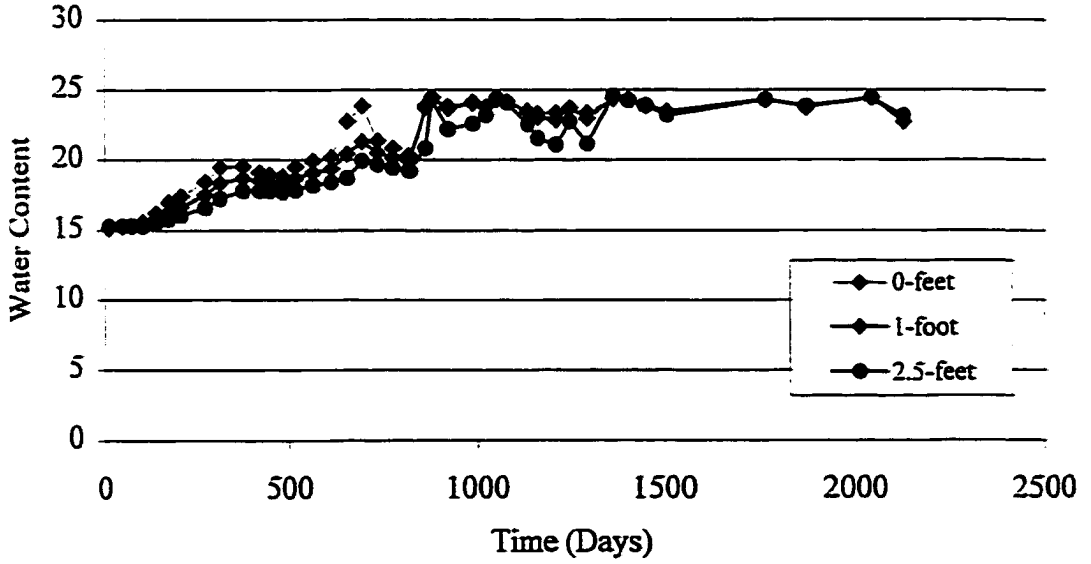

Figure 6-97 Predicted water content at a point located 5 feet inward from the east edge as a function of time – bed dip = 25°, K_h/K_v=10, with ponding in a 2-layered soil

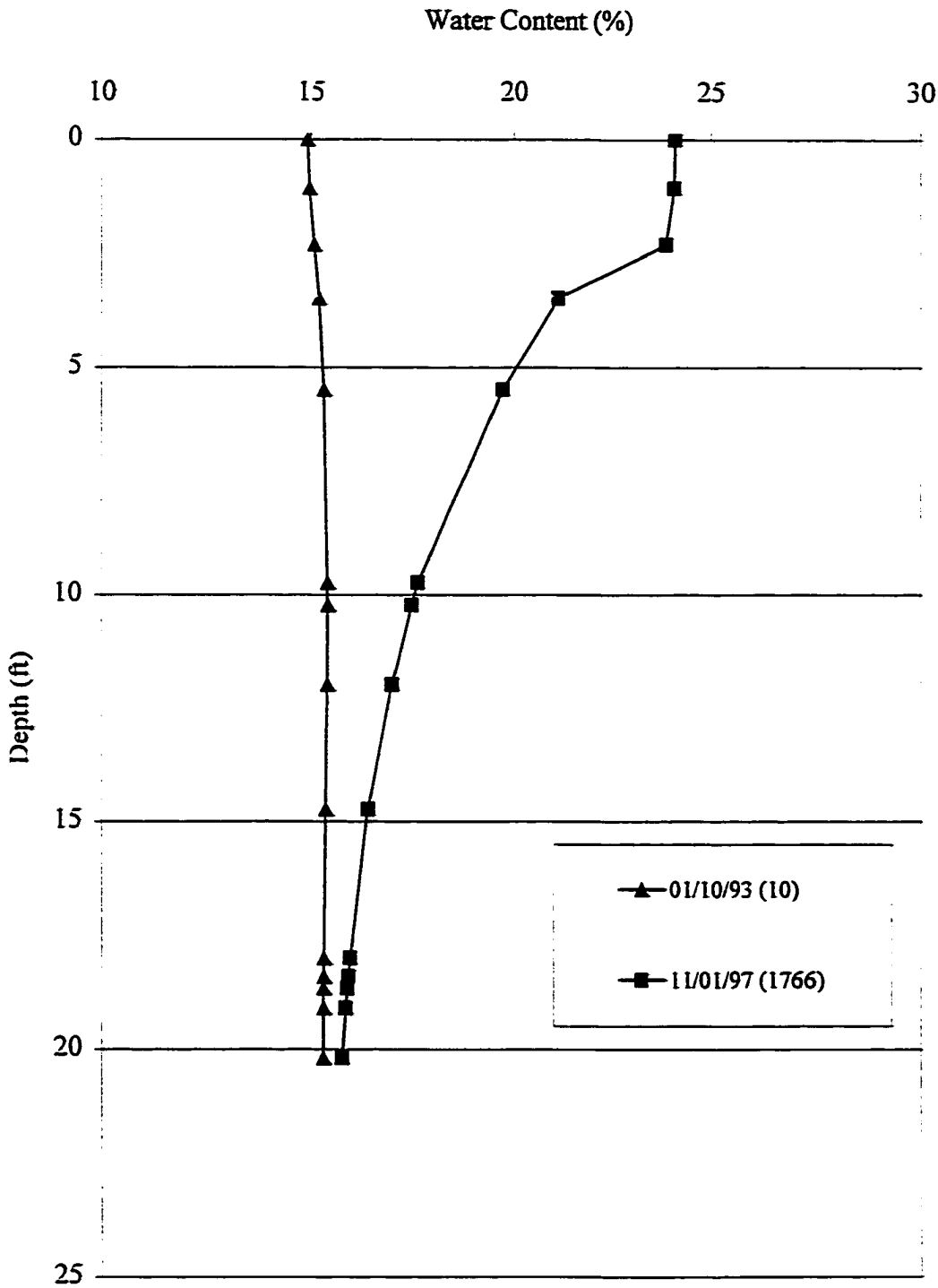

Figure 6-98 Predicted water content profile at a point located 5 feet inward from the east edge – bed dip = 25°, K_h/K_v=10, with ponding in a homogeneous soil

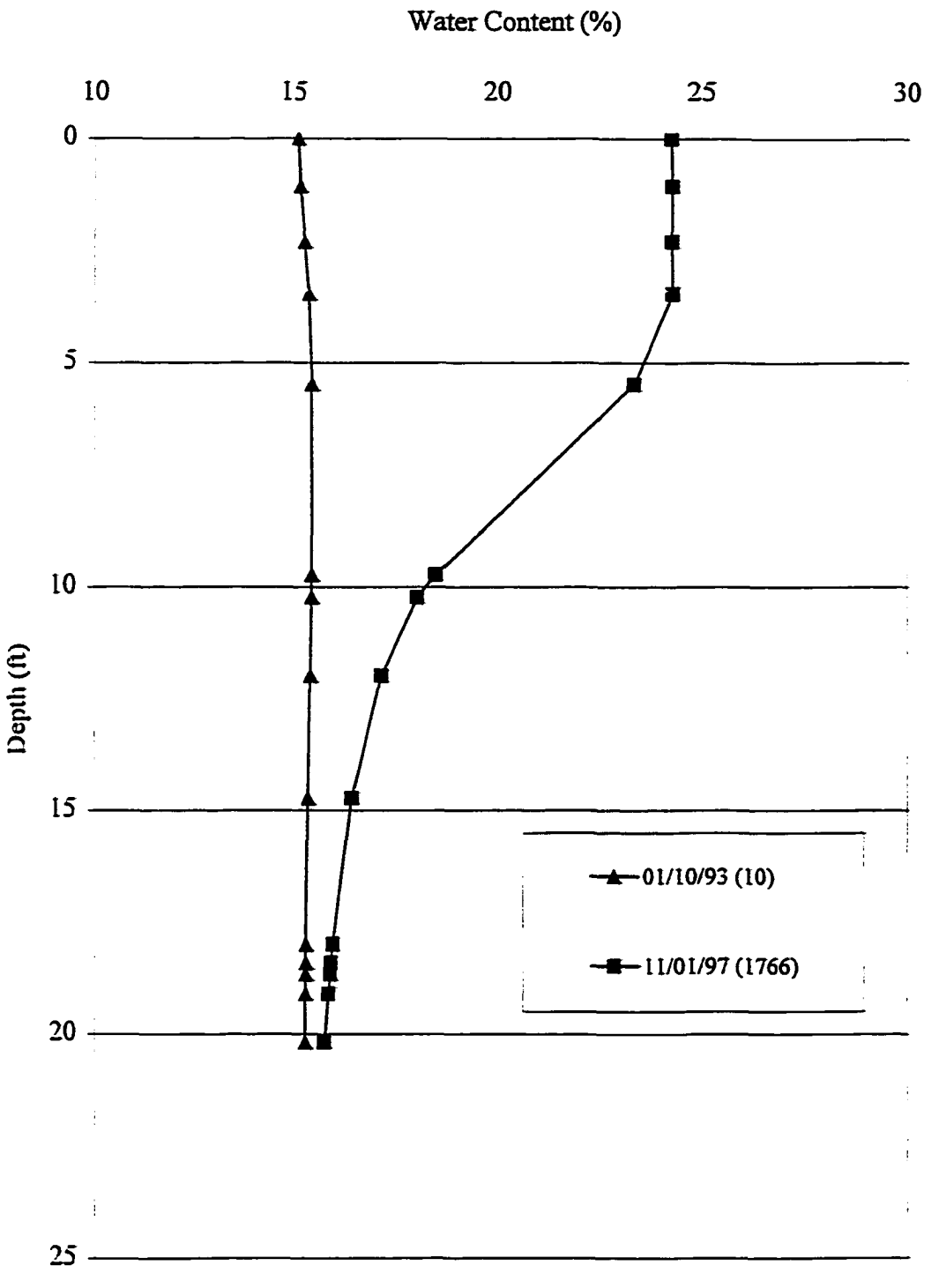

Figure 6-99 Predicted water content profile at a point located 5 feet inward from the east edge – bed dip = 25°, K_h/K_v=10, with ponding in a 2-layered soil

6.4.4 Maximum Active Zone Depth

The primary question when designing foundations on expansive soil is "how deep is the active zone"? The current state of practice for estimating active zone depth was discussed in Chapter 1. In addition, the definition of active zone depth has been examined throughout this dissertation. The modeling results presented thus far in this Chapter provide support for conceptual models proposed in this dissertation concerning the definition of active zone depth and the effects of soil properties, geologic conditions, and climate conditions.

The results presented thus far indicate that the long-term development of the active zone is controlled by the boundary conditions at the surface of the soil adjacent to the slab. In an arid climate the conditions at the surface of uncovered soils are primarily a function of the interchange of moisture due to infiltration and evaporation processes. The development of the active zone beneath the slab appears to be a function of the flow conditions in the soil adjacent to the slab and lateral flow beneath the slab.

It was demonstrated in Chapter 5.3.1 that the maximum active zone depth, based on stress conditions in the soil at the CSU site, is 35 feet. In addition, field data presented in Chapter 5 indicate that the active zone depth is continuing to increase and heave continues to occur at the surface. Numerical modeling results presented above using the soil and climate conditions at the test site and an assumed ponding scenario along the eastern side of the slab indicate that the model results, with regard to depth of wetting (active zone), agree with the field observations. The maximum depth of the active zone, 35 feet, has not been observed in the field. However, water content has been monitored

to a depth of only 20 feet. In addition the maximum depth of water content increase thus far is 18 feet, but that must be considered within the limits of measurement. It is believed that over time the depth of wetting will reach the maximum depth of active zone.

The increased water content that has developed beneath the eastern edge of the slab and has been sustained and gradually increasing since construction has not been modeled precisely. However, it is believed that the development of desiccation cracks during dry periods followed by significant precipitation, results in the inflow of water, swell of the soil, and closing of fractures, resulting in lower permeability soil that does not allow rapid upward flow and evaporation. A portion of the water that infiltrates at a high rate is then stored temporarily in the profile until the next evaporation event. During that time the excess moisture is available for lateral flow beneath the slab where evaporation effects are further reduced due to the slab at the surface.

The SoilCover model is a one-dimensional model that does not account for macro-pore flow and volume change conditions described above. As a result, the predicted evaporation rates may be higher than what actually occurs in the field. In addition, the SEEP/W model does not account for volume change. Water content is calculated based on changes in head and the SWCC in terms of volumetric water content. Therefore, the gravimetric water content values from the two-dimensional modeling presented in this dissertation are based on an average constant dry density of the soil.

6.4.4.1 Irrigation and Vegetation

In this sub-chapter the numerical modeling was expanded to include a watering cycle as would occur at a typical residence along the Front Range of Colorado. The Northern

Colorado Water Conservancy District (NCWCD) recommends the following watering schedule for typical home sites along the Front Range.

- 1 inch per week — May 1st
- 1.5 inches per week — June 15th
- 1 inch per week — August 1st – September 15th

The NCWCD watering schedule was incorporated into the SoilCover model as additional precipitation. The SoilCover model was then used to calculate the new infiltration values for use as boundary conditions in the SEEP/W model.

The results of the SoilCover modeling over the same time period as has been used in the previous simulations are shown in Figures 6-100 and 6-101. The cumulative infiltration is shown for the conditions of an irrigated soil and a non-irrigated soil. In the case of the irrigated soil, two types of vegetation were considered. The first case assumed the native vegetation was left in place and watered in accordance with NCWCD recommendations. The second case assumed that Kentucky bluegrass was planted and watered in accordance with NCWCD recommendations. Although the watering schedules are the same for both cases, the root depths and leaf area index of these two vegetation types are different. The native vegetation was discussed in Chapter 6.2.1.2 and is characterized by root depths of 0.5 to 5 feet. The leaf area index of the native vegetation was assumed to be consistent with that of poor grass. Most roots of Kentucky bluegrass are found in the upper 3 inches (FEIS, 1996). The leaf area index of the Kentucky bluegrass was assumed to be consistent with that of excellent grass.

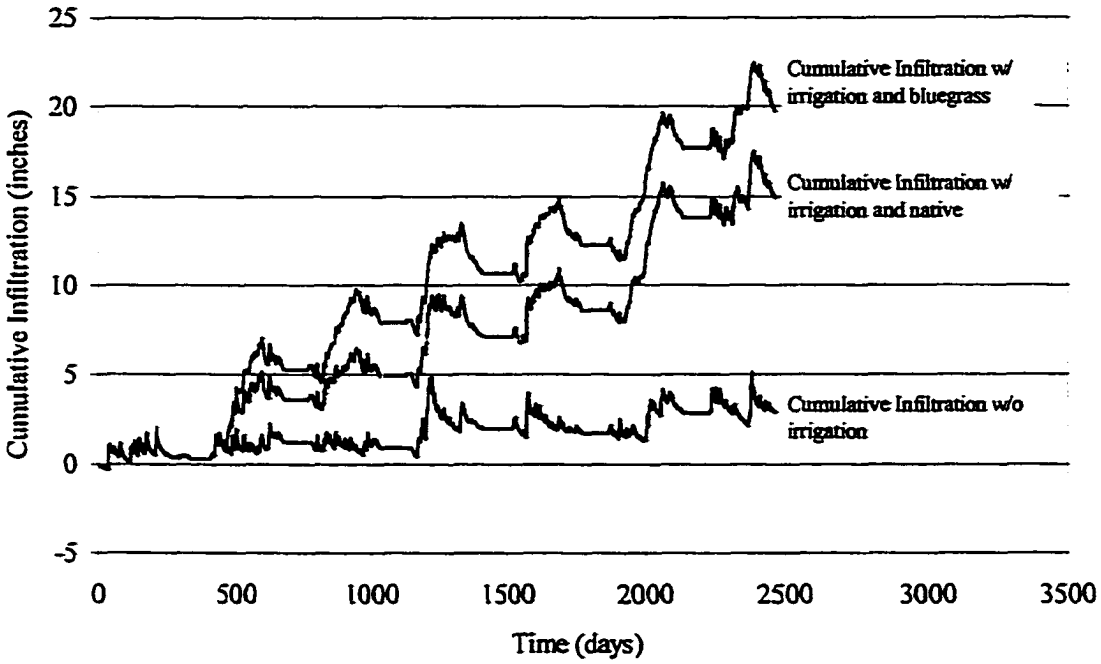

Figure 6-100 Predicted infiltration at the CSU site based on the results of SoilCover simulations

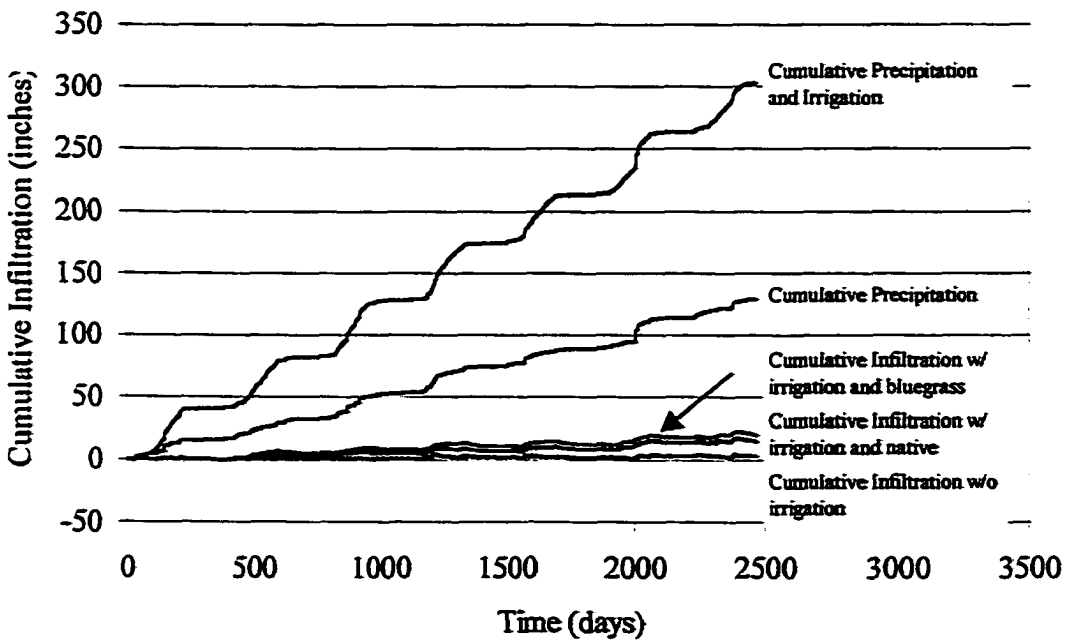

Figure 6-101 Cumulative infiltration and precipitation at the CSU site

The results in Figure 6-100 indicate that the typical irrigation schedule for the Front Range area increases the infiltration by 300 to 400 percent depending on the type of vegetation. The limitations of the vegetation algorithm used in the SoilCover model have been discussed. However, these results provide insight into the effects of irrigation and root depth on the development of the active zone. In general the infiltration rate is increased by the addition of water, as expected. However, based on these results, this condition is also exacerbated at the CSU site by replacement of the native vegetation with Kentucky bluegrass.

Figure 6-101 shows the cumulative precipitation and irrigation with the infiltration results. The results shown in Figure 6-101 indicate that a significant portion of precipitation and irrigation is lost to evaporation or runoff. Given the homogeneous nature of the soil used in the model simulations, these results are believed to be non-conservative. In general macro-pore flow and infiltration through loosely placed backfill would tend increase the depth of the active zone more rapidly.

6.4.4.2 Long-Term Conditions

The CSU site conditions were used to model long-term active zone development of an irrigated site. The soil profile was modeled after the CSU profile shown in Figure 3-4. The two-layered soil that was modeled in Chapter 6.4.3 was modified to include the bentonite seams and the shattered weathered clayshale shown in Figure 3-4.

The hydraulic conductivity of the bentonite seams was assumed to be 7.8E-09 feet per second, an order of magnitude lower than the reddish brown weathered clayshale. The SWCC for the bentonite seams was determined based on the water content profiles

presented in Chapter 5 (Figures 5-9 through 5-14). In general, the profiles indicate that the water content in the bentonite seams is 5 percent higher than the soil above and below the bentonite seams. For example, the water content at a depth of 16 feet in access tube B-5 is approximately 5 percent higher than the water content at a depth of 15 and 17 feet. The suction in this range is assumed to be approximately constant with depth, hence the water holding capacity of the bentonite seam is greater than the weathered clayshale. Therefore, it was assumed that the SWCC for the bentonite seam has the same general shape as the SWCC for the weathered clayshale, and that they are offset by 5 percent water content.

The shattered weathered clayshale was modeled with the same soil properties as the weathered clayshale except that the hydraulic conductivity was assumed to be 7.8E-07 feet per second, an order of magnitude higher than the weathered clayshale.

The long-term conditions were evaluated by modeling the CSU site conditions from 1992 to 2019. Development of the long-term active zone was evaluated from the results shown in Figures 6-102 and 6-103. The water content profiles from locations measuring approximately 5 feet from the eastern edge of the slab and 4 feet from the western edge of the slab are shown in Figures 6-102 and 6-103, respectively. The results indicate that the water content increases gradually throughout the profile. The magnitude of increase is small, on the order of 1.5 percent water content, however as mentioned previously, these small changes in water content are associated with relatively large changes in suction and hence heave. The depth of water content increase was as high as 35 feet; the maximum active zone depth based on stress conditions. Modeling was not conducted

below 35 feet, although the bottom elements of the mesh were considered to be infinite elements.

Figures 6-104 and 6-105 show the time rate of change in water content near the surface beneath the slab at the two points located approximately 5 feet inward from the eastern edge of the slab and 4 feet inward from the western edge of the slab, respectively. The results shown in Figures 6-104 and 6-105 indicate that the rate of water content increase is relatively high. After approximately 2,000 days (5 to 6 years) the rate of increase is lower, however, the seasonal fluctuations continue, particularly on the western edge of the slab. In addition, although the rate of increase is less, the long-term conditions after approximately 27 years indicate that the water content is still increasing.

These results indicate that the water content beneath a slab foundation constructed at the CSU site where irrigation has been applied in accordance with local guidelines will continue to increase throughout the depth of potential heave, 35 feet, for at least 27 years, the time considered in this investigation. There are several important considerations associated with these findings. .

- The rate of increase is slow and the water content changes shown would not be identifiable with typical field sampling methods.
- The depth of wetting shown in Figures 6-102 and 6-103 does not manifest itself in the form of a "wetting front" but rather wetting occurs throughout the profile. This is not consistent with expected trends based on field.
- Typical slab-on-grade construction practices along the Front Range of Colorado that assume the depth of seasonal moisture fluctuation is equal to the active zone, are inadequate for controlling heave of lightly loaded structures. This can also be extended to pier and grade beam construction practices where the depth of piers is typically 10 to 15 feet.
- These results are not considered to be conservative given that macro pore flow, volume change of the soil, and additional sources of water such as impounded water or broken utilities have not been considered.

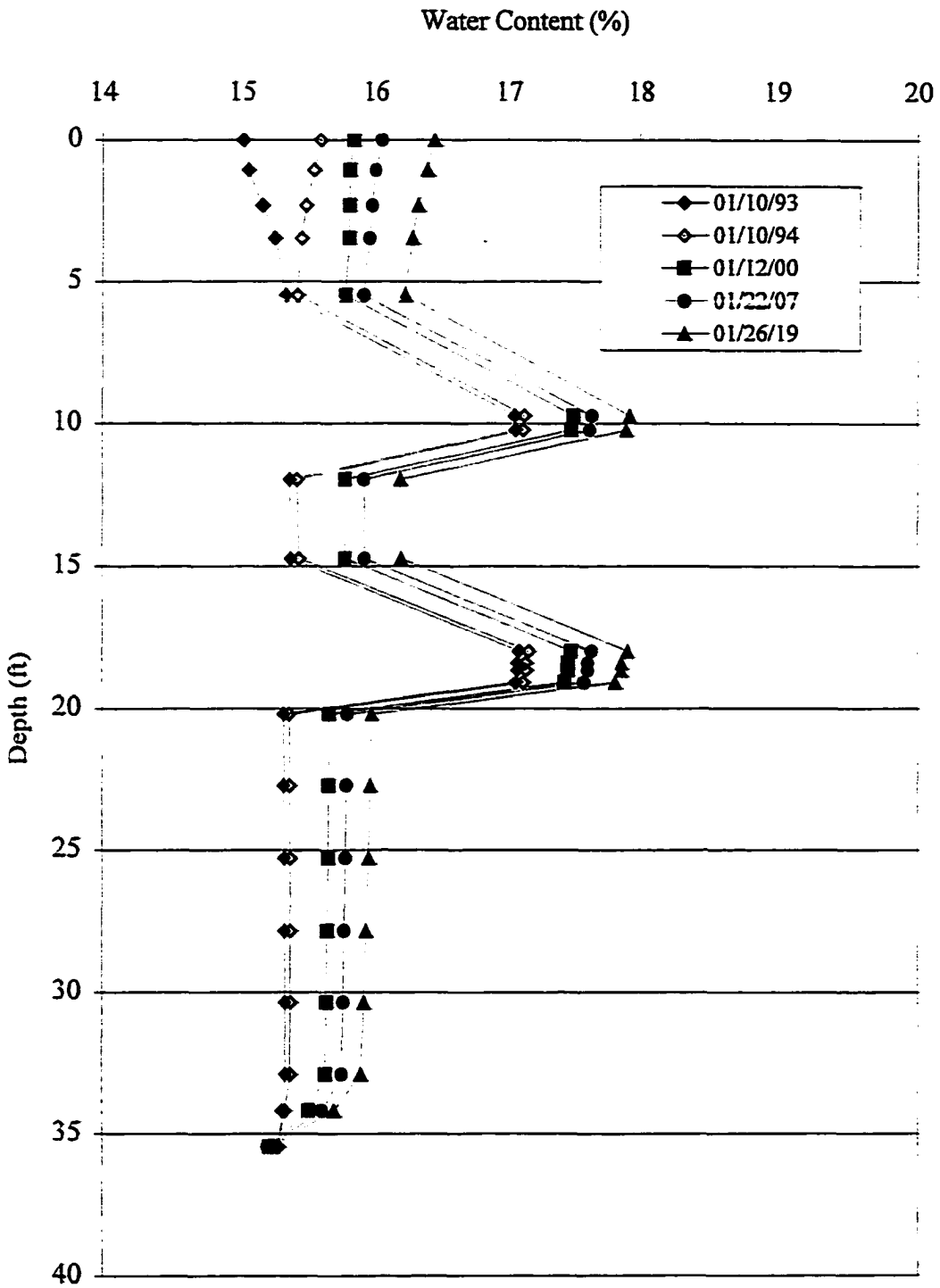

Figure 6-102 Water content profiles 5 feet inward from the eastern edge of the slab based on the long-term model results

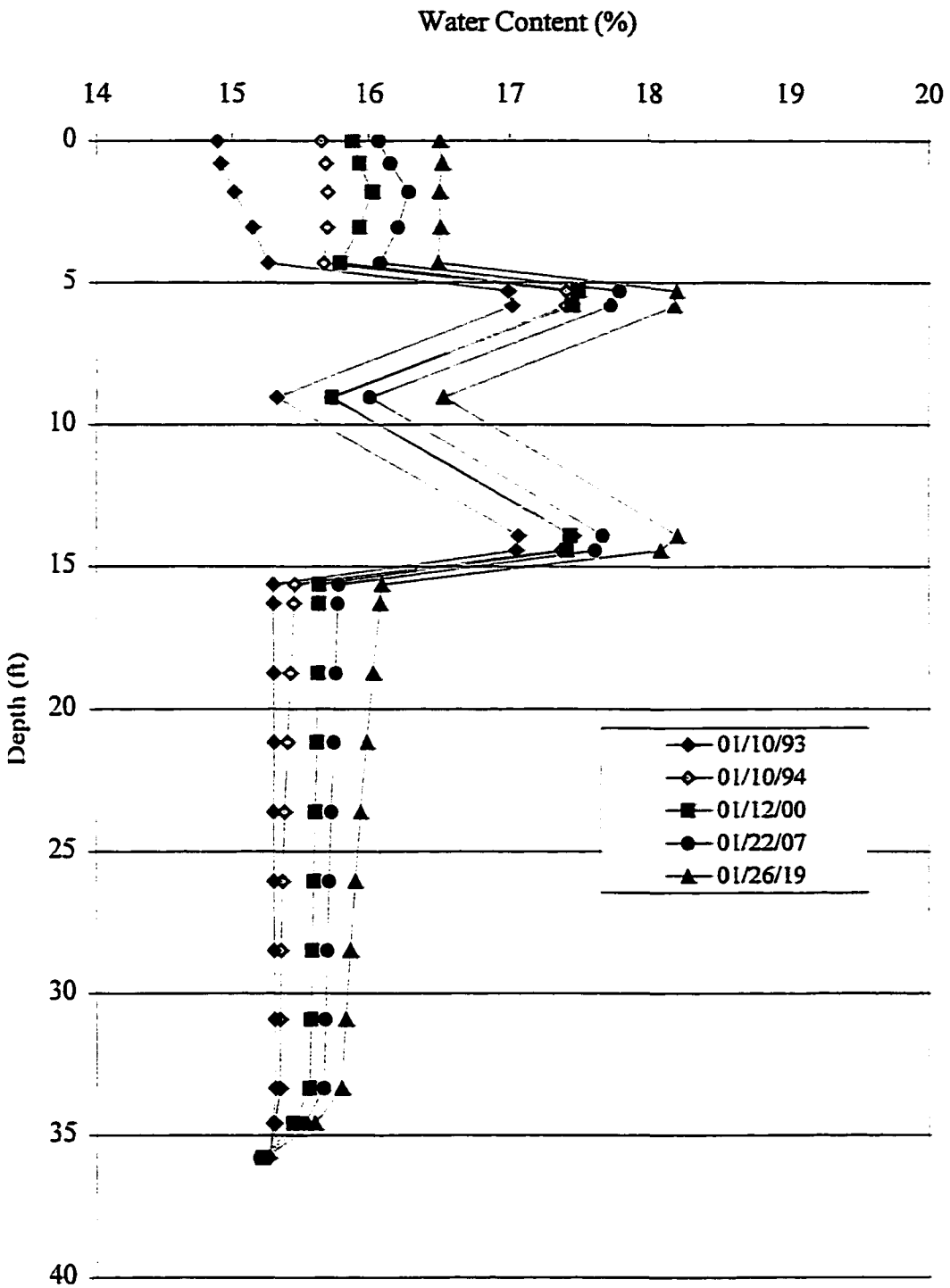

Figure 6-103 Water content profiles 4 feet inward from the western edge of the slab based on the long-term model results

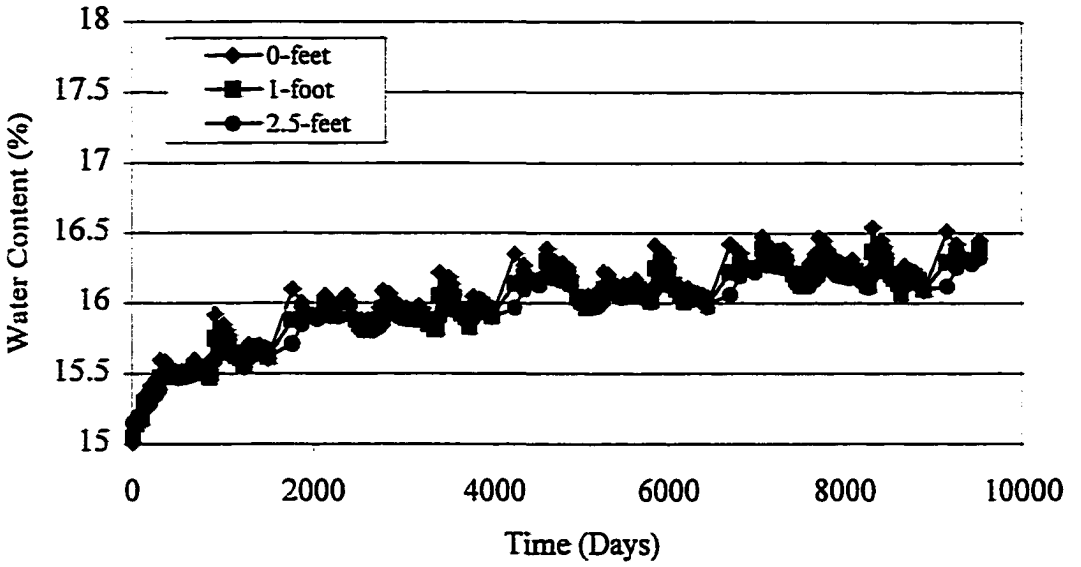

Figure 6-104 Time rate of change in water content near the surface 5 feet inward from the eastern edge of the slab based on the long-term model results

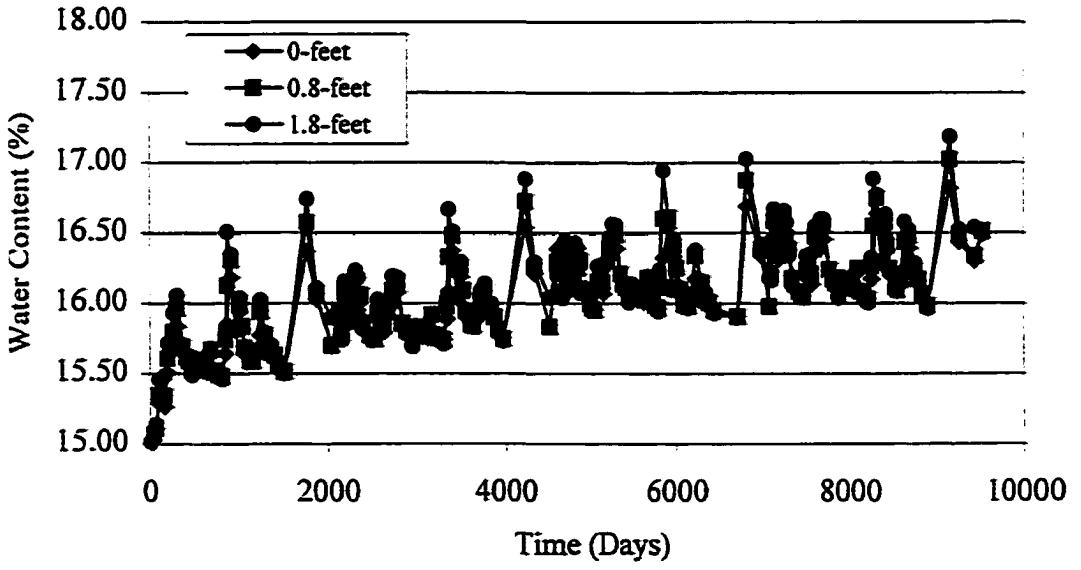

Figure 6-105 Time rate of change in water content near the surface 4 feet inward from the western edge of the slab based on the long-term model results

CHAPTER 7

SUMMARY AND CONCLUSIONS

The primary objectives of this dissertation, as stated in Chapter 1 were as follows:

1. Examine the previously proposed definitions and develop rigorous definitions for the term's "active zone depth" and "edge moisture variation distance".

2. Monitor water content, suction, and heave beneath a simulated slab foundation under controlled conditions where the evapo-transpiration has been significantly reduced.

3. Determine the active zone depth and edge moisture variation distance in terms of the observed moisture migration and heave patterns.

4. Characterize the active zone depth and edge moisture variation distance in terms of the effects of environmental conditions, geologic conditions, and soil properties.

5. Evaluate the active zone depth and edge moisture variation distance using numerical techniques to simulate boundary conditions not considered in the field investigation.

The results of the field, laboratory, and numerical investigations carried out indicate the study objectives have been met.

The historical definitions of active zone depth and edge moisture variation distance were reviewed in Chapters 1 and 2. In addition, a new definition that accounts of the time-dependent and spatially dependent nature of the active zone depth was proposed in Chapter 1. Details of the field test sites were presented in Chapter 3. The results of a laboratory investigation were presented in Chapter 4 and used in support of the numerical modeling presented in Chapter 6. The results of monitoring at the field-test sites and an evaluation of active zone depth and edge moisture variation distance in terms of observed

moisture migration and heave patterns were presented in Chapter 5. The effects of environmental conditions, geologic conditions, and soil properties were evaluated in Chapter 5 based on the field test site results and further with numerical methods in Chapter 6. The proposed definition for active zone depth appears to be appropriate based on the results from the field investigation and from the numerical models.

7.1 Key Observations and Conclusions

The foundation design parameters referred to as active zone depth and edge moisture variation distance were studied in this investigation. Observations and conclusions resulting from this investigation are summarized below.

1. Review of the literature indicated that active zone depth was not clearly defined. Previous attempts to define active zone depth were based on techniques for approximating its value. As such, a quantitative method for estimating or measuring the depth of the active zone does not exist.

2. The zone of seasonal moisture fluctuation and the depth of wetting are not necessarily the same as the depth of the active zone (as shown in Figure 5-20). Practitioners have historically used these two depths to predict the depth of the active zone. The zone of seasonal moisture fluctuation is the zone of soil in which environmental conditions, primarily water content, fluctuate due to seasonal climatic changes. For this investigation the water content distribution below the zone of seasonal fluctuation is referred to as the equilibrium water content. The depth of wetting is the zone in the soil where the water content increases due to external factors to values greater than the equilibrium water content. This zone, or portions of it, may or may not contribute to heave depending on soil conditions, swelling pressure, overburden, and applied stress.

3. The term active zone depth has been defined in this research as "the zone in the soil beneath a structure that is contributing to the actual heave that takes place at some point at the surface, at a given time (t)." As such, the depth of the active zone is time dependent and spatially dependent and is limited by two conditions (as shown in Figure 1-1).

- The depth of the active zone can not be deeper than the depth at which the overburden pressure is equal to the swell pressure.
- The depth of the active zone can not be deeper than the depth of expansive soil.

4. The historical definition of edge moisture variation distance is appropriate however; methods of estimating it have not been sufficiently tested. Review of the literature indicated that the term edge moisture variation distance has been historically defined as the distance measured inward from the edge of the slab over which moisture changes occur in response to seasonal climate variations, and result in soil movement.

5. Field data from the CSU site presented in this dissertation indicate the zone of seasonal moisture fluctuation based on water content data, represents an underestimate of the depth of the active zone. Water content profiles from uncovered soil, based on over 6 years of data, indicate that the zone of seasonal moisture fluctuation is approximately 5 to 7 feet (Figure 5-14). Water content profiles from the covered soil in the same location indicate that the depth of the active zone is at least 18 feet (Figures 5-9 and 5-10).

6. Two modes of development of the active zone were observed at the CSU site. In general the initial water content at the site ranged from approximately 10 to 12 percent in the upper 5 to 7 feet to approximately 15 percent below 7 feet, and was relatively constant to a depth of 20 feet. The water content on the western side and center of the slab increased to approximately the equilibrium water content, 15 percent, as defined in Chapter 5. In those locations the active zone is approximately equal to the depth of seasonal moisture fluctuation, 5 to 7 feet. Along the eastern side the water content has increased to values between 25 and 30 percent and the depth of the active zone is 18 feet, the depth of wetting. The differential wetting pattern is attributed to water that is impounded along the eastern side of the slab as a result of large precipitation events and snow melt.

7. Field data from the FSH site presented in this dissertation indicate that the zone of seasonal moisture fluctuation at that site is approximately 5 feet. Since the depth of expansive soil at the FSH site is limited to the upper 5 to 6 feet, the depth of seasonal moisture fluctuation is approximately equal to the maximum depth of the active zone.

8. Increases in the depth of water content increase (active zone) at the CSU site generally follow short periods of no increase and tend to coincide with an increase in the rate of rainfall accumulation. The rate of rainfall accumulation typically increases in the spring when there is also an increase in temperature. The increased surface temperature results in a thermal gradient that causes an increase in downward flow from the warmer to the cooler regions of the soil. Since May 1995 the depth of water content increase has remained constant indicating that for the

current boundary conditions the soil has reached steady-state water content distribution and the depth of the active zone is 18 feet.

9. The depth of water content increase is greatest along the edge of the slab and decreases incrementally in access tubes located inward from the edge of the slab. In addition the time for the water content to increase is greater with greater distance from the edge, indicating that the source of water is from outside the boundaries of the slab where water is periodically impounded or where water is introduced by extreme climatic events. This indicates that an edge lift condition exists at the site and that although cyclical changes in water content occur near the edge due to climate fluctuations, the slab has not reached a condition of steady-state or equilibrium.

10. Based on water content data from a depth of 1 foot beneath the slab (Figures 5-24-5-31) the edge moisture variation distance at the CSU site is equal to half the slab width, 15 feet in the north-south direction. However, in this investigation the slab was exposed to atmospheric conditions and temperature fluctuations at the surface. This would not typically be the case for a residential foundation where the structure is maintained at a constant temperature. The temperature changes contributed to moisture fluctuations in the center of the slab. Therefore, the distinction must be made between edge effects and surface effects in order to determine edge moisture variation distance as defined above. However, it is believed that the PTI (1980) method, which uses the Thornthwaite moisture index method, underestimates the edge moisture variation distance. The maximum edge moisture variation distance for this site from the PTI (1980) method is less than 6 ft.

11. Elevation data from the CSU site indicates that the majority of heave at the site has occurred along the eastern side as would be expected from the water content data. However, heave is continuing to increase in the center and on the western side of the slab where it appears that water content changes have not recently occurred. It is believed that the elevation changes occurring in the center and along the western side of the slab are due to small changes in water content that are not detectable with the field instrumentation used in this investigation.

12. Heave predictions that utilize the depth of water content increase presented above show good agreement with measured heave at the site. This indicates that the water content increases beneath the slab, observed below the depth of seasonal moisture fluctuation are contributing to heave at the surface. If the zone of seasonal moisture fluctuation of 5 to 7 feet were used in the calculations, the predictions would not be conservative.

13. The maximum predicted heave values at the CSU and FSH sites based on the maximum active zone depth, are 8.23 and 5.62 inches, respectively. These

maximum heave values are also based on the assumption of a final saturated soil condition.

14. Suction data measured at depths of 17 feet indicates that the zone of seasonal fluctuation is at least 17 feet. This indicates that the suction method (McKeen and Johnson, 1990) may have some merit for predicting active zone depth. However, measurements were not taken below 17 feet.

15. Suction measurements 2 feet beneath the slab have been at or very close to zero since approximately one year after installation. However, based on water content and density measurements in the center of the slab, the initial and final degree of saturation profiles in the center of the slab indicate that the degree of saturation in the upper few feet of soil has ranged from 40 percent to 65 percent. The lower limit of suction measurement with a TCP is approximately 33 feet (100 kPa) (see Fredlund and Rahardjo, 1993). This indicates that significant increases in the degree of saturation and heave are still possible even though the suction measurements near the surface are close to zero.

16. Although the theory of unsaturated soils and flow through unsaturated soils in particular has advanced significantly in the last 10 to 20 years, the current state of technology with regard to numerical modeling of infiltration, evaporation, and moisture migration in expansive soil is limited. The governing equations for modeling flow have been extended to account for deformable soils with some success (Edgar, 1983). However, expansive soils along the Front Range of Colorado and elsewhere present a particular challenge with regard to modeling flow.

    - Pierre shale at the CSU test site consists of highly overconsolidated weathered clayshale with a low degree of saturation and high expansive potential. The soils in the upper 5 to 7 feet cycle through conditions of relatively high degree of saturation (low suction) and very low degree of saturation and desiccation (high suction). The volume changes that occur during large suction changes contribute to the complexity of modeling infiltration. Constitutive parameters and soil hydraulic properties for these soil types are not well understood. In particular the SWCC and hydraulic conductivity functions are not well defined and do not account for desiccation and volume changes that occur near the soil surface.

    - The deeper weathered Pierre shale (below 5 to 7 feet) at the CSU site consists of a relatively dry, fissile, shale that appears to exhibit different characteristics of micro and macro pore flow. Constitutive relationships for flow through this soil type also have not been developed.

17. Reasonable results with regard to modeling water content changes in unsaturated Pierre shale at the CSU site were obtained from the SoilCover model using

saturated hydraulic conductivity values determined in the laboratory and the method developed by Brooks and Corey (1964) for unsaturated conditions. An adjustment for volume change based on the Kozeny-Carmen equation was also utilized. This approach was considered acceptable for this research application however; it is evident that rigorously evaluated analyses of these important hydraulic functions are necessary for future development of moisture flow modeling in expansive soils.

18. Reasonable results with regard to modeling suction changes in unsaturated Pierre shale at the CSU site were obtained using the SWCC data from Chao (1995), fit with the Fredlund and Xing (1994) method. However, the main limitations with regard to modeling suction changes are the inability of the model to account for volume changes and hysteresis effects. In addition the SWCC was shown to be a function of temperature, a condition that is typically not considered when modeling flow.

19. There was very close agreement between field measured soil temperature and soil temperature obtained from the SoilCover model. This indicates that the SoilCover model is appropriate for modeling heat flow through soil.

20. Results from the field investigation and model simulations indicate that the water content beneath the center of a slab-on-grade foundation increases to a steady state value to a depth that is approximately equal to the depth of seasonal moisture fluctuation. The magnitude of the steady state water content is a function of the SWCC and the equilibrium suction of the soil, and the time rate of development is primarily a function of hydraulic conductivity. The edge effects, and the reduction in the upward gradient for flow upon wetting of the upper soil layers, limit the magnitude and depth of initial increase.

21. Boundary changes at the surface adjacent to the structure control the long-term development of active zone depth and edge moisture variation distance. The results of numerical simulations that incorporated a ponding scenario along the eastern side of the slab (Figures 6-78 through 6-82) closely matched the water content measurements (Figures 6-73 through 6-77) from the field test site.

22. Model results that incorporated a layered soil for the purposes of accounting for density and hydraulic conductivity variation with depth indicated that the water content beneath the slab increases faster and to greater depth as the density of the deeper soils is increased. By decreasing the hydraulic conductivity of the deeper soil the water that infiltrated from the soils adjacent to the slab migrated laterally beneath the slab more rapidly.

23. As expected, the infiltration rate is increased by the addition of water for irrigation purposes. In addition, these results indicate that this condition is exacerbated at the CSU site by replacement of the native vegetation with Kentucky bluegrass.

24. The results of long term modeling of the CSU site utilizing a four layered soil profile and typical irrigation schedule as recommended by NCWCD indicate that increases in water content beneath the slab begin immediately after irrigation is initiated. The water content increase is gradual and in general the magnitude of increase is less than would be detectable using typical field instrumentation for water content monitoring. However, given the limitations with regard to state-of-the-art for modeling flow in expansive soil, the model results presented herein indicate that irrigation in accordance with standard practice for residential landscape design results in continued increases in the depth of water content increase. This indicates that it is possible for water content increases to occur at depths approaching the maximum active zone depth, which at the CSU site is 35 feet, based on the depth of potential heave.

In summary, the results of this study provide insight into the measurement of active zone depth and edge moisture variation distance. The observed trends can be used by practicing engineers as aid in the design of foundations on expansive soil. The conclusions are based on the results of research at two specific sites. It must be noted that the active zone depth and edge moisture variation distance are site specific design parameters and that the actual values presented in this study are not necessarily representative of other areas. Also, a longer period of record will provide a basis on which more definite conclusions can be made.

7.2 Recommendations for Additional Research

The primary objectives of this research were to examine the definitions of active zone depth and edge moisture variation distance in expansive soil and characterize these parameters with respect to climate conditions, geologic conditions, and soil properties. Although these objectives have been achieved, further investigations will improve our understanding of these parameters and result in better application to engineering practice. The most immediate research recommendations are summarized below.

- The field test site at CSU should be modified by removing the berm on the eastern side of the slab. Continued monitoring will further verify the effects of the berm and impounded water in that area. It is believed that the water content on the eastern side of the slab would decrease as a result of removing the berm.
- After a reasonable amount of time to allow observations of the effects of removing the berm the CSU site should be modified to include an irrigation system that is operated in accordance with NCWCD recommendations. This could include several forms of vegetation to evaluate their effects as well.
- Laboratory unsaturated hydraulic conductivity tests should be conducted that utilize flexible-wall permeameters and measurement or control of suction, volume change, and temperature. The results of these tests can be used to evaluate the currently available methods for estimating the SWCC and unsaturated hydraulic conductivity functions and possibly be extended to develop new methods that are more appropriate for expansive soils.
- Currently available numerical models for flow in unsaturated soils provide reasonably close agreement to field measured results and can be relied upon with confidence for evaluating general trends in expansive soil. However, the results from this investigation indicate that modification of these models to account for macro-pore flow and volume change would greatly enhance their application to expansive soil problems.

REFERENCES

Altmeyer, W.T. (1955). "Discussion of Engineering Properties of Expansive Clays," *Proc. Am. Soc. Civil Engr.* 81 (separate No. 658): 17-19.

ASTM Standards (1991). Natural Building Stones : Soil and Rock. Annual Book of ASTM Standards, Vol. 4, Philadelphia.

Bach, L.B. (1992). "Soil Water Movement In Response to Temperature Gradients: Experimental Measurements and Model Evaluation," *Soil Sci. Soc. Am. Jnl.* 56: 37-46.

Barden, L., Madedor, A.O., and Sides, G.R. (1969). "Volume Change Characteristics of Unsaturated Clay," *Soil Mechanics and Foundation Division*, ASCE 95 (SM1) Jan: 33-52.

Bishop, A.W. (1959). "The Principle of Effective Stress," Lecture delivered in Oslo, Norway, in 1955; published in *Teknisk Ukeblad*, Vol. 106, No. 39: 859-863.

Bishop, A.W. and Blight, G.E. (1963). "Some Aspects of Effective Stress In Saturated and Unsaturated Soils," *Geotechnique*, Vol. 13, No. 3: 177-197.

Brooks, R. H. and Corey, A.T. (1964). "Hydraulic Properties of Porous Media," Colorado State University Hydrology Paper, No. 3, 27 pp., March

Bruce, R.R. and Klute, A. (1956). "The Measurement of Soil Moisture Diffusivity," *Soil Sci. Soc. Am. Proc.* 27: 123-126.

Campanella, R.G. and Mitchell, J.K. (1968). "Influence of Temperature Variations on Soil Behavior," *Soil Mechanics and Foundation Division Jnl.*, ASCE (SM3) May: 709-733.

Chen, F.H. (1988). Foundations on Expansive Soils American Elsevier Science Publishing. New York.

Chen, X.Q., Lu, Z.W. and He, X.F. (1981). "Moisture Movement and Deformation of Expansive Soil," Academy of Building Research, Beijing, China: 2389-2392.

Chao, K.C. (1995). "Hydraulic Properties and Heave Prediction for Expansive Soil," Partial Fulfillment of Requirements for Master of Science Degree at Colorado State University.

Chao, K.C., Durkee, D.B., Miller, D.J., and Nelson, J.D. (1998). "Soil Water Characteristic Curve for Expansive Soil," *Thirteenth Southeast Asian Geotechnical Conference*, Taipei, Taiwan, ROC November.

Cheng, H.W. (1994). "The Soil Water Diffusivity of Unsaturated Soil," Partial Fulfillment of Requirements for Master of Science Degree at Colorado State University.

Corey, A. T. (1986). Mechanics of Immiscible Fluids in Porous Media, Water Resources Publication, Littleton, Colorado, 255 pp.

Corey, A.T. and Klute, A. (1985). "Application of the Potential Concept to Soil Water Equilibrium and Transport," *Soil Sci. Soc. Am. Jnl.* 49: 3-11.

CPN (1984). Campbell Pacific Nuclear Corp. Operating Manual, 501DR Depth Probe, Martinez, Ca. 94553.

Dakshanamurthy, V. and Fredlund, D.G. (1981) "Transient Flow Processes in Unsaturated Soils Temperature, Relative Humidity, Evaporation And Infiltration," CD-16.4 Transportation and Geotechnical. Group, University of Saskatchewan, Saskatoon, Saskatchewan Canada, 1981, 92 pp.

Donaldson, G.W. (1965). "A Study of Level Observations on Buildings as Indications of Moisture Movement in Underlying Soil," Moisture Equilibria and Moisture Changes in Soil Beneath Covered Areas, Buttersworth, Australia: 156-169.

Durnford, D.S. and Lorentz, S.A. (1991). Tests of Hydraulic and Leaching Properties of the Vadose Zone and Groundwater (in press).

Edgar, T.V. (1983). "Moisture Movement in Nonisothermal Deformable Media," Partial Fulfillment of the Requirements for Ph.D., Colorado State University.

Edgar, T.V., Nelson, J.D. and McWhorter, D.B. (1989). "Nonisothermal Consolidation in Unsaturated Soil," *Geotechnical Engineering Division Jnl.*, ASCE Vol. 115, No. 10, Oct: 1351-1372.

Edlefsen, N.E. and Anderson, A.B.C. (1943). "Thermodynamics of Soil Moisture," *Hilgardia*, 17(2) 31-298.

Fire Effects Information System (FEIS) (1996). Prescribed Fire and Fire Effects Research Work Unit, Rocky Mountain Research Station, September. Available online: www.fs.fed.us/database/feis/ [1998,March 12]

Fredlund, D.G. (1979). "Appropriate Concepts and Technology for Unsaturated Soils," *Canadian Geotechnical Jnl.*, V. 16 No. 1 p 121-138, Feb.

Fredlund, D.G. (1983). "Prediction of Ground Movements in Swelling Clays," 31st Annual Soil Mechanics and Foundation Engineering Conference, Univ. of Minnesota at Minneapolis, Feb.

Fredlund, D.G. and Hasan, J.U. (1979). "One-dimensional Consolidation Theory: Unsaturated Soils," *Canadian Geotechnical Journal*, 16(3): 521-531.

Fredlund, D.G. and Morgenstern, N.R. (1977). "Stress State Variables for Unsaturated Soils," *Geotechnical Engineering Division Jnl.* ASCE, GT5 May: 447-465.

Fredlund, D.G. and Rahardjo, H. (1993). Soil Mechanics for Unsaturated Soils, John Wiley and Sons.

Fredlund, D.G. and Xing, A. (1994). "Equations for the Soil-Water Characteristic Curve," *Canadian Geotechnical Jnl.*, 31 p 521-532.

Fredlund, D.G., Xing, A., and Huang, S. (1994). "Predicting the Permeability Function for Unsaturated Soils using the Soil-Water Characteristic Curve," *Canadian Geotechnical Jnl.*, 31 p 533-546.

Gardner, W.R. (1958). "Some Steady State Solutions of the Unsaturated moisture Flow Equation with Application to Evaporation from a Water-Table," *Soil Sci.*, Vol. 85, No. 4.

Geo2000, Ltd.,(1997). SoilCover User's Manual. Version 4.01 *Geo-Analysis 2000, Ltd.*, September.

GEO-SLOPE, International., (1991). SEEP/W for finite element seepage analysis. *GEO-SLOPE International Ltd.*, Calgary, Alberta, Canada.

Gibson, R.E., England, G.L., and Hussey, M.J.L. (1967). "The Theory of One-dimensional Consolidation of Saturated Clays," *Geotechnique*, 17(3): 261-273.

Gibson, R.E., Schiffmann, R.L., and Cargill, K.W. (1981). "The Theory of One-dimensional Consolidation of Saturated Clays, II; Finite Non-Linear Consolidation of Thick Homogeneous Layers," *Canadian Geotechnical Journal*, 18(3): 280-293.

Goode, J.C. (1982). "Heave Prediction and Moisture Migration Beneath Slabs on Expansive Soils," Partial Fulfillment of requirements for a M.S. degree at Colorado State University.

Hamberg, D.J. (1985). "A Simplified Method for Predicting Heave in Expansive Soils," Partial Fulfillment of requirements for a M.S. degree at Colorado State University.

Hamberg, D.J. and Nelson, J.D. (1984). "Prediction of Floor Slab Heave," *5th Int. Conf. Expansive Soils*, Adelaide, S. Australia. 137-217

Holtz, R.D. and Kovacs, W.D. (1981). An Introduction to Geotechnical Engineering, Prentice-Hall, Englewood Cliffs, NJ: 733 pp.

Holtz, W.G. and Gibbs, H.J. (1956). "Engineering Properties of Expansive Clays," Transactions American Society of Civil Engineers 121 Paper No. 2814: 641-677.

Jacob, C.E. (1940). "On The Flow of Water in an Elastic Artesian Aquifer," Trans. Am. Geophys. Union, 20(1): 574-586.

Jennings, J.E.B. and Burland, J.B. (1962) "Limitations to the Use of Effective Stress in Partly Saturated Soils," *Geotechnique*, 12(2): 125-144.

Johnson, L.D. (1977). "Evaluation of Laboratory Suction Tests for Prediction of Heave in Foundation Soils," Army Engr. Waterways Exp. Station, Vicksburg, MS, Rep. WES-TR-S-77-7, August.

Koerner, R. M. (1990). Designing with Geosynthetics, 2nd Edition, Prentice Hall, Englewood Cliffs, NJ.

Krahn, J. and Fredlund, D.G. (1972). "On Total Matric and Osmotic Suction," *Jnl. Soil Sci.*, Vol. 114, No. 5, pp. 339-348.

Lambe, T.W. and Whitman, R.V. (1969). Soil Mechanics. New York, Wiley, pp. 559.

Lapham, W.W. (1987). "Use of Temperature Profiles Beneath Streams to Determine Rates of Vertical Groundwater Flow and Vertical Hydraulic Conductivity," Source of report unknown: 1-34.

Lloret, A. and Alonso, E.E. (1980). "Consolidation of Unsaturated Soils Including Swelling and Collapse Behavior," *Geotechnique* 30(14): 405-418.

Matyas, E.I. and Radhakrishna, H.S. (1968). "Volume Change Characteristics of Partially Saturated Soils," *Geotechnique* 18: 432-448.

McKeen, R.G. and Johnson, L.D. (1990). "Climate Controlled Soil Design Parameters for Mat Foundations," *Geotechnical Engineering Division Jnl.* ASCE, Vol.116, No. July: 1073-1093.

McNabb, A. (1960). "A Mathematical Treatment Of One-dimensional Soil Consolidation," *Quar. Appl. Math.* 17(4): 337-347.

Miller, D.J. (1996)."Osmotic Suction as a Valid Stress State Variable in Unsaturated Soils," Partial Fulfillment of Requirements for Ph.D. degree at Colorado State University.

Miller, D.J., Durkee, D.B., Chao, K.C., and Nelson, J.D. (1995). "Simplified Heave Prediction for Expansive Soils," *1st Intl. Conf. Unsaturated Soils*, Paris, September

Mitchell, P.W. (1979). "The Structural analysis of Footings on Expansive Soil," *Research Report No. 1*, Kenneth W.G. Smith and Associates, Adelaide, South Australia.

Northern Colorado Water Conservancy District (NCWCD) Website address www.ncwcd.org. 1250 North Wilson Avenue, Loveland, CO (970) 667-2437.

Nassar, I.N. and Horton, R. (1989). "Water Transport in Unsaturated Nonisothermal Salty Soil: I. Experimental Results," *Soil Sci. Soc. Am. Jnl.* 53: 1323-1329.

Nelson, J.D. and Edgar, T.V. (1978). "Moisture Migration Beneath Impermeable Membranes," *Proc. 15th Annu. Symp. Engr. Geol. Soil Engr.* Idaho Dept. of Highways, Boise, Idaho, April.

Nelson, J.D. and Miller, D.J. (1992). Expansive Soils, Problems and Practice in Foundation and Pavement Engineering, John Wiley and Sons, 259 pp.

Nelson, J.D., Durkee, D.B., and Bonner, J.P. (1998). "Prediction of Free Field Heave Using Oedometer Test Data," *46th Annual Geotechnical Engineering Conference*, University of Minnesota, St. Paul, Minnesota.

Philip, J.R. and DeVries, D.A. (1957). "Moisture Movement In Porous Materials Under Temperature Gradients," *Trans. Am. Geophys. Union*, 38(2): 222-232.

Porter, A.A. and Nelson, J.D. (1980). "Strain Controlled Testing of Soils," *Proc. 4th Intl. Conf. Exp. Soils, ASCE and ISSMFE*, Denver, June: 34-44.

PTI (1980). Design and Construction of Post-Tensioned Slabs-on-Ground, Post-Tensioning Institute. Phoenix, Arizona.

O'Neill, M.W. and Poormoayed, N. (1980). "Methodology for Foundations on Expansive Clays," *ASCE Jnl. of Geotechnical Engineering Division*, p. 1345-1364.

Raats, P.A.C. and Klute, A. (1968a). "Transport in Soils: The Balance of Mass," *Soil Sci. Soc. Am. Proc.*, 32(2): 161-166.

Raats, P.A.C. and Klute, A. (1968b). "Transport in Soils: The Balance of Momentum," *Soil Sci. Soc. Am. Proc.*, 32(4): 452-456.

Raats, P.A.C. and Klute, A. (1969). "One-dimensional Simultaneous Motion of the Aqueous Phase and the Solid Phase of Saturated and Partially Saturated Porous Media," *Soil Sci. Soc. Am. Proc.*, 32(4): 452-456.

Richards, L.A. (1931). "Capillary Conduction of Liquids Through Porous Medium," *Physics*, Vol., No.2 318-333.

Seed, H.B., Woodward, R.J., and Lundgren, R. (1962b). "Prediction of Swelling Potential for Compacted Clays," *Soil Mechanics and Foundations Division Jnl.*, ASCE, 88 (SM3): 53-87.

Stallman, R.W. (1965). "Steady One-dimensional Fluid Flow in a Semi-Infinite Porous Medium with Sinusoidal Surface Temperature," *Jnl. of Geophys. Res.* Vol. 70, No. 12, June: 2821-2827.

Taylor, D.W. (1948). Fundamentals of Soil Mechanics, John Wiley & Sons, Inc., New York, pp. 700.

Thermocouple Psychrometer Meter Model 85 Instruction Manual, J.R.D. Merrill Specialty Equipment, Logan, Utah 84321.

Theis, C.V. (1935). "The Relationship Between the Lowering of the Piezometric Surface and the Rate and Duration of Discharge of a Well Using Ground Water Storage," *Trans. Am. Geophys. Union*, 16(1): 519-524.

Thompson, R.W., (1997) "Evaluation Protocol for Repair of Residences Damaged By Expansive Soils," ASCE *GeoInstitute Geotechnical Special Publication*, No.68, Unsaturated Soil Engineering Practice

Troxler Manual for Model 105 Moisture Probe and Model 2651 Scaler Ratemeter. Troxler Laboratories, Raleigh, North Carolina.

Tucker, R.L. and Poor, A.R. (1978). "Field Study of Moisture Effects on Slab Movements," *Geotechnical Engineering Division Jnl.*, ASCE, Vol. 104, No. GT4, April: 403-414.

Uppal, H.L. (1965). "Field Study on the Movement of Moisture in Black Cotton Soils under Road Pavements," *Moisture Equilibria and Moisture Changes in Soils beneath Covered Areas*, Buttersworth, Australia: 165-174.

Wilson, G.W. (1990). "Soil Evaporative Fluxes for Geotechnical Engineering Problems," Partial Fulfillment of the Requirements for the Degree or Doctor of Philosophy. Dept. of Civil Engineering, University of Saskatchewan.

Wray, W.K. (1978). "Development of a Design Procedure for Residential and Light Commercial Slabs-On-Ground Constructed Over Expansive Soils," Partial Fulfillment of Requirements for a Ph.D. degree, Texas A&M University College Station, Texas.

Wray, W.K. (1992). "Comparison of Predicted Heave to Field Measurements," *7th Intl. Conf. Exp. Soils*: 331-336.

Yeo, H. (1995). "The Comparison of Thermocouple Psychrometer and Filter Paper," Partial Fulfillment of Requirements for Master of Science Degree at Colorado State University.

APPENDIX A

Nuclear Gauge Calibration

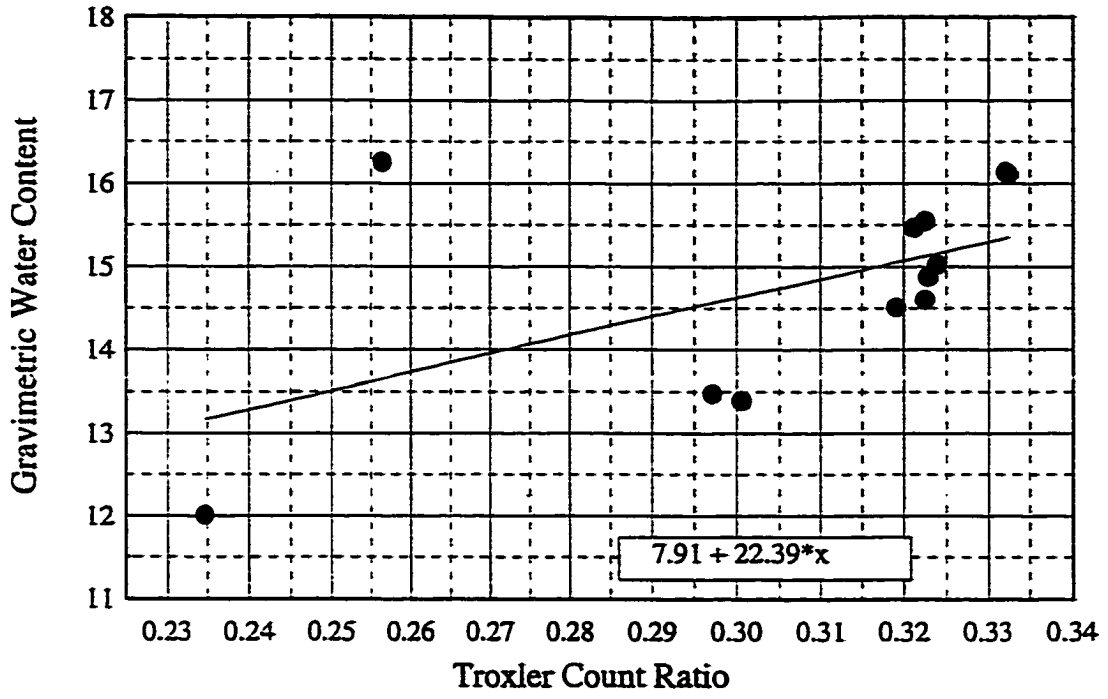

Calibration for the Troxler nuclear moisture gauge used at FSH.

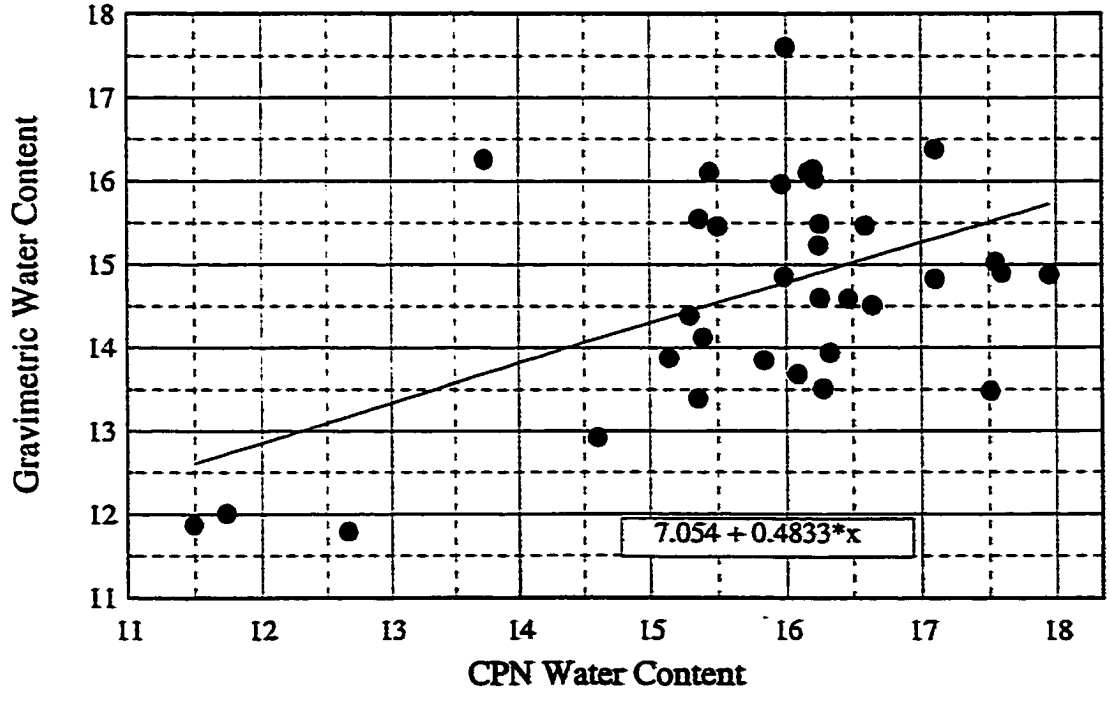

Calibration for the Campbell Pacific nuclear moisture-density gauge used at CSU.

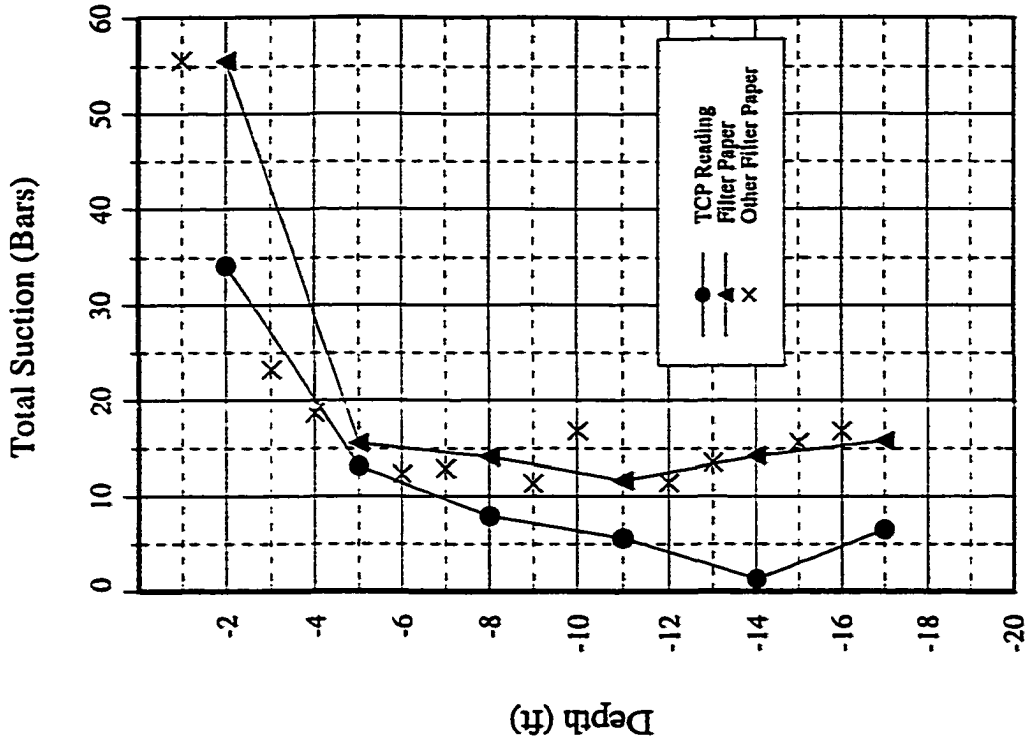

Comparison of TCP suction measurements to filter paper measurements.

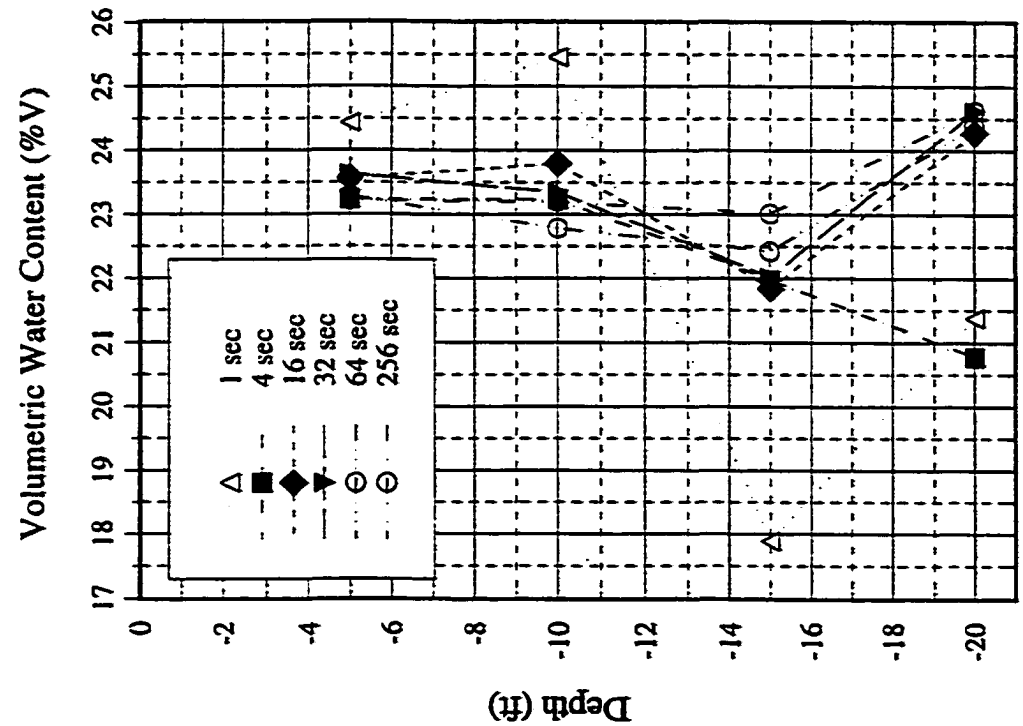

Effect of count time on water content readings from the CPN gauge.

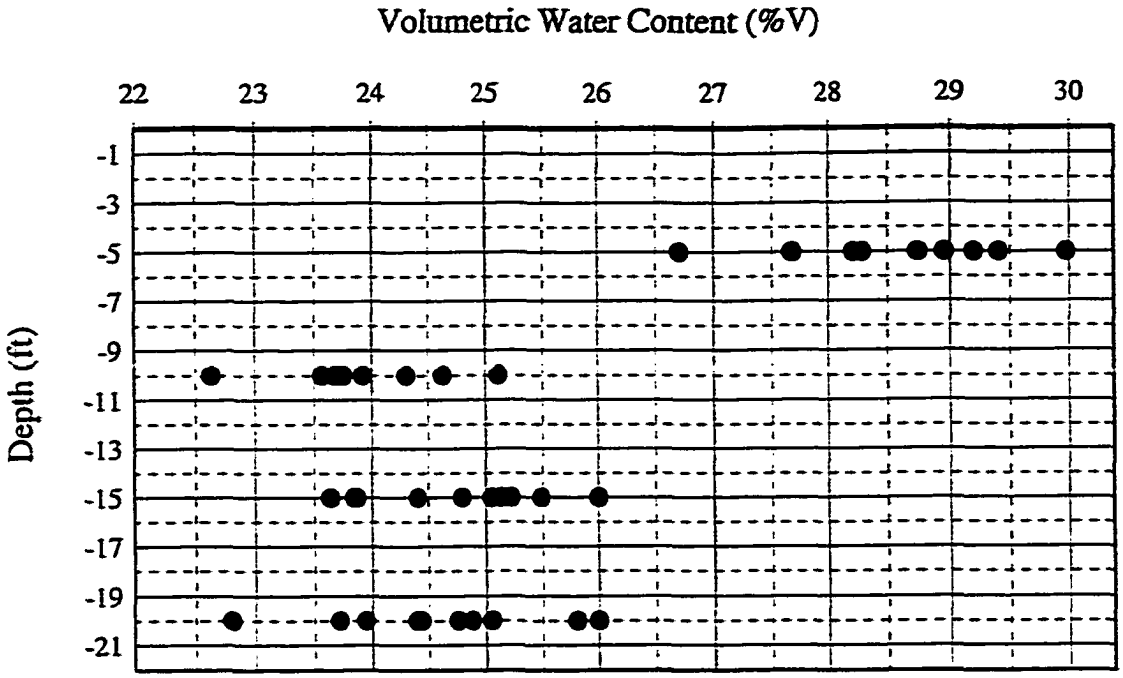

Reproducibility of data taken with the CPN gauge in access tube A-1 at CSU.

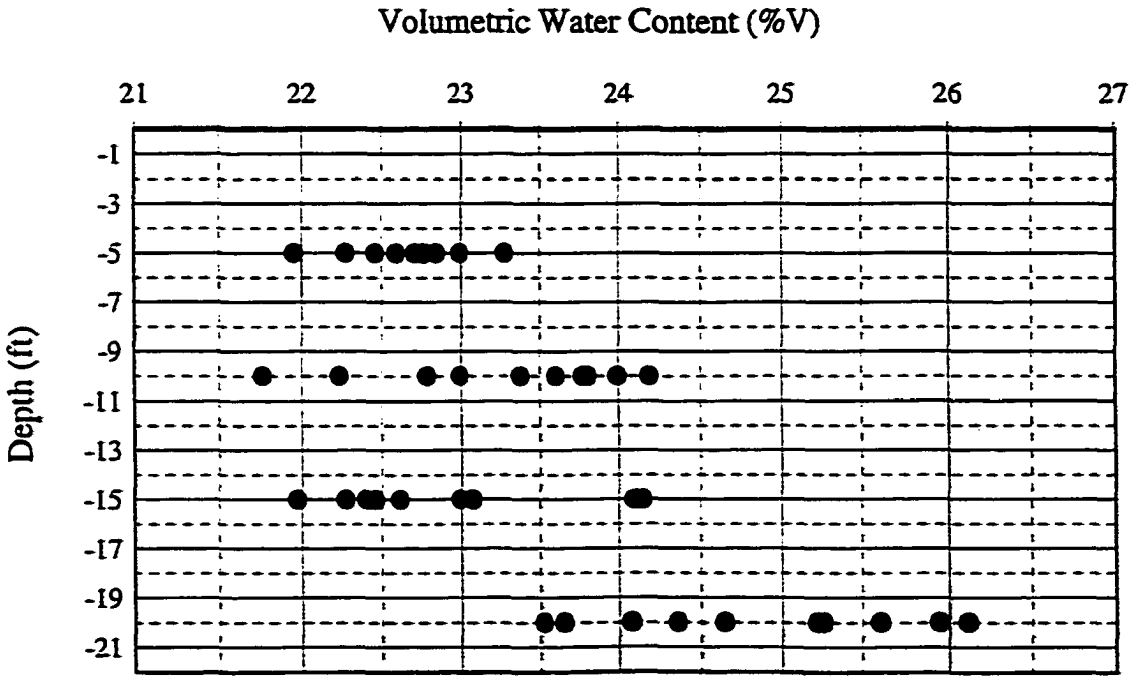

Reproducibility of data taken with the CPN gauge in access tube E-5 at CSU.

APPENDIX B

Laboratory Data

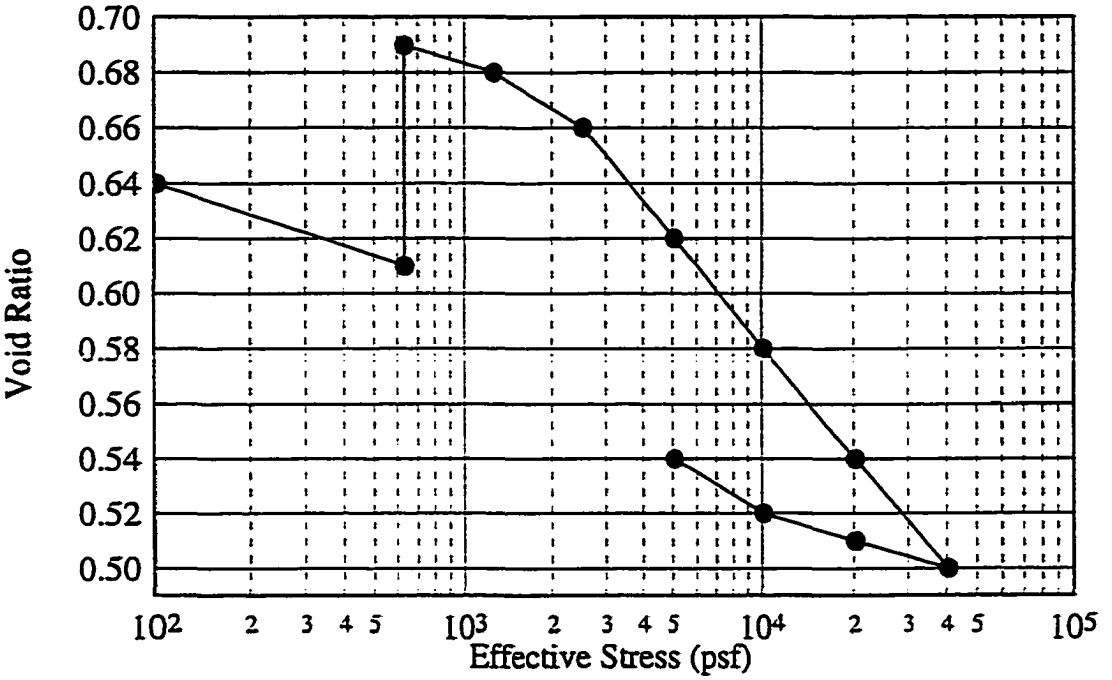

Consolidation swell test for soil from 5 feet at CSU.

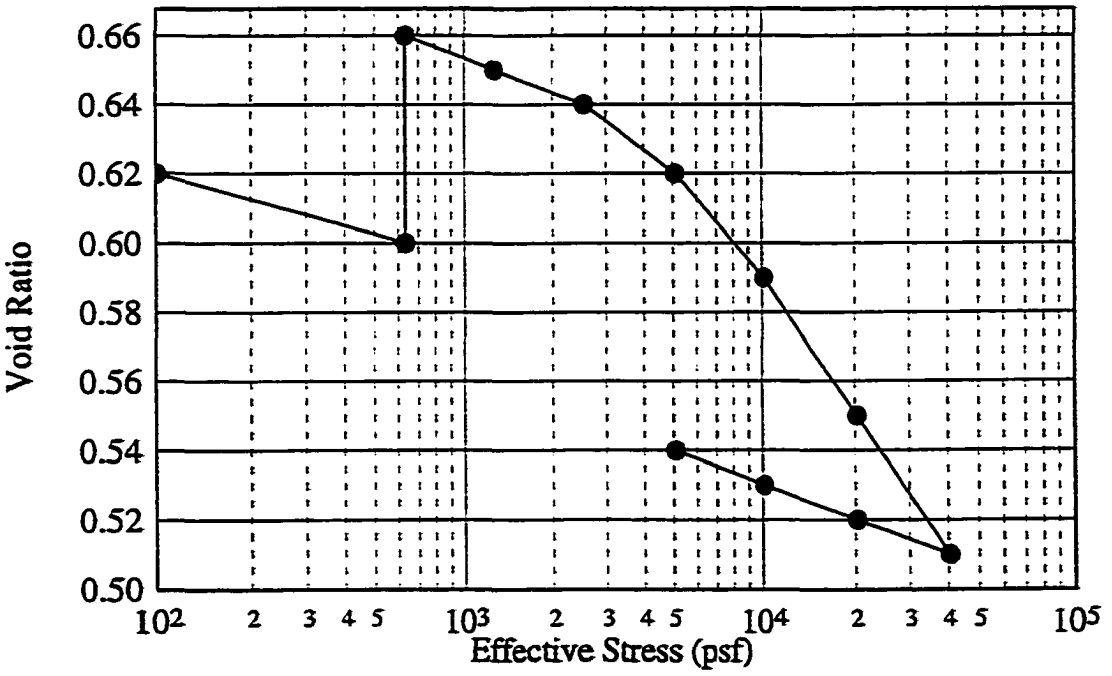

Consolidation swell test for soil from 8.5 feet at CSU.

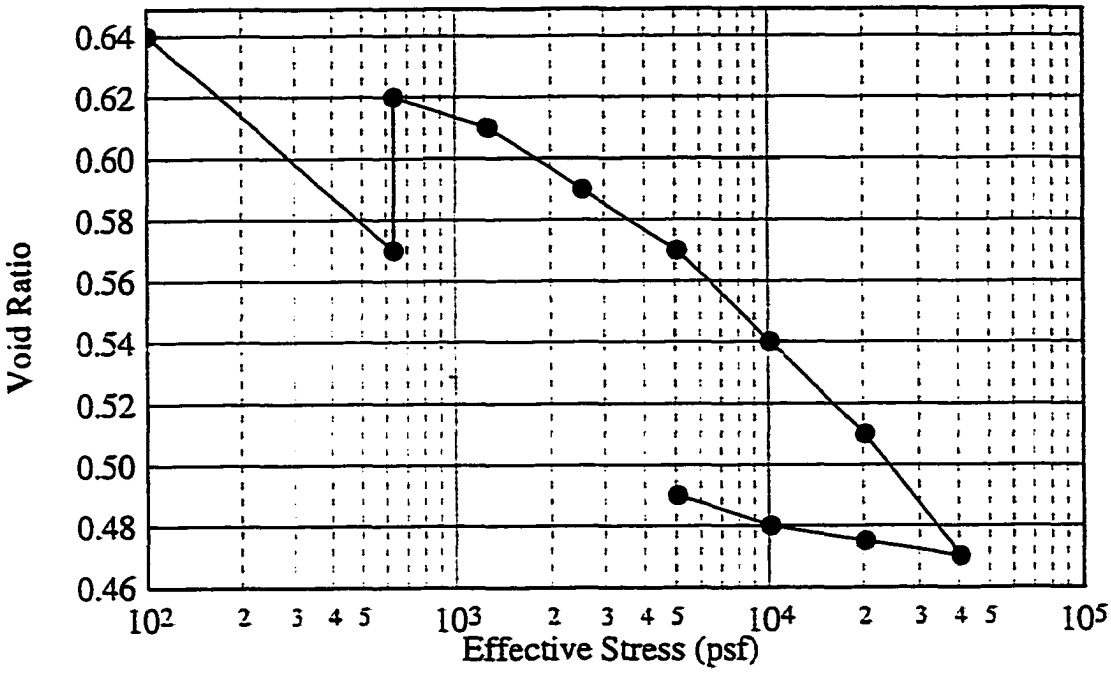

Consolidation swell test for soil from 12.5 feet at CSU.

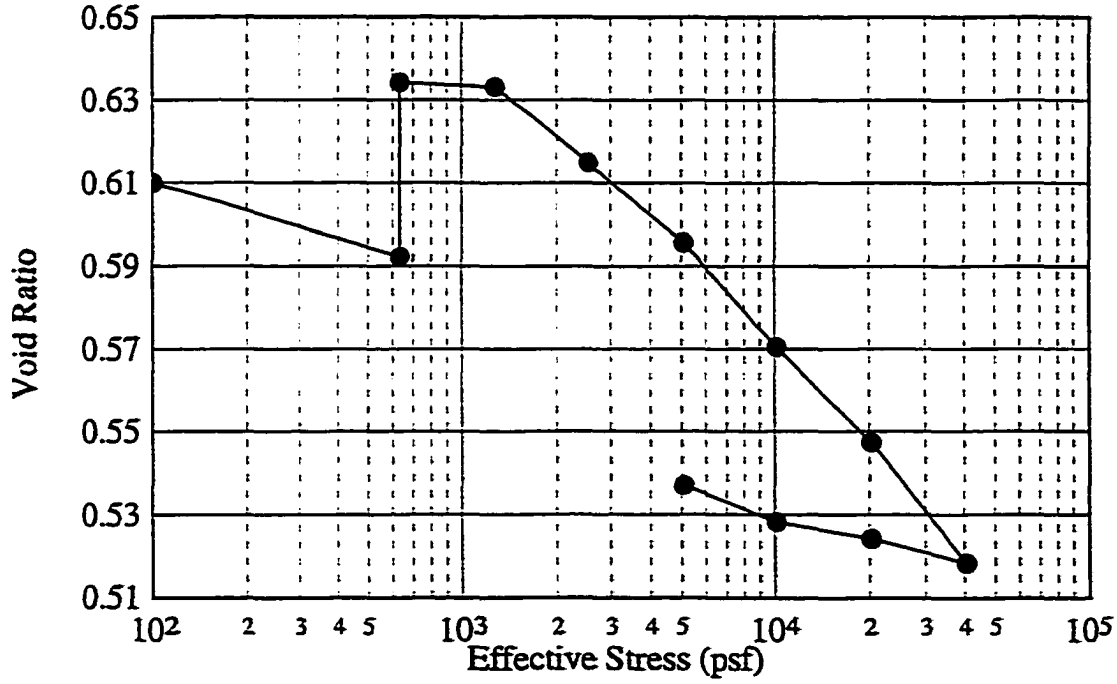

Consolidation swell test for soil from 17.5 feet at CSU

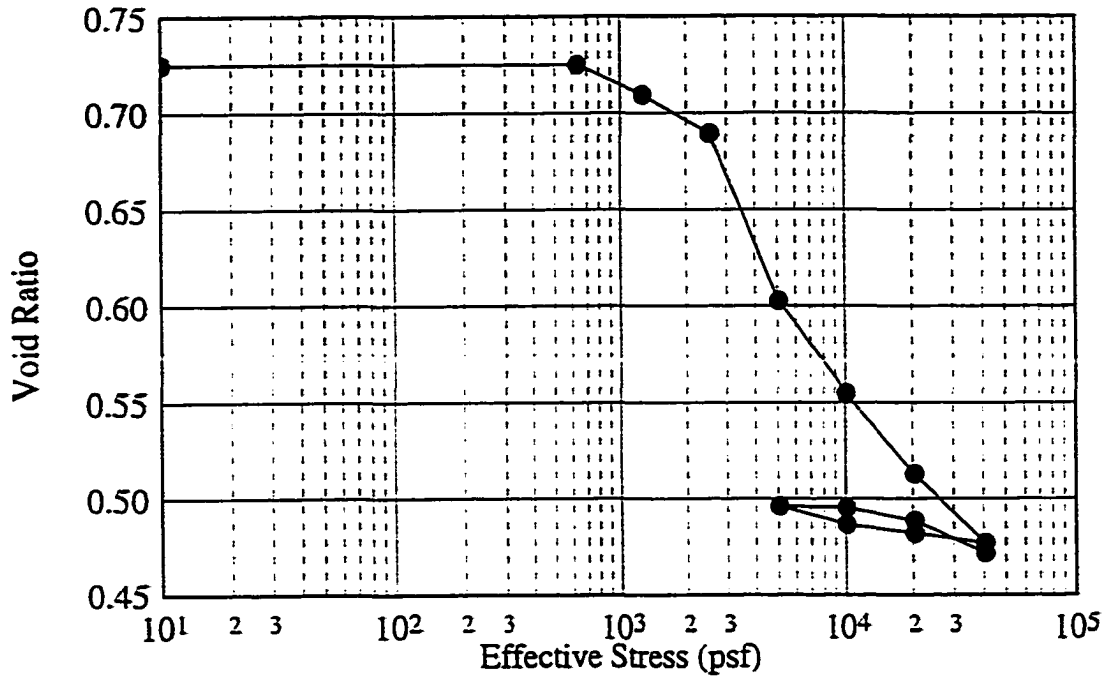

Controlled strain test for soil from 2 feet at CSU.

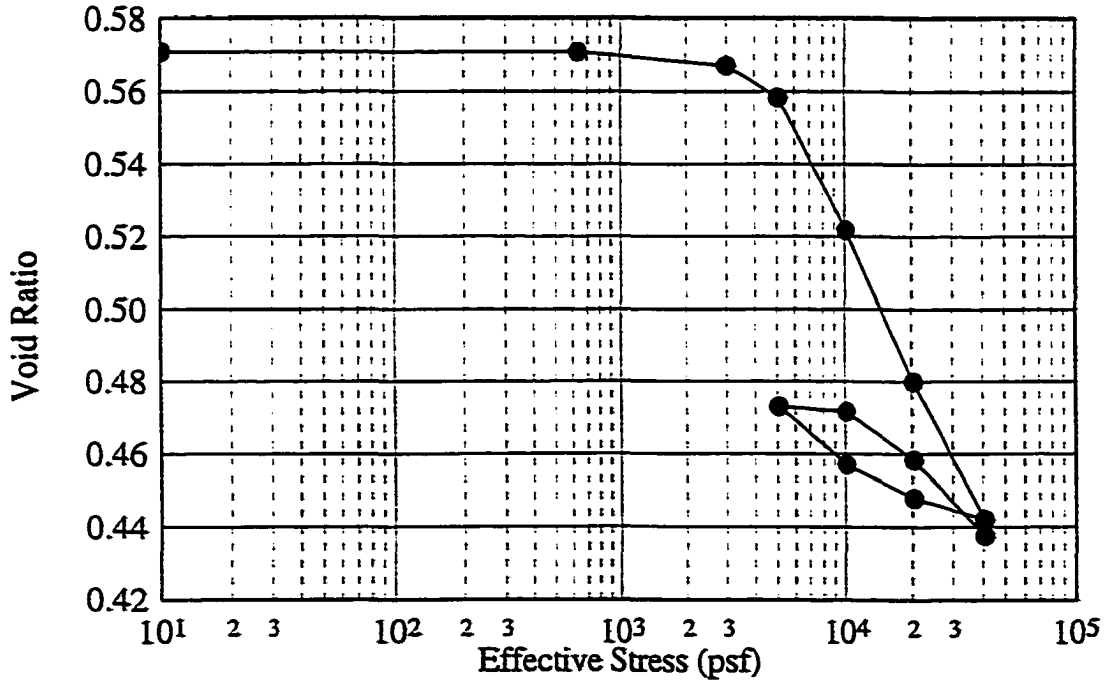

Controlled strain test for soil from 5 feet at CSU.

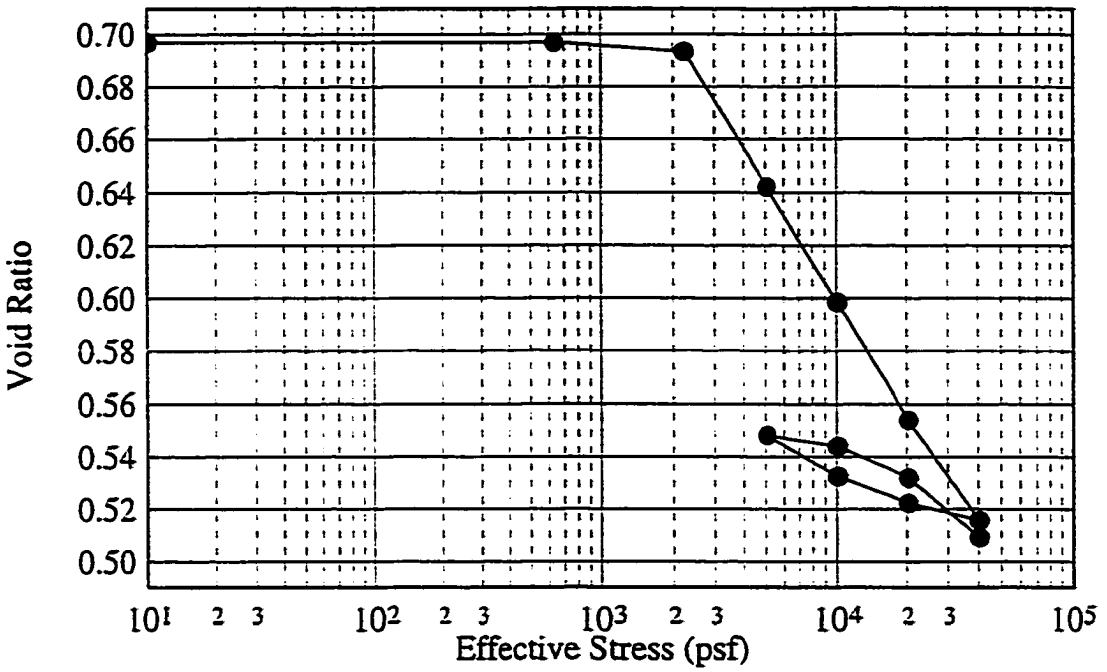

Controlled strain test for soil from 10 feet at CSU.

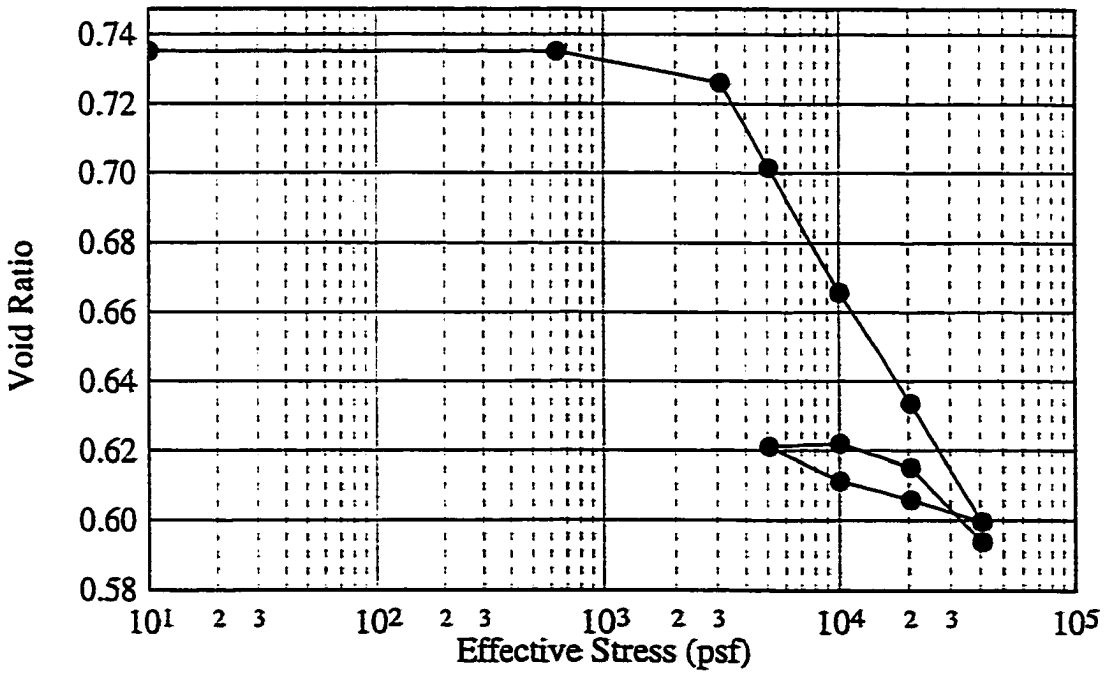

Controlled strain test for soil from 17 feet at CSU.

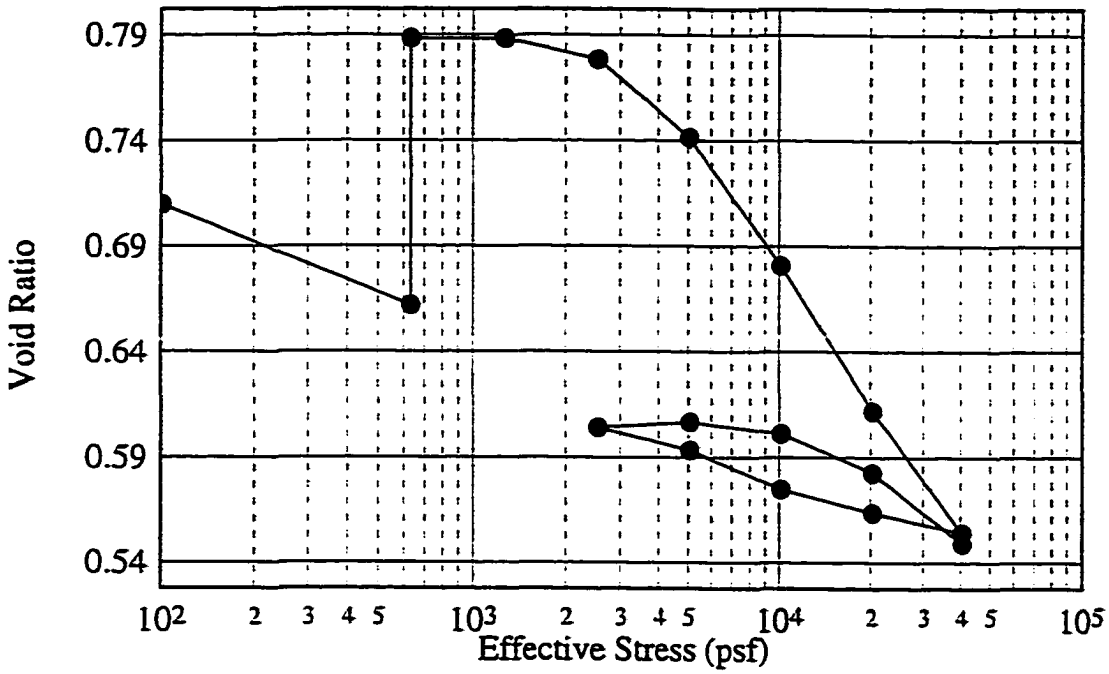

Consolidation swell test for soil from 1.5 feet at FSH.

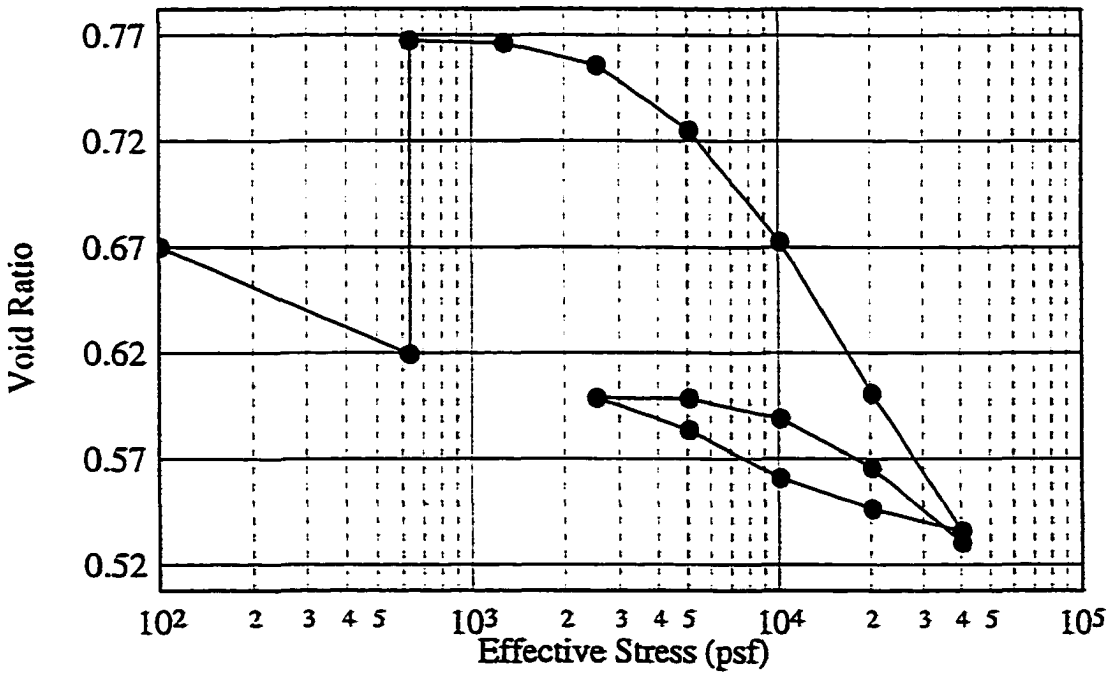

Consolidation swell test for soil from 3 feet at FSH.

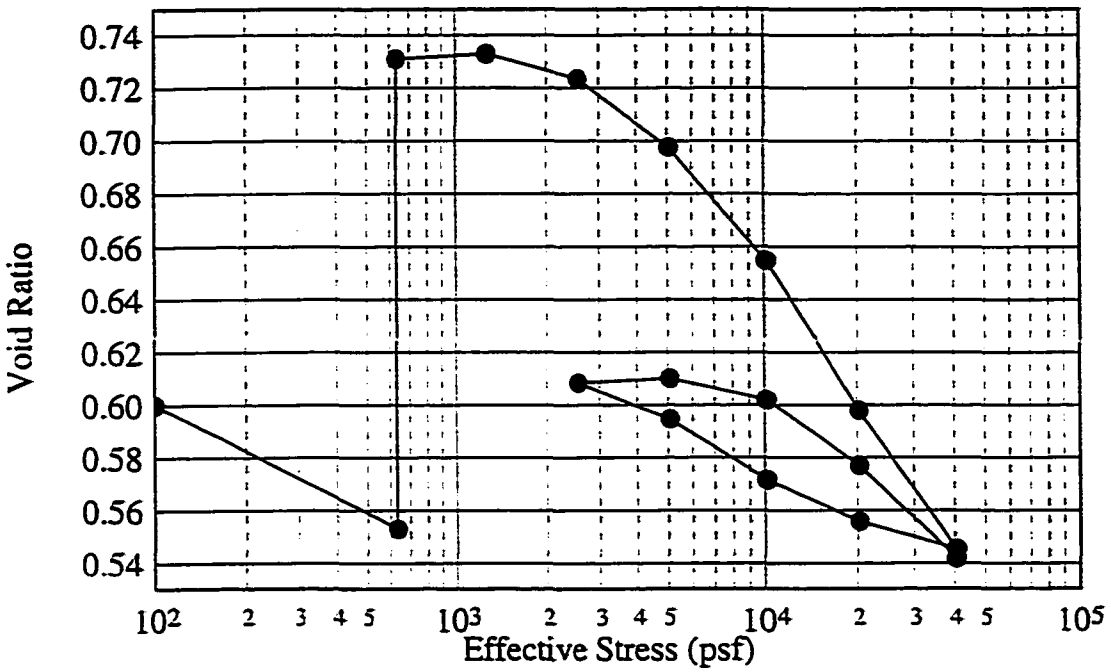

Consolidation swell test for soil from 4.5 feet at FSH.

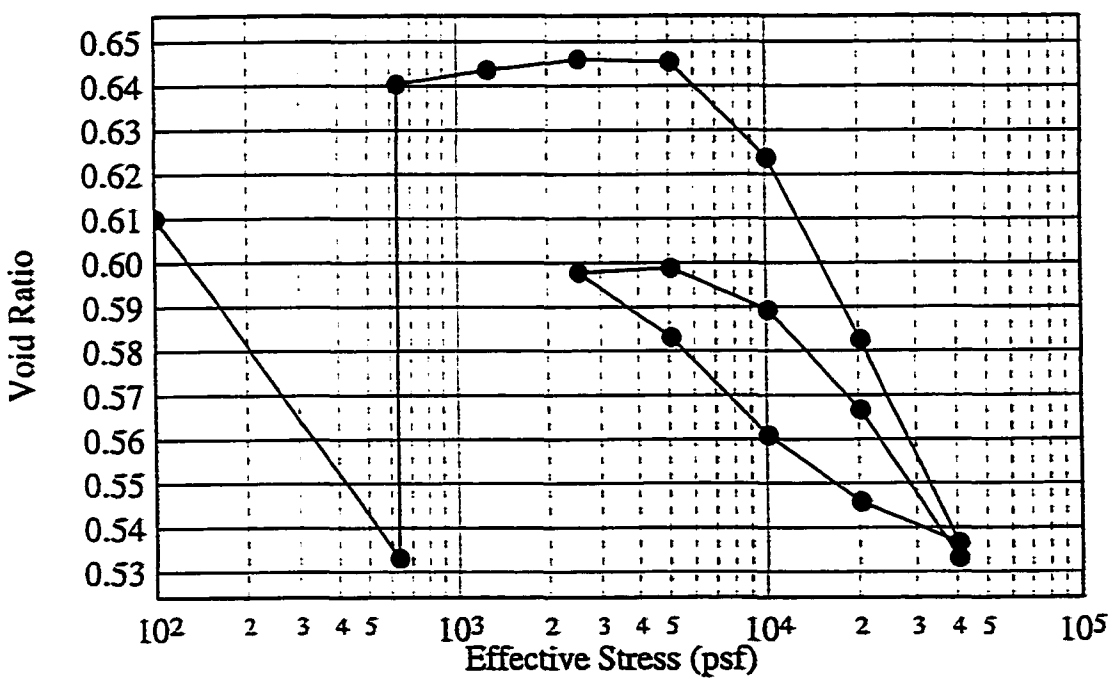

Consolidation swell test for soil from 5 feet at FSH.

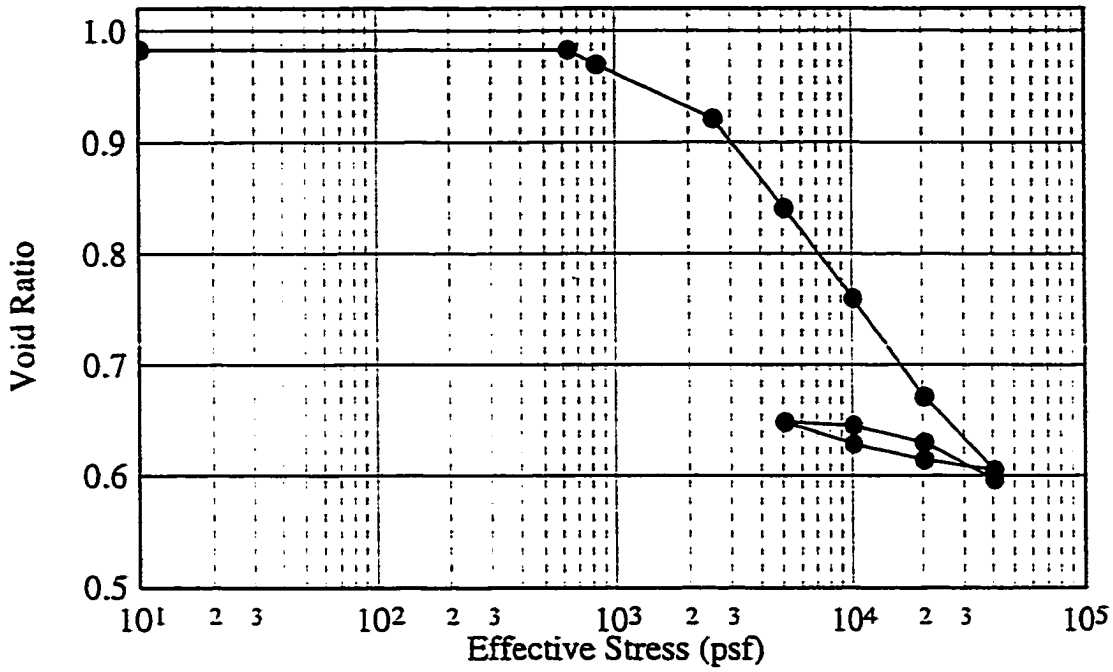

Controlled strain test for soil from 1.5 feet at FSH.

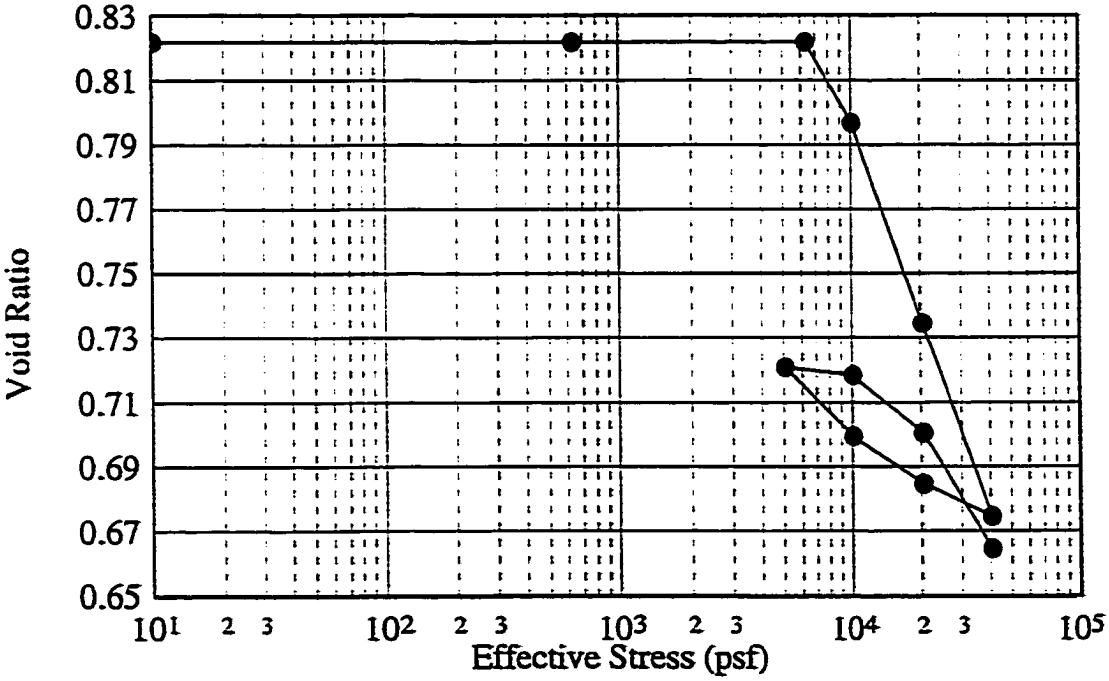

Controlled strain test for soil from 3.5 feet at FSH.

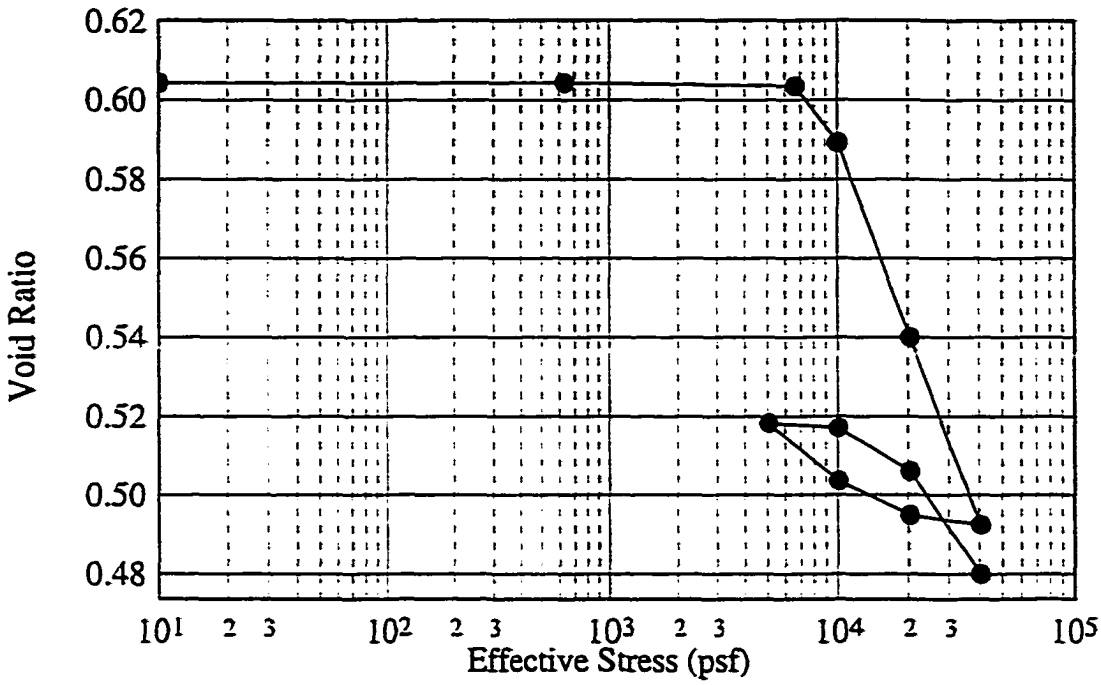

Controlled strain test for soil from 5 feet at FSH

WES Expansive Soil Project
Steady State Hydraulic Conductivity Experiment
Falling Head water-Rising Tail water Method

Test #1
Pierre Shale

6-12-95

HW Accumulater Area, A: 10.75
TW Accumulater Area: 0.62

Sample Area: 53.07
Sample Length: 7.7

Date	Time	Elapsed Time (min)	Headwater Pressure (cm)	Height of Headwater (cm)	Height of Tailwater (cm)	Hydraulic Conductivity (cm/sec)	Elapsed Time (days)	
6-13-95	11:50a	0	351.7	21.3	50.6	*****	0.00	
6-14-95	7:35a	1185	351.7	21	52.8	9.31E-09	0.82	
6-14-95	1:00p	1510	351.7	20.9	53.3	8.19E-09	1.05	
6-15-95	8:20a	2670	351.7	20.8	55.3	8.06E-09	1.85	
6-16-95	7:52a	4018	351.7	20.7	57.3	6.99E-09	2.79	
6-17-95	11:23a	5669	351.7	20.3	59.8	7.94E-09	3.94	
6-19-95	8:11a	8357	351.7	19.9	63.8	7.49E-09	5.80	
6-20-95	8:09a	9795	351.7	19.8	65.7	6.43E-09	6.80	
6-21-95	9:25a	11311	351.7	19.6	67.9	7.06E-09	7.85	
6-22-95	8:10a	12676	351.7	19.4	69.4	6.18E-09	8.80	
6-23-95	9:55a	14221	351.7	19.3	71.2	5.80E-09	9.88	
6-24-95	9:30a	15636	351.7	19.3	72.3	3.68E-09	10.86	
6-24-95	9:38a	0	351.7	33.1	52	3.68E-09	10.86	Reset TW
6-25-95	9:40a	1442	351.7	33	54.1	6.52E-09	11.86	
6-26-95	5:35p	3357	351.7	32.9	56.6	5.84E-09	13.19	
6-28-95	1:09p	5973	351.7	32.6	59.9	5.98E-09	15.01	
6-29-95	3:00p	7524	351.7	32.4	61.8	5.94E-09	16.09	
6-30-95	10:30a	8694	351.7	32.2	63.1	5.65E-09	16.90	
7-3-95	8:45a	12909	351.7	31.9	67.7	5.18E-09	19.82	
7-5-95	1:00p	15534	351.7	31.6	71.1	6.36E-09	21.65	
7-6-95	8:45a	16359	351.7	31.4	72.2	7.17E-09	22.22	
7-7-95	3:15p	18189	351.7	31.3	73.5	3.50E-09	23.49	
7-7-95	3:15p	0	351.7	31.3	59.1	3.50E-09	23.49	Reset TW
7-10-95	8:10a	3895	351.7	31	63.4	5.21E-09	26.20	
7-11-95	5:25p	5890	351.7	30.8	65.2	4.46E-09	27.58	
7-13-95	6:00a	8085	351.7	30.7	67.5	4.90E-09	29.11	
7-14-95	7:00a	9585	351.7	30.5	68.8	4.51E-09	30.15	
7-15-95	1:00p	11385	351.7	30.3	70.6	5.04E-09	31.40	

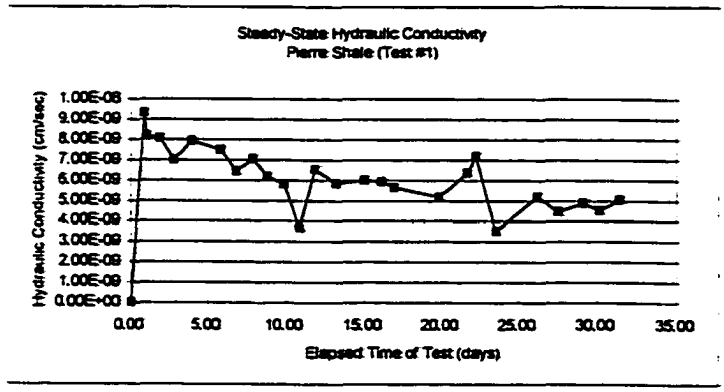

WES Expansive Soil Project
Steady State Hydraulic Conductivity Experiment
Falling Head water-Rising Tail water Method

Test #2
Texas Soil

6-12-95

HW Accumulater Area, A: 10.75
TW Accumulater Area: 0.79

Sample Area: 53.07
Sample Length: 7.7

Date	Time	Elapsed Time (min)	Headwater Pressure (cm)	Height of Headwater (cm)	Height of Tailwater (cm)	Hydraulic Conductivity (cm/sec)	Elapsed Time (days)	
6-13-95	12:28p	0	351.7	32.2	49.7	*****	0	
6-14-95	7:45a	1877	351.7	31.3	52.4	1.24E-08	1.30	
6-14-95	1:00p	2192	351.7	31	53.1	2.06E-08	1.52	
6-15-95	8:21a	3353	351.7	30.3	55.6	1.80E-08	2.33	
6-16-95	7:53a	4765	351.7	29.5	57.4	1.21E-08	3.31	
6-17-95	11:24a	6416	351.7	28.6	59.7	1.29E-08	4.46	
6-19-95	8:13a	7665	351.7	27.6	63.1	2.37E-08	5.32	
6-20-95	8:11a	9103	351.7	27.3	64.9	9.93E-09	6.32	
6-21-95	9:25a	10607	351.7	26.7	66.8	1.14E-08	7.37	
6-22-95	8:10a	11972	351.7	26.4	68.3	9.09E-09	8.31	
6-23-95	9:55a	13517	351.7	25.9	70.1	1.03E-08	9.39	
6-24-95	9:39a	14941	351.7	25.5	71.6	9.33E-09	10.38	
6-25-95	9:40a	16382	351.7	25.1	73.2	9.76E-09	11.38	
6-26-95	5:40p	18302	351.7	24.5	75.3	9.97E-09	12.71	
6-28-95	1:11p	19473	351.7	23.8	78	2.08E-08	13.52	
6-29-95	3:02p	21024	351.7	23.6	79.7	8.85E-09	14.60	
6-30-95	10:30a	22192	351.7	23.2	80.7	8.71E-09	15.41	
7-3-95	8:45a	0	351.7	22.1	56.2	8.71E-09	15.41	Reset TW
7-5-95	1:00p	3135	351.7	21.6	59.6	8.44E-09	17.59	
7-6-95	8:45a	4380	351.7	21.1	60.8	9.35E-09	18.45	
7-7-95	3:16p	6211	351.7	20.9	62.8	8.28E-09	19.72	
7-10-95	8:10a	10095	351.7	20.5	66.1	6.63E-09	22.42	
7-11-95	5:25p	12100	351.7	20.4	67.9	6.65E-09	23.81	
7-13-95	6:00a	14295	351.7	20.3	69.8	6.44E-09	25.34	
7-14-95	7:00a	15795	351.7	20.1	71	6.63E-09	26.38	
7-15-95	1:30p	17625	351.7	19.9	72.7	7.42E-09	27.65	

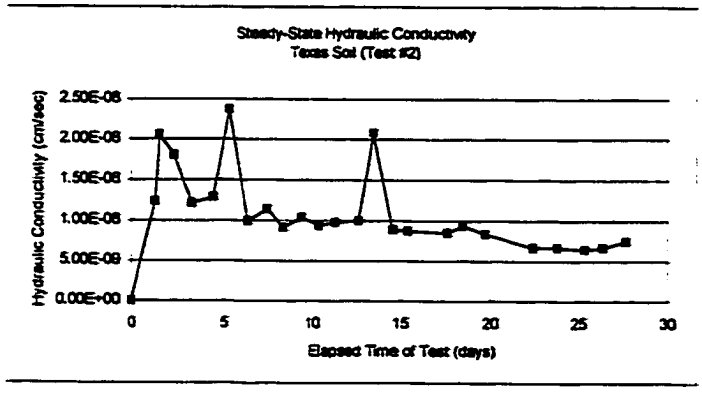

WES Expansive Soil Project
Steady State Hydraulic Conductivity Experiment
Falling Head water-Rising Tail water Method

Test #4
Texas Soil

6-12-95

HW Accumulater Area, A: 10.75
TW Accumulater Area: 0.62

Sample Area: 44.65
Sample Length: 7.8

Date	Time	Elapsed Time (min)	Headwater Pressure (cm)	Height of Headwater (cm)	Height of Tailwater (cm)	Hydraulic Conductivity (cm/sec)	Elapsed Time (days)
6-19-95	8:15a	0	351.7	22.5	75.9	*****	0.00
6-20-95	8:14a	1439	351.7	20.4	75.9	1.54E-07	1.00
6-21-95	9:29a	2954	351.7	18.7	75.9	1.19E-07	2.05
6-22-95	8:11a	3596	351.7	17.1	75.9	2.66E-07	2.50
6-23-95	9:55a	4420	351.7	15.8	75.9	1.69E-07	3.07
6-26-95	5:45p	0	351.7	35.3	75.9	4.58E-07	3.07
6-28-95	1:15p	2610	351.7	33	75.9	8.90E-08	4.88
6-29-95	3:12p	4167	351.7	32	75.9	6.52E-08	5.96
6-30-95	10:30a	5325	351.7	31.3	75.9	6.15E-08	6.77
7-3-95	8:50a	9545	351.7	29.4	75.9	4.60E-08	9.70
7-6-95	8:50a	13865	351.7	28.4	75.9	2.38E-08	12.70
7-7-95	3:17p	15692	351.7	28.1	75.9	1.69E-08	13.97
7-10-95	8:10a	19585	351.7	27.7	75.9	1.06E-08	16.67
7-11-95	5:25p	21460	351.7	27.3	75.9	2.20E-08	17.97
7-14-95	7:00a	25155	351.7	27.2	75.9	2.80E-09	20.54
7-15-95	1:30p	26985	351.7	26.8	75.9	2.26E-08	21.81

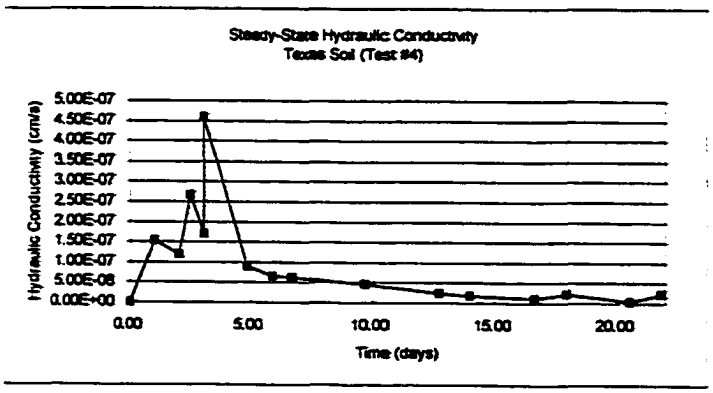

APPENDIX C

Field Data

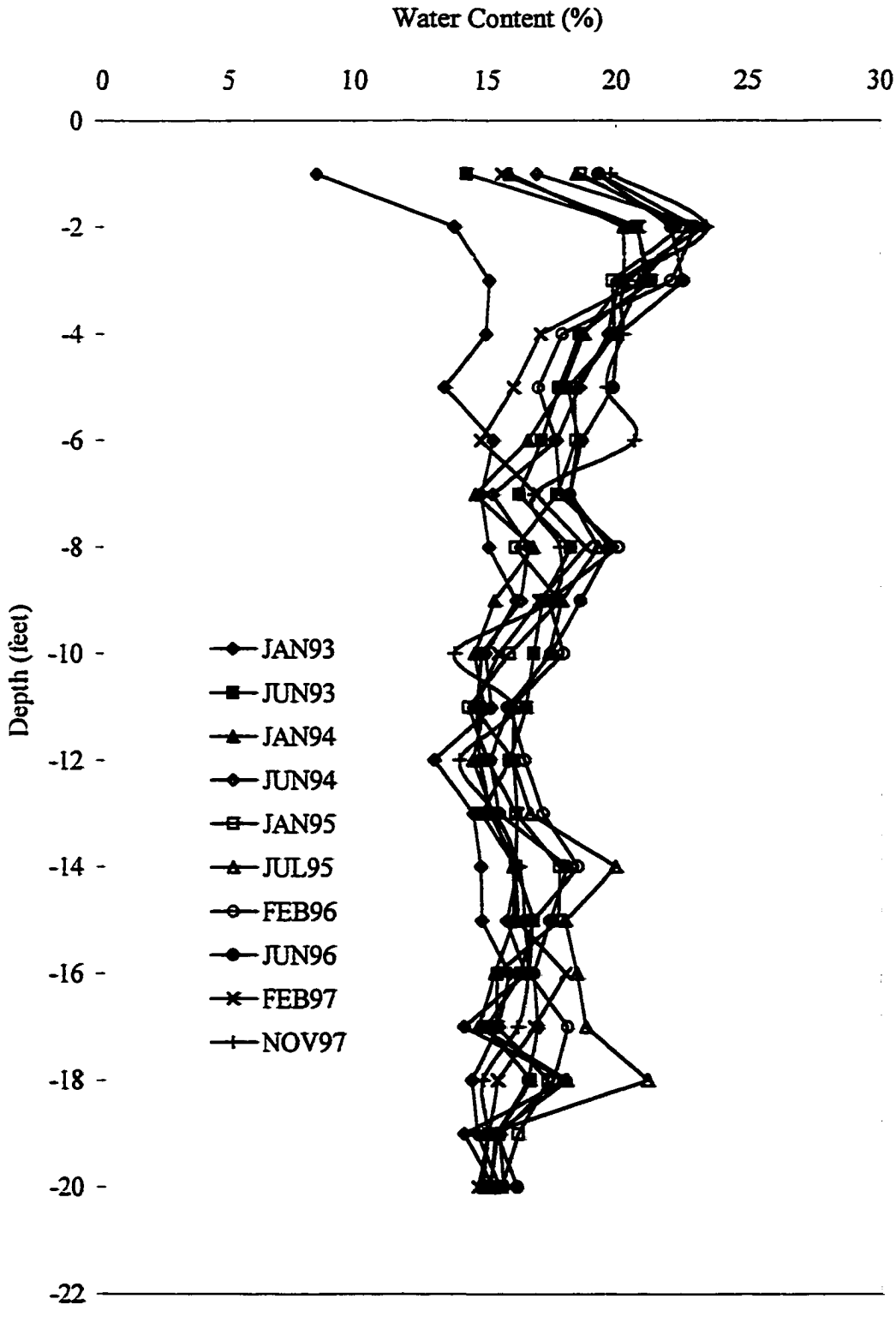

CSU Access Tube A-1

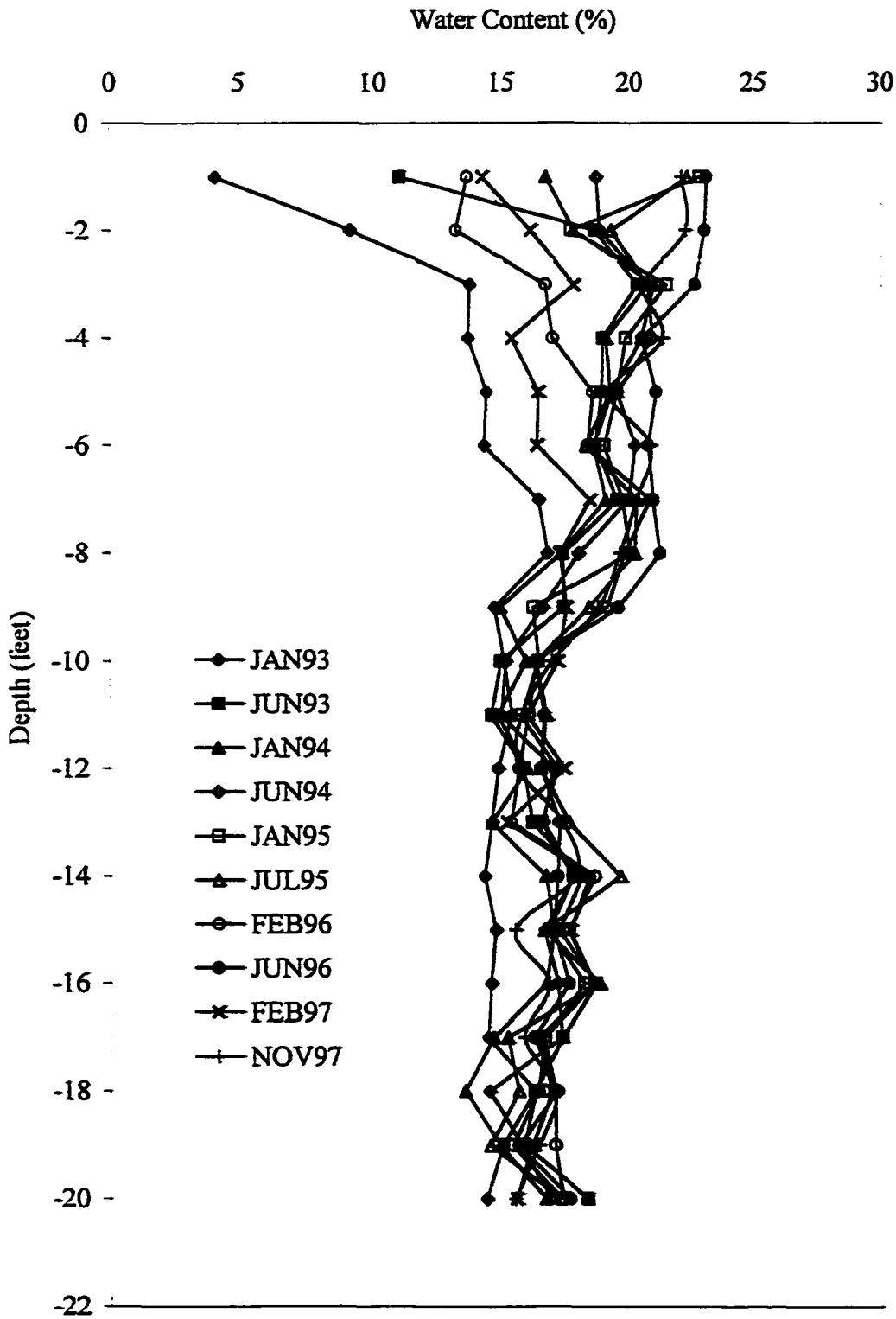

CSU Access Tube A-3

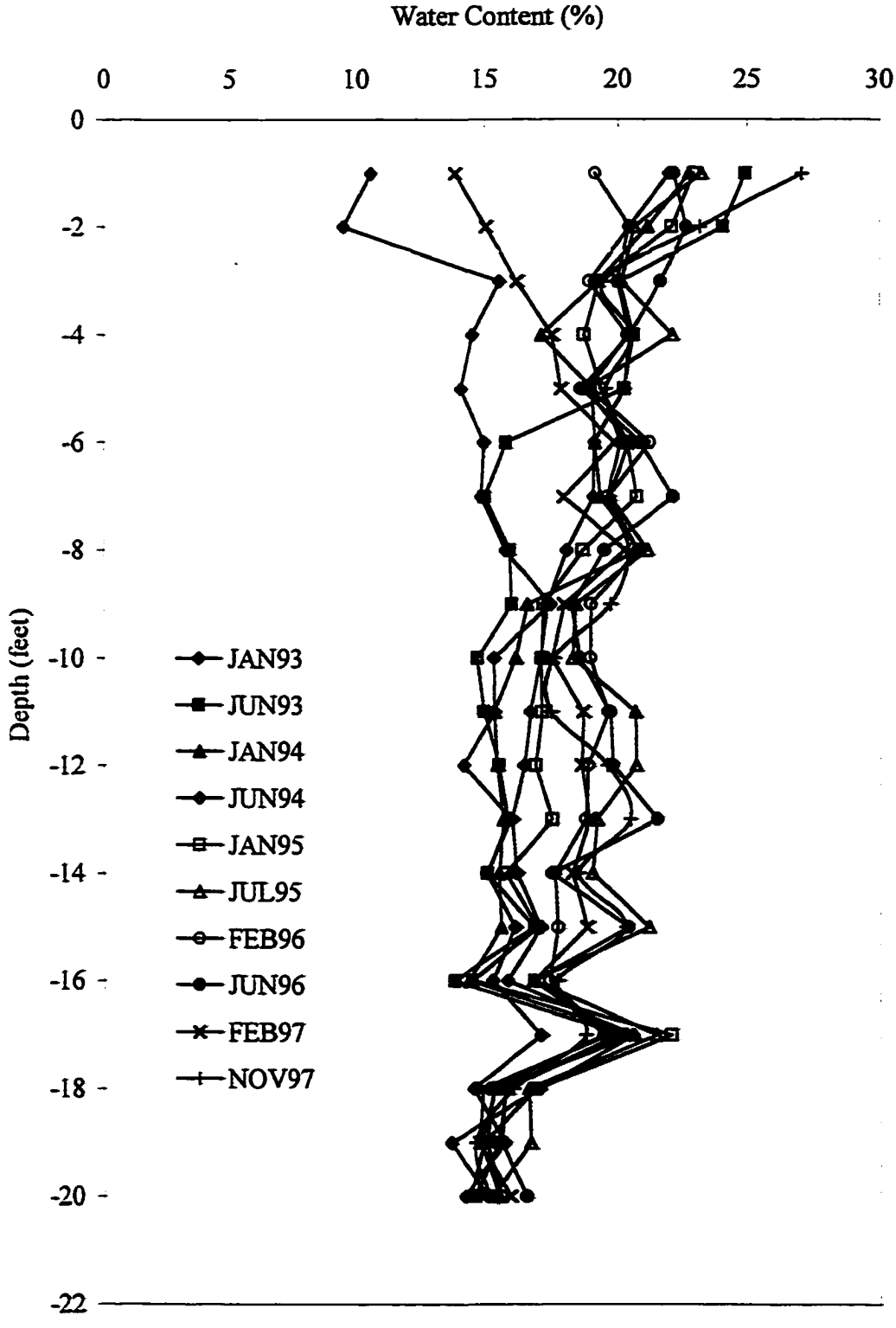

CSU Access Tube A-5

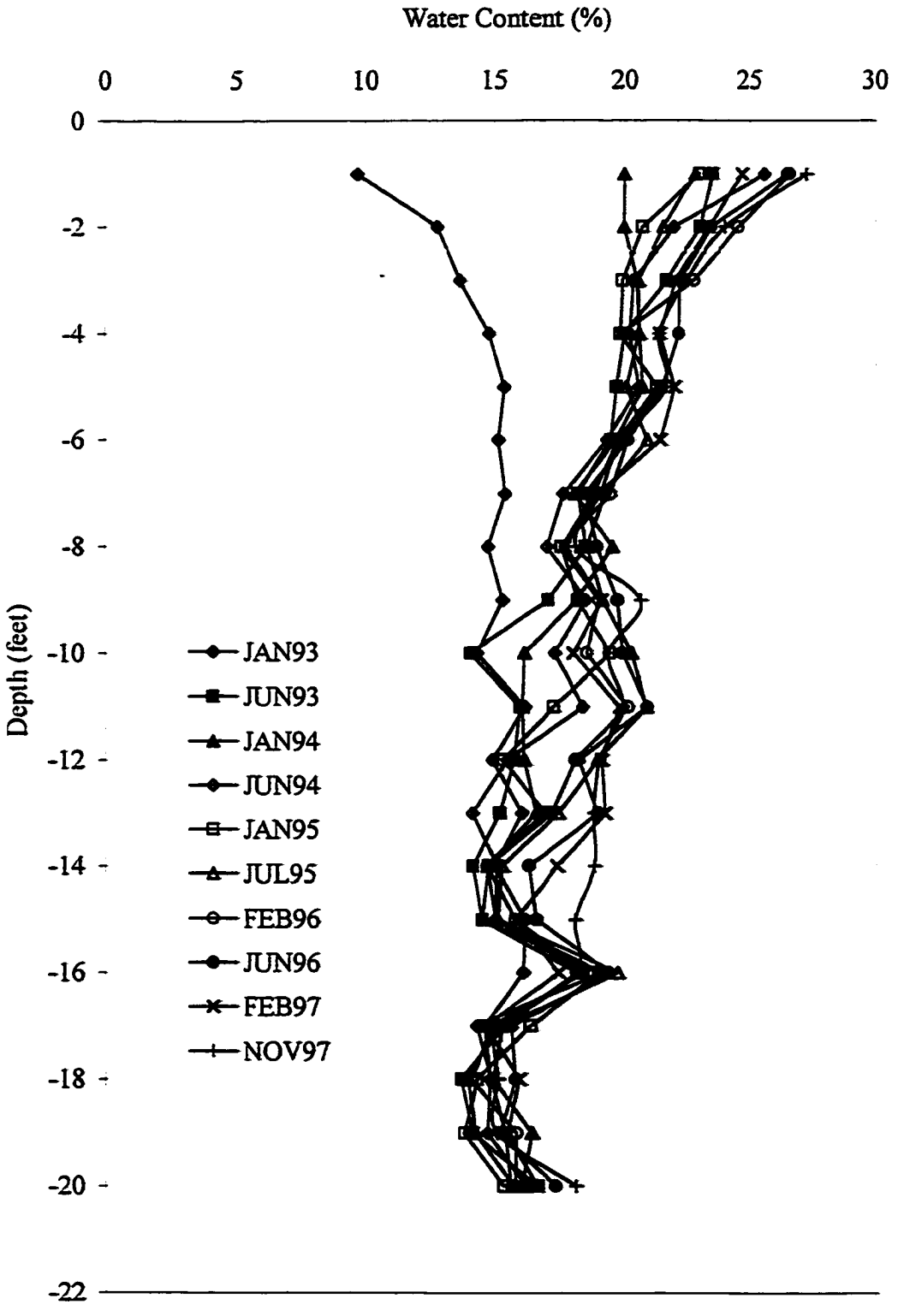

CSU Access Tube A-9

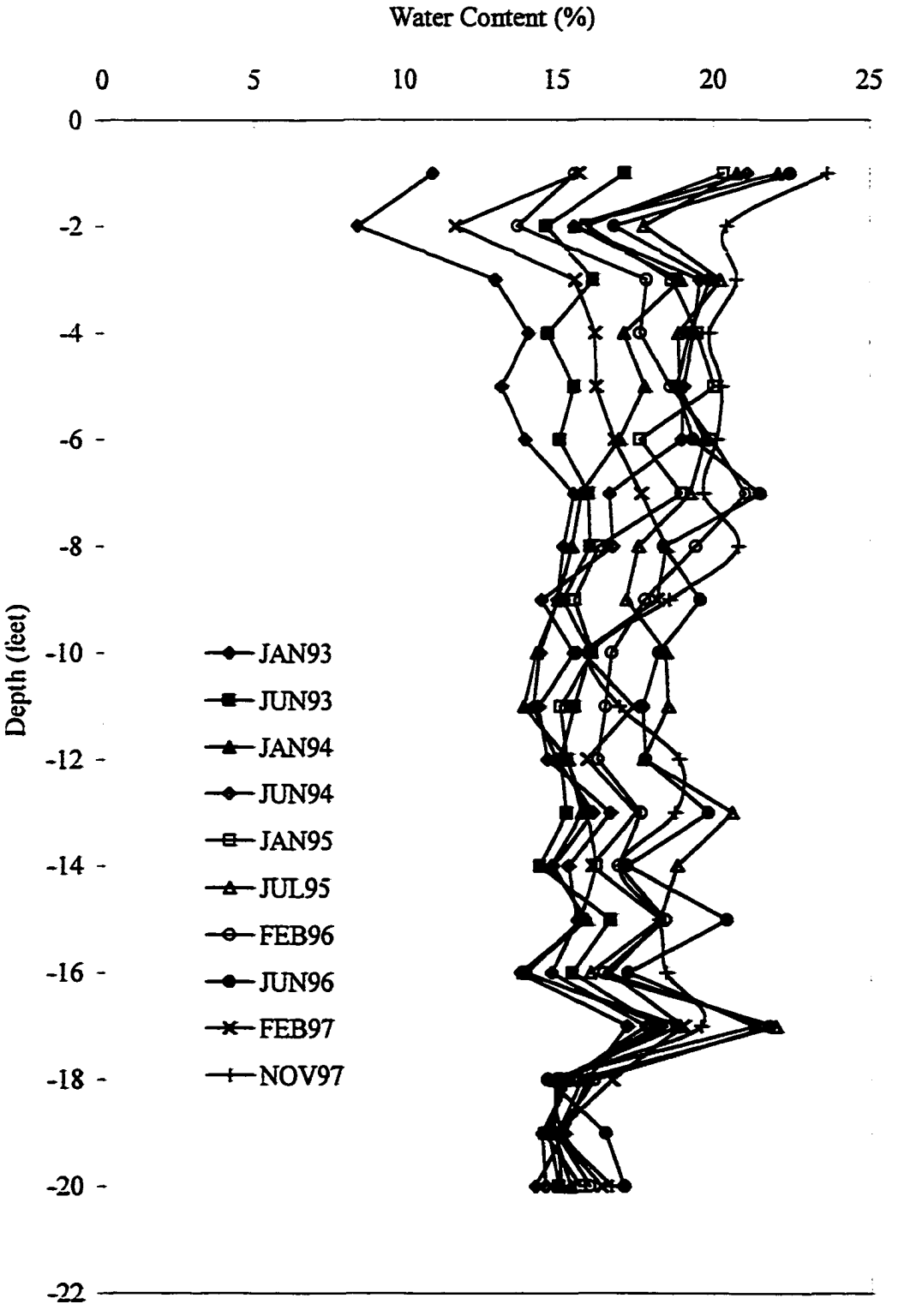

CSU Access Tube A.5-3

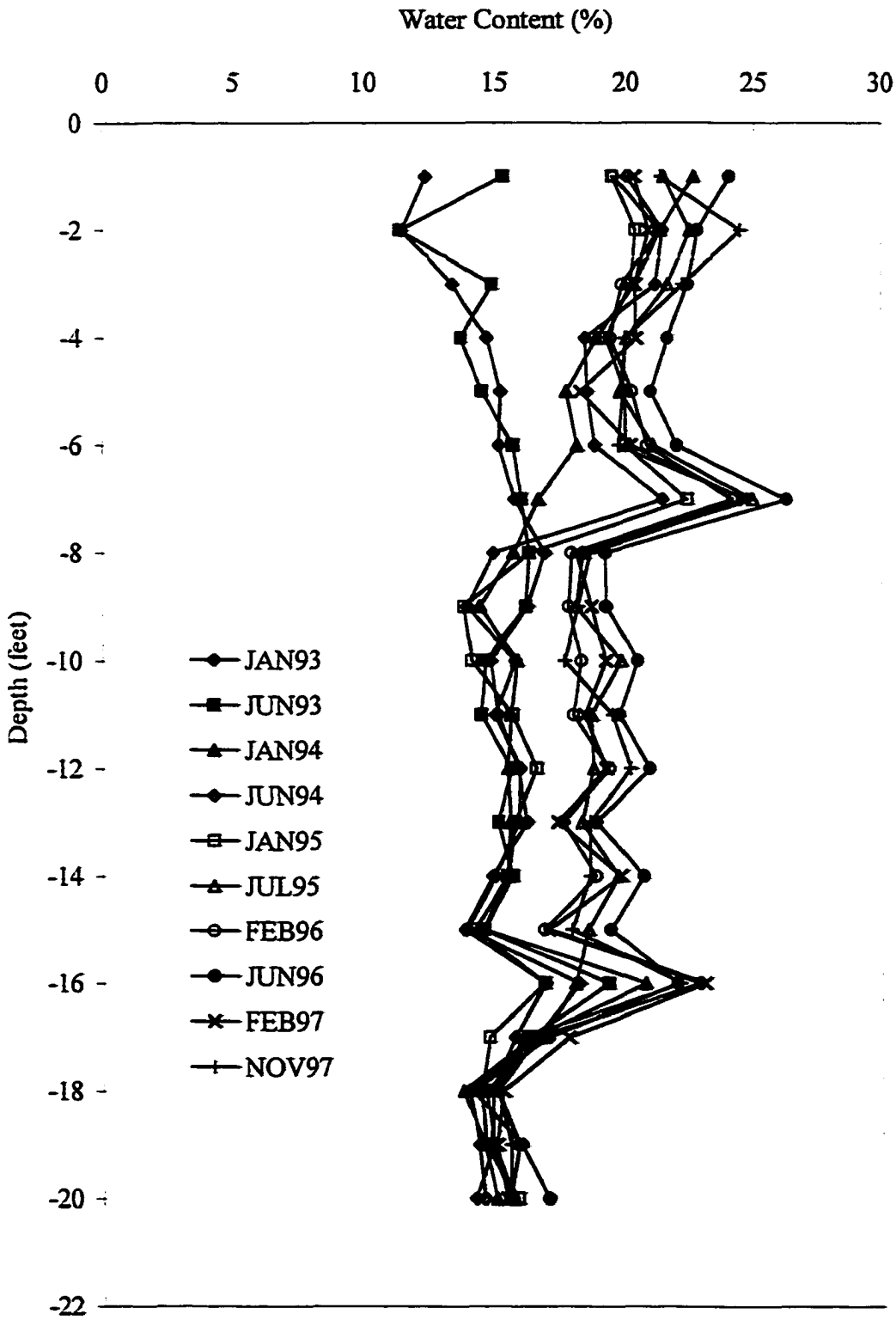

CSU Access Tube B-5

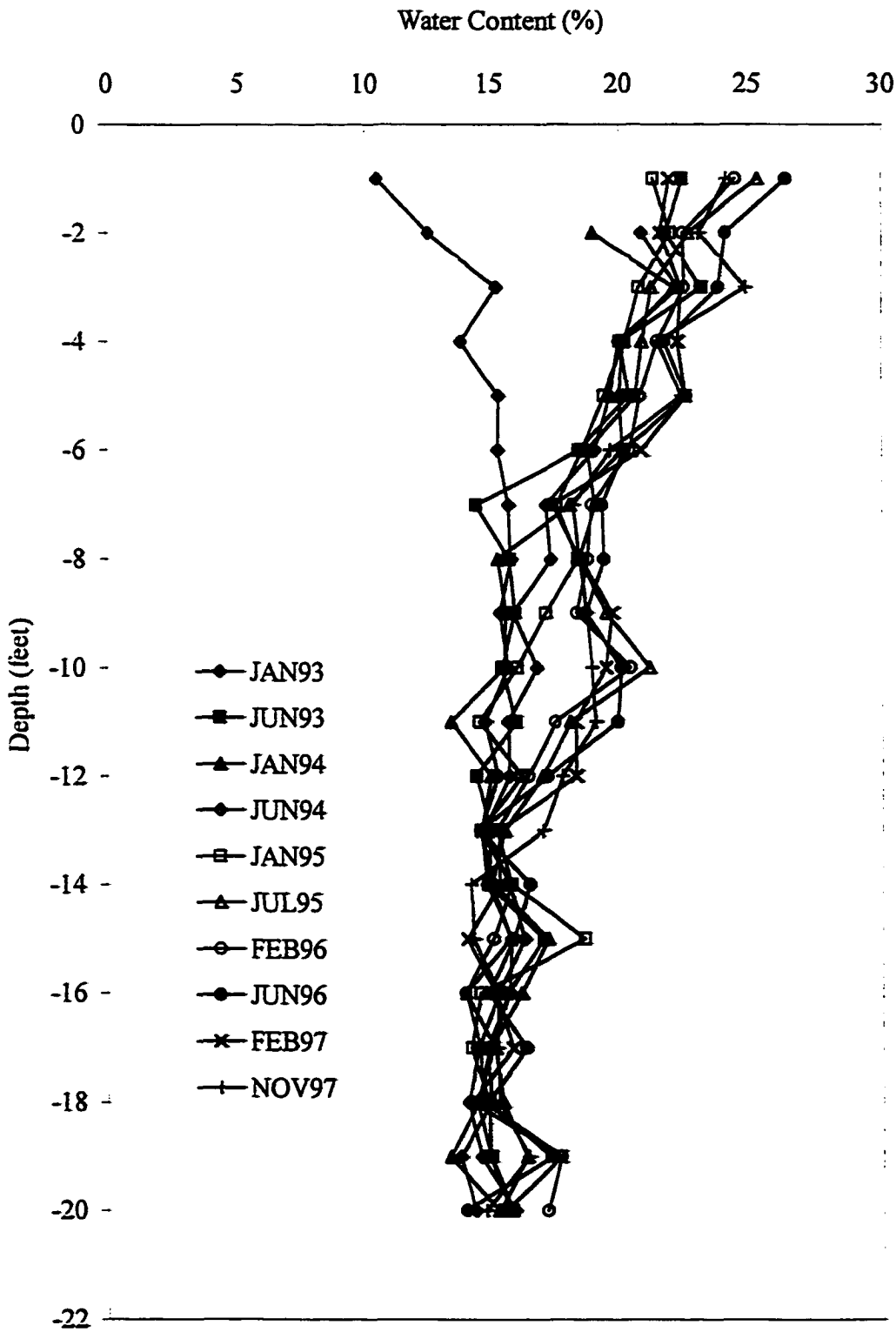

CSU Access Tube B-8

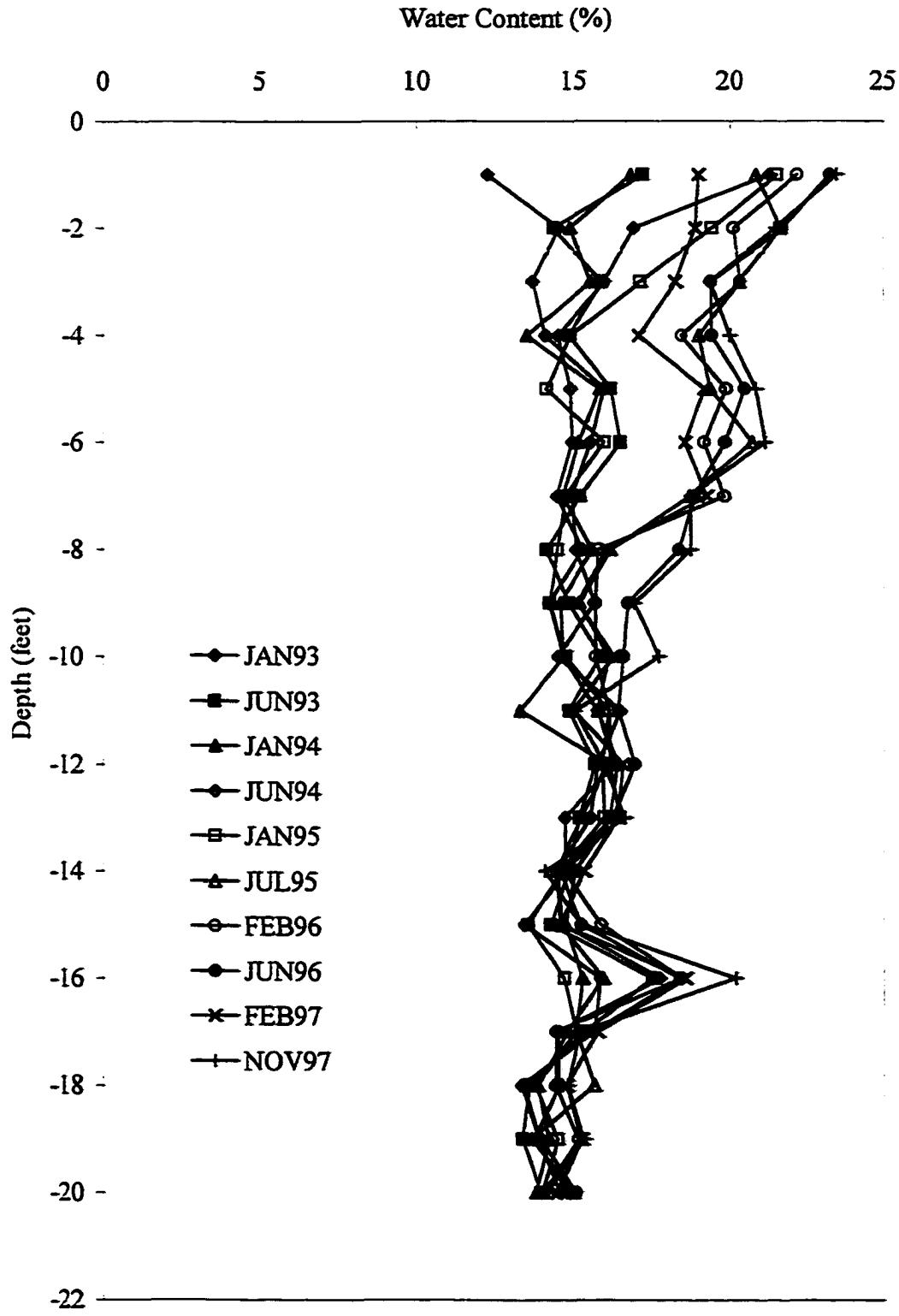

CSU Access Tube B.5-3

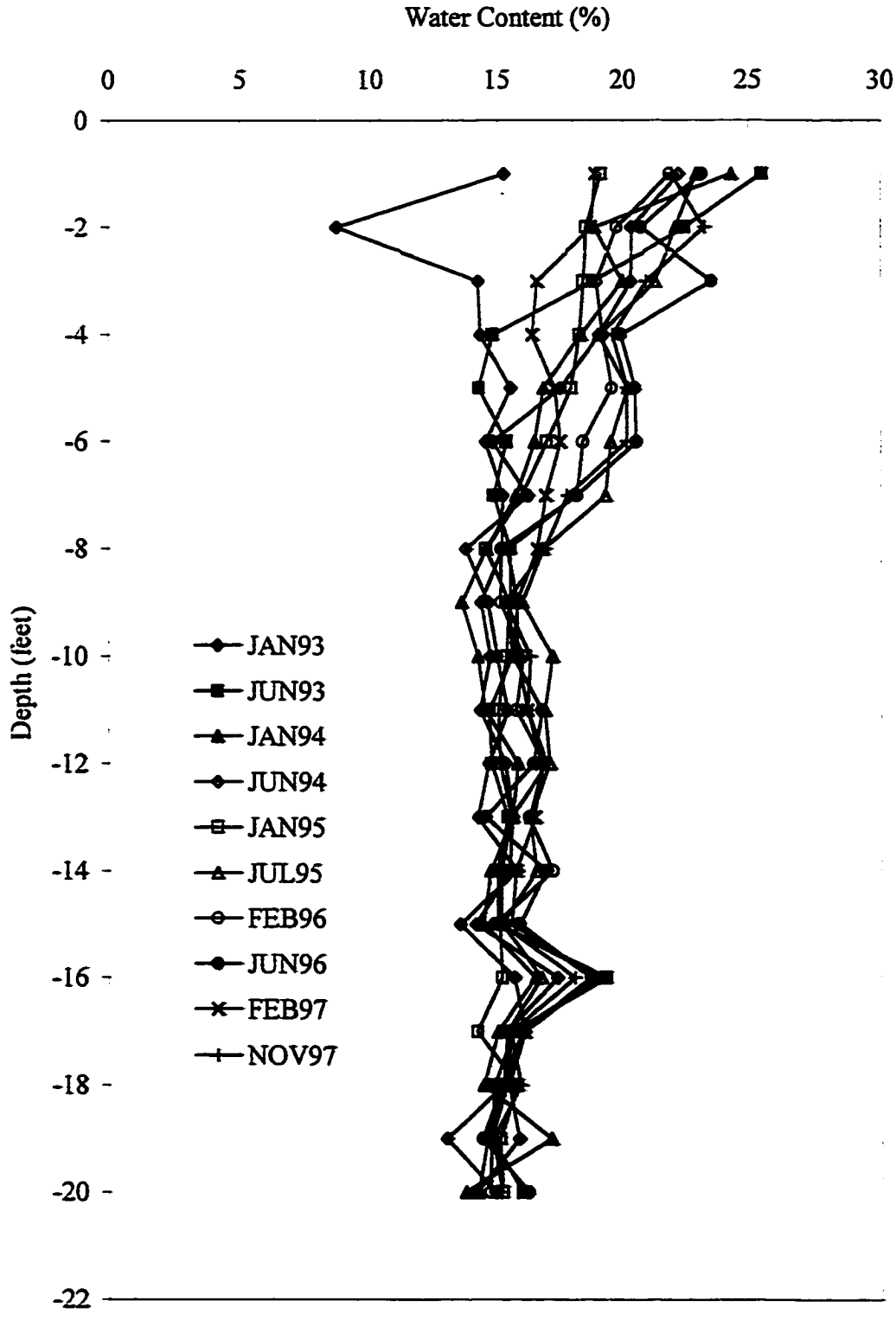

CSU Access Tube C-1

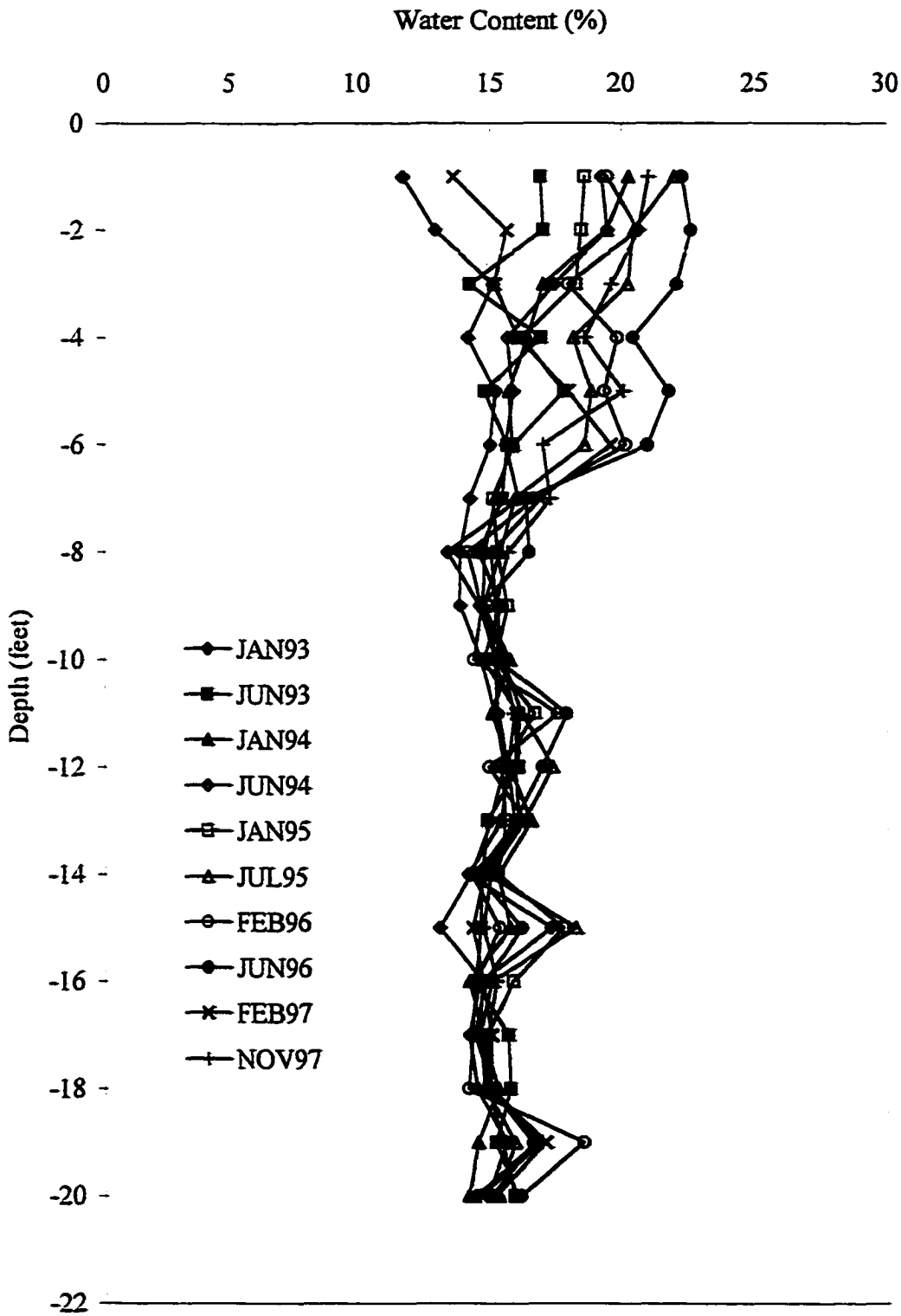

CSU Access Tube C-1.6

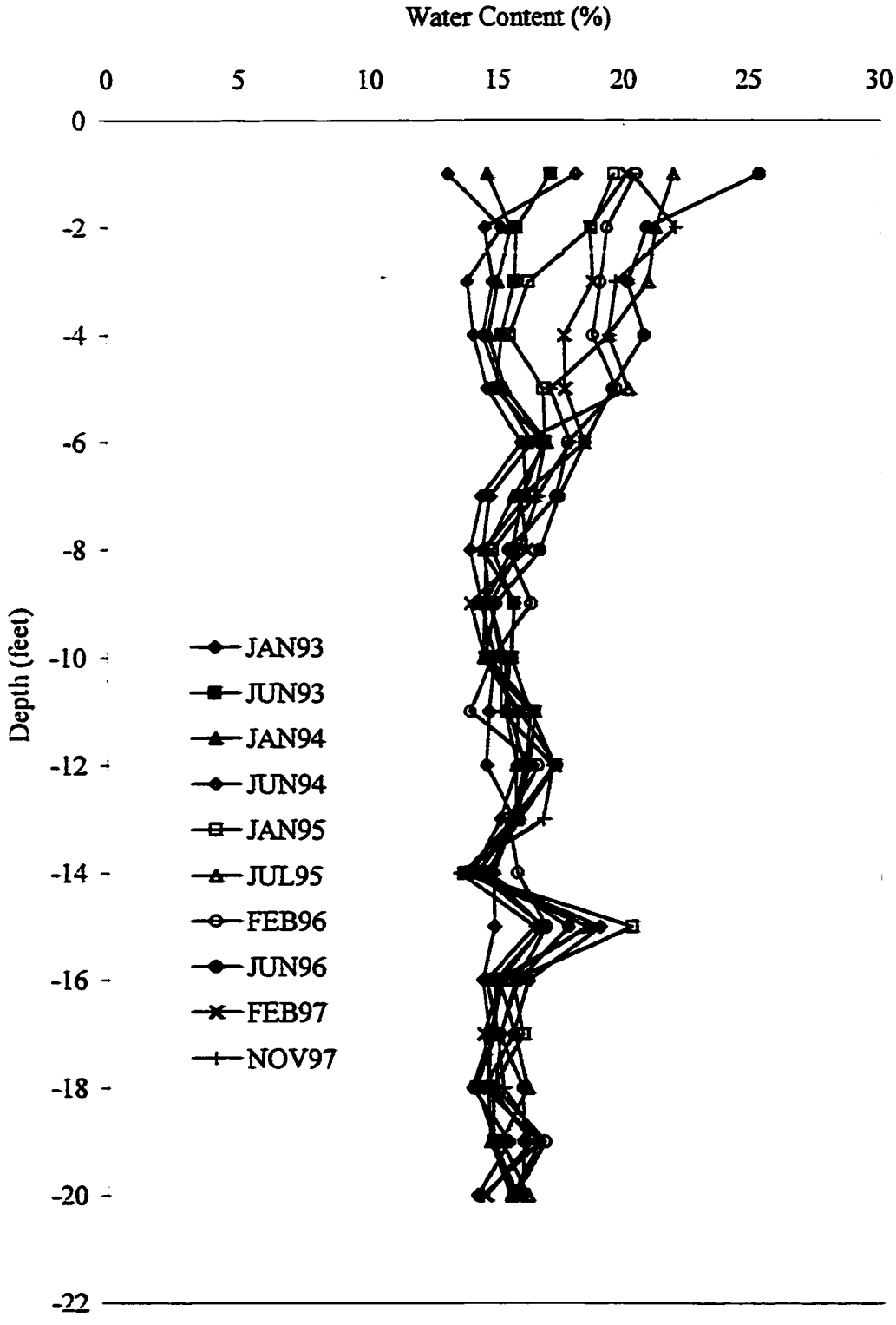

CSU Access Tube C-2.3

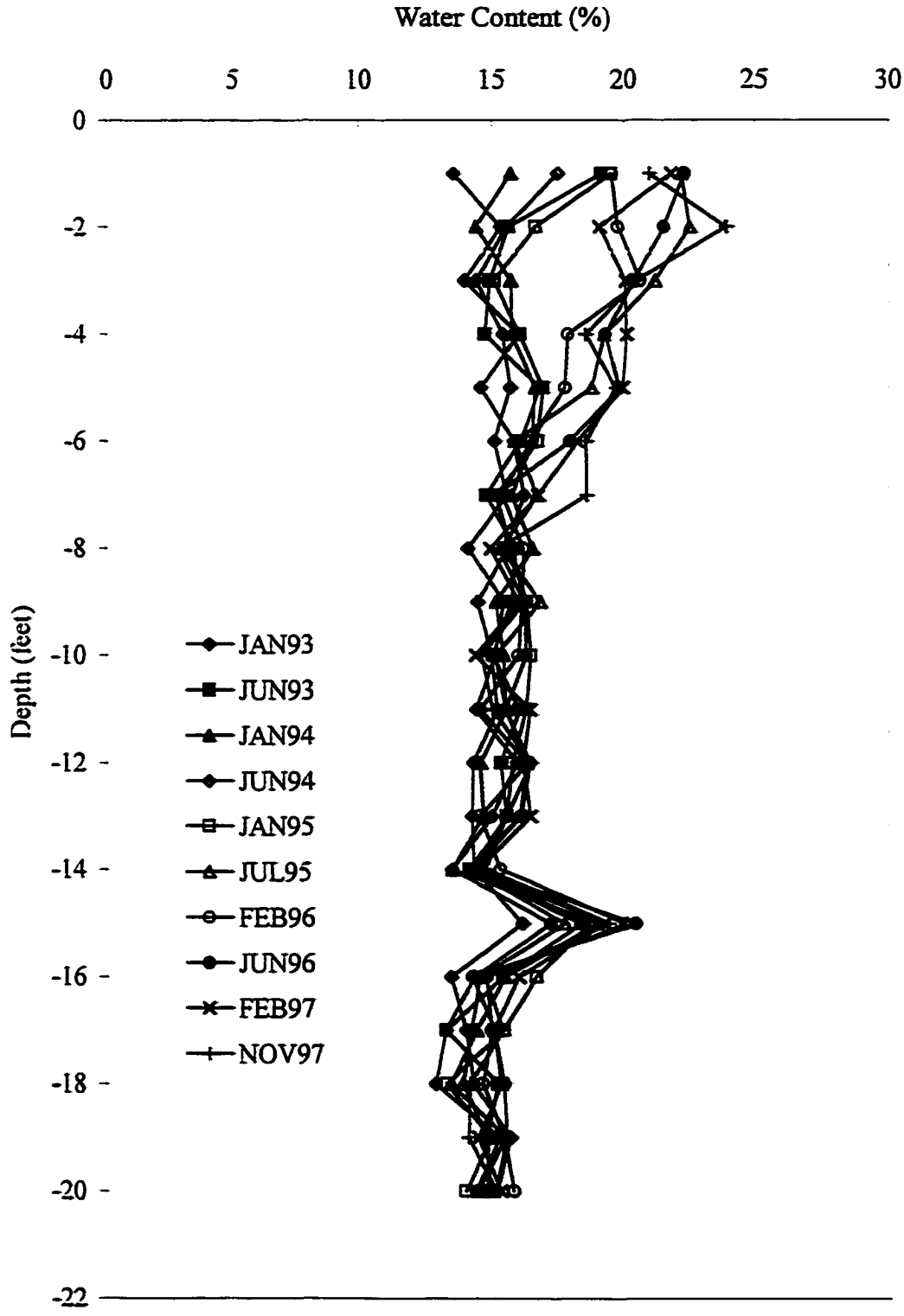

CSU Access Tube C-3

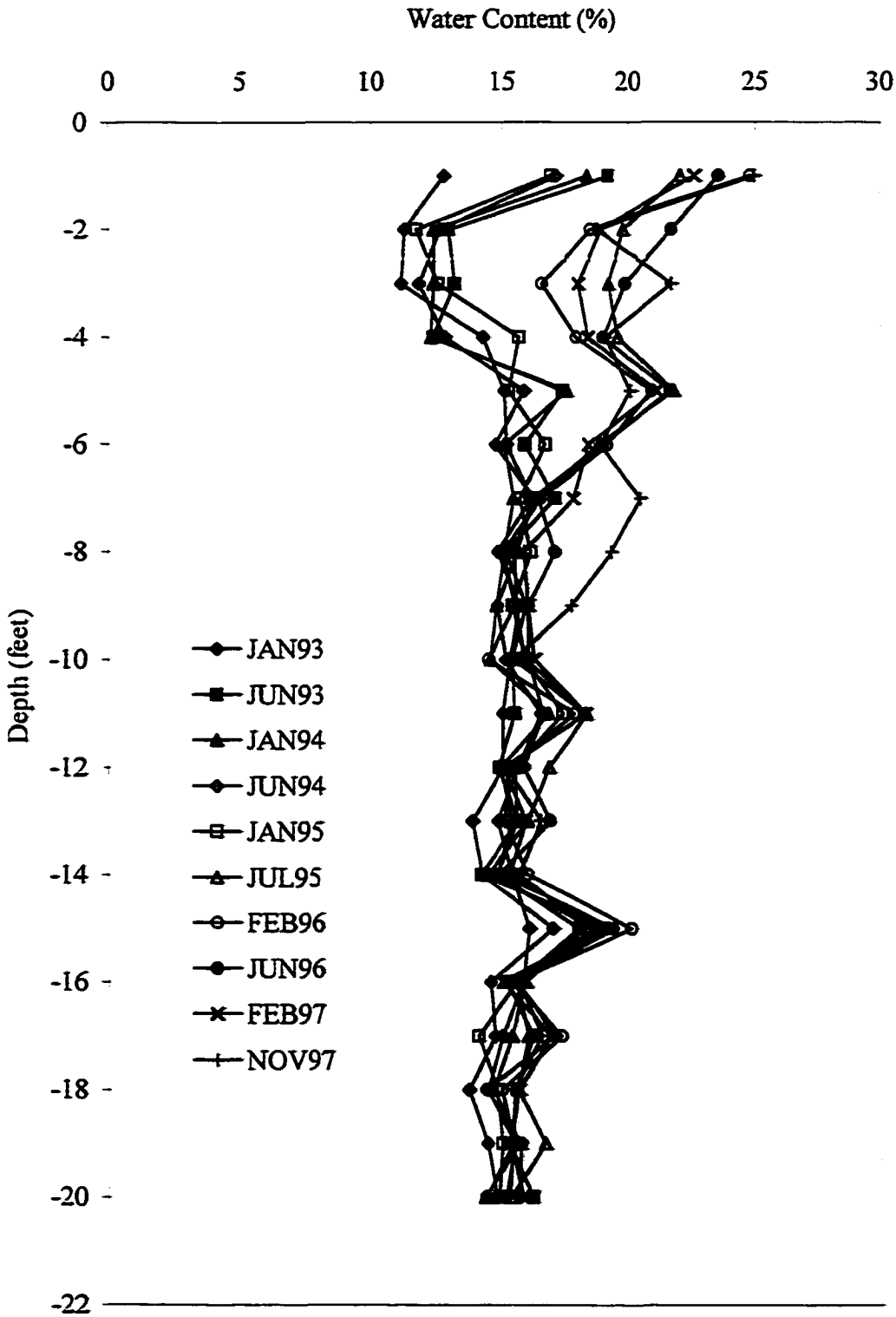

CSU Access Tube C-4

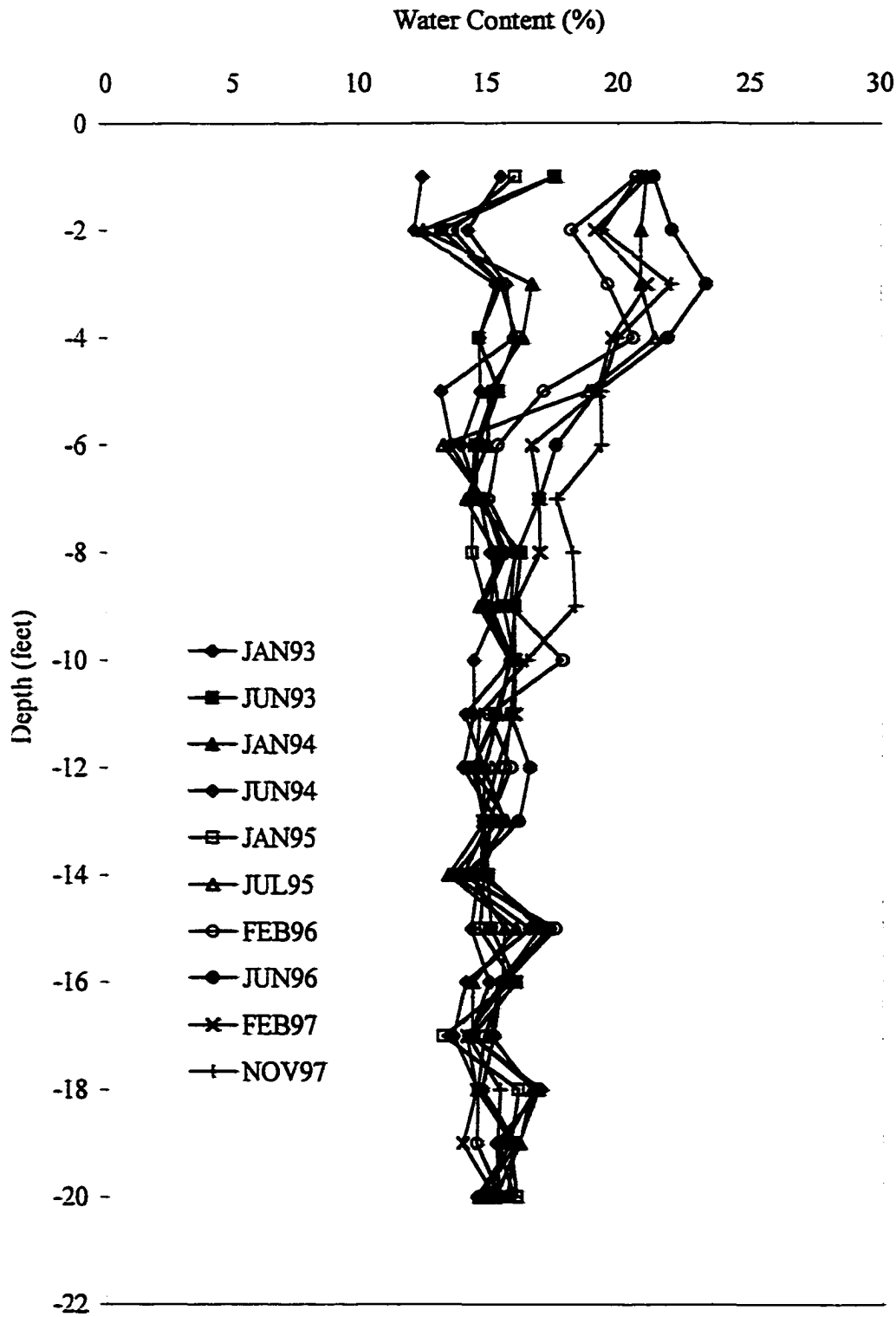

CSU Access Tube C-5

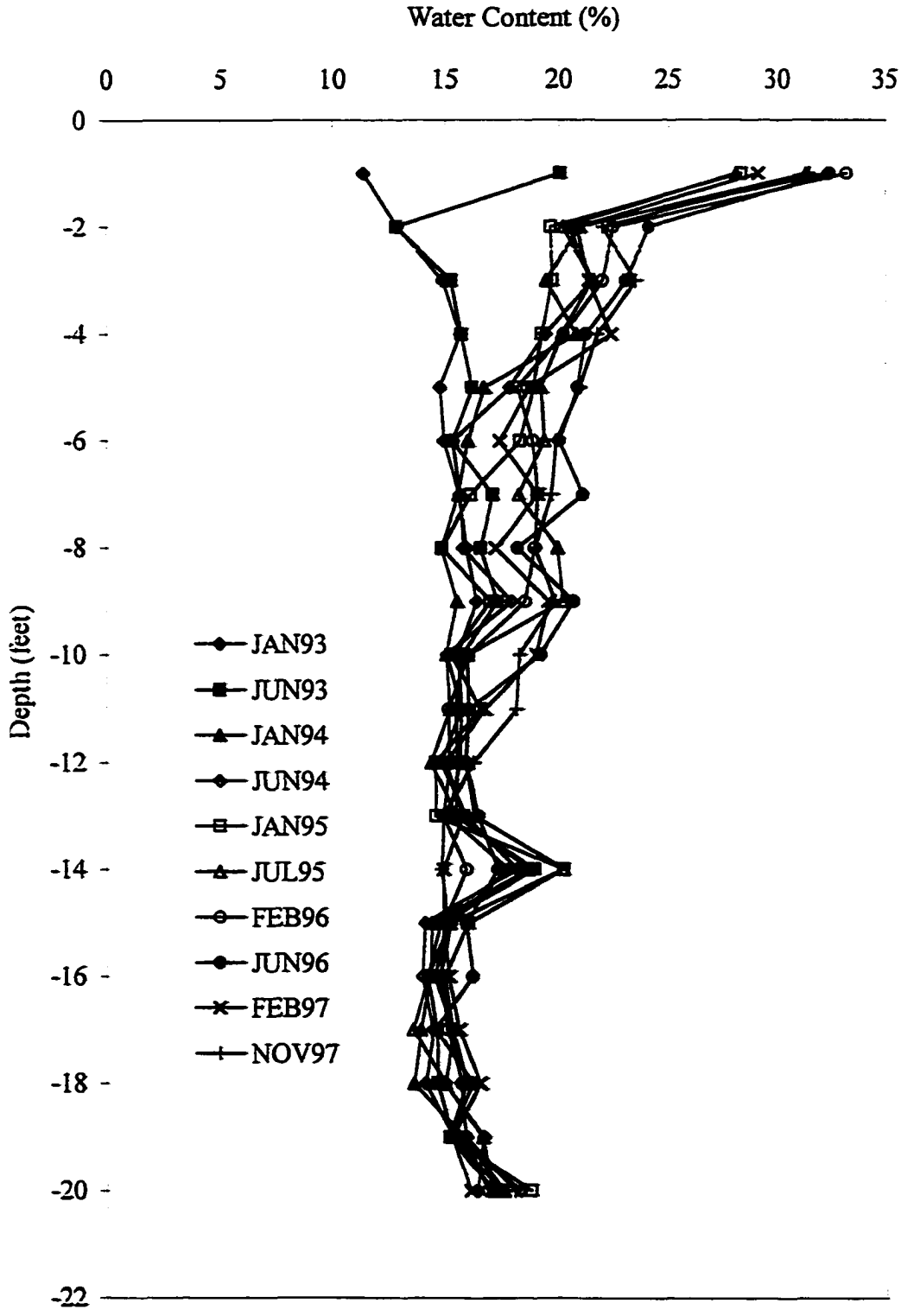

CSU Access Tube C-7

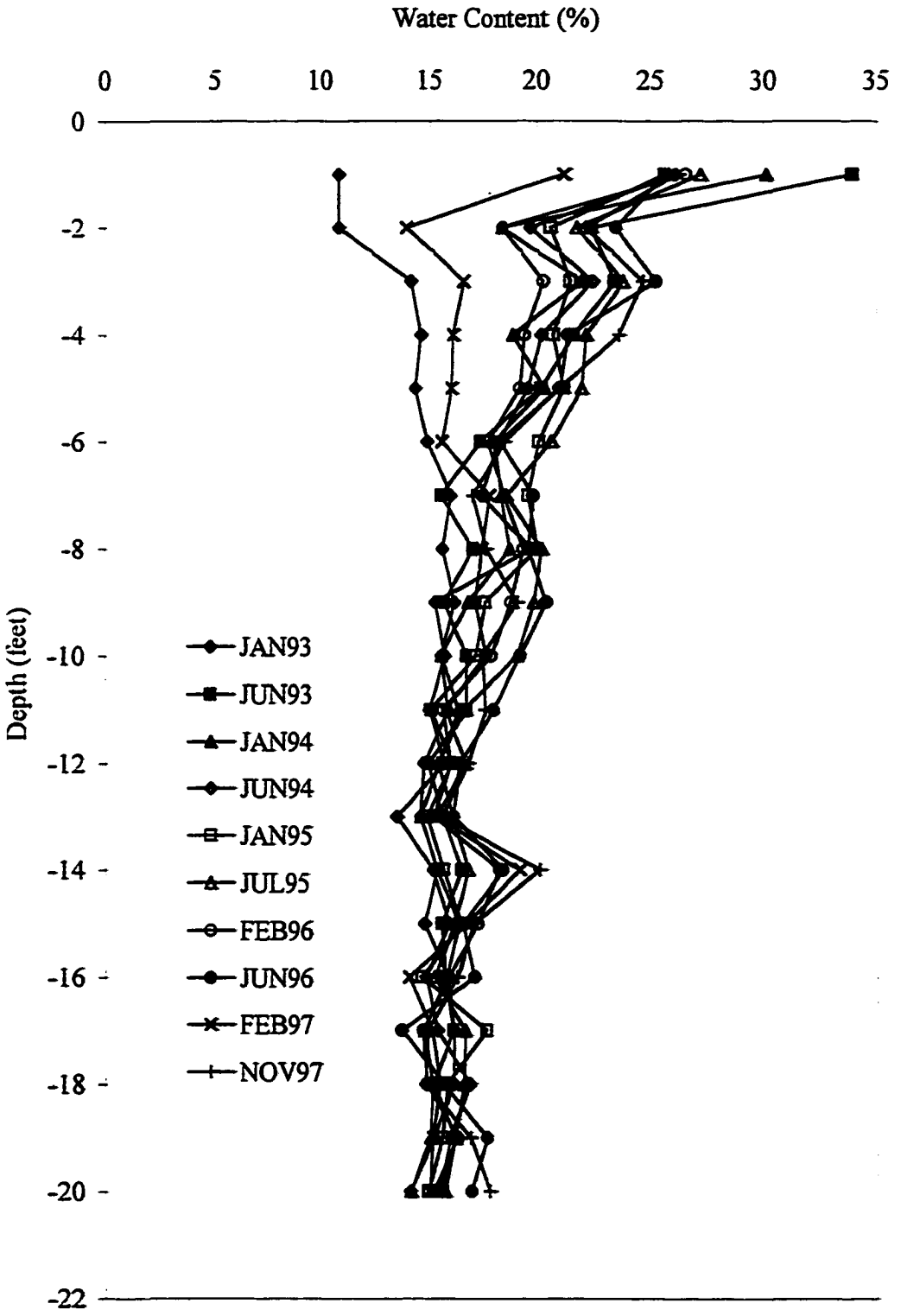

CSU Access Tube C-9

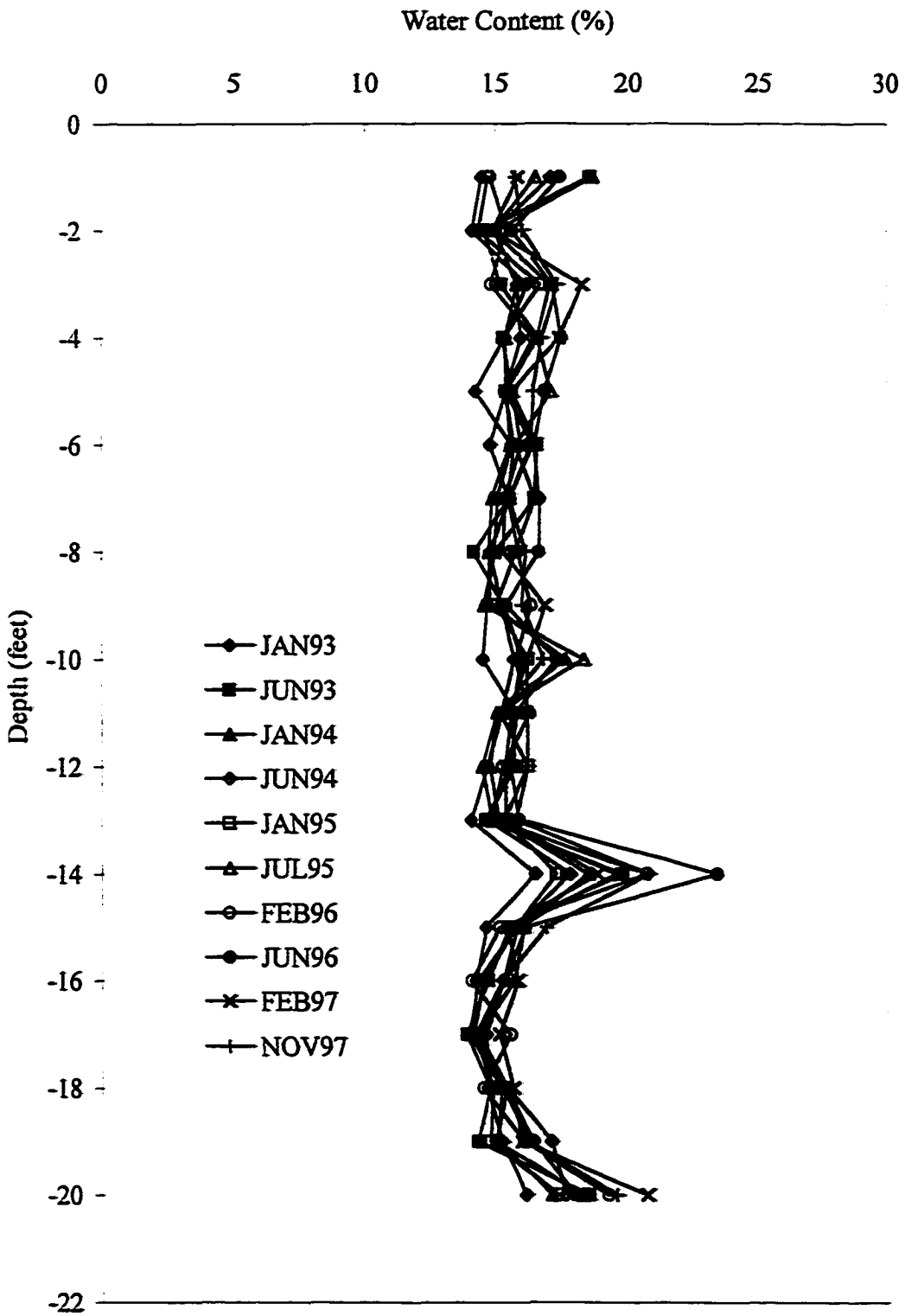

CSU Access Tube D-3

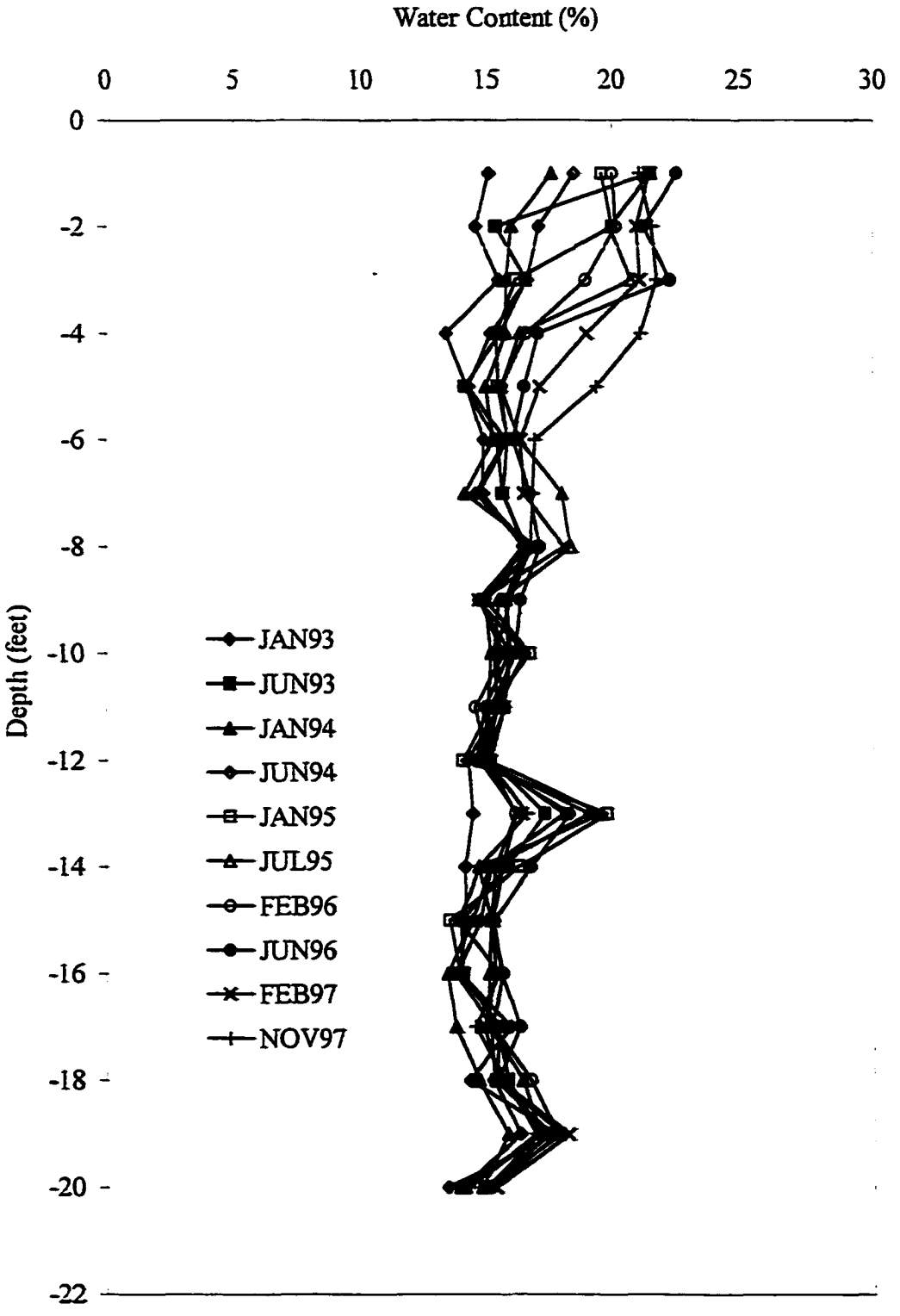

CSU Access Tube D-5

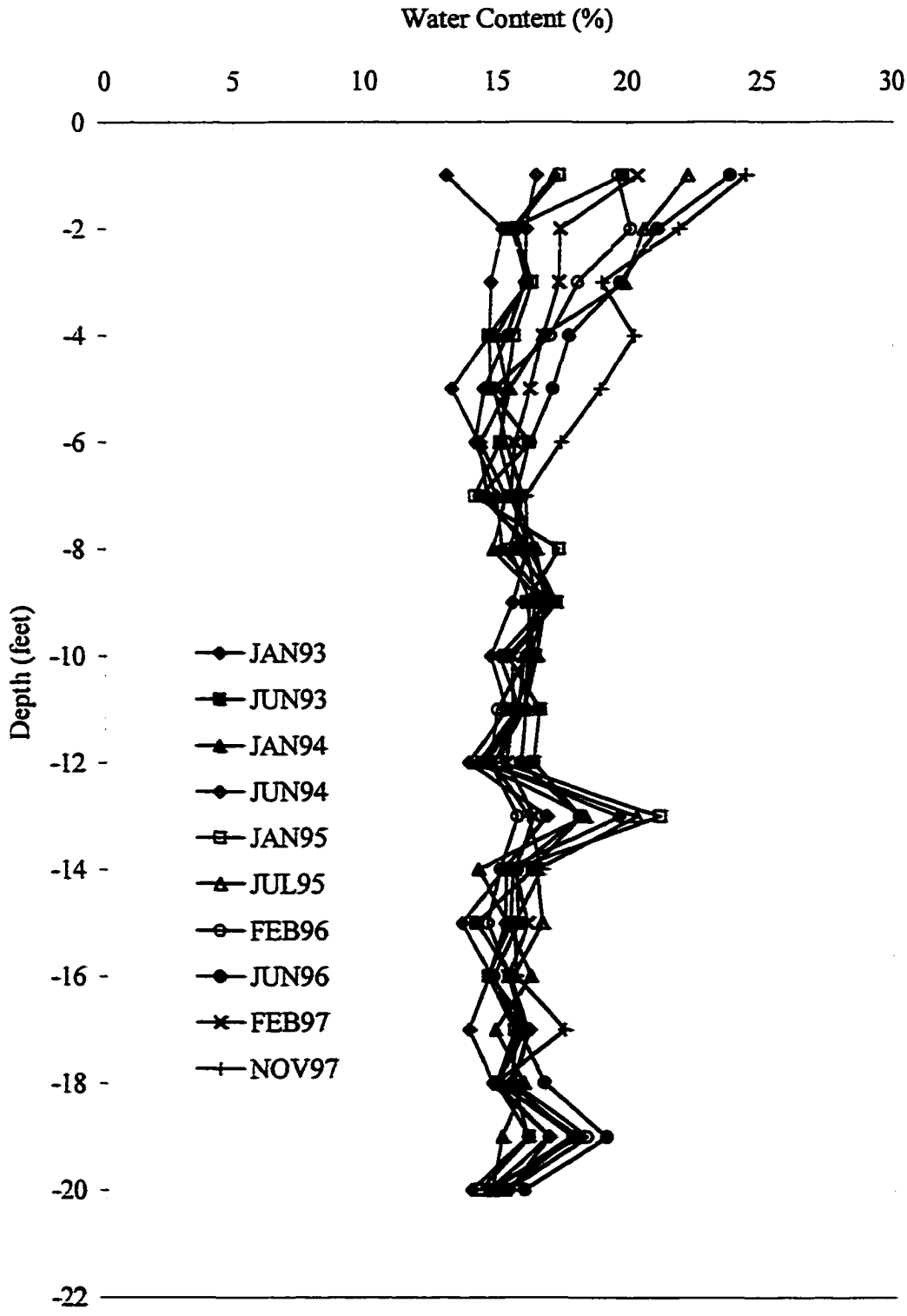

CSU Access Tube E-1

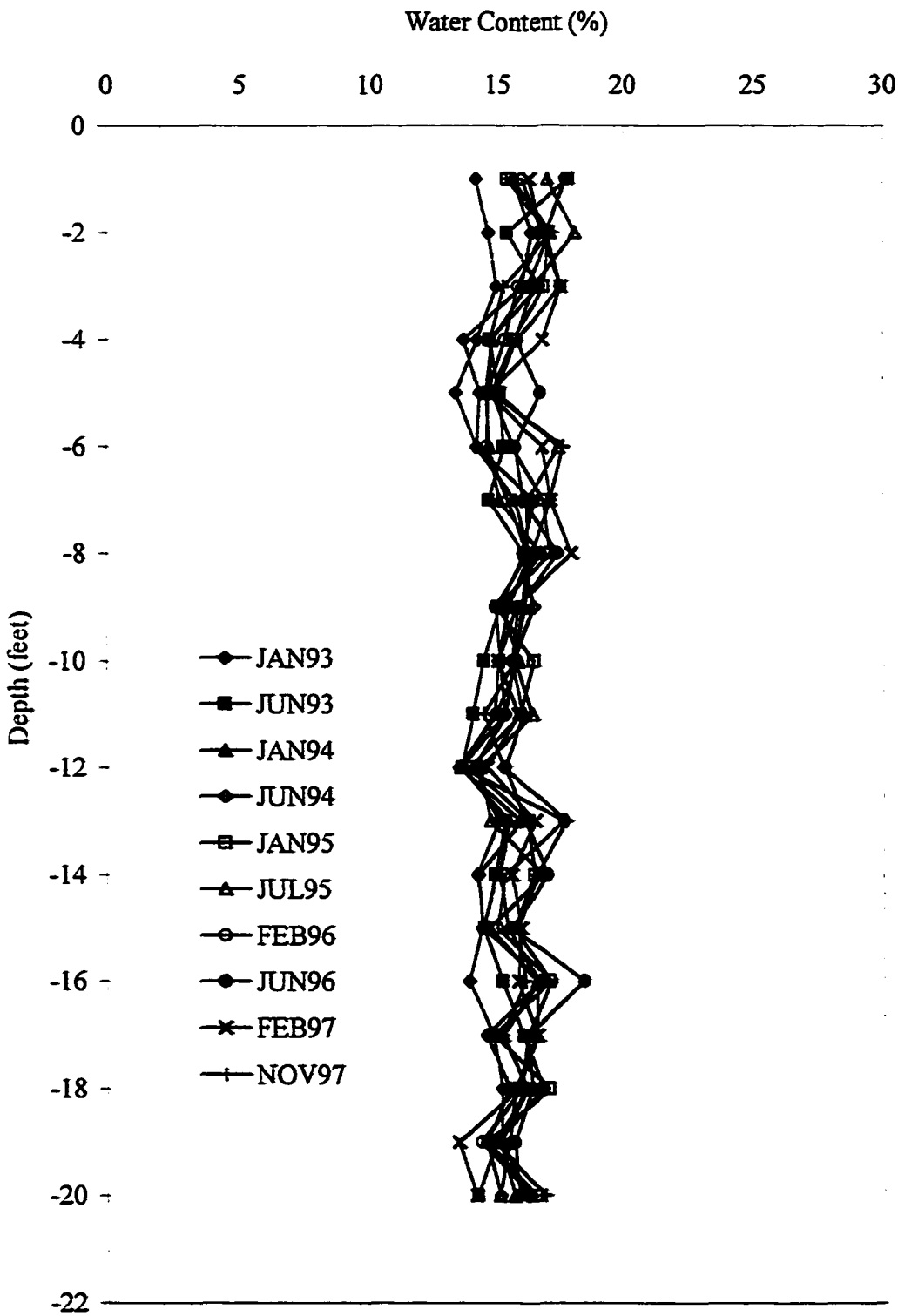

CSU Access Tube E-3

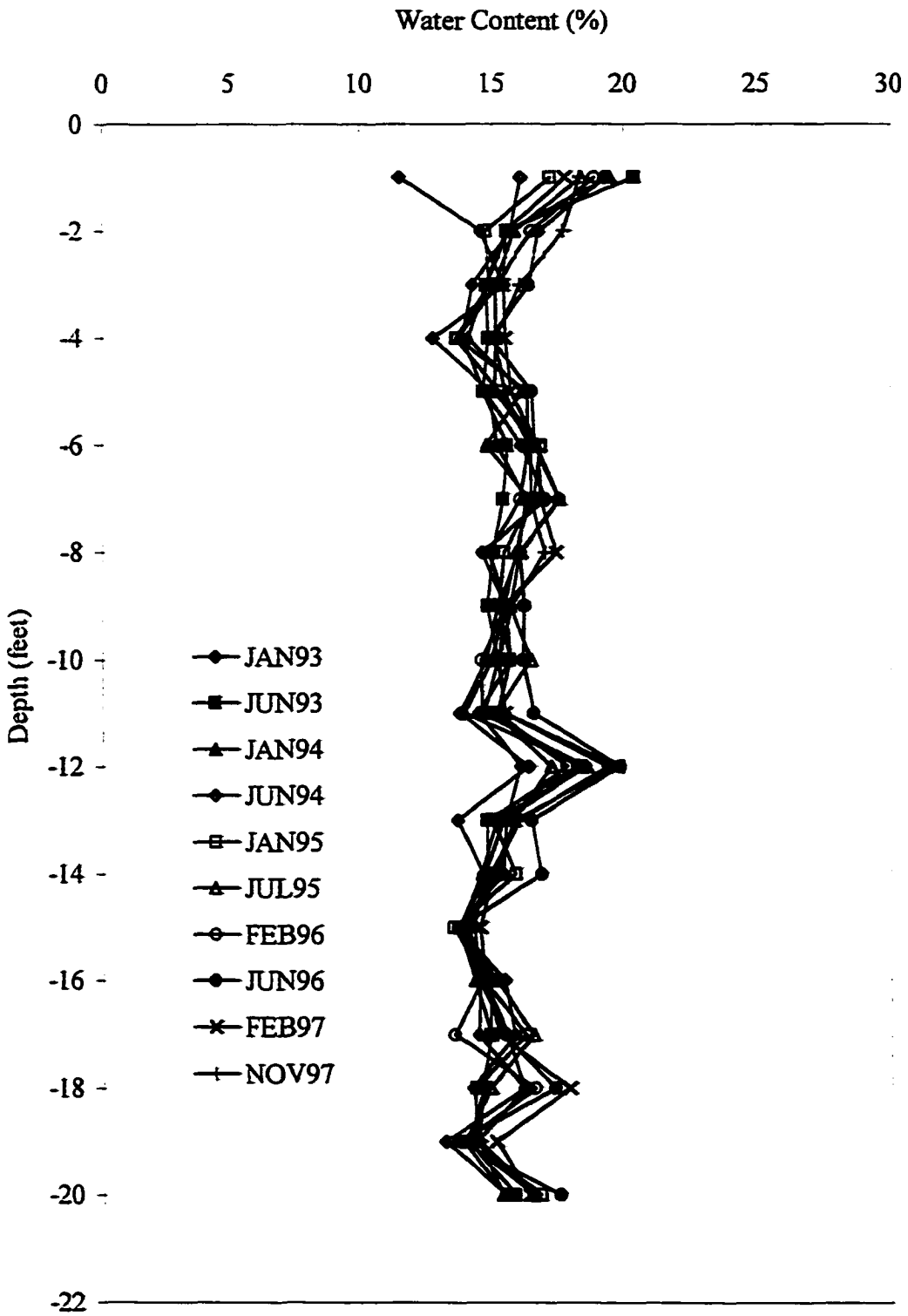

CSU Access Tube E-5

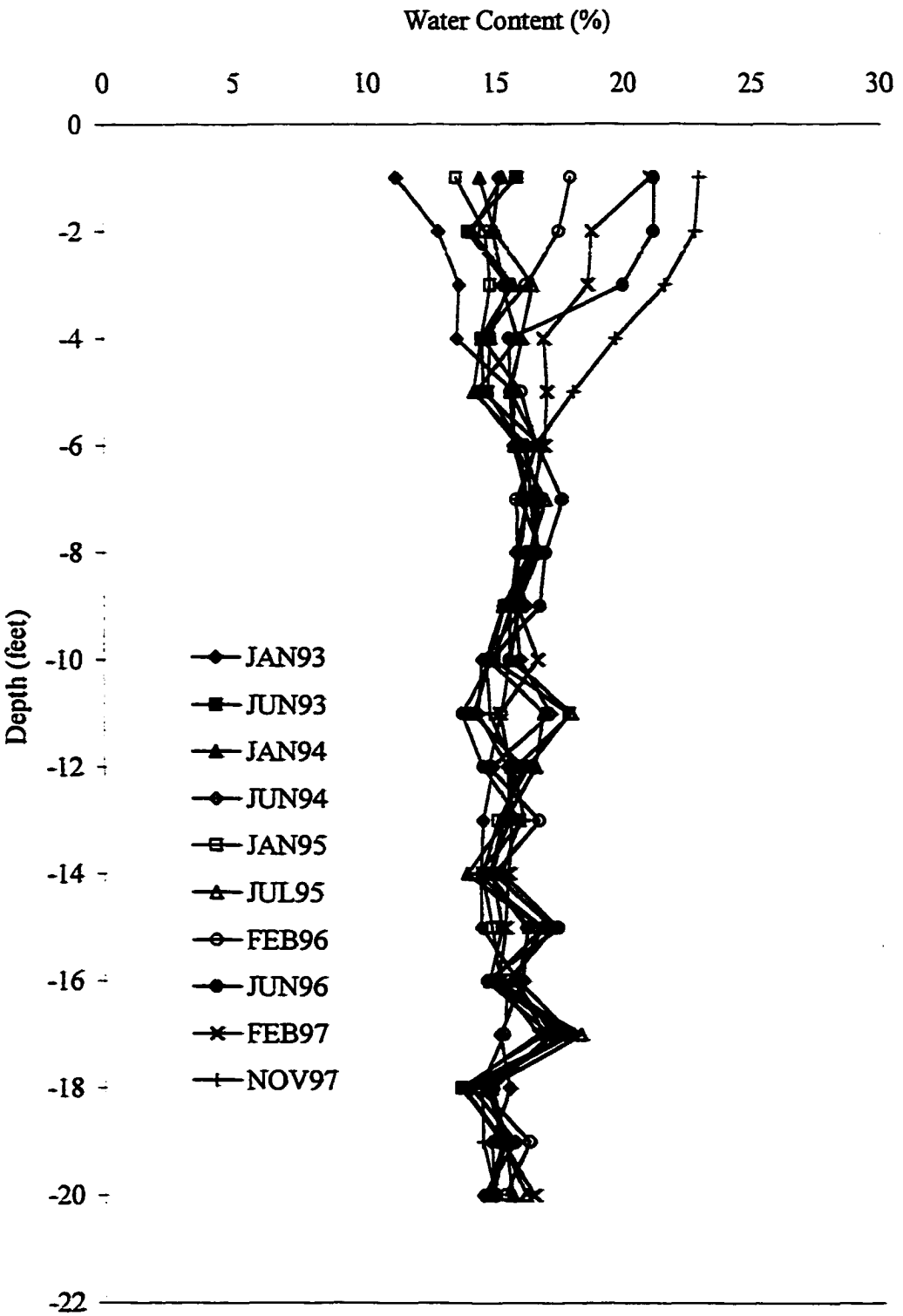

CSU Access Tube E-7

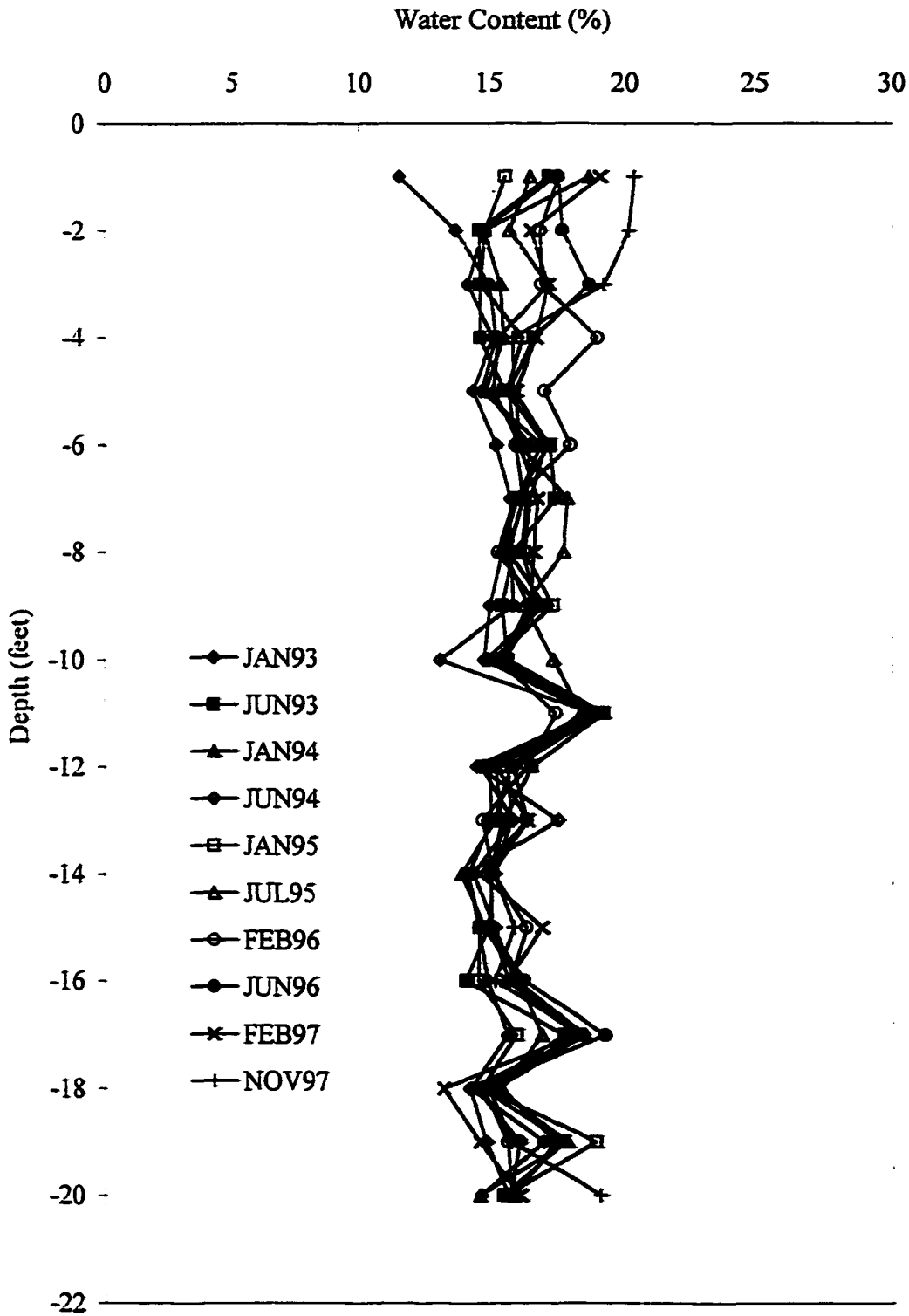

CSU Access Tube E-8

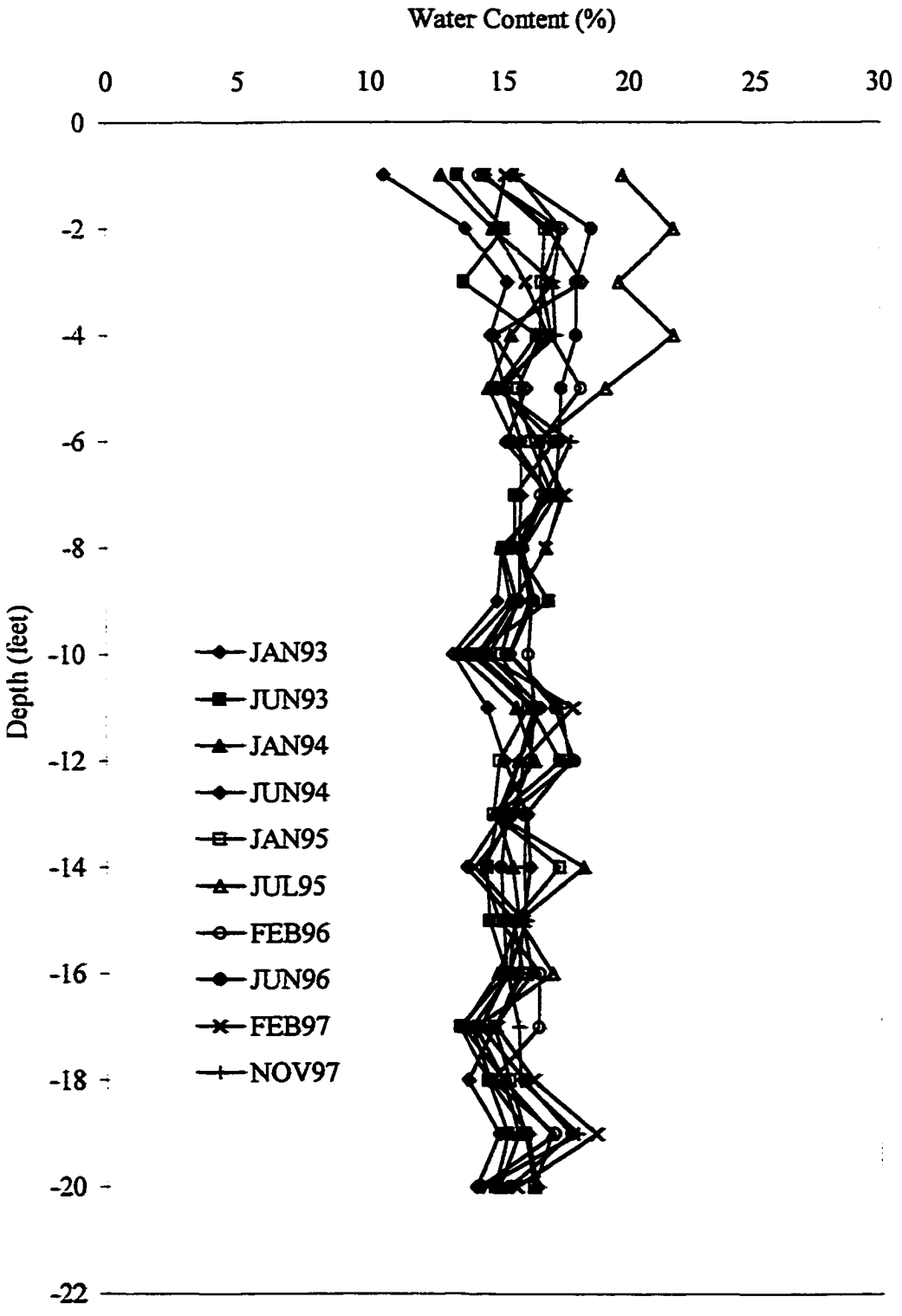

CSU Access Tube E-9

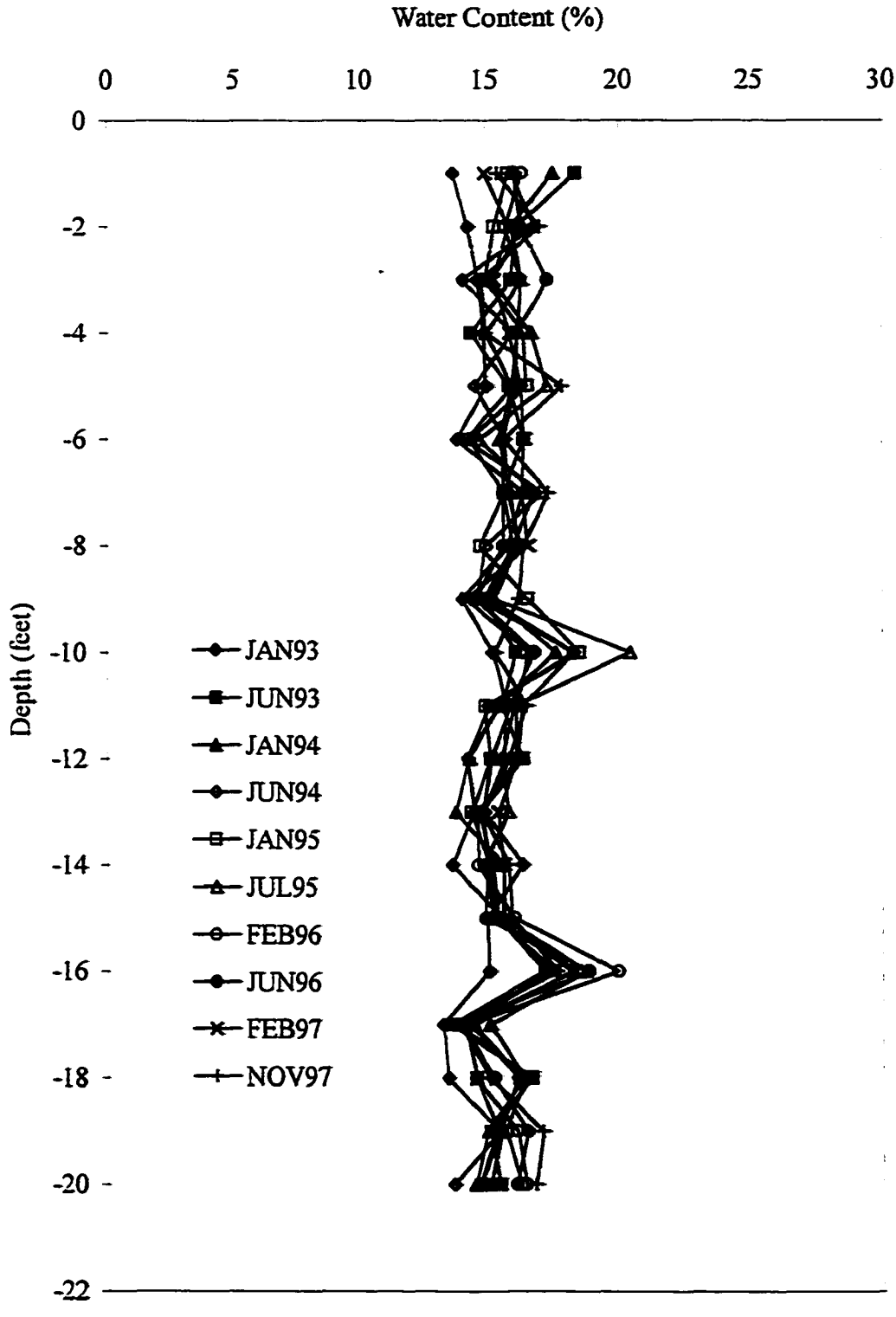

CSU Access Tube F-5

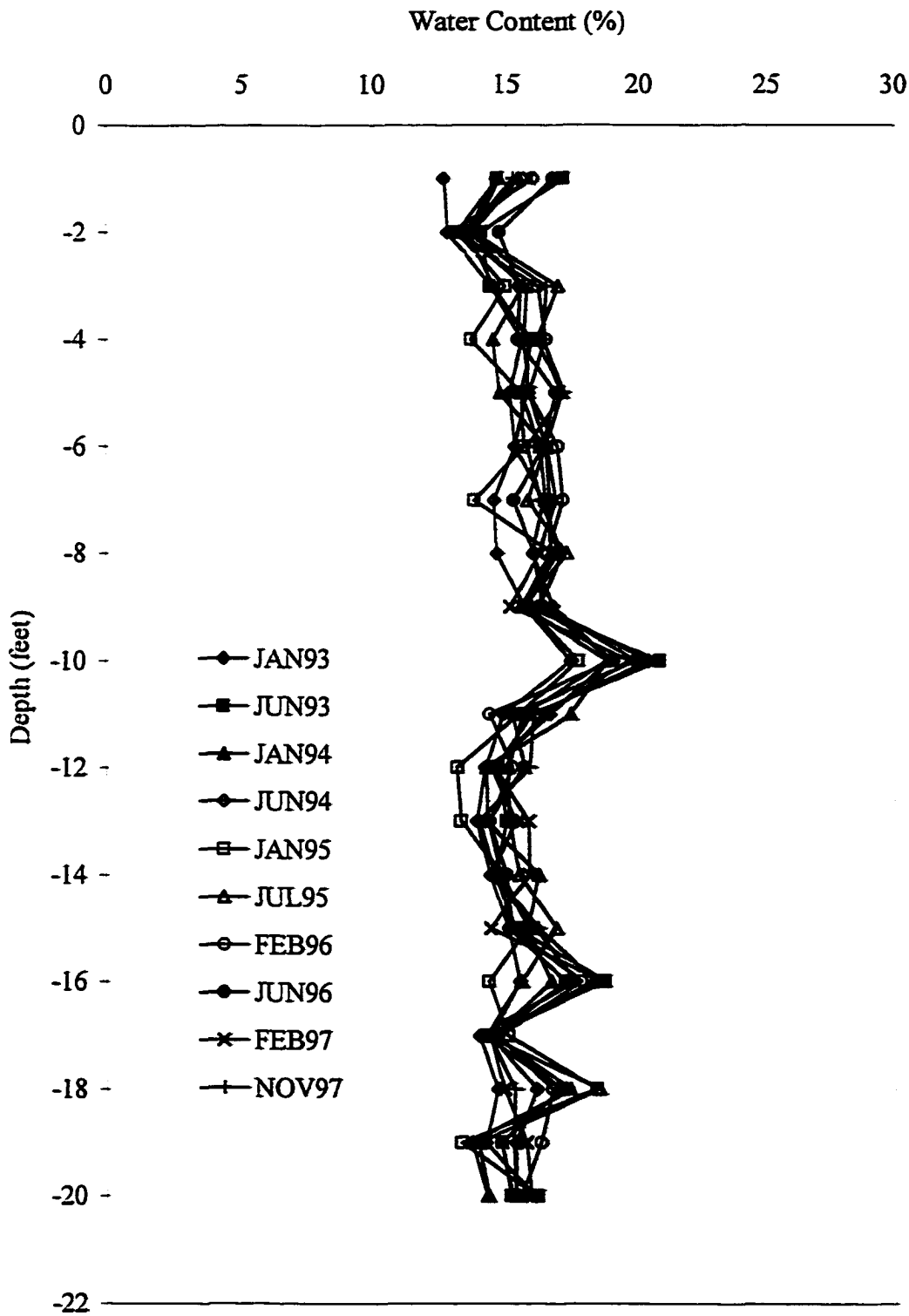

CSU Access Tube F-7

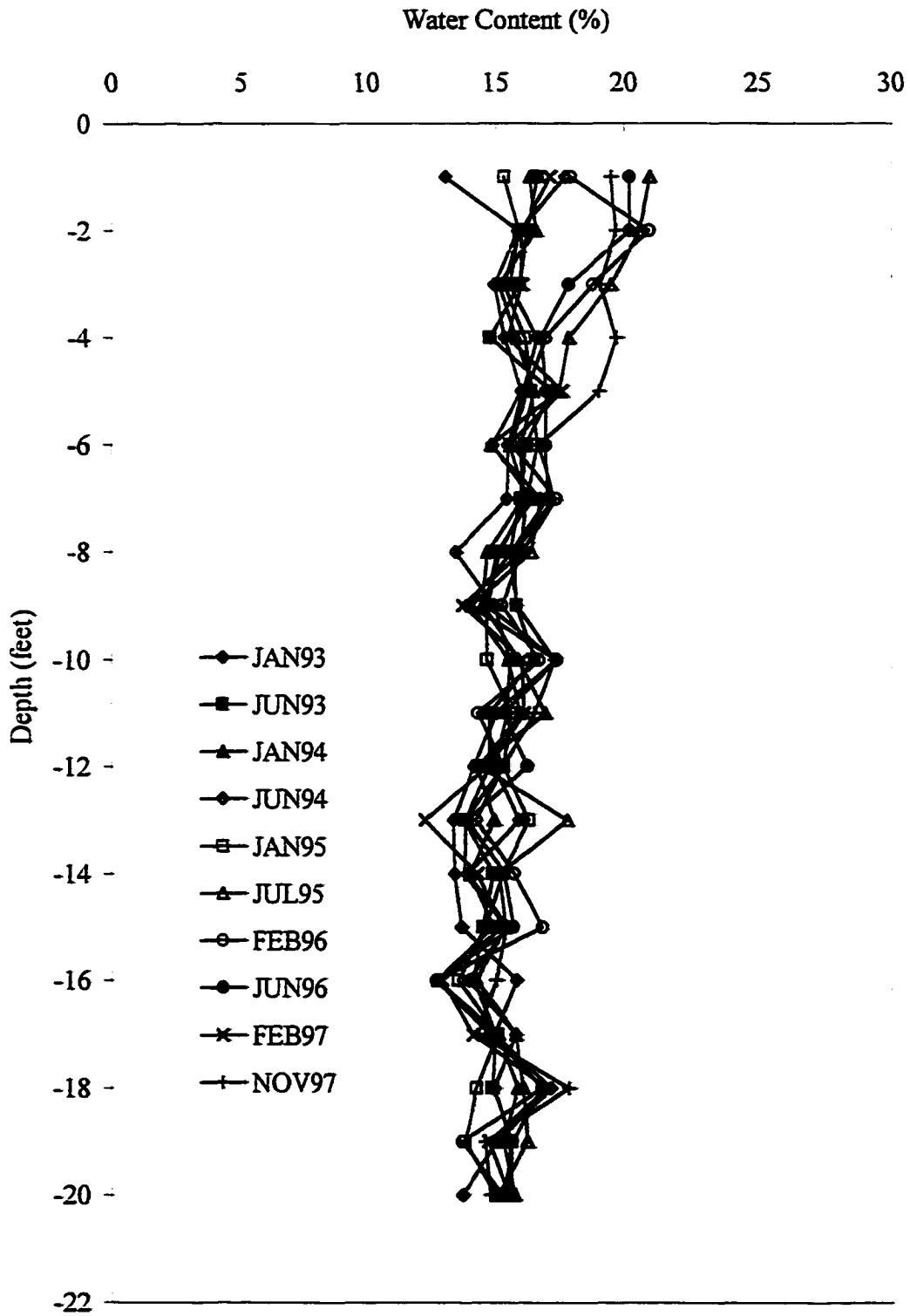

CSU Access Tube G-1

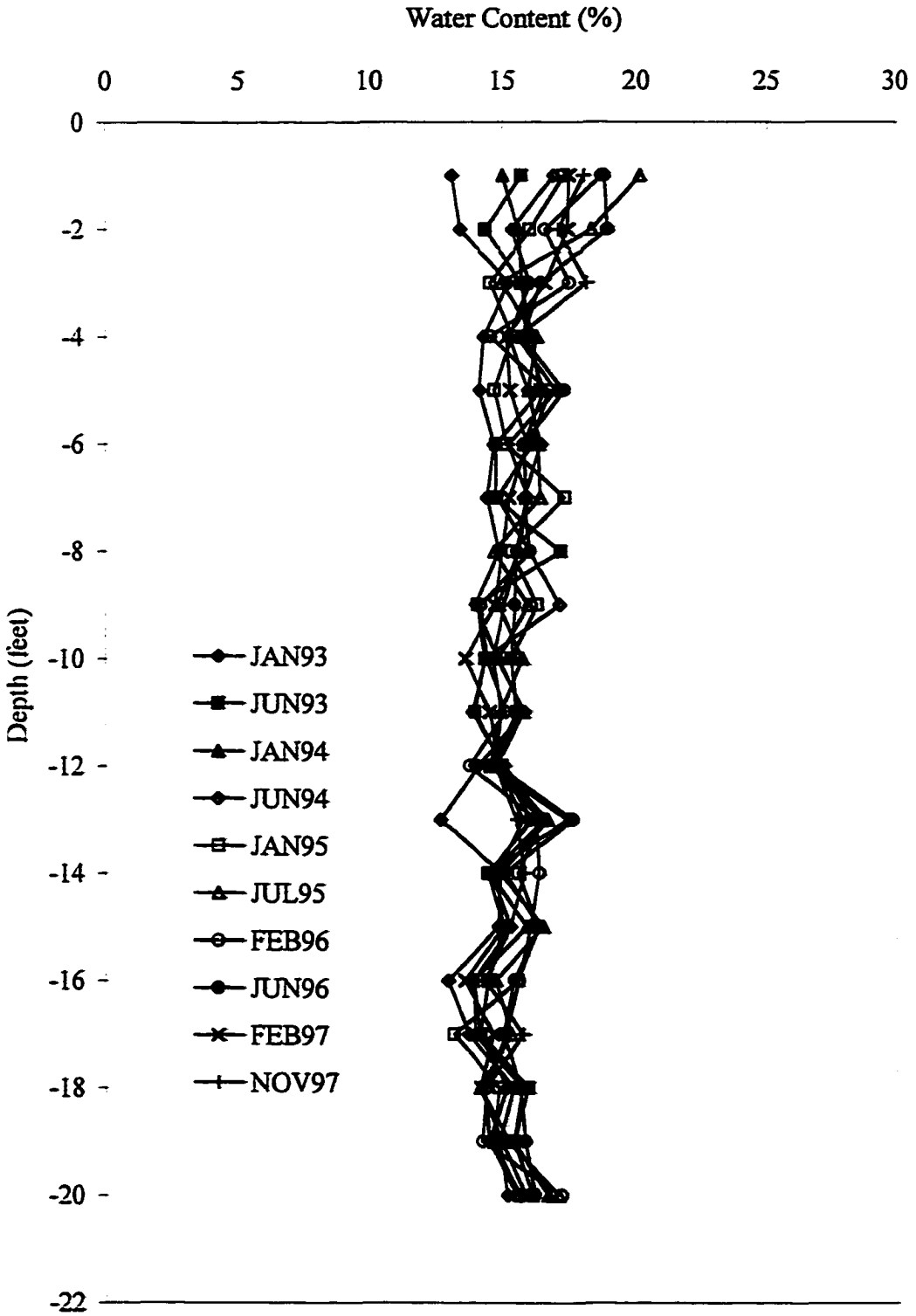

CSU Access Tube G-3

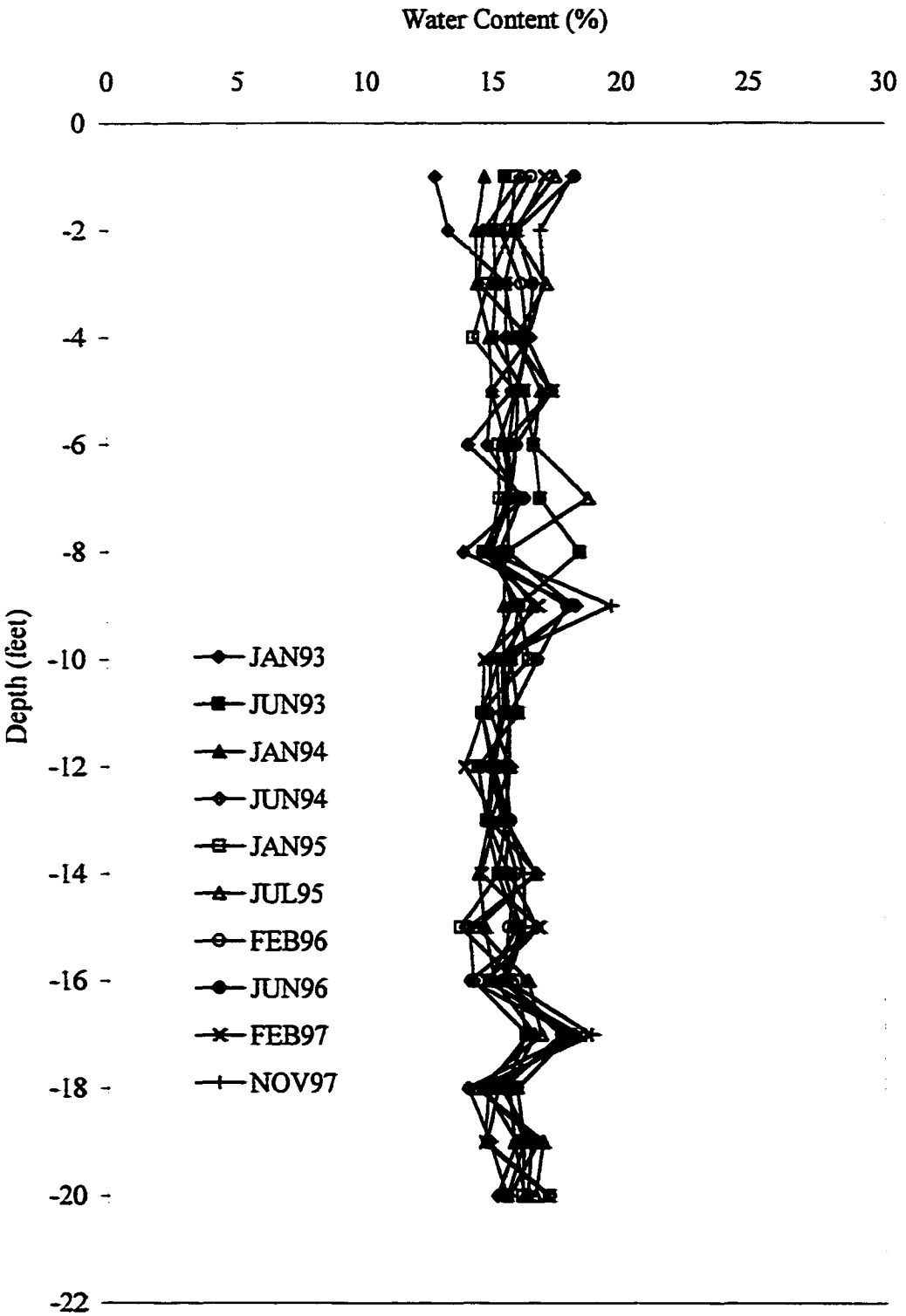

CSU Access Tube G-5

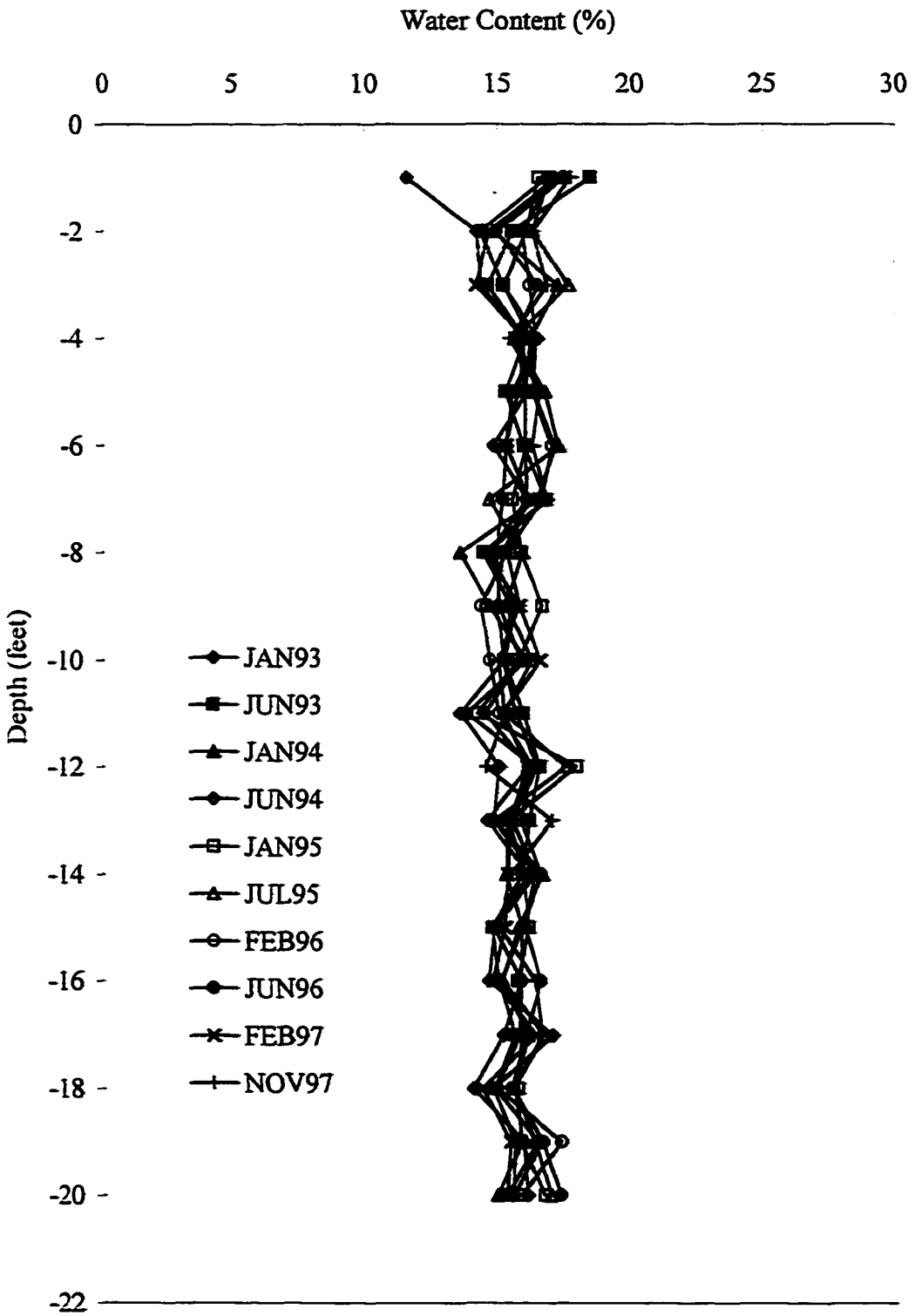

CSU Access Tube G-6

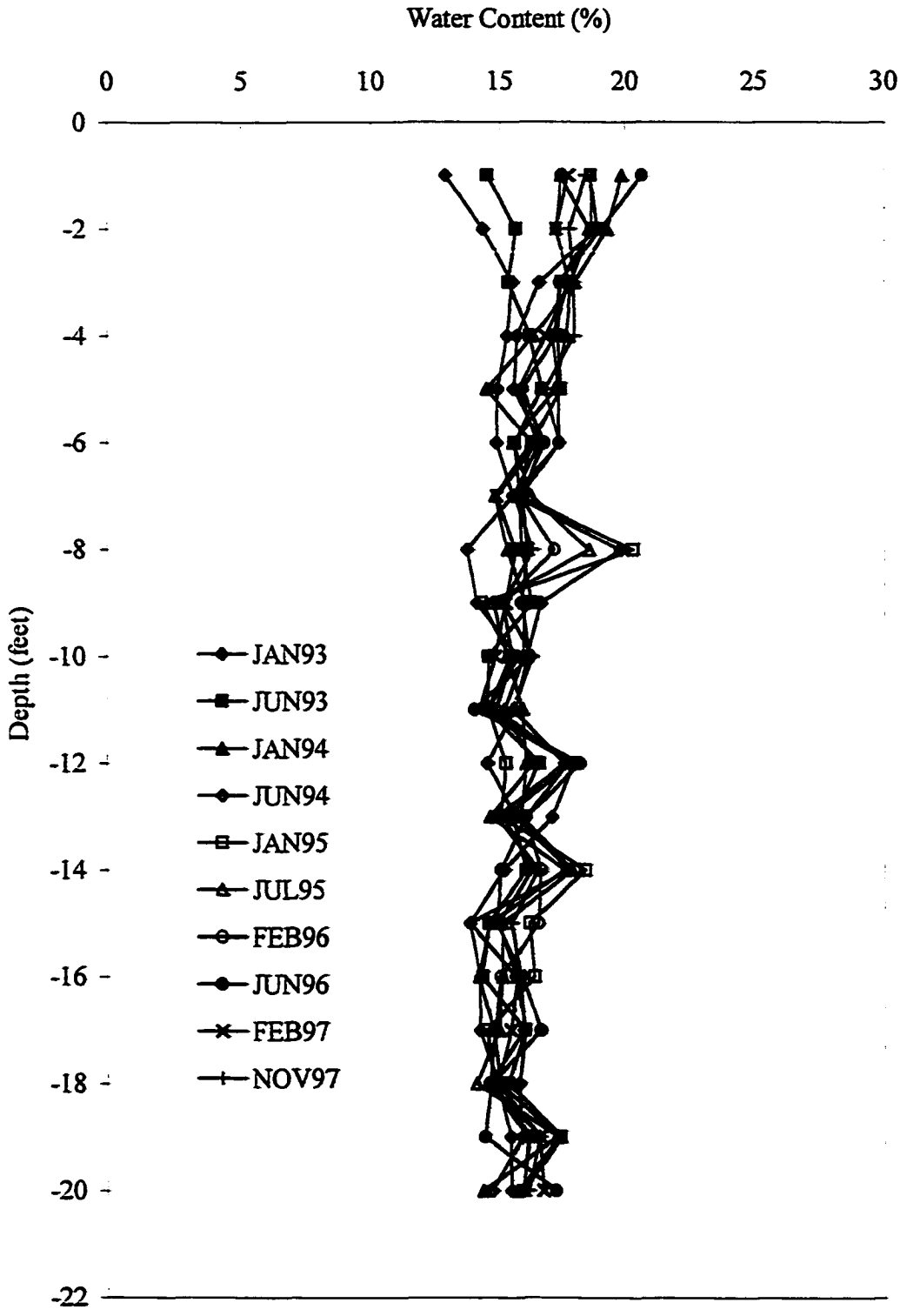

CSU Access Tube G-7

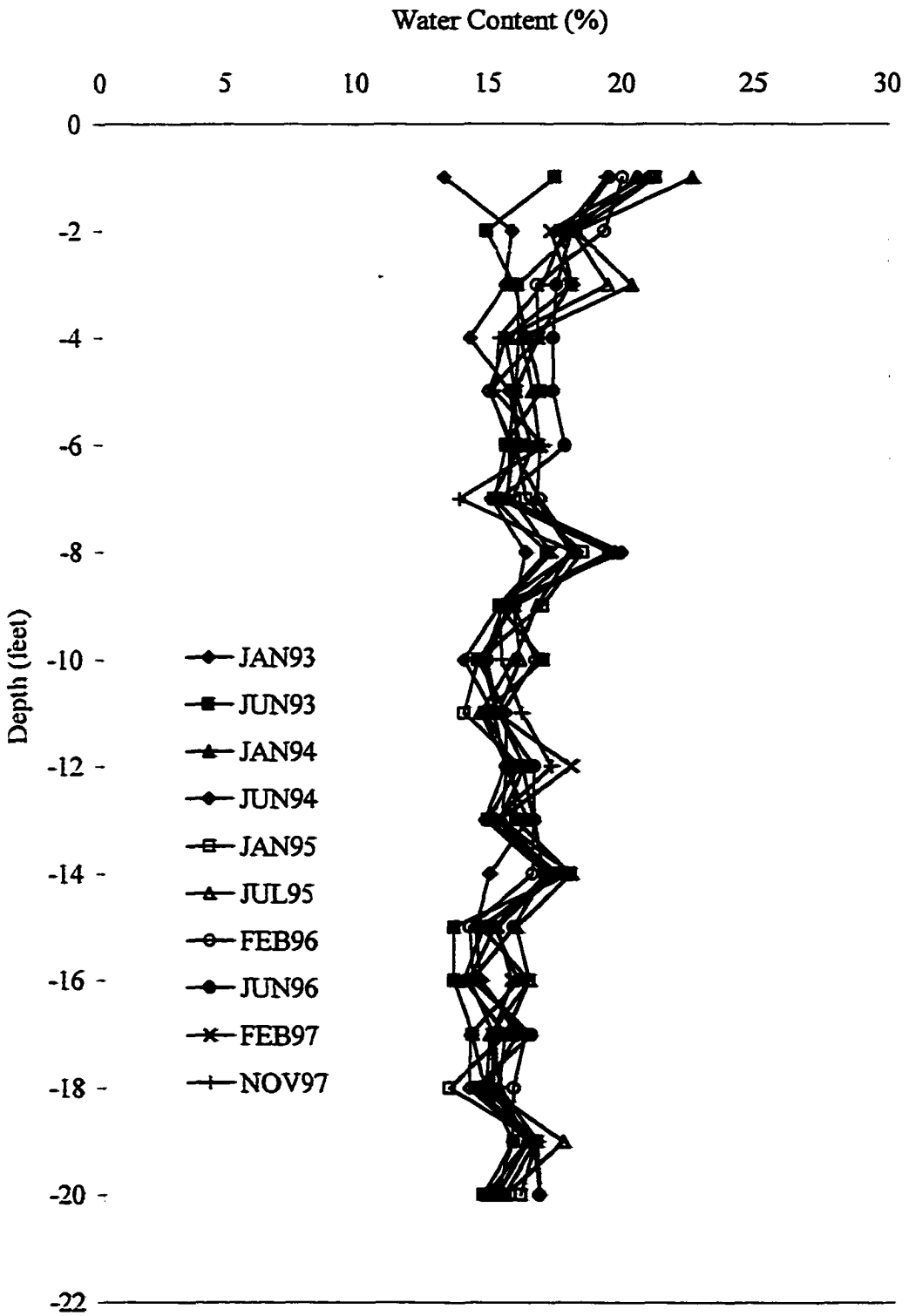

CSU Access Tube G-7.6

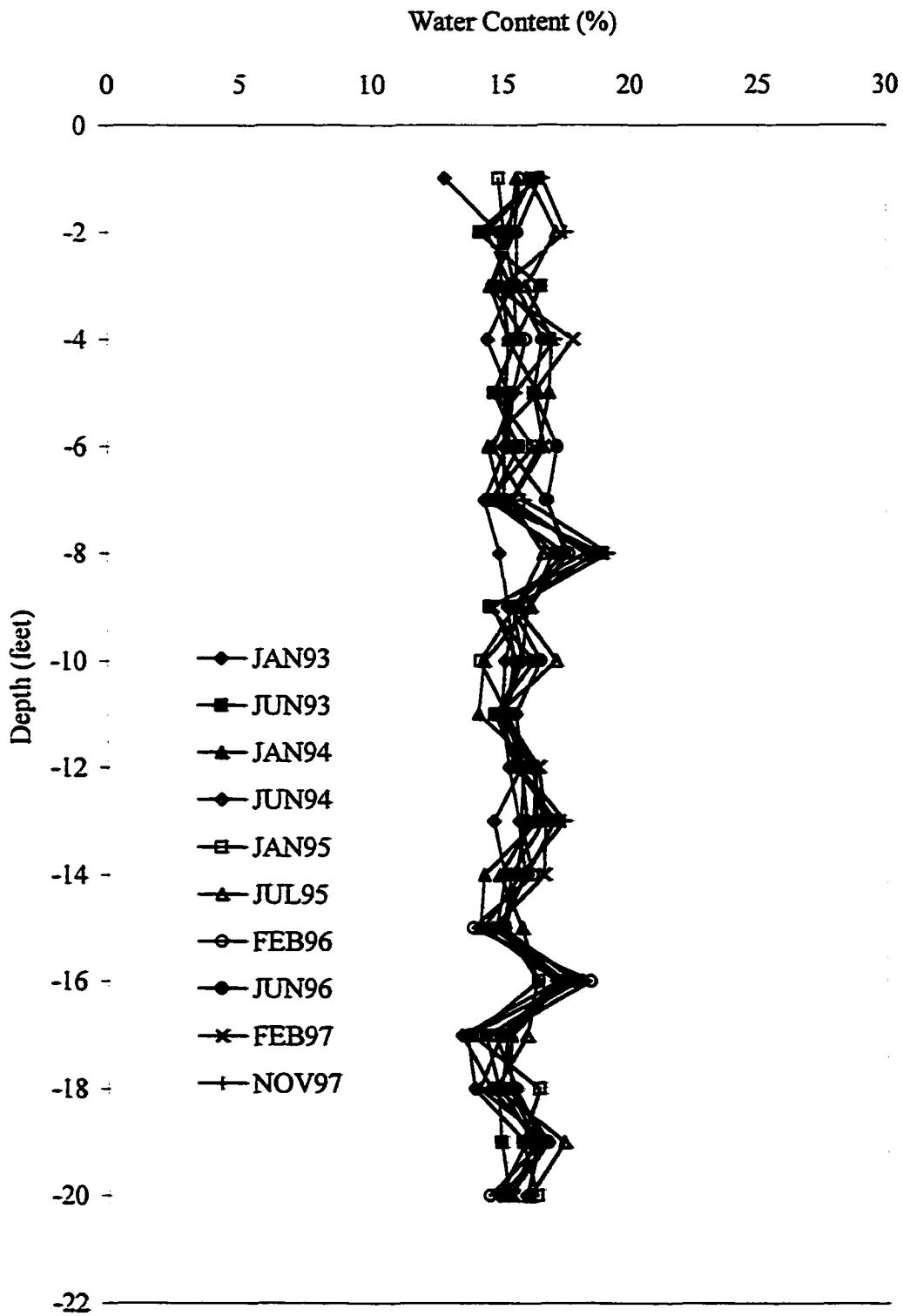

CSU Access Tube G-8.3

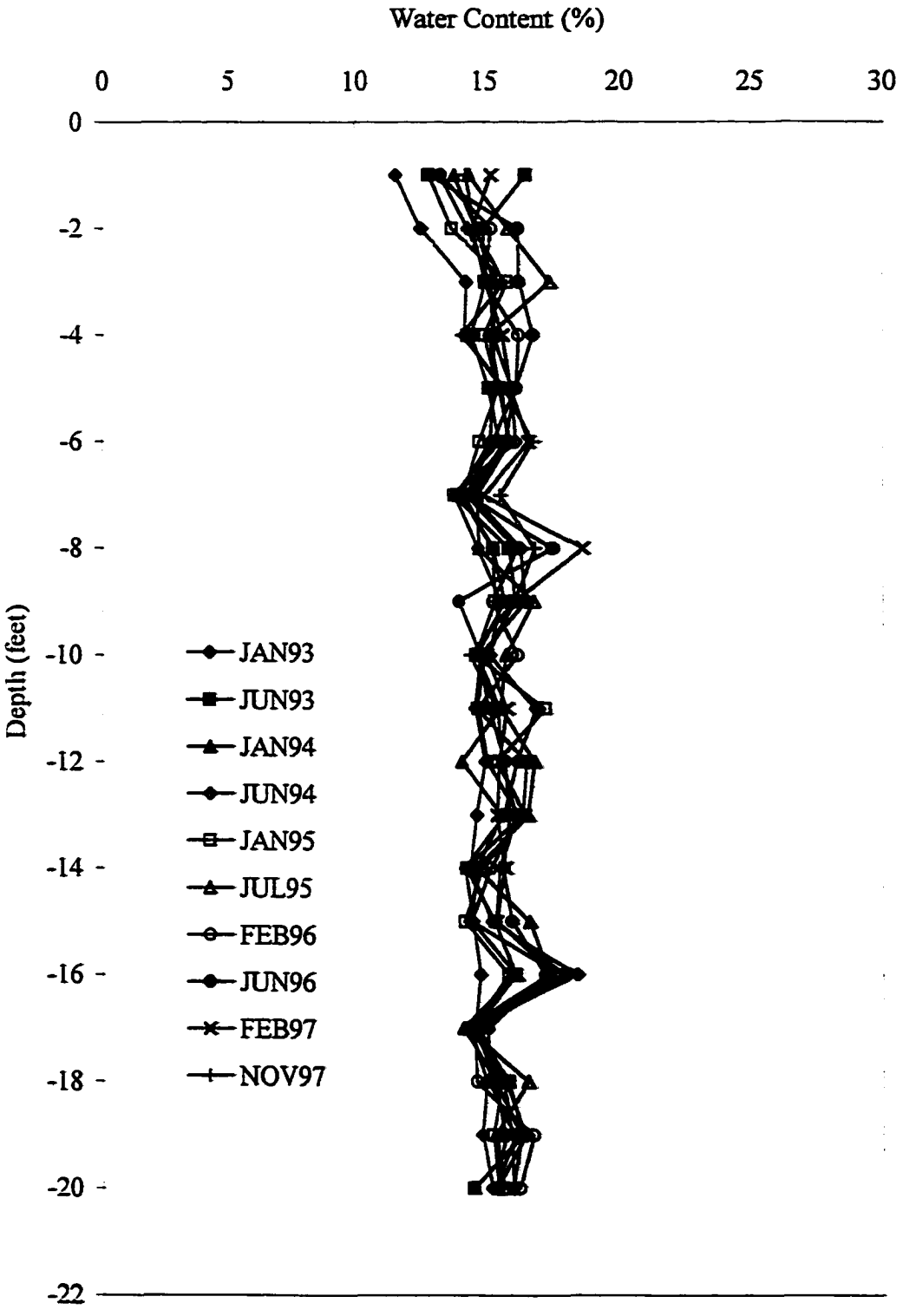

CSU Access Tube G-9

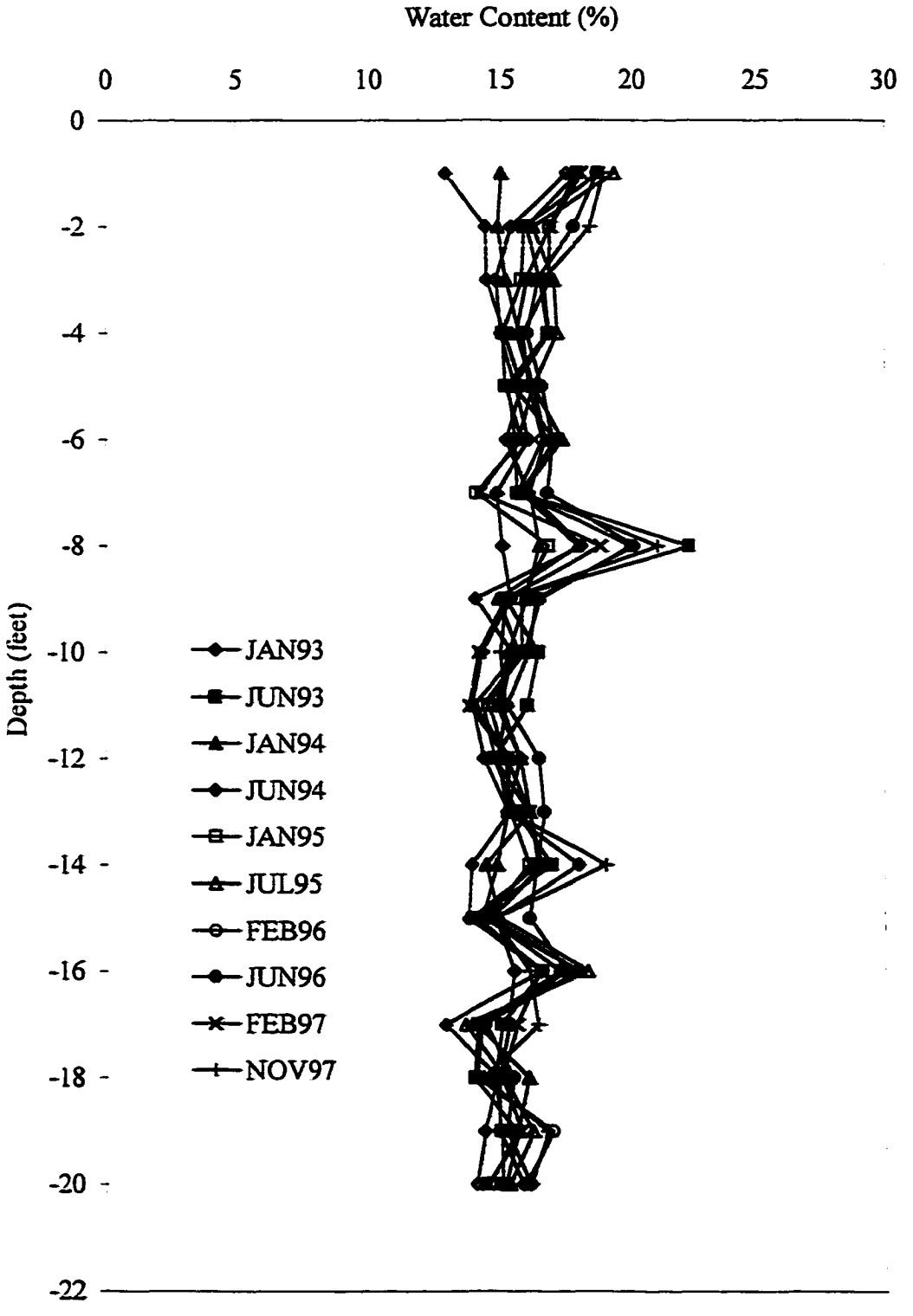

CSU Access Tube G.5-5

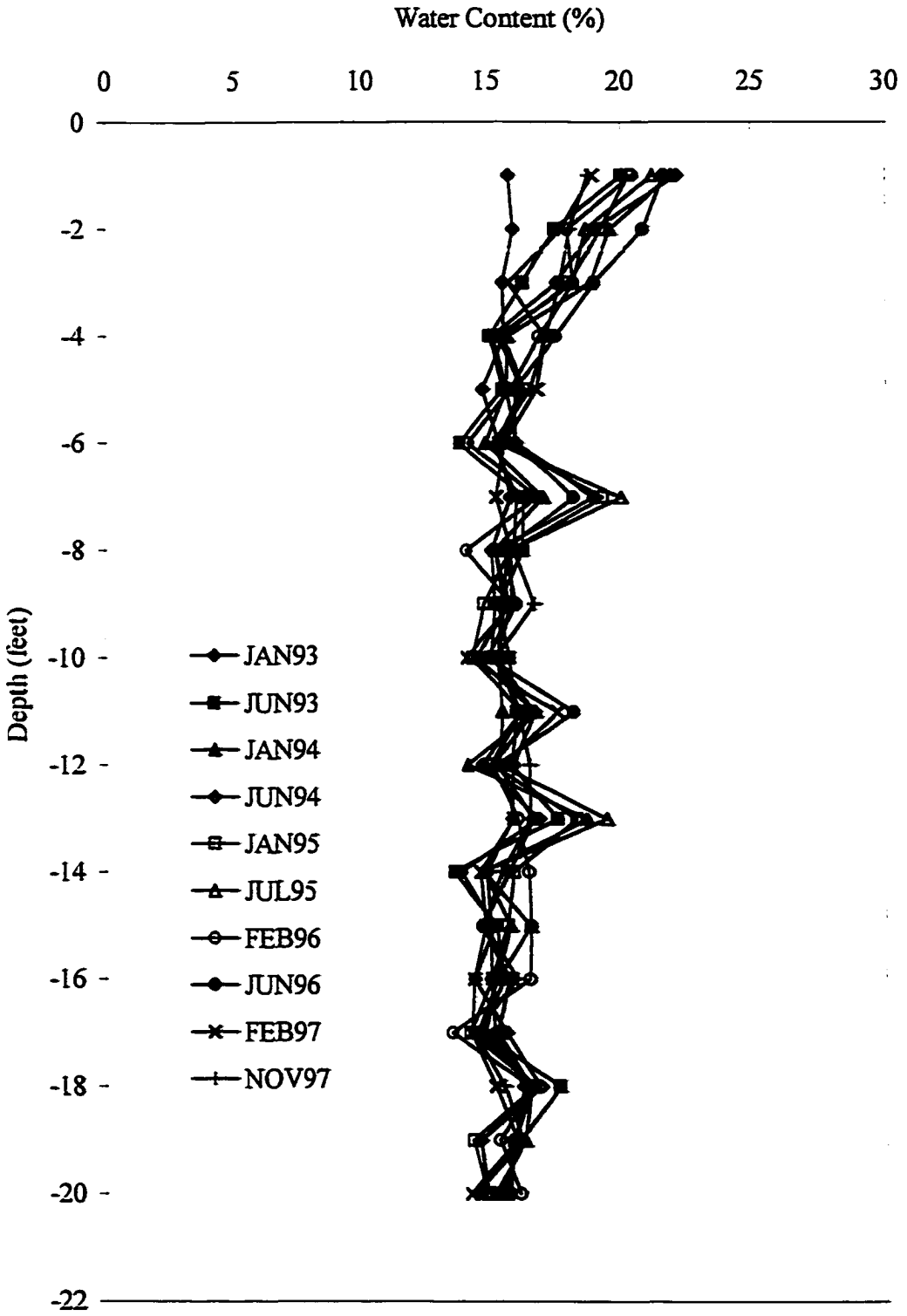

CSU Access Tube G.5-7

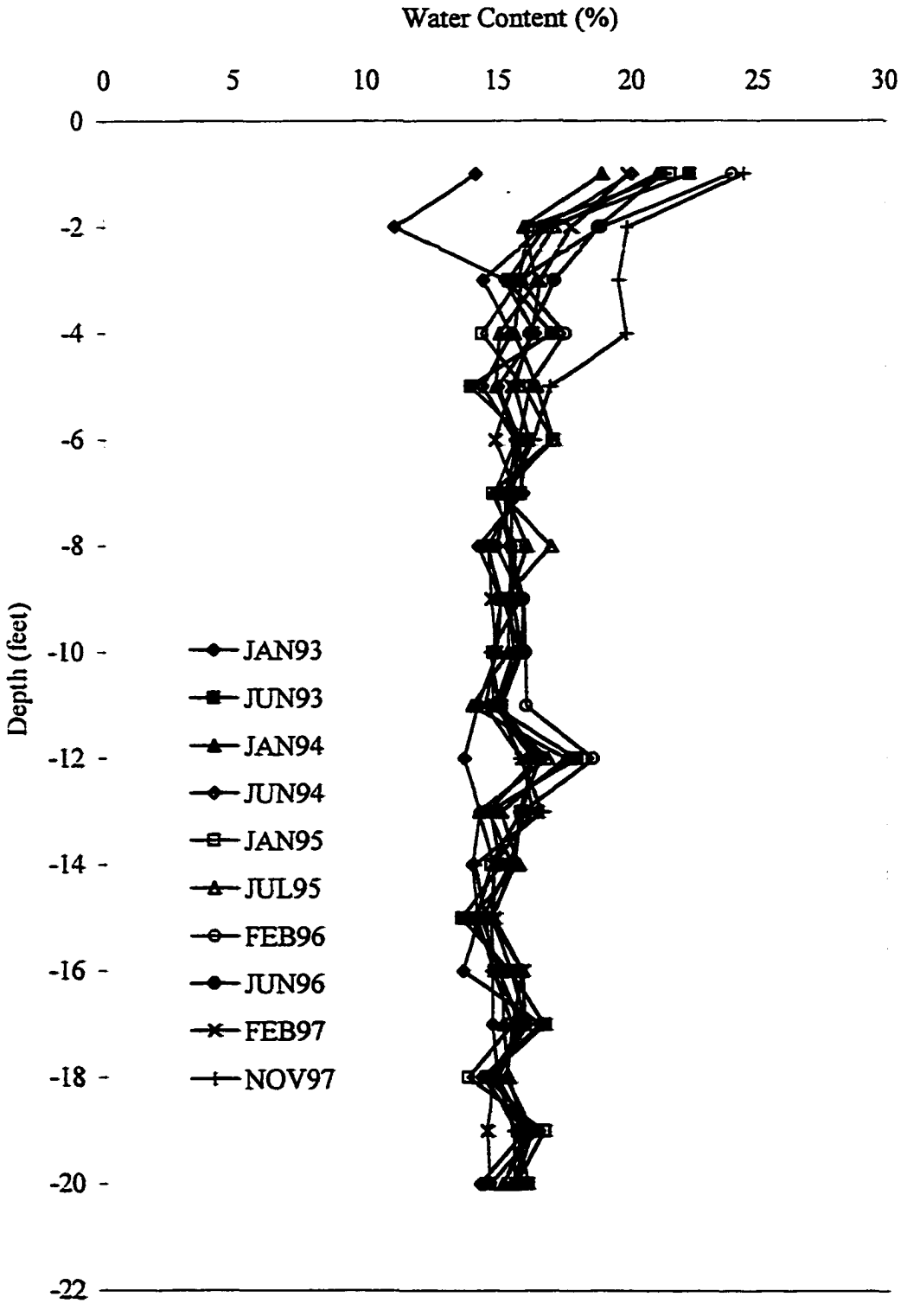

CSU Access Tube H-2

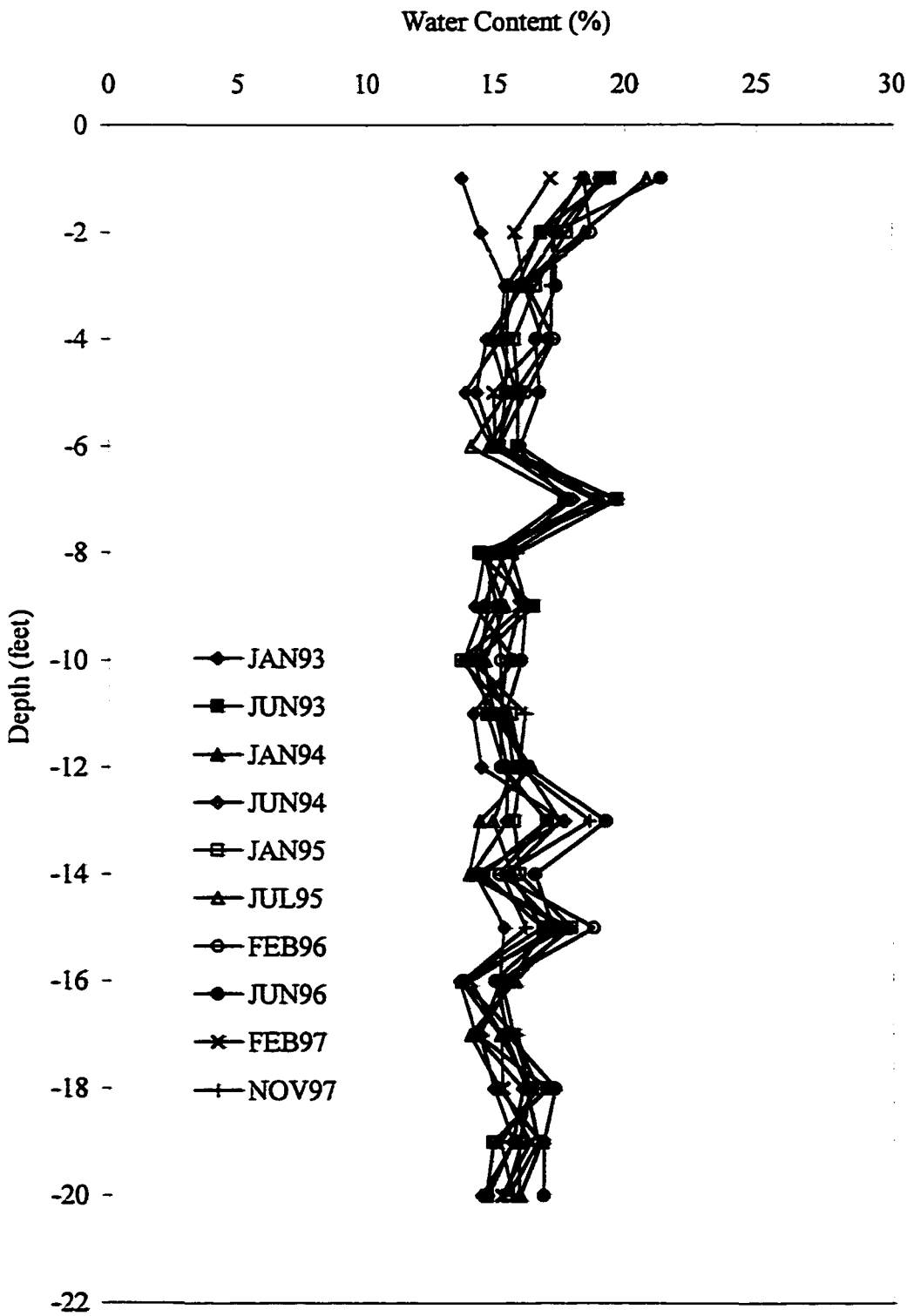

CSU Access Tube H-5

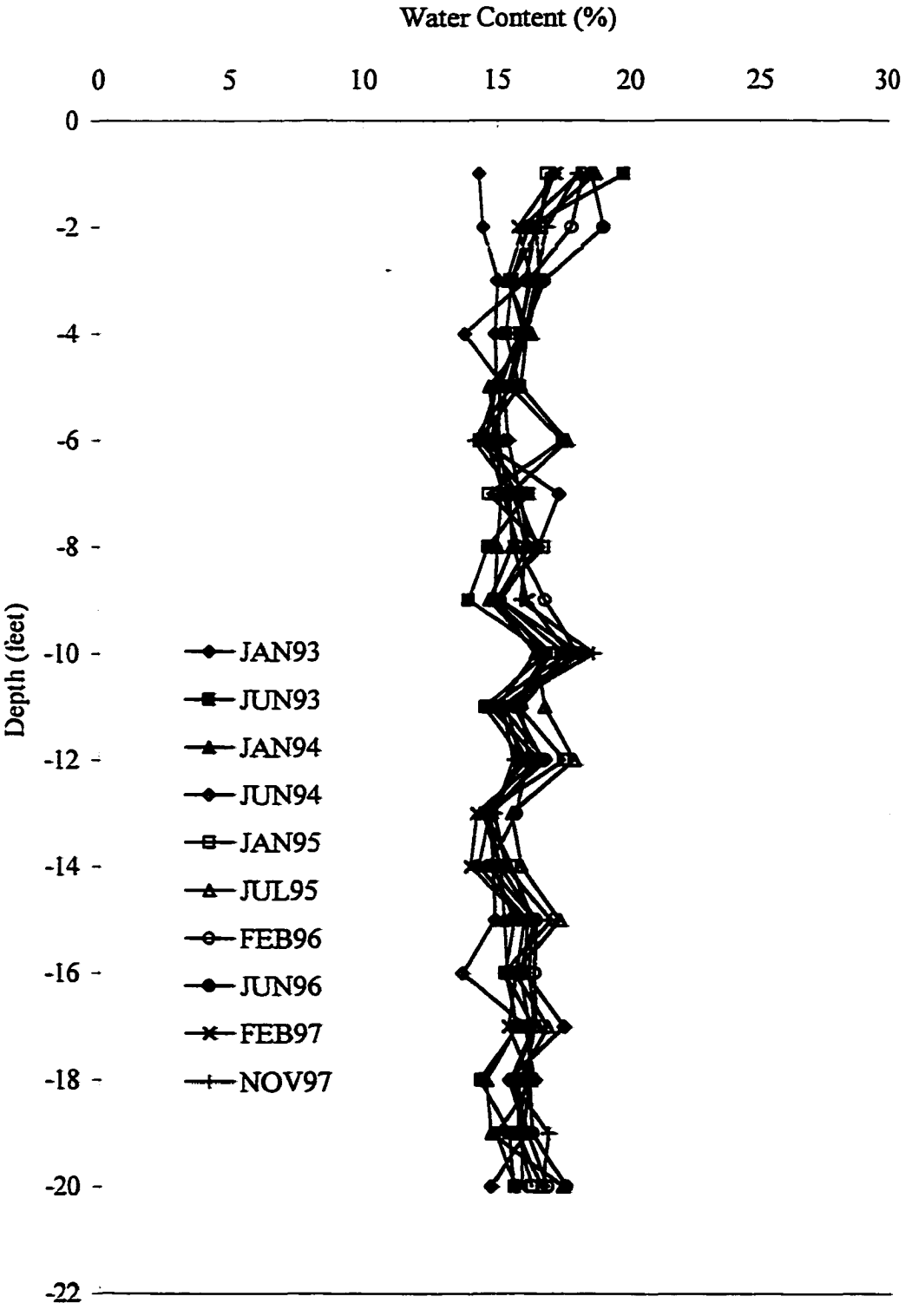

CSU Access Tube H-7

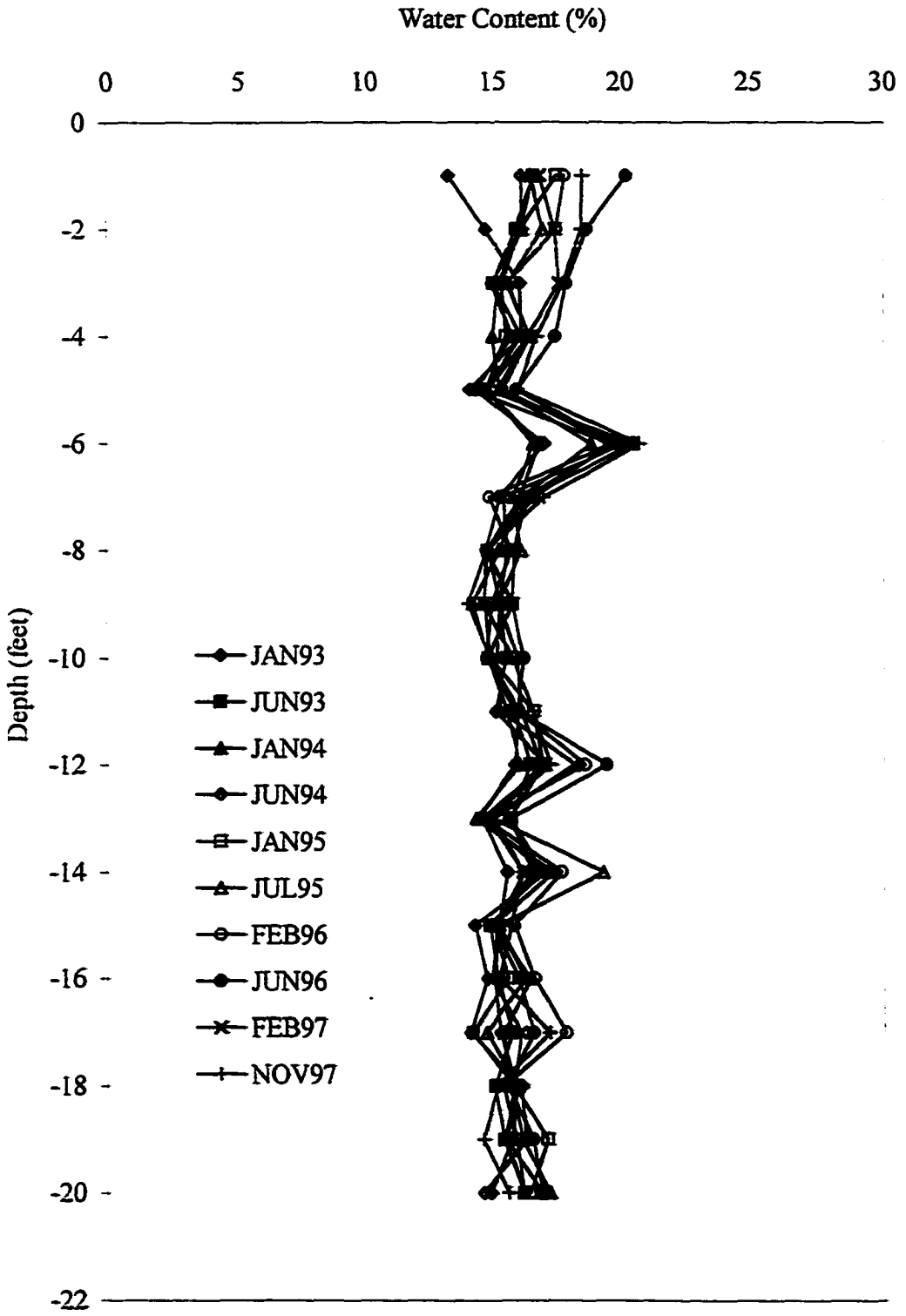

CSU Access Tube H.5-5

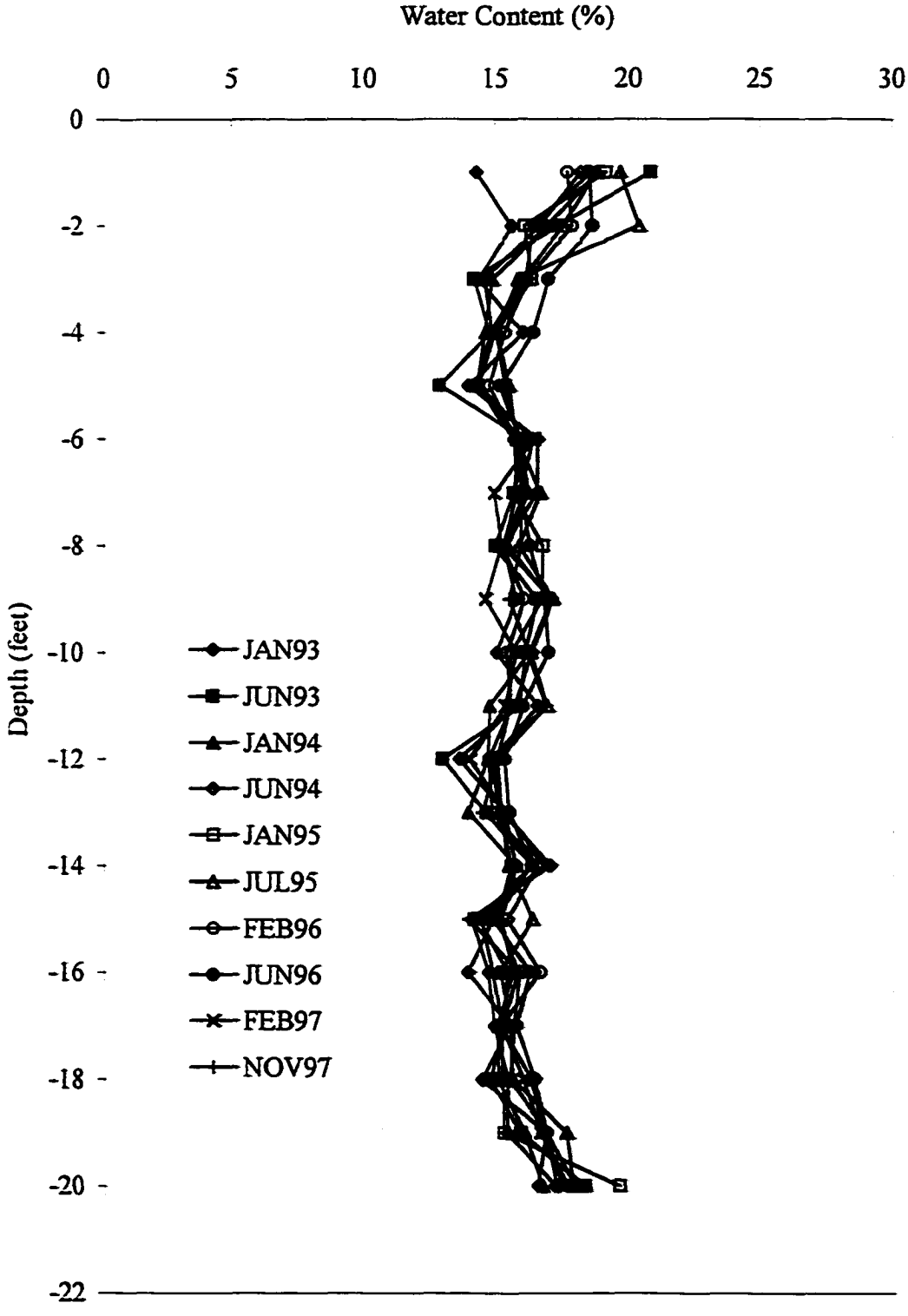

CSU Access Tube H.5-7

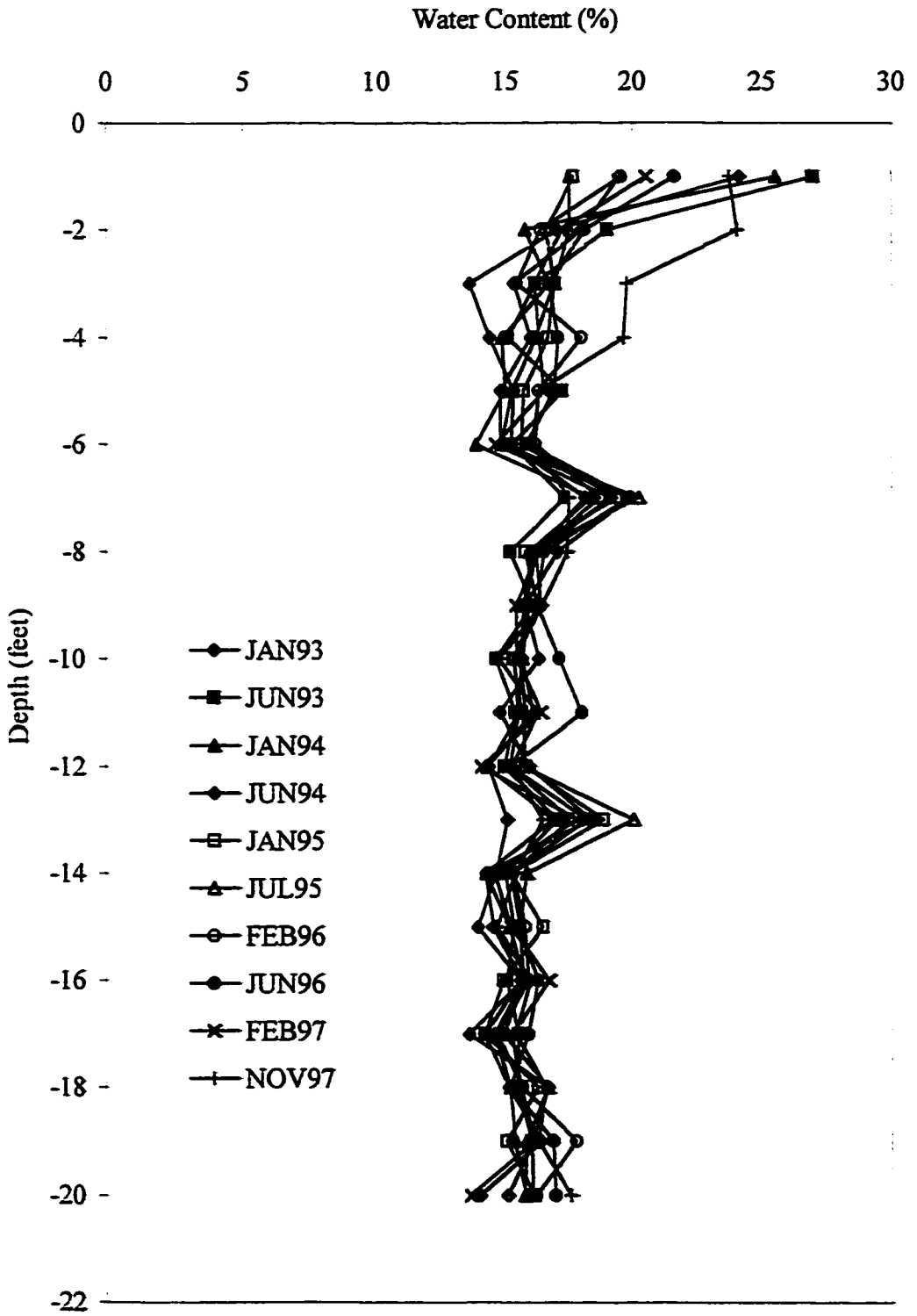

CSU Access Tube I-1

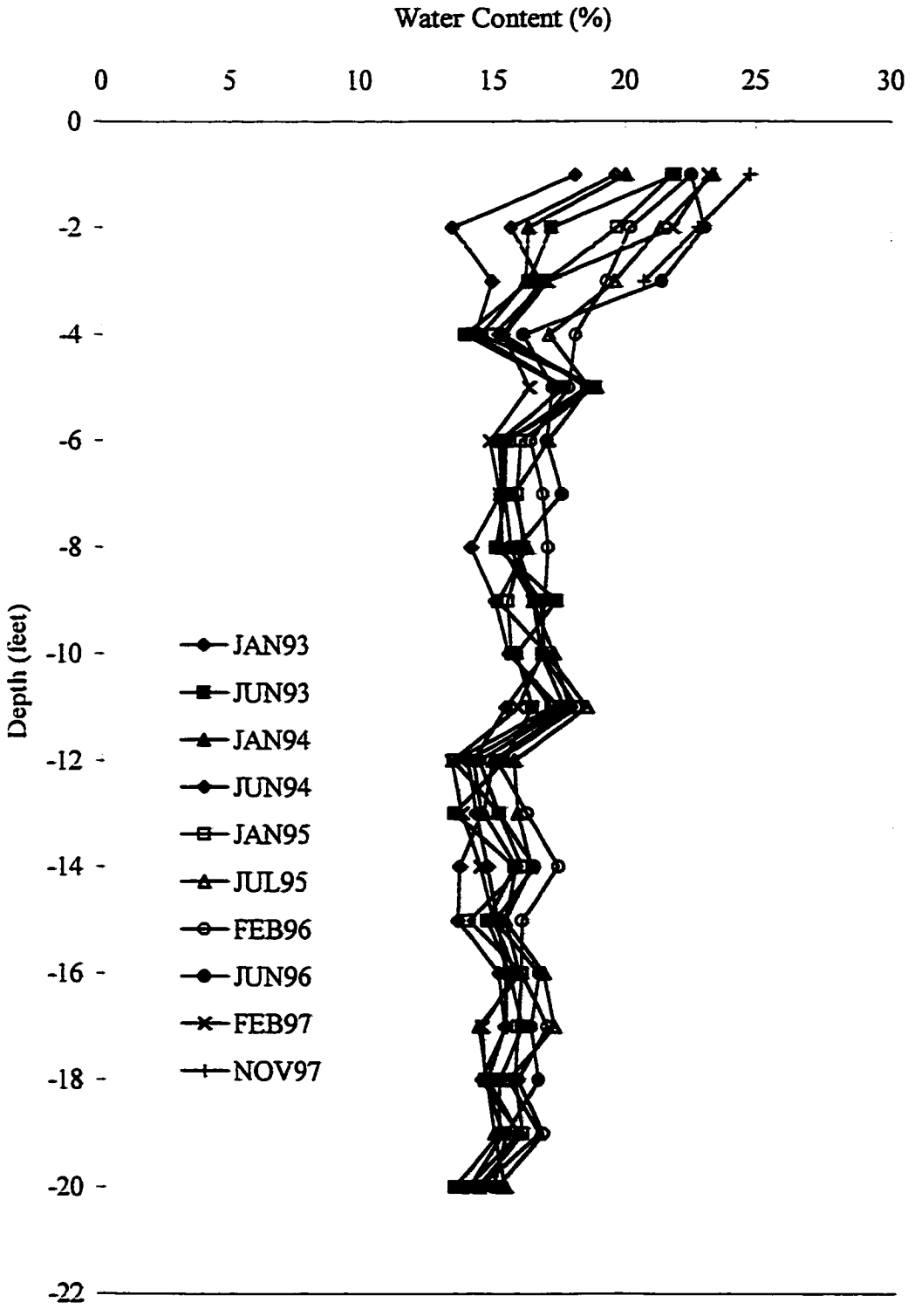

CSU Access Tube I-5

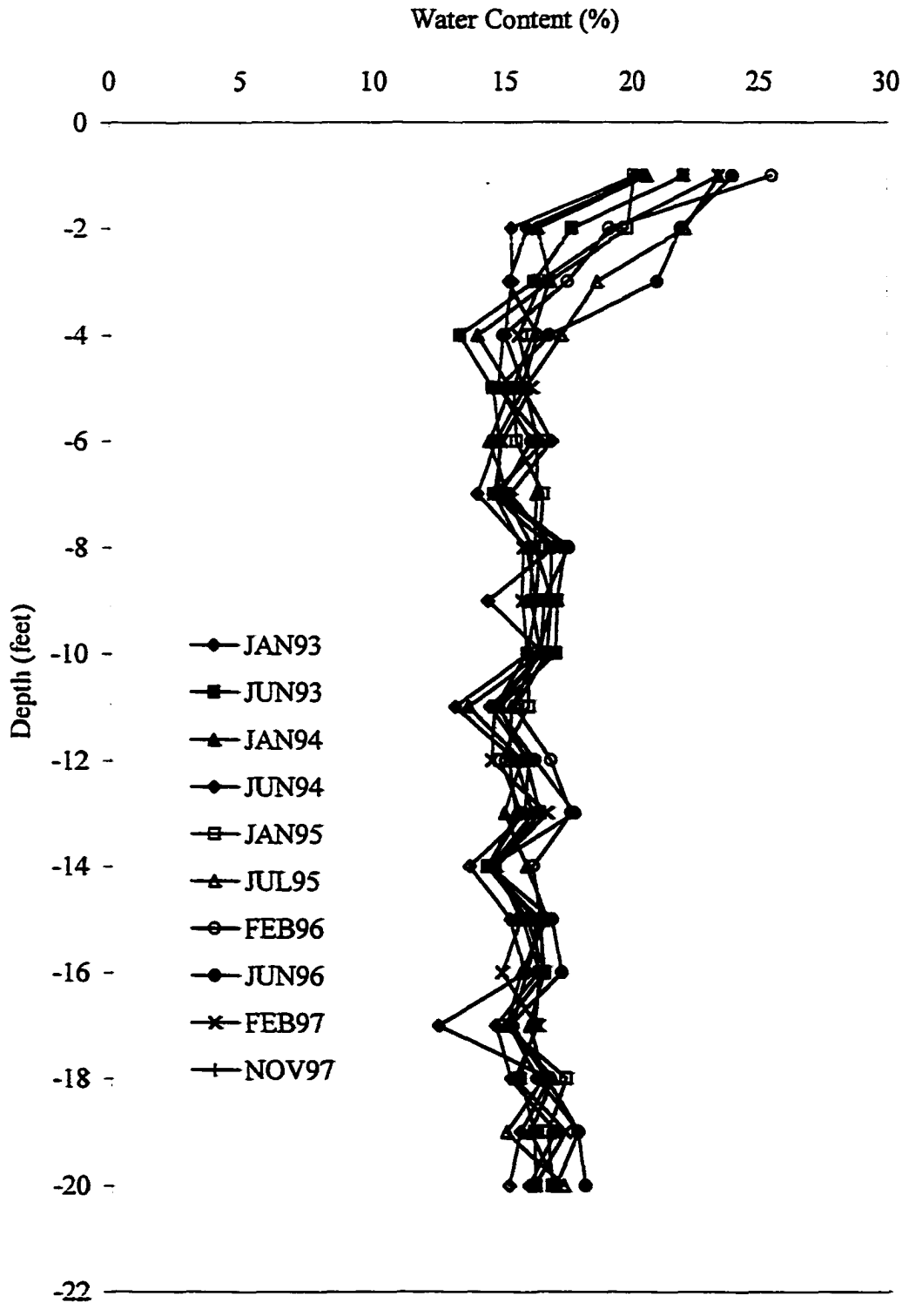

CSU Access Tube I-7

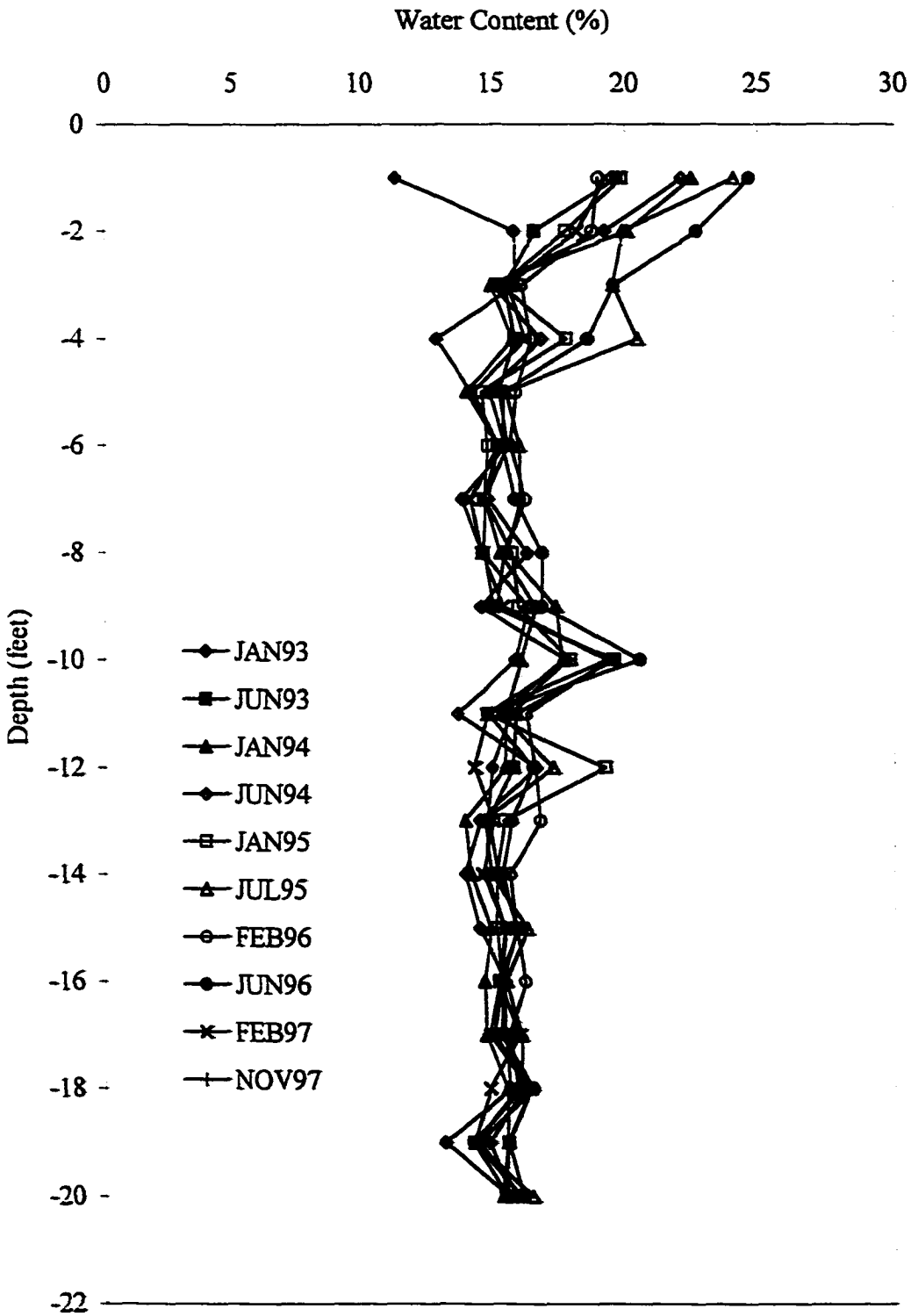

CSU Access Tube I-9

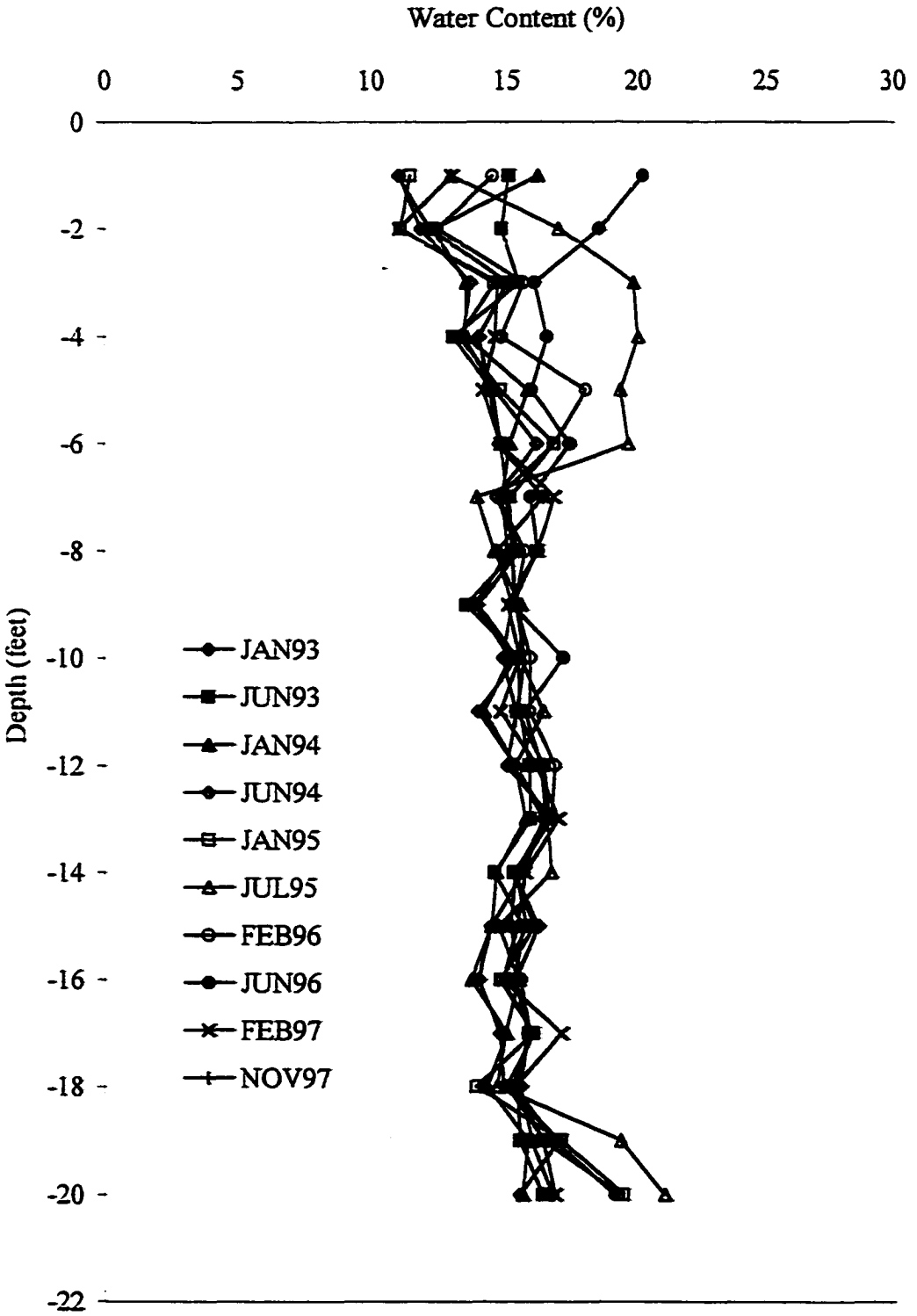

CSU Access Tube X-5

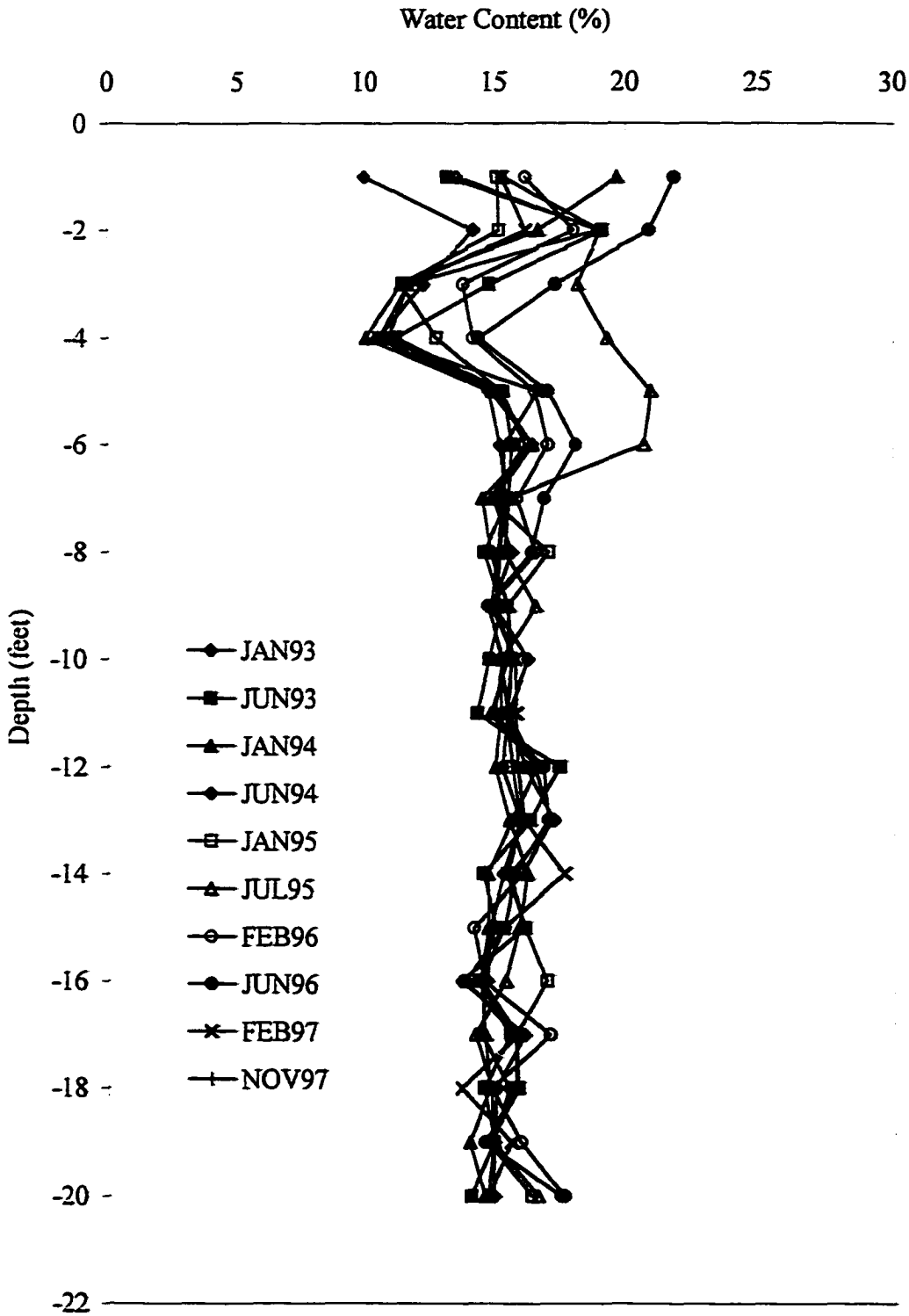

CSU Access Tube E-0

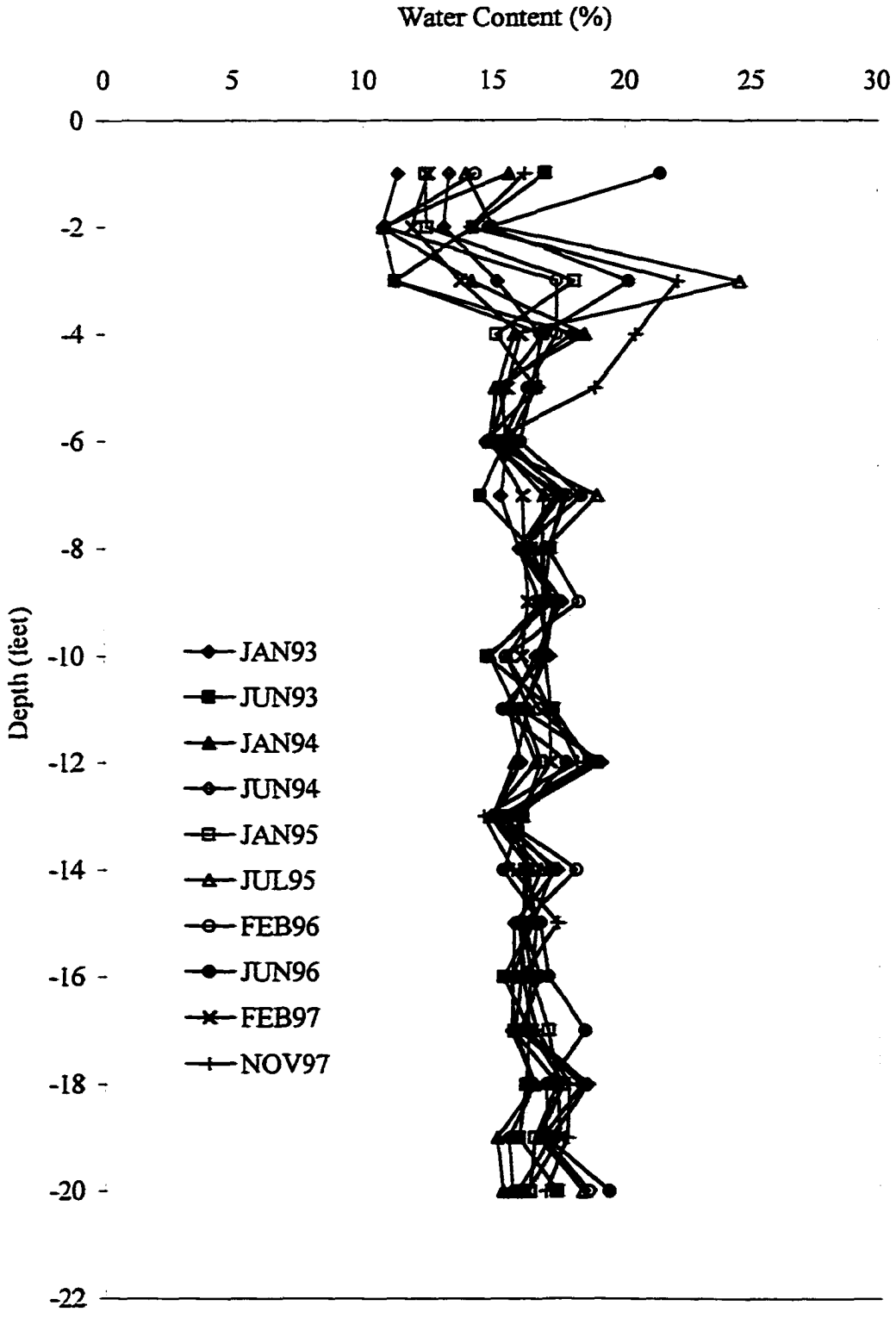

CSU Access Tube J-5

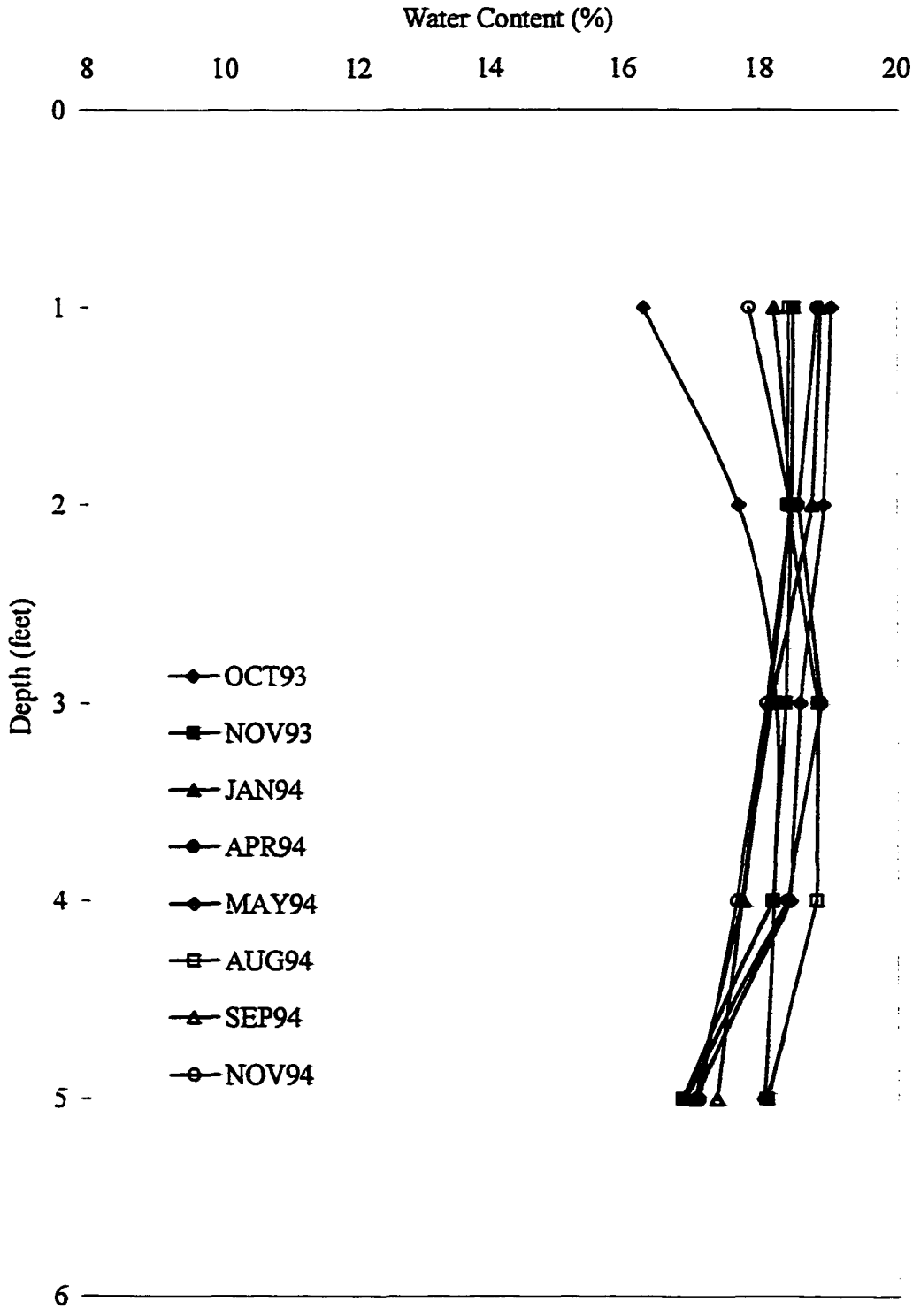

FSH Access Tube A-1

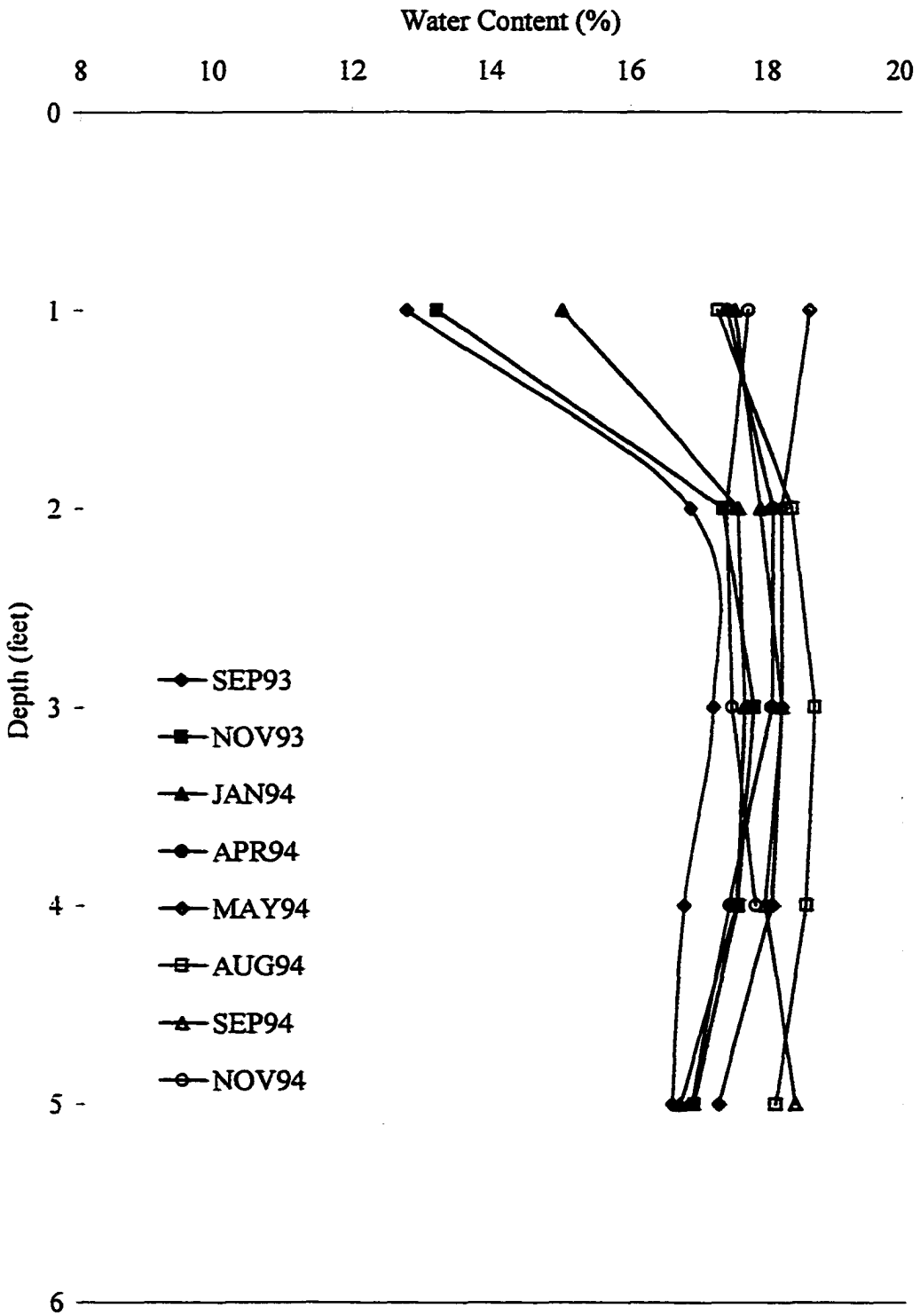

FSH Access Tube A-3

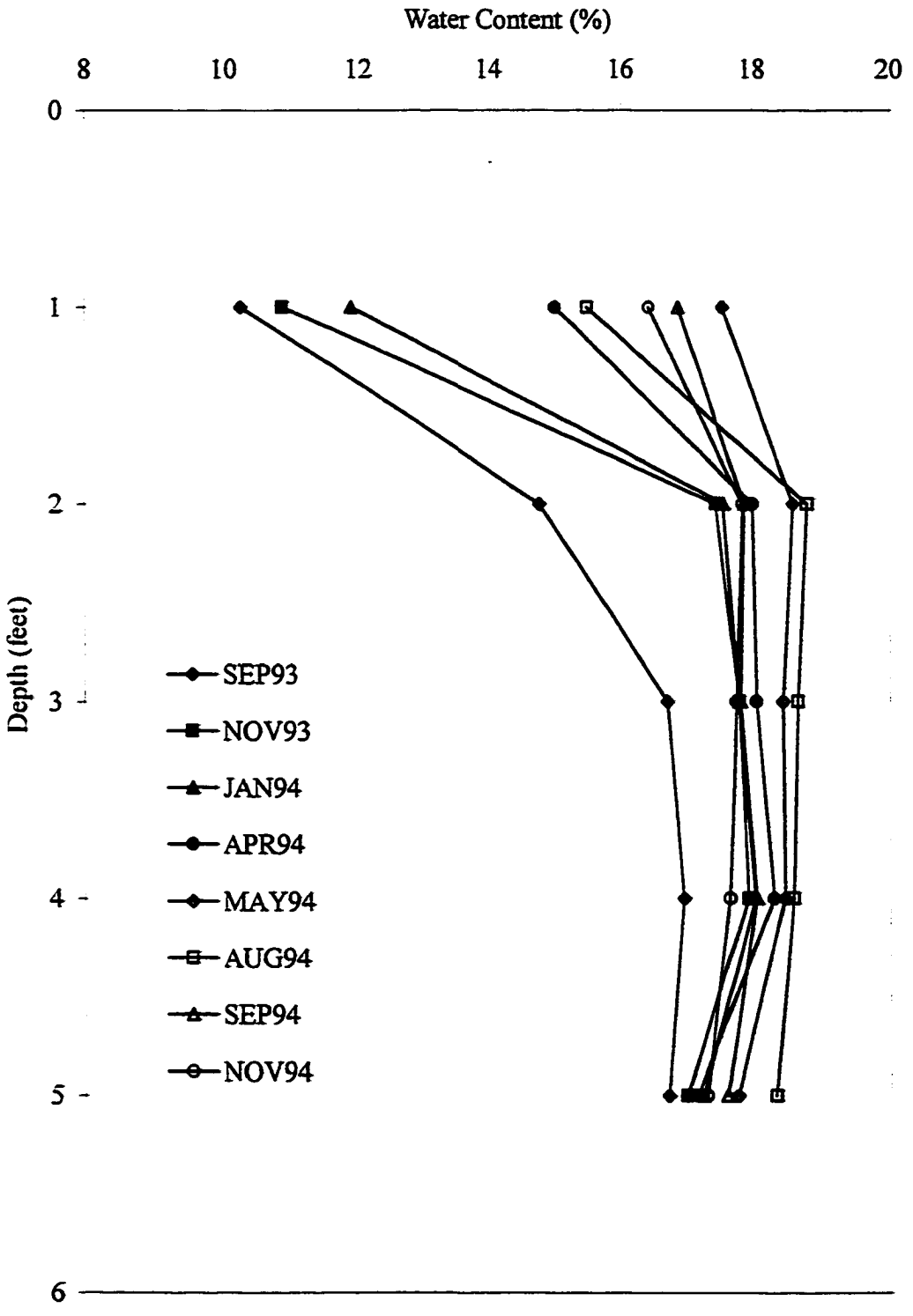

FSH Access Tube A-5

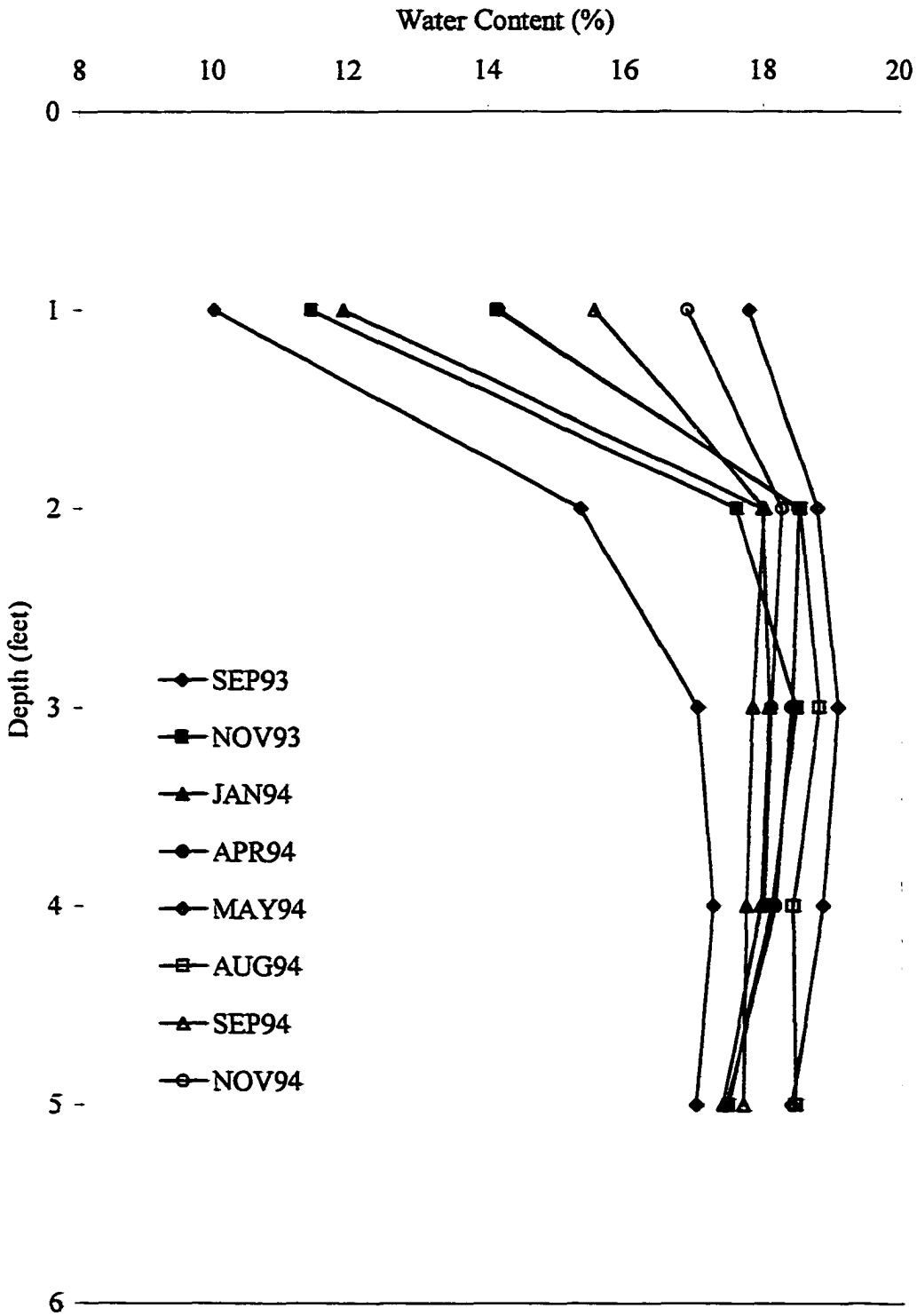

FSH Access Tube A-9

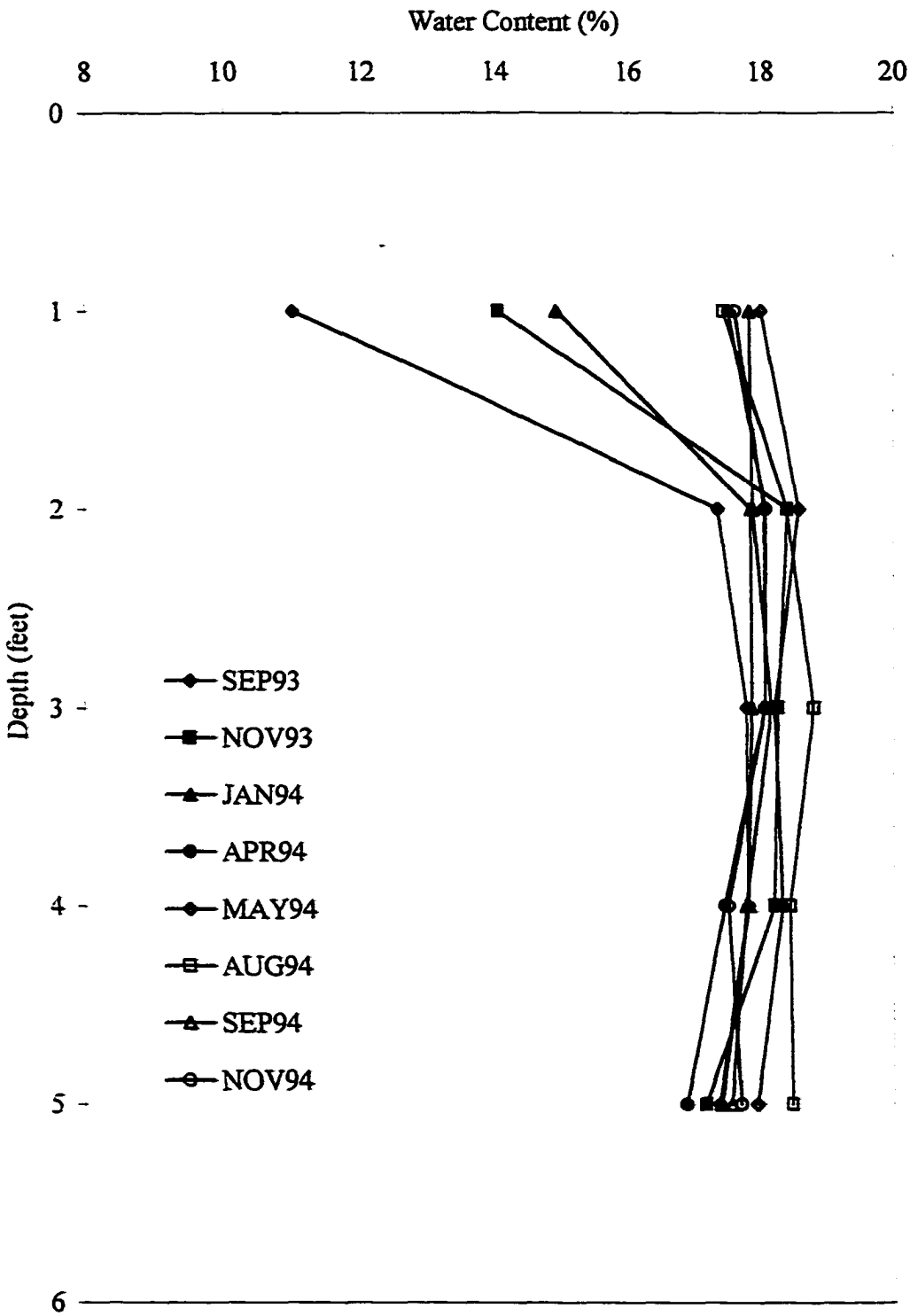

FSH Access Tube A.5-3

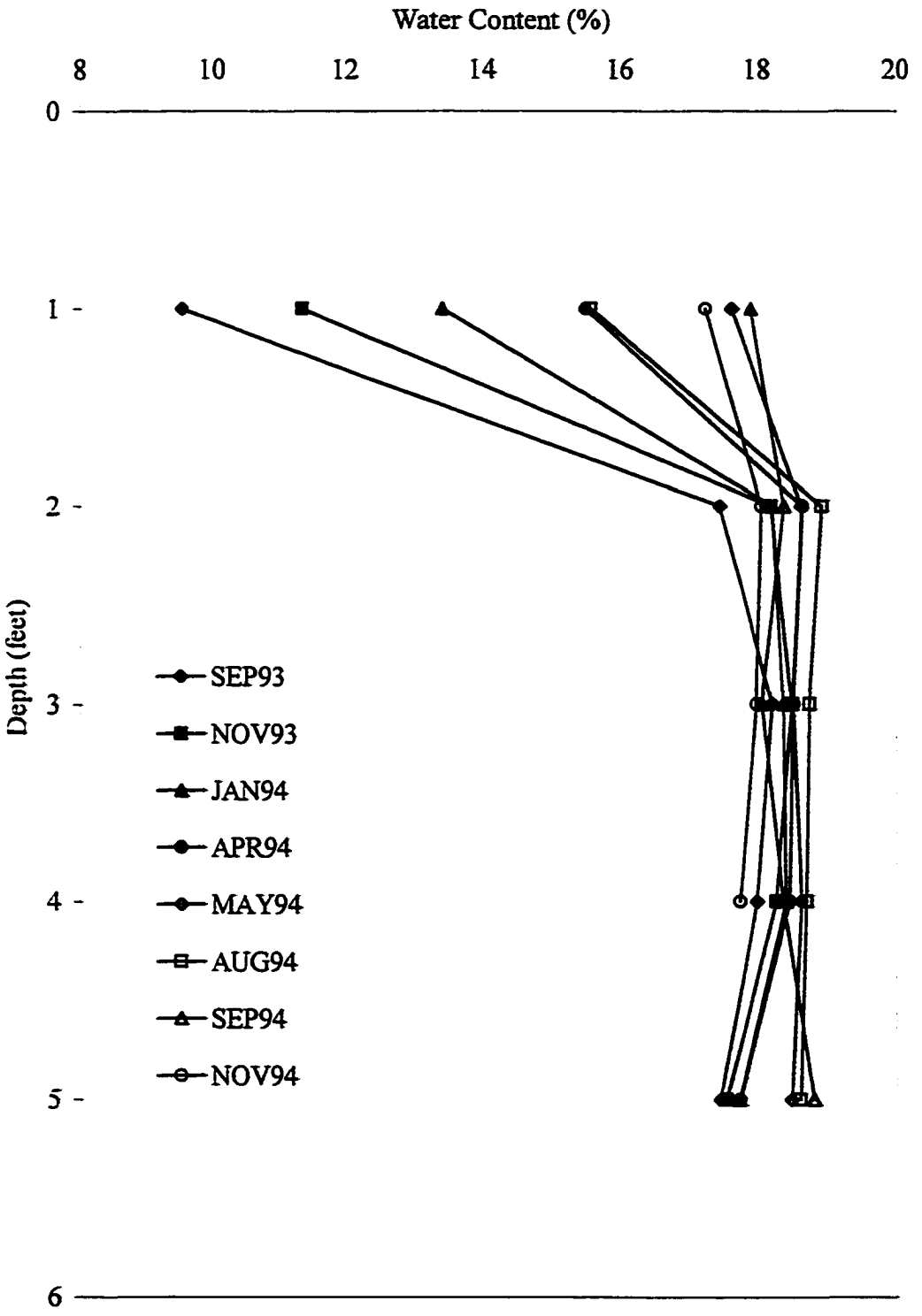

FSH Access Tube A.5-5

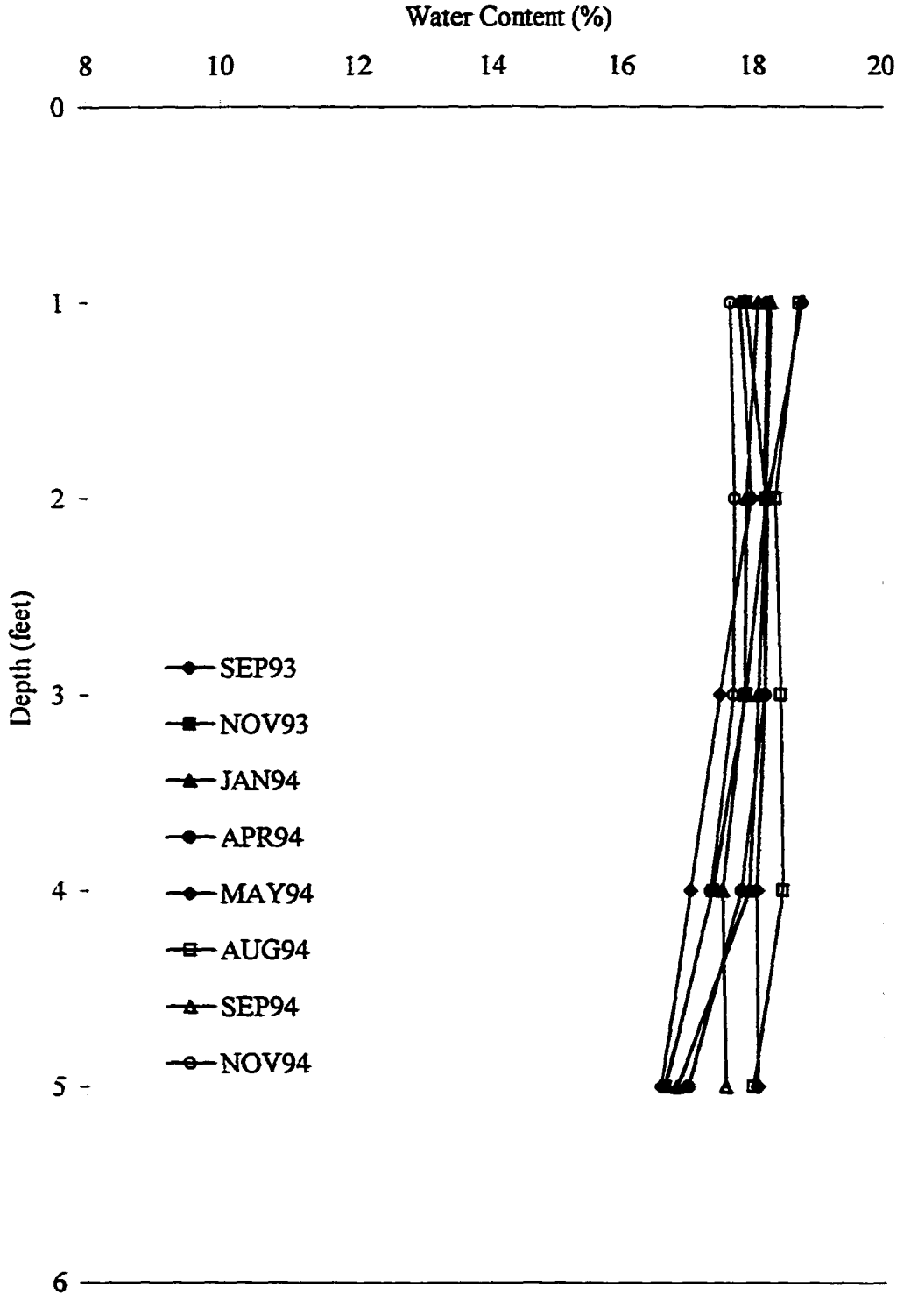

FSH Access Tube B-3

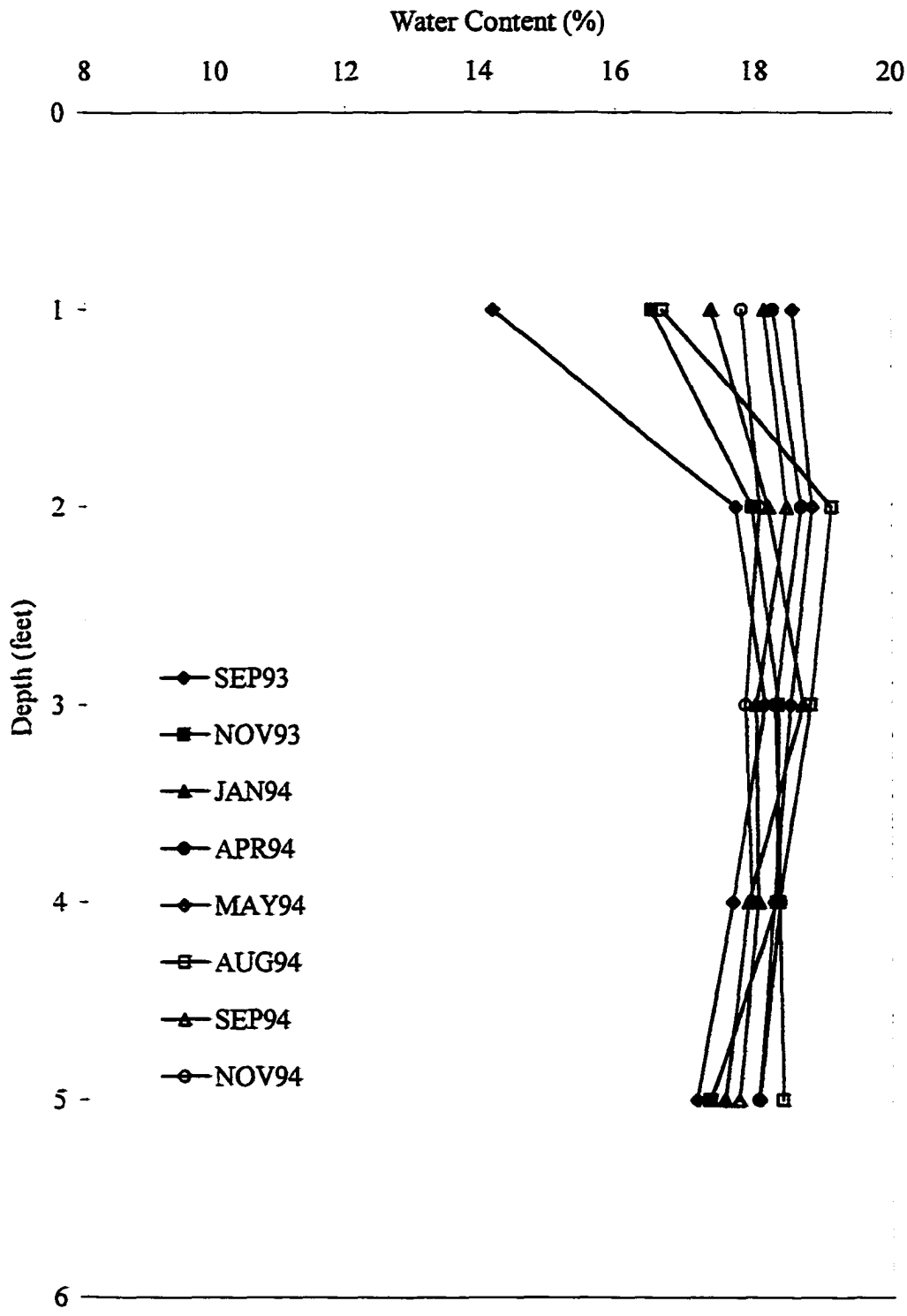

FSH Access Tube B-5

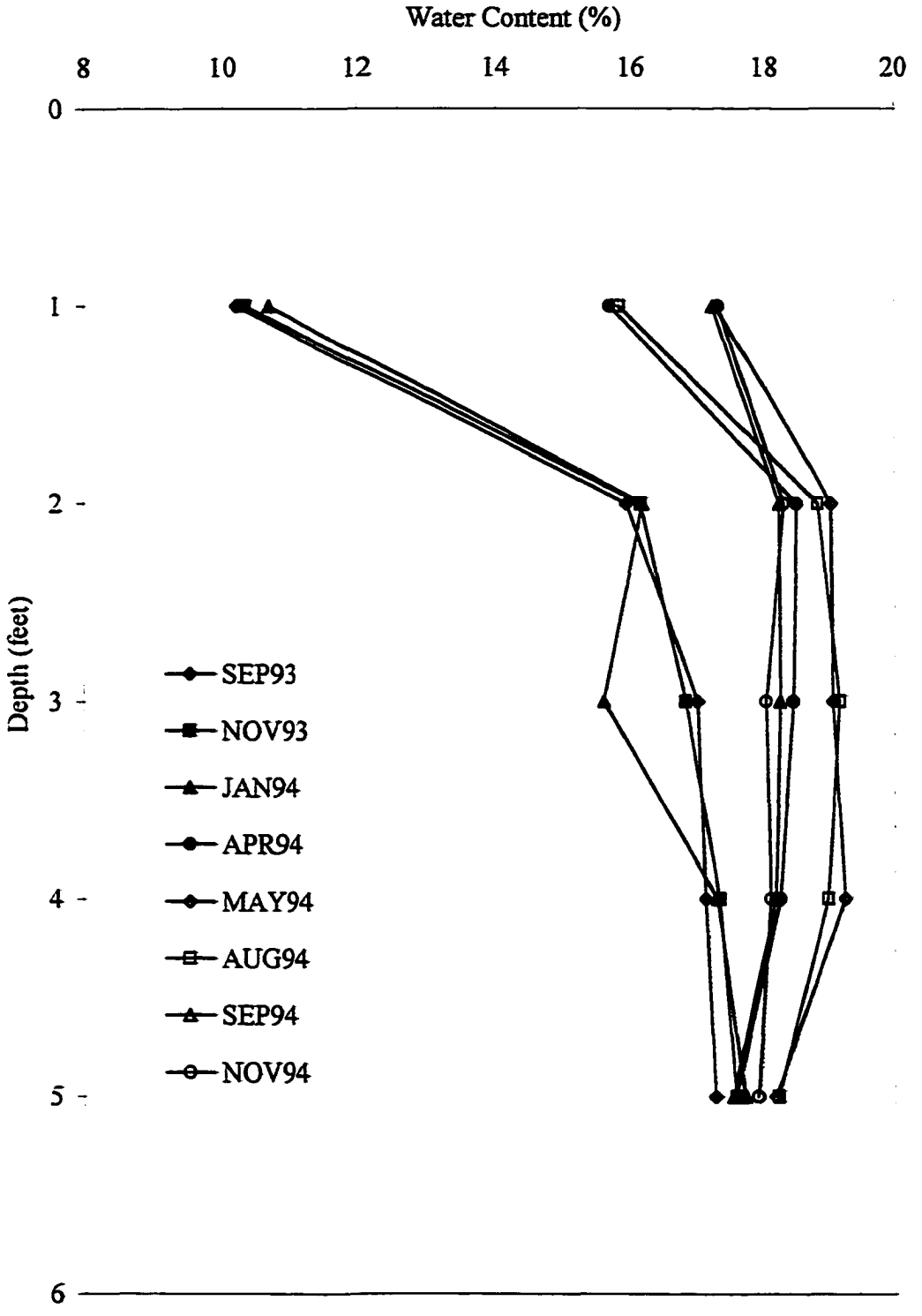

FSH Access Tube B-8

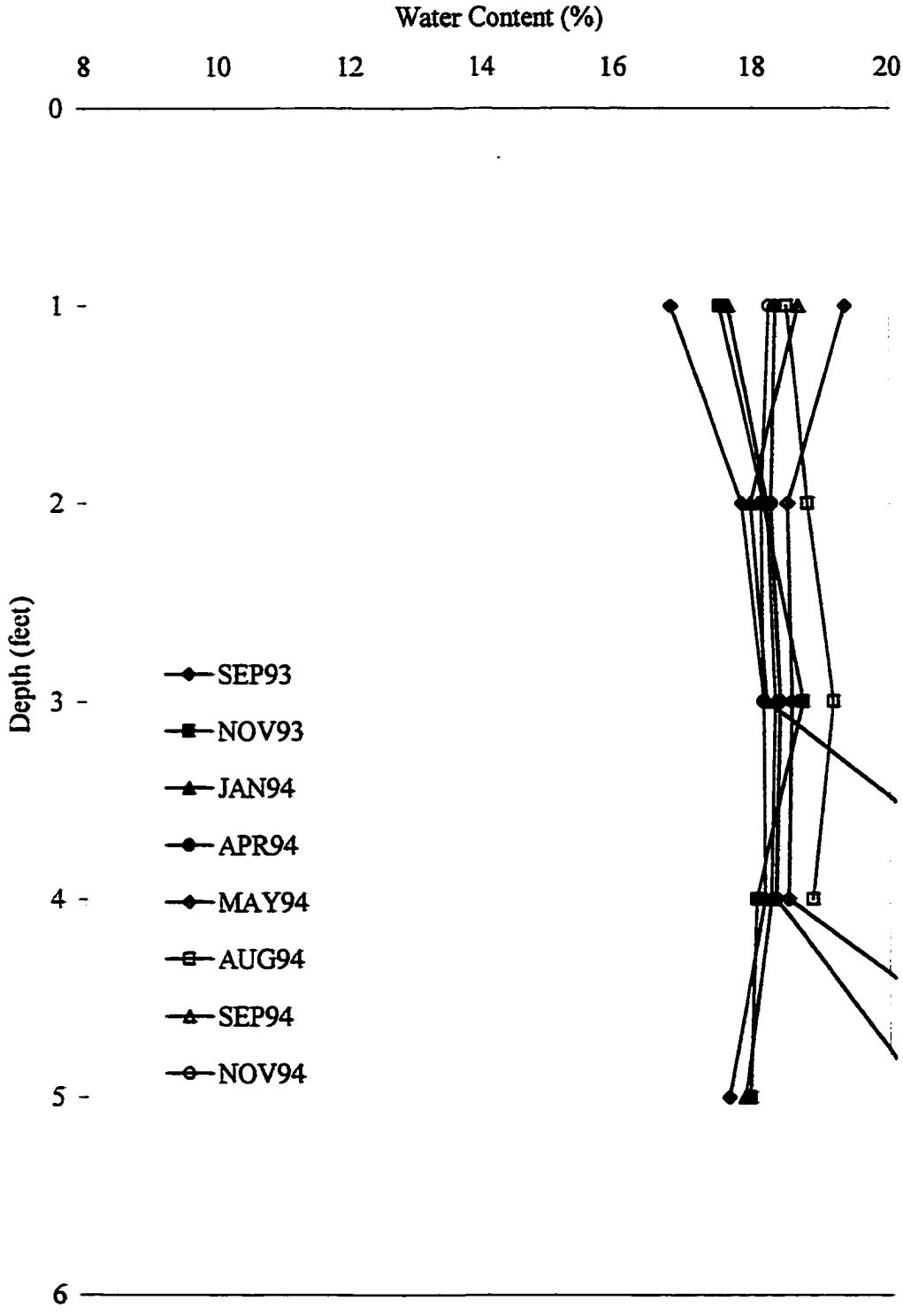

FSH Access Tube B.5-3

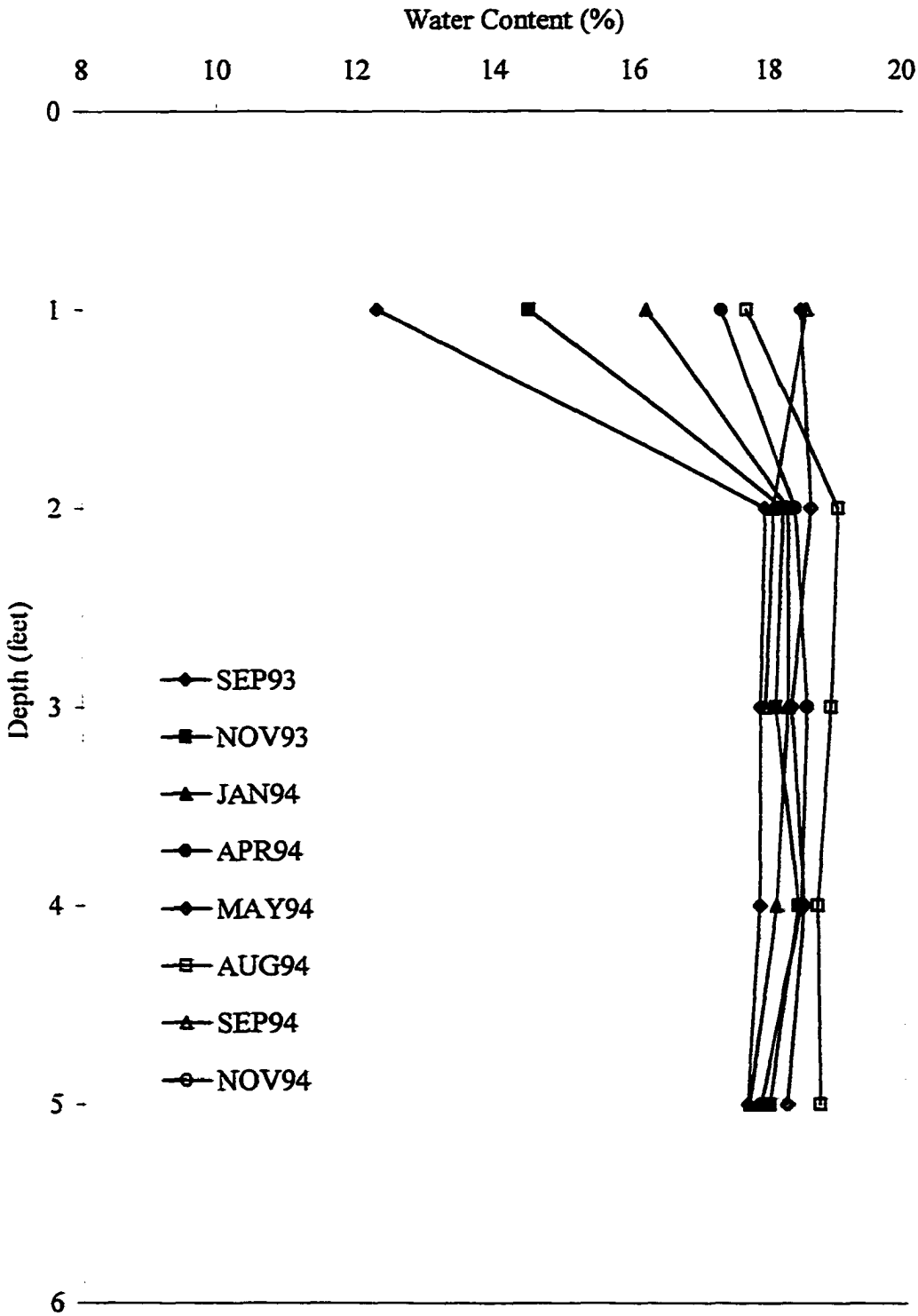

FSH Access Tube B.5-5

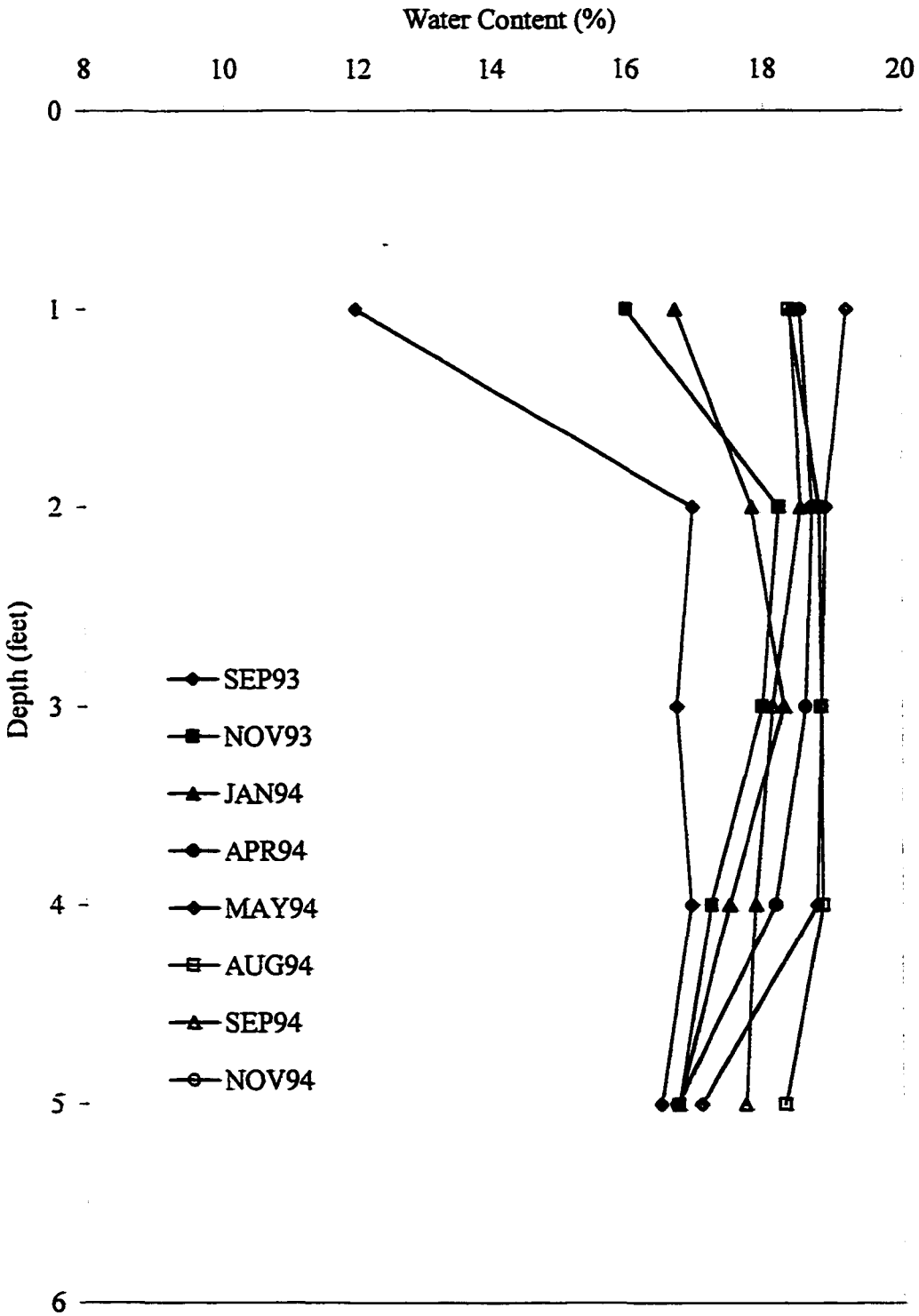

FSH Access Tube C-1

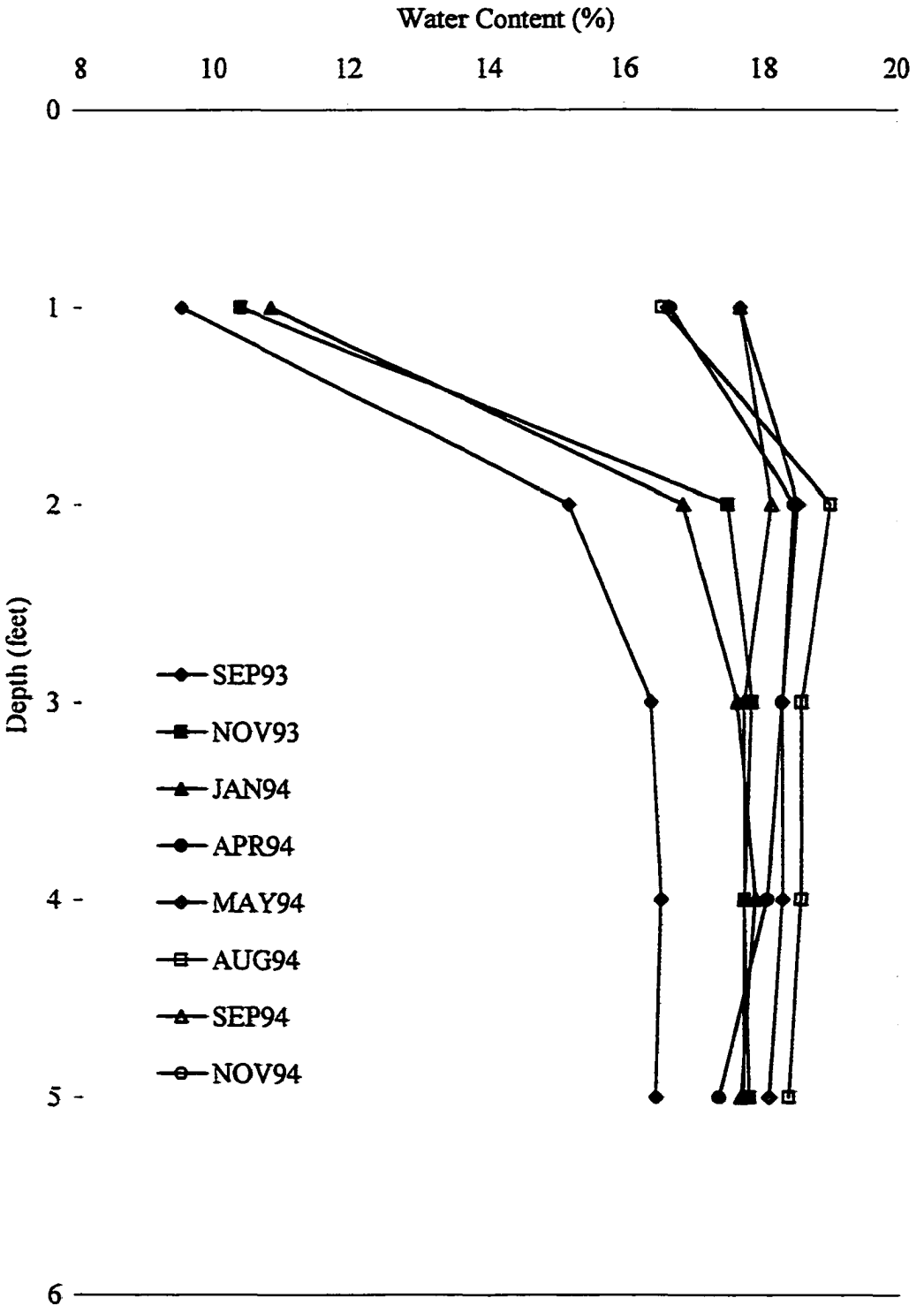

FSH Access Tube C-1.6

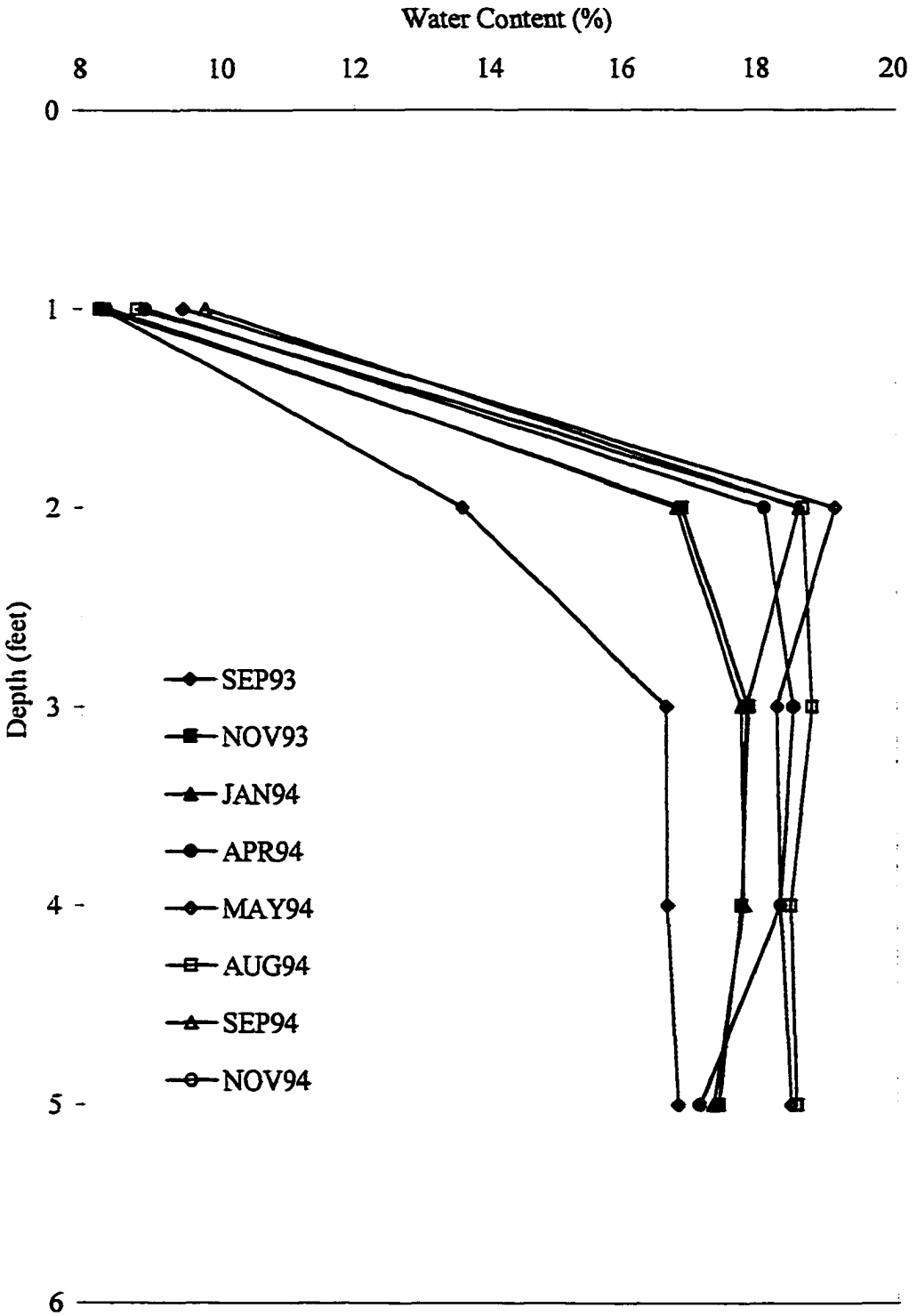

FSH Access Tube C-2.3

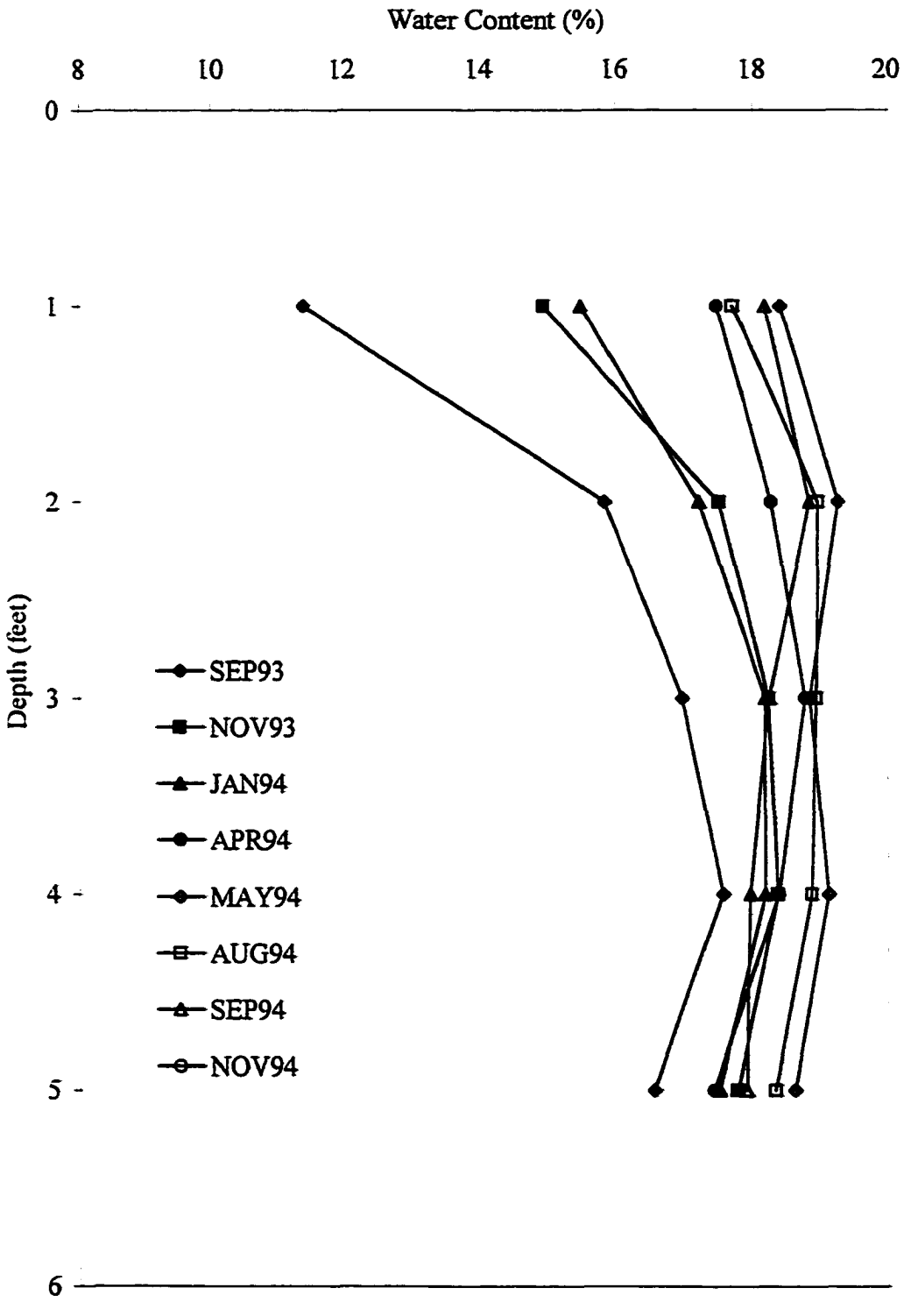

FSH Access Tube C-3

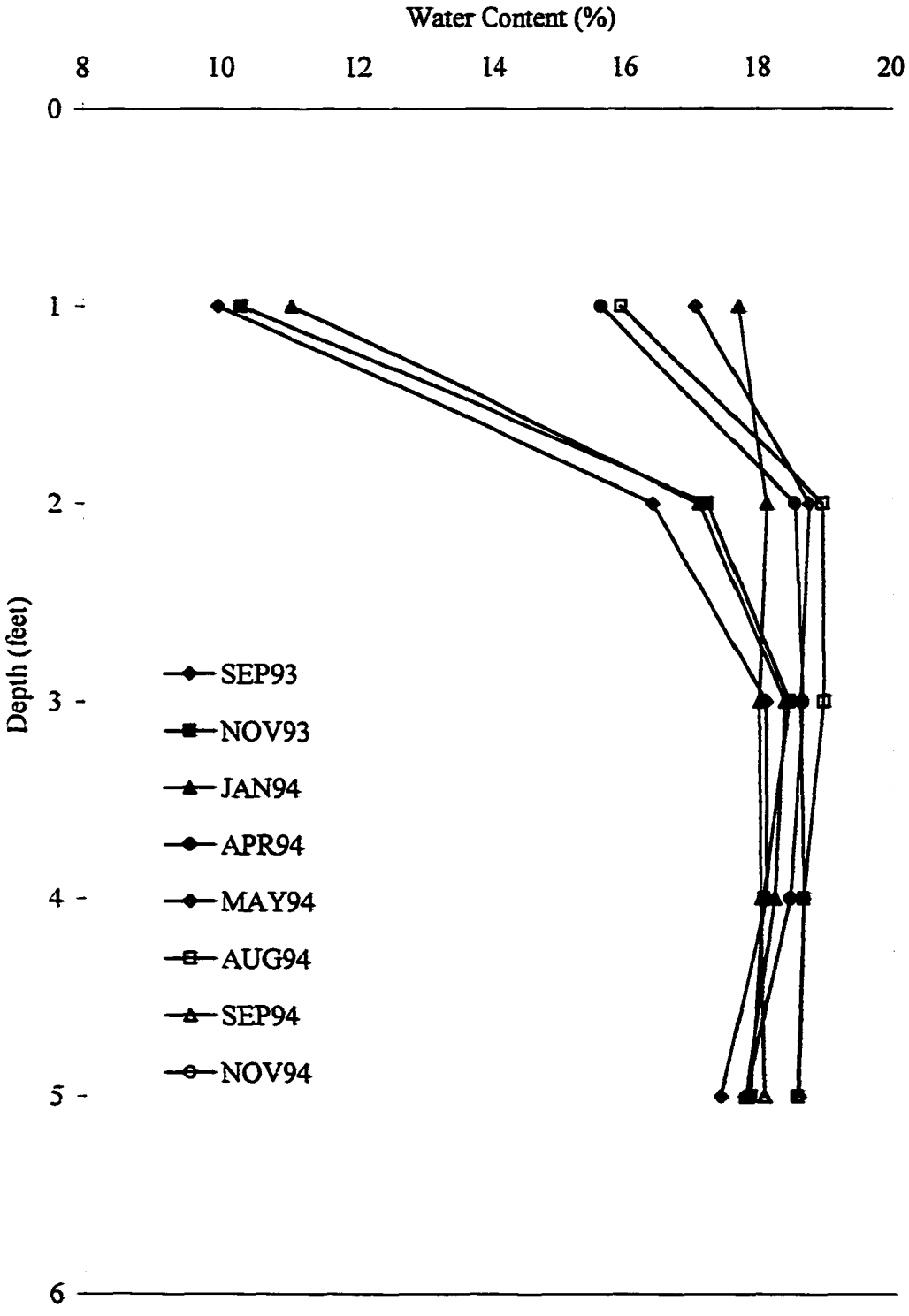

FSH Access Tube C-4

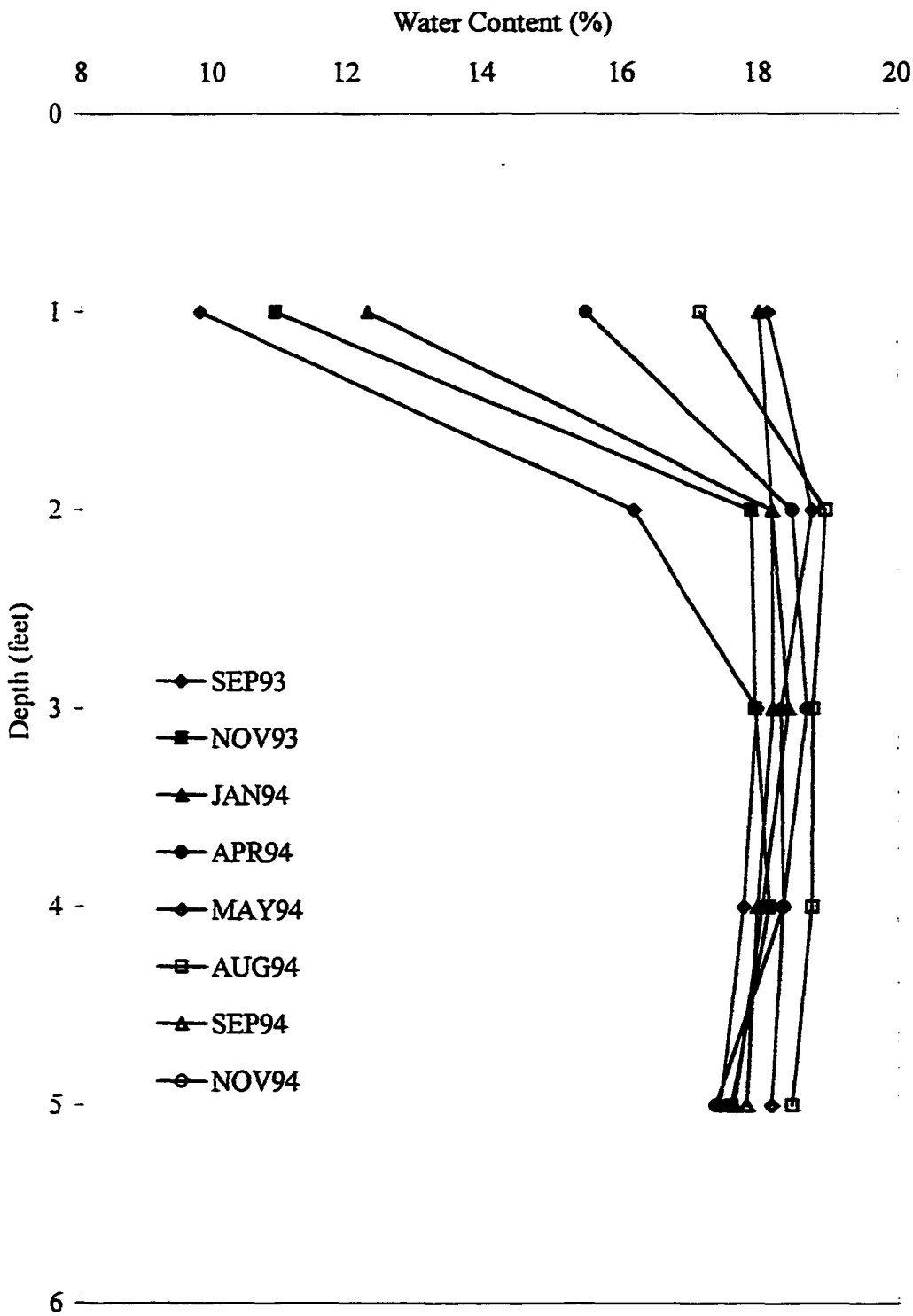

FSH Access Tube C-5

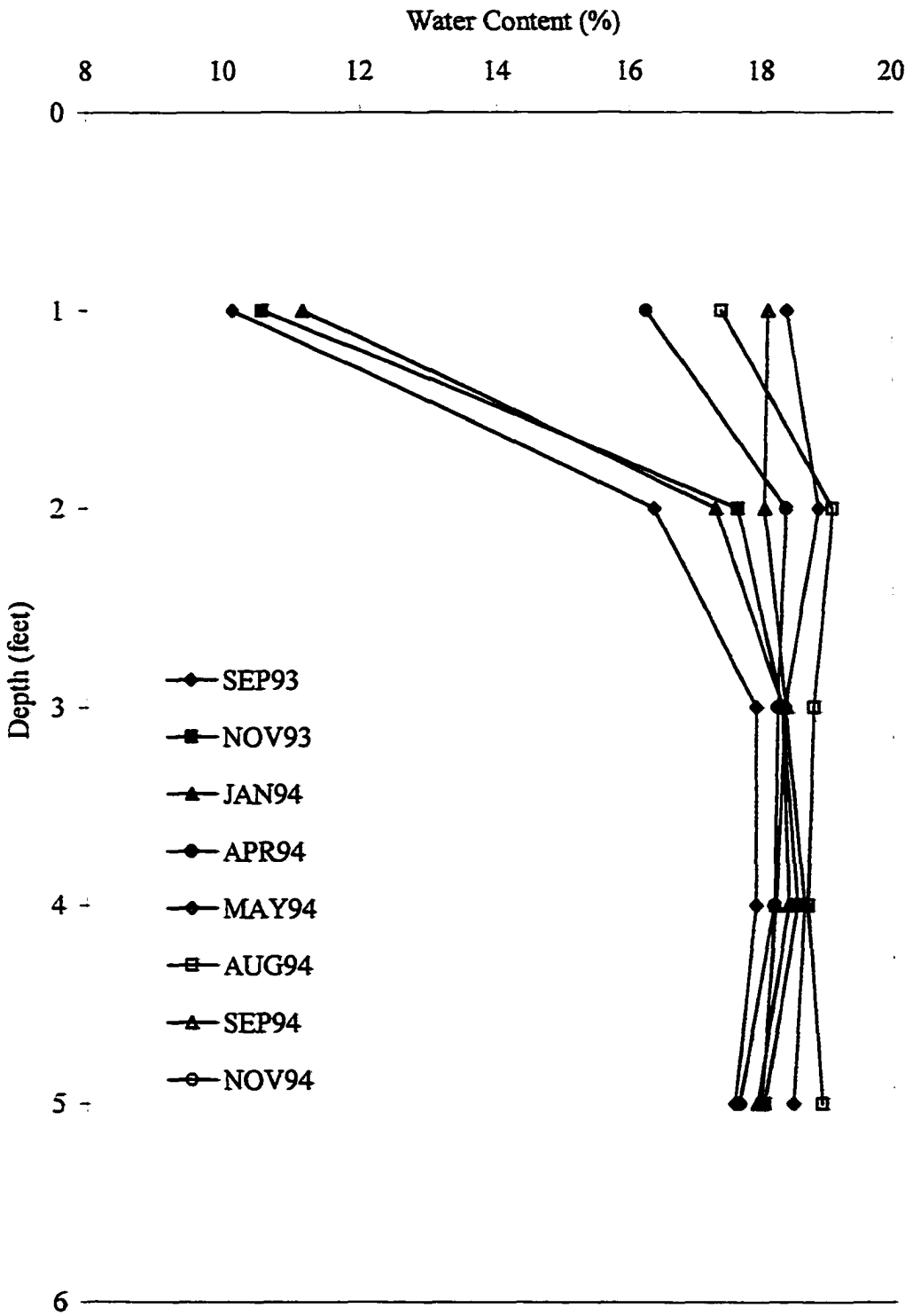

FSH Access Tube C-7

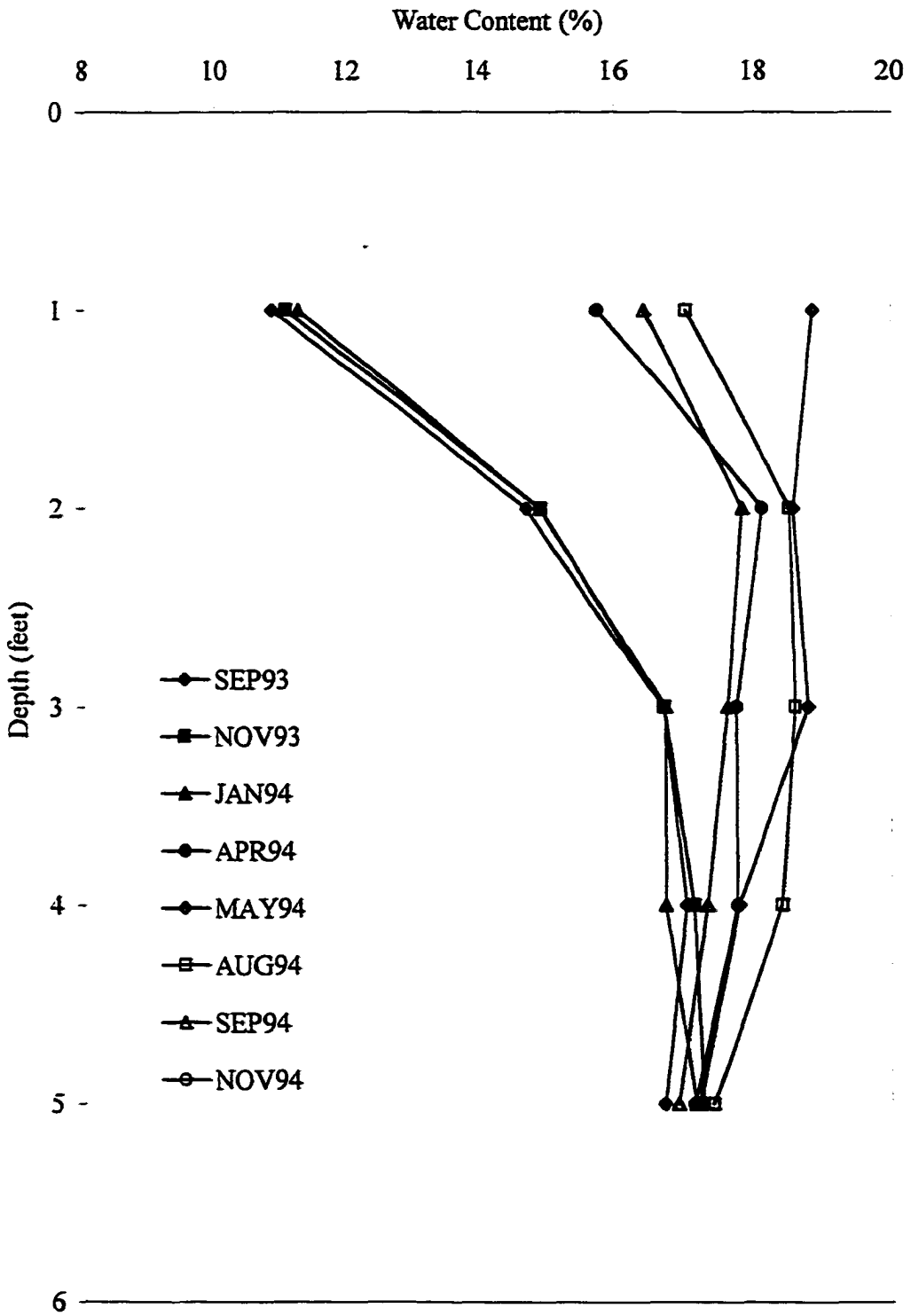

FSH Access Tube C-9

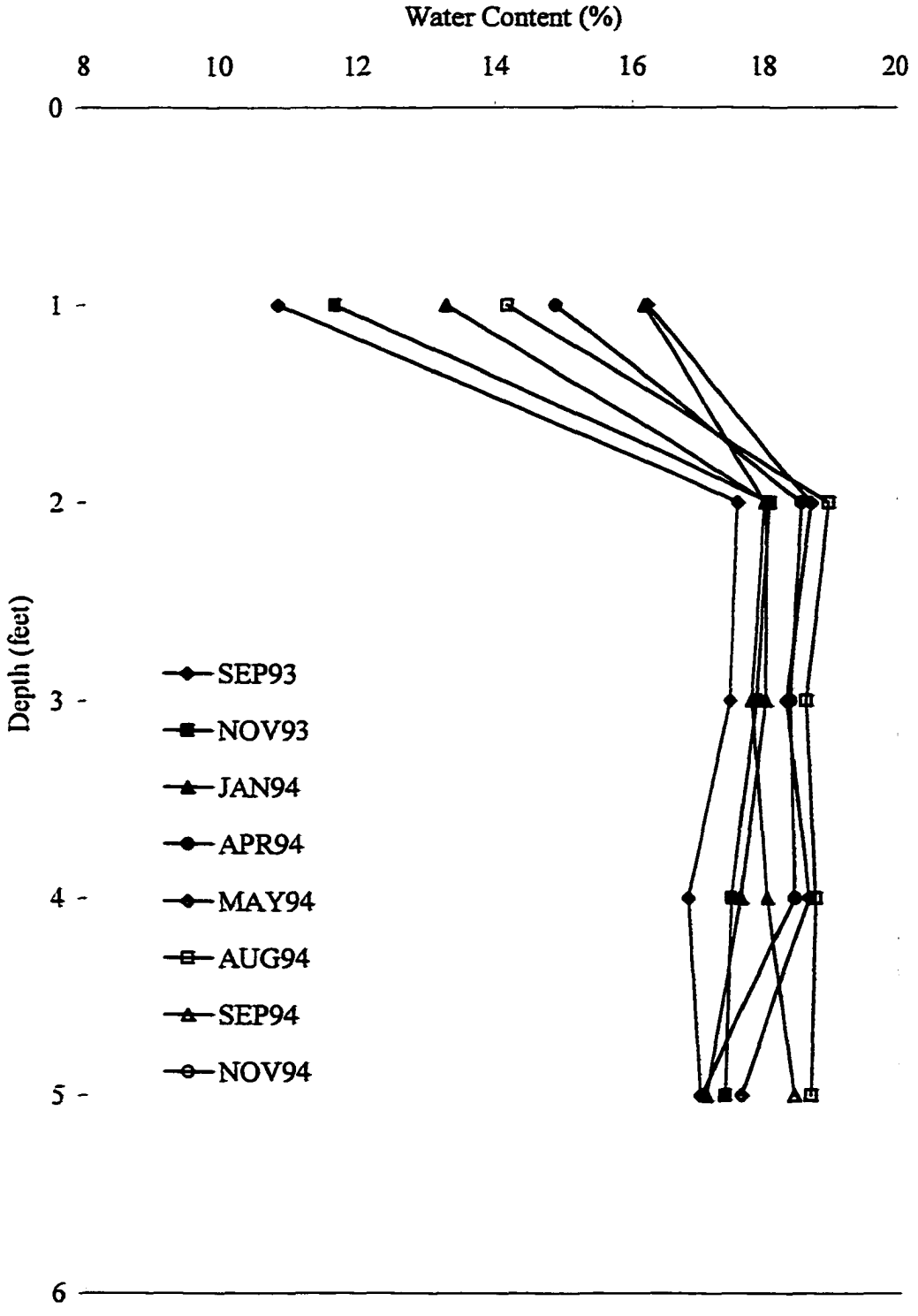

FSH Access Tube D-3

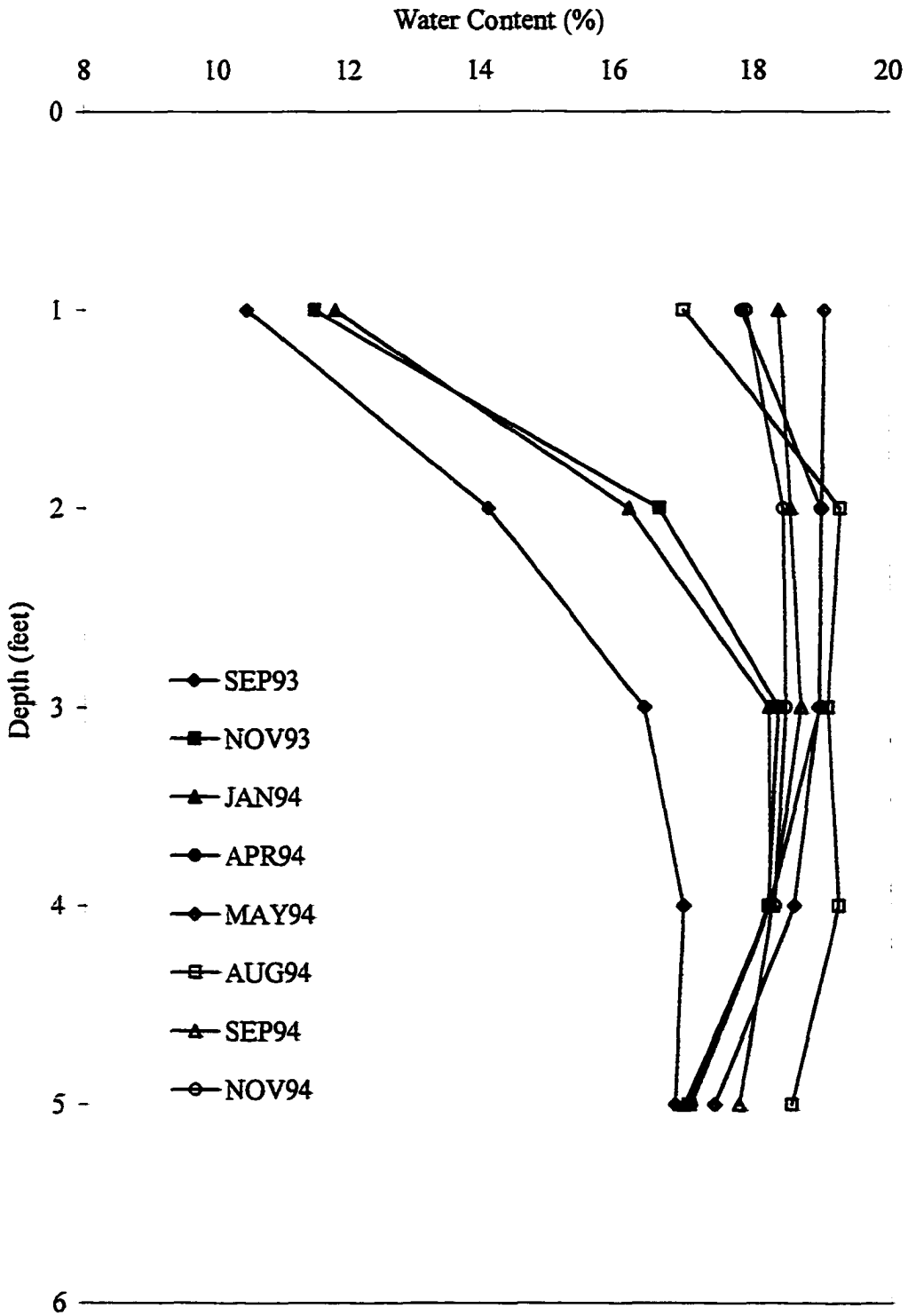

FSH Access Tube D-5

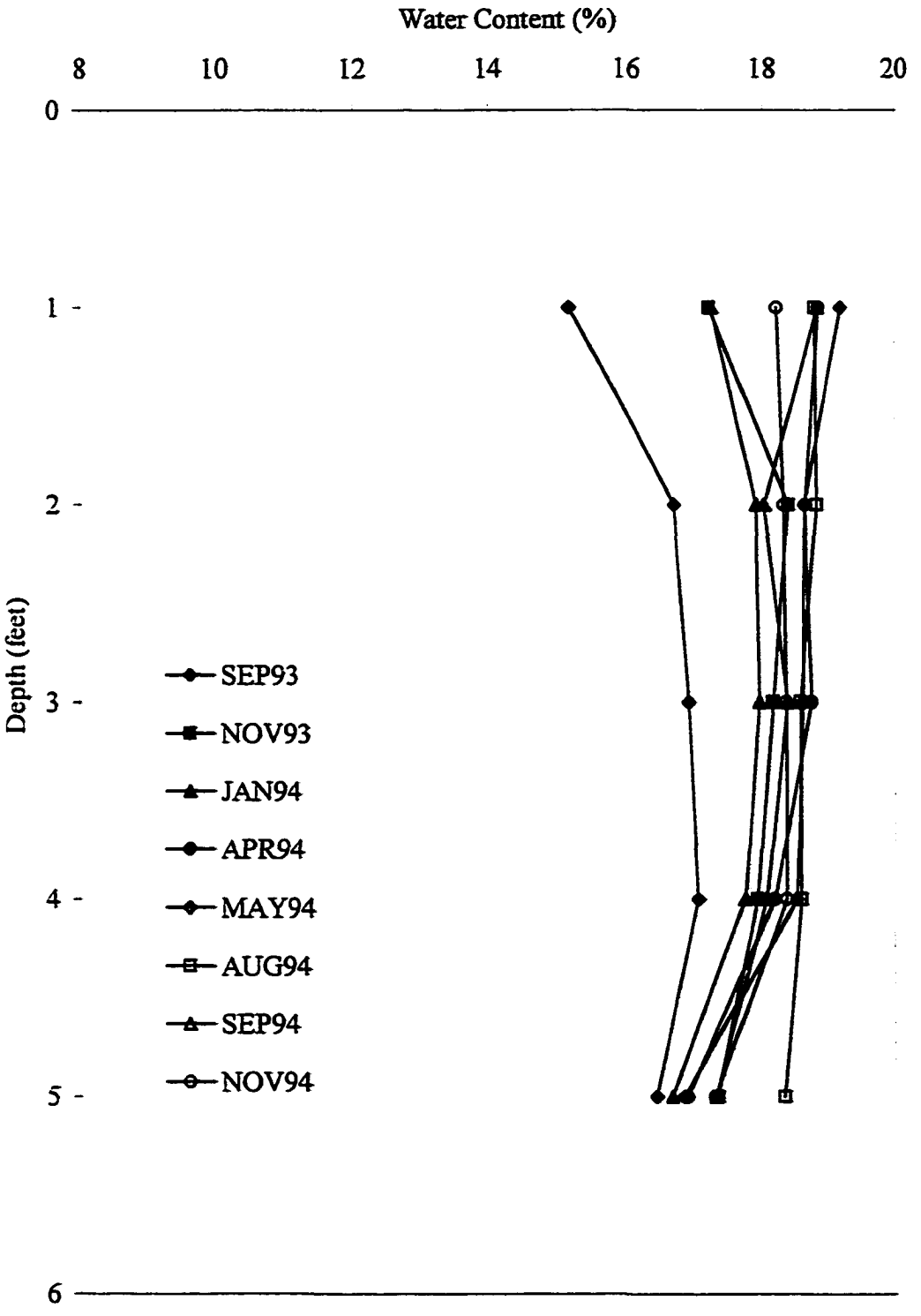

FSH Access Tube E-1

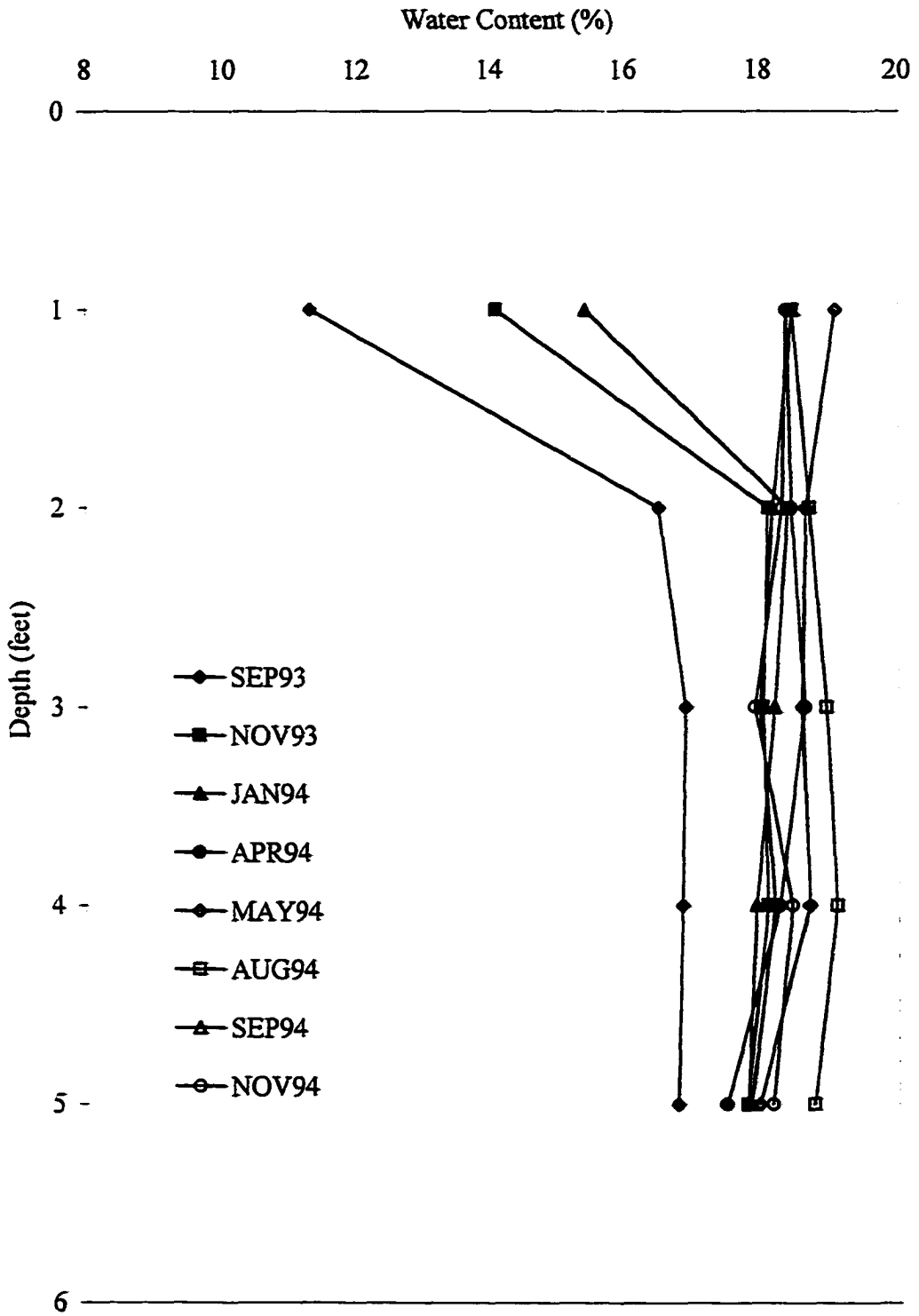

FSH Access Tube E-2

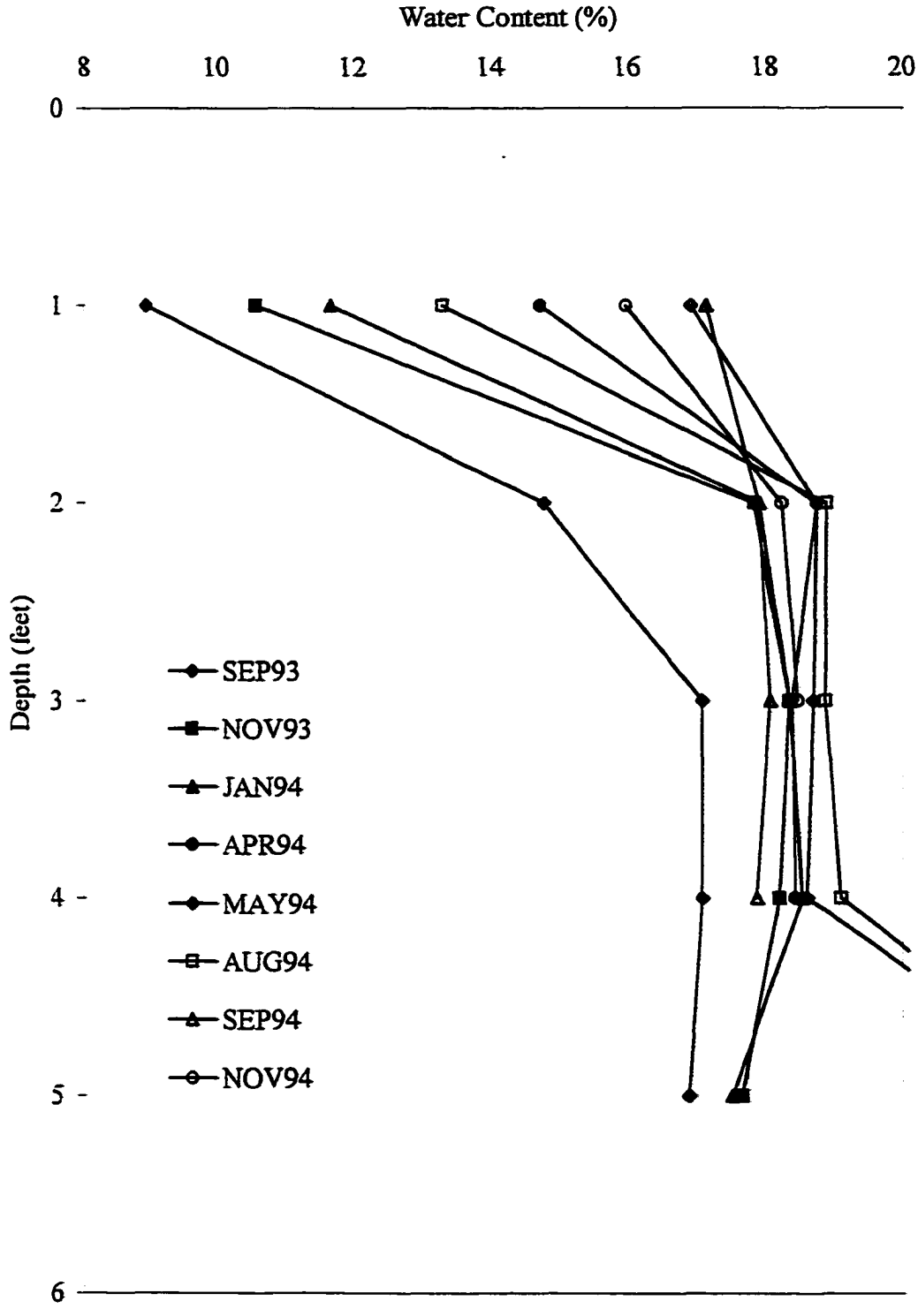

FSH Access Tube E-3

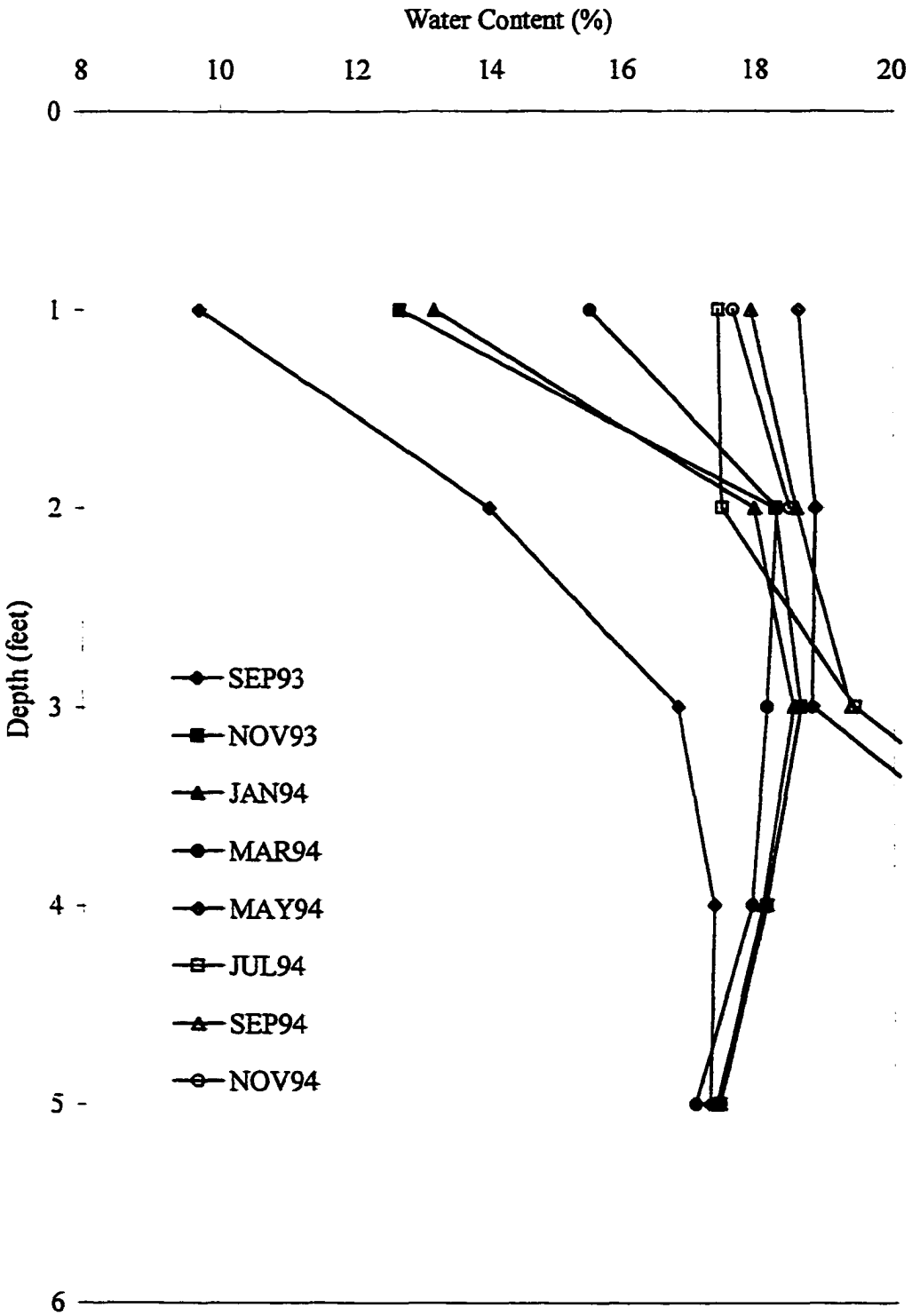

FSH Access Tube E-5

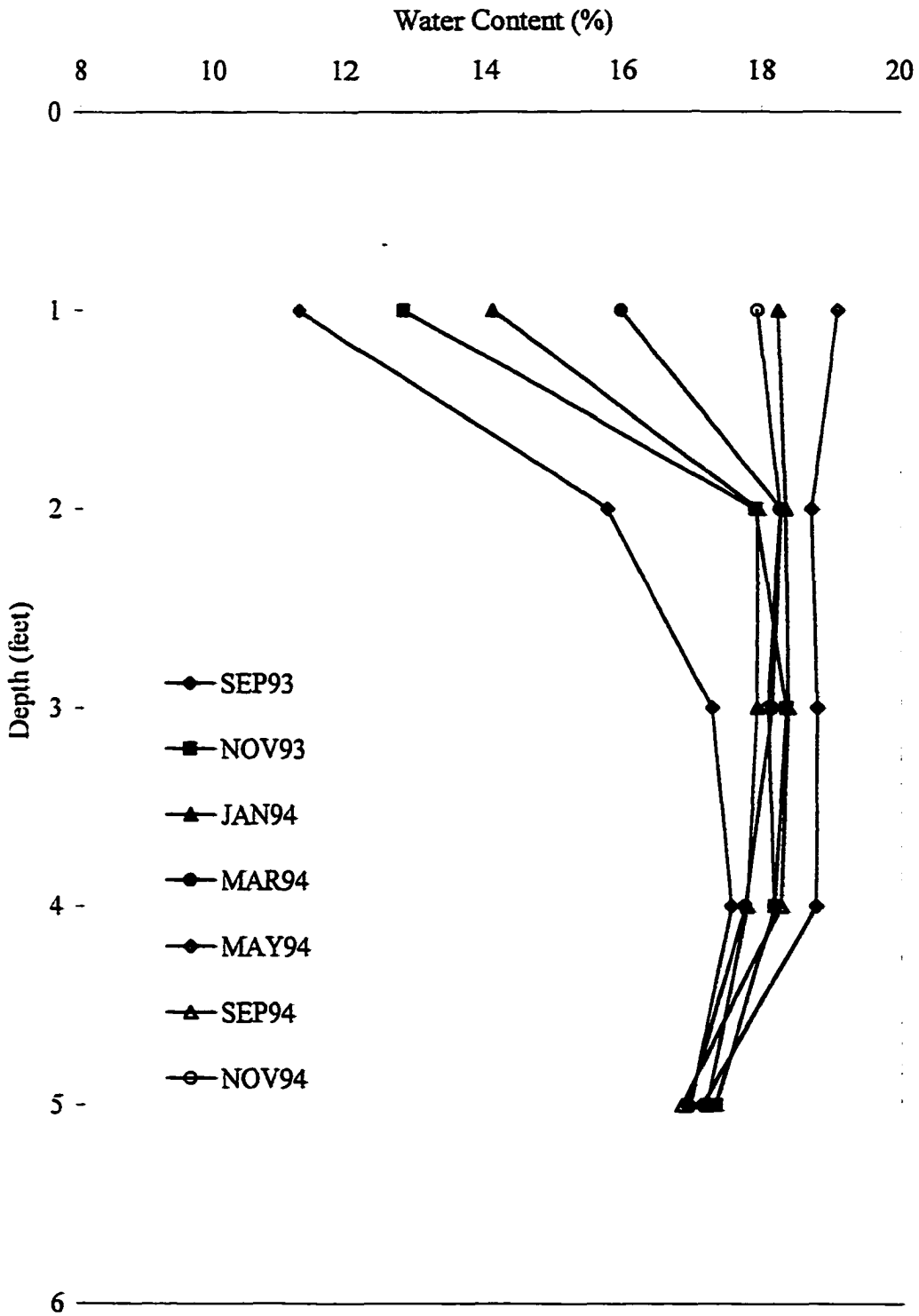

FSH Access Tube E-7

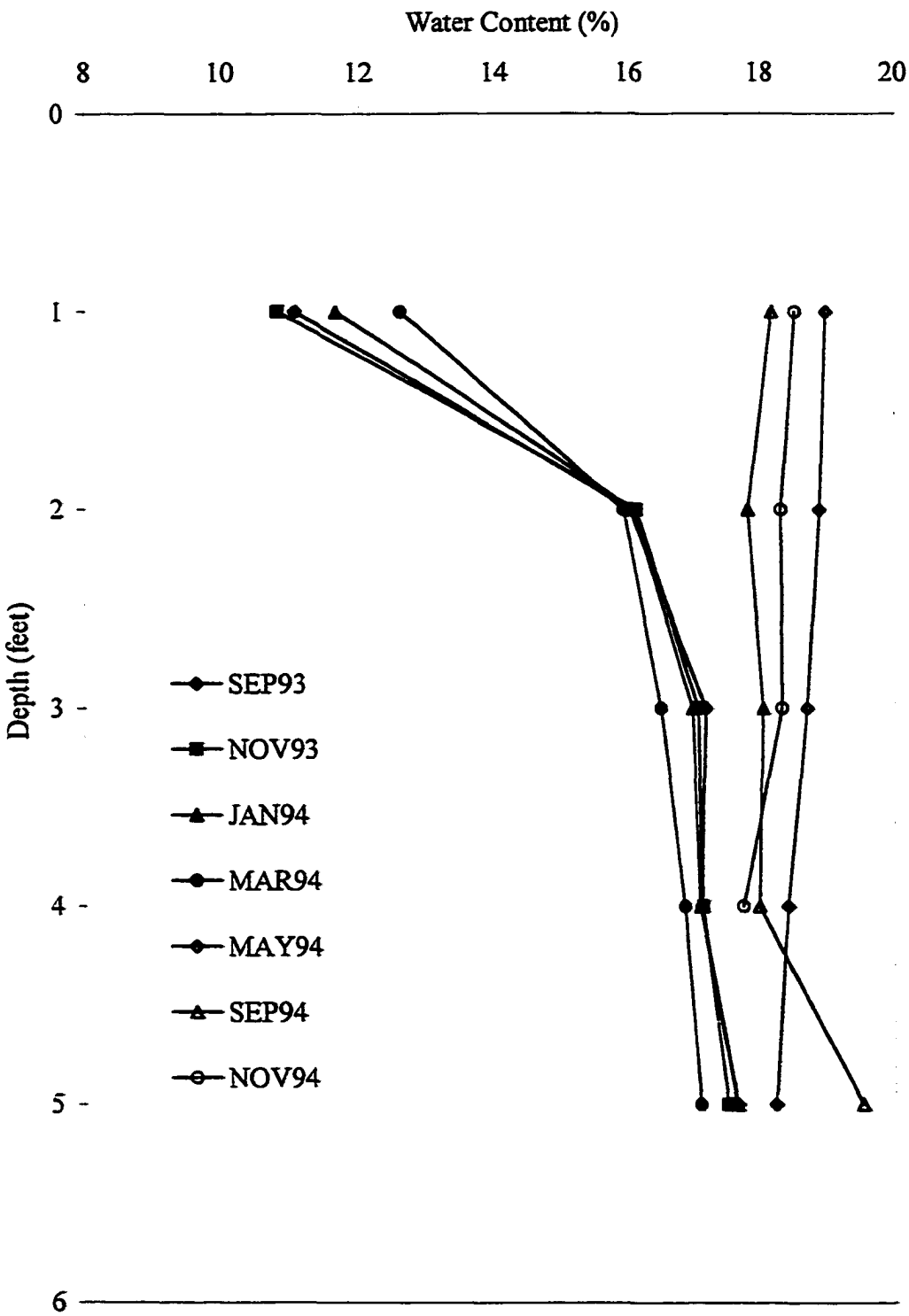

FSH Access Tube E-9

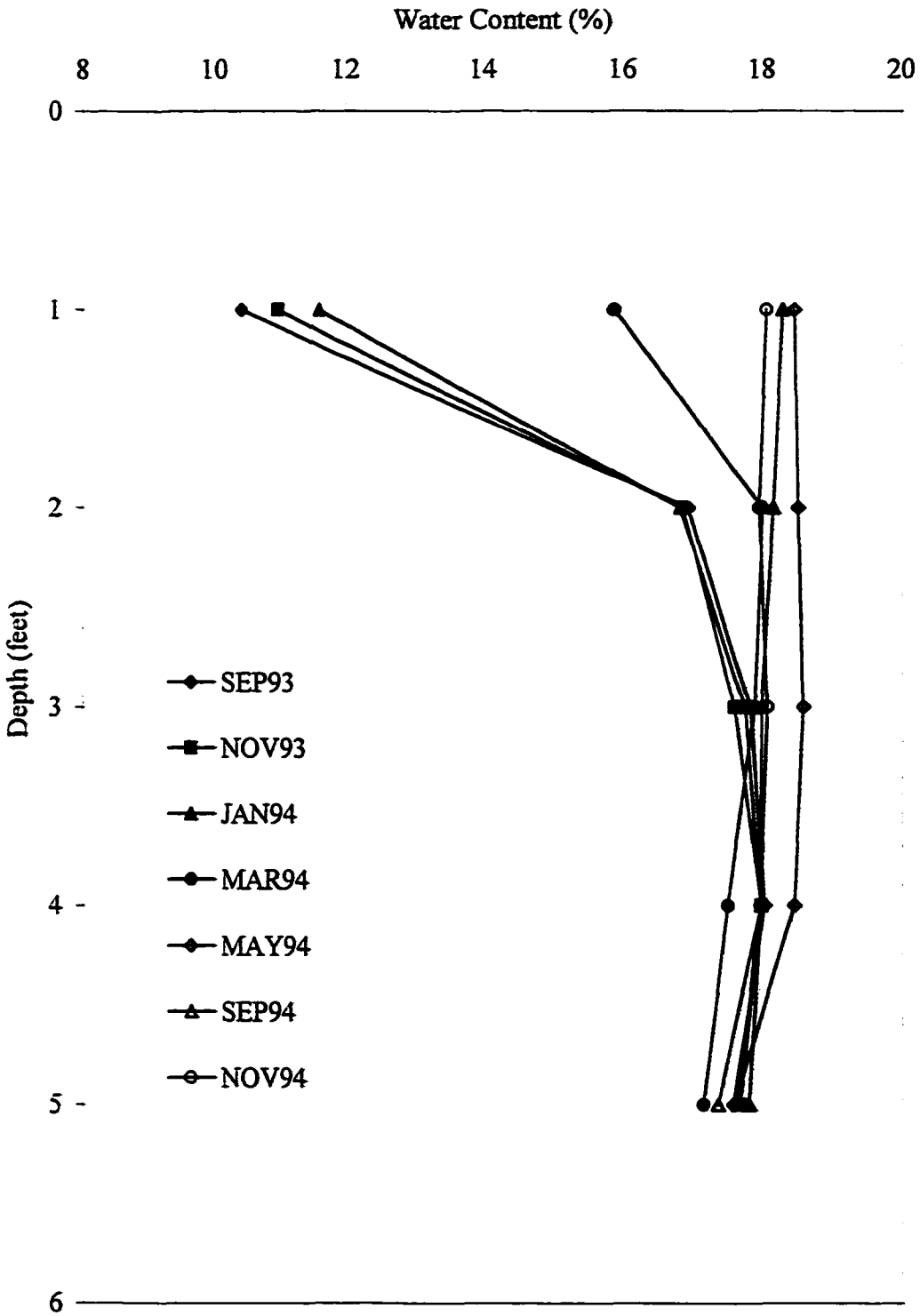

FSH Access Tube F-5

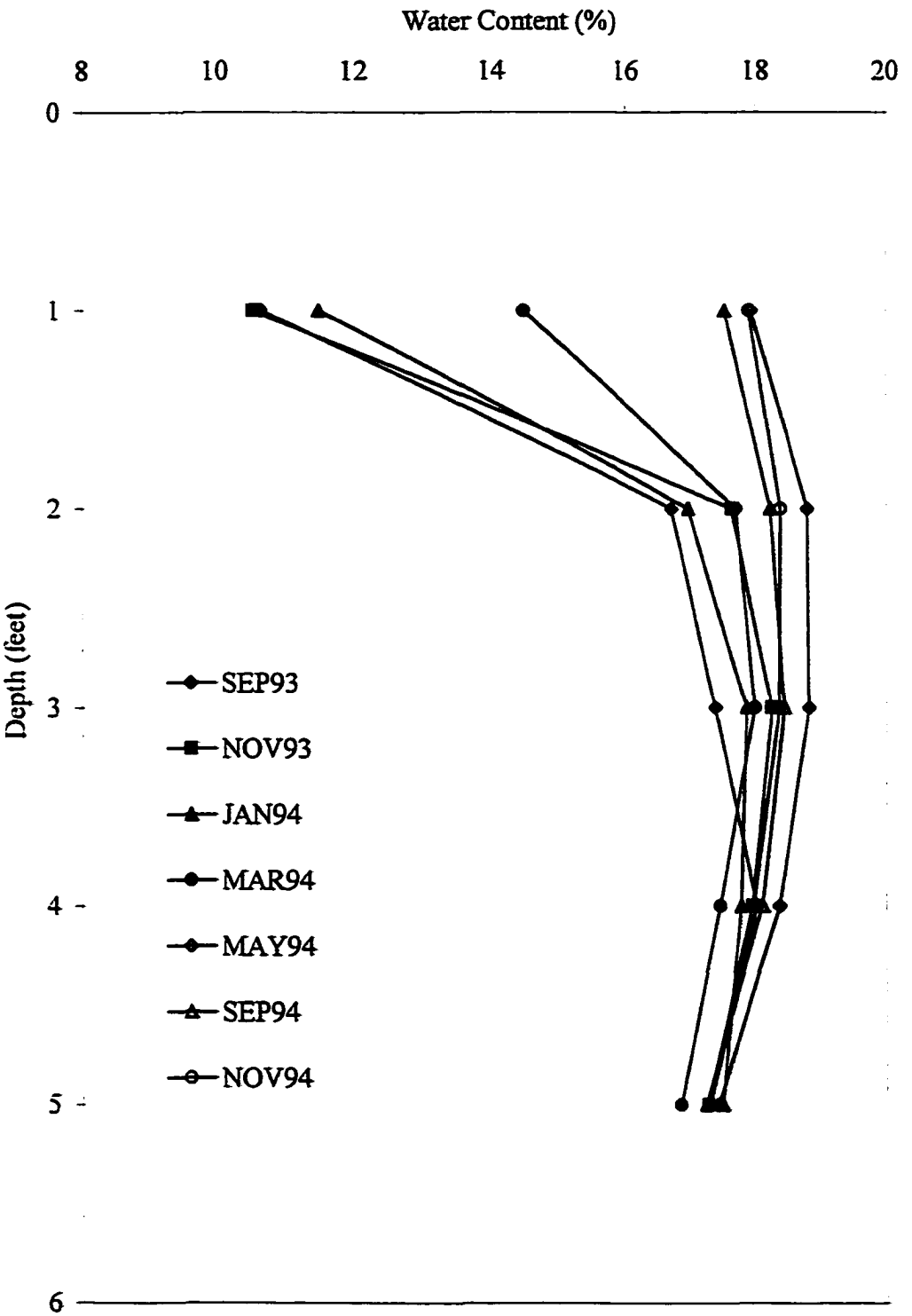

FSH Access Tube F-7

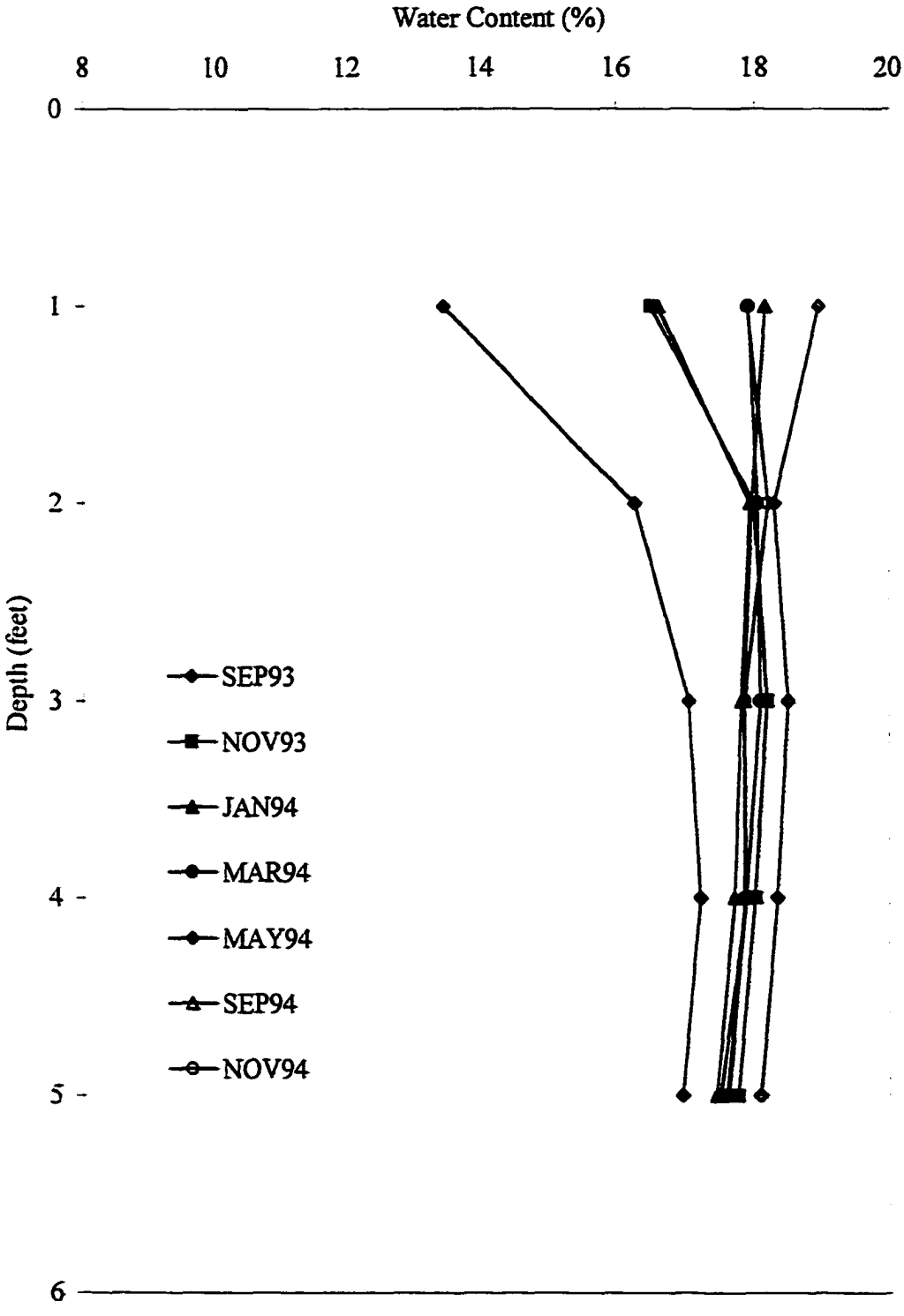

FSH Access Tube G-1

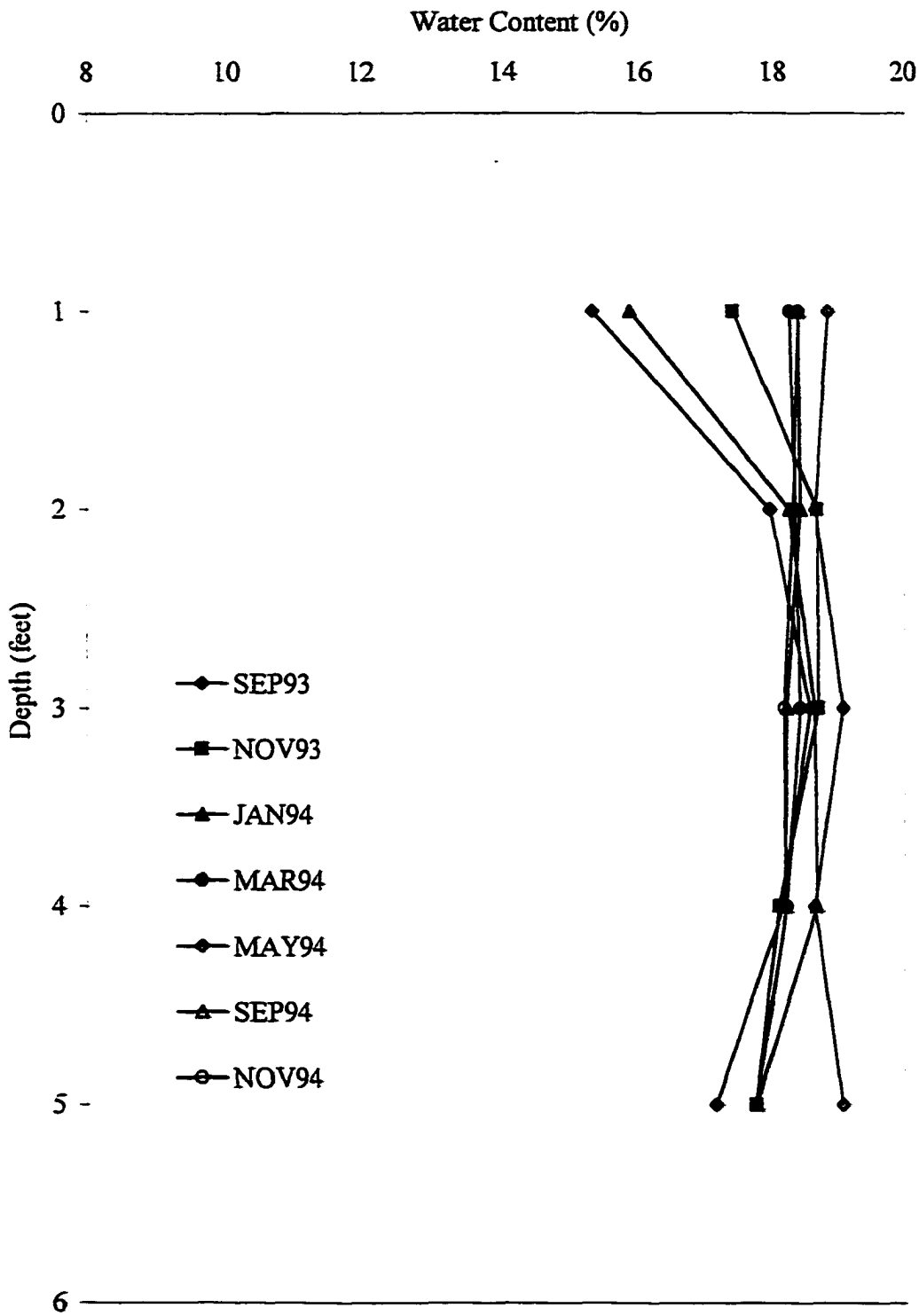

FSH Access Tube G-3

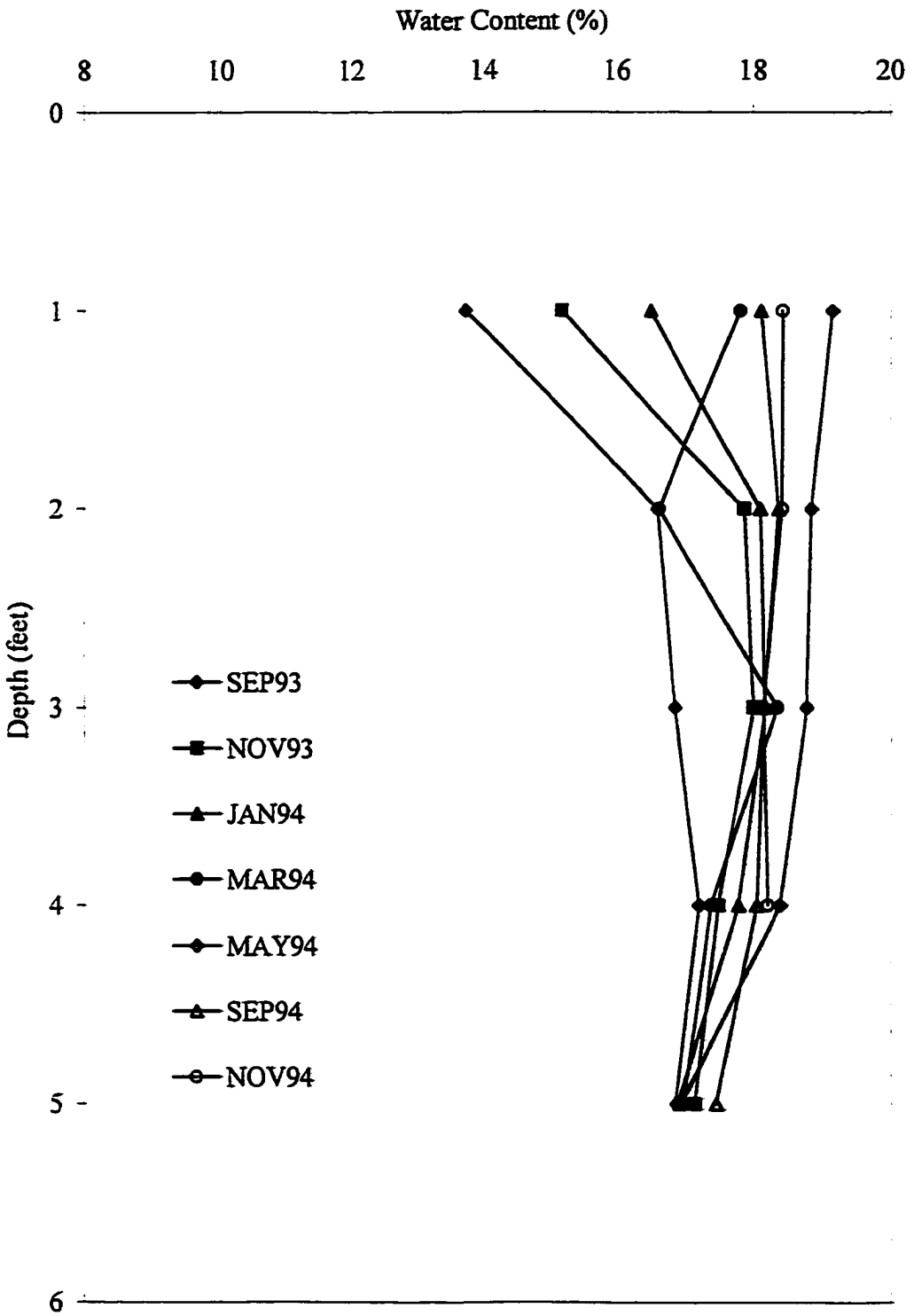

FSH Access Tube G-5

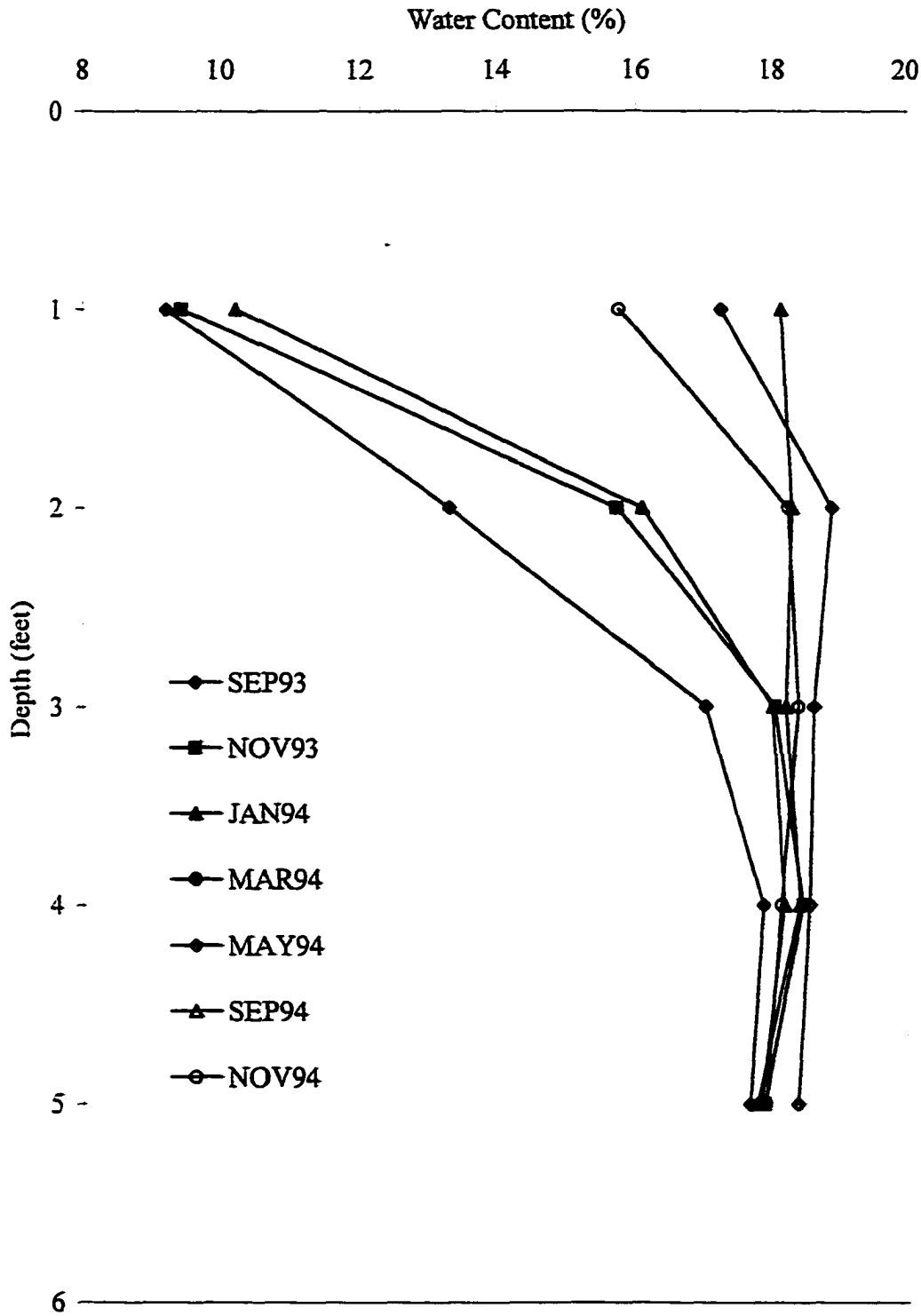

FSH Access Tube G-6

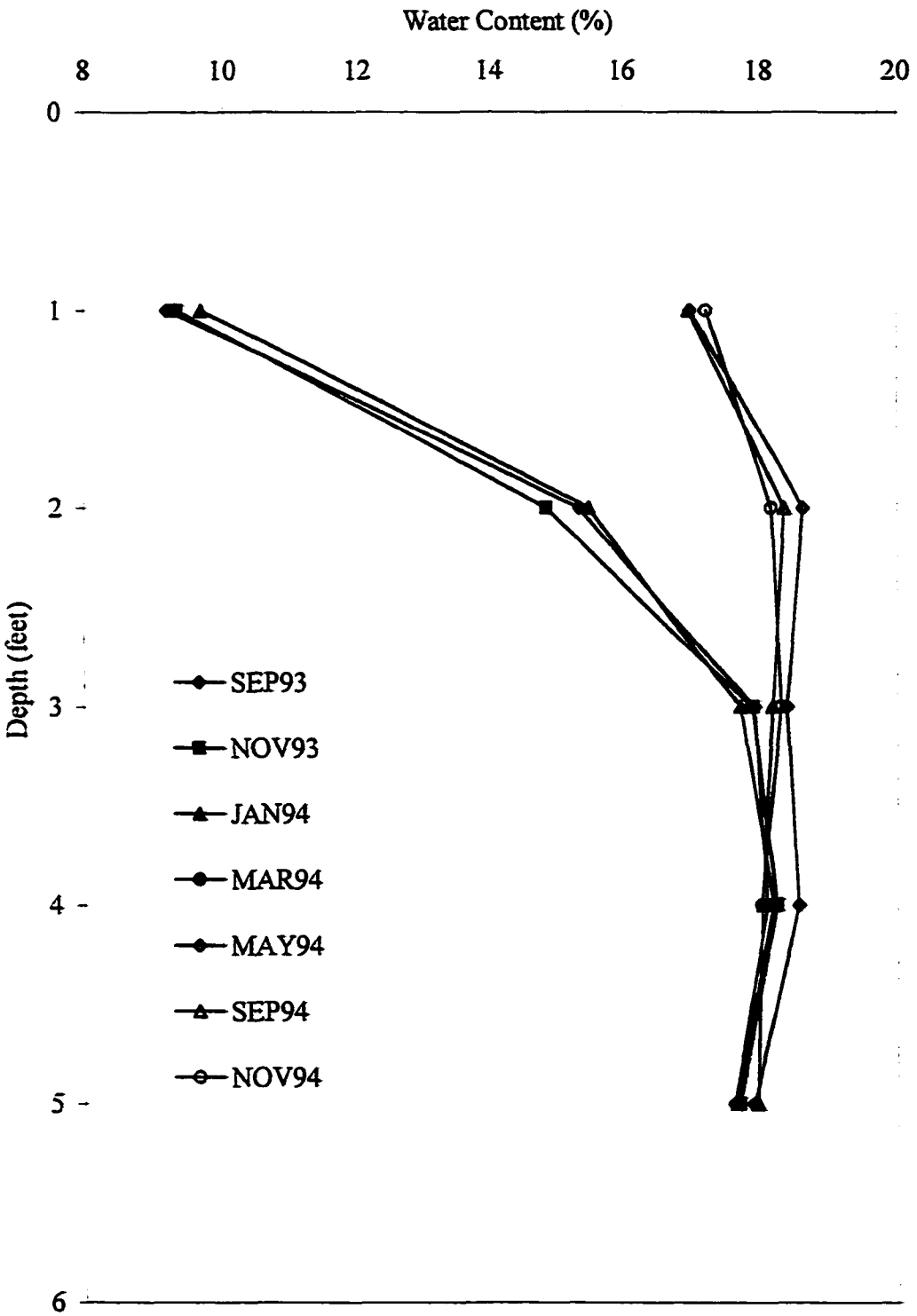

FSH Access Tube G-7

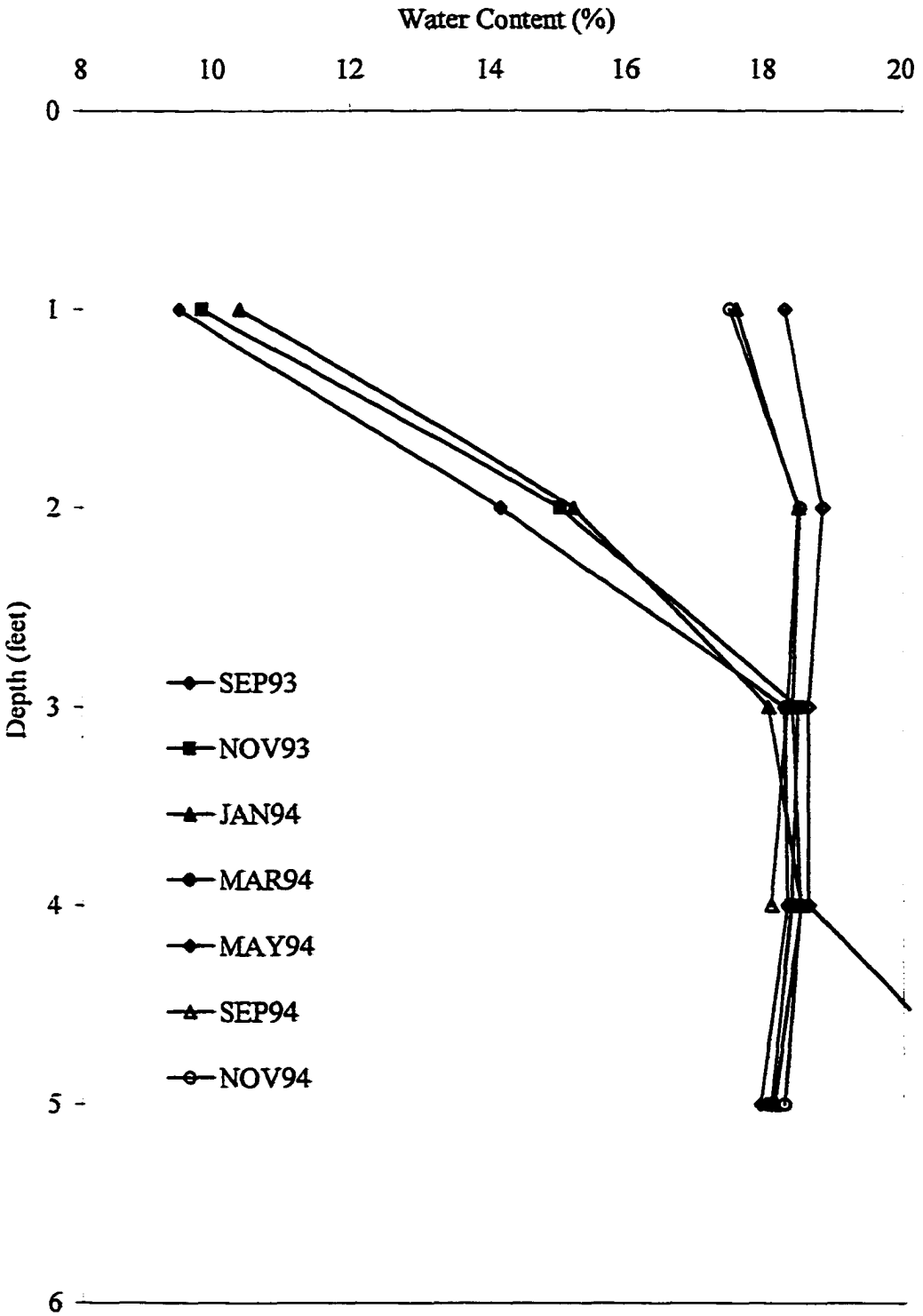

FSH Access Tube G-7.6

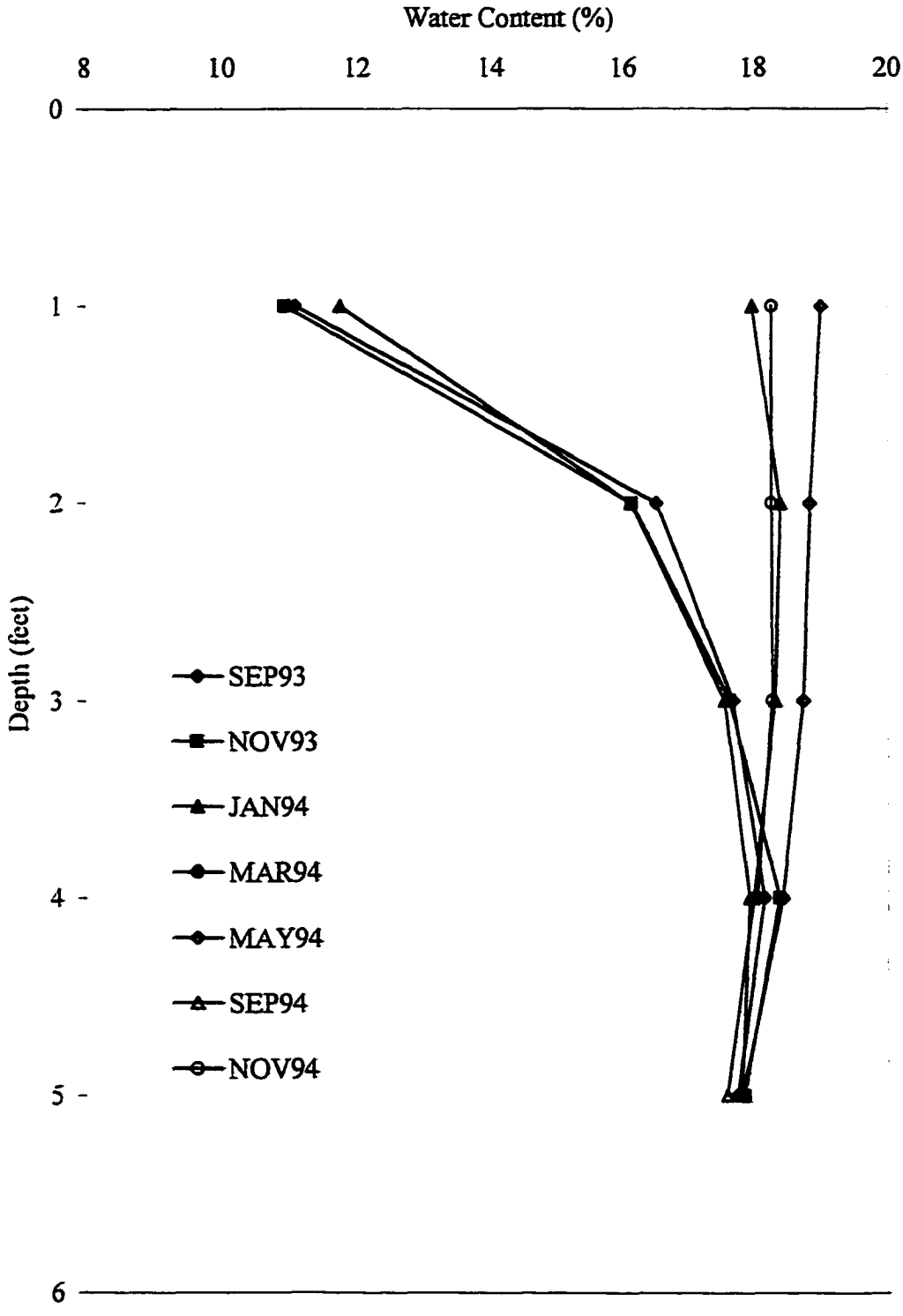

FSH Access Tube G-8.3

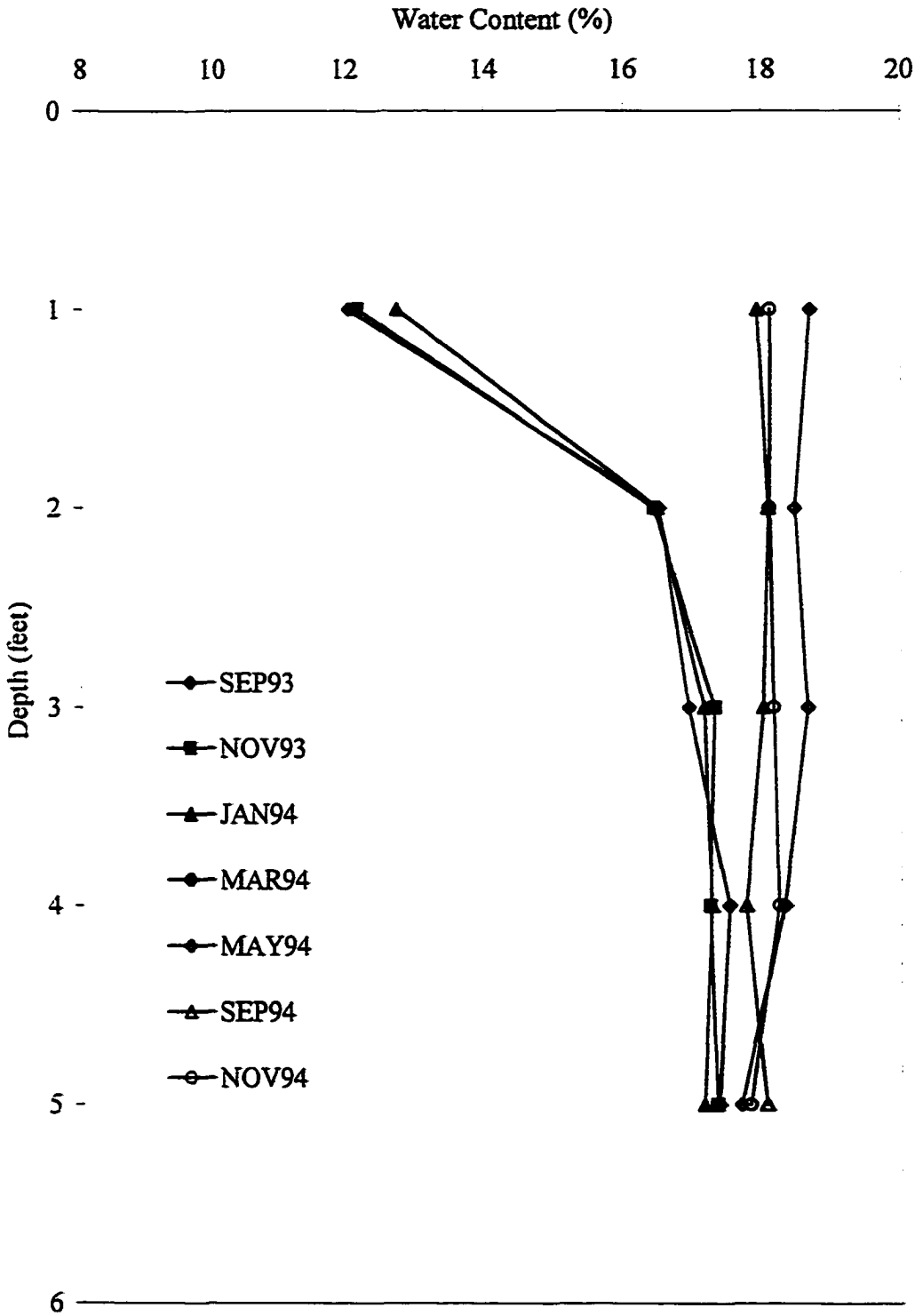

FSH Access Tube G-9

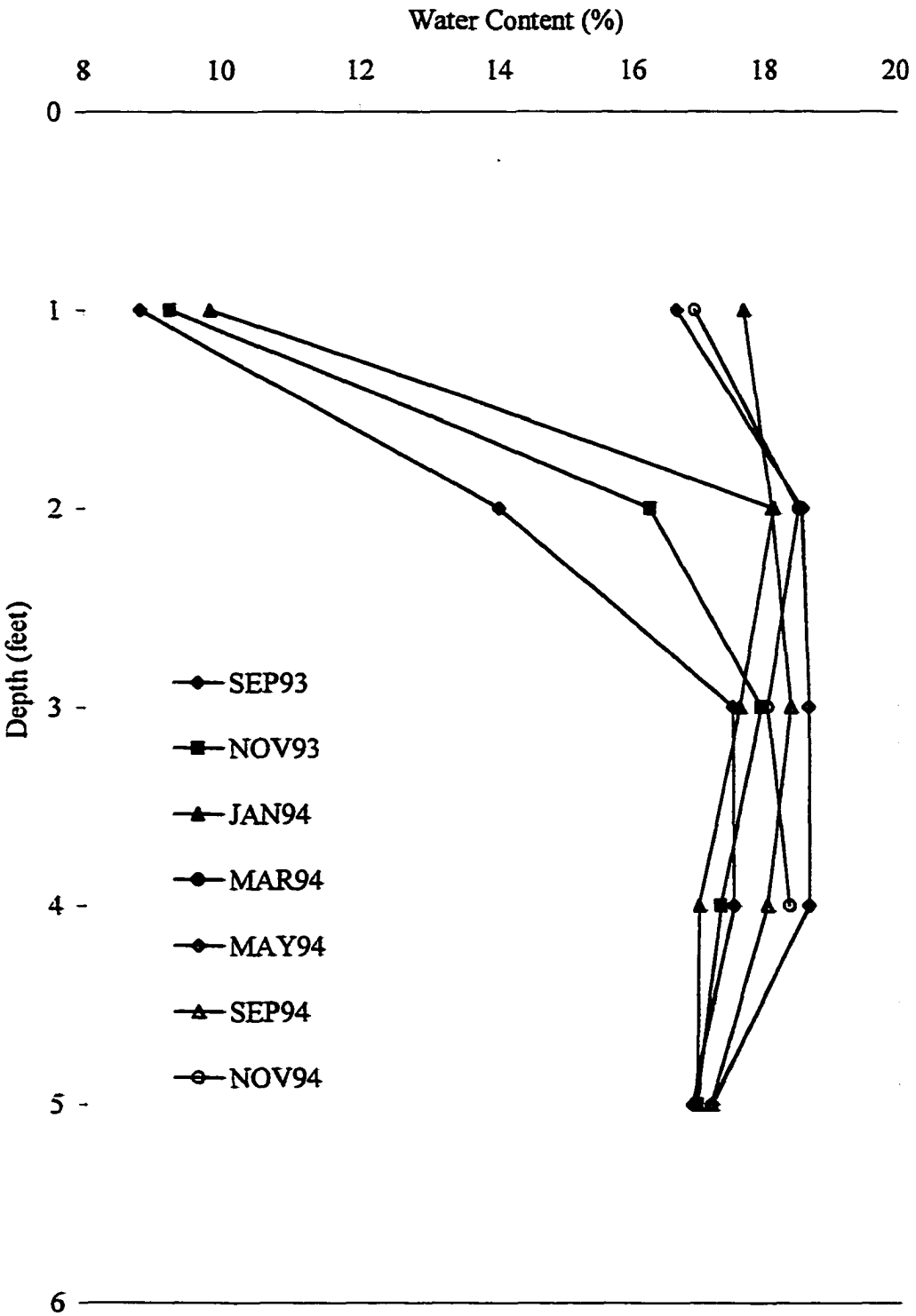

FSH Access Tube G.5-7

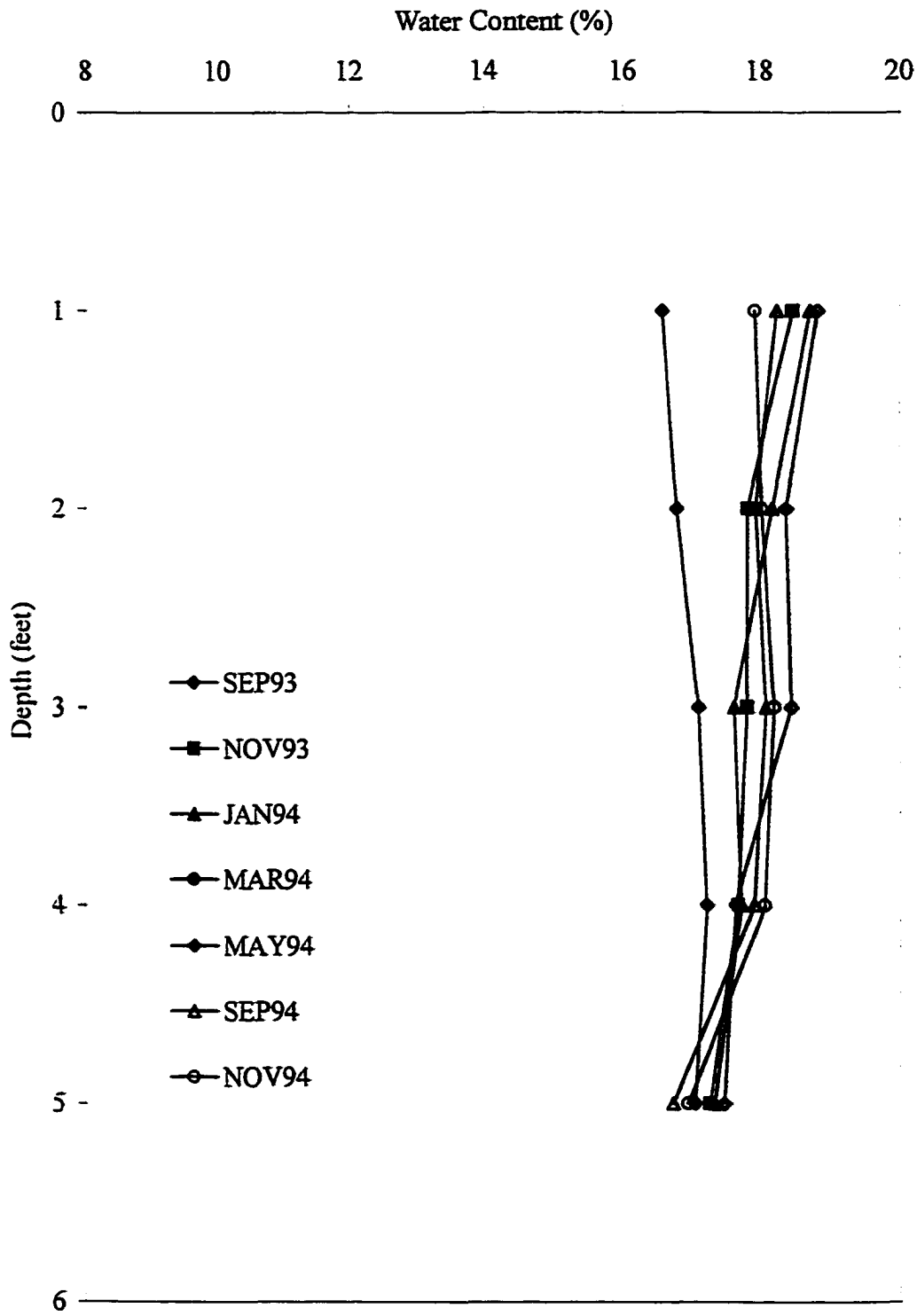

FSH Access Tube H-2

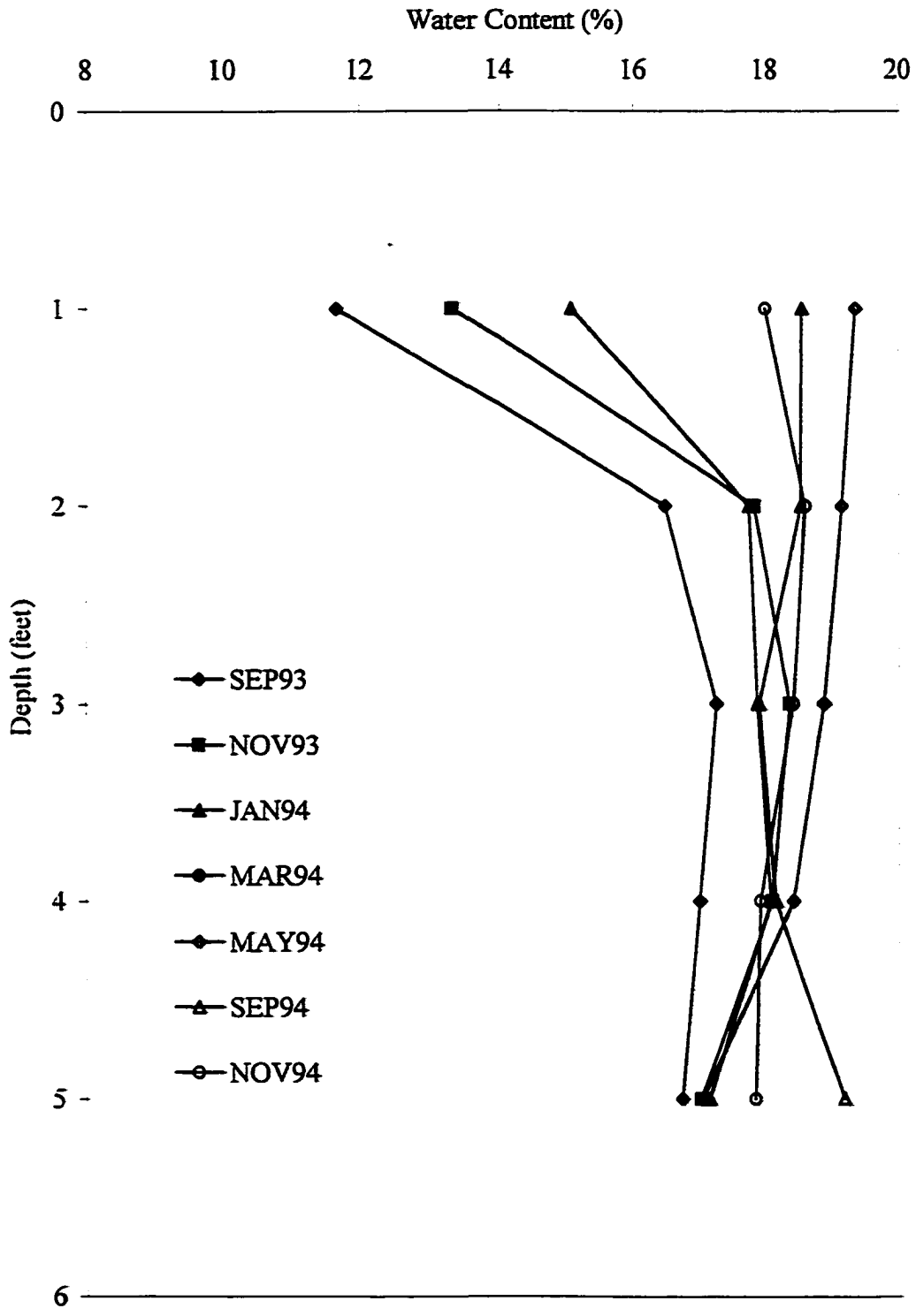

FSH Access Tube H-5

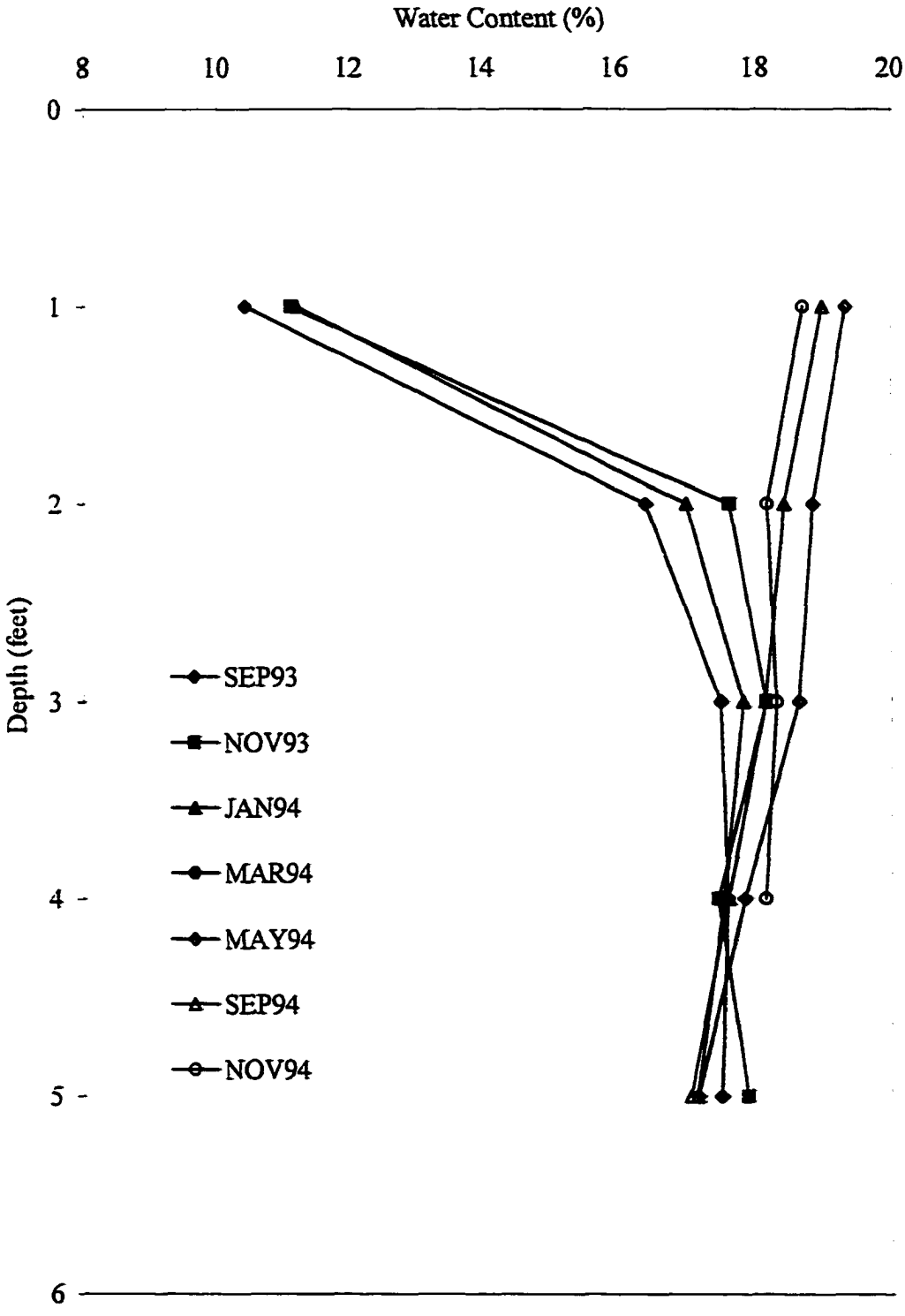

FSH Access Tube H-7

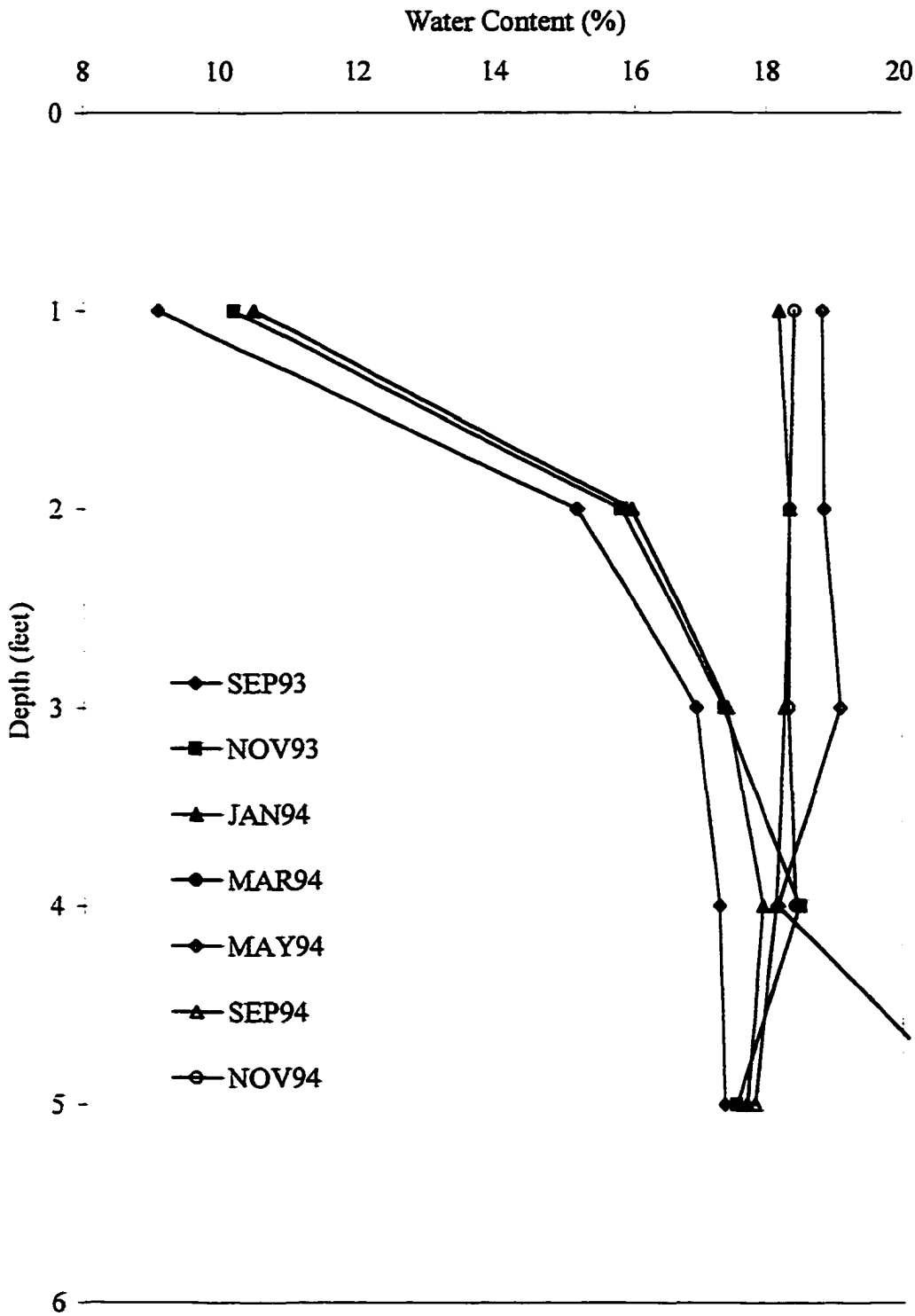

FSH Access Tube H.5-7

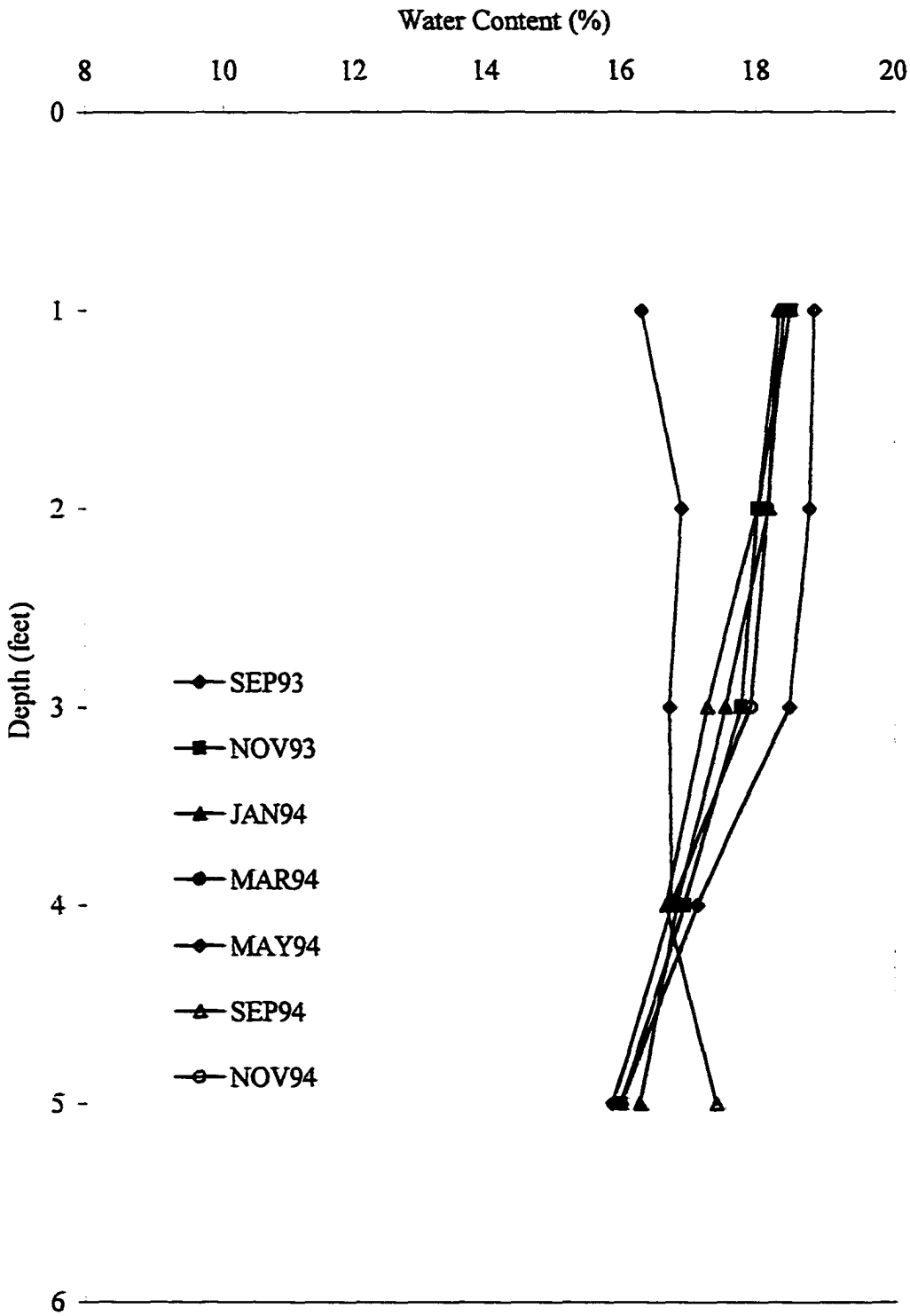

FSH Access Tube I-1

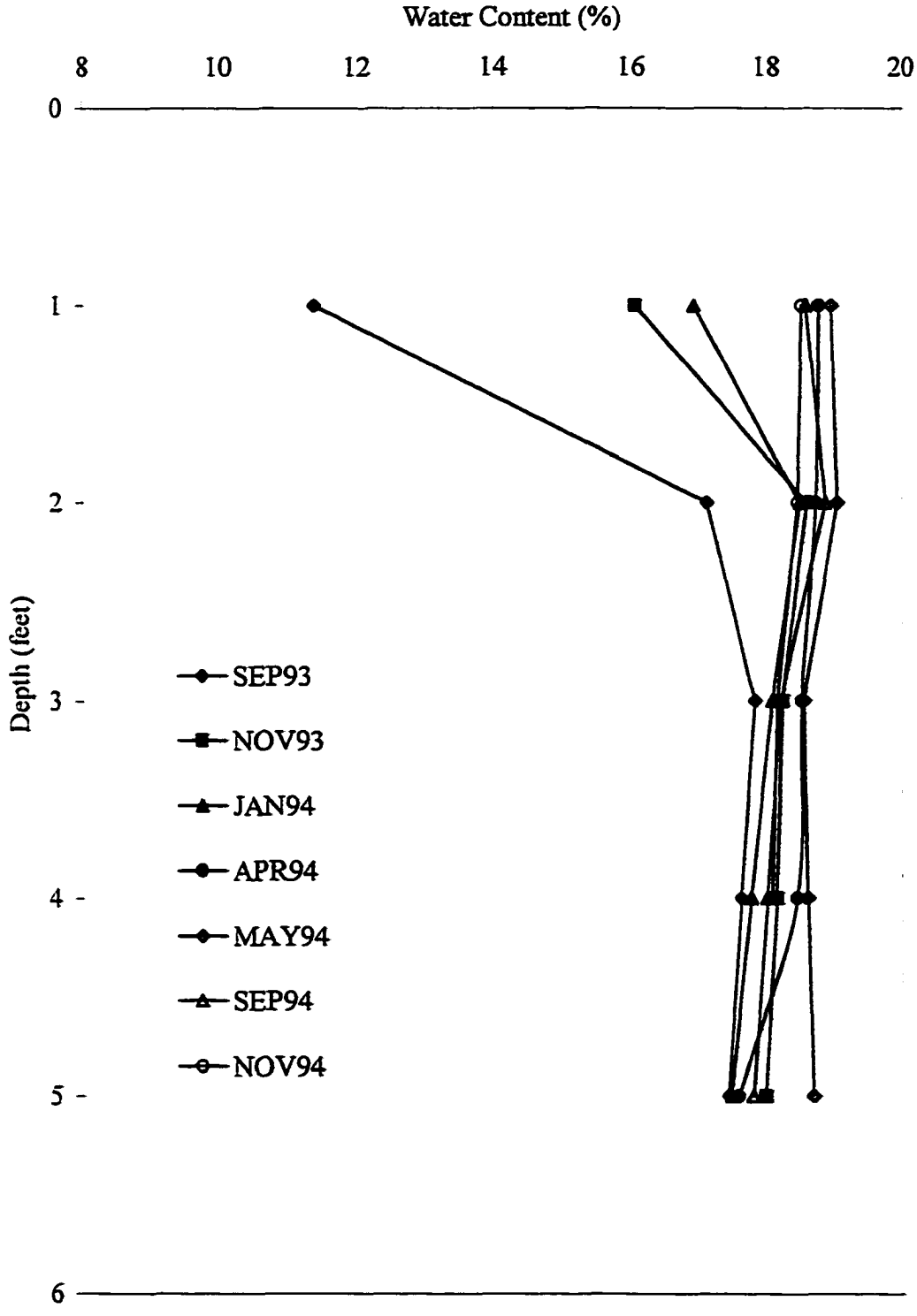

FSH Access Tube I-5

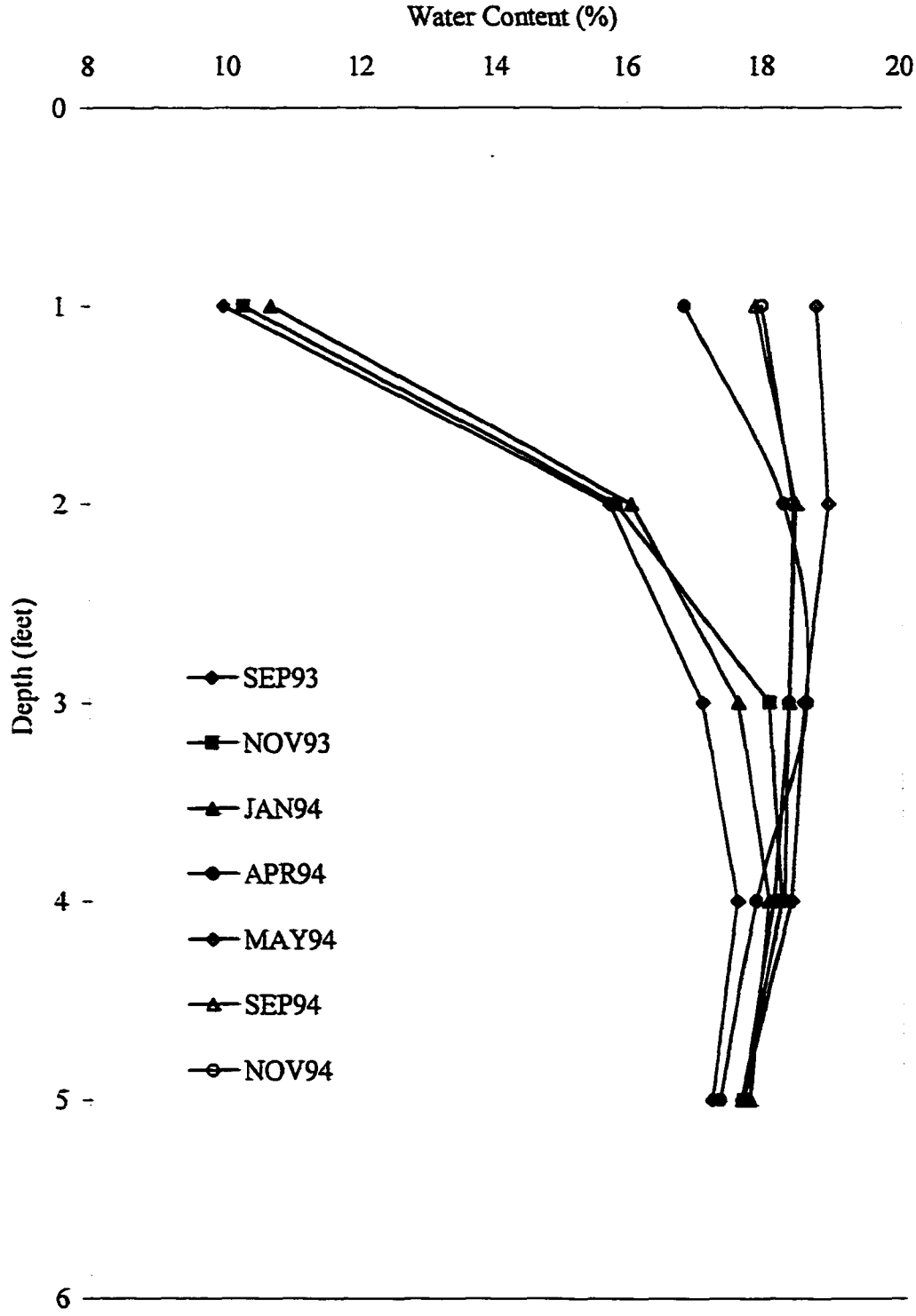

FSH Access Tube I-7

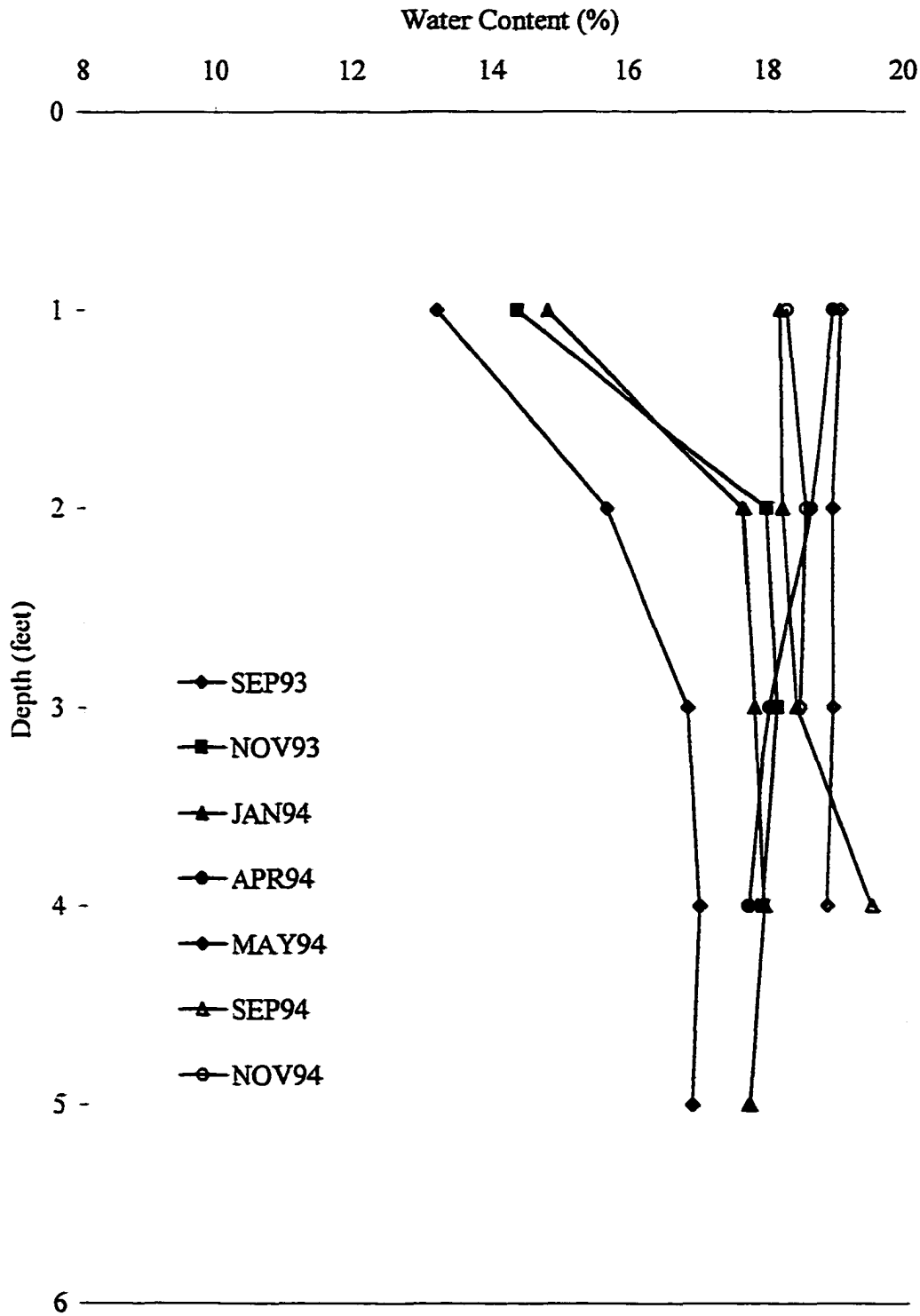

FSH Access Tube I-9

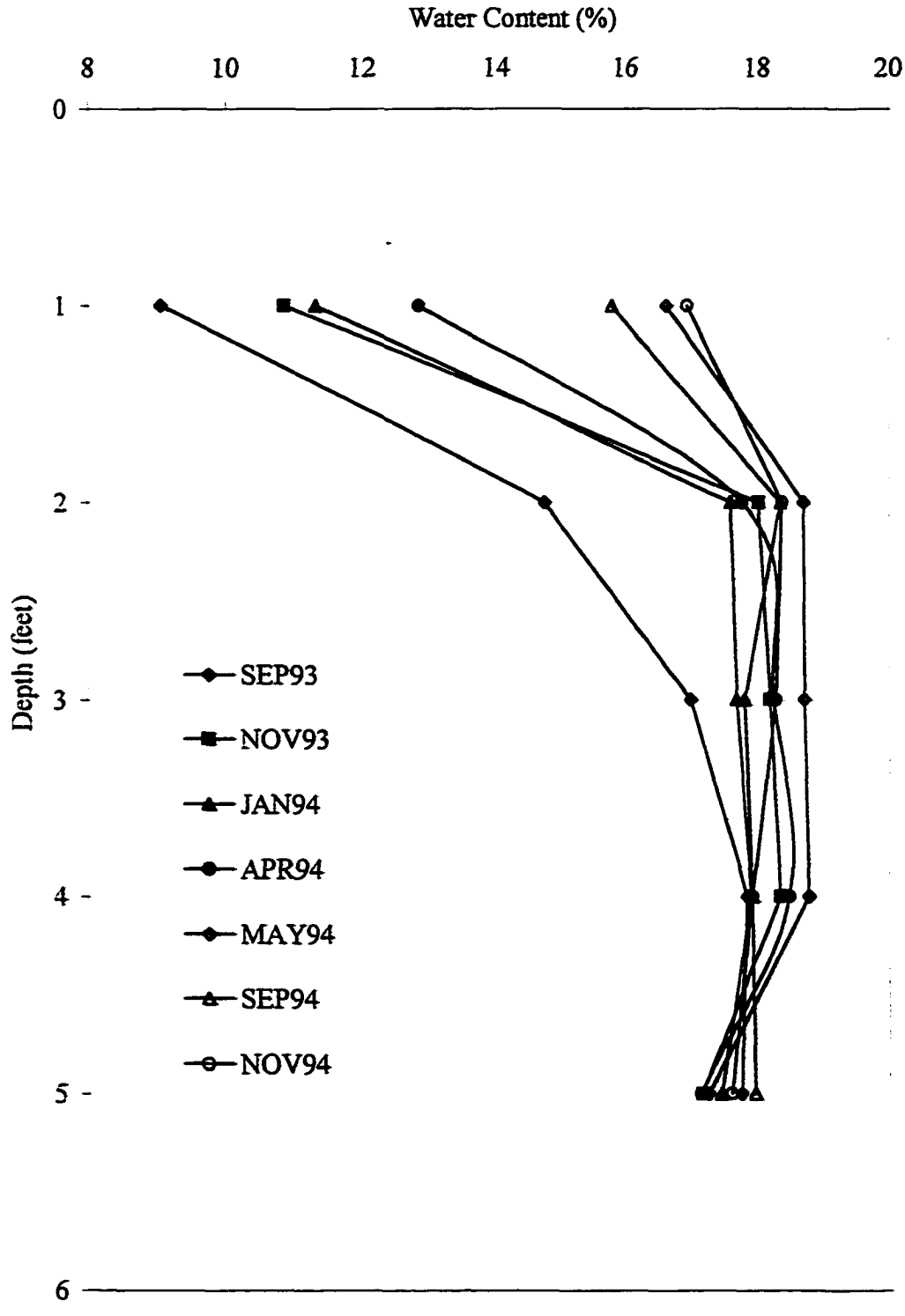

FSH Access Tube J-5

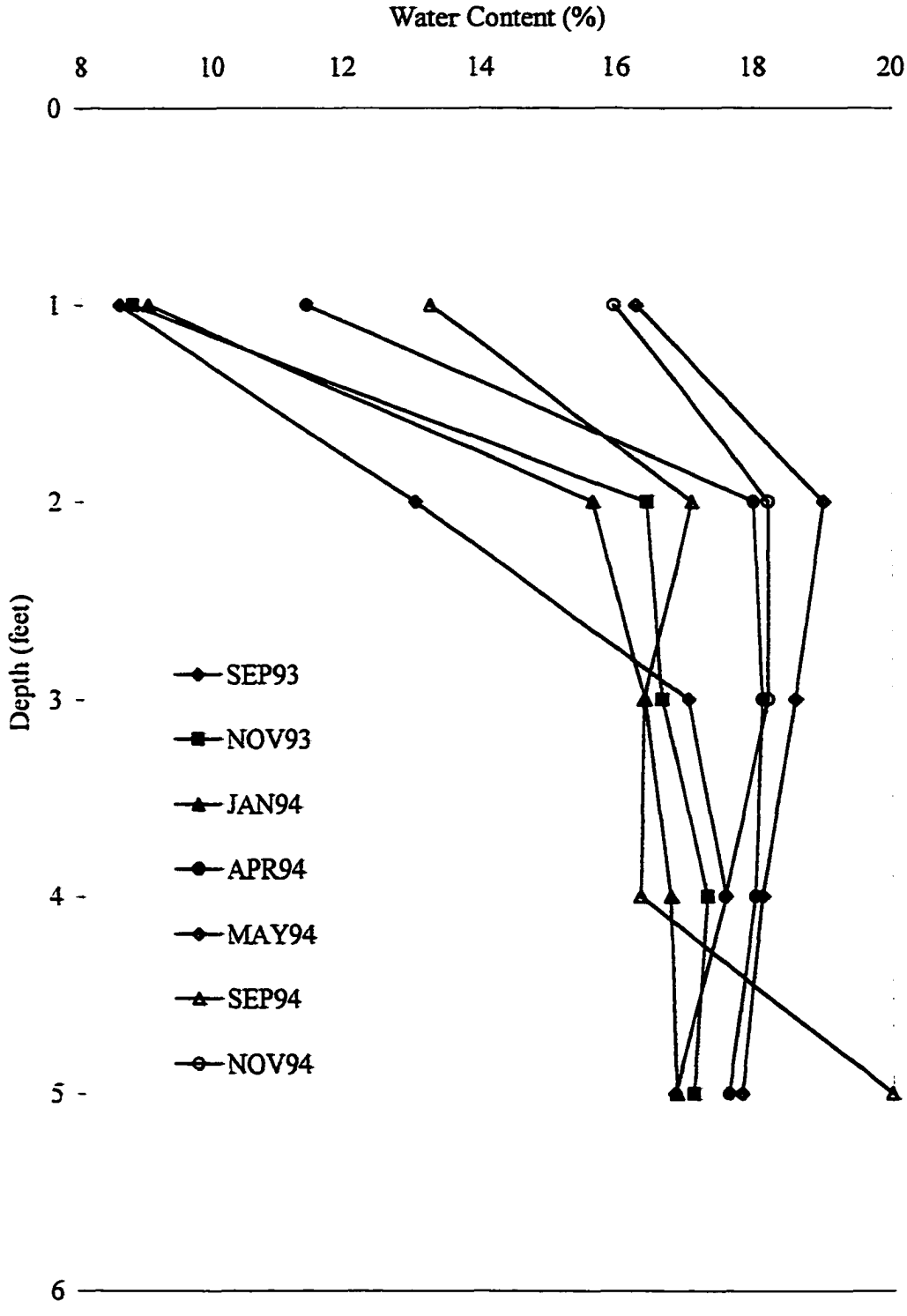

FSH Access Tube E-10

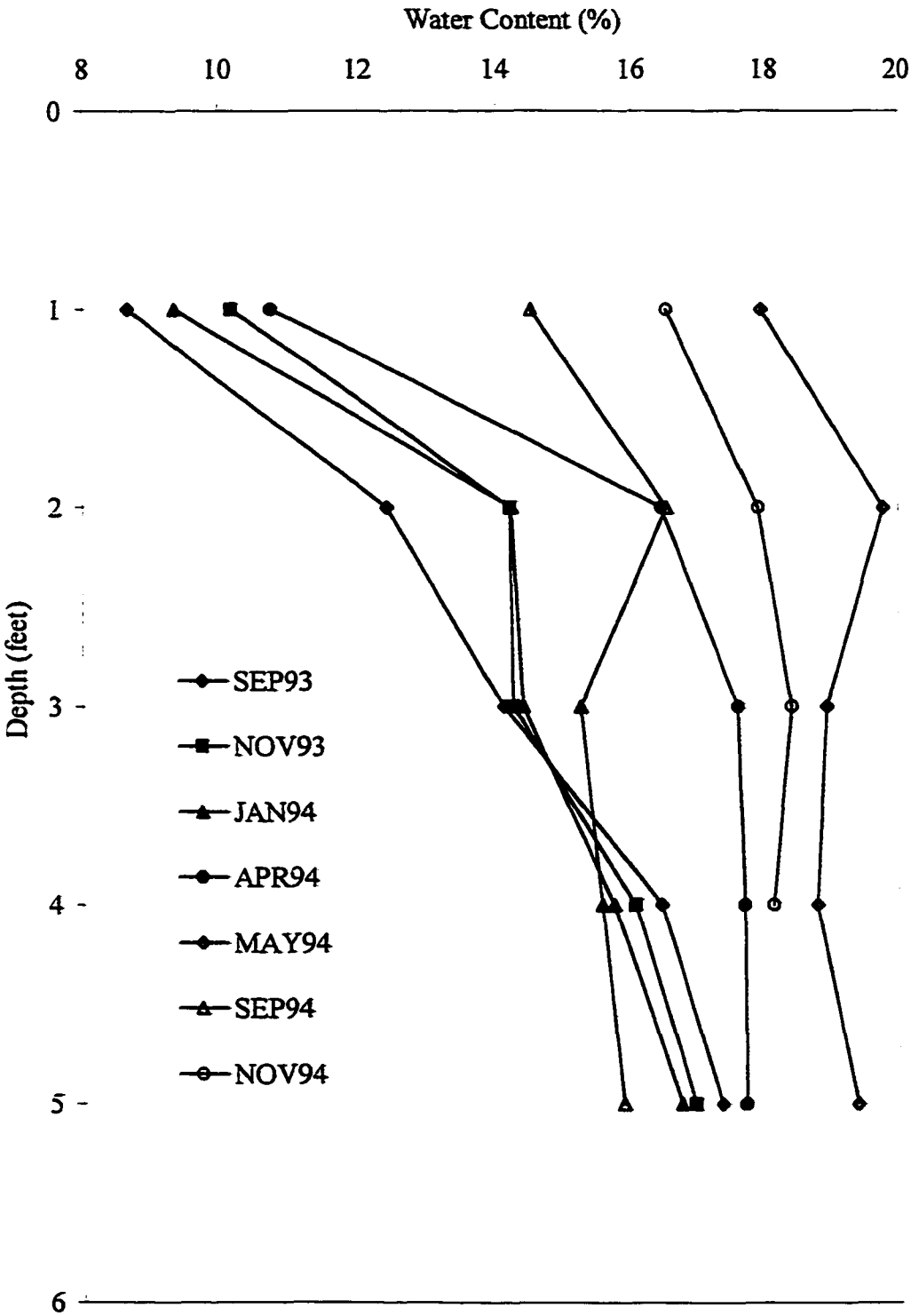

FSH Access Tube X-5

Elevation Data
Colorado State Site

Date:			01/8/93	01/8/93	01/28/93	01/28/93	02/19/93	02/19/93	03/15/93	03/15/93	04/16/93	04/16/93
Survey			Elevation	Difference	Elevation	Difference	Elevation	Difference	Elevation	Difference	Elevation	Difference
Marker	x-coordinate	y-coordinate	feet	feet	feet	feet	feet	feet	feet	feet	feet	feet
Benchmark			12.61		12.665		12.97		12.66		12.645	
A-2	40	26.25	4.54	8.07	4.61	-0.015	4.885	0.015	4.585	0.025	4.7	0.075
A-4	40	18.75	4.5	8.11	4.57	-0.015	4.85	0.01	4.525	0.025	4.69	0.045
A-6	40	11.25	4.6	8.01	4.665	-0.01	4.95	0.01	4.6	0.05	4.69	0.145
A-7	40	7.5	4.725	7.885	4.79	-0.01	5.07	0.015	4.705	0.07	4.975	-0.015
A-8	40	3.75	4.995	7.615	4.985	0.065	5.26	0.095	4.88	0.165	5.04	0.19
B-1	35	30	4.29	8.33	4.26	0.075	4.535	0.105	4.19	0.14	4.29	0.225
B-2	35	26.25	4.59	8.02	4.56	0.085	4.845	0.105	4.52	0.12	4.685	0.16
B-4	35	18.75	4.68	7.93	4.65	0.085	4.935	0.105	4.615	0.115	4.76	0.155
B-6	35	11.25	4.69	7.72	4.66	0.085	5.145	0.105	4.825	0.115	4.97	0.155
B-7	35	7.5	4.93	7.68	4.955	0.03	5.235	0.055	4.92	0.06	5.05	0.115
C-6	30	11.25	4.665	7.945	4.72	0	5	0.025	4.685	0.03	4.83	0.07
C-8	30	3.75	4.645	7.965	4.665	0.035	4.945	0.06	4.63	0.065	4.755	0.125
D-1	25	30	3.755	8.855	3.8	0.01	4.075	0.04	3.76	0.045	3.9	0.09
D-2	25	26.25	4.08	8.53	4.14	-0.005	4.42	0.02	4.105	0.025	4.25	0.065
D-4	25	18.75	4.355	8.255	4.41	0	4.69	0.025	4.38	0.025	4.525	0.065
D-6	25	11.25	4.555	8.055	4.61	0	4.89	0.025	4.575	0.03	4.72	0.07
D-7	25	7.5	4.62	7.99	4.68	-0.005	4.96	0.02	4.645	0.025	4.79	0.065
D-8	25	3.75	4.6	8.01	4.655	0	4.935	0.025	4.62	0.03	4.765	0.07
D-9	25	0	4.585	8.025	4.64	0	4.925	0.02	4.6	0.035	4.705	0.115
E-2	20	26.25	3.81	8.8	3.87	-0.005	4.15	0.02	3.84	0.02	3.985	0.06
E-4	20	18.75	4.24	8.37	4.3	-0.005	4.58	0.02	4.265	0.025	4.41	0.065
E-6	20	11.25	4.495	8.115	4.55	0	4.83	0.025	4.525	0.02	4.66	0.07
F-1	15	30	3.455	9.155	3.51	0	3.79	0.025	3.48	0.025	3.625	0.065
F-2	15	26.25	3.885	8.725	3.9	0.04	4.18	0.065	3.865	0.07	4.01	0.11
F-3	15	22.5	4.14	8.47	4.18	0.035	4.44	0.06	4.125	0.065	4.27	0.105
F-4	15	18.75	4.2	8.41	4.26	-0.005	4.53	0.03	4.225	0.025	4.365	0.07
F-6	15	11.25	4.405	8.205	4.46	0	4.74	0.025	4.425	0.03	4.575	0.065
F-8	15	3.75	4.45	8.16	4.505	0	4.785	0.025	4.475	0.025	4.62	0.065
F-9	15	0	4.385	8.225	4.44	0	4.715	0.03	4.405	0.03	4.55	0.07
G-2	10	26.25	3.93	8.68	3.985	0	4.265	0.025	3.995	-0.015	4.095	0.07
G-4	10	18.75	4.27	8.34	4.325	0	4.605	0.025	4.295	0.025	4.435	0.07
H-1	5	30	3.345	9.265	3.4	0	3.675	0.03	3.365	0.03	3.51	0.07
H-3	5	22.5	3.995	8.615	4.05	0	4.325	0.03	4.01	0.035	4.155	0.075
H-6	5	11.25	4.3	8.31	4.35	0.005	4.615	0.045	4.315	0.035	4.46	0.075
H-8	5	3.75	4.375	8.235	4.43	0	4.705	0.03	4.385	0.04	4.53	0.08
H-9	5	0	4.42	8.19	4.485	0.01	4.75	0.03	4.445	0.025	4.585	0.07
I-2	0	26.25	3.79	8.82	3.845	0	4.12	0.03	3.82	0.02	3.965	0.06
I-3	0	22.5	3.935	8.675	3.99	0	4.27	0.025	3.97	0.015	4.11	0.06
I-4	0	18.75	3.895	8.615	3.95	0.1	4.24	0.115	4.03	0.015	4.175	0.055
I-6	0	11.25	4.125	8.485	4.17	0.01	4.44	0.045	4.14	0.035	4.27	0.09
I-8	0	3.75	4.13	8.48	4.185	0	4.455	0.035	4.17	0.01	4.31	0.055

Date:			05/21/93	05/21/93	06/22/93	06/22/93	07/27/93	07/27/93	09/30/93	09/30/93	11/12/93	11/12/93
Survey Marker	x-coordinate	y-coordinate	Elevation feet	Difference feet	Elevation feet	Difference feet	Elevation feet	Difference feet	Elevation feet	Difference feet	Elevation feet	Difference feet
Benchmark			12.75		12.885		12.625		12.81		12.925	
A-2	40	26.25	4.66	0.02	4.75	0.065	4.485	0.09	4.64	0.1	4.72	0.135
A-4	40	18.75	4.6	0.04	4.69	0.085	4.41	0.105	4.585	0.115	4.655	0.16
A-6	40	11.25	4.64	0.1	4.745	0.13	4.465	0.15	4.63	0.17	4.71	0.205
A-7	40	7.5	4.74	0.125	4.845	0.155	4.585	0.175	4.74	0.185	4.815	0.225
A-8	40	3.75	4.915	0.22	5.025	0.245	4.755	0.255	4.93	0.265	5.01	0.3
B-1	35	30	4.26	0.16	4.385	0.17	4.105	0.19	4.29	0.19	4.38	0.215
B-2	35	26.25	4.63	0.1	4.75	0.115	4.485	0.14	4.645	0.145	4.72	0.185
B-4	35	18.75	4.73	0.09	4.855	0.1	4.57	0.125	4.74	0.14	4.805	0.19
B-6	35	11.25	4.94	0.09	5.05	0.115	4.76	0.145	4.92	0.17	4.99	0.225
B-7	35	7.5	5.005	0.065	5.1	0.105	4.805	0.14	4.985	0.165	5.035	0.21
C-6	30	11.25	4.805	0	4.94	0	4.665	0.015	4.86	0.005	4.945	0.035
C-8	30	3.75	4.73	0.055	4.83	0.09	4.54	0.12	4.7	0.145	4.765	0.195
D-1	25	30	3.87	0.025	4.005	0.025	3.725	0.045	3.93	0.025	4.025	0.045
D-2	25	26.25	4.225	-0.005	4.36	-0.005	4.085	0.01	4.28	0	4.38	0.015
D-4	25	18.75	4.5	-0.005	4.64	-0.01	4.355	0.015	4.56	-0.005	4.655	0.015
D-6	25	11.25	4.69	0.005	4.83	0	4.55	0.02	4.73	0.025	4.805	0.065
D-7	25	7.5	4.76	0	4.9	-0.005	4.62	0.015	4.82	0	4.905	0.03
D-8	25	3.75	4.735	0.005	4.865	0.01	4.57	0.045	4.765	0.035	4.83	0.085
D-9	25	0	4.66	0.065	4.79	0.07	4.505	0.095	4.68	0.105	4.755	0.145
E-2	20	26.25	3.995	-0.045	4.095	-0.01	3.82	0.005	4.02	-0.01	4.115	0.01
E-4	20	18.75	4.385	-0.005	4.525	-0.01	4.245	0.01	4.445	-0.005	4.54	0.015
E-6	20	11.25	4.635	0	4.77	0	4.5	0.01	4.7	-0.005	4.79	0.02
F-1	15	30	3.6	-0.005	3.745	-0.015	3.465	0.005	3.665	-0.01	3.76	0.01
F-2	15	26.25	3.99	0.035	4.125	0.035	3.85	0.05	4.045	0.04	4.145	0.055
F-3	15	22.5	4.245	0.035	4.37	0.045	4.1	0.055	4.29	0.05	4.38	0.075
F-4	15	18.75	4.34	0	4.48	-0.005	4.205	0.01	4.4	0	4.495	0.02
F-6	15	11.25	4.545	0	4.69	-0.01	4.41	0.01	4.615	-0.01	4.705	0.015
F-8	15	3.75	4.595	-0.005	4.74	-0.015	4.46	0.005	4.66	-0.01	4.75	0.015
F-9	15	0	4.525	0	4.67	-0.01	4.39	0.01	4.595	-0.01	4.76	-0.06
G-2	10	26.25	4.07	0	4.21	-0.005	3.93	0.015	4.135	-0.005	4.225	0.02
G-4	10	18.75	4.41	0	4.555	-0.01	4.275	0.01	4.475	-0.005	4.56	0.025
H-1	5	30	3.49	-0.005	3.625	-0.005	3.35	0.01	3.555	-0.01	3.645	0.015
H-3	5	22.5	4.13	0.005	4.27	0	3.99	0.02	4.18	0.015	4.255	0.055
H-6	5	11.25	4.43	0.01	4.575	0	4.3	0.015	4.5	0	4.585	0.03
H-8	5	3.75	4.505	0.01	4.65	0	4.375	0.015	4.57	0.005	4.66	0.03
H-9	5	0	4.56	0	4.705	-0.01	4.43	0.005	4.63	-0.01	4.72	0.015
I-2	0	26.25	4.03	-0.1	4.08	-0.015	3.805	0	4.02	-0.03	4.105	0
I-3	0	22.5	4.09	-0.015	4.23	-0.02	3.955	-0.005	4.15	-0.015	4.245	0.005
I-4	0	18.75	4.15	-0.015	4.3	-0.03	4.02	-0.01	4.22	-0.025	4.31	0
I-6	0	11.25	4.25	0.015	4.39	0.01	4.11	0.03	4.315	0.01	4.4	0.04
I-8	0	3.75	4.285	-0.015	4.35	0.055	4.16	-0.015	4.365	-0.035	4.445	0

Date:			12/21/93	12/21/93	01/11/94	01/11/94	02/22/94	02/22/94	3/25/94	3/25/94	4/26/94	4/26/94
Survey Marker	x-coordinate	y-coordinate	Elevation feet	Difference feet	Elevation feet	Difference feet	Elevation feet	Difference feet	Elevation feet	Difference feet	Elevation feet	Difference feet
Benchmark			12.585		12.98		12.605		12.58		12.51	
A-2	40	26.25	4.37	0.145	4.76	0.15	4.405	0.13	4.345	0.145	4.3	0.14
A-4	40	18.75	4.3	0.175	4.69	0.18	4.375	0.12	4.28	0.17	4.23	0.17
A-6	40	11.25	4.36	0.215	4.745	0.225	4.39	0.205	4.33	0.22	4.285	0.215
A-7	40	7.5	4.465	0.235	4.855	0.24	4.5	0.22	4.44	0.235	4.39	0.235
A-8	40	3.75	4.665	0.305	5.05	0.315	4.7	0.29	4.635	0.31	4.59	0.305
B-1	35	30	4.03	0.225	4.425	0.225	4.075	0.2	4.02	0.21	3.97	0.21
B-2	35	26.25	4.315	0.25	4.76	0.2	4.405	0.18	4.345	0.195	4.3	0.19
B-4	35	18.75	4.455	0.2	4.845	0.205	4.49	0.185	4.43	0.2	4.38	0.2
B-6	35	11.25	4.625	0.24	5.01	0.25	4.66	0.225	4.595	0.245	4.55	0.24
B-7	35	7.5	4.685	0.22	5.065	0.235	4.715	0.21	4.65	0.23	4.605	0.225
C-6	30	11.25	4.605	0.035	4.99	0.045	4.64	0.02	4.58	0.035	4.53	0.035
C-8	30	3.75	4.42	0.2	4.8	0.215	4.45	0.19	4.39	0.205	4.345	0.2
D-1	25	30	3.695	0.035	4.085	0.04	3.74	0.01	3.685	0.02	3.63	0.025
D-2	25	26.25	4.05	0.005	4.44	0.01	4.09	-0.015	4.035	-0.005	3.99	-0.01
D-4	25	18.75	4.325	0.005	4.715	0.01	4.37	-0.02	4.31	-0.005	4.265	-0.01
D-6	25	11.25	4.47	0.06	4.86	0.065	4.51	0.04	4.455	0.05	4.41	0.045
D-7	25	7.5	4.57	0.025	4.96	0.03	4.61	0.005	4.555	0.015	4.505	0.015
D-8	25	3.75	4.49	0.085	4.875	0.095	4.525	0.07	4.465	0.085	4.42	0.08
D-9	25	0	4.41	0.15	4.8	0.155	4.45	0.13	4.39	0.145	4.35	0.135
E-2	20	26.25	3.79	-0.005	4.18	0	3.83	-0.025	3.77	-0.01	3.73	-0.02
E-4	20	18.75	4.215	0	4.605	0.005	4.26	-0.025	4.205	-0.015	4.16	-0.02
E-6	20	11.25	4.465	0.005	4.86	0.005	4.51	-0.02	4.45	-0.005	4.41	-0.015
F-1	15	30	3.43	0	3.82	0.005	3.475	-0.025	3.42	-0.015	3.37	-0.015
F-2	15	26.25	3.82	0.04	4.205	0.05	3.86	0.02	3.805	0.03	3.76	0.025
F-3	15	22.5	4.045	0.07	4.44	0.07	4.085	0.05	4.025	0.065	3.985	0.055
F-4	15	18.75	4.17	0.005	4.56	0.01	4.21	-0.015	4.155	-0.005	4.11	-0.01
F-6	15	11.25	4.38	0	4.77	0.005	4.425	-0.025	4.37	-0.015	4.325	-0.02
F-8	15	3.75	4.425	0	4.81	0.01	4.47	-0.025	4.415	-0.015	4.37	-0.02
F-9	15	0	4.355	0.005	4.75	0.005	4.405	-0.025	4.35	-0.015	4.3	-0.015
G-2	10	26.25	3.9	0.005	4.29	0.01	3.945	-0.02	3.89	-0.01	3.845	-0.015
G-4	10	18.75	4.23	0.015	4.62	0.02	4.27	-0.005	4.305	-0.005	4.17	0
H-1	5	30	3.325	-0.005	3.71	0.005	3.36	-0.02	3.31	-0.015	3.26	-0.015
H-3	5	22.5	3.925	0.045	4.315	0.05	3.97	0.02	3.915	0.03	3.87	0.025
H-6	5	11.25	4.265	0.01	4.65	0.02	4.31	-0.015	4.36	-0.11	4.21	-0.01
H-8	5	3.75	4.335	0.015	4.73	0.015	4.38	-0.01	4.33	-0.005	4.285	-0.01
H-9	5	0	4.39	0.005	4.79	0	4.445	-0.03	4.385	-0.015	4.34	-0.02
I-2	0	26.25	3.775	-0.01	4.165	-0.005	3.815	-0.03	3.765	-0.025	3.715	-0.025
I-3	0	22.5	3.91	0	4.3	0.005	3.96	-0.03	3.9	-0.015	3.86	-0.025
I-4	0	18.75	3.995	-0.015	4.375	-0.01	4.035	-0.045	3.98	-0.035	3.94	-0.045
I-6	0	11.25	4.075	0.025	4.465	0.03	4.12	0	4.06	0.015	4.02	0.005
I-8	0	3.75	4.13	-0.025	4.51	-0.01	4.17	-0.045	4.125	-0.045	4.07	-0.04

Date: Survey Marker	x-coordinate	y-coordinate	6/2/94 Elevation feet	6/2/94 Difference feet	7/19/94 Elevation feet	7/19/94 Difference feet	9/8/94 Elevation feet	9/8/94 Difference feet	10/20/94 Elevation	10/20/94 Difference	12/1/94 Elevation	12/1/94 Difference	2/21/95 Elevation
Benchmark			12.6		12.315		12.95		13.01		12.49		12.68
A-2	40	26.25	4.37	0.16	4.085	0.16	4.7	0.18	4.76	0.18	4.245	0.175	4.43
A-4	40	18.75	4.31	0.18	4.02	0.185	4.635	0.205	4.7	0.2	4.18	0.2	4.36
A-6	40	11.25	4.36	0.23	4.08	0.225	4.695	0.245	4.75	0.25	4.235	0.245	4.41
A-7	40	7.5	4.47	0.245	4.19	0.24	4.805	0.26	4.86	0.265	4.34	0.265	4.525
A-8	40	3.75	4.67	0.315	4.39	0.31	5.005	0.33	5.06	0.335	4.545	0.33	4.725
B-1	35	30	4.05	0.22	3.77	0.215	4.405	0.215	4.46	0.22	3.945	0.215	4.13
B-2	35	26.25	4.37	0.21	4.085	0.21	4.695	0.235	4.76	0.23	4.245	0.225	4.43
B-4	35	18.75	4.46	0.21	4.17	0.215	4.775	0.245	4.83	0.25	4.32	0.24	4.5
B-6	35	11.25	4.62	0.26	4.33	0.265	4.94	0.29	5	0.29	4.475	0.295	4.66
B-7	35	7.5	4.68	0.24	4.4	0.235	5.005	0.265	5.065	0.265	4.545	0.265	4.73
C-6	30	11.25	4.605	0.05	4.32	0.05	4.92	0.085	4.975	0.09	4.45	0.095	4.63
C-8	30	3.75	4.42	0.215	4.14	0.21	4.75	0.235	4.82	0.225	4.29	0.235	4.48
D-1	25	30	3.71	0.035	3.43	0.03	4.07	0.025	4.19	-0.035	3.63	0.005	3.82
D-2	25	26.25	4.075	-0.005	3.79	-0.005	4.41	0.01	4.475	0.005	3.965	-0.005	4.15
D-4	25	18.75	4.35	-0.005	4.07	-0.01	4.685	0.01	4.75	0.005	4.24	-0.005	4.43
D-6	25	11.25	4.49	0.055	4.21	0.05	4.825	0.07	4.88	0.075	4.365	0.07	4.555
D-7	25	7.5	4.58	0.03	4.29	0.035	4.895	0.065	4.96	0.06	4.44	0.08	4.62
D-8	25	3.75	4.5	0.09	4.21	0.095	4.82	0.12	4.885	0.115	4.37	0.11	4.56
D-9	25	0	4.425	0.15	4.15	0.14	4.805	0.12	4.89	0.095	4.375	0.09	4.56
E-2	20	26.25	3.81	-0.01	3.53	-0.015	4.145	0.005	4.21	0	3.7	-0.01	3.89
E-4	20	18.75	4.24	-0.01	3.96	-0.015	4.575	0.005	4.685	-0.045	4.125	-0.005	4.32
E-6	20	11.25	4.49	-0.005	4.21	-0.01	4.82	0.015	4.89	0.005	4.38	-0.005	4.565
F-1	15	30	3.45	-0.005	3.17	-0.01	3.795	0	3.95	-0.095	3.35	-0.015	3.54
F-2	15	26.25	3.84	0.035	3.56	0.03	4.18	0.045	4.245	0.04	3.73	0.035	3.92
F-3	15	22.5	4.065	0.065	3.785	0.06	4.405	0.075	4.47	0.07	3.95	0.07	4.14
F-4	15	18.75	4.19	0	3.91	-0.005	4.53	0.01	4.59	0.01	4.08	0	4.27
F-6	15	11.25	4.405	-0.01	4.12	-0.01	4.74	0.005	4.81	-0.005	4.3	-0.015	4.485
F-8	15	3.75	4.45	-0.01	4.17	-0.015	4.785	0.005	4.85	0	4.34	-0.01	4.53
F-9	15	0	4.38	-0.005	4.1	-0.01	4.72	0.005	4.79	-0.005	4.28	-0.015	4.465
G-2	10	26.25	3.925	-0.005	3.645	-0.01	4.35	-0.08	4.33	0	3.815	-0.005	4.005
G-4	10	18.75	4.25	0.01	3.965	0.01	4.585	0.025	4.65	0.02	4.135	0.015	4.32
H-1	5	30	3.345	-0.01	3.06	-0.01	3.68	0.005	3.755	-0.01	3.23	-0.005	3.425
H-3	5	22.5	3.95	0.035	3.67	0.03	4.285	0.05	4.36	0.035	3.84	0.035	4.025
H-6	5	11.25	4.29	0	4.01	-0.005	4.63	0.01	4.7	0	4.18	0	4.37
H-8	5	3.75	4.365	0	4.08	0	4.705	0.01	4.77	0.005	4.25	0.005	4.45
H-9	5	0	4.36	0.05	4.14	-0.015	4.76	0	4.83	-0.01	4.315	-0.015	4.51
I-2	0	26.25	3.8	-0.02	3.51	-0.015	4.13	0	4.2	-0.01	3.68	-0.01	4.87
I-3	0	22.5	3.945	-0.02	3.66	-0.02	4.28	-0.005	4.345	-0.01	3.825	-0.01	4.02
I-4	0	18.75	4.02	-0.035	3.735	-0.035	4.35	-0.015	4.42	-0.025	3.9	-0.025	4.09
I-6	0	11.25	4.105	0.01	3.82	0.01	4.44	0.025	4.51	0.015	3.99	0.015	4.185
I-8	0	3.75	4.15	-0.03	3.875	-0.04	4.5	-0.03	4.58	-0.05	4.06	-0.05	4.25

Date:			2/21/95	4/4/95	4/4/95	5/16/95	5/16/95	7/13/95	7/13/95	9/17/95	9/17/95	10/21/95	10/95/95	11/19/95	11/19/95
Survey			Difference	Elevation	Difference	Elevation	Difference	Elevation	Difference	Elevation	Difference	Elevation	Difference	Elevation	Difference
Marker	x-coordinate	y-coordinate													
														14.055	
Benchmark				12.66		12.64		13.42		13.215		15.13		13.8	
A-2	40	26.25	0.18	4.4	0.21	4.565	0.205	5.13	0.22	4.98	0.165	6.88	0.18	5	0.73
A-4	40	18.75	0.21	4.33	0.24	4.5	0.23	5.065	0.245	4.9	0.205	6.79	0.23	4.93	0.76
A-6	40	11.25	0.26	4.38	0.29	4.55	0.28	5.13	0.28	4.92	0.285	6.81	0.31	4.96	0.83
A-7	40	7.5	0.27	4.485	0.31	4.66	0.295	5.24	0.295	5.04	0.29	6.93	0.315	5.09	0.825
A-8	40	3.75	0.34	4.69	0.375	4.86	0.365	5.45	0.355	5.24	0.36	7.13	0.385	5.3	0.885
B-1	35	30	0.22	4.1	0.25	4.27	0.24	4.82	0.27	4.66	0.225	6.54	0.26	4.69	0.76
B-2	35	26.25	0.23	4.4	0.26	4.57	0.25	5.12	0.28	4.9	0.295	6.82	0.29	5	0.76
B-4	35	18.75	0.25	4.465	0.285	4.63	0.28	5.18	0.31	4.96	0.325	6.86	0.34	5.07	0.8
B-6	35	11.25	0.3	4.625	0.335	4.79	0.33	5.36	0.34	5.12	0.375	7.03	0.38	5.27	0.81
B-7	35	7.5	0.27	4.69	0.31	4.86	0.3	5.44	0.3	5.21	0.325	7.11	0.34	5.36	0.76
C-6	30	11.25	0.105	4.59	0.145	4.75	0.145	5.29	0.185	5.05	0.22	6.95	0.235	5.29	0.565
C-8	30	3.75	0.235	4.44	0.275	4.615	0.26	5.18	0.275	4.95	0.3	6.86	0.305	5.21	0.625
D-1	25	30	0.005	3.79	0.035	3.965	0.02	4.47	0.095	4.26	0.1	6.17	0.105	4.5	0.445
D-2	25	26.25	0	4.12	0.03	4.305	0.005	4.875	0.015	4.64	0.145	6.55	0.05	4.91	0.36
D-4	25	18.75	-0.005	4.4	0.025	4.58	0.005	5.18	-0.015	4.84	0.12	6.86	0.015	5.26	0.285
D-6	25	11.25	0.07	4.52	0.105	4.705	0.08	5.25	0.115	5.02	0.14	6.93	0.145	5.37	0.375
D-7	25	7.5	0.07	4.59	0.1	4.76	0.09	5.29	0.14	5.06	0.165	6.96	0.18	5.41	0.4
D-8	25	3.75	0.11	4.525	0.145	4.7	0.13	5.235	0.175	5.025	0.18	6.93	0.19	5.36	0.41
D-9	25	0	0.095	4.525	0.13	4.69	0.125	5.205	0.19	5.09	0.1	7.01	0.095	5.47	0.305
E-2	20	26.25	-0.01	3.86	0.02	4.04	0	4.64	-0.02	4.41	0.005	6.32	0.01	4.78	0.22
E-4	20	18.75	-0.01	4.29	0.02	4.47	0	5.07	-0.02	4.84	0.005	6.75	0.01	5.25	0.18
E-6	20	11.25	0	4.53	0.035	4.72	0.005	5.31	-0.005	5.09	0.01	6.98	0.035	5.51	0.175
F-1	15	30	-0.015	3.505	0.02	3.69	-0.005	4.25	0.015	4.02	0.04	5.93	0.045	4.44	0.205
F-2	15	26.25	0.035	3.89	0.065	4.07	0.045	4.67	0.025	4.44	0.05	6.35	0.055	4.89	0.185
F-3	15	22.5	0.07	4.11	0.1	4.29	0.08	4.895	0.055	4.67	0.075	6.58	0.08	5.14	0.19
F-4	15	18.75	0	4.24	0.03	4.42	0.01	5.02	-0.01	4.79	0.015	6.71	0.01	5.29	0.1
F-6	15	11.25	-0.01	4.45	0.025	4.63	0.005	5.235	-0.02	5.01	0	6.92	0.005	5.54	0.055
F-8	15	3.75	-0.01	4.5	0.02	4.68	0	5.27	-0.01	5.05	0.005	6.96	0.01	5.6	0.04
F-9	15	0	-0.01	4.43	0.025	4.615	0	5.145	0.05	4.94	0.05	6.86	0.045	5.5	0.075
G-2	10	26.25	-0.005	3.97	0.03	4.155	0.005	4.75	-0.01	4.53	0.005	6.44	0.01	5.06	0.06
G-4	10	18.75	0.02	4.29	0.05	4.47	0.03	5.07	0.01	4.84	0.035	6.75	0.04	5.42	0.04
H-1	5	30	-0.01	3.39	0.025	3.575	0	4.13	0.025	3.92	0.03	5.83	0.035	4.5	0.035
H-3	5	22.5	0.04	3.99	0.075	4.17	0.055	4.775	0.03	4.55	0.05	6.46	0.055	5.19	-0.005
H-6	5	11.25	0	4.33	0.04	4.515	0.015	5.12	-0.01	4.89	0.015	6.8	0.02	5.6	-0.11
H-8	5	3.75	-0.005	4.41	0.035	4.59	0.015	5.19	-0.005	4.96	0.02	6.88	0.015	5.7	-0.135
H-9	5	0	-0.02	4.47	0.02	4.65	0	5.23	0	4.96	0.065	6.93	0.01	5.76	-0.15
I-2	0	26.25	-1.01	3.84	0.02	4.02	0	4.61	-0.01	4.4	-0.005	6.31	0.00	5.09	-0.11
I-3	0	22.5	-0.015	3.98	0.025	4.165	0	4.76	-0.015	4.55	-0.01	6.47	-0.015	5.29	-0.185
I-4	0	18.75	-0.025	4.06	0.005	4.24	-0.015	4.84	-0.035	4.62	-0.02	6.54	-0.025	5.39	-0.205
I-6	0	11.25	0.01	4.15	0.045	4.33	0.025	4.92	0.015	4.7	0.03	6.62	0.025	5.52	-0.205
I-8	0	3.75	-0.05	4.21	-0.01	4.395	-0.035	4.96	-0.02	4.77	-0.035	6.68	-0.03	5.6	-0.26

Date: Survey Marker	x-coordinate	y-coordinate	12/16/95 Elevation	12/16/95 Difference	2/10/96 Elevation	2/10/96 Difference	3/9/96 Elevation	3/9/96 Difference	4/27/96 Elevation	4/27/96 Difference	6/4/96 Elevation	6/4/96 Difference	7/21/96 Elevation	7/21/96 Difference	8/18/96 Elevation
											11.3				
Benchmark			10.99		10.54		11.45		11.34		11.4		13.55		13.66
A-2	40	26.25	2.74	0.18	2.29	0.18	3.19	0.19	3.04	0.23	2.365	0.945	5.27	0.21	5.43
A-4	40	18.75	2.64	0.24	2.2	0.23	3.1	0.24	2.98	0.25	2.32	0.97	5.17	0.27	5.325
A-6	40	11.25	2.65	0.33	2.21	0.32	3.11	0.33	3.04	0.29	2.31	1.08	5.19	0.35	5.32
A-7	40	7.5	2.76	0.345	2.32	0.335	3.23	0.335	3.16	0.295	3.22	0.295	5.305	0.36	5.42
A-8	40	3.75	2.97	0.405	2.63	0.395	3.43	0.405	3.38	0.345	3.435	0.35	5.51	0.425	5.625
B-1	35	30	2.39	0.27	1.94	0.27	2.85	0.27	2.72	0.29	2.78	0.29	4.95	0.27	5.11
B-2	35	26.25	2.66	0.31	2.23	0.29	3.13	0.3	3.02	0.3	3.07	0.31	5.21	0.32	5.35
B-4	35	18.75	2.7	0.36	2.27	0.34	3.17	0.35	3.09	0.32	3.14	0.33	5.245	0.375	5.36
B-6	35	11.25	2.87	0.4	2.44	0.38	3.34	0.39	3.27	0.35	3.33	0.35	5.41	0.42	5.62
B-7	35	7.5	2.95	0.36	2.62	0.34	3.42	0.35	3.37	0.29	3.42	0.3	5.5	0.37	5.61
C-6	30	11.25	2.8	0.245	2.36	0.235	3.27	0.235	3.21	0.185	3.26	0.195	5.34	0.265	5.45
C-8	30	3.75	2.7	0.325	2.27	0.305	3.17	0.315	3.13	0.245	3.18	0.255	5.25	0.335	5.36
D-1	25	30	2.02	0.115	1.59	0.095	2.49	0.105	2.38	0.105	2.49	0.115	4.61	0.085	4.75
D-2	25	26.25	2.39	0.07	1.97	0.04	2.87	0.05	2.77	0.04	2.83	0.04	4.95	0.07	5.065
D-4	25	18.75	2.7	0.035	2.27	0.015	3.17	0.025	3.1	-0.015	3.15	-0.005	5.25	0.045	5.36
D-6	25	11.25	2.76	0.175	2.33	0.155	3.23	0.165	3.18	0.105	3.22	0.125	5.31	0.185	5.41
D-7	25	7.5	2.8	0.2	2.37	0.18	3.27	0.19	3.22	0.13	3.265	0.145	5.335	0.225	5.445
D-8	25	3.75	2.77	0.21	2.35	0.18	3.24	0.2	3.2	0.13	3.245	0.145	5.32	0.22	5.45
D-9	25	0	2.86	0.105	2.42	0.095	3.32	0.105	3.28	0.035	3.3	0.075	5.39	0.135	5.54
E-2	20	26.25	2.17	0.02	1.74	0	2.64	0.01	2.55	-0.01	2.605	-0.005	4.73	0.02	4.84
E-4	20	18.75	2.6	0.02	2.17	0	3.07	0.01	3	-0.03	3.05	-0.02	5.18	0.02	5.26
E-6	20	11.25	2.82	0.055	2.4	0.025	3.3	0.035	3.24	-0.015	3.29	-0.005	5.375	0.08	5.48
F-1	15	30	1.78	0.055	1.35	0.035	2.25	0.045	2.15	0.035	2.205	0.04	4.34	0.055	4.45
F-2	15	26.25	2.2	0.085	1.77	0.045	2.67	0.055	2.58	0.035	2.63	0.045	4.765	0.08	4.87
F-3	15	22.5	2.42	0.1	1.99	0.08	2.89	0.09	2.8	0.07	2.86	0.07	4.98	0.1	5.09
F-4	15	18.75	2.55	0.03	2.12	0.01	3.02	0.02	2.95	-0.02	3	-0.01	5.11	0.03	5.22
F-6	15	11.25	2.76	0.025	2.34	-0.005	3.24	0.005	3.18	-0.045	3.24	-0.045	5.33	0.015	5.44
F-8	15	3.75	2.8	0.03	2.38	0	3.28	0.01	3.25	-0.07	3.3	-0.06	5.37	0.02	5.49
F-9	15	0	2.7	0.085	2.28	0.035	3.18	0.045	3.16	-0.045	3.21	-0.035	5.28	0.045	5.4
G-2	10	26.25	2.29	0.02	1.85	0.01	2.76	0.01	2.66	0	2.715	0.005	4.845	0.025	4.96
G-4	10	18.75	2.6	0.05	2.16	0.04	3.07	0.04	3	0	3.04	0.02	5.16	0.05	5.27
H-1	5	30	1.68	0.045	1.24	0.035	2.15	0.035	2.05	0.025	2.095	0.04	4.25	0.035	4.365
H-3	5	22.5	2.29	0.085	1.87	0.055	2.77	0.065	2.68	0.045	2.735	0.05	4.87	0.065	4.98
H-6	5	11.25	2.64	0.04	2.22	0.01	3.12	0.02	3.08	-0.03	3.15	-0.06	5.205	0.035	5.32
H-8	5	3.75	2.72	0.035	2.29	0.015	3.19	0.025	3.14	-0.035	3.19	-0.025	5.28	0.035	5.39
H-9	5	0	2.78	0.02	2.35	0	3.25	0.01	3.21	-0.06	3.26	-0.05	5.34	0.02	5.45
I-2	0	26.25	2.16	0.01	1.74	-0.02	2.63	0	2.52	0	2.57	0.01	4.73	0	4.84
I-3	0	22.5	2.31	0.005	1.88	-0.015	2.78	-0.005	2.69	-0.025	2.74	-0.015	4.88	-0.005	5
I-4	0	18.75	2.36	-0.005	1.95	-0.025	2.86	-0.025	2.77	-0.045	2.82	-0.035	4.955	-0.02	5.07
I-6	0	11.25	2.46	0.045	2.03	0.025	2.93	0.035	2.86	-0.005	2.905	0.01	5.02	0.045	5.13
I-8	0	3.75	2.53	-0.02	2.1	-0.04	3	-0.03	2.94	-0.08	2.98	-0.06	5.09	-0.02	5.21

Date:			8/16/96	9/29/96	9/29/96	11/10/96	11/10/96	1/1/97	1/1/97	2/16/97	2/16/97	4/6/97	4/6/97	5/26/97	5/26/97
Survey Marker	x-coordinate	y-coordinate	Difference	Elevation	Difference	Elevation	Difference	Elevation	Difference	Elevation	Difference	Elevation	Difference	Elevation	Difference
Benchmark				13.48		13.62		10.69		11.47		11.68		11.11	
A-2	40	26.25	0.16	5.29	0.12	5.44	0.11	2.51	0.110	3.24	0.160	3.45	0.160	2.87	0.170
A-4	40	18.75	0.225	5.18	0.19	5.335	0.175	2.39	0.190	3.14	0.220	3.39	0.180	2.75	0.260
A-6	40	11.25	0.33	5.15	0.32	5.29	0.32	2.35	0.330	3.1	0.360	3.31	0.360	2.75	0.350
A-7	40	7.5	0.355	5.24	0.355	5.39	0.345	2.45	0.355	3.19	0.395	3.41	0.385	2.86	0.365
A-8	40	3.75	0.42	5.445	0.42	5.59	0.415	2.65	0.425	3.4	0.455	3.62	0.445	3.07	0.425
B-1	35	30	0.22	4.96	0.19	5.11	0.18	2.17	0.190	2.89	0.250	3.11	0.240	2.55	0.230
B-2	35	26.25	0.29	5.21	0.25	5.38	0.22	2.44	0.230	3.21	0.240	3.43	0.230	2.85	0.240
B-4	35	18.75	0.37	5.2	0.35	5.36	0.33	2.42	0.340	3.18	0.360	3.4	0.350	2.84	0.340
B-6	35	11.25	0.42	5.445	0.315	5.49	0.41	2.64	0.430	3.32	0.430	3.52	0.440	2.98	0.410
B-7	35	7.5	0.37	5.43	0.37	5.57	0.37	2.64	0.370	3.39	0.400	3.62	0.380	3.06	0.370
C-6	30	11.25	0.265	5.27	0.265	5.41	0.265	2.49	0.255	3.22	0.305	3.46	0.285	2.91	0.255
C-8	30	3.75	0.335	5.185	0.33	5.33	0.325	2.4	0.325	3.15	0.355	3.37	0.345	2.83	0.315
D-1	25	30	0.055	4.585	0.04	4.73	0.035	1.82	0.015	2.56	0.055	2.79	0.035	2.26	-0.005
D-2	25	26.25	0.065	4.9	0.05	5.05	0.04	2.12	0.040	2.88	0.060	3.1	0.050	2.57	0.010
D-4	25	18.75	0.045	5.18	0.045	5.33	0.035	2.41	0.025	3.14	0.075	3.36	0.065	2.82	0.035
D-6	25	11.25	0.195	5.235	0.19	5.38	0.185	2.45	0.185	3.2	0.215	3.43	0.195	2.88	0.175
D-7	25	7.5	0.225	5.27	0.22	5.41	0.22	2.49	0.210	3.24	0.240	3.46	0.230	2.9	0.220
D-8	25	3.75	0.2	5.29	0.18	5.43	0.18	2.5	0.180	3.24	0.220	3.46	0.210	2.9	0.200
D-9	25	0	0.095	5.37	0.085	5.52	0.075	2.59	0.075	3.33	0.115	3.54	0.115	2.97	0.115
E-2	20	26.25	0.02	4.665	0.015	4.81	0.01	1.9	-0.010	2.66	0.010	2.89	-0.010	2.32	-0.010
E-4	20	18.75	0.03	5.09	0.02	5.24	0.01	2.32	0.000	3.07	0.030	3.29	0.020	2.75	-0.010
E-6	20	11.25	0.065	5.3	0.065	5.45	0.055	2.53	0.045	3.27	0.085	3.5	0.065	2.94	0.055
F-1	15	30	0.055	4.27	0.055	4.42	0.045	1.5	0.035	2.25	0.065	2.49	0.035	1.95	0.005
F-2	15	26.25	0.065	4.69	0.065	4.84	0.055	1.93	0.035	2.69	0.055	2.91	0.045	2.36	0.025
F-3	15	22.5	0.1	4.91	0.1	5.06	0.09	2.13	0.090	2.89	0.110	3.12	0.090	2.57	0.070
F-4	15	18.75	0.03	5.45	-0.38	5.2	0.01	2.27	0.010	3.02	0.040	3.245	0.025	2.7	0.000
F-6	15	11.25	0.015	5.26	0.015	5.41	0.005	2.49	-0.005	3.24	0.025	3.46	0.015	2.92	-0.015
F-8	15	3.75	0.01	5.3	0.02	5.45	0.01	2.53	0.000	3.28	0.030	3.49	0.030	2.98	-0.010
F-9	15	0	0.035	5.23	0.025	5.38	0.015	2.45	0.015	3.21	0.035	3.42	0.035	2.89	-0.005
G-2	10	26.25	0.02	4.76	0.02	4.92	0.02	2.02	-0.010	2.88	-0.090	2.99	0.010	2.44	-0.010
G-4	10	18.75	0.05	5.09	0.05	5.24	0.04	2.32	0.030	3.08	0.050	3.31	0.030	2.75	0.020
H-1	5	30	0.03	4.19	0.025	4.34	0.015	1.42	0.005	2.19	0.015	2.4	0.015	1.88	-0.015
H-3	5	22.5	0.065	4.805	0.06	4.95	0.055	2.03	0.045	2.8	0.055	3.02	0.045	2.47	0.025
H-6	5	11.25	0.03	5.14	0.03	5.29	0.02	2.35	0.030	3.12	0.040	3.34	0.030	2.81	-0.010
H-8	5	3.75	0.035	5.21	0.035	5.36	0.025	2.43	0.025	3.2	0.035	3.41	0.035	2.87	0.005
H-9	5	0	0.02	5.275	0.015	5.43	0	2.5	0.000	3.26	0.020	3.48	0.010	2.93	-0.010
I-2	0	26.25	0	4.67	-0.01	4.82	-0.02	1.9	-0.030	2.66	-0.010	2.88	-0.020	2.32	-0.030
I-3	0	22.5	-0.015	4.82	-0.015	4.97	-0.025	2.05	-0.035	2.81	-0.015	3.02	-0.015	2.48	-0.045
I-4	0	18.75	-0.025	4.91	-0.045	5.07	-0.065	2.13	-0.055	2.91	-0.055	3.12	-0.055	2.57	-0.075
I-6	0	11.25	0.045	4.96	0.035	5.11	0.025	2.19	0.015	2.94	0.045	3.16	0.035	2.62	0.005
I-8	0	3.75	-0.03	5.04	-0.04	5.18	-0.04	2.25	-0.040	3.01	-0.020	3.23	-0.030	2.67	-0.040

Date:			7/26/97	7/26/97	9/10/97	9/10/97	12/21/97	12/21/97	6/20/98	6/20/98
Survey Marker	x-coordinate	y-coordinate	Elevation	Difference	Elevation	Difference	Elevation	Difference	Elevation	Difference
Benchmark			11.18		11.18		10.88		10.83	
A-2	40	26.25	2.96	0.150	2.86	0.250	2.53	0.280	2.45	0.310
A-4	40	18.75	2.84	0.230	2.75	0.320	2.44	0.330	2.36	0.360
A-6	40	11.25	2.83	0.340	2.8	0.370	2.49	0.380	2.4	0.420
A-7	40	7.5	2.93	0.365	2.9	0.395	2.59	0.405	2.51	0.435
A-8	40	3.75	3.15	0.415	3.11	0.455	2.8	0.465	2.72	0.495
B-1	35	30	2.66	0.190	2.57	0.280	2.25	0.300	2.18	0.320
B-2	35	26.25	2.93	0.230	2.84	0.320	2.53	0.330	2.44	0.370
B-4	35	18.75	2.89	0.360	2.85	0.400	2.54	0.410	2.44	0.460
B-6	35	11.25	3.01	0.450	3.01	0.450	2.72	0.440	2.63	0.480
B-7	35	7.5	3.11	0.390	3.1	0.400	2.8	0.400	2.74	0.410
C-6	30	11.25	2.94	0.295	2.95	0.285	2.64	0.295	2.55	0.335
C-8	30	3.75	2.86	0.355	2.86	0.355	2.55	0.365	2.46	0.405
D-1	25	30	2.3	0.025	2.18	0.145	1.9	0.125	1.84	0.135
D-2	25	26.25	2.6	0.050	2.58	0.070	2.28	0.070	2.21	0.090
D-4	25	18.75	2.84	0.085	2.85	0.075	2.54	0.085	2.45	0.125
D-6	25	11.25	2.92	0.205	2.91	0.215	2.6	0.225	2.54	0.235
D-7	25	7.5	2.95	0.240	2.95	0.240	2.63	0.260	2.54	0.300
D-8	25	3.75	2.97	0.200	2.93	0.240	2.62	0.250	2.51	0.310
D-9	25	0	3.06	0.095	2.99	0.165	2.7	0.155	2.58	0.225
E-2	20	26.25	2.37	0.010	2.35	0.030	2.06	0.020	1.98	0.050
E-4	20	18.75	2.78	0.030	2.78	0.030	2.49	0.020	2.42	0.040
E-6	20	11.25	2.98	0.085	2.99	0.075	2.66	0.105	2.58	0.135
F-1	15	30	1.98	0.045	1.94	0.085	1.65	0.075	1.59	0.085
F-2	15	26.25	2.39	0.065	2.39	0.065	2.1	0.055	2.03	0.075
F-3	15	22.5	2.61	0.100	2.61	0.100	2.32	0.090	2.26	0.100
F-4	15	18.75	2.75	0.020	2.74	0.030	2.45	0.020	2.4	0.020
F-6	15	11.25	2.96	0.015	2.95	0.025	2.68	0.015	2.6	0.025
F-8	15	3.75	2.99	0.030	3	0.020	2.7	0.020	2.63	0.040
F-9	15	0	2.93	0.025	2.92	0.035	2.63	0.025	2.54	0.065
G-2	10	26.25	2.49	0.010	2.46	0.040	2.16	0.040	2.1	0.050
G-4	10	18.75	2.79	0.050	2.8	0.040	2.5	0.040	2.44	0.050
H-1	5	30	1.91	0.005	1.82	0.095	1.52	0.095	1.5	0.065
H-3	5	22.5	2.51	0.055	2.52	0.045	2.22	0.045	2.16	0.055
H-6	5	11.25	2.85	0.020	2.85	0.020	2.54	0.030	2.48	0.040
H-8	5	3.75	2.91	0.035	2.91	0.035	2.61	0.035	2.5	0.095
H-9	5	0	2.98	0.010	2.96	0.030	2.65	0.040	2.59	0.050
I-2	0	26.25	2.36	0.000	2.35	0.010	2.03	0.030	1.99	0.020
I-3	0	22.5	2.51	-0.005	2.52	-0.015	2.22	-0.015	2.15	0.005
I-4	0	18.75	2.62	-0.055	2.59	-0.025	2.3	-0.035	2.24	-0.025
I-6	0	11.25	2.65	0.045	2.63	0.065	2.32	0.075	2.25	0.095
I-8	0	3.75	2.73	-0.030	2.66	0.040	2.36	0.040	2.31	0.040

FSH Corrected Heave																	
Marker	x	y	9-9-93	10-7-93	11-2-93	12-7-93	1-4-94	2-11-94	3-11-94	4-19-94	5-17-94	6-14-94	7-14-94	8-16-94	9/13/94	10/14/94	11/10/94
A-2	50	26.25	0	-0.065	0.2	-0.055	0.2	0.24	0.36	0.13	0.16	0.17	0.17	0.15	0.16	0.17	0.19
A-4	50	18.75	0	-0.025	0.15	-0.11	0.145	0.17	0.28	0.095	0.125	0.14	0.14	0.145	0.15	0.15	0.165
A-6	50	11.25	0	0.02	0.155	-0.12	0.145	0.145	0.245	0.09	0.145	0.16	0.16	0.165	0.17	0.175	0.185
A-7	50	7.5	0	0.05	0.21	-0.08	0.18	0.175	0.265	0.09	0.135	0.145	0.16	0.155	0.16	0.165	0.175
A-8	50	3.75	0	0.07	0.185	-0.105	0.15	0.135	0.22	0.08	0.125	0.135	0.14	0.14	0.125	0.12	0.135
B-1	43.75	30	0	-0.115	0.22	-0.035	0.19	0.36	0.485	0.2	0.22	0.23	0.23	0.205	0.215	0.23	0.24
B-2	43.75	26.25	0	-0.1	0.175	-0.095	0.16	0.255	0.375	0.115	0.145	0.16	0.165	0.17	0.175	0.18	0.185
B-4	43.75	18.75	0	0.005	0.245	-0.04	0.245	0.285	0.38	0.08	0.1	0.11	0.11	0.115	0.115	0.12	0.125
B-6	43.75	11.25	0	-0.015	0.26	-0.03	0.225	0.28	0.375	0.105	0.125	0.135	0.145	0.15	0.155	0.16	0.16
B-7	43.75	7.5	0	-0.02	0.195	-0.105	0.16	0.18	0.26	0.08	0.105	0.12	0.12	0.125	0.125	0.135	0.135
B-9	43.75	0	0	0.015	0.175	-0.14	0.135	0.15	0.22	0.065	0.105	0.12	0.12	0.105	0.07	0.095	0.12
C-6	37.5	11.25	0	-0.1	0.2	-0.08	0.165	0.23	0.31	0.02	0.035	0.045	0.045	0.055	0.05	0.06	0.06
C-8	37.5	3.75	0	-0.05	0.23	-0.075	0.175	0.235	0.31	0.06	0.085	0.1	0.1	0.105	0.105	0.11	0.115
D-1	31.25	30	0	-0.245	0.16	-0.1	0.11	0.335	0.45	0.12	0.145	0.16	0.165	0.155	0.155	0.17	0.18
D-2	31.25	26.25	0	-0.23	0.15	-0.095	0.1	0.28	0.37	0.11	0.135	0.15	0.16	0.165	0.175	0.18	0.19
D-4	31.25	18.75	0	-0.175	0.245	-0.025	0.215	0.365	0.45	0.115	0.14	0.155	0.165	0.17	0.175	0.185	0.19
D-6	31.25	11.25	0	-0.145	0.165	-0.11	0.11	0.205	0.285	0.075	0.1	0.115	0.12	0.125	0.125	0.13	0.135
D-7	31.25	7.5	0	-0.125	0.17	-0.1	0.095	0.215	0.28	0.065	0.1	0.11	0.115	0.12	0.12	0.125	0.13
D-8	31.25	3.75	0	-0.105	0.19	-0.095	0.125	0.205	0.27	0.085	0.125	0.135	0.135	0.14	0.14	0.145	0.15
D-9	31.25	0	0	-0.095	0.19	-0.1	0.1	0.2	0.255	0.055	0.13	0.045	0.145	0.145	0.14	0.145	0.155
E-4	25	18.75	0	-0.28	0.125	-0.12	0.045	0.215	0.31	0.04	0.07	0.085	0.09	0.1	0.11	0.115	0.11
E-6	25	11.25	0	-0.205	0.24	-0.03	0.145	0.32	0.4	0.095	0.12	0.125	0.135	0.14	0.14	0.145	0.15
E-8	25	3.75	0	-0.155	0.26	-0.035	0.16	0.295	0.37	0.1	0.125	0.14	0.14	0.145	0.15	0.17	0.175
F-1	18.75	30	0	-0.355	0.22	-0.025	0.175	0.415	0.515	0.16	0.18	0.18	0.18	0.155	0.155	0.165	0.175
F-2	18.75	26.25	0	-0.33	0.23	-0.01	0.14	0.405	0.505	0.12	0.135	0.15	0.16	0.155	0.16	0.16	0.16
F-3	18.75	22.5	0	-0.295	0.265	0.03	0.25	0.48	0.565	0.165	0.18	0.19	0.195	0.21	0.21	0.205	0.205
F-4	18.75	18.75	0	-0.275	0.22	-0.03	0.155	0.415	0.51	0.12	0.135	0.145	0.155	0.16	0.16	0.17	0.175
F-6	18.75	11.25	0	-0.255	0.215	0.075	0.115	0.295	0.375	0.035	0.06	0.065	0.07	0.07	0.075	0.085	0.08
F-8	18.75	3.75	0	-0.21	0.21	-0.085	0.105	0.28	0.34	0.105	0.135	0.14	0.145	0.145	0.145	0.15	0.155
F-9	18.75	0	0	-0.2	0.21	-0.09	0.12	0.285	0.36	0.085	0.1	0.105	0.105	0.11	0.105	0.065	0.12
G-2	12.5	26.25	0	-0.402	0.183	-0.067	0.098	0.443	0.523	0.095	0.11	0.11	0.105	0.11	0.1	0.11	0.105
G-4	12.5	18.75	0	-0.34	0.25	-0.01	0.155	0.44	0.525	0.11	0.125	0.13	0.13	0.135	0.14	0.15	0.145
H-1	6.25	30	0	-0.45	0.28	0.04	0.185	0.52	0.61	0.16	0.185	0.19	0.18	0.145	0.125	0.14	0.16
H-3	6.25	22.5	0	-0.405	0.255	-0.025	0.16	0.46	0.535	0.09	0.11	0.12	0.115	0.12	0.165	0.165	0.16
H-4	6.25	18.75	0	-0.39	0.215	-0.065	0.12	0.41	0.495	0.09	0.11	0.12	0.125	0.08	0.125	0.135	0.13
H-6	6.25	11.25	0	-0.36	0.275	-0.02	0.2	0.45	0.51	0.1	0.115	0.13	0.135	0.14	0.145	0.155	0.16
H-8	6.25	3.75	0	-0.335	0.22	-0.085	0.09	0.34	0.39	0.095	0.115	0.12	0.13	0.135	0.135	0.14	0.145
H-9	6.25	0	0	-0.32	0.255	-0.07	0.14	0.4	0.45	0.135	0.155	0.165	0.165	0.165	0.16	0.17	0.18
I-2	0	26.25	0	-0.475	0.26	0.015	0.17	0.51	0.585	0.115	0.135	0.14	0.14	0.1	0.085	0.09	0.115
I-4	0	18.75	0	-0.38	0.42	0.155	0.335	0.645	0.71	0.195	0.215	0.215	0.215	0.2	0.195	0.2	0.21
I-6	0	11.25	0	-0.405	0.29	-0.01	0.165	0.485	0.555	0.145	0.17	0.18	0.185	0.185	0.185	0.19	0.2
I-8	0	3.75	0	-0.38	0.27	-0.05	0.13	0.455	0.49	0.13	0.155	0.17	0.17	0.165	0.165	0.175	0.185

APPENDIX D

Heave Calculation

(a) Pierre Shale

Active Zone (ft)	Layer	Thickness of Layer (ft)	Initial Void Ratio*	Cw From Wetting Curve	Average Min. Field-Measured Water Content* (%)	Average Max. Field-Measured Water Content* (%)	Delta W (%)	Delta Zi (ft)	Total Heave Prediction (ft)
8	1 (0-1 ft)	1	1.09	0.016	11.63	21.16	9.53	0.07	
	2 (1-2 ft)	1	0.99	0.016	9.95	19.25	9.30	0.07	
	3 (2-3 ft)	1	0.84	0.016	13.20	20.47	7.27	0.06	
	4 (3-4 ft)	1	0.82	0.016	14.37	19.44	5.07	0.04	
	5 (4-5 ft)	1	0.75	0.016	14.19	18.80	4.61	0.04	
	6 (5-6 ft)	1	0.76	0.019	14.55	19.86	5.31	0.06	
	7 (6-7 ft)	1	0.95	0.019	15.61	19.90	4.29	0.04	
	8 (7-8 ft)	1	0.82	0.019	16.00	16.04	0.04	0.00	0.40
8	1 (0-1 ft)	1	1.10	0.016	11.40	21.19	9.79	0.07	
	2 (1-2 ft)	1	1.11	0.016	12.00	21.45	9.45	0.07	
	3 (2-3 ft)	1	1.03	0.016	14.32	20.28	5.96	0.05	
	4 (3-4 ft)	1	0.76	0.016	14.27	20.36	6.09	0.06	
	5 (4-5 ft)	1	0.79	0.016	15.25	18.19	2.94	0.03	
	6 (5-6 ft)	1	0.81	0.019	15.22	19.07	3.85	0.04	
	7 (6-7 ft)	1	1.00	0.019	15.70	20.15	4.45	0.04	
	8 (7-8 ft)	1	0.85	0.019	16.30	16.50	0.20	0.00	0.36
8	1 (0-1 ft)	1	1.19	0.016	11.08	28.19	17.11	0.13	
	2 (1-2 ft)	1	0.97	0.016	11.84	19.67	7.83	0.06	
	3 (2-3 ft)	1	0.97	0.016	14.48	20.92	6.44	0.05	
	4 (3-4 ft)	1	0.86	0.016	15.11	20.12	5.01	0.04	
	5 (4-5 ft)	1	0.78	0.016	14.51	18.49	3.98	0.04	
	6 (5-6 ft)	1	0.78	0.019	14.87	17.74	2.87	0.03	
	7 (6-7 ft)	1	0.79	0.019	15.77	16.78	1.01	0.01	
	8 (7-8 ft)	1	0.83	0.019	15.72	17.77	2.05	0.02	0.38
8	1 (0-1 ft)	1	0.85	0.016	6.34	21.05	14.71	0.13	
	2 (1-2 ft)	1	0.93	0.016	11.42	20.12	8.70	0.07	
	3 (2-3 ft)	1	0.86	0.016	14.38	20.22	5.84	0.05	
	4 (3-4 ft)	1	0.78	0.016	14.29	19.35	5.06	0.05	
	5 (4-5 ft)	1	0.83	0.016	13.87	18.32	4.45	0.04	
	6 (5-6 ft)	1	0.75	0.019	14.74	17.98	3.24	0.04	
	7 (6-7 ft)	1	0.77	0.019	15.58	19.34	3.76	0.04	
	8 (7-8 ft)	1	0.78	0.019	15.90	18.32	2.42	0.03	0.44
12	1 (0-1 ft)	1	0.88	0.016	7.35	22.19	14.84	0.13	
	2 (1-2 ft)	1	0.98	0.016	9.30	19.74	10.44	0.08	
	3 (2-3 ft)	1	0.88	0.016	14.63	19.58	4.95	0.04	
	4 (3-4 ft)	1	0.83	0.016	14.08	19.18	5.10	0.04	
	5 (4-5 ft)	1	0.81	0.016	14.23	18.82	4.59	0.04	
	6 (5-6 ft)	1	0.70	0.019	14.61	18.52	3.91	0.04	
	7 (6-7 ft)	1	0.80	0.019	15.63	20.14	4.51	0.05	
	8 (7-8 ft)	1	0.76	0.019	16.27	19.58	3.31	0.04	
	9 (8-9 ft)	1	0.77	0.019	16.09	17.29	1.20	0.01	
	10 (9-10 ft)	1	0.74	0.019	15.19	15.53	0.34	0.00	
	11 (10-11 ft)	1	0.73	0.019	15.36	15.96	0.60	0.01	
	12 (11-12 ft)	1	0.75	0.019	14.49	15.83	1.34	0.01	0.50
14	1 (0-1 ft)	1	1.13	0.016	10.13	21.69	11.56	0.09	
	2 (1-2 ft)	1	1.00	0.016	11.11	22.14	11.03	0.09	
	3 (2-3 ft)	1	0.91	0.016	14.60	19.59	4.99	0.04	
	4 (3-4 ft)	1	0.86	0.016	14.64	19.32	4.68	0.04	
	5 (4-5 ft)	1	0.79	0.016	14.70	19.37	4.67	0.04	
	6 (5-6 ft)	1	0.77	0.019	15.03	19.96	4.93	0.05	
	7 (6-7 ft)	1	0.76	0.019	15.10	19.87	4.77	0.05	
	8 (7-8 ft)	1	0.73	0.019	15.25	18.53	3.28	0.04	
	9 (8-9 ft)	1	0.79	0.019	16.37	18.03	1.66	0.02	
	10 (9-10 ft)	1	0.75	0.019	14.81	17.46	2.65	0.03	
	11 (10-11 ft)	1	0.78	0.019	15.73	16.73	1.00	0.01	
	12 (11-12 ft)	1	0.79	0.019	14.51	15.86	1.35	0.01	
	13 (12-13 ft)	1	0.78	0.019	15.98	16.70	0.72	0.01	
	14 (13-14 ft)	1	0.77	0.019	15.01	15.60	0.59	0.01	0.52

(b) Texas Soil

Active Zone (ft)	Layer	Thickness of Layer (ft)	Initial Void Ratio*	Cw From Wetting Curve	Average Min. Field-Measured Water Content* (%)	Average Max. Field-Measured Water Content* (%)	Delta W (%)	Delta Zi (ft)	Total Heave Prediction (ft)
5	1 (0-1 ft)	1	0.97	0.023	14.5	19.0	4.5	0.05	
	2 (1-2 ft)	1	0.97	0.023	15.5	18.9	3.4	0.04	
	3 (2-3 ft)	1	0.97	0.023	17.5	18.8	1.3	0.02	
	4 (3-4 ft)	1	0.97	0.023	17.5	18.6	1.1	0.01	
	5 (4-5 ft)	1	0.97	0.023	17.2	18.0	0.8	0.01	0.13
5	1 (0-1 ft)	1	0.97	0.023	11.6	18.5	6.9	0.08	
	2 (1-2 ft)	1	0.97	0.023	13.9	18.3	4.4	0.05	
	3 (2-3 ft)	1	0.97	0.023	16.5	18.4	1.9	0.02	
	4 (3-4 ft)	1	0.97	0.023	16.9	18.5	1.6	0.02	
	5 (4-5 ft)	1	0.97	0.023	16.8	18.4	1.6	0.02	0.19
5	1 (0-1 ft)	1	0.97	0.023	12.1	18.0	5.9	0.07	
	2 (1-2 ft)	1	0.97	0.023	14.7	18.2	3.5	0.04	
	3 (2-3 ft)	1	0.97	0.023	17.3	18.5	1.3	0.01	
	4 (3-4 ft)	1	0.97	0.023	17.3	18.5	1.2	0.01	
	5 (4-5 ft)	1	0.97	0.023	17.2	18.4	1.2	0.01	0.15

SOIL PROFILE AND PROPERTIES
WES PROJECT

SMI Project No.: n/a
File: c:wes\elevation\Heave-Pier_4.xls

Sources: FSH Boring Log
CSU Geotechnical Laboratory Result

Computed by: DBD Date: 1/14/00
Checked by: Date:

Ground Surface

Depth (ft) 0.0

		w =	11.1 %	% Swell =	7.8 %
	Clay 1	γ_d =	102 pcf	$(\sigma_s')_{c-s}$ =	12,400 psf
		γ_t =	113 pcf	Adj. $(\sigma_s')_{c-s}$ =	7,640 psf
		Inundation Pressure =	500 psf	$C_p/(1+e_o)$ =	0.066
1.0					
		w =	14.7 %	% Swell =	9.2 %
	Clay 2	γ_d =	105 pcf	$(\sigma_s')_{c-s}$ =	17,000 psf
		γ_t =	120 pcf	Adj. $(\sigma_s')_{c-s}$ =	10,400 psf
		Inundation Pressure =	500 psf	$C_p/(1+e_o)$ =	0.070
2.0					
		w =	16.7 %	% Swell =	11.6 %
	Clay 3	γ_d =	109 pcf	$(\sigma_s')_{c-s}$ =	38,000 psf
		γ_t =	127 pcf	Adj. $(\sigma_s')_{c-s}$ =	23,000 psf
		Inundation Pressure =	500 psf	$C_p/(1+e_o)$ =	0.070
3.0					
		w =	17.3 %	% Swell =	7.2 %
	Clay 4	γ_d =	110 pcf	$(\sigma_s')_{c-s}$ =	46,000 psf
		γ_t =	129 pcf	Adj. $(\sigma_s')_{c-s}$ =	27,800 psf
		Inundation Pressure =	500 psf	$C_p/(1+e_o)$ =	0.041

E.O.B = 6.0 feet

HEAVE PREDICTION
WES PROJECT

SMI Project No.: n/a
File: c:\wes\elevation\Heave-Pier_4.xls

Total Heave
@ Max. Depth of Potential Heave: -45.83 inches

Computed by: DBD Date: 1/14/00
Checked by: Date:

(1) Soil Profile and Properties:

	Depth Below G.S. (feet)	Soil Type	Total Unit Weight (pcf)	% Swell, S (%)	Adj. $(\sigma_s')_{o\text{-}s}$ * (psf)	$C_p/(1+e_o)$
	0.0					
	1.0	Clay 1	113	7.8	7,640	0.066
	2.0	Clay 2	120	9.2	10,400	0.070
	3.0	Clay 3	127	11.6	23,000	0.070
>	3.0	Clay 4	129	7.2	27,800	0.041
	E.O.B. =	6.0	feet			

(2) Assumed Depth of Footing: 0 feet
(3) Soil Layers: 35 layers
(4) Depth of Potential Heave Below Footing: 215.49 feet
(5) Calculation of Heave Prediction:

* Adj. $(\sigma_s')_{o\text{-}s} = 0.6\,((\sigma_s')_{o\text{-}s}$ - Inudation Pressure) + Inudation Pressure

Depth Below G.S. (feet)	Depth Below Footing (feet)	Interval (feet)	Soil Type	Total Unit Weight (pcf)	Incr. Load @ midlayer (psf)	Overburden Stress (psf)	Predicted Heave (inches)	Cumulative Heave (inches)
0.00	0.00							
6.16	6.16	6.16	Clay 4	129	397.54	397.54	-5.62	-5.62
12.31	12.31	6.16	Clay 4	129	397.54	1192.62	-4.17	-9.79
18.47	18.47	6.16	Clay 4	129	397.54	1987.70	-3.49	-13.28
24.63	24.63	6.16	Clay 4	129	397.54	2782.78	-3.05	-16.33
30.78	30.78	6.16	Clay 4	129	397.54	3577.85	-2.71	-19.05
36.94	36.94	6.16	Clay 4	129	397.54	4372.93	-2.45	-21.49
43.10	43.10	6.16	Clay 4	129	397.54	5168.01	-2.23	-23.72
49.26	49.26	6.16	Clay 4	129	397.54	5963.09	-2.04	-25.76
55.41	55.41	6.16	Clay 4	129	397.54	6758.17	-1.87	-27.63
61.57	61.57	6.16	Clay 4	129	397.54	7553.25	-1.73	-29.36
67.73	67.73	6.16	Clay 4	129	397.54	8348.33	-1.59	-30.95
73.88	73.88	6.16	Clay 4	129	397.54	9143.40	-1.47	-32.42
80.04	80.04	6.16	Clay 4	129	397.54	9938.48	-1.36	-33.78
86.20	86.20	6.16	Clay 4	129	397.54	10733.56	-1.26	-35.04
92.35	92.35	6.16	Clay 4	129	397.54	11528.64	-1.17	-36.21
98.51	98.51	6.16	Clay 4	129	397.54	12323.72	-1.08	-37.29
104.67	104.67	6.16	Clay 4	129	397.54	13118.80	-0.99	-38.28
110.82	110.82	6.16	Clay 4	129	397.54	13913.88	-0.92	-39.20
116.98	116.98	6.16	Clay 4	129	397.54	14708.95	-0.84	-40.04
123.14	123.14	6.16	Clay 4	129	397.54	15504.03	-0.77	-40.81
129.29	129.29	6.16	Clay 4	129	397.54	16299.11	-0.71	-41.52
135.45	135.45	6.16	Clay 4	129	397.54	17094.19	-0.64	-42.16
141.61	141.61	6.16	Clay 4	129	397.54	17889.27	-0.58	-42.75
147.77	147.77	6.16	Clay 4	129	397.54	18684.35	-0.53	-43.27
153.92	153.92	6.16	Clay 4	129	397.54	19479.43	-0.47	-43.74
160.08	160.08	6.16	Clay 4	129	397.54	20274.50	-0.42	-44.16
166.24	166.24	6.16	Clay 4	129	397.54	21069.58	-0.37	-44.53
172.39	172.39	6.16	Clay 4	129	397.54	21864.66	-0.32	-44.85
178.55	178.55	6.16	Clay 4	129	397.54	22659.74	-0.27	-45.12
184.71	184.71	6.16	Clay 4	129	397.54	23454.82	-0.23	-45.34
190.86	190.86	6.16	Clay 4	129	397.54	24249.90	-0.18	-45.52
197.02	197.02	6.16	Clay 4	129	397.54	25044.98	-0.14	-45.66
203.18	203.18	6.16	Clay 4	129	397.54	25840.06	-0.10	-45.76
209.33	209.33	6.16	Clay 4	129	397.54	26635.13	-0.06	-45.81
215.49	215.49	6.16	Clay 4	129	397.54	27430.21	-0.02	-45.83
							Total	-45.83

SOIL PROFILE AND PROPERTIES
WES PROJECT

SMI Project No.: n/a
File: c:wes\elevation\Heave-Pier_4.xls

Sources: CSU Boring Log
CSU Geotechnical Laboratory Result

Computed by: DBD Date: 1/14/00
Checked by: Date:

Ground Surface

Depth (ft) 0.0

		w =	13.3 %	% Swell =	5.0 %
	Clay	γ_d =	84 pcf	$(\sigma_s')_{c-s}$ =	6,000 psf
		γ_t =	96 pcf	Adj. $(\sigma_s')_{c-s}$ =	3,800 psf
		Inundation Pressure =	500 psf	$C_p/(1+e_o)$ =	0.057
5.0					
		w =	15.1 %	% Swell =	3.8 %
	W. Clayshale 1	γ_d =	98 pcf	$(\sigma_s')_{c-s}$ =	9,000 psf
		γ_t =	112 pcf	Adj. $(\sigma_s')_{c-s}$ =	5,600 psf
		Inundation Pressure =	500 psf	$C_p/(1+e_o)$ =	0.036
10.0					
		w =	15.7 %	% Swell =	1.9 %
	W. Clayshale 2	γ_d =	96 pcf	$(\sigma_s')_{c-s}$ =	4,400 psf
		γ_t =	111 pcf	Adj. $(\sigma_s')_{c-s}$ =	2,840 psf
		Inundation Pressure =	500 psf	$C_p/(1+e_o)$ =	0.025
15.0					
		w =	15.8 %	% Swell =	3.8 %
	W. Clayshale 3	γ_d =	95 pcf	$(\sigma_s')_{c-s}$ =	6,000 psf
		γ_t =	110 pcf	Adj. $(\sigma_s')_{c-s}$ =	3,800 psf
		Inundation Pressure =	500 psf	$C_p/(1+e_o)$ =	0.043

E.O.B = 20.0 feet

HEAVE PREDICTION
WES PROJECT

SMI Project No.: n/a
File: c:wes\elevation\Heave-Pier_4.xls

Total Heave
@ Max. Depth of Potential Heave: -8.23 inches

Computed by: DBD Date: 1/14/00
Checked by: Date:

(1) Soil Profile and Properties:

Depth Below G.S. (feet)	Soil Type	Total Unit Weight (pcf)	% Swell, S (%)	Adj. $(\sigma_s')_{c-s}$* (psf)	$C_c/(1+e_o)$
0.0					
5.0	Clay	96	5.0	3,800	0.057
10.0	W. Clayshale 1	112	3.8	5,600	0.036
15.0	W. Clayshale 2	111	1.9	2,840	0.025
> 15.0	W. Clayshale 3	110	3.8	3,800	0.043
E.O.B. =	20.0	feet			

(2) Assumed Depth of Footing: 0 feet
(3) Soil Layers: 35 layers
(4) Depth of Potential Heave Below Footing: 35.10 feet
(5) Calculation of Heave Prediction:

* Adj. $(\sigma_s')_{c-s} = 0.6\,((\sigma_s')_{c-s}$ - Inudation Pressure) + Inudation Pressure

Depth Below G.S. (feet)	Depth Below Footing (feet)	Interval (feet)	Soil Type	Total Unit Weight (pcf)	Incr. Load @ midlayer (psf)	Overburden Stress (psf)	Predicted Heave (inches)	Cumulative Heave (inches)
0.00	0.00							
1.00	1.00	1.00	Clay	96	47.95	47.95	-1.30	-1.30
2.01	2.01	1.00	Clay	96	47.95	143.86	-0.97	-2.27
3.01	3.01	1.00	Clay	96	47.95	239.77	-0.82	-3.09
4.01	4.01	1.00	Clay	96	47.95	335.68	-0.72	-3.81
5.01	5.01	1.00	W. Clayshale 1	112	56.35	439.99	-0.48	-4.28
6.02	6.02	1.00	W. Clayshale 1	112	56.35	552.70	-0.43	-4.72
7.02	7.02	1.00	W. Clayshale 1	112	56.35	665.41	-0.40	-5.11
8.02	8.02	1.00	W. Clayshale 1	112	56.35	778.12	-0.37	-5.48
9.03	9.03	1.00	W. Clayshale 1	112	56.35	890.83	-0.34	-5.83
10.03	10.03	1.00	W. Clayshale 2	111	55.70	1002.88	-0.14	-5.96
11.03	11.03	1.00	W. Clayshale 2	111	55.70	1114.29	-0.12	-6.09
12.04	12.04	1.00	W. Clayshale 2	111	55.70	1225.69	-0.11	-6.20
13.04	13.04	1.00	W. Clayshale 2	111	55.70	1337.09	-0.10	-6.30
14.04	14.04	1.00	W. Clayshale 2	111	55.70	1448.49	-0.09	-6.39
15.04	15.04	1.00	W. Clayshale 3	110	54.99	1559.18	-0.20	-6.59
16.05	16.05	1.00	W. Clayshale 3	110	54.99	1669.17	-0.19	-6.77
17.05	17.05	1.00	W. Clayshale 3	110	54.99	1779.16	-0.17	-6.94
18.05	18.05	1.00	W. Clayshale 3	110	54.99	1889.15	-0.16	-7.10
19.06	19.06	1.00	W. Clayshale 3	110	54.99	1999.13	-0.14	-7.25
20.06	20.06	1.00	W. Clayshale 3	110	54.99	2109.12	-0.13	-7.38
21.06	21.06	1.00	W. Clayshale 3	110	54.99	2219.11	-0.12	-7.50
22.07	22.07	1.00	W. Clayshale 3	110	54.99	2329.10	-0.11	-7.61
23.07	23.07	1.00	W. Clayshale 3	110	54.99	2439.09	-0.10	-7.71
24.07	24.07	1.00	W. Clayshale 3	110	54.99	2549.07	-0.09	-7.80
25.07	25.07	1.00	W. Clayshale 3	110	54.99	2659.06	-0.08	-7.88
26.08	26.08	1.00	W. Clayshale 3	110	54.99	2769.05	-0.07	-7.95
27.08	27.08	1.00	W. Clayshale 3	110	54.99	2879.04	-0.06	-8.01
28.08	28.08	1.00	W. Clayshale 3	110	54.99	2989.02	-0.05	-8.07
29.09	29.09	1.00	W. Clayshale 3	110	54.99	3099.01	-0.05	-8.11
30.09	30.09	1.00	W. Clayshale 3	110	54.99	3209.00	-0.04	-8.15
31.09	31.09	1.00	W. Clayshale 3	110	54.99	3318.99	-0.03	-8.18
32.09	32.09	1.00	W. Clayshale 3	110	54.99	3428.98	-0.02	-8.21
33.10	33.10	1.00	W. Clayshale 3	110	54.99	3538.96	-0.02	-8.22
34.10	34.10	1.00	W. Clayshale 3	110	54.99	3648.95	-0.01	-8.23
35.10	35.10	1.00	W. Clayshale 3	110	54.99	3758.94	0.00	-8.23
							Total	-8.23

APPENDIX E

SoilCover Model Input Pages and SEEP/W Mesh

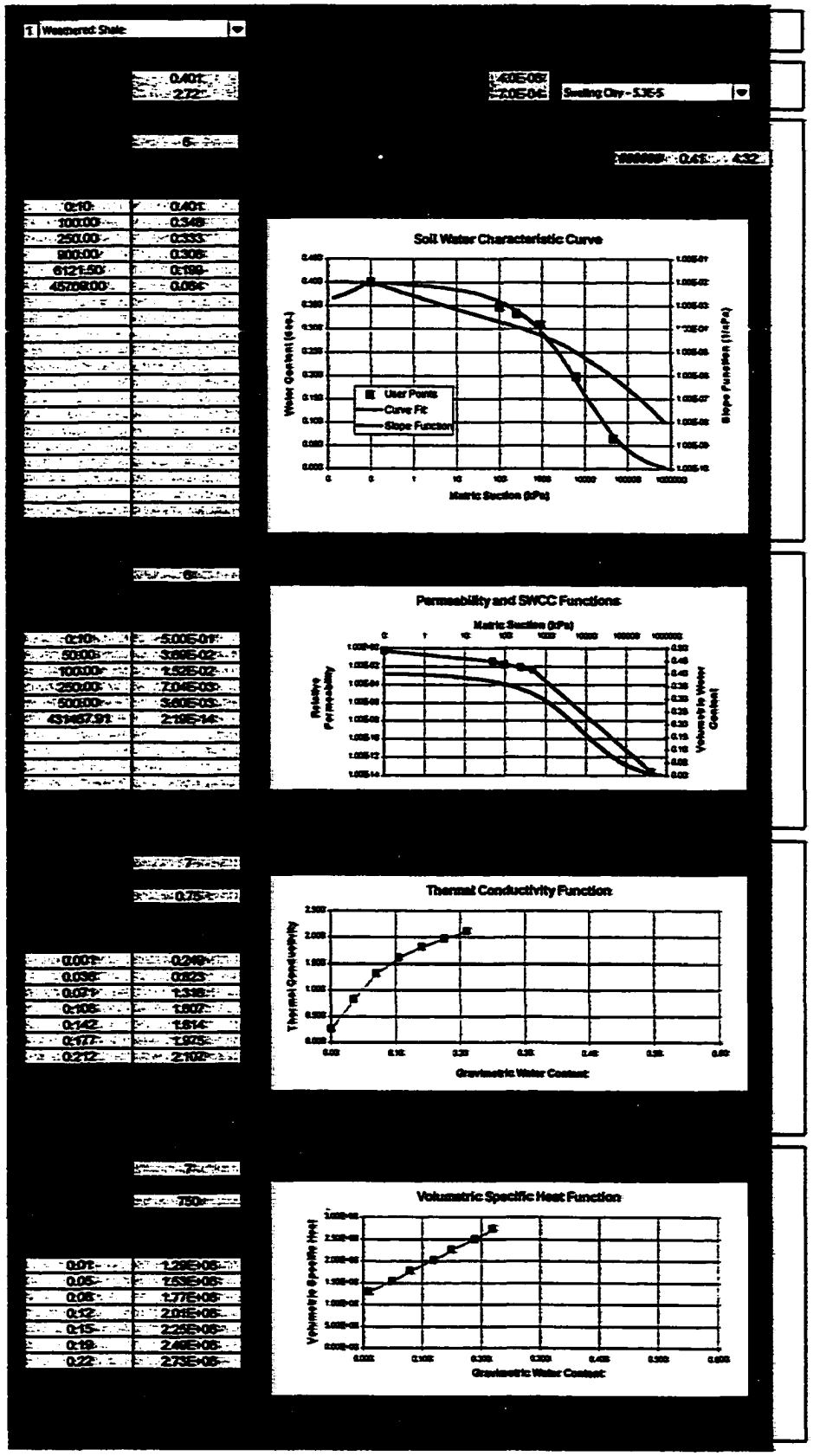

Note: Boundary Conditions TYPES and value UNITS can be:
0 - Pressure (kPa) 3 - Rain / Snow Melt (m/s/day)
1 - Volumetric Water Cont (dec.) 2 - Gravimetric Water Cont (dec.)

		Weather Data Section:						Moisture Boundaries Section:							Other Daily Data Section:			
199																		
200																		
201																		
202	1	12.36	4.33	4.67160667	0.408	0.229	21.09583333	3	0	0	24	2	0.15		12.5		0	
203	2	10.43	-3.38	-4.955558614	1.041	0.346	15.25	3	0	0	24	2	0.15		12.5		0	
204	3	1.25	-6.39	1.58549474	0.653	0.522	23.02916667	3	0	0	24	2	0.15		12.5		0	
205	4	1.57	-8.91	4.251684691	0.878	0.556	8.741666667	3	0	0	24	2	0.15		12.5		0	
206	5	4.06	-8.48	0.247353281	0.913	0.517	4.0875	3	1.27	0	24	2	0.15		12.5		0	
207	6	8.12	-4.40	4.320022935	0.971	0.403	5.891666667	3	0.254	0	24	2	0.15		12.5		0	
208	7	11.42	-5.67	3.030745829	0.959	0.365	3.829166667	3	0	0	24	2	0.15		12.5		0	
209	8	12.40	-3.20	2.191917303	0.907	0.303	5.95	3	0	0	24	2	0.15		12.5		0	
210	9	12.44	-3.47	4.188541685	0.866	0.122	12.175	3	0	0	24	2	0.15		12.5		0	
211	10	4.33	-4.60	-1.125047941	0.914	0.324	7.941666667	3	0	0	24	2	0.15		12.5		0	
212	11	7.42	-6.05	4.256686681	0.912	0.382	6.895833333	3	0	0	24	2	0.15		12.5		0	
213	12	5.98	-6.57	0.331063819	0.824	0.47	7.15	3	0	0	24	2	0.15		12.5		0	
214	13	11.43	-7.98	2.578273497	0.9	0.376	6.3	3	0	0	24	2	0.15		12.5		0	
215	14	14.90	-3.28	3.072061254	0.816	0.33	6.858333333	3	0	0	24	2	0.15		12.5		0	
216	15	16.48	-2.80	3.650973736	0.808	0.285	5.204166667	3	0	0	24	2	0.15		12.5		0	
217	16	14.87	-1.13	-1.75215736	0.829	0.304	4.129166667	3	0	0	24	2	0.15		12.5		0	
218	17	12.89	-1.53	3.653296796	0.83	0.429	4.354166667	3	0	0	24	2	0.15		12.5		0	
219	18	11.93	-3.58	0.120198836	1.057	0.446	4.841666667	3	1.27	0	24	2	0.15		12.5		0	
220	19	3.33	-5.48	-4.301098552	1.057	0.913	4.55	3	0	0	24	2	0.15		12.5		0	
221	20	0.50	-2.36	-4.851529227	1.062	1.004	4.291666667	3	0.254	0	24	2	0.15		12.5		0	
222	21	0.95	-14.86	1.092725243	1.061	0.7	5.108333333	3	0	0	24	2	0.15		12.5		0	
223	22	-1.40	-17.42	-3.458951808	1.031	0.872	2.7	3	0	0	24	2	0.15		12.5		0	
224	23	-0.29	-8.32	-2.16361885	1.038	0.782	9.570833333	3	0	0	24	2	0.15		12.5		0	
225	24	-4.77	-17.24	0.689186376	0.834	0.514	7.854166667	3	0	0	24	2	0.15		12.5		0	
226	25	-2.41	-18.17	2.278106188	0.957	0.477	3.508333333	3	0	0	24	2	0.15		12.5		0	
227	26	5.35	-14.83	3.363136167	0.921	0.396	4.395833333	3	0.762	0	24	2	0.15		12.5		0	
228	27	5.01	-13.06	3.178288753	0.832	0.329	3.7	3	1.778	0	24	2	0.15		12.5		0	
229	28	3.58	-12.08	-0.882334734	1.018	0.438	4.575	3	0.762	0	24	2	0.15		12.5		0	
230	29	0.97	-17.26	2.307961286	1.026	0.47	5.670833333	3	0	0	24	2	0.15		12.5		0	
231	30	10.26	-15.20	2.518199867	0.958	0.093	9.804166667	3	0.254	0	24	2	0.15		12.5		0	
232	31	8.73	-10.36	2.609199642	0.949	0.286	16.85416667	3	0	0	24	2	0.15		12.5		0	
233	32	0.10	-13.24	2.708548901	0.965	0.536	6.495833333	3	0	0	24	2	0.15		12.5		0	
234	33	-5.40	-11.10	-3.22000854	0.991	0.787	7.420833333	3	0	0	24	2	0.15		12.5		0	
235	34	-4.83	-21.40	2.799363818	0.991	0.592	3.420833333	3	0	0	24	2	0.15		12.5		0	
236	35	-7.48	-19.84	-2.97474836	1	0.803	5.116666667	3	0	0	24	2	0.15		12.5		0	
237	36	-1.63	-16.17	1.505965116	1.001	0.684	3.7375	3	0	0	24	2	0.15		12.5		0	
238	37	3.22	-16.52	2.763556817	0.956	0.385	3.395833333	3	0.254	0	24	2	0.15		12.5		0	
239	38	5.76	-13.37	0.758632854	0.785	0.405	4.9	3	1.016	0	24	2	0.15		12.5		0	
240	39	9.69	-10.08	0.597374046	0.707	0.389	12.15416667	3	2.302	0	24	2	0.15		12.5		0	
241	40	7.18	-8.54	1.772372445	0.91	0.421	8.383333333	3	0	0	24	2	0.15		12.5		0	
242	41	9.62	-6.00	-0.171220059	0.913	0.466	5.079833333	3	0	0	24	2	0.15		12.5		0	
243	42	0.96	-5.91	-3.16323823	0.939	0.632	5.25	3	0	0	24	2	0.15		12.5		0	
244	43	-3.26	-8.25	-1.915787111	0.823	0.565	15.47916667	3	0	0	24	2	0.15		12.5		0	
245	44	-7.35	-15.85	1.858065887	0.962	0.52	5.054166667	3	0	0	24	2	0.15		12.5		0	
246	45	4.81	-4.46	-2.534178048	0.868	0.527	9.3375	3	0	0	24	2	0.15		12.5		0	
247	46	-2.78	-10.67	-2.917189024	0.995	0.63	5.079166667	3	0	0	24	2	0.15		12.5		0	
248	47	-1.48	-15.49	1.468581939	1.003	0.635	3.883333333	3	0	0	24	2	0.15		12.5		0	
249	48	2.25	-12.40	-0.403223214	1.018	0.489	4.508333333	3	0	0	24	2	0.15		12.5		0	
250	49	-4.32	-18.94	-3.622135146	1.02	0.951	4.391666667	3	0	0	24	2	0.15		12.5		0	
251	50	4.27	-19.70	0.272282899	0.97	0.306	8.604166667	3	0	0	24	2	0.15		12.5		0	
252	51	2.23	-11.64	1.776860805	0.711	0.372	7.004166667	3	0	0	24	2	0.15		12.5		0	
253	52	5.84	-11.24	1.627078337	0.736	0.308	11.81666667	3	0	0	24	2	0.15		12.5		0	
254	53	-0.24	-16.62	1.678841744	0.965	0.544	6.216666667	3	0	0	24	2	0.15		12.5		0	
255	54	12.57	-16.89	0.930580563	0.97	0.198	11.825	3	0	0	24	2	0.15		12.5		0	
256	55	2.70	-12.46	2.074891232	0.963	0.561	4.991666667	3	0	0	24	2	0.15		12.5		0	
257	56	11.32	-14.27	1.863861775	0.845	0.157	7.825	3	0	0	24	2	0.15		12.5		0	
258	57	7.38	-8.40	1.698672963	0.513	0.215	5.045833333	3	0	0	24	2	0.15		12.5		0	
259	58	0.47	-7.15	-1.0244717	1.035	0.472	5.616666667	3	0	0	24	2	0.15		12.5		0	
260	59	1.34	-8.84	-0.18026803	1.036	0.657	4.15	3	0	0	24	2	0.15		12.5		0	
261	60	9.44	-8.61	-1.28995139	1.02	0.375	10.03333333	3	0	0	24	2	0.15		12.5		0	
262	61	-0.41	-11.07	1.458831948	1.03	0.707	4.995833333	3	0	0	24	2	0.15		12.5		0	
263	62											2	0.15		12.5		0	
264	63											2	0.15		12.5		0	
265	64											2	0.15		12.5		0	
266	65											2	0.15		12.5		0	
267	66											2	0.15		12.5		0	
268	67											2	0.15		12.5		0	
269	68											2	0.15		12.5		0	
270	69											2	0.15		12.5		0	
271	70											2	0.15		12.5		0	
272	71											2	0.15		12.5		1	
273	72											2	0.15		12.5		0	
274	73											2	0.15		12.5		0	
275	74											2	0.15		12.5		0	
276	75											2	0.15		12.5		0	
277	76											2	0.15		12.5		0	
278	77											2	0.15		12.5		0	
279	78											2	0.15		12.5		0	
280	79											2	0.15		12.5		0	
281	80											2	0.15		12.5		0	
282	81											2	0.15		12.5		0	
283	82											2	0.15		12.5		0	
284	83											2	0.15		12.5		0	
285	84											2	0.15		12.5		0	
286	85											2	0.15		12.5		0	

	A	B	C	D	E	F	G	H	I	J	K	L	M	N	O	P	Q	R	S
287	86											2	0.15		12.5		0		
288	87											2	0.15		12.5		0		
289	88											2	0.15		12.5		0		
290	89											2	0.15		12.5		0		
291	90											2	0.15		12.5		0		
292	91											2	0.15		12.5		0		
293	92											2	0.15		12.5		0		
294	93											2	0.15		12.5		0		
295	94											2	0.15		12.5		0		
296	95											2	0.15		12.5		0		
297	96											2	0.15		12.5		0